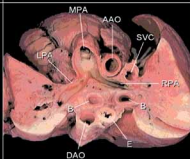Enrico M. Chiappa
Andrew C. Cook
Gianni Botta
Norman H. Silverman

Echocardiographic Anatomy in the Fetus

Springer

Enrico M. Chiappa • Andrew C. Cook
Gianni Botta • Norman H. Silverman

Echocardiographic Anatomy in the Fetus

Enrico M. Chiappa
Maternal and Perinatal Cardiology Unit
Division of Pediatric Cardiology
"Meyer" Children's Hospital
Florence, Italy

Andrew C. Cook
British Heart Foundation
Cardiac Morphology Unit
Institute of Child Health
University College London
London, United Kingdom

Gianni Botta
Fetal and Maternal Pathology
Department of Pathology
"O.I.R.M. – S. Anna"
Children & Women's Hospital
Turin, Italy

Norman H. Silverman
Pediatric and Fetal Echocardiography Laboratories
Division of Pediatric Cardiology
Lucile Packard Children's Hospital
Stanford University Medical Center
Palo Alto, California, USA

With a contribution by
Rabih Chaoui (Chapter 20)
Center for Prenatal Diagnosis
and Human Genetics
Berlin, Germany

To our parents, who paved the way of our lives

Preface

by Norman H. Silverman

Over the last two decades, the value of examining the fetal heart has moved from an experimental procedure of diagnostic curiosity to a front-line form of evaluating fetal cardiac health and disease. There have been numerous advances in the associated technology, including high-resolution imaging, the introduction of reliable color flow and pulse Doppler, and M-Mode and continuous-wave Doppler recordings in some instruments. Such advances continue, with the potential for 3D imaging using spatiotemporal image correlation (STIC) and full-volume fetal technology.

The techniques used by obstetric sonographers in all fields, including physicians from the fields of radiology, obstetrics, and pediatric cardiology, together with technologists who support and do most of the scanning, require a fundamental understanding of ultrasound as well as anatomy, physiology, and the various cardiac pathologies that occur in the fetus. This book addresses these fundamentals, providing correlations by means of diagrams and images of fetal cardiac morphology and pathology. The scans are quite unique, having been collected over several years by the principal author, Dr. Enrico M. Chiappa, from his laboratories in Italy, and provide exquisite echocardiography of normal and congenitally malformed hearts. These are complemented by the excellent pathological images of Dr. Andrew C. Cook and Dr. Gianni Botta, who provided high-quality images of normal and pathological fetal heart conditions, which are displayed as support for the echocardiographic images.

The organization of this book is oriented toward practitioners. The first section provides general guidelines for imaging the fetal body and heart, for segmental analysis, and for diagnosis. The second section takes a view-oriented approach, describing first the transverse views and then the longitudinal views of the fetal body and how each echocardiographic projection best displays a particular pathological entity. The third section contains essential information pertaining to the new technique of 3D/4D echocardiography and the role of the pathologist in heart disease, which expands further the value of this text for providing references and comparisons with standard imaging techniques.

The authors obviously gave a great deal of thought to this project – from the choice of images in the text, which include the clearest descriptions and labels, to the accompanying DVD, which contains complex moving echocardiographic images. The objective is to provide the reader with something greater than a static representation of the fetal cardiac morphology while retaining the ability to refer directly to morphological comparisons and consult with the text for greater detail. This work will have great appeal to physicians and technologists involved in obtaining and interpreting such images and will provide the obstetric, cardiological, and radiological communities with an excellent reference for comparing cases seen in their daily practice.

Preface

by Enrico M. Chiappa

The number of congenital heart diseases detected in utero is still low, even in countries with well-advanced screening programs. Only 20% of new cases of congenital heart disease come from traditional high-risk pregnancies. Ultrasound screening of all pregnancies is therefore necessary to improve the detection rate of congenital heart diseases and to manage them most effectively. However, prenatal screening studies have shown widely divergent results, with low detection rates in most cases. Several reasons have been advocated to explain why these programs seem to fail, and different solutions have been proposed to improve the success rate. There is a broad consensus that examiner skill plays a crucial role in this setting and that appropriate training is mandatory.

It is our belief that people responsible for fetal cardiology units in centers of excellence should invest resources to fully educate the personnel involved in prenatal ultrasound screening. To do this, a fundamental step is to improve, simply and comprehensibly, their knowledge about the anatomy of the fetal cardiovascular system. As Prof. Robert Anderson beautifully stated in a recent review [Anderson RH, Razavi R, Taylor AM (2004) Cardiac anatomy revisited. J Anat 205:159-177], one convention of the human anatomy is that all structures should be described in the setting of their anatomical position within the body and of the relationship of organs to each other. This convention has not always been strictly applied when describing the heart. In the past, the so-called Valentine approach has prevailed, that is, the convention of representing the heart isolated from the surrounding structures and balanced on its apex, with the atria above the ventricles. This approach generated confusion, particularly in the field of congenital heart disease, where the position of the heart and the location of the cardiac segments is variable. Therefore, as Prof. Anderson wrote: "students should be introduced to the anatomy of the heart as it lies within the body, as revealed with clinical tomographic images". To this purpose, the use of tomographic sections of isolated hearts, frequently used in textbooks of echocardiography, is only partially effective in prenatal ultrasound examination, where the views of the surrounding structures are much wider and the approaches to the fetal thorax more variable than in the postnatal setting.

We decided, therefore, to perform image sections of the whole fetal body to obtain tomographic views of the heart, thus showing the relationship between cardiac and extracardiac structures. As indicated in Chapter 21, tomographic sections of the fetal body were obtained in a limited number of fetuses under the gestational age of 20 weeks following informed consent of parents and in strict adherence with the Italian legislation on this subject. The idea to obtain these types of sections stemmed from almost 20 years of fundamental work by Alf Staudach [Staudach A (1989) Sectional fetal anatomy in ultrasound. Springer], with the advantages of computer technology in photographic and ultrasound images.

Rather than systematically describing congenital heart diseases in the fetus, the goal of this work is to provide a basic tool for understanding the normal and abnormal echocardiographic anatomy of the fetal heart. In this way, this textbook is complementary and not alternative to the more extensive publications on this subject.

The first section of this book describes the basic principles of diagnosis, illustrating assessment of the laterality of the fetal body, the visceroatrial arrangement, and the cardiac position. This order reproduces the logical sequence the examiner should follow when studying the fetal heart. In the second section, all echocardiographic projections in the fe-

tus are described, from those most familiar to obstetric sonographers, to those usually obtained only by pediatric cardiologists. Particular emphasis is given to imaging the short-axis sections of the fetal body, which has recently proven to be a powerful method for complete examination of the fetal heart. The chapters pertaining to echocardiographic projection are in logical sequence in two series: the transverse views of the fetal thorax, presented from the bottom to the top, and the sagittal and parasagittal views, presented from the right side to the left side. The sequence of these planes in some ways imitates the changes of the scanning plane that can be obtained by the examiner tilting or translating the probe manually with traditional probes or electronically with modern 3D ultrasound.

The third section consists of two chapters. The first describes the essential use of modern 3D/4D ultrasound techniques to image the fetal heart, including new volume manipulation, such as spatial and temporal image correlation (STIC), and rendering, such as glass-body, minimum-transparent, and inversion modes. The second chapter emphasizes the importance of autopsy in providing information regarding anomalies of the fetal heart and describes optimal techniques for dissection and photography of the autopsic specimens. This section emphasizes the crucial role of the echocardiographic projections described elsewhere in this book, which maintain their fundamental role in the comprehension of new advances in ultrasound and the future application of MRI/CT in postmortem studies of the fetal heart. These two different chapters are incorporated in this section because the approach to volume data sets of 3D/4D sonography and to blocks of pathological specimens shows many similarities. The information displayed by either technique depends on the level at which the examiner cuts the cardiac volume, no matter if a digital tool or a pathologist's blade is used. Moreover, some image-rendering techniques are comparable with the fine-art photographic technique available to the pathologist to display with outstanding clarity the subtle details of congenital heart disease in fetal heart specimens.

The problem of image orientation was thoroughly discussed with cardiac morphologists Andrew C. Cook, Gianni Botta, and Robert H. Anderson from the very beginning of the editorial phase of this book. The reader will notice that some anatomical images of the transverse sections of the thorax do not "at first sight" match the echocardiographic images. We decided to maintain the echocardiographic images in their original caudocranial orientation, a standard that is accepted in MR and CT imaging, rather than flip them horizontally, which would reduce the resolution of the digital clips on the accompanying DVD. We decided, instead, to display a compass with every image, thus illustrating its orientation.

As to the abnormal heart, rather than fully describe a single congenital heart disease in different projections, the book and DVD describe how a specific projection appears in the normal heart and in some abnormal conditions. Although we understand that this is not sufficient for a comprehensive assessment of a specific disease, we believe this type of presentation reproduces the usual approach of the examiner, who is initially unaware whether the case being examining is normal or abnormal. The more the examiner understands the normal anatomy, the easier it is to recognize what is wrong.

Ultrasound assessment of the heart, whether in fetal life or postnatally, is based on moving images, and books therefore have limited value in teaching echocardiography. With recent advances in ultrasound systems, storing multiple digital frames and clips with superb image quality has become a reality. These advances have brought innovative applications to the clinical field and can be utilized as powerful multimedia presentations for teaching purposes. The accompanying DVD is such a tool. This is a complex DVD that includes more than 300 clips of normal and abnormal views of the fetal heart frames of each topic, with 11–13, representing a single cardiac cycle, each of which is displayed in a loop. The DVD in many respects is not simply a copy of the book. The text window contains essential information of the case being presented, and – in the four-chamber section in particular – a short unit describes the essential features of each specific congenital heart disease. We believe this presentation will be a highly useful tool for all those interested in the echocardiographic study of the fetal heart.

Acknowledgements

We are particularly indebted to Giuliano Kraft – efficiently supported in the final phase of this work by Tiziano Carducci – for the patience and strength he showed as time went on and it became apparent that the work was evolving beyond our expectations. Thanks to his creativity and professional ability in the digital world, he contributed brilliantly to the shape and construction of the complex structure of the accompanying DVD.

We also thank the staff at Springer-Verlag Italia, and in particular Antonella Cerri, executive editor, for first approaching us with, and then believing in, this project; Marie Thompson, for her outstanding work in copyediting the manuscript; and Alessandra Born and Barbara Ferrario, assistant editors, for their efficiency in helping to keep everything straight and on track.

Finally, my deep appreciation to Gabriella, my lovely companion in life, who believed in me and tolerated many lonely evenings and weekends over the long period it took to complete this project. The authors' wish only that through this work, many families will gain more than our families have lost.

Florence, August 2008   E.M. Chiappa

Contents

PART II   Echocardiographic Projections

A   Transverse Views of the Fetal Body

C Oblique Views of the Fetal Body

PART III Echocardiographic and Morphologic Overview

PART I

Basic Principles of Diagnosis

CHAPTER 1 General Guidelines

Introduction

Congenital heart diseases are the most common congenital malformations, affecting six to eight per 1,000 live births [1-3], and their prevalence in abortuses has been shown to be even higher [4, 5]. Moreover, heart diseases are the leading cause of death among infants with congenital anomalies, causing nearly 20% of neonatal deaths and up to 50% of infant deaths due to congenital anomalies. Recent studies have demonstrated a positive impact of prenatal diagnosis in morbidity and mortality rates in specific groups of congenital heart disease [6-8]. Only 20% of congenital heart disease in the fetus occurs in high-risk pregnancies; therefore, routine screening of all pregnancies is necessary. Prenatal screening cannot be conferred solely to pediatric cardiologists because of the limited number of these specialists. The alternative, chosen in many developed countries, is to assess the heart in a simplified form – the four-chamber view – during routine "anomaly scan" at 18-20 weeks' gestation and to provide extra training for all obstetric sonographers. The anticipated potential of the four-chamber view to detect most of the severe cardiac anomalies has been disproved by discouraging false-negative rates of congenital heart disease in many screening programs utilizing this projection only [9-11]. Most forms of conotruncal anomalies, such as transposition of the great arteries, tetralogy of Fallot, truncus arteriosus, and double-outlet right ventricle, may appear completely normal in the four-chamber view. Some screening programs have demonstrated that the detection rate for congenital heart disease is significantly improved by an extended cardiac examination [12-16]. Therefore, there is a growing consensus that assessment of the ventriculoarterial connection should be included in the routine fetal anomaly scan [17, 18]. Detailed fetal echocardiography may identify most significant congenital heart diseases, but it is time consuming and requires special knowledge of the normal and abnormal cardiovascular system, which is not a requirement for every examiner. Most authors agree that to improve results in fetal echocardiography, efforts are needed to expand the skills of the operator involved with a clear and effective educational method. Positive results of training sonographers to recognize cardiac abnormality in the fetus have been proven [19, 20]. We believe the information provided in this work will be most useful to that end.

The background of this project comes from two main considerations. First, whether in fetal life or postnatally, echocardiographic diagnosis is based on moving images. Consequently, books have limited value in teaching echocardiography, and the use of videotapes is time consuming and relies on inconsistent image quality. With recent advances in ultrasound systems, storing multiple digital frames and clips with superb image quality has become a reality. These advances have brought innovative applications into the clinical field and can be utilized in powerful multimedia presentations for teaching purposes. Second, imaged sections of cardiac specimens are usually compared with their corresponding echocardiographic views in textbooks of echocardiography. These sections are mainly obtained from isolated hearts because they are technically easier and less time consuming to obtain. Nevertheless, imaged sections of the whole body are better tools by which to understand the relationship between cardiac and extracardiac structures. This understanding is particularly necessary in fetal echocardiography, where the number of visible structures around the heart is much greater and the approaches to the fetal thorax are more variable.

For this project, we created a digital presentation, included in the DVD, in which images from tomographic sections of the whole fetal body are combined with dynamic echocardiographic images of normal fetuses and of some of the most common congenital heart defects. All projections are accompanied by schemes and full text for better understanding. We believe this collection will be a major tool for all those interested in studying the fetal heart.

Equipment

A thorough discussion of the principles of ultrasound in prenatal diagnosis is beyond the scope of this project, and the reader must refer to papers and books that extensively cover this subject [21-24].

General guidelines for instrumentation in fetal echocardiography recommend high-resolution ultrasound machines. Impressive progress has been made in ultrasound probe resolution over the past decade, thanks also to the very fast frame rate achieved by parallel processing in which the transducer transmits one line and receives two, resulting in a doubling of the previous rate (Fig. 1.1). Using modern probes, fetal echocardiography can now be performed transvaginally at 11-14 weeks gestational age and transabdominally at 12-15 weeks gestational age [25, 26]. Because of its effectiveness in identifying fetuses at risk for chromosomal and cardiac anomalies, nuchal translucency screening is creating an increasing population of fetuses in need of complete echocardiography [27-29]. Although diagnostic examination can be obtained at an early gestational age in selected cases, further scan between 18-22 weeks gestational age is recommended [30-32].

Transducer frequency should be as high as possible to obtain the best resolution. In the second trimester, a 5-8 MHz transducer is suitable in most cases. Nevertheless, a 3 MHz transducer may be required when deep penetration is necessary due to maternal overweight, an anterior placenta, polyhydramnios, or an unfavorable fetal position. Either sector or convex probes may be used, with advantages and disadvantages for each. Sector probes are the ones most preferred by cardiologists because they are designed to give the best performance in cardiac applications. Moreover, because of their diverging beam, sector probes are most useful when the acoustic window is limited. In the presence of polyhydramnios or increased thickness of the maternal wall, a sector transducer, thanks to its small footprint, can be placed into the umbilical cavity to get closer to the fetus and thus improve image quality. On the other hand, because of the divergent direction of the ultrasound beam from the probe surface, line density (and lateral resolution) decreases as depth increases.

Conversely, convex probes allow for a more ample angle of visualization, making orientation on the fetal body easier and guaranteeing a more homogeneous resolution over the whole area of investigation.

Because of the moving structures of the heart and the high heart rate in the fetus, the primary goal in ultrasound setting is to obtain a frame rate as high as possible. Cross-sectional imaging (Fig. 1.2a) is still the modality most commonly used to study the fetal heart. In this setting, a presetting with compressed gray scale, narrow ultrasound beam, single focus, and absent or very low persistence is recommended. For inexperienced obstetric sonographers, it is important to remember that such a presetting exists and must be selected because an obstetrical presetting employs a frame rate too low to reliably image the fetal heart. To avoid damage to the fetus, cardiac presetting
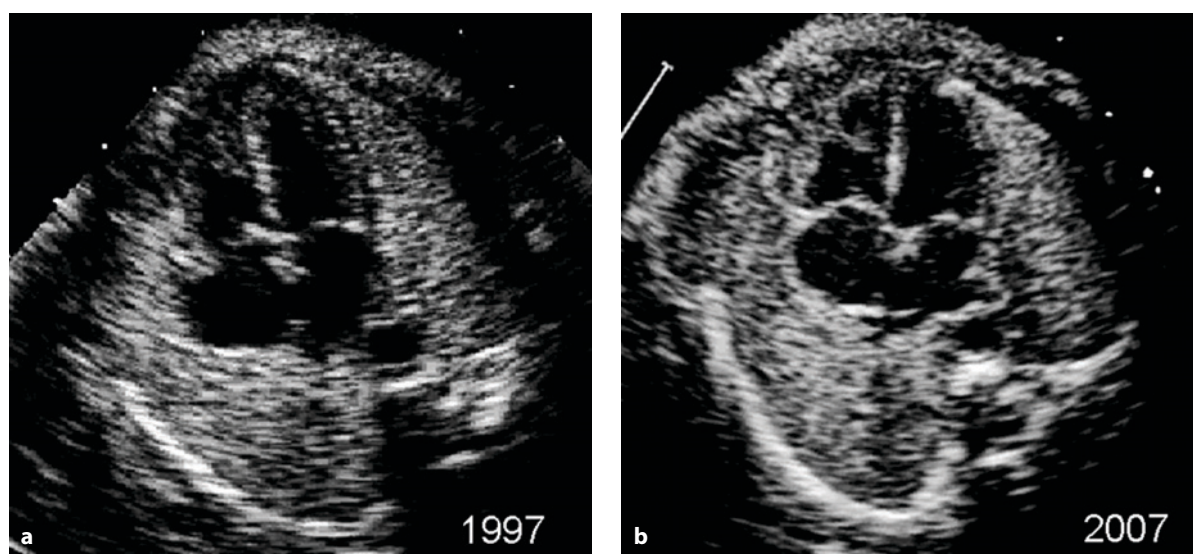
Fig. 1.1 • Ten years separates these two (**a**, **b**) four-chamber echocardiographic sections (**a** 1997; **b** 2007). The improvement in resolution of the new generation of probes is seen in the 2007 image, where a higher degree of anatomic detail is appreciated

should also be used to ensure that spatial temporal average power output for color and pulsed Doppler is less than 100 mW/cm^2.

The possibility of image magnification using the zoom allows for better definition of the size and structure of the fetal heart, whereas the cine loop now makes it possible to record a long series of consecutive digital images that can be immediately reexamined as single frames. This function is particularly useful for identifying structural or flow anomalies that may be overlooked should the images be evaluated in real time only. With recent instrumentation, storing digital clips on the hard disk of the built-in computer is possible. Instruments equipped with cine-loop and digital-clip storing capabilities provide a user-friendly system in which moving clips and still-frame digital images are readily accessible for review – a powerful means for off-line analysis and case discussion that is largely superior to professional videotape recorders.

When investigating the fetal heart, the use of Doppler is complementary to the morphological study with the cross-sectional technique. To allow an accurate flow evaluation, the insonation angle should be as parallel as possible to the estimated flow direction under study. The estimated error of flow velocity is negligible for insonation angles less than 20-30°. Routine use of color flow mapping (CFM) (Fig. 1.2b) is helpful to assess the symmetry of ventricular filling and to detect significant regurgitation of the atrioventricular valves related to major congenital heart defects. CFM facilitates positioning of the sample volume of pulsed Doppler in the region of interest. On CFM evaluation, the color box should be kept as small as possible, with maximum scale velocity around 50-90 cm/s in arterial districts and 7-20 cm/s in venous districts. On pulsed Doppler (Fig. 1.2c), the sample volume must be kept small (2-4 mm), with a wall filter at 150-300 Hz for arterial vessels and 50-100 Hz for venous vessel. Pulsed Doppler tracings should be obtained during periods of fetal apnea to avoid the flow waveform modifications produced by respiratory movement. Continuous Doppler is considered optional but may be necessary to assess precisely the peak velocity of high-velocity jets, such as those in tricuspid valve regurgitation in pulmonary valve atresia with intact ventricular septum (Fig. 1.2d).
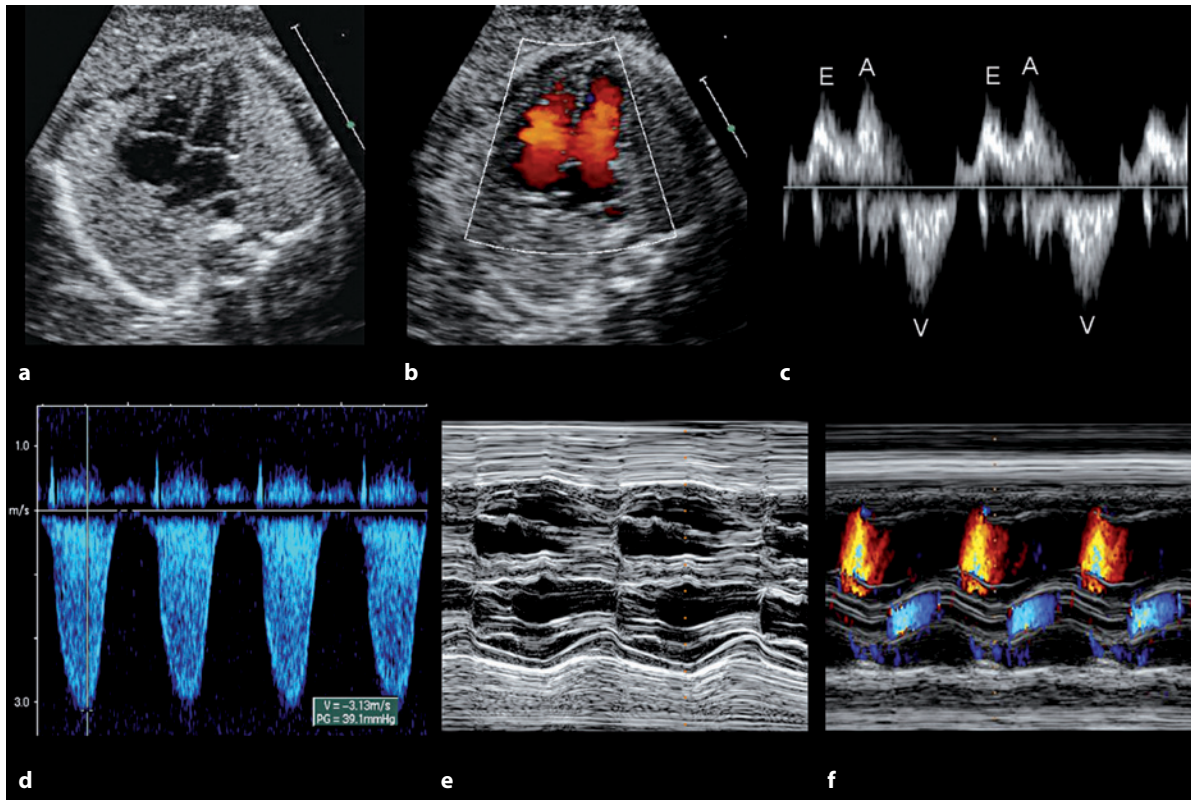
Fig. 1.2 • Some of the most common applications of echocardiography in the fetal heart: cross sectional (**a**), color flow mapping (**b**), pulsed Doppler (**c**), continuous Doppler (**d**), M-mode (**e**), and color M-mode (**f**)

Due to the high frame rate and time resolution, M-mode tracing (Fig. 1.2e) is the most accurate method to provide information on wall thickness, ventricular diameter, and shortening fraction. However, the application of M-mode in the fetus is limited because M-mode measurements require an ultrasound beam orientation that is difficult and sometimes impossible to obtain. Color M-mode color (Fig. 1.2f) combined with pulsed Doppler has been demonstrated to be an invaluable tool in assessing fetal arrhythmias.

Major Planes of the Body and Heart

The major planes of the body are the sagittal, coronal, and transverse planes (Fig. 1.3) as detailed in the following:

- The *sagittal plane*, also called the median plane, runs in a true anteroposterior direction. When traced through the median axis, the body is divided into right and left halves.
- The *coronal plane*, also called frontal plane, is a long-axis plane of the body perpendicular to the sagittal plane. When it is traced through the central axis, it divides the body into anterior and posterior halves.
- The *transverse plane*, also called the horizontal plane, is a short-axis plane of the body perpendicular to the sagittal and coronal planes. It divides the body into superior and inferior portions.

The long axis of the heart in postnatal life lies in a plane that runs from the left hypochondrium, where the cardiac apex is located, to the right shoulder. In the adult, it is typically inclined 45° to each major
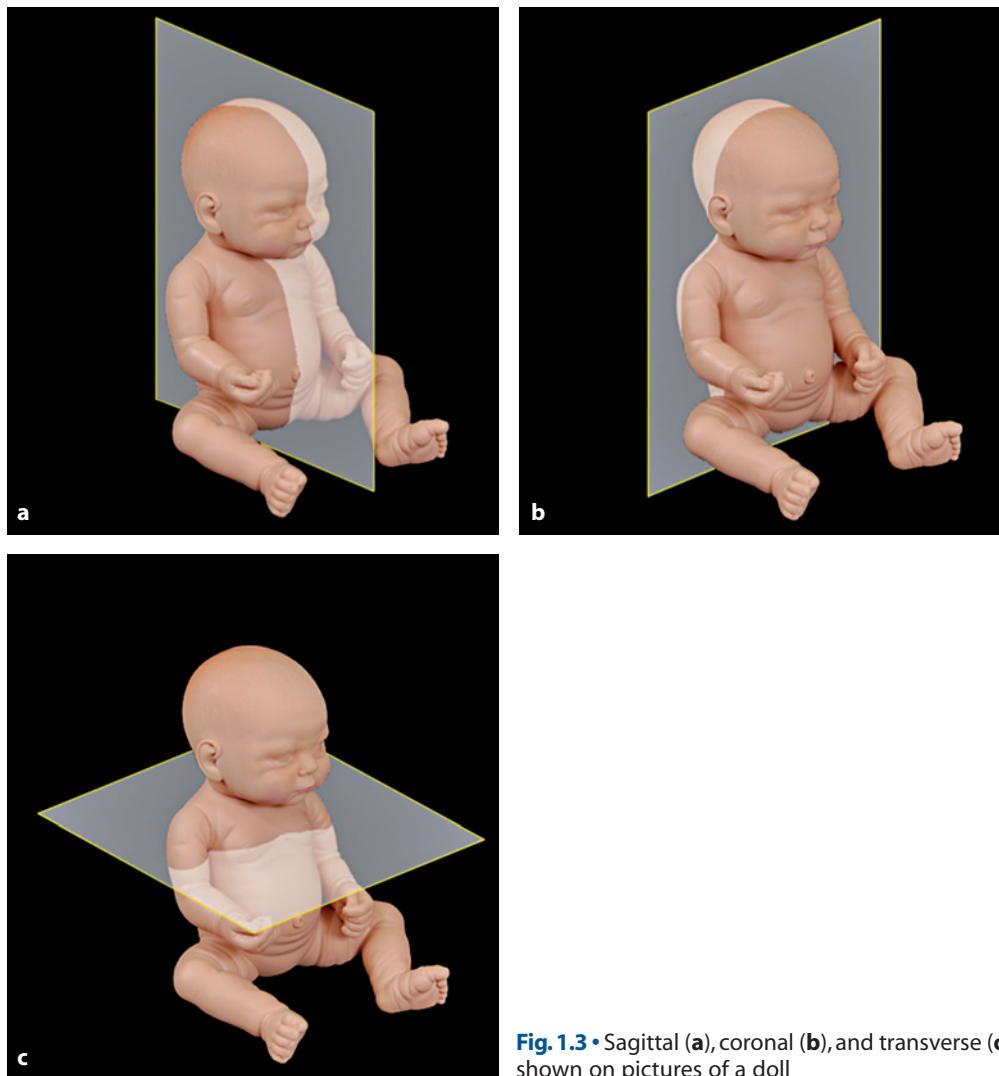
Fig. 1.3 • Sagittal (**a**), coronal (**b**), and transverse (**c**) planes of the body shown on pictures of a doll

body plane. However, inclination of the cardiac long axis relative to the transverse plane may change with the positions of the diaphragm. In the fetus, the heart is more horizontal than in postnatal life because the lungs are deflated and the liver is relatively large. Therefore, the cardiac long axis sits on a plane nearly parallel to a transverse plane of the fetal body. On the contrary, the short axis of the heart, which is perpendicular to the long axis, is almost parallel to the sagittal plane of the fetal body (Fig. 1.4).

By convention, two major planes can be distinguished along the long axis of the heart: the four-chamber plane and the two-chamber plane. The first plane is perpendicular to the inlet and trabecular ventricular septum, whereas the second plane is parallel to it (Fig. 1.5a). The short-axis plane includes a series of parallel planes, all perpendicular to the long axis of the heart. Classically, the short-axis plane at the level of the mitral valve and the level of the papillary muscles of the left ventricle are considered (Fig. 1.5b).

Fig. 1.4 • Long and short axis of the fetal heart and body are simulated on a picture of a doll

Basic Probe Manipulations

In general, echocardiographic study of the fetal heart requires small probe manipulations. In fact, because of the small size of heart and the relatively large distance from the application point of the probe, small movements of the transducer produce great changes in the scan plane.

In ultrasound examination, the section plane can be modified by three fundamental manipulations of the probe: rotation, angulation, and translation (Fig. 1.6):

- With rotation, the scan plane is changed by turning the transducer clockwise or counterclockwise while maintaining the footprint in a fixed position.
- With angulation, the scan plane is modified by tilting the probe in the cranial, caudal, right, or left direction. In this case also, the application point of the probe is maintained relatively fixed.
- In translation, the scan plane is left unchanged while its application point is changed by sliding the transducer on the skin.
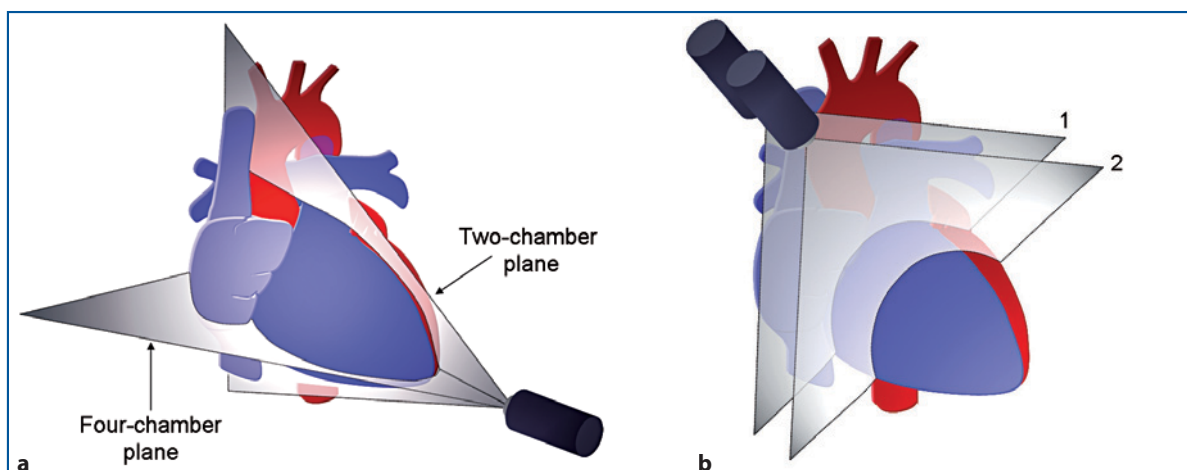
Fig. 1.5 • The two planes along the long axis of the heart are shown on a heart diagram, simulating an apical approach with the probe (**a**). The two basic short-axis planes of the heart are shown on a heart diagram: at the level of the mitral valve (or the base of the heart) (*1*) and at the level of the papillary muscles (*2*) (**b**). (See more in the respective chapter)
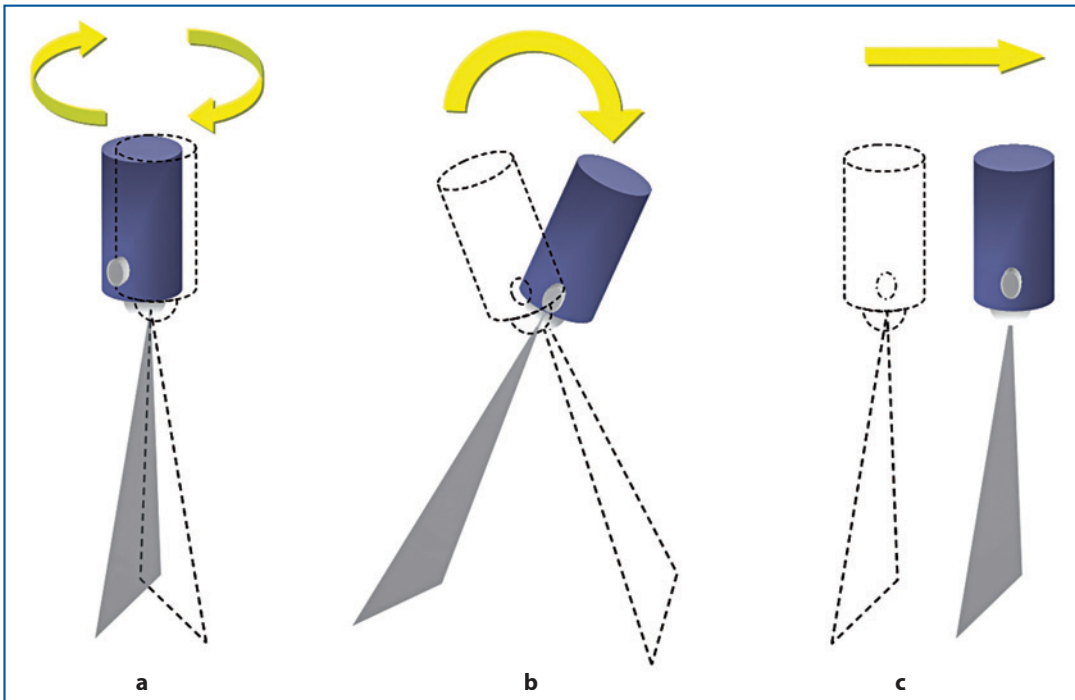
Fig. 1.6 • Diagram showing the three basic manipulations of the probe: rotation (**a**), angulation (**b**), and translation (**c**)
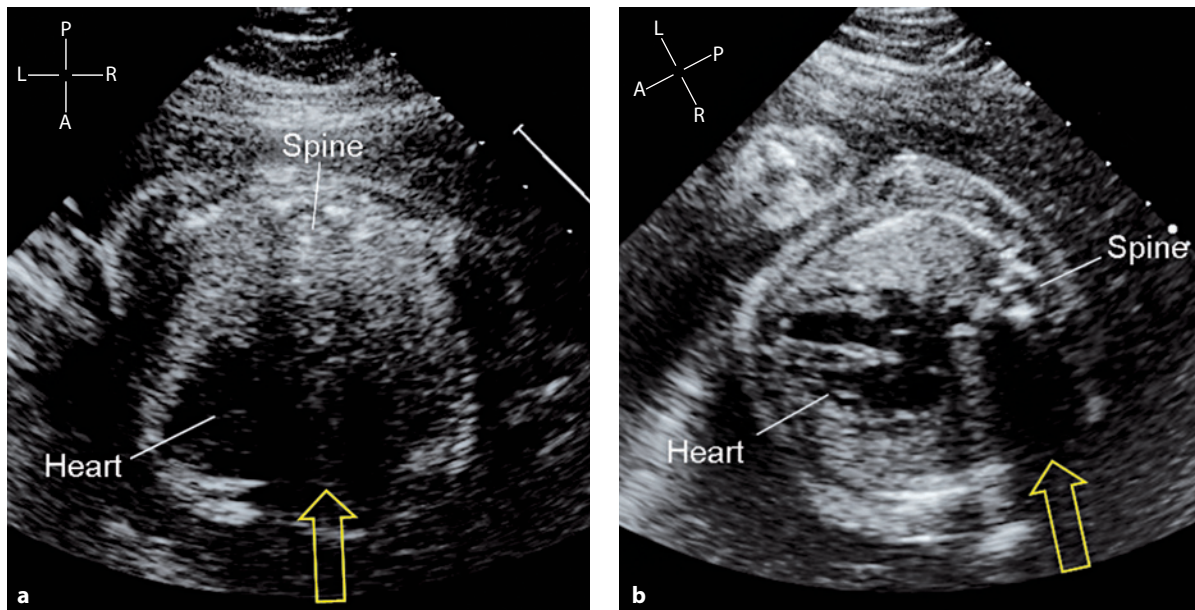
Fig. 1.7 • Four-chamber view in the same fetus with unfavorable anterior presentation of the spine. The shadow of the spine (**a**) (*yellow open arrow*) masks the heart, which is barely visible. The heart is brought out of the shadow (**b**) (*yellow open arrow*) by translating the probe to the left side of the spine. A four-chamber view of reasonable quality is obtained from the posterior part of the left hemithorax

Translation of the scan plane is more difficult to learn but is particularly useful in prenatal ultrasound examination because it provides a similar projection from different scanning angles. This allows, for example, the targeted organ to be brought out of the shadow of proximal structures (Fig. 1.7).

Translation of the scan plane may also improve the definition of cardiac structures by allowing examination
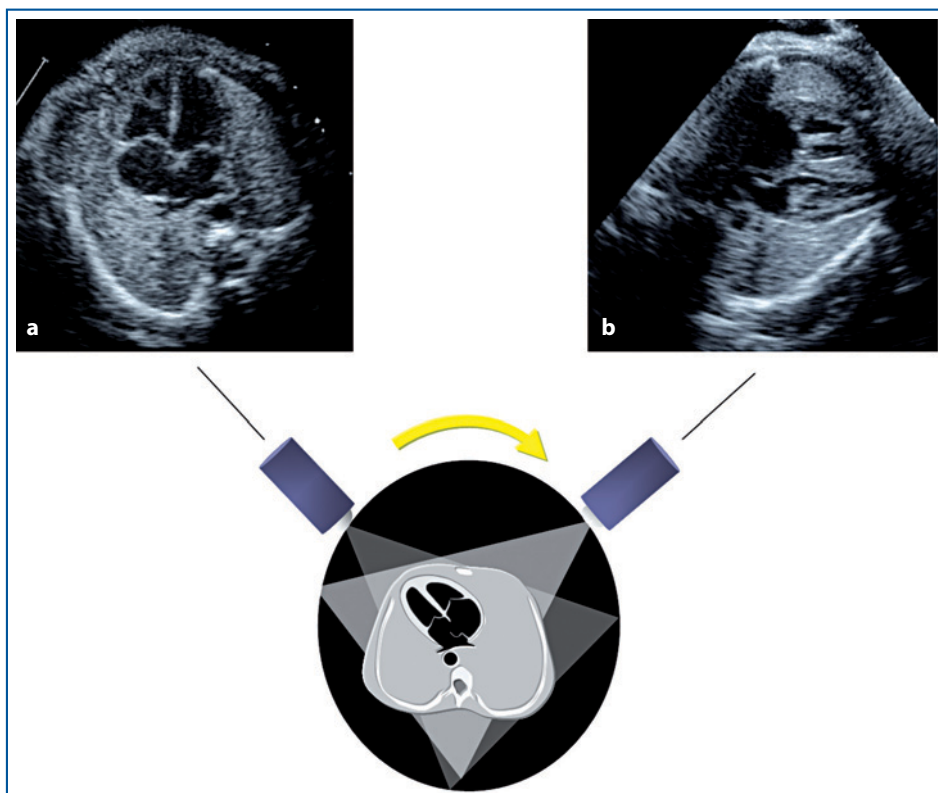
Fig. 1.8 • Diagram simulating a transverse section of the fetal thorax at the level of the four-chamber view within the amniotic cavity (*black area*). The apical four-chamber view (**a**) can be changed to a transverse four-chamber view (**b**) by translating the probe (*yellow arrow*) on the mother's abdomen while maintaining the section plane unchanged

with axial instead of lateral resolution (Fig. 1.8). In fetal echocardiography, similar projections of the heart can be obtained from different positions of the transducer because the lungs do not represent an obstacle to imaging, as they are filled with fluid and not air. This allows projections through the rib cage, even from the back, which are unobtainable postnatally (Fig. 1.7). Nevertheless, projections from the back produce attenuation of the ultrasonic energy, particularly in the third trimester when bony structures of the thoracic cage absorb most of the ultrasound energy.

In general, the best definition of cardiac structures is achieved through the fetal abdomen. If initially unfavorable, fetal presentation may change for the better by translating the scan plane or by turning the mother on her side, having her empty a full bladder, or having her take a little walk. Sometimes, the examination must be postponed for hours or a few days.

Axial and Lateral Resolution

The axial resolution is the shortest distance between two points lying on the same insonation axis, which

the ultrasound system is able to represent as separate. The lateral resolution refers to the shortest distance between two adjacent points that an ultrasound system is able to represent as distinct. In virtually all cross-sectional ultrasound systems, the axial resolution is better than the lateral resolution. This implies that structures that are orthogonal to the ultrasound beam will be better represented than structures that are parallel. The four-chamber view provides one of the best examples to explain this concept. This view can be obtained in apical or transverse orientation. Despite showing sections of the fetal thorax across identical structures, the apical and transverse four-chamber views provide different information. In fact, in the apical approach, the moderator band, the atrioventricular valves, and the venoatrial connection are better represented; in the transverse approach, ventricular-wall thickness, ventricular transverse diameter, and foramen ovale morphology and function are more precisely assessed. Conversely, in the apical approach, it is difficult to identify the endocardial borders of the heart chambers and assess precisely ventricular-wall thickness and transverse diameter of cardiac cham-
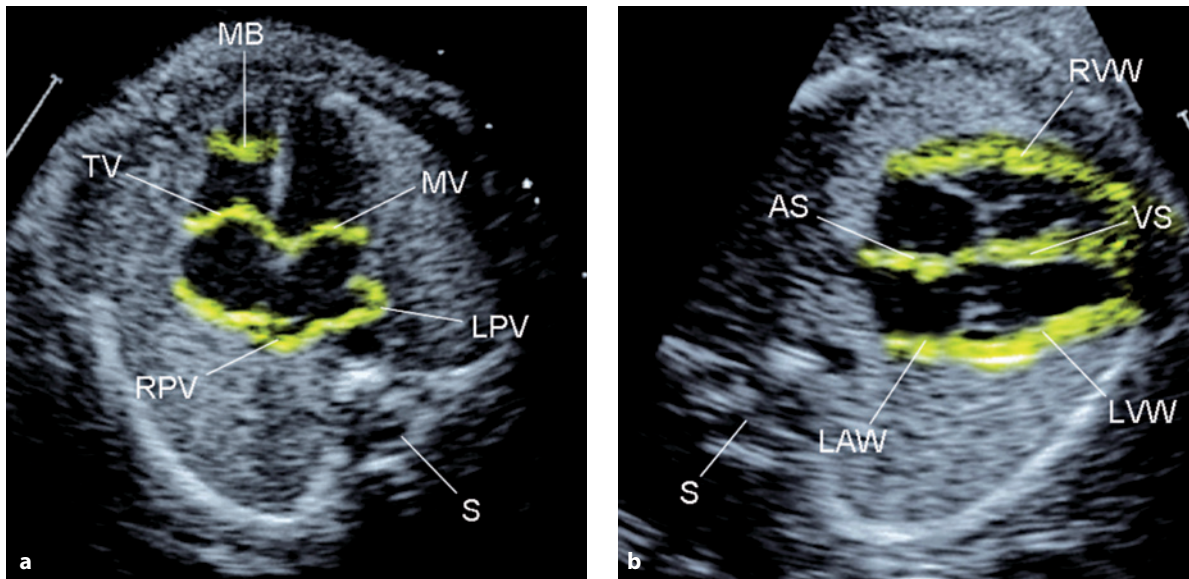
Fig. 1.9 • Normal four-chamber view in apical (**a**) and transverse (**b**) approach. The *yellow highlighted areas* indicate structures that are better defined in each view. *AS* atrial septum, *LAW* left atrial wall, *LPV* left pulmonary vein, *LVW* left ventricular wall, *MV* mitral valve, *RPV* right pulmonary vein, *RVW* right ventricular wall, *TV* tricuspid valve, *S* spine, *VS* ventricular septum

bers, whereas in the transverse approach, the moderator band and atrioventricular valves are usually undefined (Fig. 1.9). These differences are even better appreciated on moving images than in still frames.

Method for Comprehensive Cardiac Evaluation

As already stated, most authors agree that the routine fetal anomaly scan should include assessment of ventriculoarterial connection, and this can be achieved by different methods. Some authors favor incorporating the views of the two so-called ventricular outlets [16, 17]. Others suggest using a series of short-axis sections of the fetal thorax for complete cardiac examination [33-36].

In complete assessment of the fetal heart, the experienced examiner should understand the echocardiographic anatomy so thoroughly that he or she uses the standard views not as ends in themselves but only as reference points during a scan sequence, including a series of parallel sections from bottom to top, from side to side, and from front to back. However, demanding such knowledge from all obstetric sonographers for routine examination is highly unreasonable. Our teaching experience over the past 10 years has shown us that beginners or first-level sonographers can understand and more easily assess the fetal heart using transverse or sagittal views of the fetal body; that is, by orienting the scan plane or-
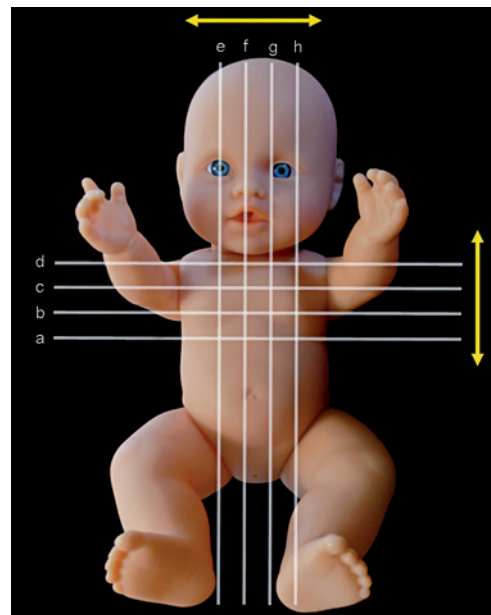
Fig. 1.10 • *White lines* on the picture of a doll simulate a consecutive series of sections with which one can investigate the fetal body along the transverse plane, from bottom to top (*a-d*), and along the sagittal plane, from right to left (*e-h*)

thogonal or parallel to the long axis of the fetal body (Fig. 1.10). This is because the long axis of the fetal body is a reference line easier to identify than the major axis of the fetal heart.

In particular, the transverse sections of the fetal upper abdomen and thorax have gained a growing

reputation in recent years in imaging the fetal heart. These sections resemble those obtained with magnetic resonance imaging (Fig. 1.11).

We believe that a complete assessment of the fetal heart can be obtained through a series of transverse sections of the fetal body (Fig. 1.12) and can be adopted as a standardized technique for cardiac evaluation in screening [35].

Our goal for this project is that the reader will gain greater knowledge of the fetal cardiac anatomy to be able to obtain a mental three-dimensional reconstruction of the fetal heart and surrounding structures. Moreover, a specific chapter describes new ultrasound technologies dedicated to the three-dimensional study of the fetal heart. After introduction of the spatiotemporal image correlation (STIC) technique, three-dimensional study of the fetal heart has changed and will change rapidly over the coming decade [37-45]. Once a volume data set is acquired, the heart can be examined using multiple section planes, some of which are unobtainable with cross-sectional ultrasound [44]. In addition, digitally stored volumes can be sent to experts for analysis or second opinions. Three-dimensional echocardiography has the potential for making the examination less operator dependent. For example, with spatial com-

Fig. 1.11 • Postnatal four-camber view obtained with magnetic resonance imaging. Courtesy of G. Festa, CNR Massa Carrara, Italy
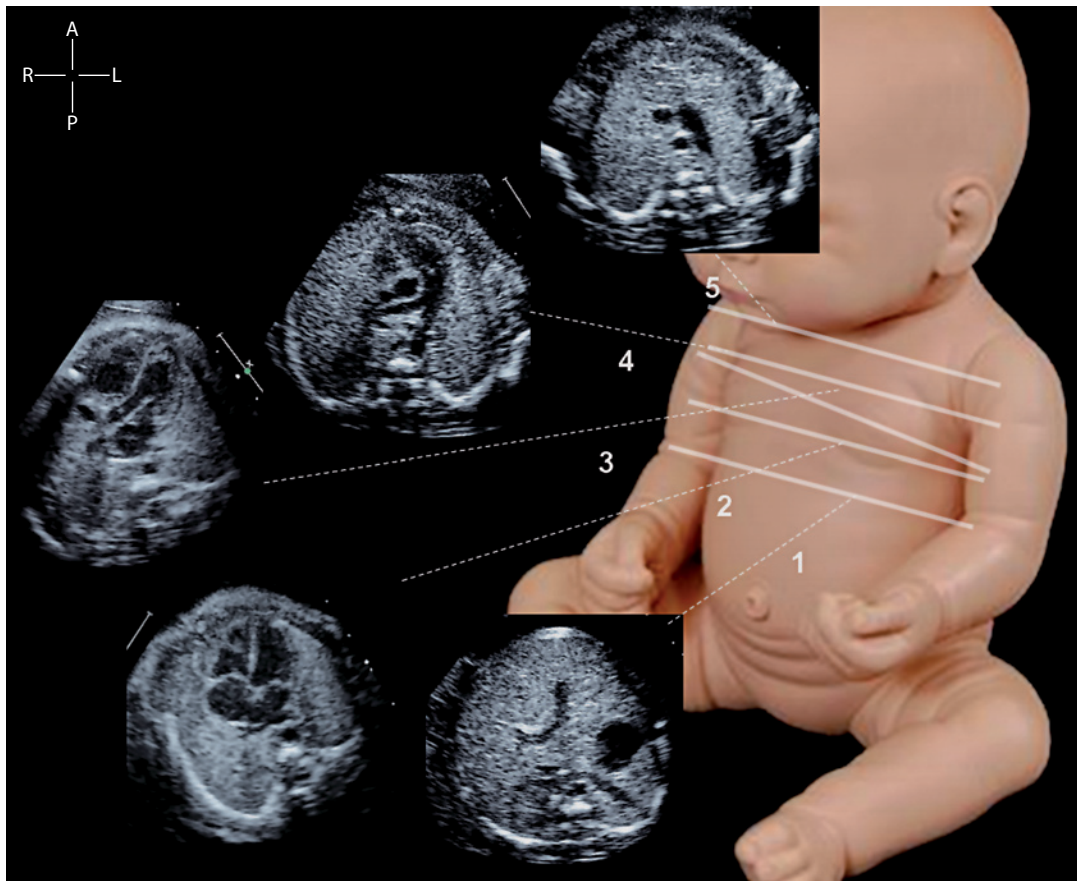
Fig. 1.12 • The five fundamental transverse sections of the fetal body and their respective section planes shown on a picture of a doll: the upper abdomen (*1*), the four-chamber view (*2*), the five-chamber view (*3*), the arterial duct transverse view (three-vessel view variant) (*4*), and the aortic arch transverse view (*5*)
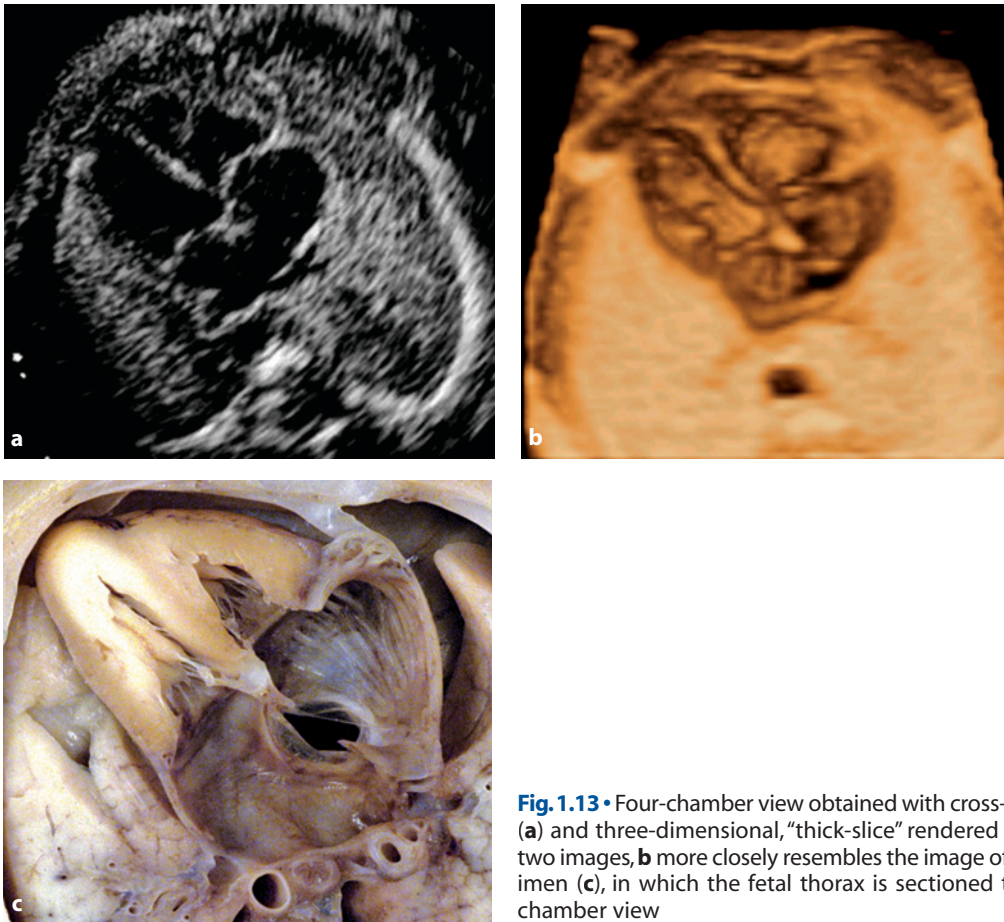
Fig. 1.13 • Four-chamber view obtained with cross-sectional technique (**a**) and three-dimensional, "thick-slice" rendered image (**b**). Of these two images, **b** more closely resembles the image of the anatomic specimen (**c**), in which the fetal thorax is sectioned to imitate the four-chamber view

pounding, which is still limited by a low frame rate, the acquired volume can be sectioned automatically in a series of parallel slices similar to those obtained by manipulating the probe with "traditional" techniques.

Progress in echocardiography is likely to reduce image acquisition time and provide more rapid and simpler recognition of defects, "mirroring" the actual morphology of the heart. Indeed, the images now produced by magnetic resonance imaging and com-

puted tomography may become so like the actual anatomical specimens that clinicians' and pathologists' views may be indistinguishable (Fig. 1.13).

Continuing developments in ultrasound already show great promise in this regard. It is also clear, however, that for the foreseeable future, the exquisite detail of cross-sectional images, such as those contained in this work, will remain the basis of fetal cardiac imaging and the standard reference tools for examining the fetal heart.

References

1. Hoffman JI (1995) Incidence of congenital heart disease: I. Postnatal incidence. Pediatr Cardiol 16:103-113
2. Hoffman J, Kaplan S (2002) The incidence of congenital heart disease. J Am Coll Cardiol 39:1890-1900
3. Kochanek KD, Smith BL (2004) Deaths: preliminary data for 2002. Natl Vital Stat Rep 52:1-47
4. Chinn A, Fitzsimmons J, Shepard TH (1989) Congenital heart disease among spontaneous abortuses and stillborn fetuses: prevalence and associations. Teratology 40:475-482
5. Hoffman JI (1995) Incidence of congenital heart disease: II. Prenatal incidence. Pediatr Cardiol 16:155-165
6. Bonnet D, Coltri A, Butera G et al (1999) Detection of transposition of great arteries in fetuses reduces neonatal morbidity and mortality. Circulation 99:916-918
7. Tworetzky W, McElhinney DB, Reddy MV et al (2001) Improved surgical outcome after fetal diagnosis of hypoplastic left heart syndrome. Circulation 103:1269-1273

8. Franklin O, Burch M, Manning N et al (2002) Prenatal diagnosis of coarctation of the aorta improves survival and reduces morbidity. Heart 87:67-69

9. Tegnander E, Eik-Nes SH, Johansen OJ et al (1995) Prenatal detection of heart defects at the routine fetal examination at 18 weeks in a non-selected population. Ultrasound Obstet Gynecol 5:373-380

10. Buskens E, Grobbee DE, Frohn-Mulder JM et al (1996) Efficacy of routine fetal ultrasound screening for congenital heart disease in normal pregnancy. Circulation 94:67-72

11. Todros T, Faggiano F, Chiappa E et al (1997) Accuracy of routine ultrasonography in screening heart disease prenatally. Gruppo Piemontese for prenatal screening of congenital heart disease. Prenatal Diagn 17:901-906

12. Achiron R, Glaser J, Gelernter et al (1992) Extended foetal echocardiographic examination for detecting cardiac malformations in low risk pregnancies. Br Med J 304:671-674

13. Bromley B, Estroff JA, Sanders SP et al (1992) Fetal echocardiography: accuracy and limitations in a population at high and low risk for heart defects. Am J Obstet Gynecol 166:1473-1481

14. Kirk JS, Riggs TW, Comstock CH et al (1994) Prenatal screening for cardiac anomalies: the value of routine addition of the aortic root to the four chamber view. Obstet Gynecol 84:427-431

15. Wyllie J, Wren C, Hunter S (1994) Screening for fetal cardiac malformations. Br Heart J 71(Suppl):20-27

16. Stumpflen I, Stumpflen A, Wimmer M et al (1996) Effect of detailed fetal echocardiography as part of routine prenatal ultrasonographic screening on detection of congenital heart disease. Lancet 348:854-857

17. Carvalho JS, Mavrides E, Shinebourne EA et al (2003) Improving the effectiveness of routine of routine prenatal screening for major congenital heart defects. Heart 88:387-391

18. Chaoui R (2003) The four-chamber view: four reasons why it seems to fail in screening for cardiac abnormalities and suggestions to improve detection rate. Ultrasound Obstet Gynecol 22:3-10

19. Hunter S, Heads A, Wyllie J et al (2000) Prenatal diagnosis of congenital heart disease in the northern region of England: benefits of a training programme for obstetric ultrasonographers. Heart 84:294-298

20. Sharland GK, Allan LD (1999) Screening for congenital heart disease prenatally. Results of a 2.5 year study in the south-east Thames region. Br J Obstet Gynaecol 99:220-225

21. Silverman NH (1993) Pediatric echocardiography. Williams & Wilkins, Baltimore

22. Maulik D (1995) Principles of Doppler signal processing and hemodynamic analysis. In: Copel JA, Reed KL (eds) Doppler ultrasound in obstetrics and gynecology. Raven Press, New York, pp 1-18

23. Beach KW (1995) Ultrasound physics and ultrasonic imaging. In: Copel JA, Reed KL (eds) Doppler ultrasound in obstetrics and gynecology. Raven Press, New York, pp 31-39

24. Dudwiesus H (1995) Principles of physics. In: Sohn C, Holzgreve W (eds) Ultraschall in gynakologie und geburtshilfe. Georg Thieme Verlag, pp 7-61

25. Achiron R, Rotstein Z, Lipitz S et al (1994) First-trimester diagnosis of fetal congenital heart disease by transvaginal ultrasonography. Obstet Gynecol 84:69-72

26. Simpson JM, Jones A (2000) Accuracy and limitations of transabdominal fetal echocardiography at 12-15 weeks of gestation in a population at high risk for congenital heart disease. Br J Obstet Gynaecol 107:1492-1497

27. Hyett JA, Perdu M, Sharland GK et al (1997) Increased nuchal translucency at 10-14 weeks of gestation as a marker for major cardiac defects. Ultrasound Obstet Gynecol 10:242-246

28. Hyett JA, Perdu M, Sharland GK, et al (1999) Using fetal nuchal translucency to screen for major congenital cardiac defects at 10-14 weeks of gestation: population based cohort study. BMJ 318:81-85

29. Snijders RJM, Noble P, Sebire N et al 1998 UK multicentre project on assessment of risk of trisomy 21 by maternal age and fetal nuchal-translucency thickness at 10-14 weeks of gestation. Lancet 352:343-346

30. Yagel S, Achiron R, Ron M et al (1995) Transvaginal sonography at early pregnancy cannot replace midtrimester targeted organ ultrasound examination in a high-risk population. Am J Obstet Gynecol 172:971-975

31. Lee W (1998) Performance of the basic fetal cardiac ultrasound examination. AIUM Technical Bulletin. J Ultrasound Med 17:601-607

32. Allan L, Dangel J, Fessolova V et al (2004) Recommendations for the practice of fetal cardiology in Europe Cardiol Young 14:109-114

33. Yoo SJ, Lee YH, Kim ES et al (1997) Three-vessel view of the fetal upper mediastinum: an easy means of detecting abnormalities of the ventricular outflow tracts and great arteries during obstetric screening. Ultrasound Obstet Gynecol 9:173-182

34. Yoo SJ, Young HL, Kyoung SC (1999) Abnormal three-vessel view on sonography: a clue to the diagnosis of congenital heart disease in the fetus. AJR Am J Roentgenol 172:825-830

35. Yagel S, Cohen SM, Achiron A (2001) Examination of the fetal heart by five short-axis views: a proposed screening method for comprehensive cardiac evaluation. Ultrasound Ostet Gynecol 17:367-369

36. Yagel S, Arbel R, Anteby EY et al (2002) The three vessels and trachea view (3VT) in fetal cardiac scanning. Ultrasound Obstet Gynecol 20:340-345

37. Scharf A, Geka F, Steinborn A (2000) 3D real-time imaging of the fetal heart. Fetal Diagn Ther 15:267-274

38. Meyer-Wittkopf M, Cooper S, Vaughan J (2001) Three-dimensional (3D) echocardiographic analysis of congenital heart disease in the fetus: comparison with cross-sectional (2D) fetal echocardiography. Ultrasound Obstet Gynecol 17:485-492

39. Timor-Tritsch IE, Platt LD (2002) Three-dimensional ultrasound experience in obstetrics. Curr Opin Obstet Gynecol 14:569-575
40. Vinals F, Poblete P, Giuliano A (2003). Spatio-temporal image correlation (STIC): a new tool for the prenatal screening of congenital heart defects. Ultrasound Obstet Gynecol 22:388-394
41. DeVore GR, Falkensammer P, Sklansky MS (2003) Spatiotemporal image correlation (STIC): new technology for evaluation of the fetal heart. Ultrasound Obstet Gynecol 22:380-387
42. DeVore GR, Polanco B, Sklansky MS (2002) The 'spin' technique: a new method for examination of the fetal outflow tracts using three-dimensional ultrasound. Ultrasound Obstet Gynecol 24:72-82
43. Chaoui R, Hoffmann J, Heling KS (2004) Three-dimensional (3D) and 4D color Doppler fetal echocardiography using spatio-temporal image correlation (STIC). Ultrasound Obstet Gynecol 23:535-545
44. Yagel S, Valsky DV, Messing B (2005) Detailed assessment of fetal ventricular septal defect with 4D color Doppler ultrasound using spatio-temporal image correlation technology. Ultrasound Obstet Gynecol 25:97-98
45. Goncalves LF, Lee W, Espinoza JR et al (2006) Examination of the fetal heart by four-dimensional (4D) ultrasound with spatio-temporal image correlation (STIC). Ultrasound Obstet Gynecol 27:336-348

CHAPTER 2

Determining the Laterality of the Fetal Body and Image Orientation

Introduction

In the normal human, the midline sagittal plane divides the body into two sides that are mirror images of each other in term of their skeletal and muscular structure. However, many organs within the body, even those that are paired (such as lungs, bronchi, kidneys), show a distinctly lateralized arrangement. This lateralization is most striking in unpaired organs. In the large majority of normal subjects, the liver is predominantly to the right of the midline, whereas the stomach and spleen are located to the left. The heart sits in the mediastinum, with two thirds in the left side of the chest and its long axis also pointing left. This pattern of lateralization is called *situs solitus*, which means usual arrangement.

Congenital heart diseases occur with increased frequency in cases with malposition of the heart and other major organs. Moreover, an abnormal heart po-sition may worsen the surgical prognosis of a particular congenital heart defect. Determining the precise location of the heart is therefore an obligatory prerequisite of the echocardiographic examination. To precisely locate organs, preliminary assessment of the laterality of the fetal body (that means understanding which is the right side and which the left side of the fetus) is necessary. In fact, if the left/right axis is not correctly identified, significant pitfalls may result in establishing the visceroatrial situs, cardiac position, and cardiac segmental analysis.

In cardiovascular medicine, there are several examples of imaging techniques where the left and right side of the body can be confused. The chest X-ray is one of the most common examples. In fact, the film can be inspected from both sides, leaving the examiner uncertain as to which is the right and which is the left side of the body (Fig. 2.1). Needless to say, the position of the heart or the stomach
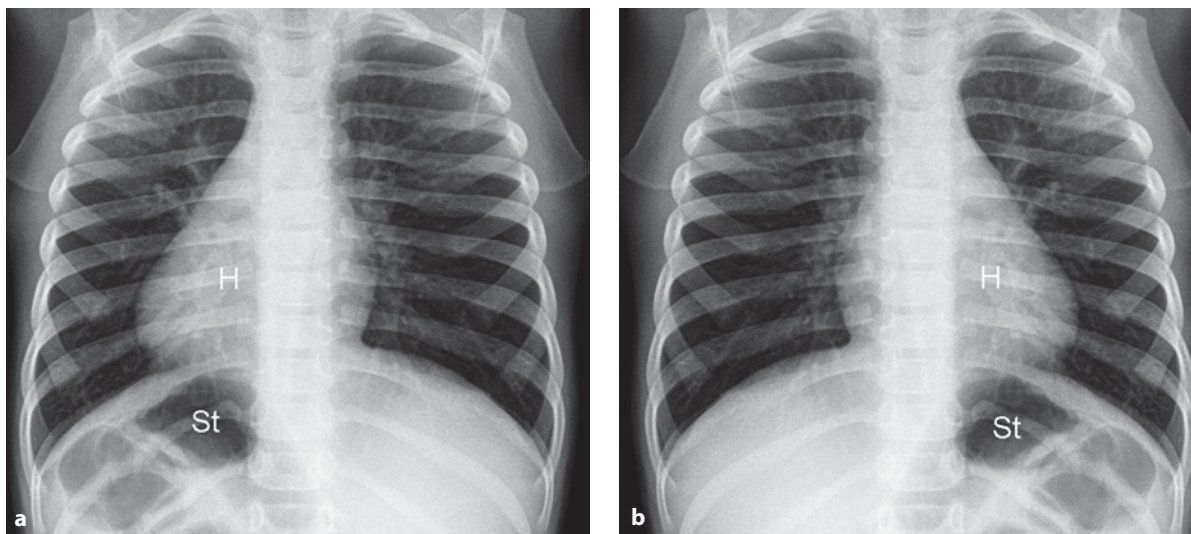
Fig. 2.1 • In this chest X-ray, no left/right axis marker is provided. The film can be examined from both sides (**a**, **b**), making impossible to establish whether the heart and stomach are in the left or right side of the body. *H* heart, *St* stomach

cannot be used to identify the left side of the body, because location of these organs may vary. If a lead marker is placed to precisely identify one of the two sides of the body (Fig. 2.2), the position of the organs can be established. However, mistakes are possible if the marker is placed on the wrong side.

Fetal echocardiography images are not immune to such left/right axis ambiguity. In fact, transverse
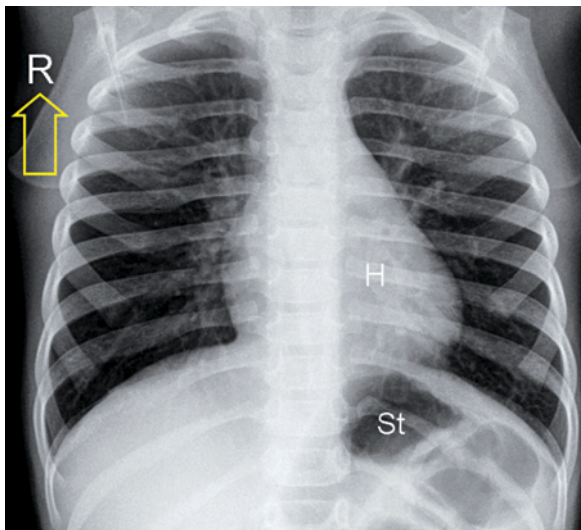
Fig. 2.2 • In this chest X-ray, a lead "R" marker (*yellow arrow*) has been place to indicate the right side of the patient. The heart and stomach can therefore be located in the left side. *H* heart, *St* stomach

sections of the fetal body can be obtained in opposite perspectives: caudocranial (the section is viewed from the feet toward the head) and craniocaudal (the section is viewed from the head toward the feet) (Fig. 2.3). The perspective must be the result of an imaging procedure that the operator must follow. Only when the examiner intentionally obtains one specific perspective is the left/right axis determined by the position of the fetal spine (Figs. 2.4, 2.5). Once again, the procedure for determining laterality must be independent from the position of the body organs, because organ location may vary.

Methods

Different methods of assessing laterality can be applied successfully in fetal ultrasound examination. Since publication in the *Journal of the American Society of Echocardiography* in 1994, the method established by Cordes and colleagues [1] has been adopted by many prenatal cardiologist. The technique is easy to learn and quick to perform. Moreover, this method is effective when the fetus is in transverse position – a condition where obstetrical methods can fail. It is recommended that the left/right axis be determined at the very beginning of the scan. When this procedure is performed systematically and recorded on videotape, assessing the visceroatrial situs and heart position is still possible, even when reviewing the images off line.
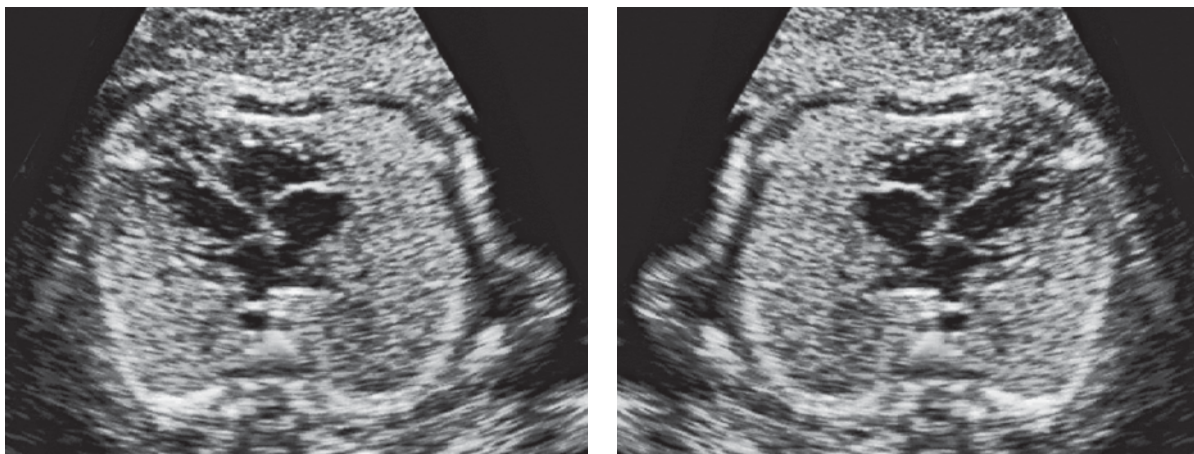
Fig. 2.3 • Transverse view of the fetal thorax at the four-chamber level of the heart. The same image is displayed in the two different perspectives: caudocranial and craniocaudal. However, if the specific perspective of each image is not known, the *left/right* axis and position of the heart cannot be established
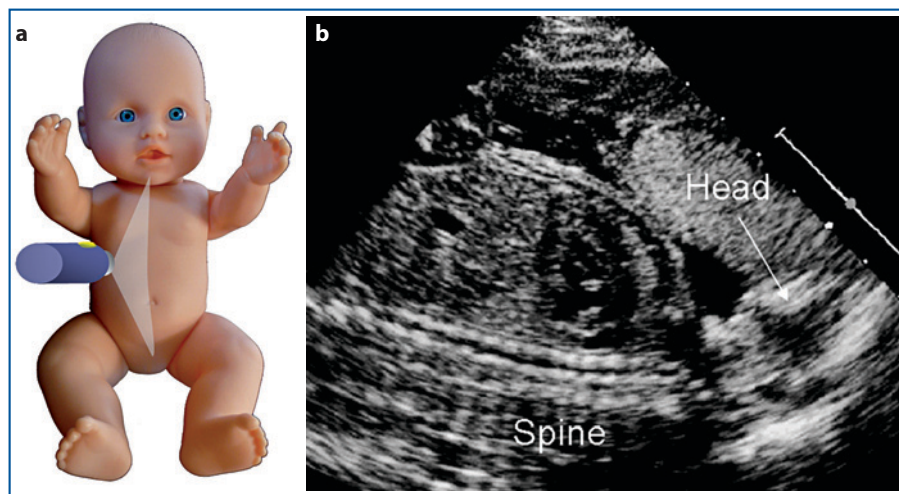
Fig. 2.4 • Simulated sagittal echocardiographic plane of the fetal body shown on the picture of a doll (**a**). A long-axis echocardiographic view of the fetal body with the fetal head displayed on the screen to the right side of the observer (**b**)

Fig. 2.5 • How to obtain a transverse view (*grey area*) of the fetal body from a sagittal view (*white broken lines*) by 90° clockwise rotation of the transducer is demonstrated on the picture of a doll (**a**). If the vertex of the scanning fan in the sagittal view is placed slightly cranial to the diaphragm, by 90° rotation of the scan plane, a transverse section of the four-chamber view is obtained (**b**). This view is in caudocranial orientation and the left/right axis is inferred by the position of the spine. Therefore, the heart is in the left side of the chest in this case
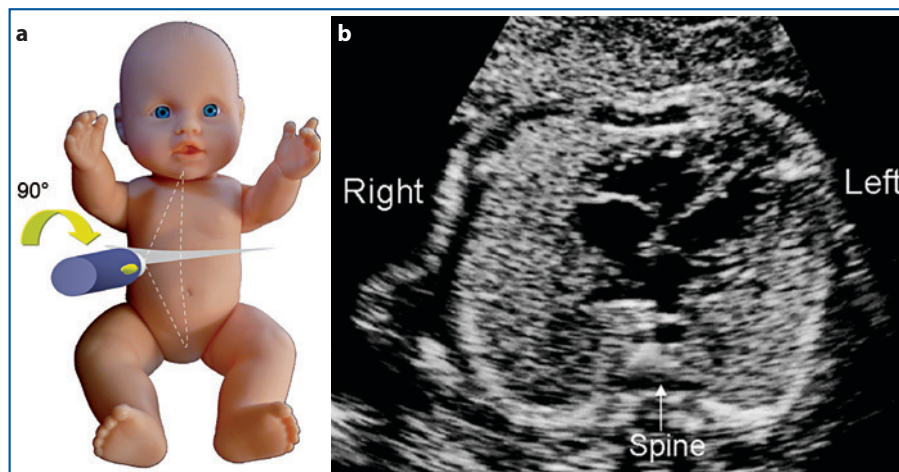
Procedure

1. Obtain a sagittal view of the fetal body, whatever its position.
2. Orient the transducer so that the fetal head is on the right side of the observer on the video screen (Fig. 2.4).
3. Rotate the transducer 90° clockwise to obtain a transverse view of the fetal body (Fig. 2.5a).
4. Transverse section thus acquired will be in caudocranial perspective (Fig. 2.5b).

It is important to remember that the sequence of these steps must not be reversed or the images electronically switched before the left/right axis assessment is completed. Otherwise, significant errors in interpreting the fetal anatomy may occur.

By systematically applying this method, the examiner will become familiar with the four basic presentations of the fetus (Fig. 2.6).

Once laterality of the fetal body is determined, the examiner checks the location of the the organs and can then assess the visceroatrial arrangement and the position of the heart and its axis. This can be obtained through two fundamental transverse sections of the fetal body: the upper abdomen, and the four-chamber view. Figure 2.7 simulates these two sections in the four basic presentations of the fetus in usual visceroatrial arrangement (situs solitus) and the heart in the left side of the chest (levocardia).
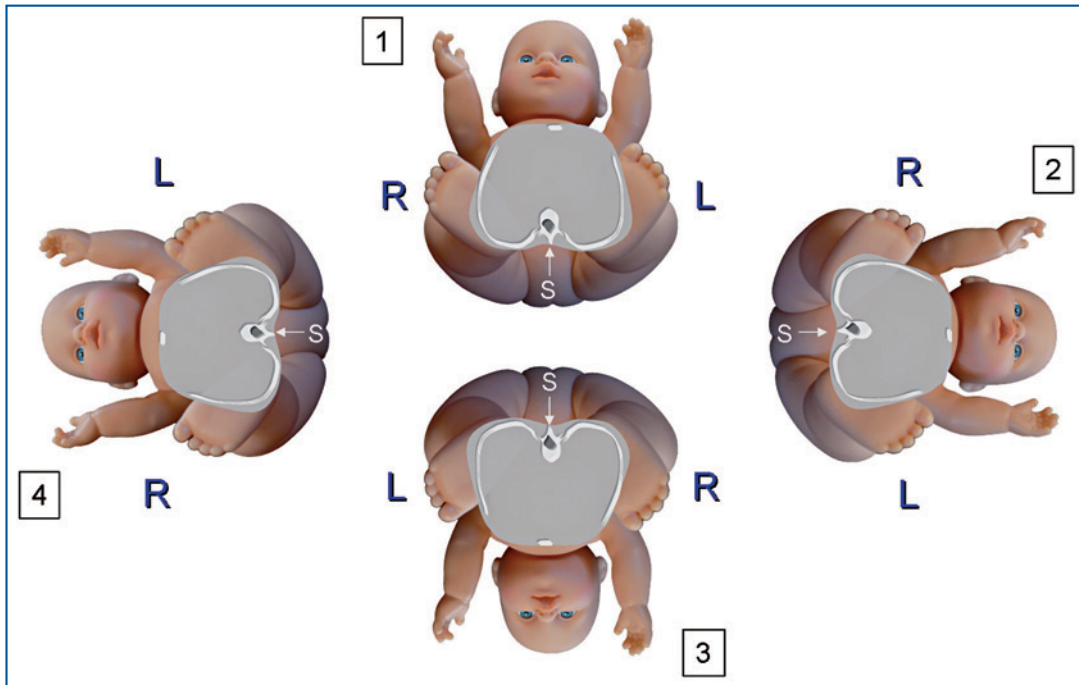
Fig. 2.6 • Transverse section of the fetal trunk in caudocranial perspective illustrating the four basic presentations: face up (*1*), right side up (*2*), face down (*3*), and left side up (*4*). Using the fetal spine as the landmark, the right and left sides of the fetal body can be determined. For clarity, the drawings are superimposed on the picture of a doll viewed from feet toward the head. *L* left, *R* right, *S* spine
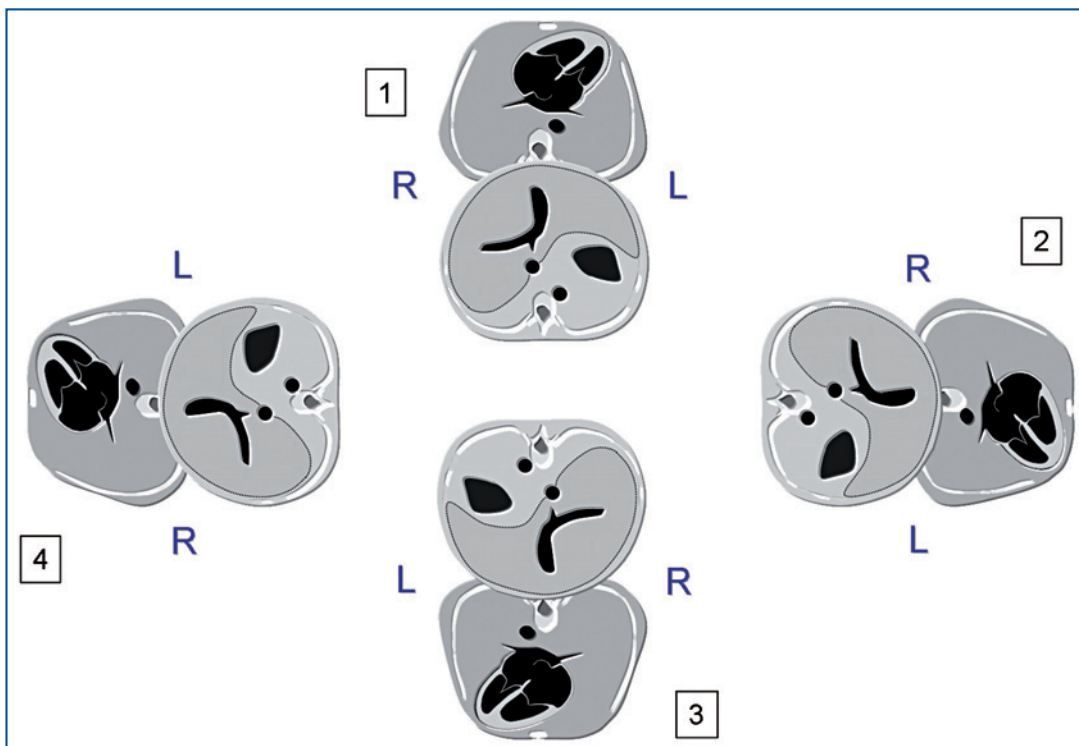
Fig. 2.7 • Diagrams of the transverse views of the fetal body (upper abdomen and four-chamber view) in visceroatrial situs solitus and levocardia. Each pair of sections, displayed in caudocranial presentation, is shown in the four basic presentations of the fetus: face up (*1*), right side up (*2*), face down (*3*), and left side up (*4*). *L* left, *R* right

Image Orientation

In prenatal ultrasound examination, the problem of orientation applies to each transverse view of the fetal body. There is no international standard regarding type of orientation of these sections. Usually, obstetricians are more familiar with images displayed in craniocaudal perspective. If images with this type of orientation are preferred, the examiner can apply Cordes' method following the same instructions with the exception of a counterclockwise rather than a clockwise rotation of the transducer in step 3.

Many cardiologists prefer to obtain sections in anatomical presentation, that is, in a manner corresponding to the anatomic position of the heart within the body (Fig. 2.8). This is obtained by switching images electronically until the desired result is obtained. However, this process is generally very difficult for beginners and noncardiologists to obtain and understand.

Because caudocranial presentation is an international standard for orienting transverse sections in magnetic resonance imaging and computer tomography, most echocardiographic images in this manual are displayed in caudocranial orientation. However, a compass will help the reader understanding the type of orientation depicted in each image.
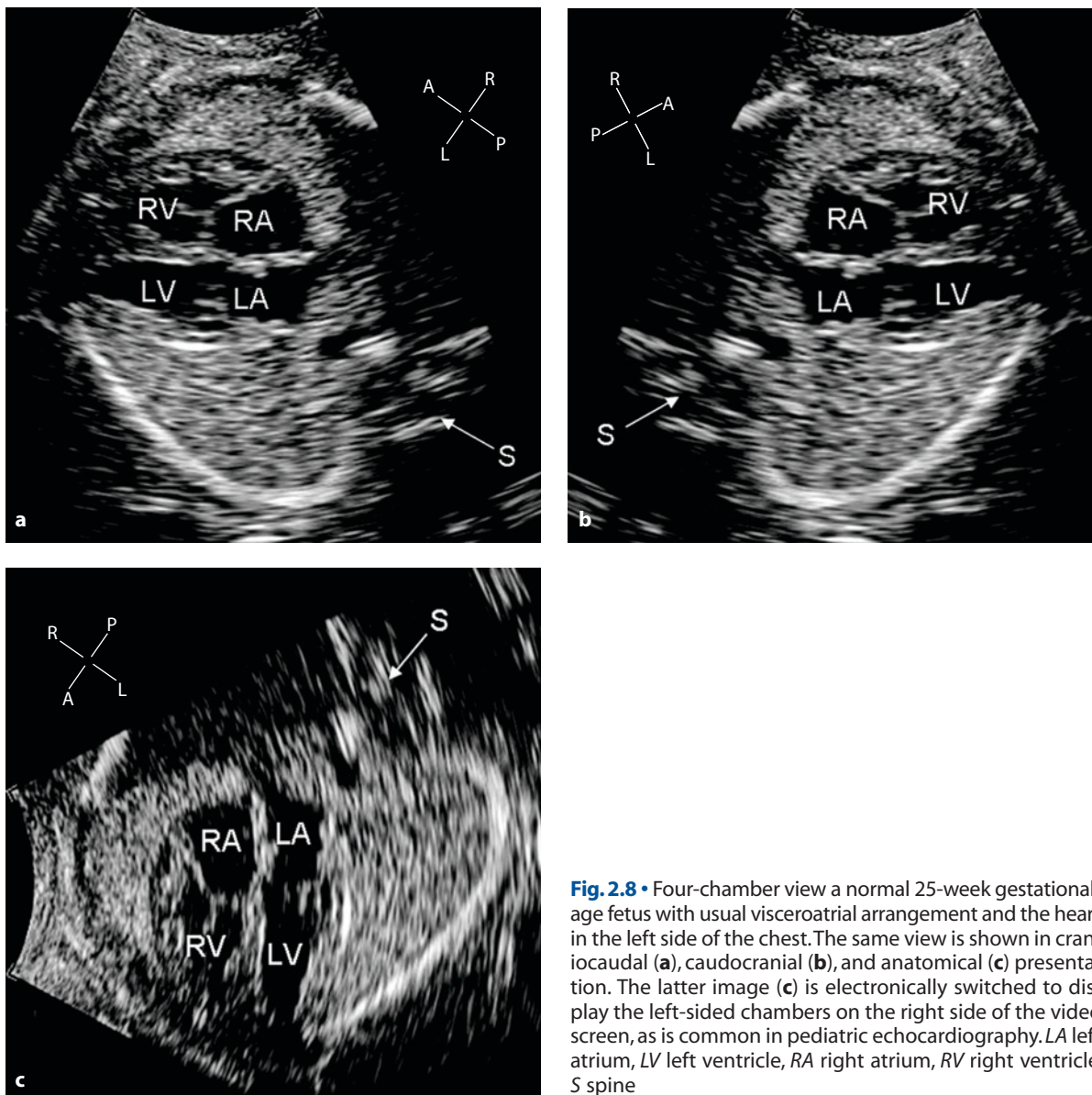
Fig. 2.8 • Four-chamber view a normal 25-week gestational-age fetus with usual visceroatrial arrangement and the heart in the left side of the chest. The same view is shown in craniocaudal (**a**), caudocranial (**b**), and anatomical (**c**) presentation. The latter image (**c**) is electronically switched to display the left-sided chambers on the right side of the video screen, as is common in pediatric echocardiography. *LA* left atrium, *LV* left ventricle, *RA* right atrium, *RV* right ventricle, *S* spine

Whatever the preferred image orientation, it must always be the result of an intentional choice by the examiner, and not random, so as to always be aware which side of the fetus is which. By following this method, it is possible to recognize an abnormal position of cardiac and extracardiac structures, whatever the level of the transverse section along the caudocranial axis of the fetal body.

In our experience, maintaining the same orientation throughout a series of transverse sections of the fetal body more readily provides the examiner with a mental three-dimensional reconstruction of the fetal anatomy.

Reference

1. Cordes TM, O'Leary PW, Seward JB, Hagler DJ (1994) Distinguishing right from left: a standardized technique for fetal echocardiography J Am Soc Echo 7:47-53

The Visceroatrial Arrangement (Situs)

Introduction

In the sequential segmental approach to diagnosing congenital heart disease, the morphological arrangement of the atria is the starting point [1, 2]. The appendages are the most constant component of the atria. Their shape and the morphology of their junction with the atria always show a morphologically right or left pattern. The morphologically left atrial appendage is tubular and hook-shaped, with a narrow junction with the venous portion of the atrium. The vestibular aspect of the left atrium is smooth, as the pectinate muscles are restricted to the appendage. The morphologically right atrial appendage is essentially triangular, with a broad junction with the venous portion of the atrium. Its internal aspect contains pectinate muscles that extend around the atrioventricular junction and reach the crux of the heart (Fig. 3.1) [3].
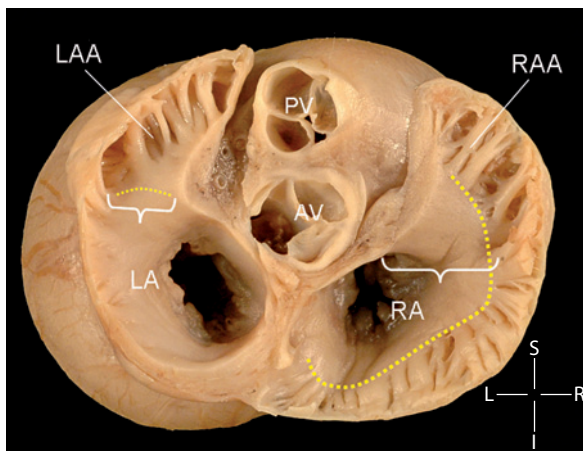
Fig. 3.1 • In this specimen of a normal heart, viewed form above, the upper portion of the atria is sectioned to show the "floor" of the atria with their appendages. The different size of the junction of the atrial appendages (*white brackes*) and different distribution of the pectinated muscles (*yellow dotted line*) within each atrium is demonstrated. *AV* aortic valve, *LA* left atrium, *LAA* left atrial appendage, *PV* pulmonary valve, *RA* right atrium, *RAA* right atrial appendage

The morphology of the atrial appendages can be identified with cross-sectional echocardiography, but in practice, this is unreliable in fetal scanning due to the small atrial appendages and their location outside the standard planes [4]. Berg et al. proposed a method of evaluating the atrial morphology in the four-chamber view that seems to differentiate between left and right isomerism in the majority of patients [5]. The atrial arrangement can be more easily recognized sonographically by a transverse section of the fetal upper abdomen. In fact, there is a close relationship between the arrangement of the atria and the position of the descending aorta and great veins at the level of the diaphragm [6-8]. There are four possible types of visceral and atrial arrangement: usual, mirror image, and left and right isomerism.

Usual Arrangement (*Situs Solitus*)

Situs solitus means the usual arrangement of the thoracic and abdominal organs found in most individuals. There is lateralized arrangement of the organs within the body and of the atrial appendages within the heart. The right lung is a three-lobed structure with a short eparterial bronchus, whereas the left lung is bilobed, and its bronchus is long and hyparterial. The stomach, spleen, and descending aorta are present on the left side of the body, and the major liver lobe and inferior vena cava are to the right of the midline (Fig. 3.2a). The left-sided atrium is morphologically of left type, and the right-sided atrium is morphologically of right type (Figs. 3.2b, 3.3). In individuals with usual atrial arrangement, a left-sided heart with apex to the left, the incidence of congenital cardiac malformations approximates that seen in the general population.

In transverse sections of the upper abdomen, the descending aorta sits close to the spine, slightly to the left of the midline. The inferior vena cava is in a more anterior position and slightly to the right of the midline. The stomach is on the left, and the portal sinus curves smoothly to the right where the predominant liver lobe is located (Fig. 3.4).
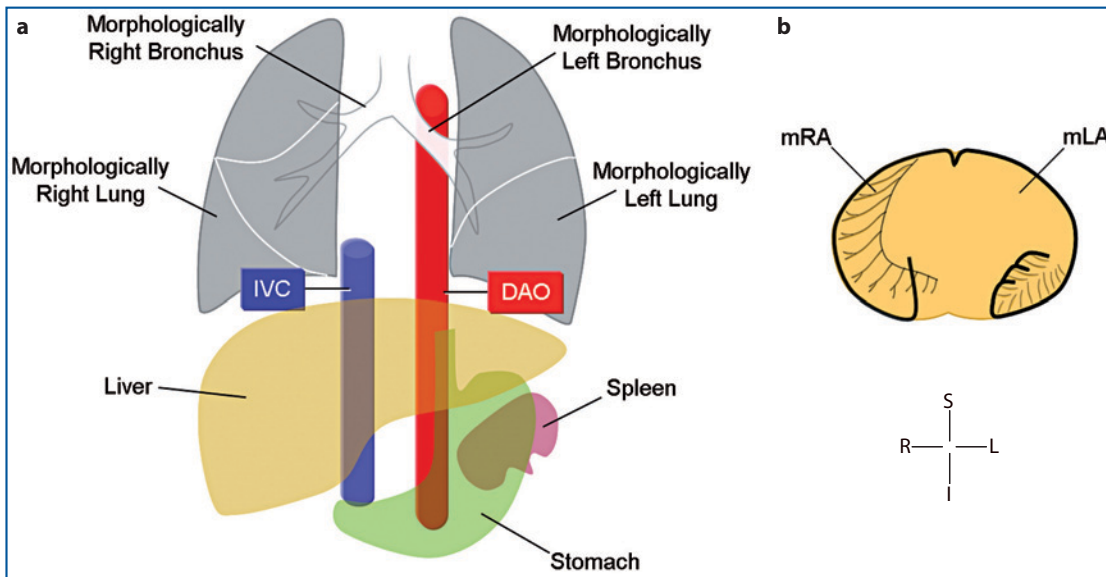
Fig. 3.2 • Representation of major body organs (**a**) and atrial appendages (**b**) in usual arrangement (*situs solitus*). *DAO* descending aorta, *IVC* inferior vena cava, *mLA* morphologically left atrium, *mRA* morphologically right atrium
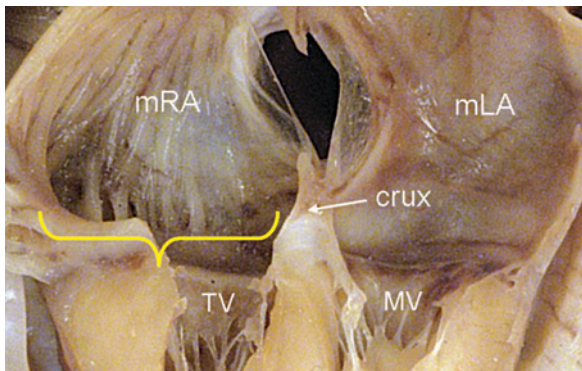
Fig. 3.3 • The inner surface of the two atria is shown in a fetal heart with usual atrial arrangement. The vestibule of the morphologically left atrium shows a smooth surface, whereas in the morphologically right atrium, there are extended pectinated muscles (*yellow bracket*) around the orifice of the tricuspid valve reaching the crux of the heart. *mLA* morphologically left atrium, *mRA* morphologically right atrium, *MV* mitral valve, *TV* tricuspid valve
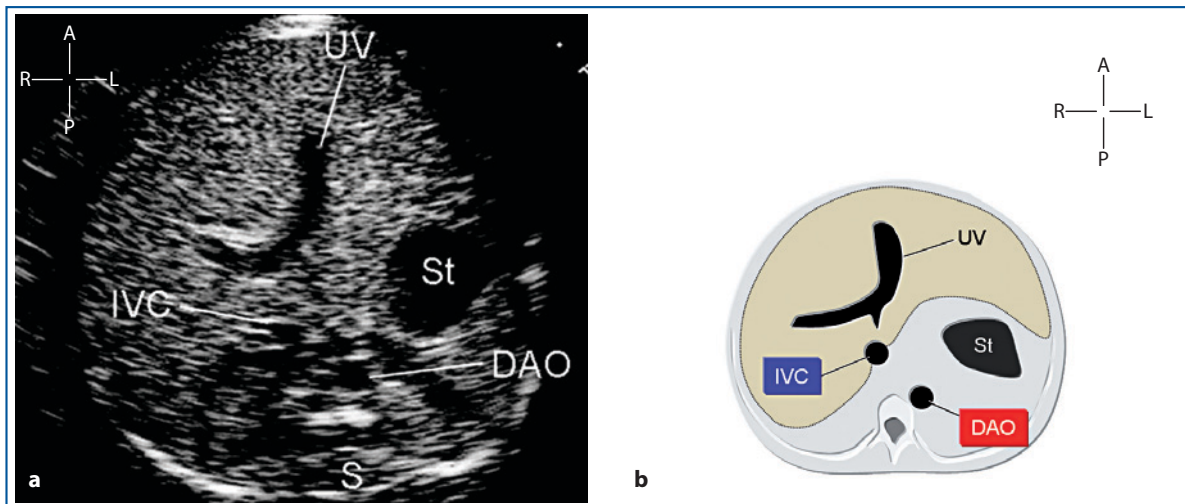
Fig. 3.4 • Transverse echocardiographic view of the upper abdomen in a fetus with usual visceroatrial arrangement (**a**) and a corresponding diagram (**b**). *DAO* descending aorta, *IVC* inferior vena cava, *S* spine, *St* stomach, *UV* umbilical vein

Mirror-Image Arrangement (*Situs Inversus*)

The other form of lateralized body arrangement is the situation in which the bodily organs are mirror-imaged. Although frequently termed *situs inversus*, this term does not describe the situation well, as it represents mirroring around a vertical axis rather than inversion around a horizontal axis. The general incidence of mirror-image arrangement is rare and approaches 0.01% of the population. All body organs are in mirror-image position, so that the morphologically right lung is on the left side with the inferior vena cava and liver major lobe, and the morphologically left lung, stomach, spleen, and descending aorta are on the right (Fig. 3.5a). Likewise, within the heart, the morphologically right atrium is left-sided, and the morphologically left atrium is right-sided (Fig. 3.5b). Usually, the bowel is rotated so that it sits in a mirror-image position. When a right-sided heart and its axis are found in a mirror-imaged atrial arrangement, the incidence of cardiac malformations is only slightly higher than in the general population – of the order of 0.3-5% [9].

However, in one major fetal series, 12 out of 19 cases with *situs inversus* had structural cardiac malformations [10]. This is probably the consequence of selected cases referred for fetal echocardiography to a tertiary care center. Mirror image arrangement was reported in a case with Turner's mosaicism [11]. In 20% of cases, mirror-image arrangement is associated with Kartagener syndrome, an autosomal recessive disease characterized by primary ciliary dyskinesia, which leads to repeated sinus and pulmonary infections and reduced fertility in postnatal life. Frequent pulmonary infections often result in bronchiectasis, which predominantly affects the lower lungs [12].

In transverse sections of the upper abdomen, the descending aorta is close to the spine and slightly to the right of the midline. The inferior vena cava is anterior and slightly to the left. The stomach is on the right, and the portal sinus curves to the left, where the predominant liver lobe is located (Fig. 3.6). When the left and right axis of the fetal body are not routinely assessed as a preliminary step in fetal scanning, this arrangement can be easily confused with usual arrangement.
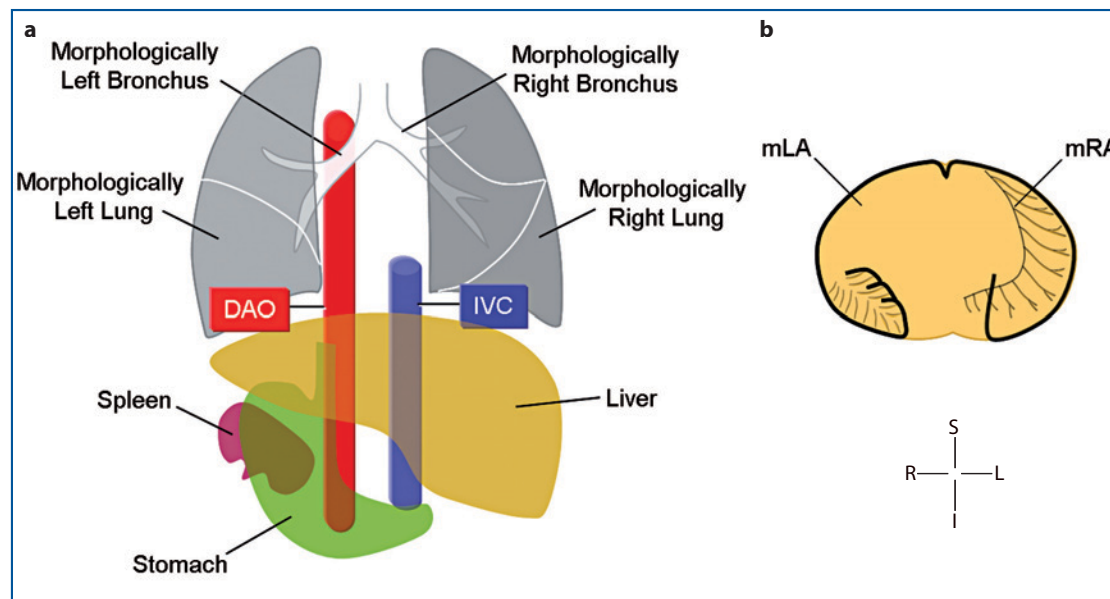
Fig. 3.5 • Representation of major body organs (**a**) and atrial appendages (**b**) in mirror-image arrangement (*situs inversus*). *DAO* descending aorta, *IVC* inferior vena cava, *mLA* morphologically left atrium, *mRA* morphologically right atrium
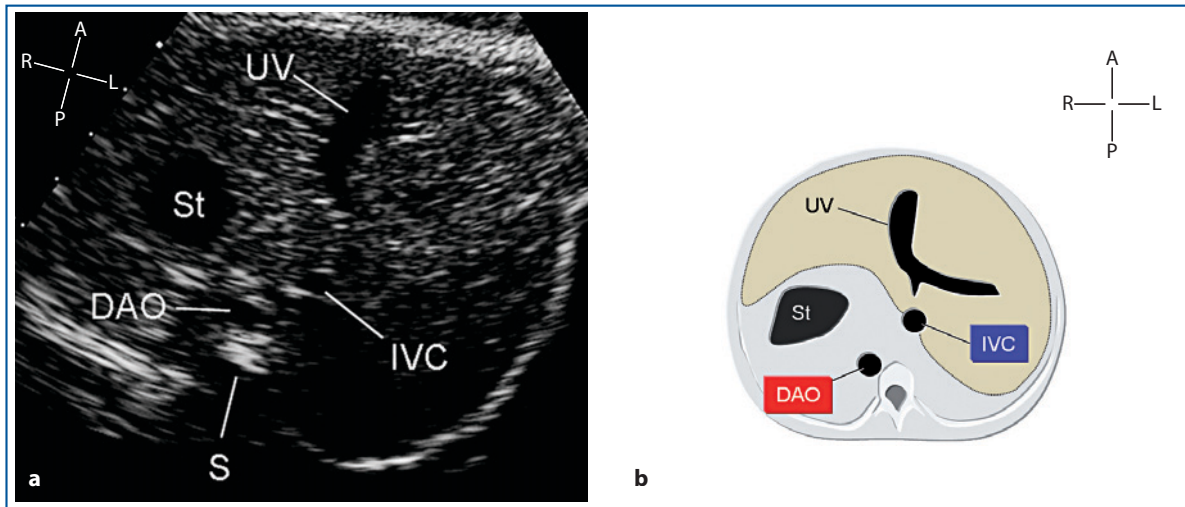
Fig. 3.6 • Transverse echocardiographic view of the upper abdomen in a fetus with mirror-image visceroatrial arrangement (**a**) and a corresponding diagram (**b**). *DAO* descending aorta, *IVC* inferior vena cava, *S* spine, *St* stomach, *UV* umbilical vein
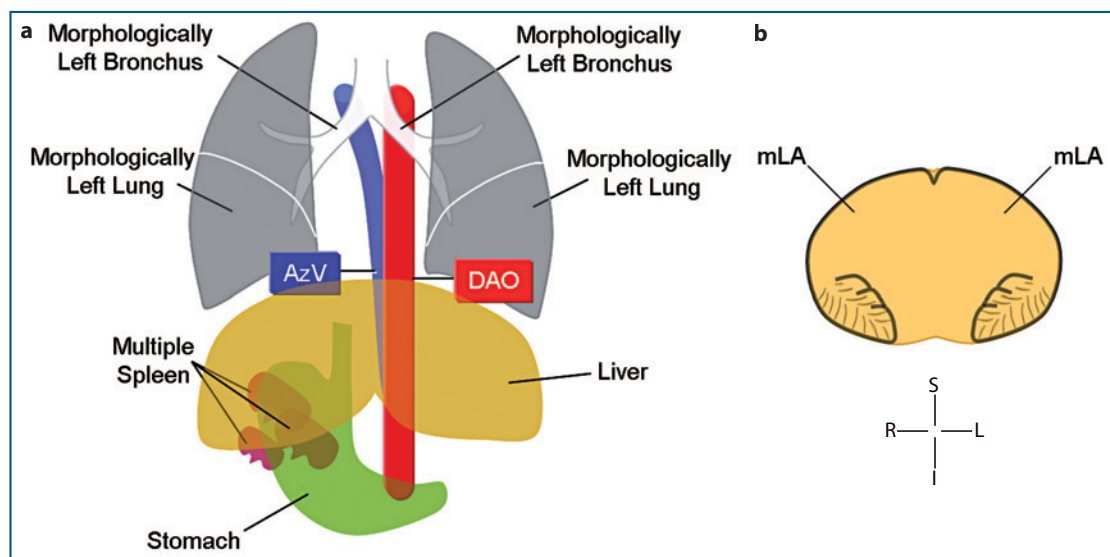
Fig. 3.7 • Representation of major body organs (**a**) and atrial appendages (**b**) in left isomerism. *DAO* descending aorta, *AzV* azygos vein, *mLA* morphologically left atrium

Left Isomerism (*Polysplenia*)

Heterotaxy is the definition commonly used to indicate an abnormal visceroatrial arrangement of the viscera that is different from usual or mirror-image arrangement. Two types of heterotaxy can be recognized: left isomerism and right isomerism. The term isomerism refers to the symmetrical development of organs that are normally asymmetrical, which characterize heterotaxy syndromes. These syndromes include a wide range of cardiac, vascular, and visceral abnormalities [12-18].

In individuals with left isomerism, both sides of the body show left morphology, and some structures normally found on the right are absent. Both lungs, therefore, are usually bilobed, with long and hyparterial bronchi (Fig. 3.7a). There are frequently multiple spleens present, giving rise to the term "polysplenia" syndrome, but this is not a universal finding. The liver is a central structure with two symmetric lobes, the inferior vena cava is interrupted in approximately 90% of cases, and venous blood from below the diaphragm drains back to the heart via the azygos or hemiazygos vein system, either or
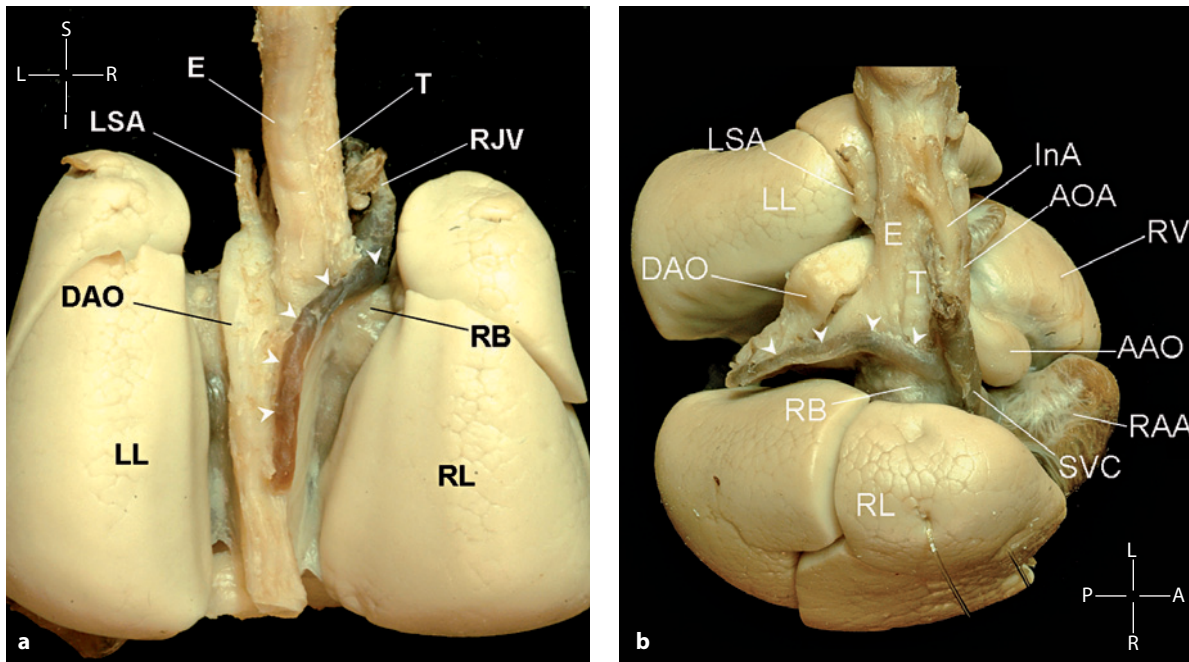
Fig. 3.8 • The normal azygos vein (*white arrowheads*) in a normal heart and lung block ensemble seen from behind (**a**) and from the right upper side (**b**). The azygos vein runs posteriorly and medial to the descending aorta then arches superiorly above the right bronchus to join the superior vena cava before its junction with the right atrium. *AAO* ascending aorta, *AOA* aortic arch, *DAO* descending aorta, *E* esophagus, *InA* innominate artery, *LL* left lung, *LSA* left subclavian artery, *SVC* superior vena cava, *RAA* right atrial appendage, *RB* right bronchus, *RJV* right jugular vein, *RL* right lung, *RV* right ventricle, *T* trachea
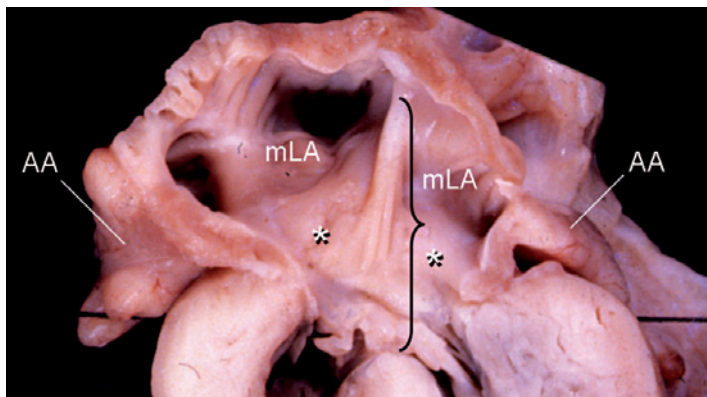
Fig. 3.9 • The inner surface of the two atria is shown in a fetal heart with left isomerism; the atrial appendage is hooked, with a narrow junction with the atria on both sides. Because both atria are morphologically left, the atrial vestibule (*white asterisk*) shows a smooth surface bilaterally. There is an atrioventricular septal defect (*black bracket*), with large atrial and relatively small ventricular component. Therefore, the crux cordis is absent. *AA* atrial appendage, *mLA* morphologically left atrium

both of which continue into the thorax to reach the superior vena cava system (Fig. 3.8). The enlarged azygos vein sits in paravertebral position always posterior to the descending aorta and can be identified by ultrasound in the fetus [19]. The position of the stomach and of the descending aorta is variable and inconsistent with the identification of this situs type. They can be located either to the left or right, on the same side, or on opposite sides. The intestines are almost always malrotated, although their precise position within the abdomen varies in each individual. Within the heart, both atrial appendages are morphologically left. They are therefore narrow tubular

structures, and the inferior aspect of the atria is smooth (Figs. 3.7b, 3.9). Other cardiac malformations are present in most cases, the commonest being:

- abnormal heart position;
- bilateral superior vena cava;
- anomalous pulmonary venous return, usually draining bilaterally;
- atrioventricular septal defect, more commonly with absent or small ventricular component;
- concordant ventriculoarterial connections;
- systemic outflow-tract obstruction;
- complete heart block, often associated with cardiomegaly and ventricular hypertrophy [19].
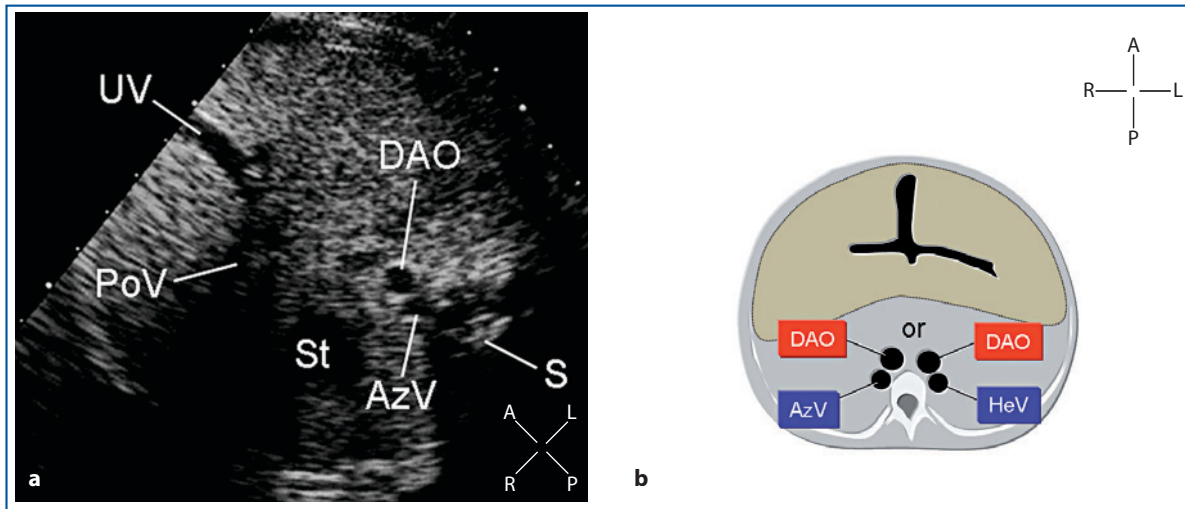
Fig. 3.10 • Transverse cross-sectional image of portal sinus in a 34-week gestational-age fetus with left isomerism (**a**). The azygos vein sits posteriorly to the descending aorta close to the spine and slightly to the right of the midline. The stomach is also on the right side. Diagram of transverse section of the upper abdomen in left isomerism (**b**). Because of their variable positions, the azygos (or hemiazygos) vein and the descending aorta are represented on both sides of the midline. The stomach is not represented because its position is variable and inconsistent with identification of this type of situs. *AzV* azygos vein, *DAO* descending aorta, *HeV* hemiazygos vein, *PoV* portal vein, *S* spine, *St* stomach, *UV* umbilical vein

In general, left isomerism has a better prognosis because of the less severe associated cardiac defects. However, the incidence of severe cardiac lesions is higher in prenatally diagnosed cases [20].

In patients with polysplenia, biliary atresia may be present. In fact, 10% of all patients with biliary atresia also have polysplenia [21, 22]. Malrotation anomalies of the intestines include a wide spectrum that ranges from nonrotation to reversed rotation and faulty peritoneal attachments. Duodenal atresia or stenosis may also be present.

In transverse sections of the upper abdomen, the inferior vena cava is nearly always interrupted, with azygos or hemiazygos continuation. In these cases, the venous channel lies in paravertebral position on the same side of and posterior to the descending aorta. Due to the symmetric liver lobes, the portal sinus often shows an ambiguous way of branching (Fig. 3.10).

Right Isomerism (Asplenia)

Right isomerism is characterized by bilateral "rightness". Consequently, both lungs are frequently trilobed with short eparterial bronchi. The descending aorta and inferior vena cava are commonly on the same side of the abdomen, although both can be right- or left-sided, and the inferior vena cava is located anterior to the descending aorta. As in left isomerism, in right isomerism, the stomach appears to be randomly positioned on the right or left but can also appear central

in some instances, with a tubular shape. The stomach and heart can both be located on the same or opposite sides (80% of cases in the Guy Hospital series) [24]. The intestines are malrotated, and the liver is a central structure with two symmetric lobes. As the spleen is normally a left-sided organ, there is frequently complete absence of the spleen (asplenia), although – again – this is not a universal finding (Fig. 3.11a). With respect to the heart, both atrial appendages are morphologically of right type. The internal aspect of both atria is rough, as the pectinate muscles extend from the tip of the appendages around the entirety of the atrioventricular junction (Fig. 3.11b).

Associated cardiac malformations are the rule in right isomerism [25]. By definition, the pulmonary veins always show anomalous connection, as there is no morphologically left atrium for them to connect to. They usually join together into a confluence behind the atria, which then drains anomalously below the diaphragm via a descending vein or to the superior vena cava via an ascending vein. Rarely, they drain directly to the atria or the coronary sinus. Other common malformations include:
- abnormal heart position;
- bilateral superior vena cava;
- totally anomalous pulmonary venous connection
- atrioventricular septal defect, often unbalanced;
- double-outlet right ventricle or discordant ventriculoarterial connections;
- pulmonary-outflow-tract obstruction;
- abnormal ventriculoarterial connections.
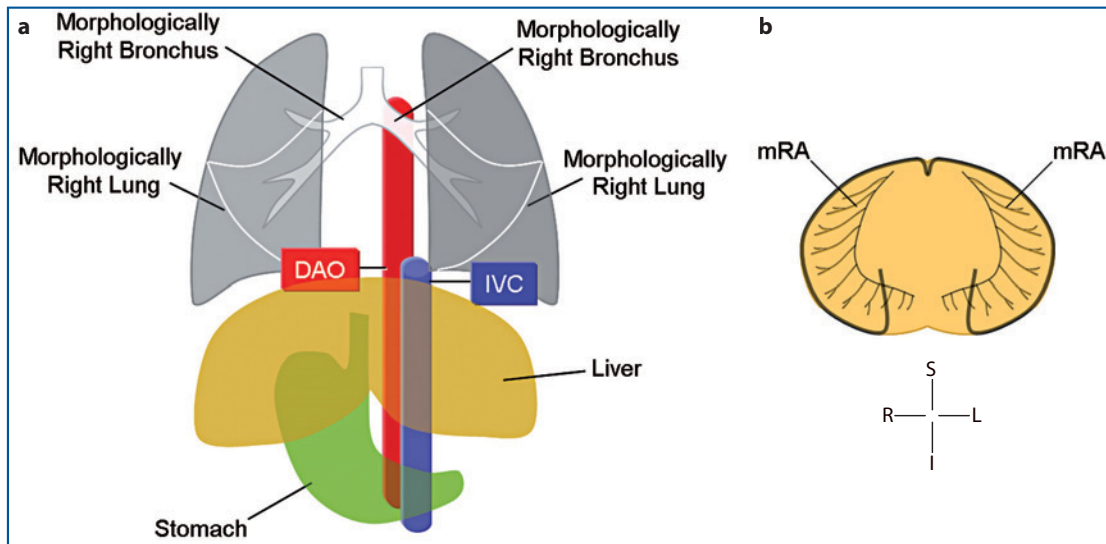
Fig. 3.11 • Representation of major body organs (**a**) and atrial appendages (**b**) in right isomerism. *DAO* descending aorta, *IVC* inferior vena cava, *mRA* morphologically right atrium
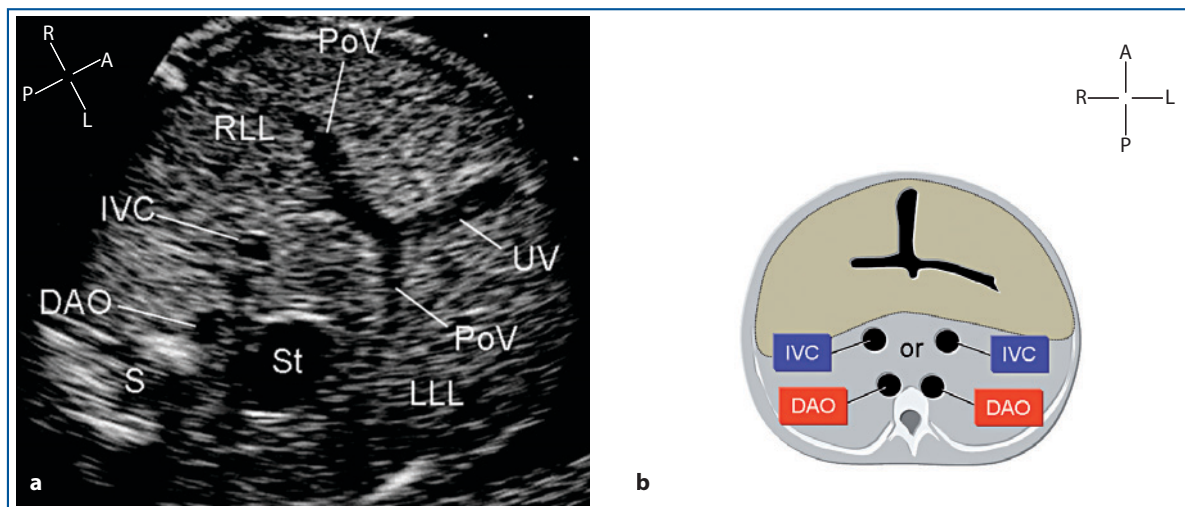
Fig. 3.12 • Transverse cross-sectional view of the portal sinus in a fetus with right isomerism (**a**). The inferior vena cava and descending aorta sit on the right side of the midline, with the inferior vena cava in anterolateral position. A tubular stomach is slightly to the left of the midline. The liver shows two nearly symmetrical lobes with a T-shaped branching of the portal sinus. These images could be mistaken for *situs solitus* by an inexperienced examiner. Diagram of transverse section of the upper abdomen in right isomerism (**b**). Because of their variable position, the inferior vena cava and descending aorta are represented on both sides of the midline. The stomach is not shown because its position is variable and inconsistent with identification of this type of situs. *DAO* descending aorta, *IVC* inferior vena cava, *LLL* left liver lobe, *PoV* portal vein, *RLL* right liver lobe, *S* spine, *St* stomach, *UV* umbilical vein

In transverse sections of the upper abdomen, the descending aorta and inferior vena cava lie on the same side of the midline, either to the left or right. The inferior vena cava sits in anterolateral position relative to the descending aorta. These two vessel can be either to the right or left of the midline. Due to the symmetric liver lobes, the portal sinus is ambiguous, often showing a T-shaped branching (Fig. 3.12). Right isomerism can be difficult to differentiate from *situs solitus* when the stomach is on the left and both great vessels at the level of the diaphragm are not imaged in a true transverse section.

References

1. Shinebourne EA, Macartney FJ, Anderson RH (1976) Sequential chamber localization – logical approach to diagnosis in congenital heart disease. Br Heart J 38:327-340

2. Anderson RH, Becker AE, Freedom RM et al (1984) Sequential segmental analysis of congenital heart disease. Pediatr Cardiol 5:281-288

3. Ho SY, Baker EJ, Rigby ML et al (1995) The normal heart. In Congenital heart disease. Mosby-Wolfe, London, pp 7-24

4. Chaoui R (2003) Cardiac malpositions and syndromes with right or left atrial isomerism. In: Gembruch U (ed) Fetal cardiology. Martin Dunitz, London, pp 173-182

5. Berg C, Geipel A, Kohl T et al (2005) Fetal echocardiographic evaluation of atrial morphology and the prediction of laterality in cases of heterotaxy syndromes Ultrasound Obstet Gynecol 26:538-545

6. Allan LD, Crawford DC, Anderson RH et al (1984) Echocardiographic and anatomical correlations in fetal congenital heart disease. Br Heart J 52:542-548

7. Silverman NH, Schmidt KG (1994) Ultrasound evaluation of the fetal heart. In Callen PW (ed) Ultrasonography in obstetrics and gynecology. WB Saunders, Philadelphia, pp 291-332

8. Bronshtein M, Gover A, Zimmer EZ (2002) Sonographic definition of the fetal situs. Obstet Gynecol 99:1129-1130

9. De Vore GR, Sarti DA, Siassi B et al (1986) Prenatal diagnosis of cardiovascular malformations in the fetus with situs inversus viscerum during the second trimester of pregnancy. J Clin Ultrasound 14:454-457

10. Bernasconi A, Azancot A, Simpson JM et al (2005) Fetal dextrocardia: diagnosis and outcome in two tertiary centres. Heart 91:1590-1594

11. Ortiga DJ, Chiba Y, Kanai H et al (2001) Antenatal diagnosis of mirror-image dextrocardia in association with situs inversus and Turner's mosaicism. J Matern Fetal Med 10:357-359

12. Holzmann D, Ott PM, Felix H (2000) Diagnostic approach to primary ciliary dyskinesia: a review. Eur J Pediatr 159(1-2):95-98

13. Sapire DW, Ho SY, Anderson RH et al (1986) Diagnosis and significance of atrial isomerism. Am J Cardiol 58:342-346

14. Ho SY, Cook A, Anderson RH et al (1991) Isomerism of the atrial appendages in the fetus. Pediatr Pathol 11:589-608

15. Allan LD, Sharland G, Cook A (1994) Atrial isomerism. In: Color atlas of fetal cardiology. Mosby-Wolfe, London, pp 33-42

16. Uemura H, Ho SY, Devine WA et al (1995) Atrial appendages and venoatrial connections in hearts from patients with visceral heterotaxy. Ann Thorac Surg 60:561-569

17. Anderson RH, Becker AE (1997) Isomerism of the atrial appendages. In: Controversies in the description of congenitally malformed hearts. Imerial College Press, London, pp 67-112

18. Berg C, Geipel A, Smrcek J et al (2003) Prenatal diagnosis of cardiosplenic syndromes: a 10-year experience. Ultrasound Obstet Gynecol 22:451-459

19. Sheley RC, Nyberg DA, Kapur R (1995) Azygous continuation of the interrupted inferior vena cava: a clue to prenatal diagnosis of the cardiosplenic syndromes. J Ultrasound Med 14:381-387

20. Schmidt KG, Ulmer HE, Silverman NH et al (1991) Perinatal outcome of fetal complete atrioventricular block: a multicenter experience. J Am Coll Cardiol 17:1360-1366

21. Phoon CK, Villegas MD, Ursell PC et al (1996) Left atrial isomerism detected in fetal life. Am J Cardiol 77:1083-1088

22. Davenport M, Howard ER (1992) Biliary atresia and the polysplenia syndrome. J Pediatr Surg 27(4):539-540

23. Chandra RS (1974) Biliary atresia and other structural anomalies in congenital polysplenia syndrome. J Pediatr 85:649-655

24. Sharland G, Cook A (2000) Heterotaxy syndromes/ isomerism of the atrial appendages. In: Textbook of fetal cardiology. Greenwich Medical Media, London, pp 335-346

25. Berg C, Geipel A, Kamil D et al (2006) The syndrome of right isomerism – prenatal diagnosis and outcome Ultraschall Med 27(3):225-233

CHAPTER 4

The Cardiac Position and Axis Orientation

Introduction

Although in most individuals two thirds of the heart is in the left side of the chest, the heart can be unusually positioned. All cardiac positions can be described in terms of overall location of the heart and orientation of its axis. The cardiac position and axis can be assessed by fetal echocardiography in the four-chamber view. In this view, by tracing the sagittal and coronal planes through the center of the thorax, four quadrants are identified. In the normal individual, the left ventricle, most of the right ventricle, and the anterior part of the left atrium, lie in the left anterior quadrant. A small part of the right ventricle and most of the right atrium fall in the right anterior quadrant, and the posterior part of the left atrium is in in the posterior quadrants (Fig. 4.1) [1].

The axis of the heart refers to its long axis. The orientation of this axis can be expressed as the angle between a line along the ventricular septum, directed toward the cardiac apex, and the midline sagittal plane of the thorax (Fig. 4.2). In the normal individual, the axis is oriented approximately 45° to the left [2]. In hearts with one large and one rudimentary ventricle, the ventricular septum can be difficult to identify. In these cases, the cardiac axis coincides with the major axis of the large ventricle.

Regarding position, the heart can be left-sided (levocardia), central (mesocardia), or right-sided (dextrocardia) within the thorax. Rarely, it can be located outside the thorax (ectopia cordis). The orientation of the cardiac axis is independent from the position of the heart. Therefore, for each heart posi-

Fig. 4.1 • Cross-sectional four-chamber view of a normal 21-week gestational-age fetus. The four quadrants, identified by the sagittal and coronal planes (*white dashed lines*) traced in the center of the thorax, are shown (see text for details.) *LA* left atrium, *LV* left ventricle, *RA* right atrium, *RV* right ventricle, *S* spine
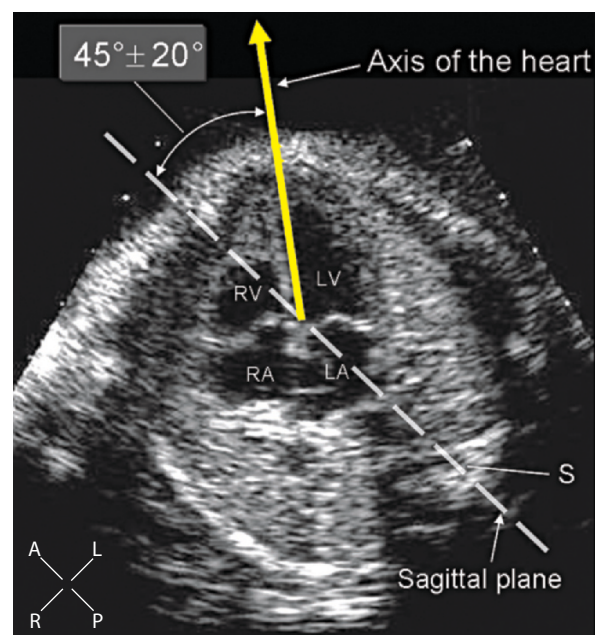
Fig. 4.2 • In this normal four-chamber view, the *yellow arrow* is traced along the ventricular septum to indicate the axis of the heart, with the *arrowhead* pointing toward the apex. The normal range of the angle between the cardiac axis and the midline sagittal plane (*white dashed line*) is indicated. *LA* left atrium, *LV* left ventricle, *RA* right atrium, *RV* right ventricle, *S* spine
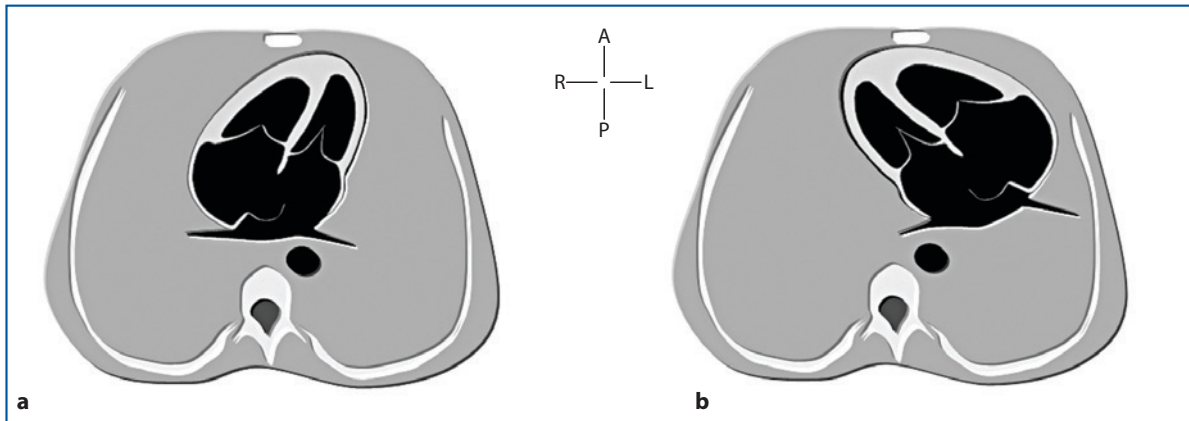
Fig. 4.3 • Two examples of different positions and axis orientations of the heart and how they can be described. **a** Central heart, axis to the left. **b** Left-sided heart, axis to the right

tion, orientation of the axis can be to the left, to the midline, or to the right and must be described separately (Fig. 4.3). Anomalies of the cardiac position or axis can occur in isolation, although many anomalies alter both.

An abnormal cardiac position frequently coexists with abnormal cardiac morphology. However, an abnormal heart position is not a disease per se and can be found in an entirely normal heart. For example, a right-sided heart is the normal situation in individuals with mirror-image visceroatrial arrangement. Therefore, cardiac position and axis must be placed in the context of a global assessment that takes into account the visceroatrial arrangement, the segmental analysis of the cardiac morphology, and the possible presence of anomalies of organs within the thorax.

As stated, the cardiac position and axis can be assessed in the four-chamber view, whereas the visceroatrial arrangement can be defined in transverse views of the upper abdomen (please refer to Chapters 3, 5, and 6).

Fig. 4.4 • Four-chamber view in a 24-week gestational-age fetus with critical pulmonary valve stenosis in usual arrangement. The heart is mostly in the left side of the chest, with its axis (*yellow arrow*) pointing to the left. However, the cardiac axis shows a pronounced leftward rotation, close to 85° from the midline sagittal plane (*white dashed line*). *DAO* descending aorta, *LA* left atrium, *LV* left ventricle, *RA* right atrium, *RV* right ventricle, *S* spine

Heart in the Left Side of the Chest (Levocardia)

As stated earlier, a left-sided heart with the axis pointing to the left is the normal pattern in individuals with usual visceroatrial arrangement. However, even in this setting, anomalies can occur. Pronounced rotation of the cardiac axis to the left has been described in pulmonary valve stenosis (Fig. 4.4) and Ebstein's anomaly. Dilatation of the right atrium has been advocated as the cause of the rotational anomaly in these cases. Leftward rotation of the cardiac axis may also be observed in conotruncal malformation, where the size of the cardiac chambers is usually nor-

mal (Fig. 4.5). Overrotation during embryogenesis has been hypothesized in axis deviation of these congenital heart diseases [3, 4]. However, abnormal cardiac axis is an inconstant finding and can be overlooked on routine examination. Only including assessment of the ventriculoarterial connections in prenatal ultrasound screening will detect most conotruncal anomalies.

A heart in the left side of the chest may show a position excessively to the left. This may happen in
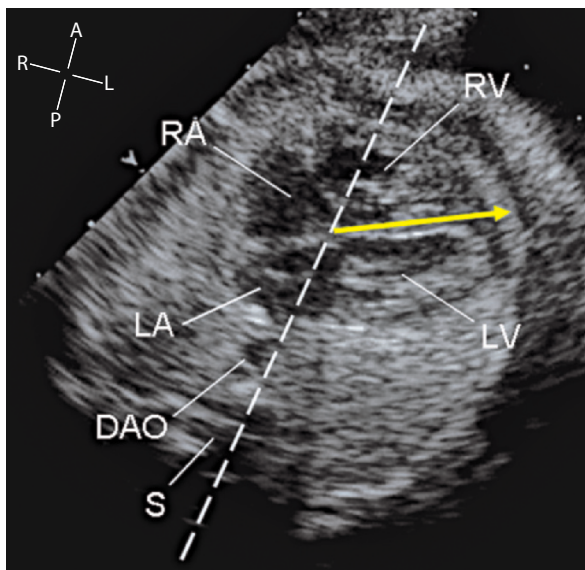
Fig. 4.5 • Four-chamber view in a 27 week-gestational-age fetus with tetralogy of Fallot in usual atrial arrangement. The heart is mostly in the left side of the chest, with the cardiac axis (*yellow arrow*) slightly overrotated to the left, approximately 70° from the midline sagittal plane (*white dashed line*). *DAO* descending aorta, *LA* left atrium, *LV* left ventricle, *RA* right atrium, *RV* right ventricle, *S* spine
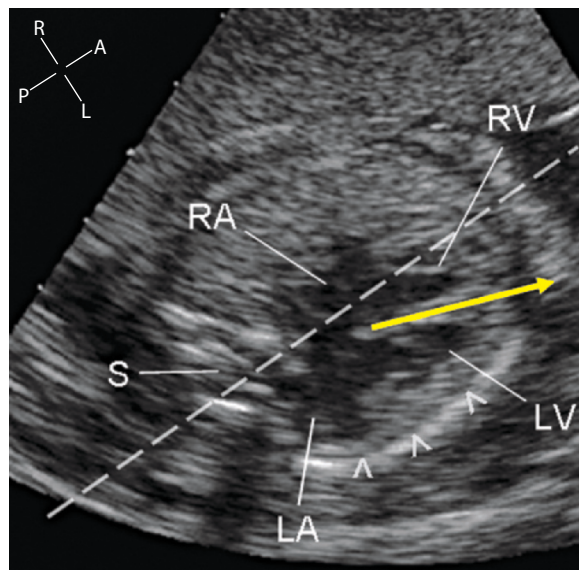
Fig. 4.6 • Four-chamber view in a 23-week gestational-age fetus with agenesia of the left lung. The cardiac axis (*yellow arrow*) is normally to the left, approximately 30° from the midline sagittal plane (*white dashed line*), but the heart is displaced to the left, reaching the most lateral part of the left hemithorax. The left atrium and ventricle are in close contact with the thoracic cage (*yellow arrowheads*). The atrial arrangement is usual. *LA* left atrium, *LV* left ventricle, *RA* right atrium, *RV* right ventricle, *S* spine

unilateral agenesia of the left lung, where the heart is displaced toward the affected hemithorax (Fig. 4.6) [5].

Because a right-sided heart is normal in mirror-image visceroatrial arrangement, if the heart is located in the left side of the chest in this setting, it will be frequently associated with congenital heart defects.

Heart in the Middle of the Chest (Mesocardia)

This is the least common type of malposition observed in postnatal autopsic series [6, 7]. In decreasing order of frequency, a central heart has been found in normal hearts and in congenitally corrected transposition (Fig. 4.7), complete transposition, and double-outlet right ventricle. In our experience (unpublished data), a central heart with apex pointing to the midline is a common cardiac finding in hearts with tricuspid atresia (Fig. 4.8).

Anomalies of cardiac position of any type can occur in lung malformations [8, 9]. In cystic adenomatoid malformation (CAM), when the disease affects both lungs, the heart can be in the central part of the chest and appear compressed by the overdistended lungs. Lung overdistension may occur also in laryngeal stenosis, as is seen in Fraser syndrome (Fig. 4.9).

Heart in the Right Side of the Chest (Dextrocardia)

Dextrocardia is a condition that includes a heterogeneous spectrum of hearts and in which the incidence of cardiac malformations varies according to the cardiac situs. Two major fetal series on this type of cardiac malposition have been published, reporting a high incidence of structural cardiac and extracardiac malformations [10, 11]. More rarely, a right-sided heart has been found in association with an abnormal karyotype [12, 13].

In usual atrial arrangement, the terms "dextroposition" and "dextroversion" have been used by many authors to distinguish two different types of hearts in the right side of the chest. The terms "levoposition" and "levoversion" have been used to indicate similar conditions in cases with mirror-image visceroatrial arrangement.

Dextroposition has been used to refer to a translational problem of the heart that is displaced in the right hemithorax but maintains a relatively normal axis orientation to the left, that is, to the side expected from the situs. In malpositions of this type, extracardiac malformations are common and often re-
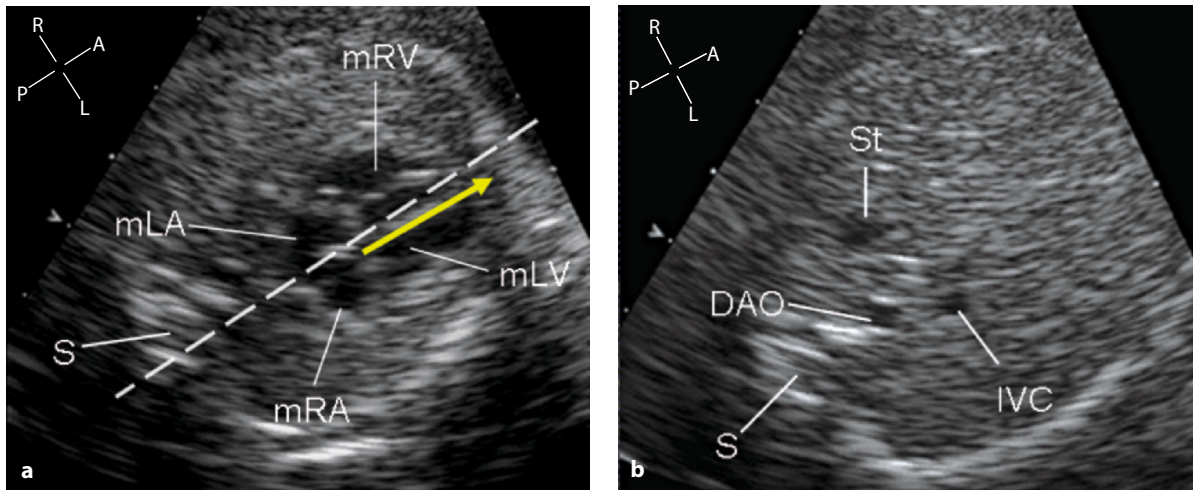
Fig. 4.7 • Four-chamber view (**a**) and transverse view of the upper abdomen (**b**) in a 22-week gestational-age fetus with the heart in the middle of the chest. Cardiac axis (*yellow arrow*) is nearly parallel to the midline sagittal plane (*white dashed line*). This malposition occurred in the context of an atrioventricular and ventriculoarterial discordance and mirror-image visceroatrial arrangement. Reversed position of the stomach and the great vessels (**b**) is seen. Mirror-image atrial arrangement occurred in two out of 14 cases of atrioventricular discordance in our initial fetal series. Precise evaluation of cardiac connections in this setting represents one of the most challenging tasks in prenatal diagnosis, with an increased risk of misinterpretation and inappropriate counseling. *DAO* descending aorta, *IVC* inferior vena cava, *mLA* morphologically left atrium, *mLV* morphologically left ventricle, *mRA* morphologically right atrium, *mRV* morphologically right ventricle, *S* spine, *St* stomach
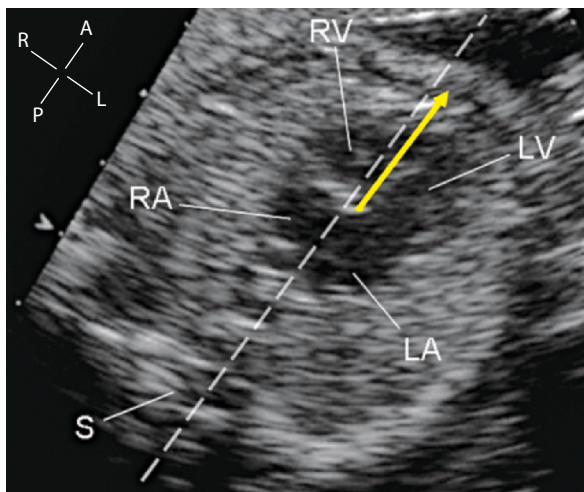
Fig. 4.8 • Four-chamber view in a 25-week gestational-age fetus with tricuspid valve atresia. The heart is in central position within the chest with its axis (*yellow arrow*) pointing to the midline (*white dashed line*). The atrial arrangement is usual. *LA* left atrium, *LV* left ventricle, *RA* right atrium, *RV* right ventricle, *S* spine

sponsible for the abnormal location of the heart. These malformations include space-occupying lesions within the thorax, such as diaphragmatic hernia (Fig. 4.10), cystic adenomatoid malformation of the lung, and tumors of the lung or the mediastinum. Congenital heart disease can be associated and must be always ruled out. Left diaphragmatic hernia represents the typical example of extracardiac malformation that can cause cardiac malpositions of this type. In up to 20% of cases, diaphragmatic hernia can be associated with congenital heart disease,

which can be of every kind [14]. An associated cardiac defect is generally an indicator of poor prognosis [15]. In the majority of cases with left diaphragmatic hernia, cardiac dimensions in general and the left heart chambers in particular are smaller than normal. However, only a minority of cases develops a true hypoplastic left heart.

Dextroversion has been used to indicate a rotational problem of the heart, as though the cardiac axis had pivoted horizontally to the right around a superoinferior axis. In malposition of this type, the heart
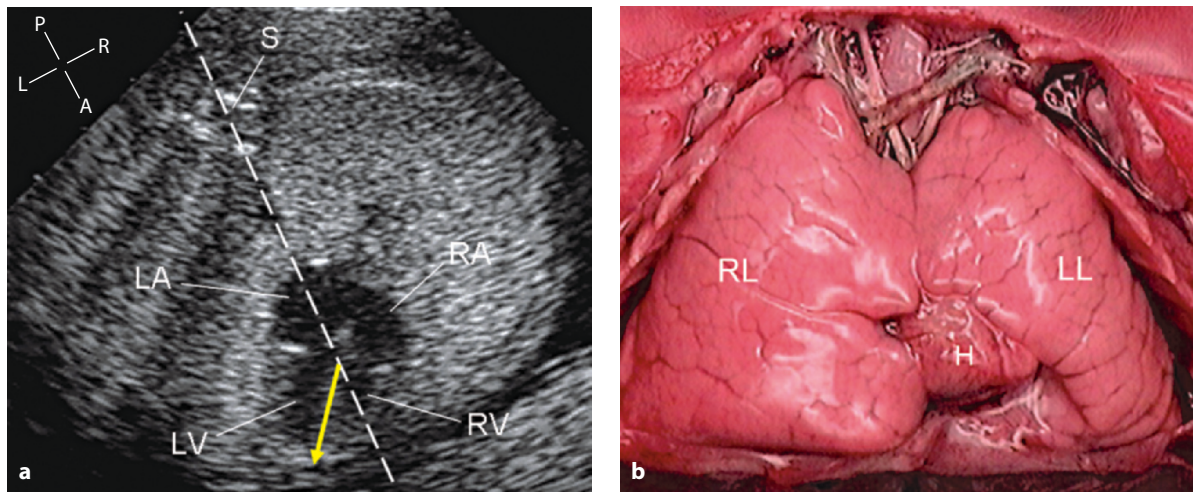
Fig. 4.9 • Four-chamber view (**a**) and the anatomic specimen of the opened chest (**b**) in a 22-week gestational-age fetus with Fraser syndrome who underwent termination. Lung overdistension, due to laryngeal stenosis, caused compression of the heart chambers, with impairment to the flow of the vena cava, increased hydrostatic pressure, and massive ascites. The echocardiographic image shows a small heart in the middle of the thorax, squeezed by two overexpanded lungs. The cardiac axis (*yellow arrow*) points to the left of the midline (*white dashed line*) in the setting of usual atrial arrangement. *H* heart, *LA* left atrium, *LL* left lung, *LV* left ventricle, *RA* right atrium, *RL* right lung, *RV* right ventricle, *S* spine
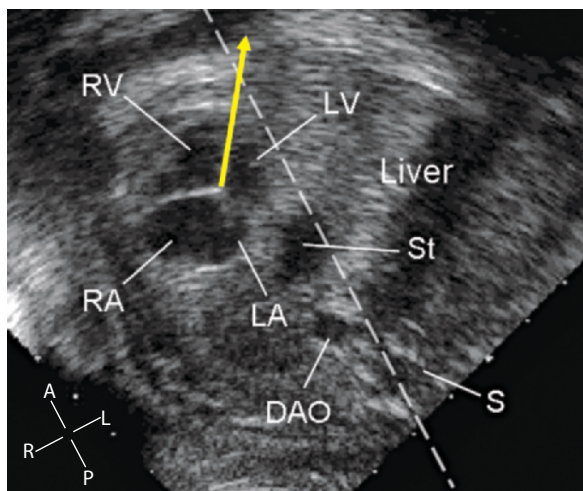
Fig. 4.10 • Four-chamber view in a 33-week gestational-age fetus with left diaphragmatic hernia. The heart is in the right side of the chest but with the apex still pointing to the left (*yellow arrow*) of the midline (*white dashed line*). Part of the herniated stomach can be seen behind the heart. The left atrium and ventricle are hypoplastic. *DAO* descending aorta, *LA* left atrium, *LV* left ventricle, *RA* right atrium, *RV* right ventricle, *S* spine, *St* stomach

is located in the right side of the chest, with its axis pointing to the right, that is, to the opposite side from that expected for the visceroatrial arrangement. Although such a right-sided heart can rarely be normal (Fig. 4.11), the large majority of cases is associated with congenital heart disease. Among these, the most common is a discordant atrioventricular connection (Fig. 4.12) [16, 17].

A diagram summarizing three common types of dextrocardia is shown in Figure 4.13.

Trying to describe in a few words different types of right-sided hearts, one can be tempted to use short definitions such as dextroposition, dex-

troversion, pivotal dextrocardia, isolated dextrocardia, or secondary dextrocardia. However, these definitions frequently do not apply to many conditions or can be simply equivocal. Cases shown in Figures 4.11 and 4.12, for example, could both fall into the definition of dextroversion, which does not tell anything about the important differences between their structural morphology and physiology.

Therefore, we agree with Prof. Robert Anderson's teaching [18] that the use of these term should be abandoned in favor of a purely descriptive segmental approach to the malformed heart.
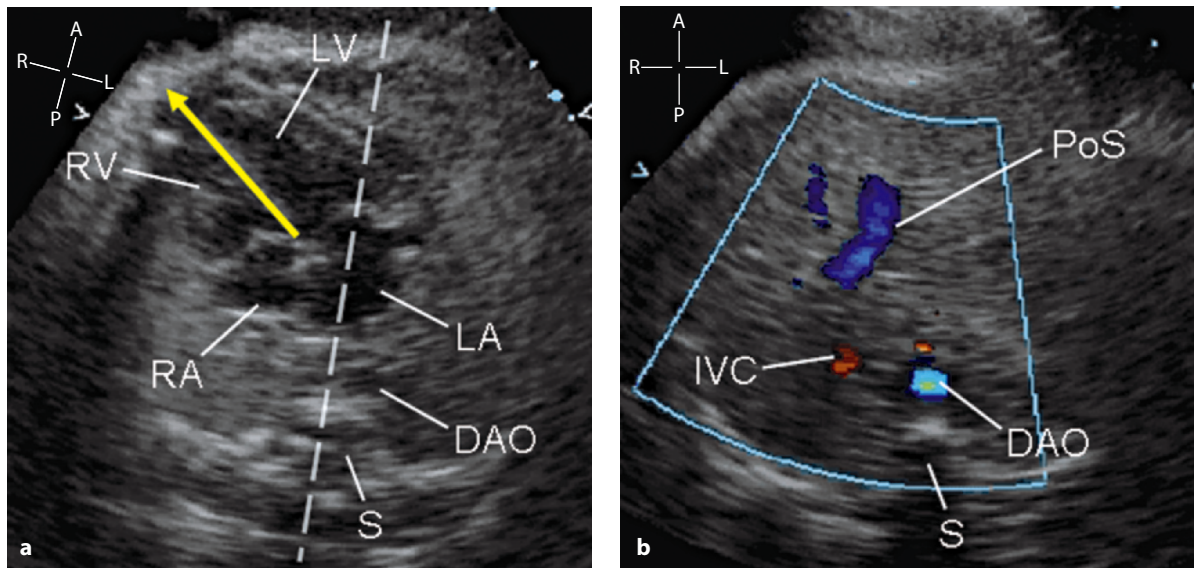
Fig. 4.11 • Four-chamber view (**a**) and transverse section of the upper abdomen (**b**) in a 26-week gestational-age fetus. The heart is located in the right chest with its axis (*yellow arrow*) to the right of the midline (*white dashed line*). The visceroatrial arrangement is usual. Sequential analysis revealed an entirely normal heart, and no associated extracardiac anomalies were identified. *DAO* descending aorta, *IVC* inferior vena cava, *LA* left atrium, *LV* left ventricle, *RA* right atrium, *RV* right ventricle, *PoS* portal sinus, *S* spine
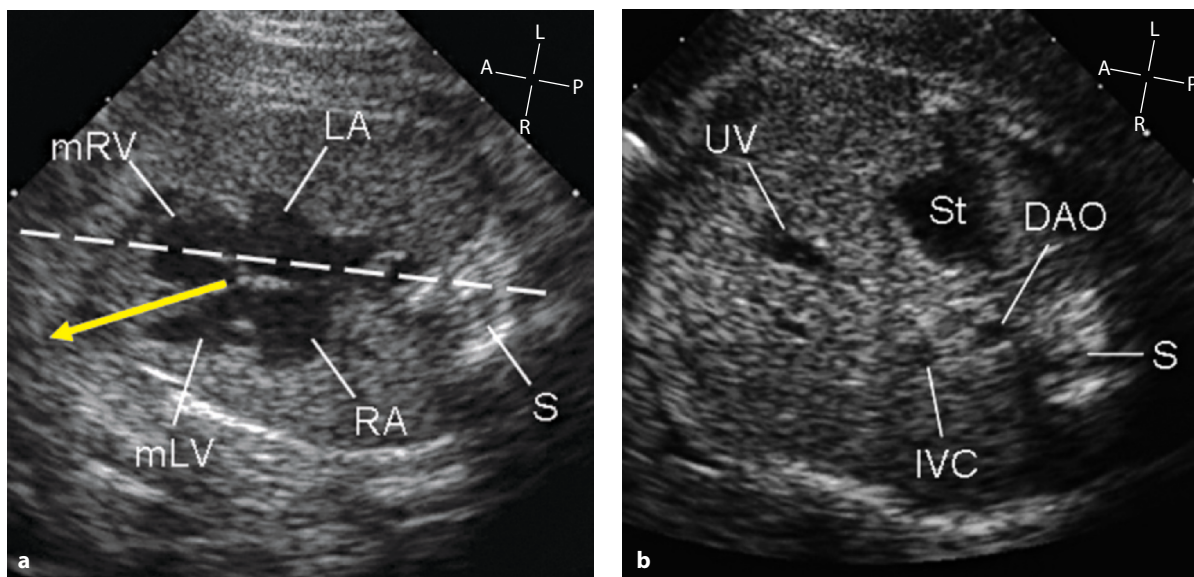
Fig. 4.12 • Four-chamber view (**a**) and transverse section of the upper abdomen (**b**) in a 32-week gestational-age fetus. The heart is mostly located in the right chest with its axis (*yellow arrow*) pointing to the right of the midline (*white dashed line*). The visceroatrial arrangement is usual. The atrioventricular connection is discordant, with the the atria being connected with ventricles of opposite morphology. Discordant ventriculoarterial connection, ventricular septal defect, and pulmonary valve stenosis are among associated cardiac defects in this case. *DAO* descending aorta, *IVC* inferior vena cava, *LA* left atrium, *mLV* morphologically left ventricle, *mRV* morphologically right ventricle, *RA* right atrium, *S* spine, *St* stomach, *UV* umbilical vein
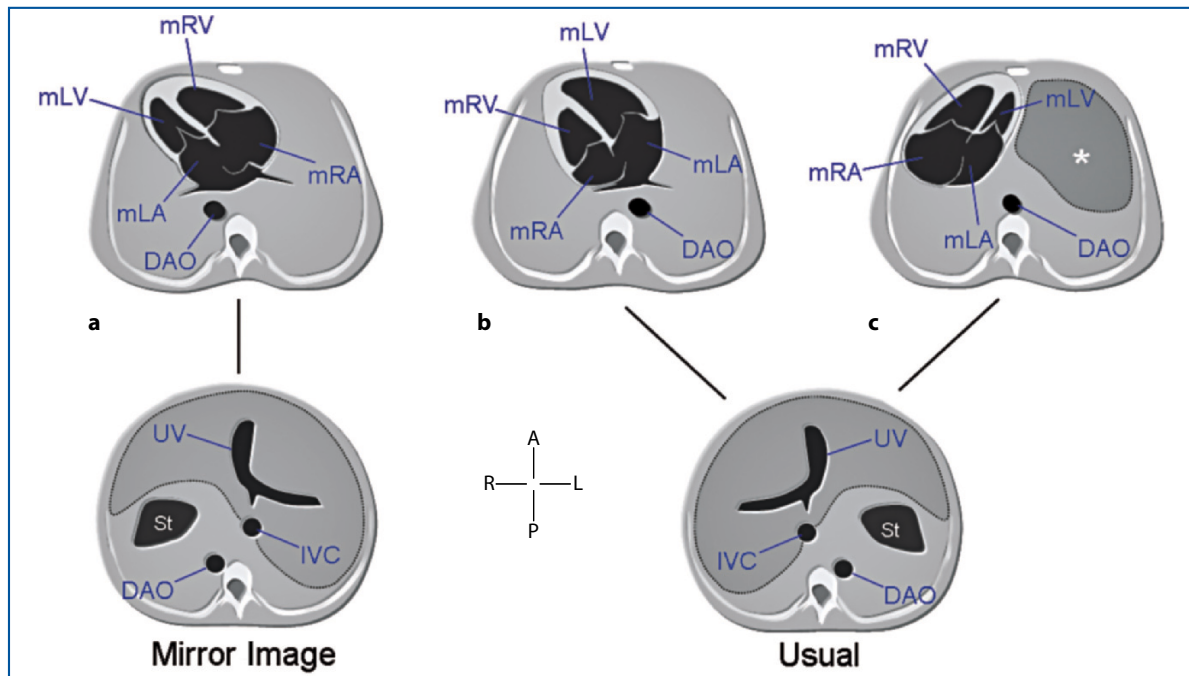
Fig. 4.13 • Diagram simulating the transverse view of the upper abdomen and the four-chamber view in three different types of hearts in the right side of the chest (dextrocardia). Right-sided heart associated with mirror-image visceroatrial arrangement (*situs inversus*) (**a**). This type of dextrocardia has also been called "mirror-image dextrocardia". Two other types of dextrocardia with usual visceroatrial arrangement are shown (**b, c**). Right-sided heart with apex to the right (**b**). This type could be defined as "dextroversion". Note that the ventricle immediately behind the sternum is the morphologically left ventricle and not the morphologically right ventricle, as observed in **a**. The left atrium is elongated and bent to the right to maintain its connection with the anterior ventricle. Right-sided heart is shown with the axis still pointing to the left (**c**). This case has been called "dextroposition" and is usually secondary to space-occupying lesions within the thorax (*white asterisk*). *DAO* descending aorta, *IVC* inferior vena cava, *mLA* morphologically left atrium, *mLV* morphologically left ventricle, *mRA* morphologically right atrium, *mRV* morphologically right ventricle, *S* spine, *UV* umbilical vein

Isomerism of the Atrial Appendages and Cardiac Position

Abnormal cardiac position has been observed in up to 60% of cases with either form of isomerism. In nearly one third of such cases, the heart is in the right side of the chest. In up to 80% of cases with right isomerism and 50% with left isomerism, the heart and stomach are located on opposite sides of the body. This finding can be easily detected by the obstetric sonographer during a routine examination and should alert to the possibility of a visceroatrial anomaly of this type (Figs. 4.14, 4.15) [19].
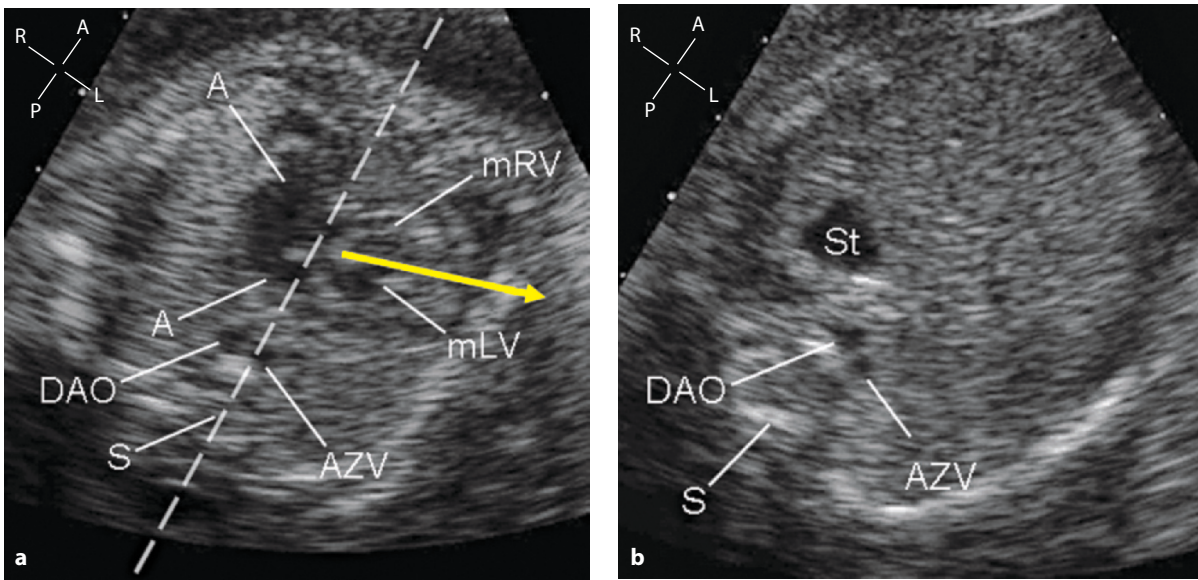
Fig. 4.14 • Four-chamber view (**a**) and transverse section of the upper abdomen (**b**) in a 21-week gestational-age fetus with left isomerism. The stomach and the heart lie on opposite sides of the body. The heart is mostly in the left side of the chest, but its axis (*yellow arrow*) shows a pronounced rotation to the left, being approximately 80° from the midline sagittal plane (*white dashed line*). Azygos continuation of the inferior vena cava, common atrium, and atrioventricular septal defect are among the associated cardiac malformations. *A* atrium, *AzV* azygos vein, *DAO* descending aorta, *mLV* morphologically left ventricle, *mRV* morphologically right ventricle, *S* spine, *St* stomach
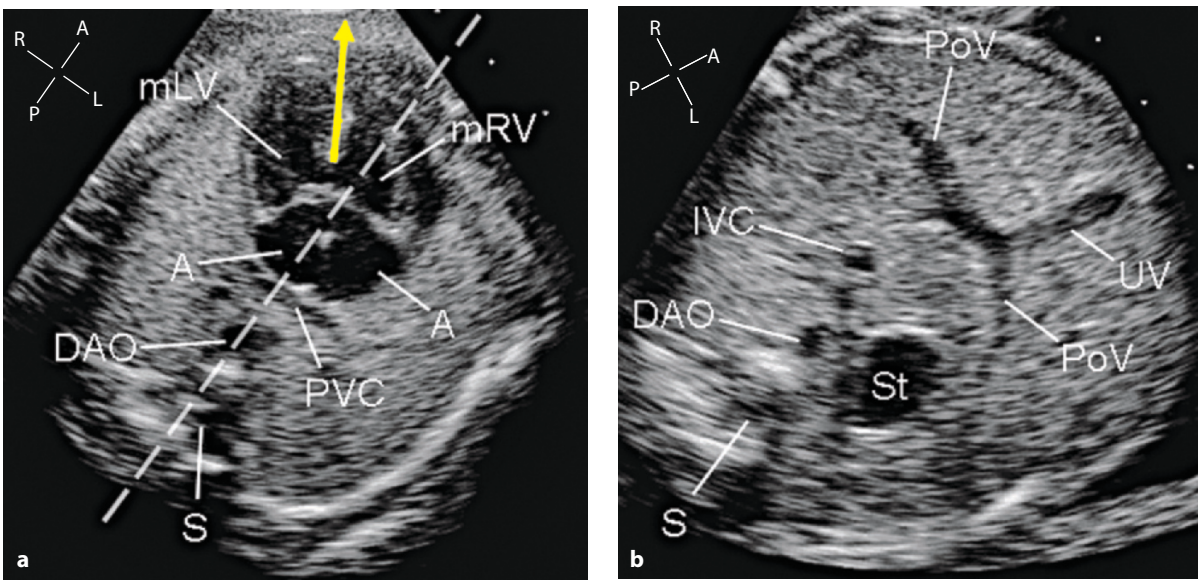
Fig. 4.15 • Four-chamber view (**a**) and transverse section of the upper abdomen (**b**) in a 27-week gestational-age fetus with right isomerism. The stomach and the heart lie on opposite sides of the body. The heart is right-sided, with its axis (*yellow arrow*) oriented 30-40° to the right of the midline sagittal plane (*white dashed line*). *A* atrium, *DAO* descending aorta, *IVC* inferior vena cava, *mLV* morphologically left ventricle, *mRV* morphologically right ventricle, *PoV* portal vein, *PVC* pulmonary veins confluence, *S* spine, *St* stomach, *UV* umbilical vein

References

1. Schmidt KG, Silverman NH (1988) Evaluation of the fetal heart by ultrasound. In: Callen PW. Ultrasonography in obstetrics and gynecology. WB Saunders, pp 165-206

2. Comstock CH (1987) Normal fetal heart axis and position. Obstet Gynecol 70:255-259

3. Shipp TD, Bromely B, Hornberg LK et al (1995) Levorotation of the fetal cardiac axis: a clue for the presence of congenital heart disease. Obstet Gynecol 85:97-102

4. Smith RS, Comstock CH, Kirk JS et al (1995) Ultrasonographic left cardiac axis deviation: a marker for fetal anomalies. Obstet Gynecol 85:187-191

5. Bromley B, Benacerraf BR (1997) Unilateral lung hypoplasia. Report of three cases. J Ultrasound Med 16:599-601

6. Stanger P, Rudolph AM, Edwards JE (1977) Cardiac malpositions: an overview based on study of sixty-five necropsy specimens. Circulation 56:159-172

7. Lev M, Liberthson RR, Golden JG et al (1971) The pathologic anatomy of mesocardia. Am J Cardiol 28:428-435

8. Rosado-de-Christenson ML, Stocker JT (1991) Congenital cystic adenomatoid malformation. RadioGraphics 11:865-886

9. Bromley B, Parad R, Estroff JA et al (1995) Fetal lung masses: prenatal course and outcome. J Ultrasound Med 14:927-936

10. Walmsley R, Hishitani T, Sandor GG et al (2004) Diagnosis and outcome of dextrocardia diagnosed in the fetus. Am J Cardiol 94:141-143

11. A Bernasconi, A Azancot, J M Simpson et al (2005) Fetal dextrocardia: diagnosis and outcome in two tertiary centres. Heart 91:1590-1594

12. Ortiga DJ, Chiba Y, Kanai H et al (2001) Antenatal diagnosis of mirror-image dextrocardia in association with situs inversus and Turner's mosaicism. J Matern Fetal Med 10:357-359

13. Pauliks LB, Friedman DM, Flynn PA (2000) Fetal diagnosis of atrioventricular septal defect with dextrocardia in trisomy 18. J Perinat Med 28:412-413

14. Allan LD, Irish MS, Glick PL (1996) The fetal heart in diaphragmatic hernia. Clin Perinatol 23:795-811

15. Sharland GK, Lockhart SM, Heward AJ et al (1992) Prognosis in fetal diaphragmatic hernia. Am J Obstet Gynecol 166:9-13

16. Winer-Muram HT, Tonkin ILD (1989) The spectrum of heterotaxic syndromes. Radiol Clin North Am 27:1147-1170

17. Hagler DJ, O'Leary PW (1995) Cardiac malpositions and abnormalities of atrial and visceral situs. In : Emmanouilides GC, Riemenschneider TA, Allen HD et al (eds) Heart disease in infants, children and adolescents including the fetus and young adult. Williams & Wilkins, Baltimore, pp 249-294

18. Calcaterra G, Anderson RH, Lau KC et al (1979) Dextrocardia: value of segmental analysis in its categorisation. Br Heart J 42:497-507

19. Sharland G, Cook A (2000) Heterotaxy syndromes/isomerism of the atrial appendages. In: Allan LD, Hornberg L, Sharland GK (eds) Textbook of fetal cardiology. Greenwich Medical Media, London, pp 335-346

CHAPTER 5

Principles of Segmental Analysis

Introduction

Once the laterality, visceroatrial arrangement, and cardiac position of the fetus have been established, the next step is to analyze the heart in a sequential segmental approach. Sequential analysis allows description of all congenital heart malformations, even the more complex ones, simply and unambiguously [1-3]. All hearts, whether normal or abnormal, can be assumed to comprise three major segments and two connections between those segments. Each segment is usually partitioned into one left-sided and one right-sided component. The three segments are the atria, the ventricles, and the arterial trunks. The connections consist of the atrioventricular connection and the ventriculoarterial connection. A fourth segment – the systemic and pulmonary veins, and its connection – the venoatrial connection, must be assessed for a complete segmental analysis. This is not discussed in this chapter because of the great variability of these structures.

In congenital heart malformations, the cardiac structures may not always be in their expected location and may be connected in an abnormal sequence. Therefore, the atria and the ventricles should be recognized by their anatomic structure and not by their location, and thus the terms "morphologically left" and "morphologically right" should be used instead of simply "left" and "right". In practice, the heart should be evaluated by following the direction of blood flow in order to assess the connection of the systemic and pulmonary veins, the atria, the atrioventricular connection, the ventricles, the ventriculoarterial connection, and the great arteries. Sequential examination must define morphology, position (relative and absolute), size, functional status, and state of septation (separation of the right-sided from the left-sided structures) of a segment or a connection. Sequential analysis represents a diagnostic fundamental basis for the clinician and the pathologist.

The Atria

Each atrium is usually composed of four basic parts: (1) the venous component, receiving the systemic or pulmonary venous return, (2) the vestibule, giving access to the atrioventricular valve, (3) the septal surface, and (4) the appendage. When these parts are considered in terms of constancy in malformed hearts, it can be demonstrated that parts 1, 2, and 3 cannot be used as a defining criterion to identify the morphologically right or left atrium. In fact, the venous return to the atria, the atrioventricular valves, and the atrial septum are variable structures in abnormal hearts and can be totally lacking. On the other hand, the appendages are the most constant component of the atria [4]. Their shape, the morphology of their junction with the body of the atrium, and the extent of the pectinate muscles within the appendage always show a morphologically right or left pattern. The morphologically left atrial appendage is tubular, hook-shaped, and has a narrow junction with the body of the atrium. The internal surface of the latter is smooth, as the pectinate muscles are restricted to the appendage. The morphologically right atrial appendage is triangular, with a broad junction with the body of the atrium. On its internal aspect, it contains pectinate muscles extending around the atrioventricular junction and reaching the crux of the heart.

As already described in the dedicated chapter, there are four possible arrangements of the atria. In usual arrangement, the left-sided atrium is morphologically of left type, and the right-sided atrium is morphologically of right type. In mirror-image arrangement, all body organs are in mirror-image position. Therefore, within the heart, the morphologically right atrium is left-sided, and the morphologically left atrium is right-sided. In left isomerism, both atrial appendages are morphologically of left type. They are therefore narrow tubular structures, and the interior aspect of both atria is smooth. In right isomerism, both atrial appendages are morphological-
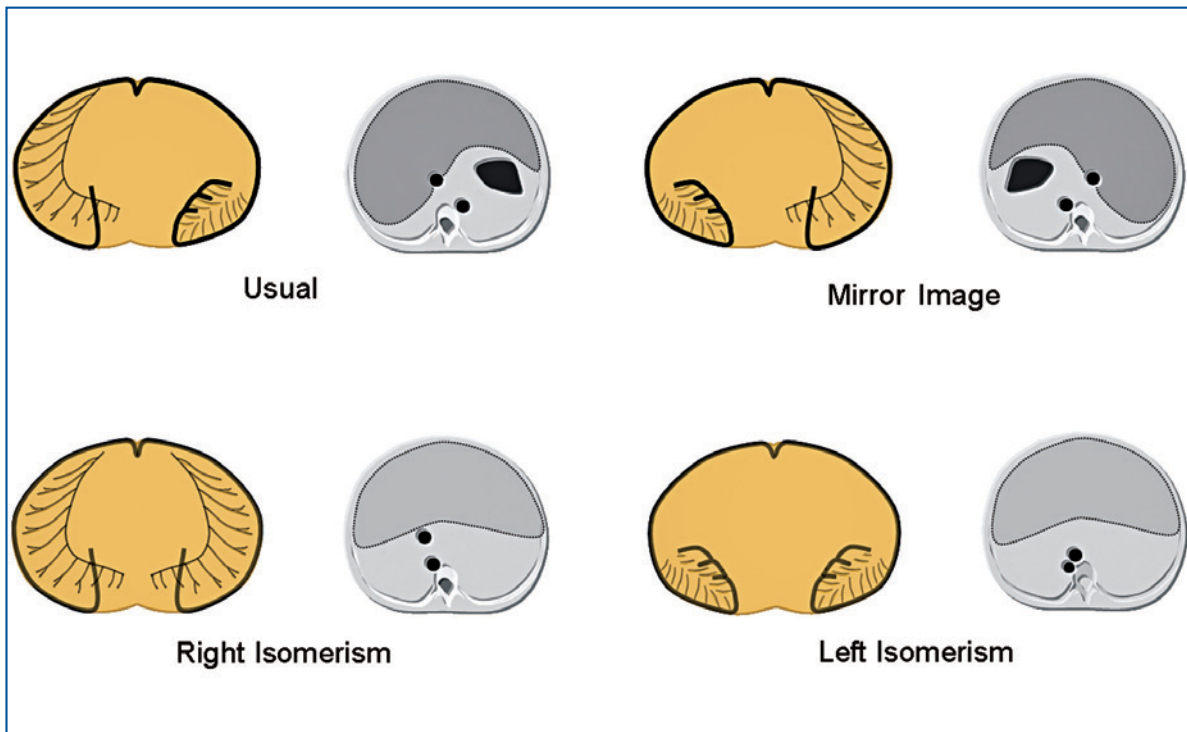
Fig. 5.1 • Diagram of the four different types of atrial arrangement and the correspondent section of the upper abdomen showing the location of the descending aorta and the inferior vena cava

ly of right type. The internal aspect of both atria will show pectinate muscles extending from the tip of the appendages around the entirety of the atrioventricular junction.

Because the morphology of the atrial appendage is very difficult to recognize directly on echocardiography, the atrial arrangement can be determined indirectly from the location of the aorta and the inferior vena cava on transverse view of the upper abdomen (Fig. 5.1) [5].

The Ventricles

The ventricular mass is the cardiac segment that extends from the atrioventricular junction to the ventriculoarterial junction. A ventricle is an endocardial-lined chamber within the ventricular mass. Almost always, there are two ventricles in the ventricular mass. Each ventricle usually consist of three parts: (1) the inlet, (2) the apical trabecular, and (3) the outlet components. Because the inlet and outlet component can be missing, a rudimentary ventricle may consist of only one or two parts. The most constant part of the ventricles is therefore the

apical trabecular component. In the morphologically right ventricle, the apical region is characterized by a coarse trabeculation, whereas in the morphologically left ventricle the trabeculation is fine (Fig. 5.2). This myocardial characteristic can be recognized even in ventricles in which only the apical part is represented. The type of ventricular trabeculation is generally recognizable by fetal echocardiography.

Other characteristic features of the normal morphologically right ventricle include the presence of tendinous cord attachments of the tricuspid valve to the ventricular septum; a complete muscular outlet supporting the pulmonary valve; a prominent septal trabeculation, the so-called septomarginal trabeculation; and an infolded ventricle roof, the supraventricular crest, which causes discontinuity between the atrioventricular and the semilunar valve. Most of these features can be recognized on fetal echocardiography (Fig. 5.3).

As for the morphologically left ventricle, characteristic features are a smooth septal surface, generally without septal attachment of the atrioventricular valve, and continuity between the atrioventricular and semilunar valve (Fig. 5.4).
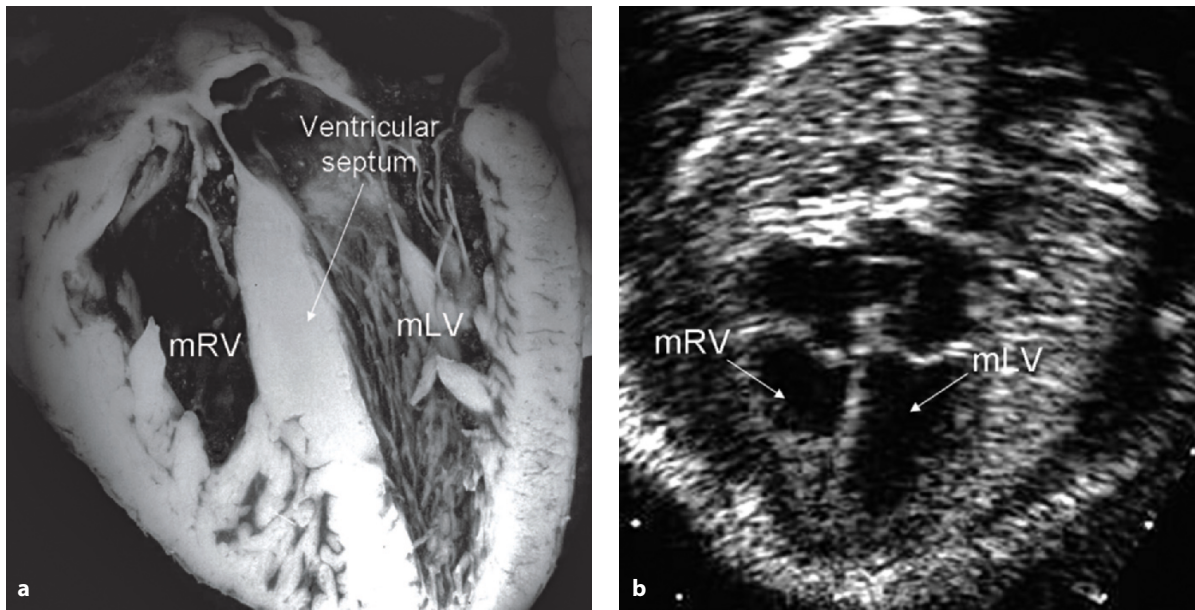
Fig. 5.2 • The different character of the apical trabeculation of the two ventricles is shown in a cardiac specimen (**a**) and in a corresponding echocardiographic view (**b**). The trabeculation is coarse in the morphologically right ventricle (*mRV*) and fine in the morphologically left ventricle (*mLV*)
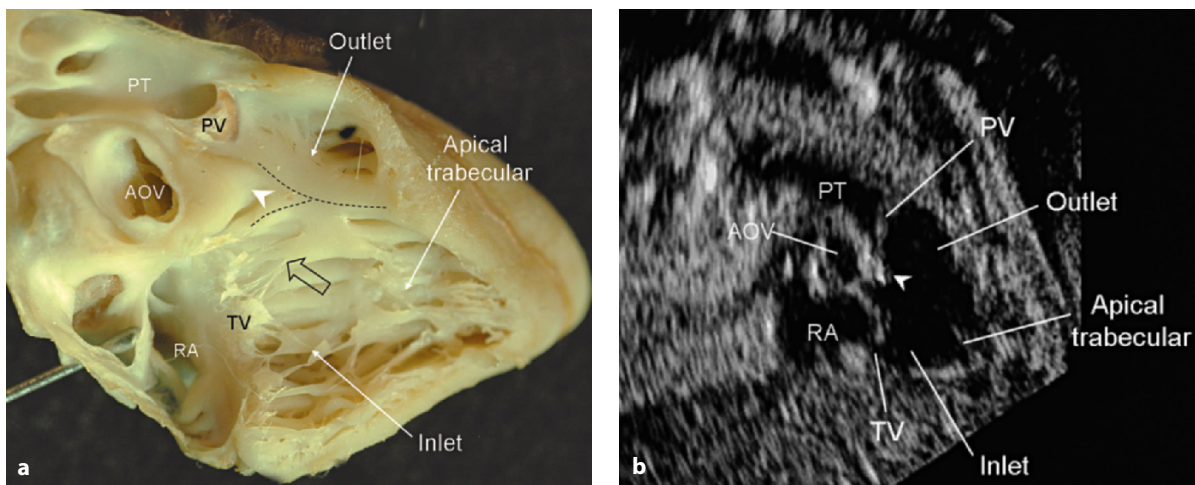
Fig. 5.3 • Morphologic characteristics of the right ventricle are shown in a fetal cardiac specimen (**a**) and in a corresponding echocardiographic view (**b**). The inlet, apical trabecular, and outlet components are seen. The *white arrowhead* indicates the supraventricular crest, separating the tricuspid valve from the pulmonary valve. The *open black arrow* points to the septal insertion of the tricuspid apparatus, and the *black dotted line* indicates the septomarginal trabeculation with its two limbs. *AOV* aortic valve, *PT* pulmonary trunk, *PV* pulmonary valve, *RA* right atrium, *TV* tricuspid valve
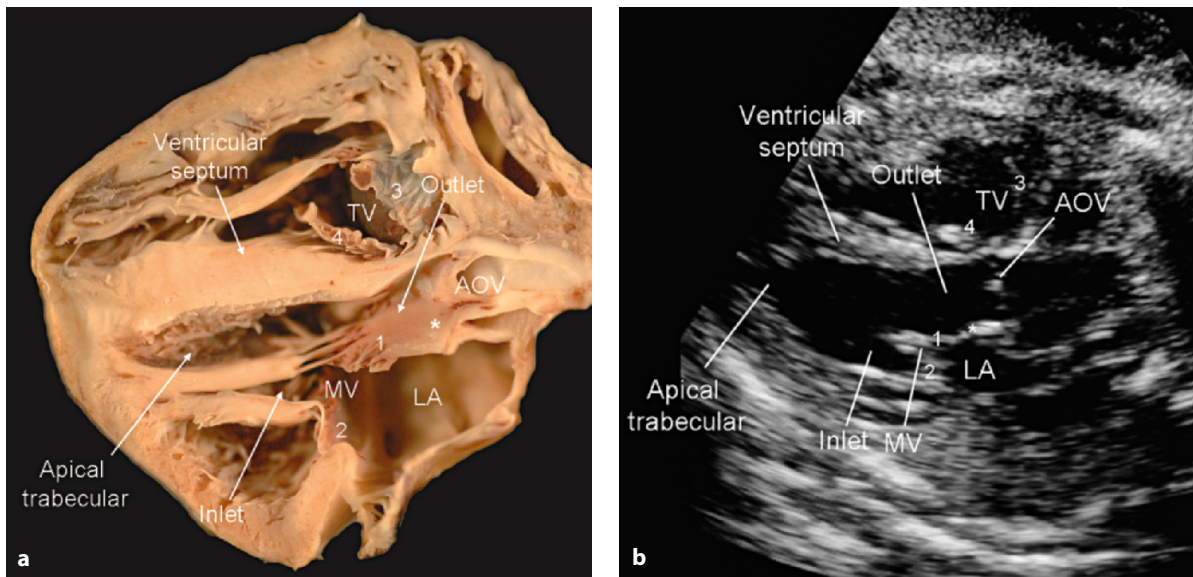
Fig. 5.4 • Characteristics of the left ventricle are displayed in a specimen (**a**) and in a corresponding echocardiographic view of a fetal heart (**b**). The inlet, the apical trabecular, and the outlet components are seen. These pictures demonstrate how the septal surface of the left ventricle is free from cordal attachment of the mitral valve. The aortic (*1*) and mural (*2*) leaflets of the mitral valve are seen. The *white asterisk* indicates the continuity between the aortic leaflet of the mitral valve and the aortic valve. The anterolateral (*3*) and septal (*4*) leaflets of the tricuspid valve are seen, with their close relationship with the right side of the ventricular septum. *AOV* aortic valve, *LA* left atrium, *MV* mitral valve, *TV* tricuspid valve

The Arterial Trunks

As for the third segment, there are four possible types of arterial trunks. The branching pattern usually allows their identification.

In the normal heart, the aorta originates in the center of the heart. The three sinuses of Valsalva in its root support the aortic valve, and from two of them, the coronary arteries originate. Whatever its connection with the ventricular mass, the aorta runs superiorly to form the aortic arch, where it gives origin to the brachiocephalic vessels: the innominate artery, the left common carotid artery, and the left subclavian artery (Fig. 5.5). Because of the caudocranial alignment of its major axis, the aorta can be imaged on parasagittal planes of the fetal body. Usually, the brachiocephalic vessels are more easily identified by fetal echocardiography than are the coronary arteries, particularly in second-trimester scans.

In the normal heart, the pulmonary trunk springs from the infundibulum, where the three sinuses of Valsalva support the pulmonary valve. The main pulmonary artery runs anteroposteriorly on a nearly horizontal plane and bifurcates early into the right and left pulmonary arteries (Fig. 5.6). In the normal heart, the main pulmonary artery connects to the descending aorta via the arterial duct. Because of the anteroposterior alignment of its major axis, the main pulmonary artery and its proximal branches are therefore seen in transverse sections of the fetal thorax.

Two other types of arterial trunks can exist: a common arterial trunk supplying all the pulmonary, coronary, and systemic arteries, and a single great artery connected to the heart, with no central pulmonary arteries. Usually, the pulmonary artery circulation is supplied from major collaterals from the descending aorta (Fig. 5.7).

The Atrioventricular Connection

As to the connection between the atria and the ventricle, the *type* and the *mode* of connection are discussed here. The *type* of atrioventricular connections describes how the atrial myocardium is joined or is not joined to the body of the ventricles. The atrioventricular connection can be biventricular or univentricular. Biventricular atrioventricular connections can be concordant or discordant. The atrioventricular connection is concordant when each atrial chamber is connected with its appropriate ventricle. On the contrary, the atrioventricular connection is discordant when each atrium is connected with the morphologically inappropriate ventricle
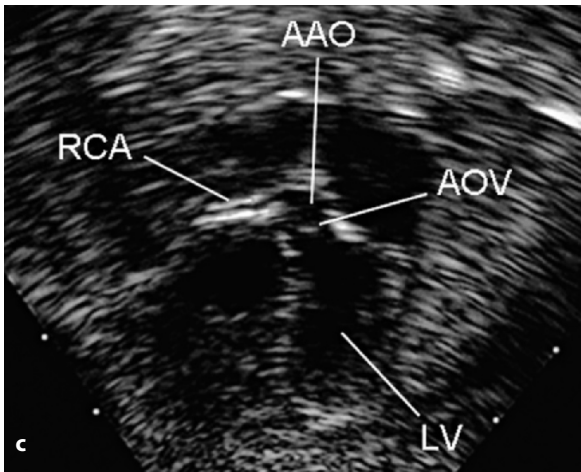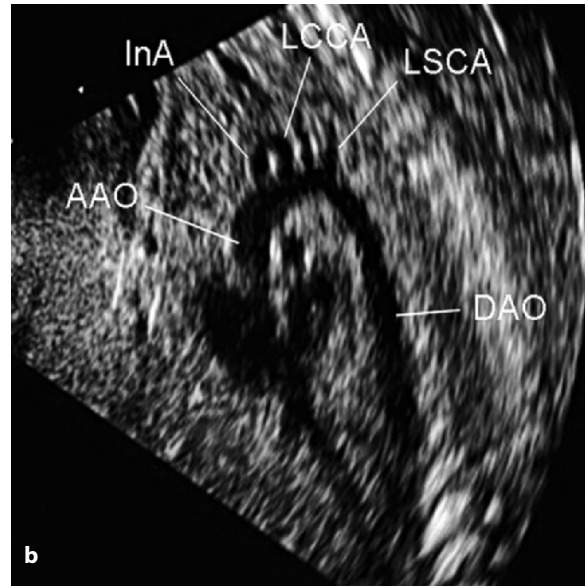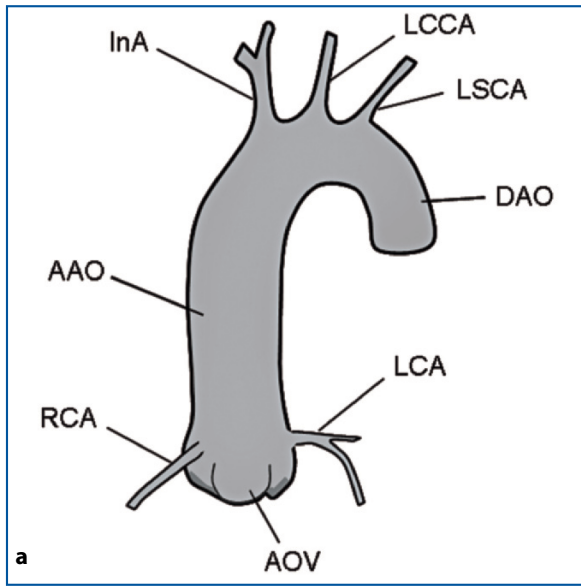
Fig. 5.5 • The coronary and brachiocephalic arteries branching from the aorta are shown in a diagram (**a**) and in two echocardiographic views of the fetal heart (**b**, **c**). The aortic arch giving rise to the brachiocephalic vessel is seen in a parasagittal view of the fetal thorax (**b**), whereas the proximal tract of the right coronary artery is seen in a slightly modified five-chamber view (**c**). *AAO* ascending aorta, *AOV* aortic valve, *DAO* descending aorta, *InA* innominate artery, *LCA* left coronary artery, *LCCA* left common carotid artery, *LSCA* left subclavian artery, *RCA* right coronary artery
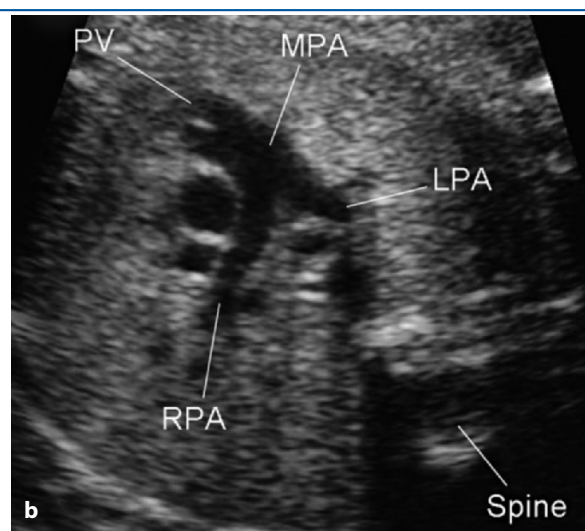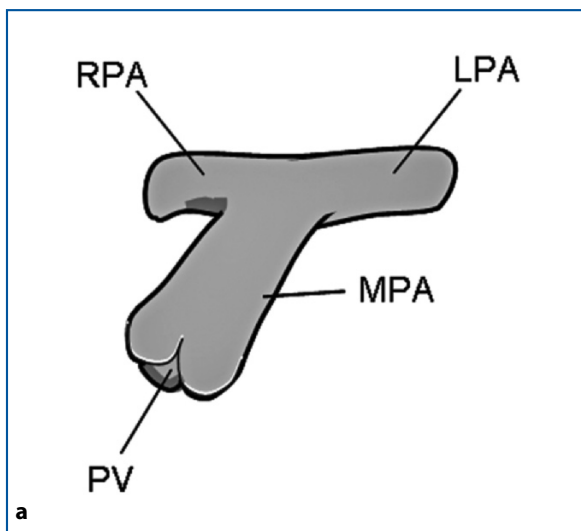
Fig. 5.6 • The pulmonary trunk branching in the right and left pulmonary artery is shown in a diagram (**a**) and in a transverse echocardiographic view (**b**) of the fetal thorax. *LPA* left pulmonary artery, *MPA* main pulmonary artery, *PV* pulmonary valve, *RPA* right pulmonary artery
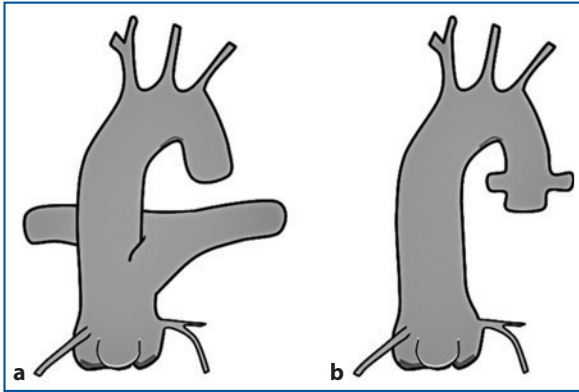
Fig. 5.7 • Diagram of a common arterial trunk (**a**) and a solitary arterial trunk (**b**)

(Fig. 5.8). Concordant and discordant atrioventricular connections may occur in usual or mirror-image arrangement of the atria.

When there is isomeric atrial arrangement, the atrioventricular connection cannot be described in terms of concordance or discordance (Figs. 5.9, 5.10). In atrial isomerism, in fact, half of the heart has concordant and half has discordant atrioventricular connections. When the atrioventricular connection is ambiguous, the three-dimensional structure of the ventricular mass must be described. One accepted method is to determine the ventricular topology by the right- or left-hand method. This method consist of examining the morphologically right ventricle and determining whether a right or left hand can be figuratively placed, with the palm upon the septal surface, so that the thumb is in the ventricular inlet and the fingers in the outlet (Fig. 5.11).

Univentricular atrioventricular connection occurs when the atria are connected with only one ventricle. The dominant ventricle, which may be morphologically left or morphologically right, is invariably associated with a rudimentary chamber of the opposite ventricle. Rudimentary ventricles of right morphology are nearly always in anterosuperior position, whereas rudimentary ventricles of left morphology are in posteroinferior position (Fig. 5.12). More rarely, the dominant ventricle is a solitary ventricular chamber with indeterminate morphology.

Atrioventricular connection *mode* describes the characteristics of the atrioventricular valves. There may be two atrioventricular valves or a common valve. One valve may be imperforated or totally absent when one atrioventricular connection is lacking. In the setting of two atrioventricular valves, one may be straddling, when its tension apparatus attaches on both sides of the interventricular septum, or overriding, when its valvular orifice lies across the interventricular septum (Fig. 5.13). Straddling and overriding frequently coexist. When more than 50% of an overriding atrioventricular valve opens into the opposite ventricle, then the atrioventricular connection becomes univentricular. This has major physiopathological and surgical implications.

The Ventriculoarterial Connection

Ventriculoarterial connection *type* describes how the ventricles are connected to the great arteries. The ventriculoarterial connection can be concordant, discordant, double outlet, or single outlet. Concordant ventriculoarterial connections exist when the
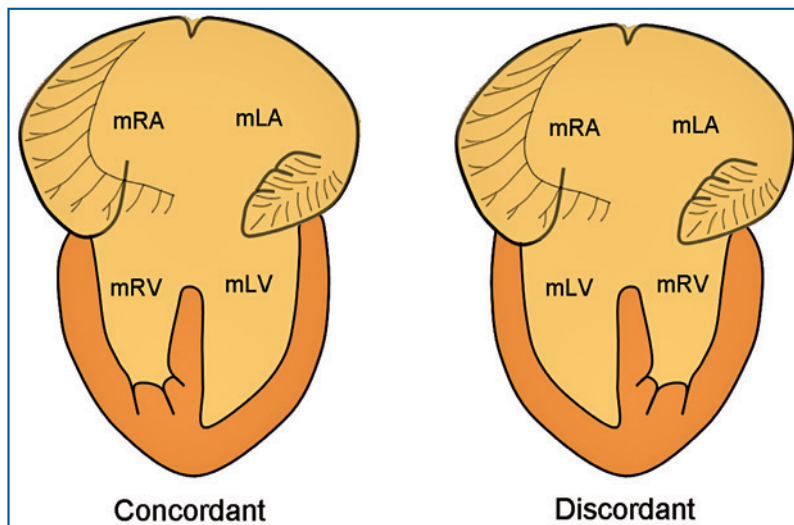
Fig. 5.8 • Diagram showing concordant and discordant atrioventricular connection in the setting of usual arrangement of the atria. *mLA* morphologically left atrium, *mLV* morphologically left ventricle, *mRA* morphologically right atrium, *mRV* morphologically right ventricle

Fig. 5.9 • Diagram of biventricular atrioventricular connection in the setting of left atrial isomerism. Right-hand (**a**) and left-hand (**b**) topology are represented. *mLA* morphologically left atrium, *mLV* morphologically left ventricle, *mRV* morphologically right ventricle
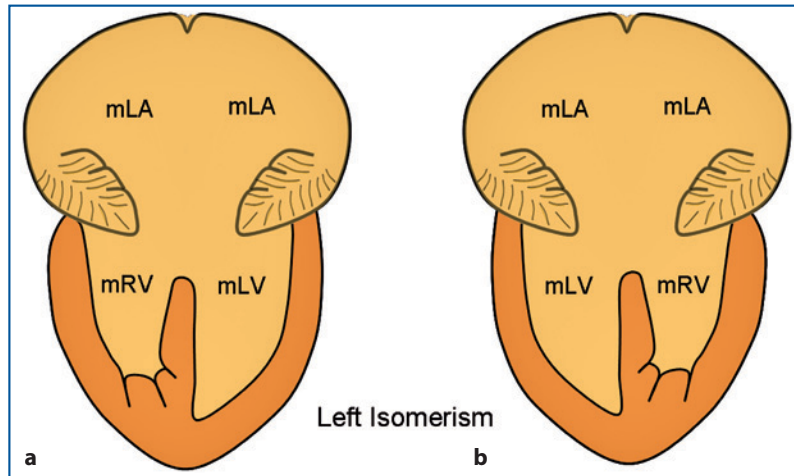
Fig. 5.10 • Diagram of biventricular atrioventricular connection in the setting of right atrial isomerism. Right-hand (**a**) and left-hand topology (**b**) are represented. *mLV* morphologically left ventricle, *mRA* morphologically right atrium, *mRV* morphologically right ventricle
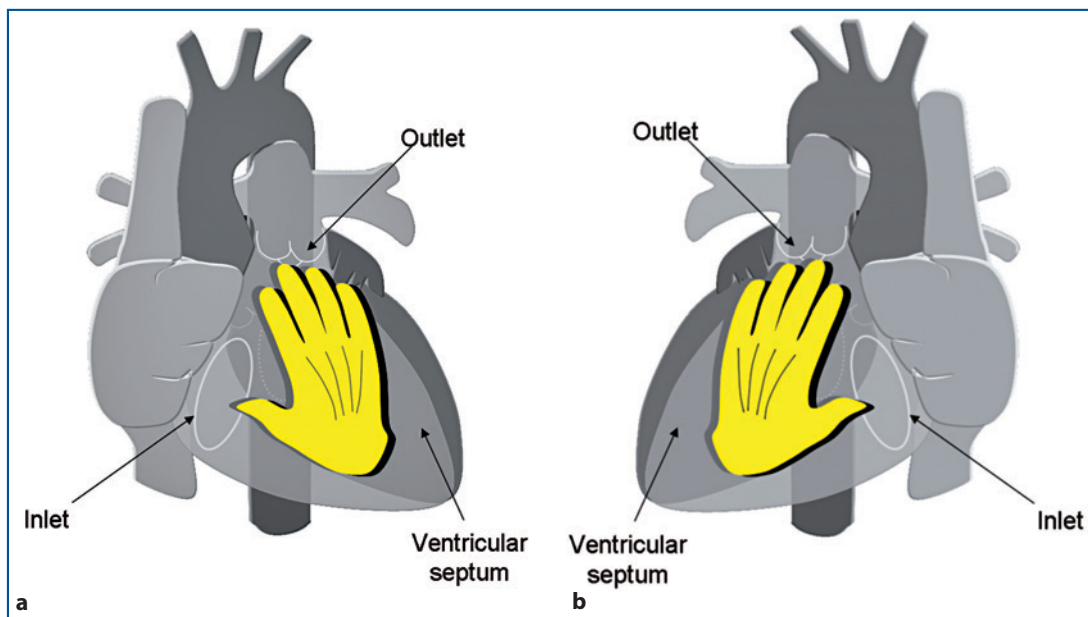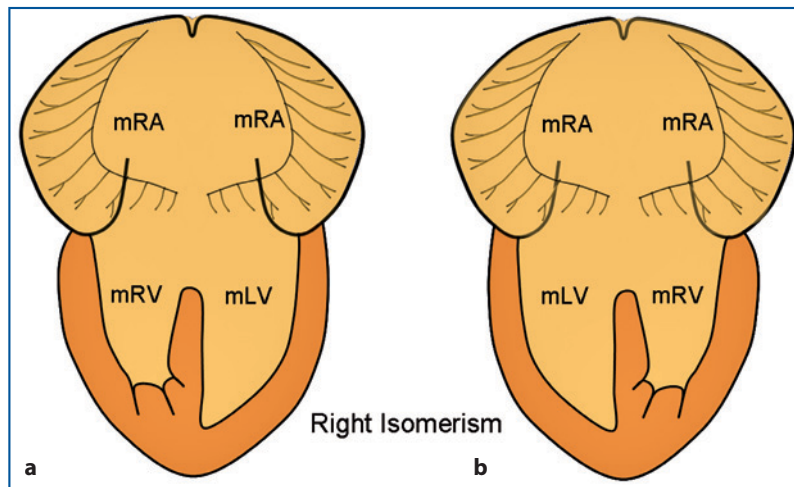
Fig. 5.11 • Diagram illustrating the right- and left-hand topology method. Right-hand (**a**) and left-hand (**b**) morphologically right ventricles
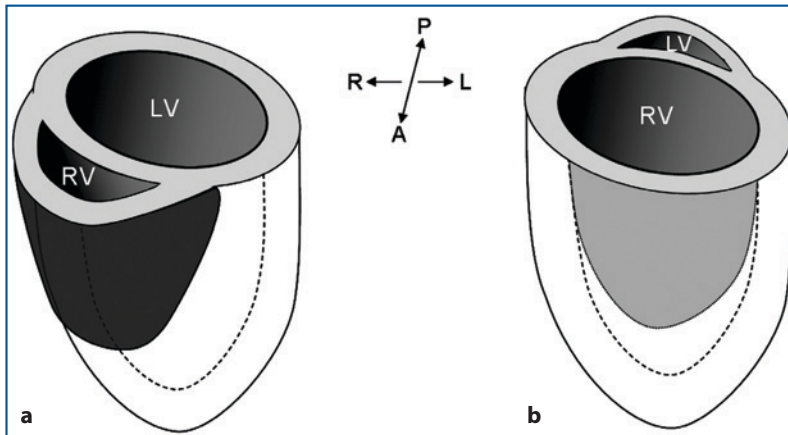
Fig. 5.12 • Diagram showing the relative position between the dominant and the rudimentary ventricle when the latter is morphologically right (**a**) or morphologically left (**b**). *LV* left ventricle, *RV* right ventricle
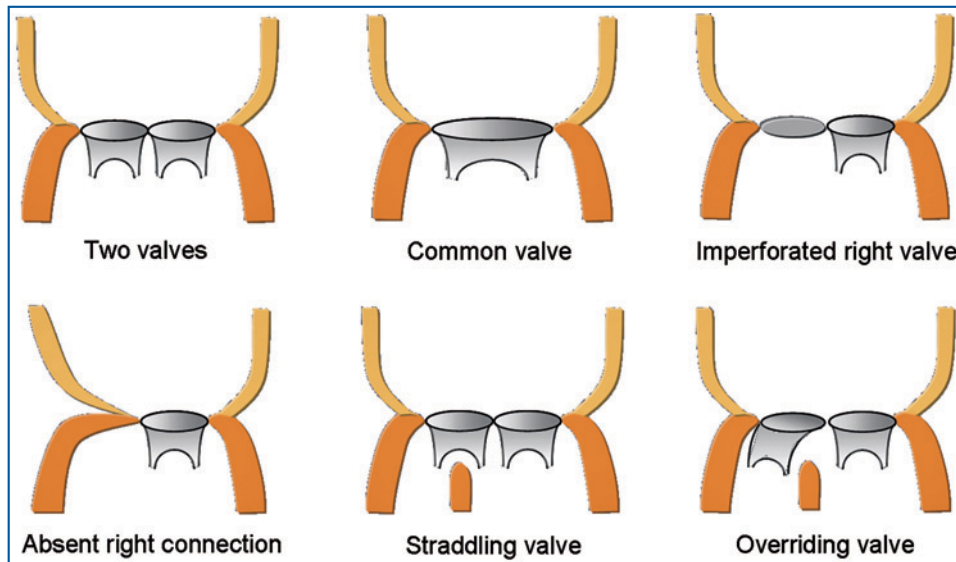
Fig. 5.13 • Diagram showing the possible modes of atrioventricular connections

morphologically right ventricle is connected to the pulmonary artery and the morphologically left ventricle is linked to the aorta. Ventriculoarterial discordance corresponds to the origin of the aorta from the morphologically right ventricle and the pulmonary artery from the morphologically left ventricle (Fig. 5.14).

Double outlet exists when both arterial trunks originate from one ventricle. This may be morphologically right, morphologically left, or indeterminate. Double-outlet right ventricle is far more common than the other two types. In double-outlet ventricles, the relative position of the great artery is variable and

is the basis of the different physiopathologic patterns in this cardiac malformation (Fig. 5.15).

Single outlet occurs when only one arterial trunk is connected to the ventricles. This can be a common arterial trunk, the aorta, or the main pulmonary artery when the other artery is atretic and its connection with a ventricle is not recognizable (Fig. 5.16).

The position of the great arteries can be defined by describing the position of the aorta relative to the pulmonary artery at the level of their semilunar valves. In the normal heart, the position of the aortic valve is right posterior (Fig. 5.17).
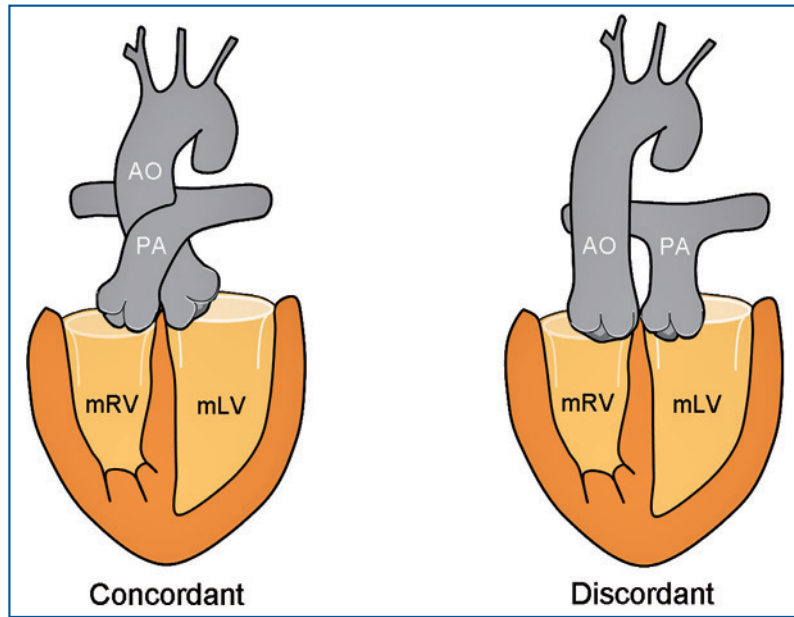
Fig. 5.14 • Diagram of concordant and discordant ventriculoarterial connection. *AO* aorta, *mLV* morphologically left ventricle, *mRV* morphologically right ventricle, *PA* pulmonary artery
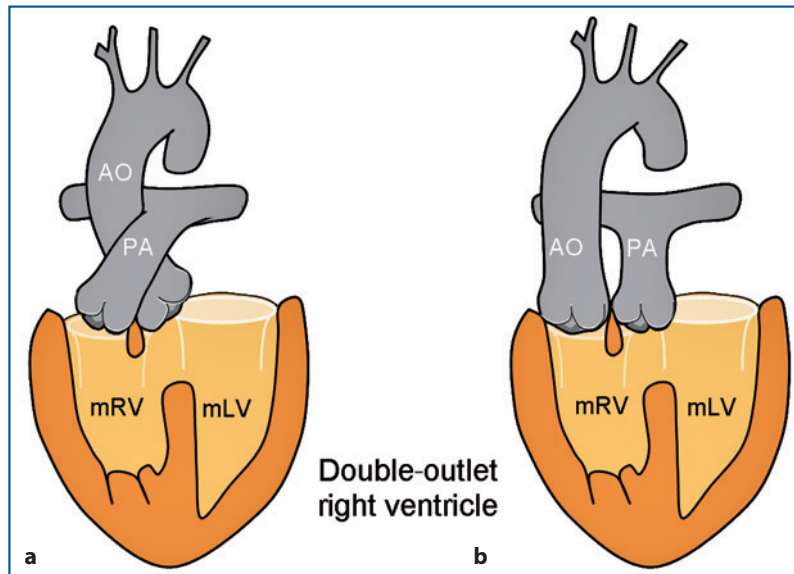
Fig. 5.15 • Diagram showing two examples of double-outlet right ventricle with different position of the great arteries: aorta posterior to the left (**a**), and side-by-side aorta to the right (**b**). *AO* aorta, *mLV* morphologically left ventricle, *mRV* morphologically right ventricle, *PA* pulmonary artery
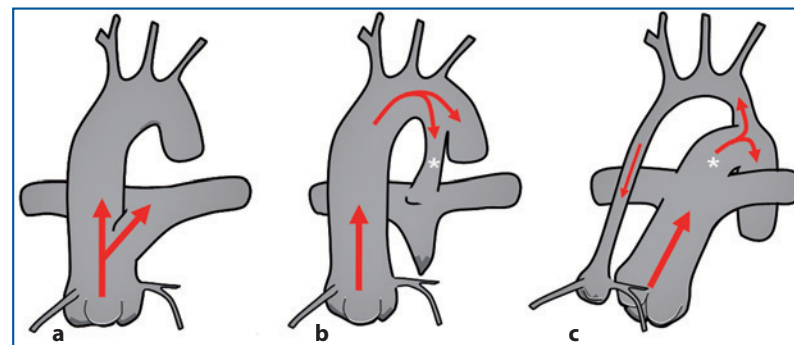
Fig. 5.16 • Diagrams of single-outlet ventriculoarterial connection to a common arterial trunk (**a**), to the aorta (**b**), and to the pulmonary artery (**c**). In **a**, the arterial trunk supplies the aorta, the pulmonary artery, and the coronary arteries. In **b**, the pulmonary artery is retrogradely perfused by the aorta through the arterial duct (*white asterisk*). In **c**, the aortic arch, the ascending aorta, and the coronary arteries are retrogradely perfused by the arterial duct (*white asterisk*)
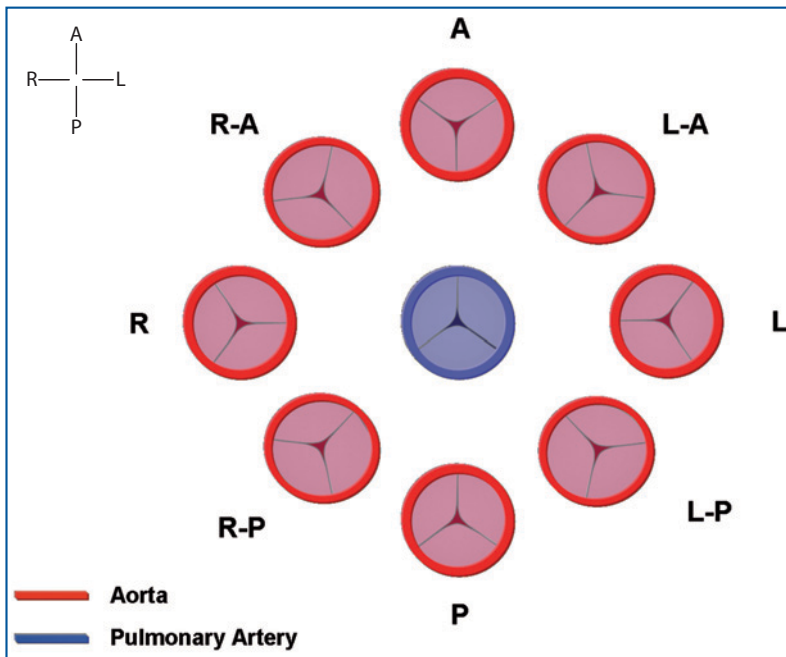
Fig. 5.17 • Diagram showing the eight different basic positions of the aortic valve relative to the pulmonary valve. *A* anterior, *L* side-by-side left, *L-A* left anterior, *L-P* left posterior, *R* side-by-side right, *R-A* right anterior, *R-P* right posterior, *P* posterior

References

1. Shinebourne EA, Macartney FJ, Anderson RH (1976) Sequential chamber localization – logical approach to diagnosis in congenital heart disease. Br Heart J 38:327-340
2. Tynan MJ, Becker AE, Macartney FJ et al (1979) Nomenclature and classification of congenital heart disease. Br Heart J 41:544-553
3. Anderson RH, Becker AE, Freedom RM et al (1984) Sequential segmental analysis of congenital heart disease. Pediatr Cardiol 5:281-288
4. Sharma S, Devine W, Anderson RH et al (1988) The determination of atrial arrangement by examination of appendage morphology in 1842 heart specimens. Br Heart J 60:227-231
5. Huta JC, Smallhorn JF, Macartney FJ (1982) Two-dimensional echocardiographic diagnosis of situs. Br Heart J 48:97-108

Echocardiographic Projections

A **Transverse Views of the Fetal Body**

PART II

Echocardiographic Projections

A **Transverse Views of the Fetal Body**

CHAPTER 6

The Transverse Views of the Upper Abdomen

Introduction

This series of transverse sections of the fetal body will be not discussed in detail here. The reader should refer to books and papers dealing with this subject. Among these sections, the portal sinus view holds a crucial role, not only because it is close to the section used for biometry of the upper abdomen, but also because it is crucial in the assessment of the visceroatrial arrangement. These views can be the starting point in Doppler flow assessment of major veins of the fetal circulatory system, such as umbilical vein and ductus venosus and suprahepatic veins [1-8].

The Umbilical Cord Insertion

In this section, we see the junction of the umbilical cord with the anterior abdominal wall. The inferior vena cava and the abdominal aorta sit within the midline between the two psoas muscles, with the aorta toward the left. This level cuts across the crest of the iliac bones, below the level of the liver, and the bowel is seen filling the abdominal cavity (Fig. 6.1).
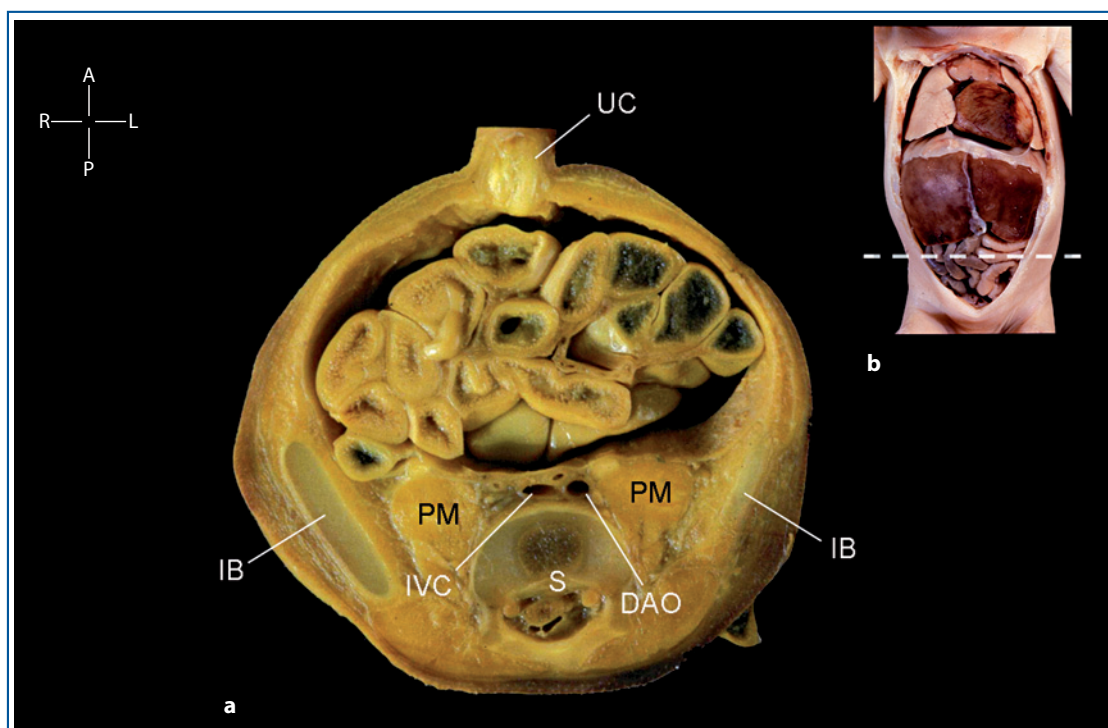
Fig. 6.1 • Transverse section of the insertion of the umbilical cord (**a**). The section level is indicated on the fetal body (**b**). *DAO* descending aorta, *IB* iliac bone, *IVC* inferior vena cava, *PM* psoas muscle, *S* spine, *UC* umbilical cord

The Lower Liver

At a slightly more cranial level from its insertion, the umbilical vein is seen in cross section running cephalad immediately behind the anterior wall of the abdomen. The lower part of the right lobe of the liver is seen in cross section, with bowel filling the left side of the abdomen. Both kidneys are seen in cross section sitting on either side of the inferior vena cava and the abdominal aorta (Fig. 6.2).

The Mid Liver

A transverse section across the mid liver shows the larger right and the smaller left lobes. The umbilical vein is now seen within the falciform ligament running posteriorly away from the anterior abdominal wall. In contrast, the inferior vena cava moves anteriorly away from the spine and is slightly increasing in size. Both adrenal glands are seen in cross section, as is the upper pole of the kidney on the left. The duodenum and distal part of the stomach are seen more centrally (Fig. 6.3).

The Portal Sinus

This is a transverse view of the upper abdomen, obtained above the level of the falciform ligament, showing the confluence of the umbilical vein with the left portal vein. This confluence is seen taking an anteroposterior course, curving smoothly toward the right. At the most posterior portion of this curve, the very first part of the ductus venosus can often be seen. The stomach lies on the left side of this view. The abdominal aorta is located posteriorly, close to the spine and to the left of the midline. The inferior vena cava is located more anteriorly and slightly to the right of the midline. The aorta and the inferior vena cava at this level are of similar size (Fig. 6.4). On ultrasound, the portal sinus view is close to the section commonly used for biometry of the upper abdomen and is crucial in the assessment of the visceroatrial arrangement (Fig. 6.5).

In transverse section of the fetal abdomen, the inferior vena cava and aorta are seen at right angle with the ultrasound beam. Because of the unfavorable insonation angle, the flow is difficult to see in these vessels, and more commonly, only the abdominal
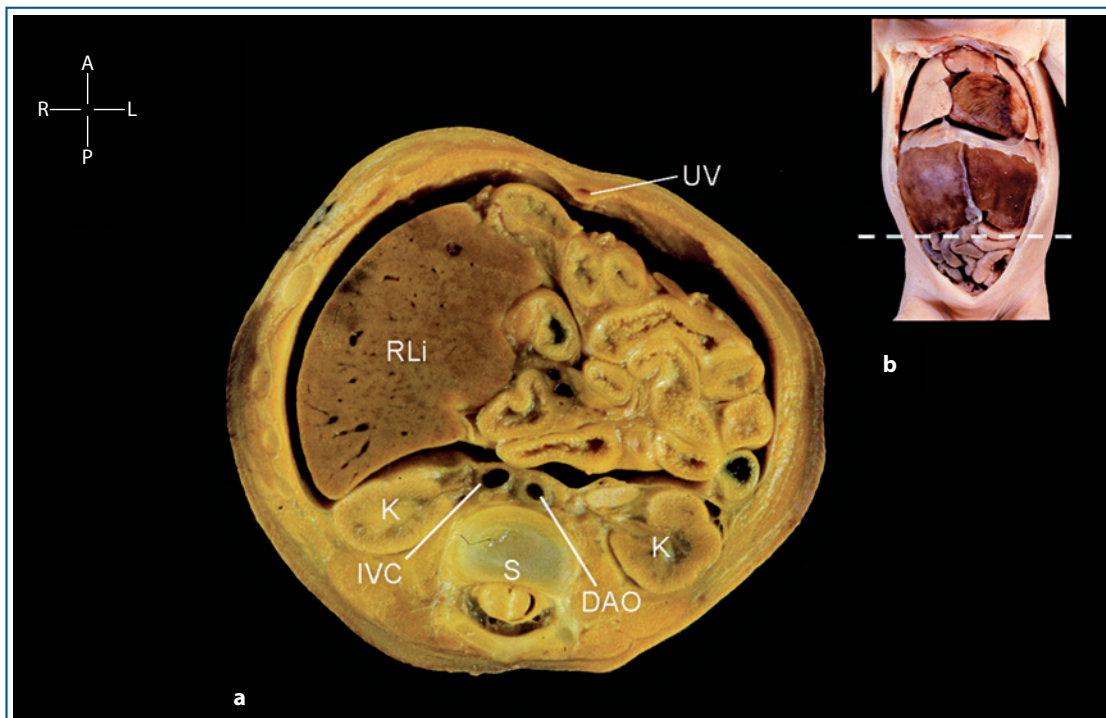
Fig. 6.2 • Transverse section of the lower liver (**a**). The section level is shown on the fetal body (**b**). *DAO* descending aorta, *IVC* inferior vena cava, *K* kidney, *RLL* right liver lobe, *S* spine, *UV* umbilical vein
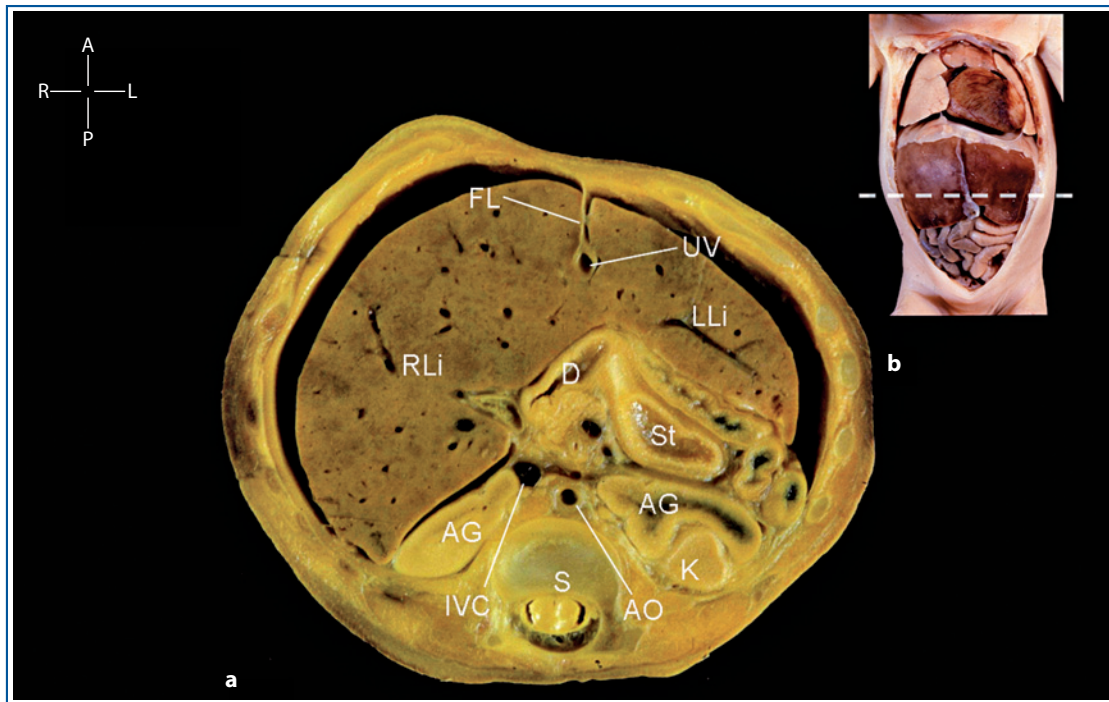
Fig. 6.3 • Transverse section of the mid liver (**a**). The section level shown on the fetal body (**b**). *AG* adrenal gland, *D* duodenum, *DAO* descending aorta, *FL* falciform ligament, *IVC* inferior vena cava, *K* kidney, *LLL* left liver lobe, *RLL* right liver lobe, *S* spine, *St* stomach, *UV* umbilical vein
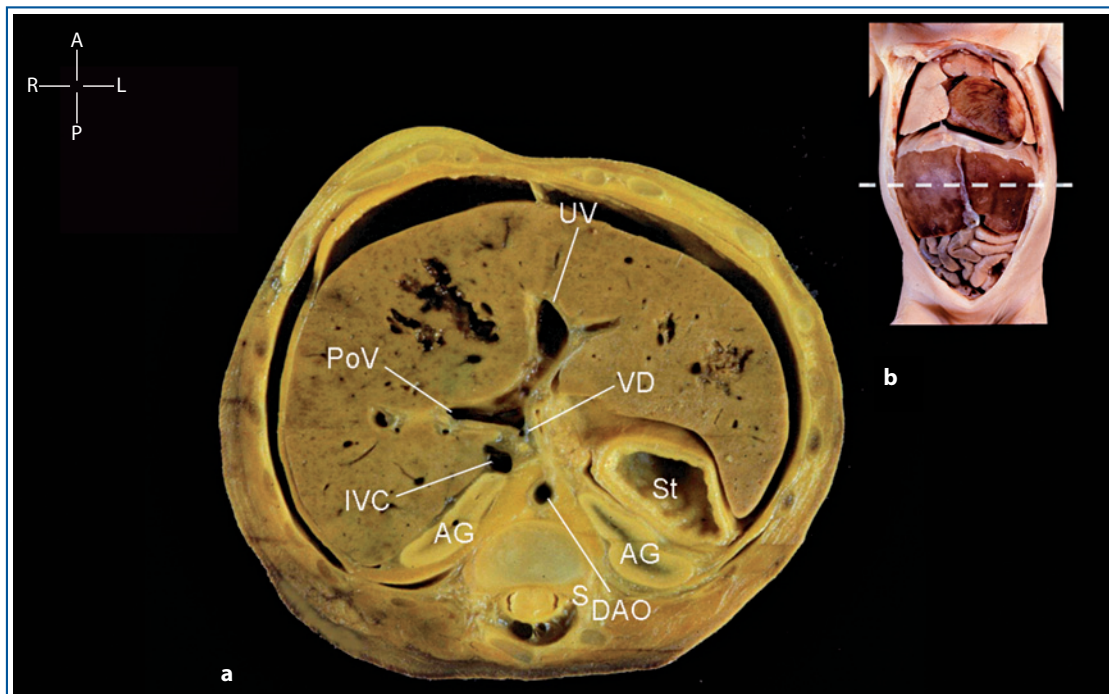
Fig. 6.4 • Transverse section of the fetal upper abdomen at the level of the portal sinus (**a**). The confluence of the umbilical vein into the portal vein is displayed, curving smoothly toward the right. The very first part of the ductus venosus is indicated. The size of the inferior vena cava and the descending aorta is very similar at this level. Part of the stomach is seen on the left side. The section level is indicated on the fetal body (**b**). *AG* adrenal gland, *DAO* descending aorta, *VD* venous duct, *IVC* inferior vena cava, *LLL* left liver lobe, *PoV* portal vein, *S* spine, *RLL* right liver lobe, *St* stomach, *UV* umbilical vein
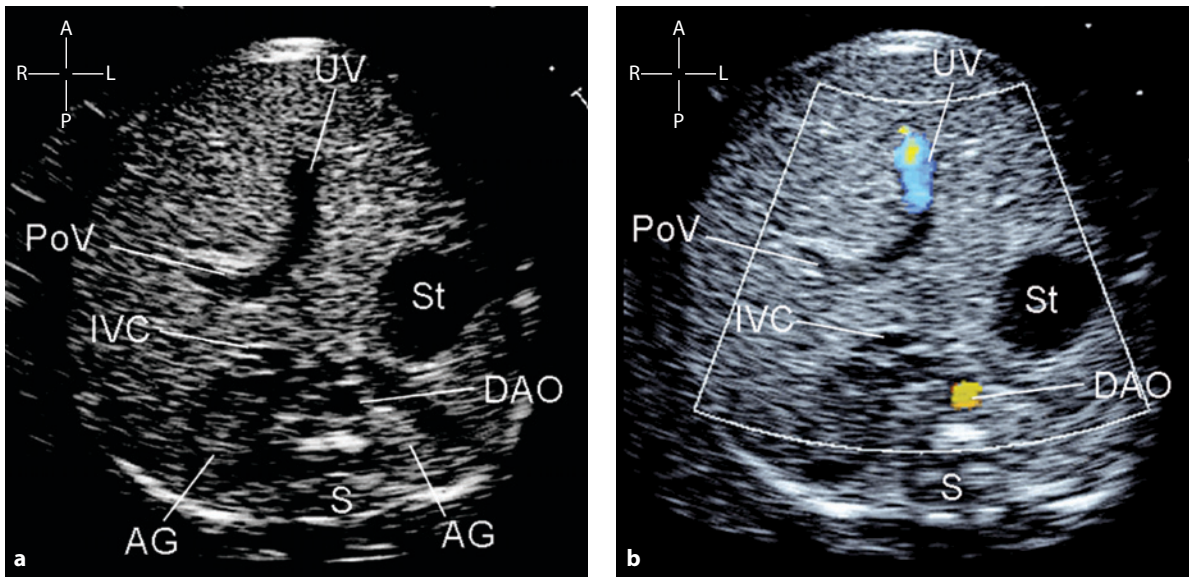
Fig. 6.5 • Cross sectional (**a**) and color flow mapping (**b**) echocardiographic views of the portal sinus in a normal 22-week gestational-age fetus. The portal vein and the inferior vena cava are not coding in color because of the unfavorable insonation angle and the low velocity of blood flow. The umbilical vein and the descending aorta are coding in color, thanks to the better insonation angle of the vein and the higher velocity of the artery (**b**). *AG* adrenal gland, *DAO* descending aorta, *IVC* inferior vena cava, *PoV* portal vein, *S* spine, *St* stomach, *UV* umbilical vein

aorta is coding in color (Fig. 6.5b). With a very low-scale setting, it is possible to see the lumen of the two vessels coded in different colors because of the opposite direction of their flow (Fig. 6.6).

Because of its upward and posteriorly oriented course, the ductus venosus can be regularly visualized in sagittal sections of the fetal body. In transverse sections of the fetal body, its narrow isthmic entrance from the portal sinus can be difficult to identify on cross-sectional examination. By using color flow mapping with a low-scale setting, the preorificial acceleration of blood at the entrance of the ductus venosus is easily recognized. When the portal sinus section is acquired with the transverse approach, the blood flow can be seen inside the portal vein because it is more parallel to the ultrasound beam (Fig. 6.7).
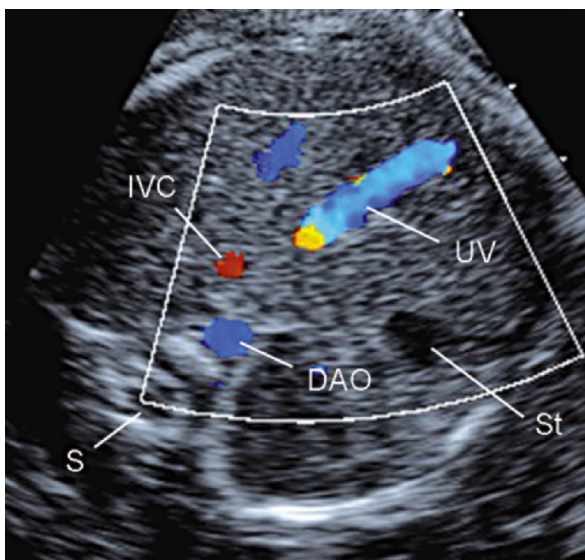
Fig. 6.6 • Portal sinus view in a 23-week gestation fetus. On color flow mapping with low-scale setting (Nyquist limit of 19 cm/s), the inferior vena cava and abdominal aorta flow are seen in different colors, *red* and *blue,* respectively. *DAO* descending aorta, *IVC* inferior vena cava, *S* spine, *St* stomach, *UV* umbilical vein
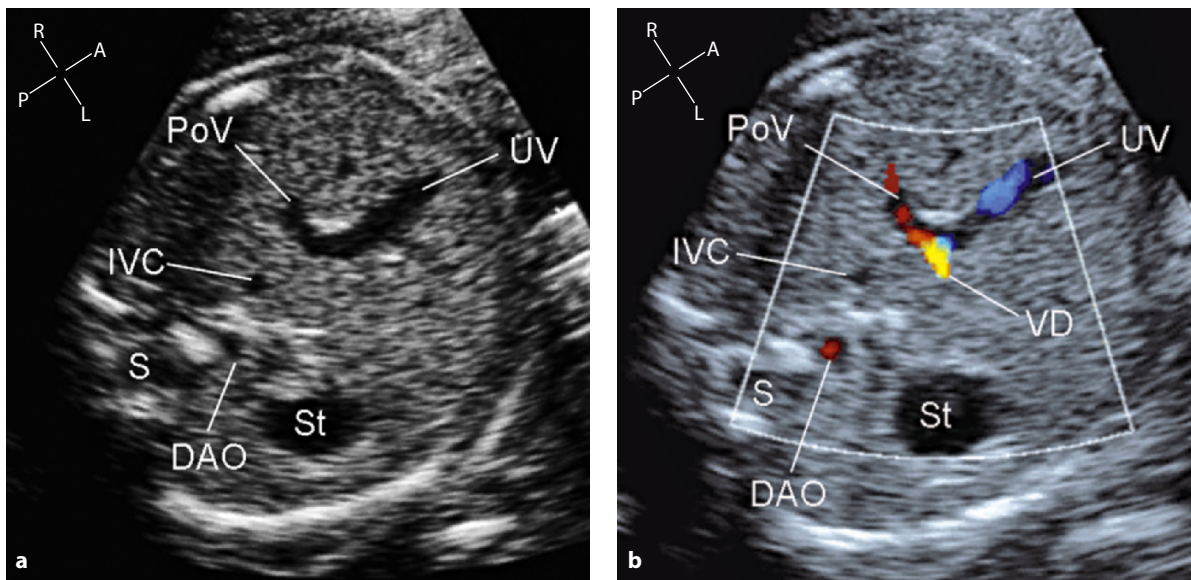
Fig. 6.7 • Cross-sectional (**a**) view of the portal sinus in a normal 20-week gestational-age fetus. On color flow mapping (**b**), the preorificial acceleration of blood at the entrance of the ductus venosus is easily recognized. Due to the transverse orientation of this view, color flow is seen in *red* filling the protal vein. The Nyquist limit was 20 cm/s. *DAO* descending aorta, *IVC* inferior vena cava, *PoV* portal vein, *S* spine, *St* stomach, *UV* umbilical vein, *VD* venous duct

The Infracardiac Vena Cava

This section shows the very distal portion of the inferior vena cava just before its junction with the floor of the right atrium. At this level, the size of the vena cava is larger and its position is more anterior than in caudal sections. This is because the inferior vena cava has already received the flow of the umbilical and suprahepatic veins. Due to the dome-shaped conformation of the diaphragm, when this section is truly horizontal, it shows both abdominal and thoracic structures at the same time. In fact, the upper parts of the right and left lobes of the liver are seen to either side of the caval orifice. Anteriorly, the inferior part of the ventricles are seen and, posteriorly, the inferior portion of the lower lobes of the lungs. The esophagus sits between the descending thoracic aorta and the inferior vena cava (Figs. 6.8, 6.9).

The Suprahepatic Veins

Slightly caudal to the section of the infracardiac vena cava, a transverse section of the confluence of the suprahepatic veins can be obtained. This confluence gives a stellate appearance, the so-called "hepatic star", to the cross section of the inferior vena cava (Fig. 6.10).
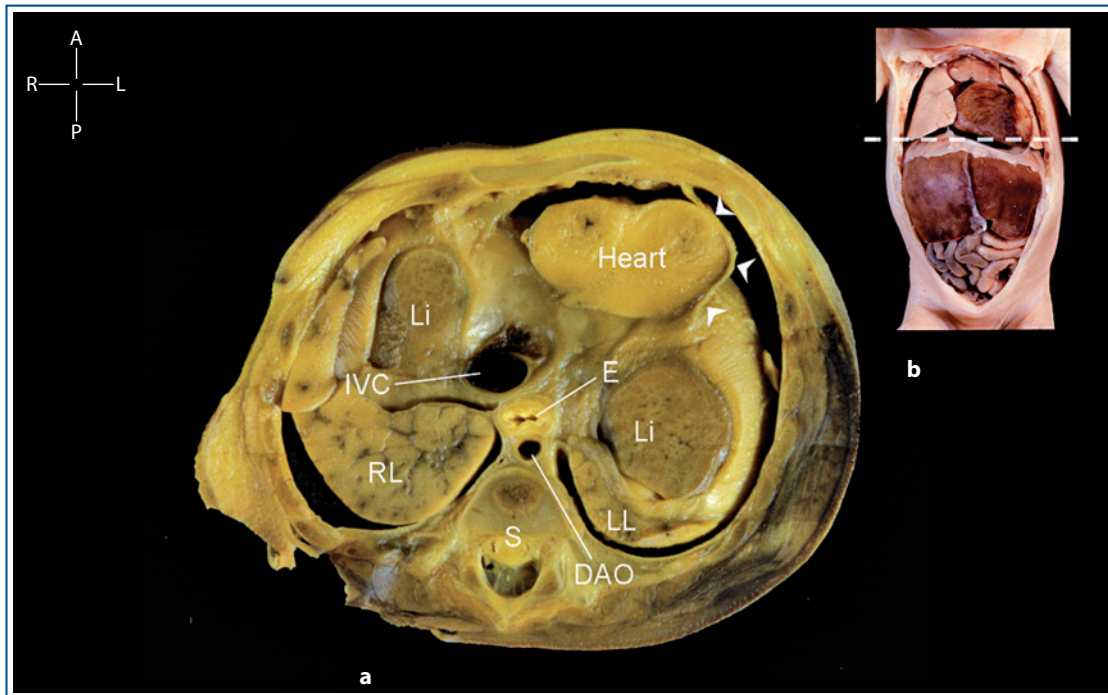
Fig. 6.8 • Morphologic section through the fetal upper abdomen at the level of the infracardiac portion of the inferior vena cava (**a**). Anteriorly, the inferior portion of the ventricles is seen encased in the pericardium (*arrowheads*). Because of the dome shape of the diaphragm, a section of the upper part of the right and left lobes of the liver is seen, with the section of the inferior lobes of the two lungs posteriorly. The section level is indicated on the fetal body (**b**). *DAO* descending aorta, *E* esophagus, *IVC* inferior vena cava, *LL* left lung, *LLL* left liver lobe, *RL* right lung, *RLL* right liver lobe, *S* spine
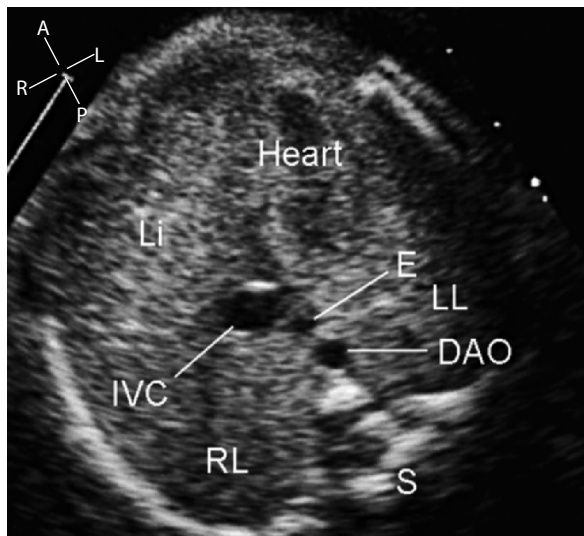
Fig. 6.9 • Transverse section of the infracardiac inferior vena cava in a 22-week gestational-age fetus. *DAO* descending aorta, *E* esophagus, *IVC* inferior vena cava, *Li* liver, *LL* left lung, *RL* right lung, *S* spine
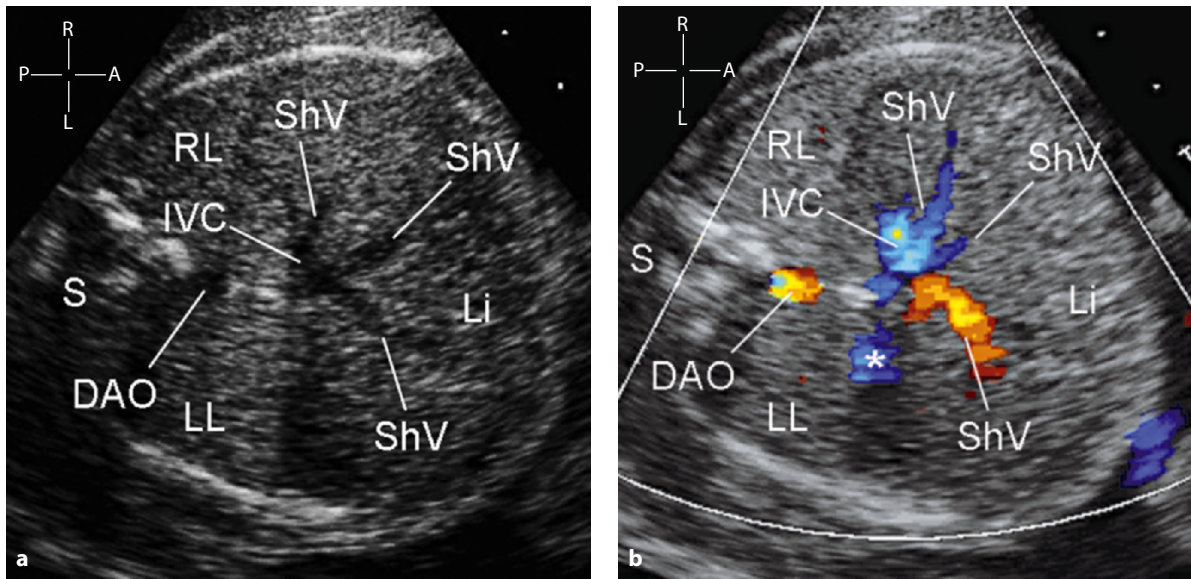
Fig. 6.10 • Transverse section of the confluence of the suprahepatic veins in a normal 25-week gestational-age fetus. On cross-sectional examination (**a**), the confluence of the suprahepatic veins gives a stellate appearance, the so-called "hepatic star," to the cross section of the inferior vena cava. Color flow mapping of the same section (**b**). The low-scale setting highlights the flow in the suprahepatic veins. On moving images, the *blue* pulsatile flow, in the center of the image, is a phantom of the flow of the inferior vena cava (*white asterisk*). *DAO* descending aorta, *E* esophagus, *IVC* inferior vena cava, *Li* liver, *LL* left lung, *RL* right lung, *S* spine, *ShV* suprahepatic vein

References

1. Hill LM, Kislak S, Rumo C (1987) An US view of the umbilical cord. Obstet Gynecol Surv 42:82-88
2. Staudach A (1989) Sectional fetal anatomy in ultrasound. Springer-Verlag, Berlin
3. Filly RA (2000) US evaluation of normal fetal anatomy. In: Callen PW (ed) US in obstetrics and gynecology. WB Saunders, Philadelphia, pp 221-276
4. Mavrides E, Moscoso G, Carvalho JS et al (2001) The anatomy of the umbilical, portal and hepatic venous system in the human fetus at 14-19 weeks of gestation. Ultrasound Obstet Gynecol 18:598-604
5. Jeanty P, Romero R, Hobbins JC (1985) Vascular Anatomy of the fetus. J Ultrasound Med 4:343-348
6. Copel JA, Reed KL (1995) Doppler ultrasound in obstetrics an gynecology. Raven Press, New York
7. Kalache K, Romero R, Goncalves LF et al (2003) Three-dimensional color power imaging of the fetal hepatic circulation Am J Obstet Gynecol 189:1401-1406
8. Kiserud T, Acharya G (2004) The fetal circulation. Prenatal Diagn 24:1049-1059

The Four-Chamber View

The Section Plane

Because the diaphragm in the fetus is at a higher level within the chest, making the heart more horizontal than it is after birth, the four-chamber view of the heart lies closer to a transverse section of the fetal thorax just above the diaphragm (Fig. 7.1) [1]. This view is easily obtained from a transverse plane of the upper abdomen by tracing the inferior vena cava to the right atrium and then angling the transducer slightly cranially until the four chambers are visualized.

The Normal Morphology

In a transverse section of the thorax (Fig. 7.2), the morphologically right ventricle is the most anterior chamber closest to the thoracic wall and can be recognized by its blunted apex. The left ventricle is in posterior position and has an ellipsoidal shape. The left atrium is the most posterior chamber, closest to the spine and the descending aorta. On closer view (Fig. 7.2b), the smooth endocardial surface of the left atrium is clear, whereas the right atrium shows extensive pectinate muscles branching from the ter-
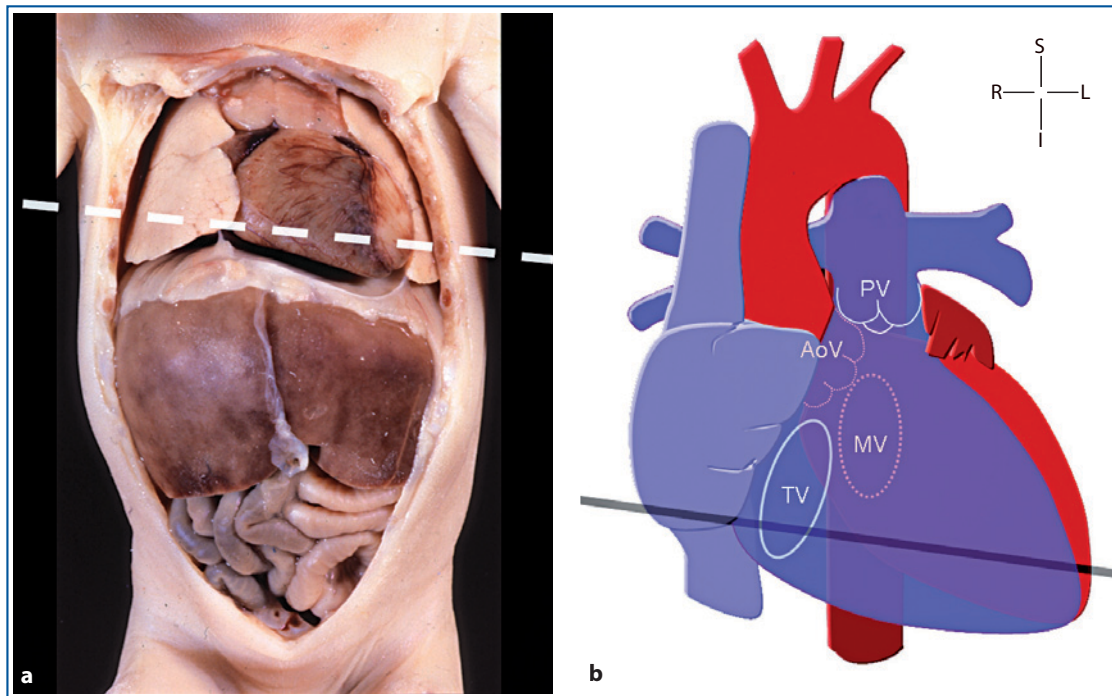
Fig. 7.1 • Level of the four-chamber view on the fetal body (**a**) and on a heart (**b**) diagram. The diagram demonstrates how the plane of this view lies along the long axis of the heart and perpendicular to the inlet of the interventricular septum. In the classical four-chamber view, the tricuspid valve and the mitral valve can be seen but not the aortic valve and the pulmonary valve, which lie on superior planes. *AoV* aortic valve, *MV* mitral valve, *PV* pulmonary valve, *TV* tricuspid valve
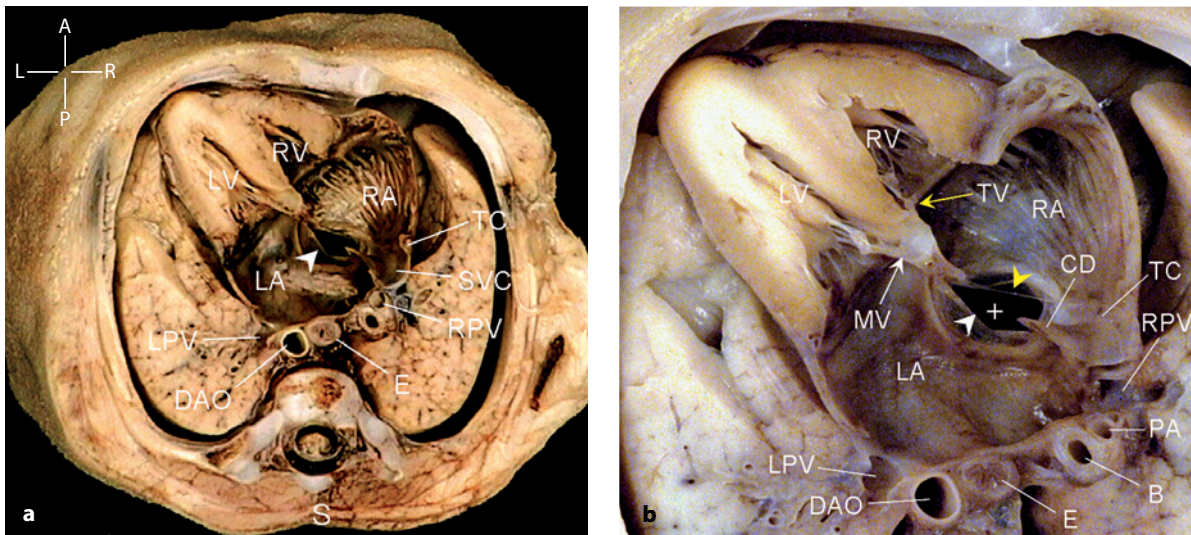
Fig. 7.2 • In this specimen, the fetal thorax has been sectioned in a simulated four-chamber view (**a**). The same specimen magnified for greater anatomical detail (**b**). The septal leaflet of the tricuspid valve (*yellow arrow*) attaches to the atrioventricular junction more apically than the aortic leaflet of the mitral valve (*white arrow*), which is effectively inserted to the underside of the atrial septum. The *yellow arrowhead* indicates the eustachian valve, which is seen anteriorly and to the right of the orifice of the inferior vena cava (*white cross*), whereas the *white arrowhead* indicates the flap valve of the foramen ovale, which forms its left posterior border and arches into the left atrium. Posteriorly, the left and right pulmonary artery joining the left atrium are displayed. The descending aorta, the esophagus, the bronchus, and the pulmonary artery of the lower lobe of the right lung are seen in between. *B* bronchus, *CD* crista dividens, *DAO* descending aorta, *E* esophagus, *LA* left atrium, *LPV* left pulmonary vein, *LV* left ventricle, *MV* mitral valve, *PA* pulmonary artery, *RA* right atrium, *RPV* right pulmonary vein, *RV* right ventricle, *S* spine, *SVC* superior vena cava, *TC* terminal crest, *TV* tricuspid valve

minal crest. The posterior portion of this latter chamber is smooth and receives the superior vena cava. The septal leaflet of the tricuspid valve attaches to the atrioventricular junction more apically than does the aortic leaflet of the mitral valve, which is effectively inserted to the underside of the atrial septum. This results in the so-called "offsetting", or "differential insertion", of the atrioventricular valves. The atrioventricular valves together with the atrial and ventricular septum meet in the center of the heart, forming an offset cross known as the "crux of the heart." In the normal heart, the two atrioventricular valves are therefore separated and nearly equal in size. The left and right lower pulmonary veins join the back of the left atrium to either side of the esophagus and the descending aorta. The inferior vena cava is seen entering the floor of the right atrium, with a small portion of the interatrial septum overriding it. Because of its overriding, this upper portion of the atrial septum is called *crista dividens*, which in Latin means "the crest which divides." This verb refers to the flow coming from the inferior vena cava. The image depicts how the most posterior and leftward portion of the inferior caval flow, which brings the most oxygenated blood coming from the venous duct and the

placenta, is diverted by this crest into the left atrium. The eustachian valve is seen anteriorly and to the right of the orifice of the inferior vena cava, whereas the flap valve forms its left posterior border, arching into the left atrium. A recent review has been published illustrating many aspects of normal and abnormal anatomy of the fetal heart and updating classical concepts of cardiac embryology [2].

The Normal Echocardiogram – 2D

The four-chamber view can be obtained echocardiographically with two basic approaches to the fetal thorax: apical (Figs. 7.3, 7.4) or transverse (Fig. 7.5). To ensure that this section is truly horizontal, one complete rib and no abdominal content should be imaged [3] (Fig. 7.3). In the four-chamber view, the examiner should identify the following features:

• Two atrial chambers of nearly equal size. The left atrium should be the most posterior chamber and closest to the spine. The right atrium is in contact with the right lung. Both atria connect with the respective ventricle via an atrioventricular valve.
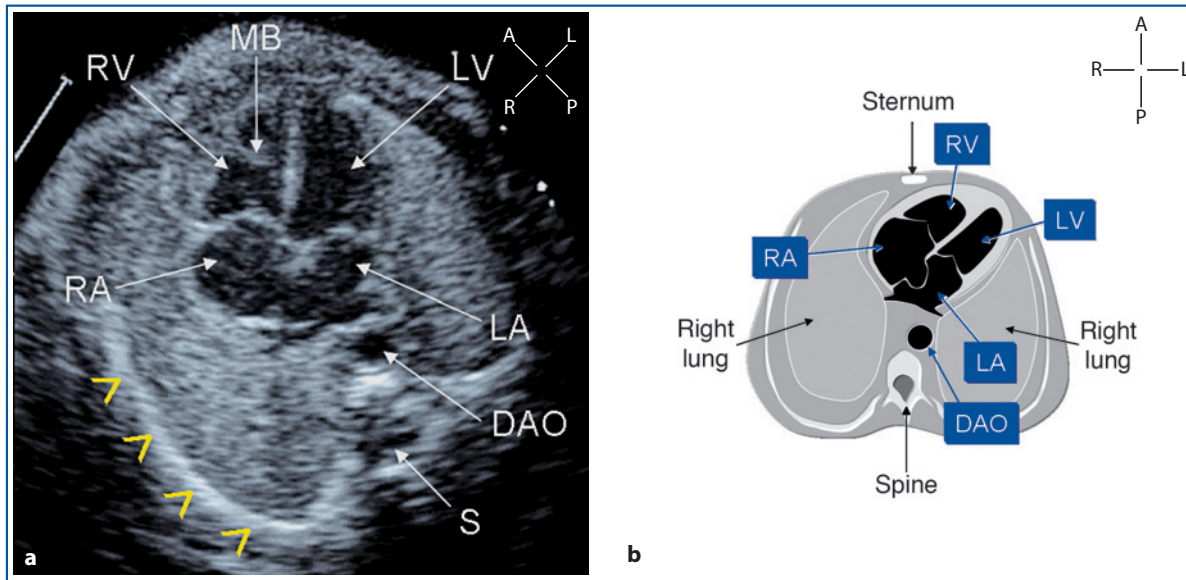
Fig. 7.3 • Cross-sectional apical view in a normal 21-week gestational-age fetus (**a**) and a corresponding diagram (**b**). This section is considered suitable when the entire thorax is seen, there is a complete rib (*yellow open arrowheads*), and no abdominal content. The spatial relationship of the heart chambers inside the chest is illustrated. *DAO* descending aorta, *LA* left atrium, *LV* left ventricle, *MB* moderator band, *RA* right atrium, *RV* right ventricle, *S* spine

Fig. 7.4 • Apical view in a normal 23-week gestational-age fetus. The morphologically right ventricle is in anterior position and characterized by the moderator band and a lower insertion of the tricuspid valve into the ventricular septum. The *white cross* indicates the crux of the heart, where the atrial septum fuses with the ventricular septum. The *white closed arrowhead* indicates the atrioventricular septum, which is delimited by the lower annular insertion of the tricuspid valve relative to the mitral valve. The *open arrowheads* indicate the flap of the oval fossa arching inside the left atrium. The left and right inferior pulmonary veins are seen entering the posterior portion of the left atrium on either side of the descending aorta. *DAO* descending aorta, *LPV* left pulmonary vein, *MB* moderator band, *MV* mitral valve, *RPV* right pulmonary vein, *SP* septum primum, *TV* tricuspid valve
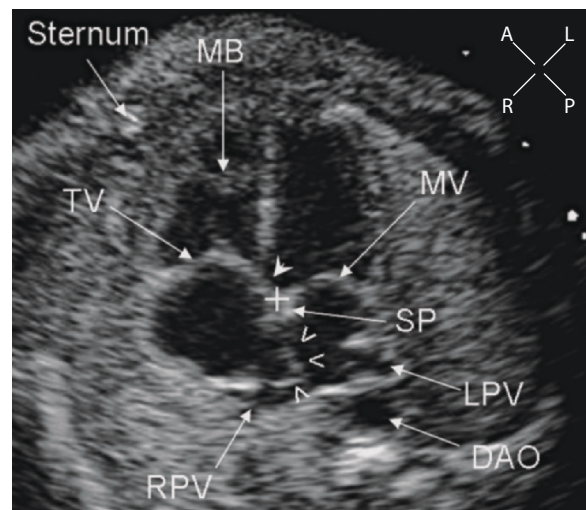
• Two ventricular chambers of nearly equal size and thickness. The morphologically right ventricle should be the most anterior chamber, lying immediately behind the anterior chest wall. The morphologically right ventricle can be recognized by its coarse trabeculation including a muscle bundle, the moderator band, which transverses the ventricular cavity and gives a characteristic blunted appearance to its apex. The left ventricle lies between the right ventricle and the left lung. The morphologically left ventricle is finely trabeculated, and its apex is normally free from muscle bundles so that the apical part of the ventricular cavity is better represented in the four-chamber view (Fig. 7.3, 7.4). On the moving images, the two ventricles should contract equally. In the second trimester, the two atria and ventricles appear equal in size, but in the last trimester, a certain degree of dominance of the right chambers is common [4-7].

• Two atrioventricular valves that can be seen to open equally and with similar annular size. The mitral valve on the left side and tricuspid valve on the right side meet the atrial and ventricular septa at the crux of the heart in an offset cross appearance. This offset is due to insertion of the tricuspid valve annulus slightly lower into the ventricular septum than the mitral valve (Fig. 7.4).
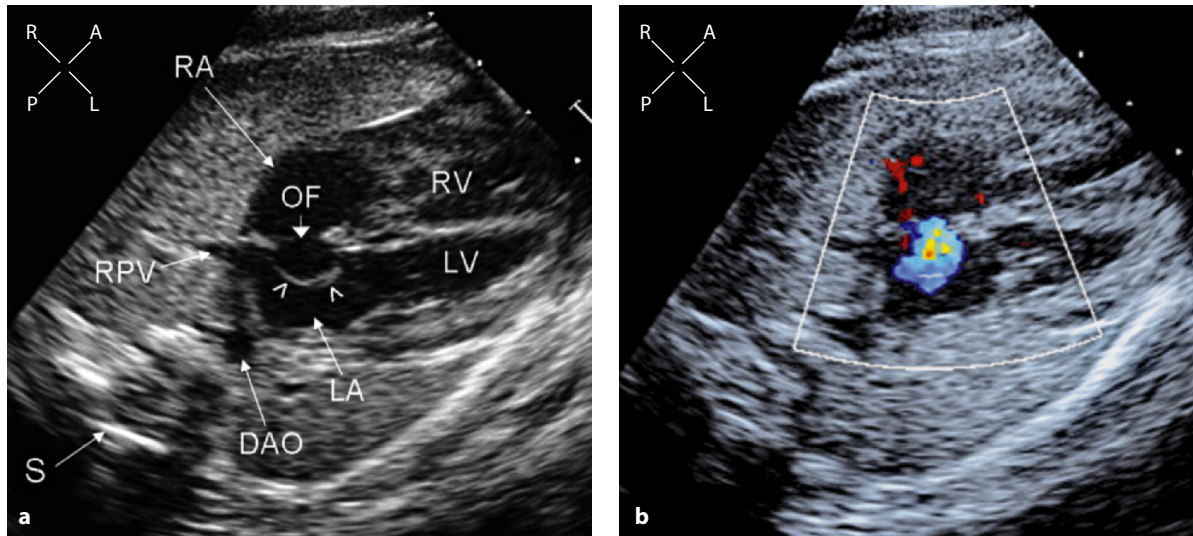
Fig. 7.5 • Transverse view in a normal 34-week gestational-age fetus (**a**). Transverse view better represents the structure of the atrial septum, because it is oriented at right angle relative to the ultrasound beam. Opening of the foramen ovale in the middle of the atrial septum and the foraminal flap (*open arrows*) arching inside of the left atrium. On color flow mapping with low scale setting (**b**), the normal right to left flow at the level of the foramen is visible in *blue*. The Niquist limit was 20 cm/s. *DAO* descending aorta, *LA* left atrium, *LV* left ventricle, *OF* oval fossa, *RA* right atrium, *RPV* right pulmonary vein, *RV* right ventricle, *S* spine
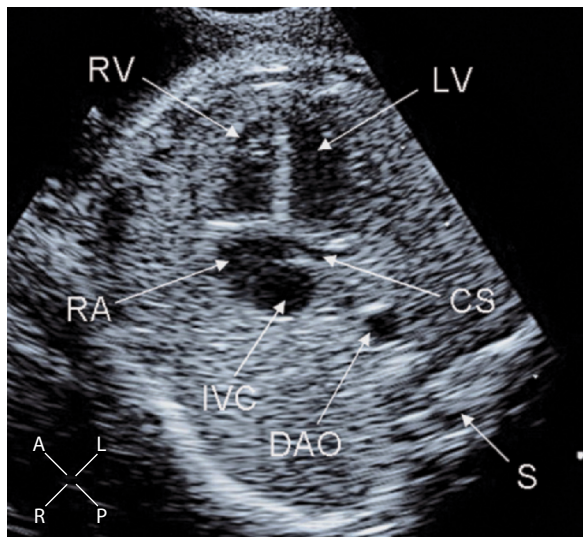
Fig. 7.6 • Cross-sectional view, obtained with slight caudal tilt from the classical four-chamber view, of the inferior venoatrial connection of the right atrium. The inferior vena cava and the coronary sinus connect with the floor of the right atrium. The cavity of the left atrium is not visualized. *CS* coronary sinus, *DAO* descending aorta, *IVC* inferior vena cava, *LV* left ventricle, *RA* right atrium, *RV* right ventricle, *S* spine

- The atrial septum should appear intact in the small portion above the atrioventricular valves where it fuses with the ventricular septum at the crux of the heart (Figs. 7.4, 7.5). A normal opening, the foramen ovale, occupies the middle third of the atrial septum and is guarded by a thin membrane, the foraminal flap, which flickers into the body of the left atrium.
- The interventricular septum should appear intact.
- With slight probe manipulation, the right and left venoatrial connection can be assessed. The two in-

ferior pulmonary veins are seen in the four-chamber view entering the back of the left atrium on either side of the descending aorta (Fig. 7.4). With caudal angulation from the classic four-chamber view, the ostium of the inferior vena cava appears on the floor of the right atrium close to the inferior part of the interatrial septum (Fig. 7.6). Immediately posterior to the left atrioventricular junction, the coronary sinus are seen entering the inferior portion of the right atrium. Because the coronary sinus is a structure coursing outside the heart along
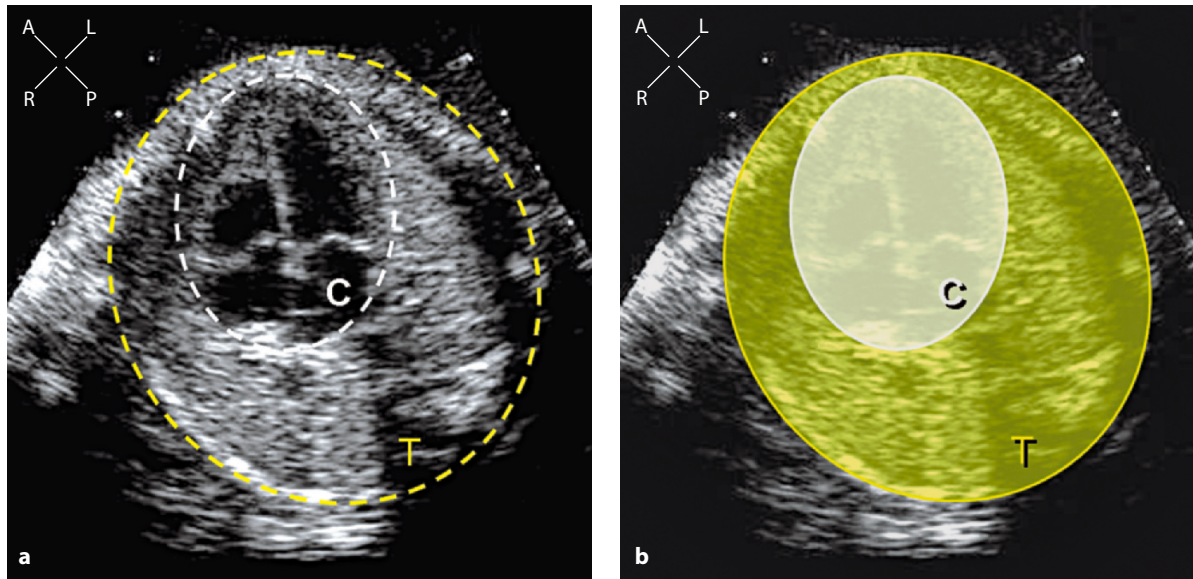
Fig. 7.7 • Circumferences (**a**) and areas (**b**) of the heart (*C*) and the thorax (*T*) can be determined at the level of the four-chamber view

the left posterior atrioventricular groove, this vessel is visualized when the scanning plane is immediately inferior to the cavity of the left atrium. Therefore, the cavity of the left atrium and the orifice of the mitral valve cannot be imaged at the same time with the coronary sinus in horizontal sections (Fig. 7.6).

Dimensions of the Heart

The ratio of the size of the heart to that of the thorax is a useful index of cardiac disease with heart failure in both pediatric and adult cardiology. In the fetus, the cardiothoracic (C/T) ratio has been proposed as a useful prognostic tool, easily obtained, in structural and functional heart disease at risk to develop heart failure. The circumference of the heart and the circumference of the thorax can be measured and express as ratio (C/T circumference ratio). A cross-sectional view is suitable for this measurement when the entire thorax is seen and includes a good four-chamber view, a complete rib, and no abdominal content (Fig. 7.7). The C/T circumference ratio is rather constant, with a mean value of 0.45 at 17 weeks and 0.50 at term [3]. Alternatively, one can calculate the ratio of the cardiac and thoracic area (C/T area ratio). This ratio also is fairly constant, with normal values between 0.25 and 0.35 throughout pregnancy [8]. When the C/T ratio is abnormal, it is important to distinguish an enlarged heart in a normal sized thorax from a normal sized heart in a small thorax. This distinction can be obtained by comparing the measured circumference of the chest with the age-related normal values.

Measurement

The four-chamber view represent one of the basic echocardiographic projection for measurement of chamber size and ventricular wall thickness. Because of its high frame rate and time resolution, M-mode tracing (Fig. 7.8) is the most accurate method not only for these measurements but also for valve and wall motion and is a useful tool in assessing cardiac arrhythmias [9]. Nevertheless, M-mode measurements must be obtained with the ultrasound beam oriented at right angle to the structures to be measured. Because this orientation is difficult and sometimes impossible to obtain, the application of M-mode in the fetus is limited.

Alternatively to M-mode tracing, fairly accurate measurements can be obtained from two-dimensional (2D) images, and this method has replaced the M-mode method in practice. Although good images can be obtained with different cardiac orientation, the transverse four-chamber view is recommended because with this orientation, the ventricular walls, the interventricular septum, and their endocardial surfaces are imaged at right angle with the ultrasound beam, with better resolution (Figs. 7.9, 7.10).
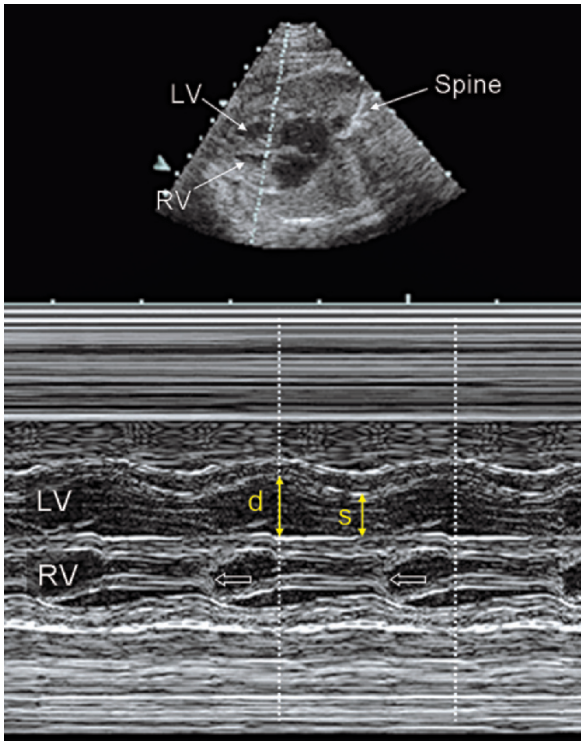
Fig. 7.8 • End-diastolic (*d*) and end-systolic (*S*) transverse diameter of the left ventricle measured by M-mode tracing. The *upper part* of this figure depicts how cross-sectional examination is utilized to identify the heart chambers in a transverse four-chamber view and to align the M-mode cursor perpendicular to the structures of interest. The cursor is placed apically to the atrioventricular valves, and measurements are performed from endocardial to endocardial surface. The diastolic diameter is taken at the end of diastole when the ventricular width is largest. This event coincides with the closure of the atrioventricular valves (*dashed line*). The systolic diameter (*s*) is taken at the end of systole when the width of the ventricle reaches its minimum, before the atrioventricular valves open. *White open arrows* indicate tricuspid valve opening. *LV* Left ventricle, *RV* right ventricle
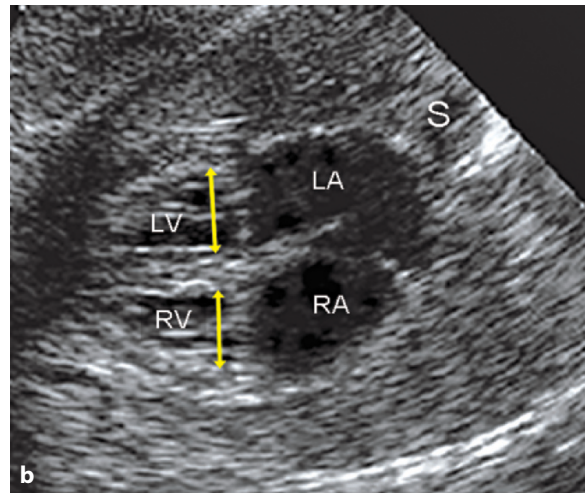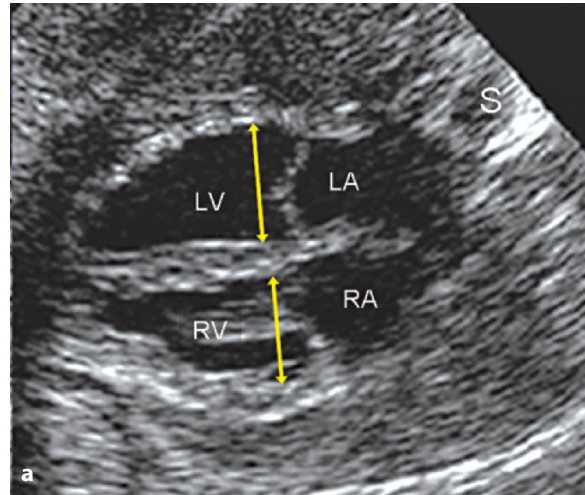
Fig. 7.9 • End-diastolic (**a**) and end-systolic (**b**) frame in a transverse view. The *yellow segments* indicate where measurements of the width of the left and right ventricles are taken. *LA* left atrium, *LV* left ventricle, *RA* right atrium, *RV* right ventricle, *S* spine
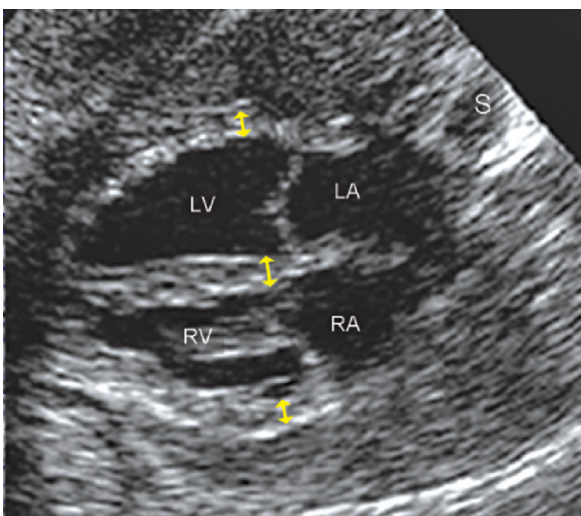
Fig. 7.10 • The same end-diastolic frame as in Figure 7.9. Measurements of the thickness of the left and right ventricular walls and of the interventricular septum (*yellow segments*). Of note, measurements of wall thickness and ventricular diastolic diameter are both taken close to the base of the heart, just below the orifice of the atrioventricular valves. The endocardial-to-endocardial method is utilized to measure the cavities, and the endocardial-to-epicardial surface to measure ventricular-wall thickness. *LA* left atrium, *LV* left ventricle, *RA* right atrium, *RV* right ventricle, *S* spine
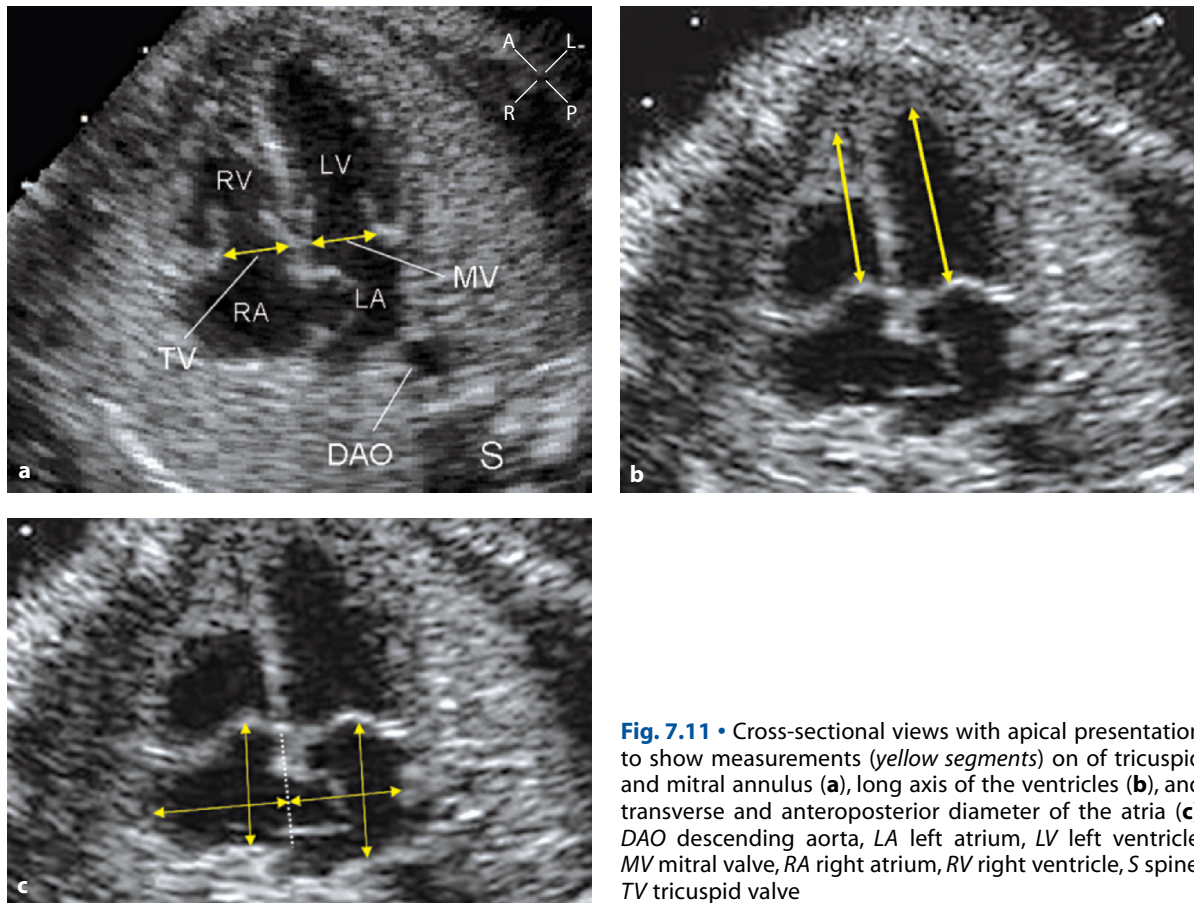
Fig. 7.11 • Cross-sectional views with apical presentation to show measurements (*yellow segments*) on of tricuspid and mitral annulus (**a**), long axis of the ventricles (**b**), and transverse and anteroposterior diameter of the atria (**c**). *DAO* descending aorta, *LA* left atrium, *LV* left ventricle, *MV* mitral valve, *RA* right atrium, *RV* right ventricle, *S* spine, *TV* tricuspid valve

Conversely to ventricular diameters and wall thickness measurement, assessment atrioventricular valve size will be obtained at the best in apical four-chamber view, because the plane of the atrioventricular valves is perpendicular to the ultrasound beam.

Moreover, the apical four-chamber view is better for measuring the long-axis diameter of both atria and ventricles (Fig. 7.11) [10-14].

Ventricular Function

As in the pediatric population, segmental abnormalities of ventricular wall motion are very rare in the fetus. Therefore, some indices of global ventricular performance derived from linear dimensions can be used as reliable estimates of left ventricular performance. The ventricular fractional shortening (FS) is most widely used among these indices, because it requires two measurements that are quick and easy to obtain

$$FS = (EDD - ESD) / EDD$$

where *EDD* is the ventricular width at the end of diastole and *ESD* is the ventricular width at the end of systole. Ventricular FS is often referred to as a percentage rather than a fraction. In general, the diameter of both the right and the left ventricles should shorten more than 28%. Serial assessment of this index can be useful in following individual patients at risk for developing fetal heart failure [15, 16].

The Normal Echocardiogram – Color Flow Mapping and Pulsed Doppler

The Atrioventricular Valves

When the four-chamber view is obtained with apical orientation, the inflow of both ventricles is parallel to the ultrasound beam. Therefore, this approach is ideal for assessing the flow of the mitral and tricuspid valves. When carrying out a pulsed Doppler inflow study of the verticles, the sample volume is to be positioned on the ventricular side of the atrioventricular valves immediately distal to their leaflets and parallel to the flow direction. The Doppler flow profile of the mitral and tricuspid valves is similar, with a diastolic pattern characterized by two peaks: the first one
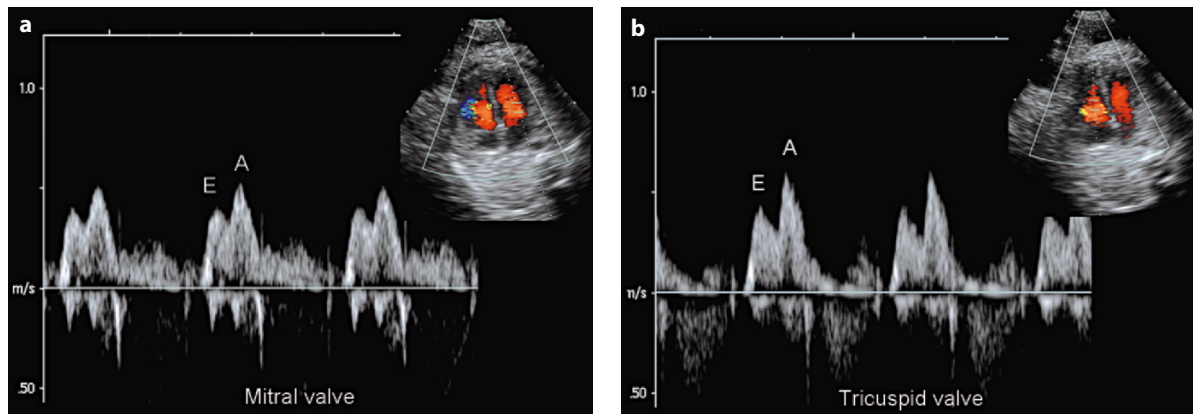
Fig. 7.12 • Pulsed Doppler tracing of normal mitral (**a**) and tricuspid (**b**) valves in a 22-week gestational-age fetus. The color flow mapping panels show that both tracings are obtained from an apical four-chamber view. The sample volume position for each valve is displayed. *A* A wave, *E* E wave
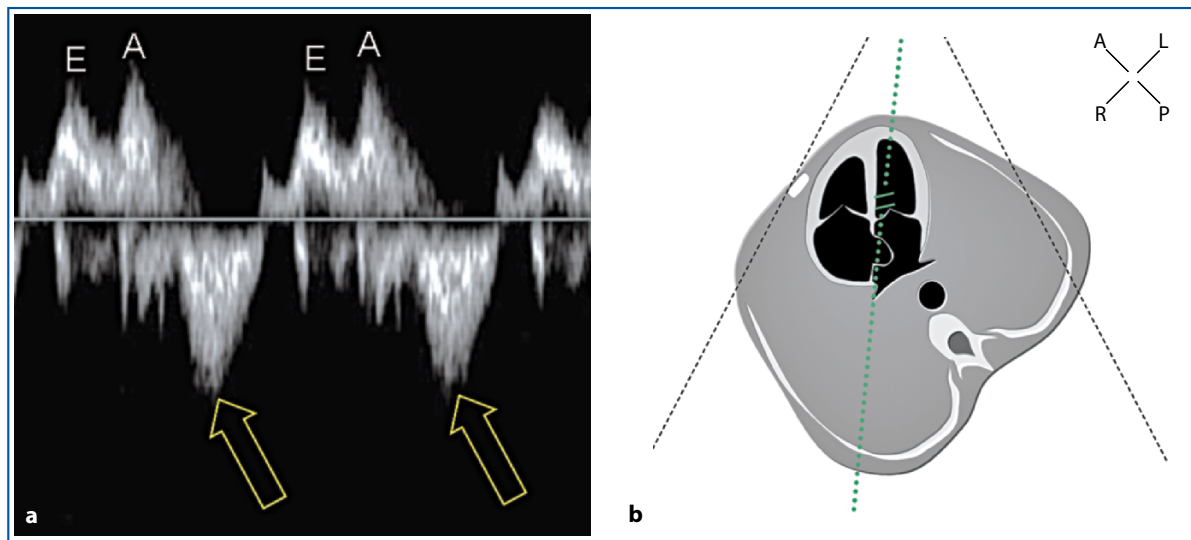
Fig. 7.13 • Pulsed Doppler tracing from the inflow–outflow of the left ventricle (**a**). The biphasic flow above the baseline is the normal transmitral flow. The monophasic flow below the baseline (*yellow open arrows*) is the outflow from the left ventricle and must not be mistaken for tricuspid regurgitation. Position of the sample volume for Doppler assessment of the inflow–outflow of the left ventricle (**b**). *A* A wave, *E* E wave

(E wave) represents the passive ventricular filling as the valve opens in the first part of diastole, whereas the second (A wave) corresponds to the active ventricular filling during atrial contraction (Fig. 7.12). These two peaks are well defined when the heart rate is in the normal ranges, but they merge into each other for heart rates over 160-170 beats/min [17, 18].

In a normal atrioventricular valve, there should be no backflow into the atria during systole. However, when examining the mitral valve, the sample volume may find itself near the left ventricular outflow. Therefore, outflow toward the aorta may be recorded during systole and must not be mistaken for a mitral regurgitation (Fig. 7.13). This position of the Doppler sample can be intentionally obtained for fetal cardiac rhythm assessment.

In contrast to postnatal life, in the normal fetus, the E-wave is smaller than the A wave. This is due to the reduced compliance of the fetal ventricular myocardium. Therefore, most ventricular filling takes place in the second part of the diastole and is dependent on the regular atrial contraction. This explains why the loss in the regular sinus rhythm may seriously compromise the fetal cardiac performance.

The atrioventricular valve velocities of the E wave increase throughout gestation with values of 25 cm/s at 16 weeks' gestation and 45 cm/s at term for the mitral valve and 30 cm/s and 50 cm/s for the tricuspid
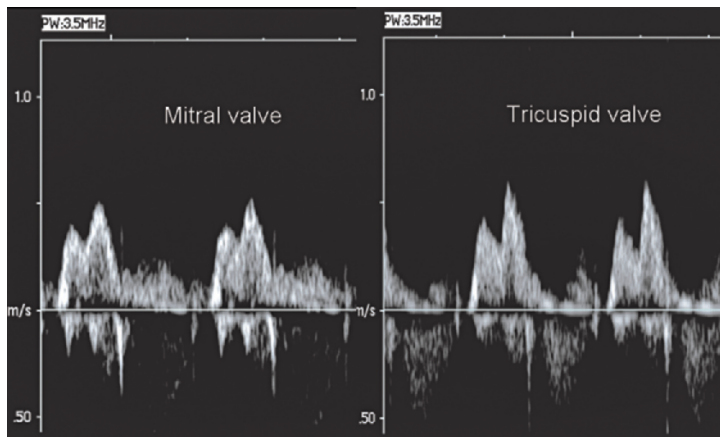
Fig. 7.14 • Mitral and tricuspid valve Doppler tracing obtained in the same patient from apical four-chamber view. Both tracings are represented with the same scale gain. The time velocity integral of the tricuspid valve flow is slightly higher than that of the mitral valve and is due to the larger output of the right ventricle in the fetal circulation
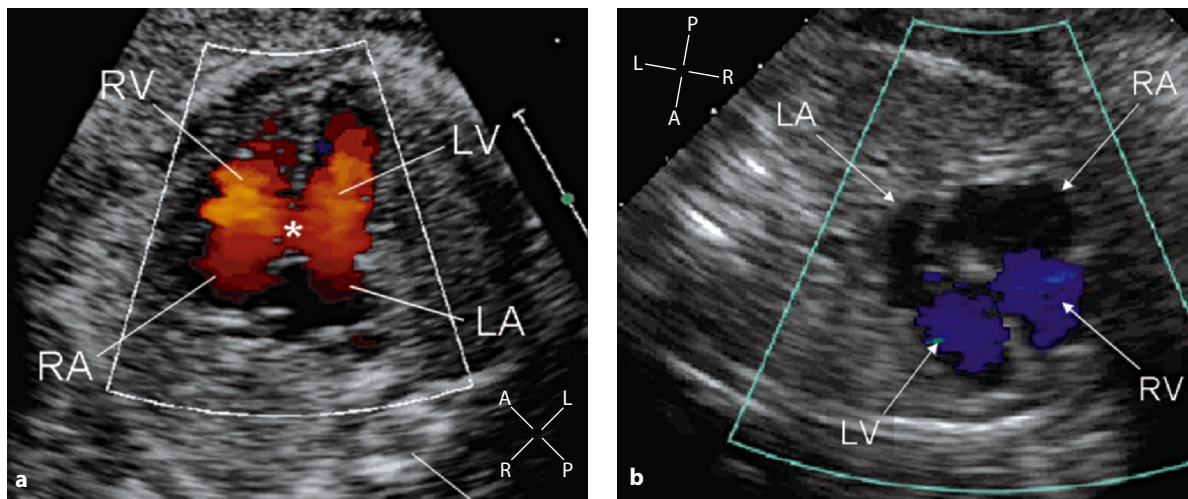
Fig. 7.15 • Color flow mapping of the apical view from ventral (**a**) and dorsal (**b**) approach: diastolic frames. The atrioventricular valve shows equal width of the flow filling the ventricles. The *asterisk* indicates a bridge of color flow over the inlet ventricular septum, simulating a defect at this level. This is a common artefact due to a high color gain setting. The atrial or ventricular septum should be orthogonal to the ultrasound beam to investigate for defects in this region. The different color of the flow in the two pictures indicates the opposite direction of the flow relative to the ultrasound source. *LA* left atrium, *LV* left ventricle, *RA* right atrium, *RV* right ventricle

valve at the same gestational ages. The A wave shows a relatively constant velocity or a mild increase during gestation, with values of 45 cm/s for the mitral valve and 50 cm/s for the tricuspid valve.

The reason the E-wave velocity increases more than that of the A wave is believed to be due to the diastolic "maturation" of the ventricles during gestation. The ratio between the peak velocity of the E and A waves on Doppler spectrum (E/A ratio) is about 0.5 at the 16th week of gestation and is around 1 near term. The slightly higher flow velocity through the tricuspid valve is mainly due to the larger output of the right ventricle in the fetal circulation (Fig. 7.14) [19].

Color Doppler is an integral part of the evaluation of the fetal heart in specialized centers and can

increase the speed and accuracy of the examination [20-26]. Its use during a routine obstetrical scan of the fetal heart is controversial.

In the normal fetus, color flow mapping evaluation in the four-chamber view shows equal and nonaliased flow through the atrioventricular valves in diastole (Fig. 7.15). In systole, there should be no evidence of regurgitation of the atrioventricular valves.

With high-resolution equipment, it is quite common to detect a trivial jet of tricuspid regurgitation limited to a couple of frames in early systole (Fig. 7.16) [27, 28].

In the four-chamber view, color Doppler is particularly useful to detect atrioventricular valve disfunction and tricuspid regurgitation in particular. Semiquantitative assessment of the severity of re-
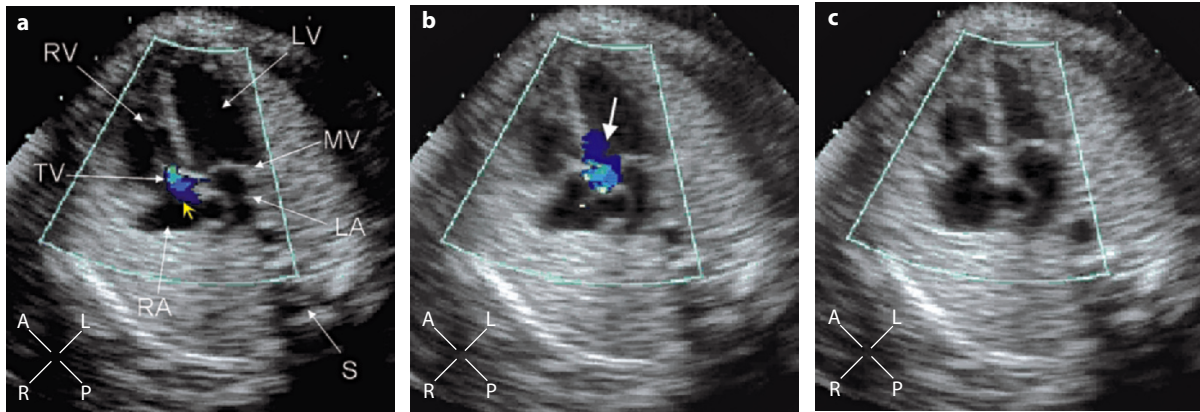
Fig. 7.16 • The heart is seen in the apical view. Color flow mapping is shown in three consecutive systolic frames. In this early systolic frame (**a**), the *yellow arrow* indicates a tiny jet of physiologic tricuspid regurgitation. The regurgitant jet has already stopped when the ejection phase into the aorta begins (**b**). *Blue* represents the flow in the left ventricular outflow tract toward the aorta (*white arrow*). No regurgitation is seen in this frame (**c**) at the end of the systole. *LA* left atrium, *LV* left ventricle, *MV* mitral valve, *RA* right atrium, *RV* right ventricle, *S* spine, *TV* tricuspid valve
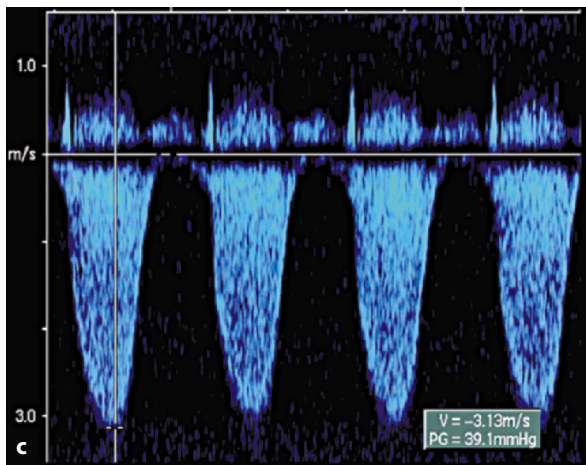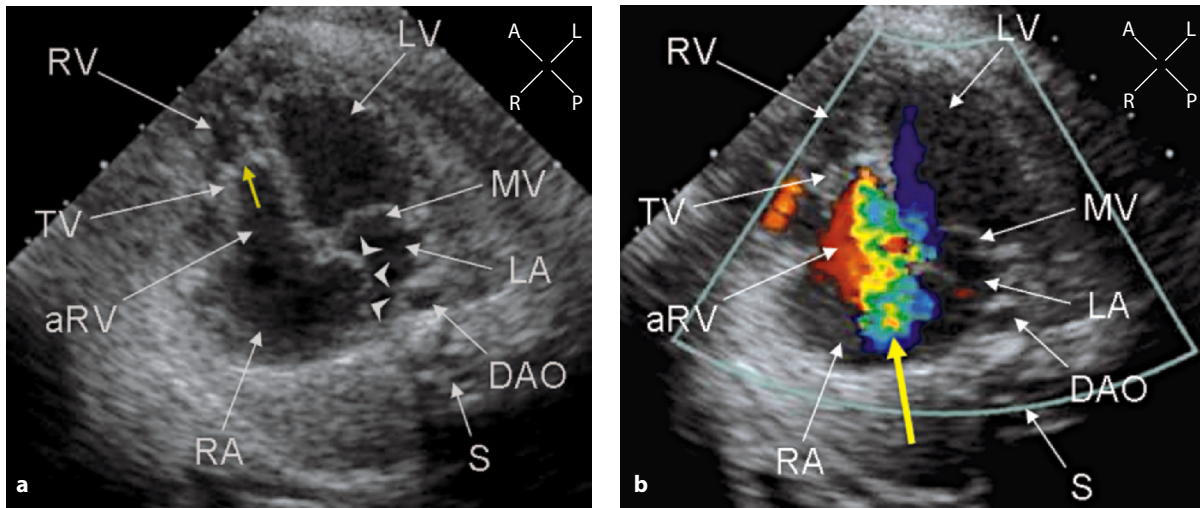
Fig. 7.17 • Apical view (**a**) in 33-week gestational-age fetus with Ebstein's malformation of the tricuspid valve. The *yellow arrow* indicates apical displacement of the septal leaflet of the tricuspid valve. Color flow mapping systolic frame (**b**) showing a jet of significant tricuspid regurgitation that originates in the body of the right ventricle at the site of coaptation of the tricuspid leaflets. Continuous Doppler tracing (**c**) of the regurgitant jet with a peak velocity around 3 m/s. *aRV* atrialized right ventricle, *DAO* descending aorta, *LA* left atrium, *LV* left ventricle, *MV* mitral valve, *RA* right atrium, *RV* right ventricle, *S* spine, *TV* tricuspid valve

gurgitation of the atrioventricular valves is usually obtained on the basis of the spatial extension of the regurgitant signal by color flow mapping and atrial size. When an area of regurgitation or a stenotic jet is identified, color flow imaging is very helpful for aligning the Doppler cursor to assess velocities and estimated gradients across these valves. Figures 7.17-7.19 illustrate cross-sectional, color flow, and Doppler
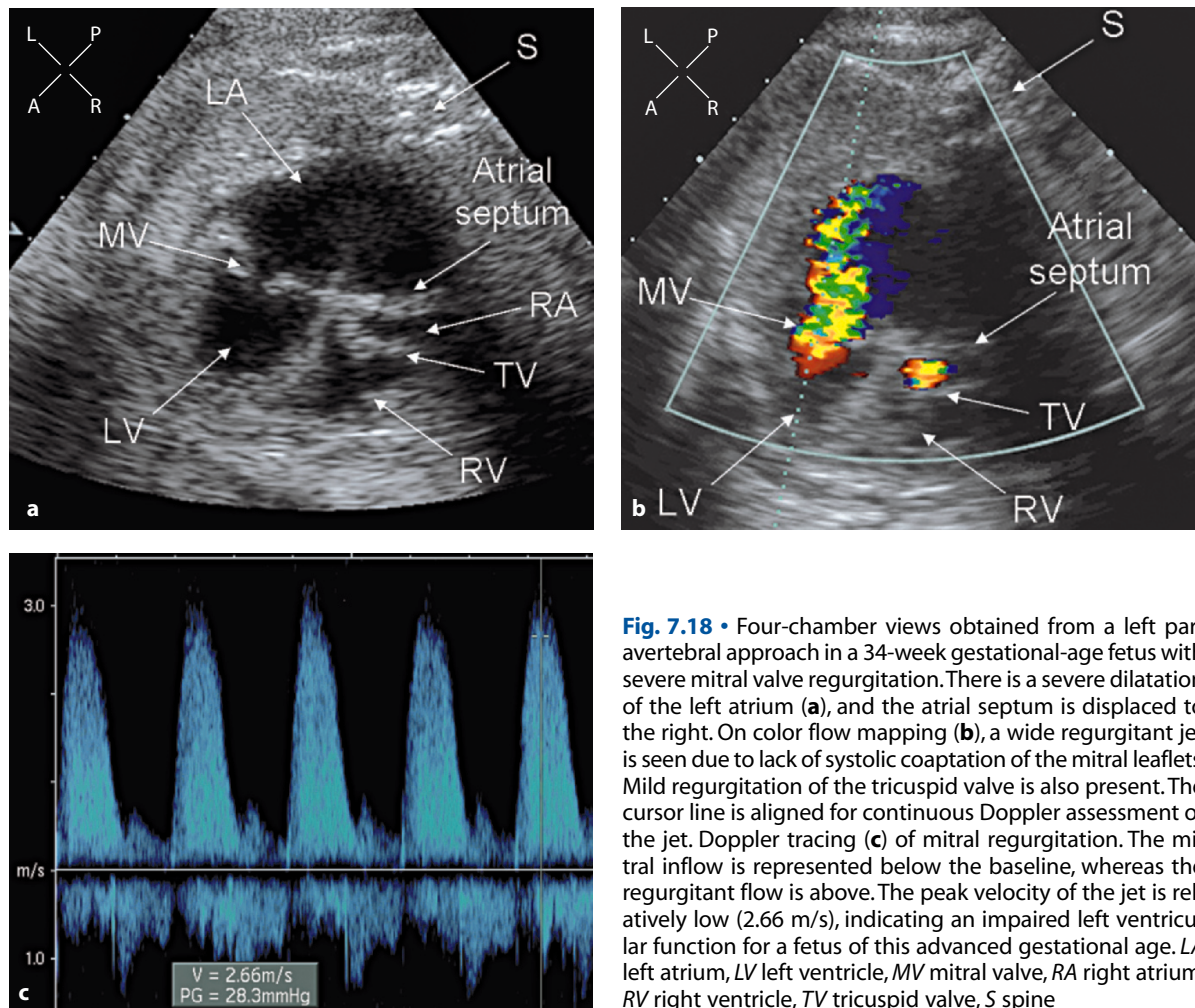
Fig. 7.18 • Four-chamber views obtained from a left paravertebral approach in a 34-week gestational-age fetus with severe mitral valve regurgitation. There is a severe dilatation of the left atrium (**a**), and the atrial septum is displaced to the right. On color flow mapping (**b**), a wide regurgitant jet is seen due to lack of systolic coaptation of the mitral leaflets. Mild regurgitation of the tricuspid valve is also present. The cursor line is aligned for continuous Doppler assessment of the jet. Doppler tracing (**c**) of mitral regurgitation. The mitral inflow is represented below the baseline, whereas the regurgitant flow is above. The peak velocity of the jet is relatively low (2.66 m/s), indicating an impaired left ventricular function for a fetus of this advanced gestational age. *LA* left atrium, *LV* left ventricle, *MV* mitral valve, *RA* right atrium, *RV* right ventricle, *TV* tricuspid valve, *S* spine

tracings obtained in the four-chamber projection in some congenital heart diseases with disfunction of the atrioventricular valve.

The Pulmonary Veins

The four-chamber view allows the best beam-flow alignment for the Doppler study of the pulmonary veins. Transverse or apical four-chamber views are utilized, depending on fetal presentation and the vein under study. It is often difficult to recognize the pulmonary veins on two-dimensional examination, whereas they are more easily evidenced by color Doppler with the low-scale setting. Color flow mapping facilitates correct alignment and positioning of the sample volume of pulsed Doppler that is to be placed in the terminal part of the veins, just before their junction with the left atrium. While examining pulmonary vein flow, it is advisable to limit the box of the color Doppler to the posterior portion of the left atrium to avoid an unclear, confused image caused by the high-velocity flow of the ventricles (Fig. 7.20).

The color Doppler profile of the pulmonary vein flow reflects the variations in pressure in the left atrium. As is observed in the vena cava, two anterograde flow peaks are present, one systolic and one protodiastolic. Although the velocity of the systolic peak may be higher than the diastolic peak, the difference is relatively modest or absent in most patients. During atrial contraction, the flow is seen to cease or a short inversion is observed (Fig. 7.21).

a

b

c
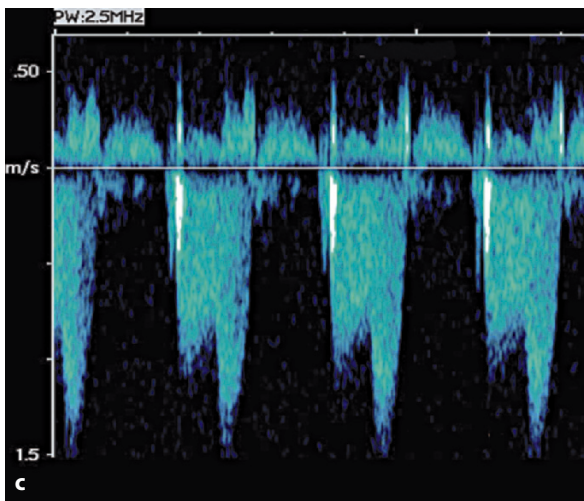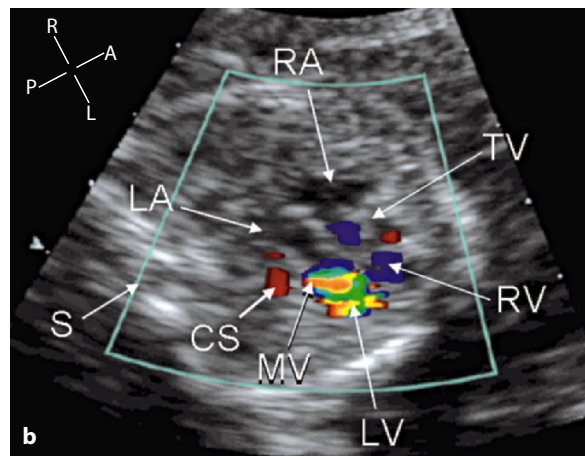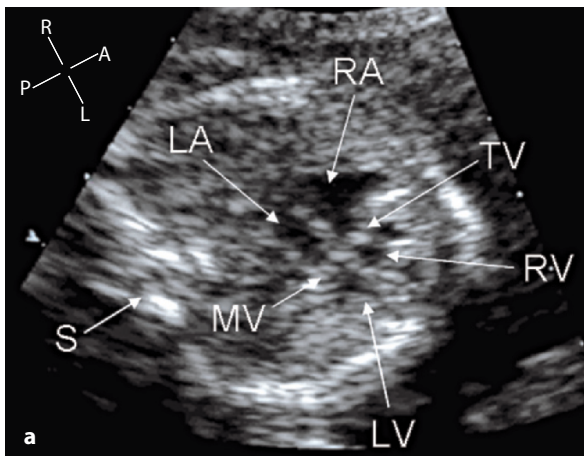
Fig. 7.19 • Four-chamber view (**a**) obtained from the right chest approach in a fetus with mitral valve stenosis. The dominance of the right heart chambers is abnormal for gestational age. The mitral annulus is small, and the valve leaflets look dysplastic. The color flow diastolic frame (**b**) shows a narrow and accelerated flow through the mitral valve, whereas that of the tricuspid valve is wider and laminar. Pulsed Doppler tracing (**c**) of the accelerated mitral valve flow. Despite the less than ideal alignment of the cursor line, the A wave peak velocity is high and close to 1.5 m/s. *CS* coronary sinus, *LA* left atrium, *LV* left ventricle, *MV* mitral valve, *RA* right atrium, *RV* right ventricle, *S* spine, *TV* tricuspid valve
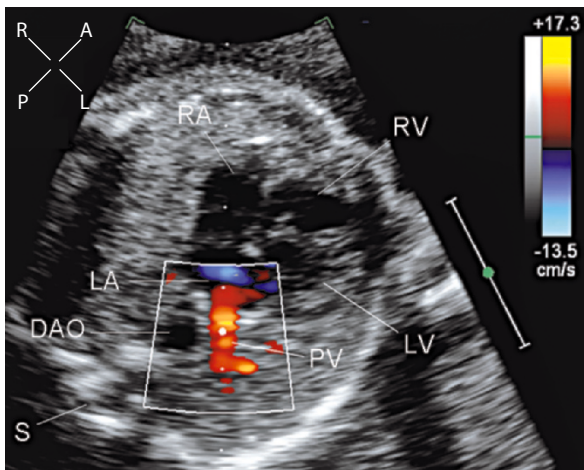
Fig. 7.20 • Four-chamber view in transverse approach in a normal 23-week gestational-age fetus. The size of the color box is intentionally limited to the posterior part of the left atrium. The low-scale setting highlights the flow in the left inferior pulmonary vein to guide the position of the sample volume (*large white dot*) for pulsed Doppler assessment. *DAO* descending aorta, *LA* left atrium, *LV* left ventricle, *PV* pulmonary vein, *RA* right atrium, *RV* right ventricle, *S* spine
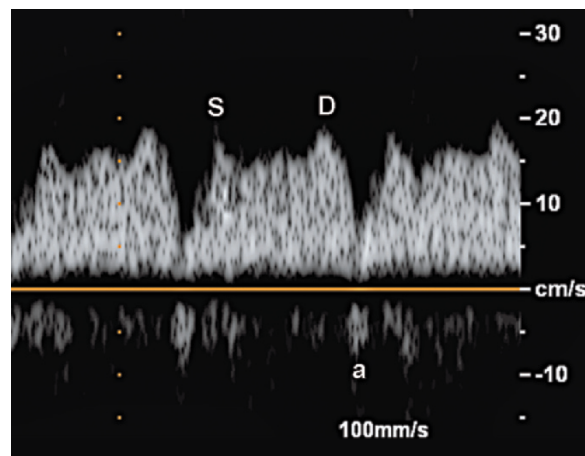
Fig. 7.21 • Pulsed Doppler spectrum of the pulmonary vein of the same fetus as in Fig. 7.20. The velocity of flow of the systolic (*S*) and protodiastolic (*D*) peak is similar. During atrial contraction, (*a*). the flow stops, and there is a small reversal
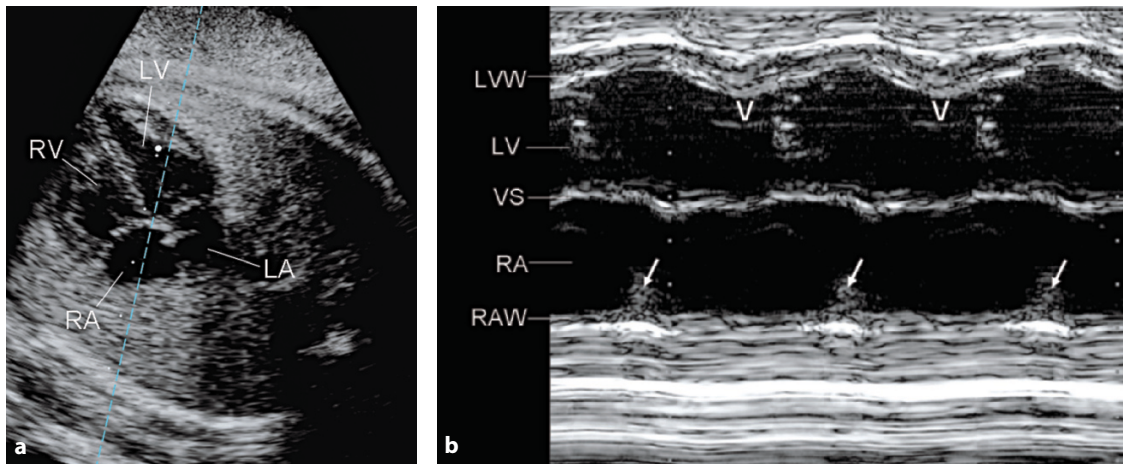
Fig. 7.22 • In a four chamber view, the M-mode cursor (*green dashed line*) is oriented through the left ventricle, ventricular septum and the right atrium (**a**). The M-mode trace (**b**) shows the regular sequence of atrial contractions (*arrows*) preceding ventricular contraction (*V*). *LV* left ventricle, *LVW* left ventricular wall, *RA* right atrium, *RAW* right atrial wall, *VS* ventricular septum
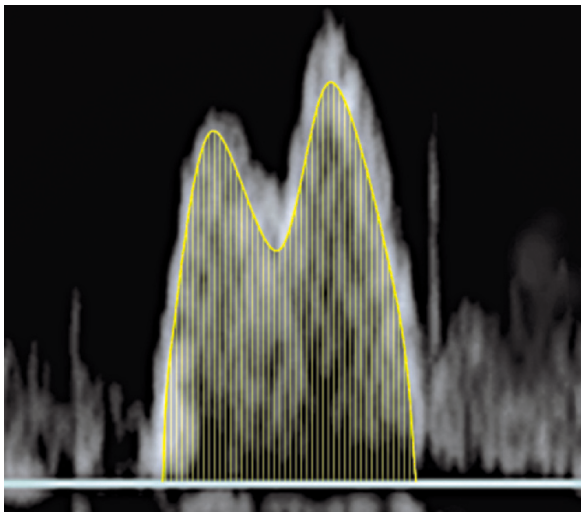
Fig. 7.23 • Doppler spectrum of the mitral valve integrated to obtain the velocity-time integral (VTI)

Cardiac Rhythm

Different techniques for assessing cardiac rhythm can be obtained by M-mode, color flow M-mode, or pulsed Doppler tracing [29–33]. The basic principle of these methods is to assess the relationship between atrial and ventricular contraction. With the M-mode method, the cursor line should be aligned so that atrial and ventricular wall movement is recorded at the same time. In the normal sinus rhythm, every atrial contraction must precede ventricular contraction action and must be relatively constant and within the normal ranges for the heart rate. Figure 7.22 shows one example of M-mode rhythm assessment in the four-chamber view.

If fetal presentation allows the apical four-chamber view to be obtained, the easiest method to evaluate the cardiac rhythm is inflow–outflow pulsed

Doppler assessment of the left ventricle. This method is described further in the chapter pertaining to the five-chamber view.

Ventricular Output

As in postnatal examination, transvalvular flow (Q) can be calculated from the formula:

$$Q \text{ (ml/min)} = VTI \, \pi \, D^2/4 \, HR$$

where *D* is the diameter of the valve annulus, *VTI* is the velocity-time integral of the Doppler flow at the same site, and *HR* represents heart rate. In the four-chamber view, left ventricular output can be calculated from the mitral annulus cross-sectional area and VTI from the flow through the mitral valve (Fig. 7.23). The right ventricular output is calculated
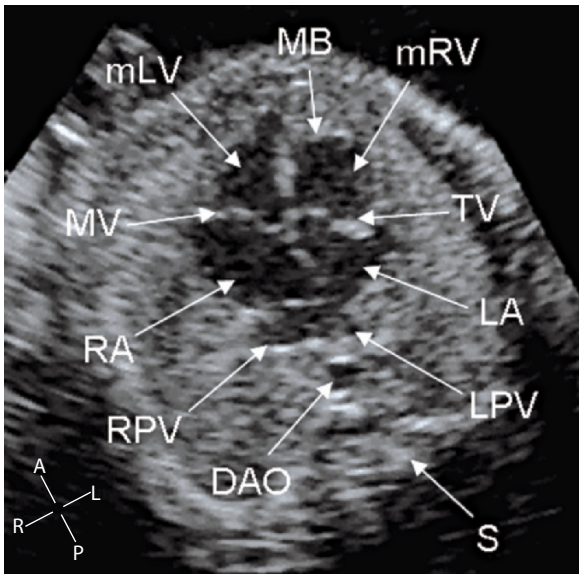
Fig. 7.24 • Apical view in a 22-week gestation-age fetus with atrioventricular discordance. The left-sided atrium, which receives the pulmonary veins, is connected with a morphologically right ventricle characterized by a moderator band and a lower insertion of the atrioventricular valve. The right-sided atrium is committed to a morphologically left ventricle with smooth endocardial surface a higher insertion of the atrioventricular valve. *DAO* descending aorta, *LA* left atrium, *LPV* left pulmonary vein, *MB* moderator band, *mLV* morphologically left ventricle, *MV* mitral valve, *RA* right atrium, *mRV* morphologically right ventricle, *RPV* right pulmonary vein, *S* spine, *TV* tricuspid valve
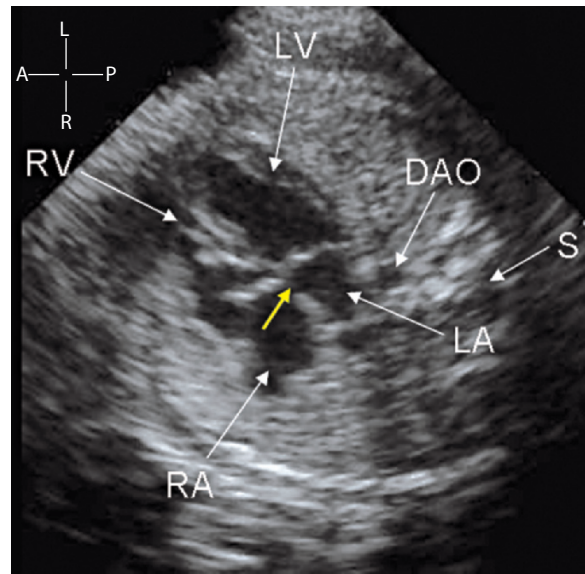
Fig. 7.25 • Atrioventricular septal defect and atrial component only in a 27-week gestational-age fetus. The *yellow arrow* indicates a small defect of the atrial septum primum immediately above the plane of the atrioventricular valves. The two atrioventricular valves lie on the same plane. Fetal karyotype revealed a trisomy 21. *DAO* descending aorta, *LA* left atrium, *LV* left ventricle, *RA* right atrium, *RV* right ventricle, *S* spine

from the tricuspid annulus cross-sectional area and the VTI from the flow of the tricuspid valve. Despite the fact that certain assumption of the above formula are not fully satisfied by atrioventricular valves (the annuli are not circular and the dimension of their orifice is not constant throughout the period of flow), reliable estimates of ventricular output have been obtained in experimental fetal animal models and in human fetuses [34-36].

Four-Chamber-View Checklist

Many examiners may expect that cardiac anomalies produce severe anatomical distortion in the four-chamber view or a clearly dilated heart. Unfortunately, some heart defects, detectable in the four-chamber view, may present with a nearly normal four-chamber anatomy, and thus are often overlooked [37, 38]. Figures 7.24 and 7.25 show two "nearly" normal four-chamber views in cases with congenital heart disease, which can go undetected by an inexperienced examiner. In both cases, the heart is of normal size and position, with two atria and two ven-

tricles of nearly equal size, two equal atrioventricular valves, an apparently intact ventricular septum, and a left atrium receiving two pulmonary veins.

Knowledge of possible anomalies and systematic adherence to a checklist is therefore mandatory for successful identification of these abnormalities [37]. The following checklist summarizes the structures that can be assessed in the four-chamber view:

- position and dimensions of the heart;
- morphology of heart chambers;
- venoatrial connection;
- morphology of the atrial septum and foramen ovale;
- morphology and function of the atrioventricular valves;
- morphology of the ventricular septum (with exception of the anterior and perimembranous portion);
- ventricular wall thickness;
- dimensions (relative and absolute) of heart chambers;
- ventricular function;
- cardiac rhythm.

It has been proposed also that color flow mapping Doppler, if available, should be used routinely
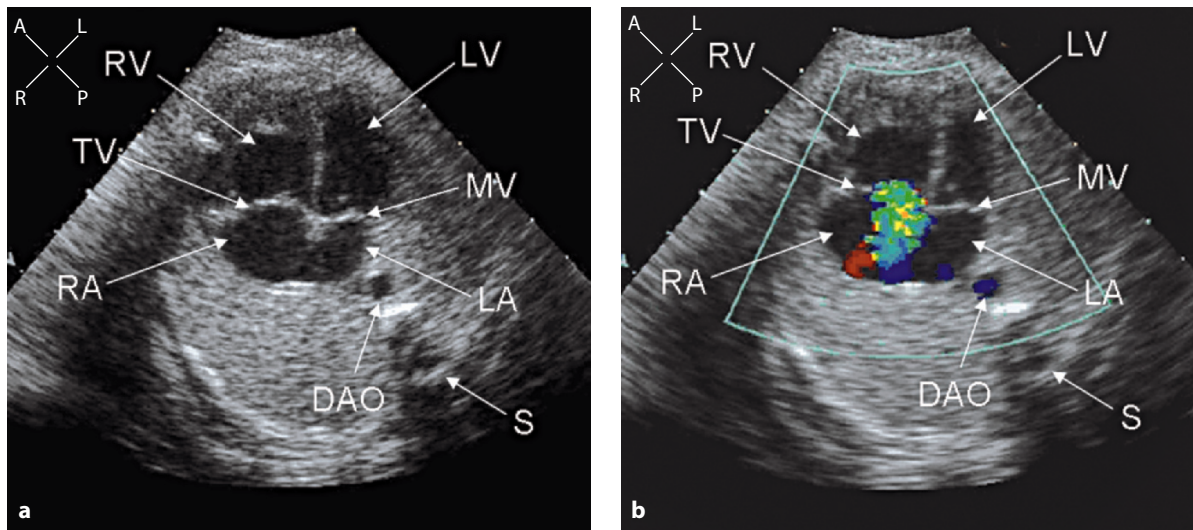
Fig. 7.26 • Apical view in a 32-week gestational-age fetus. Cross-sectional view (**a**) shows a right ventricular dominance apparently within the normal ranges for gestational age. Color flow mapping (**b**) reveals an unexpected tricuspid regurgitation, at least of moderate degree. In a third-level scan, severe constriction of the arterial duct is identified. *DAO* descending aorta, *LA* left atrium, *LV* left ventricle, *MV* mitral valve, *RA* right atrium, *RV* right ventricle, *S* spine, *TV* tricuspid valve
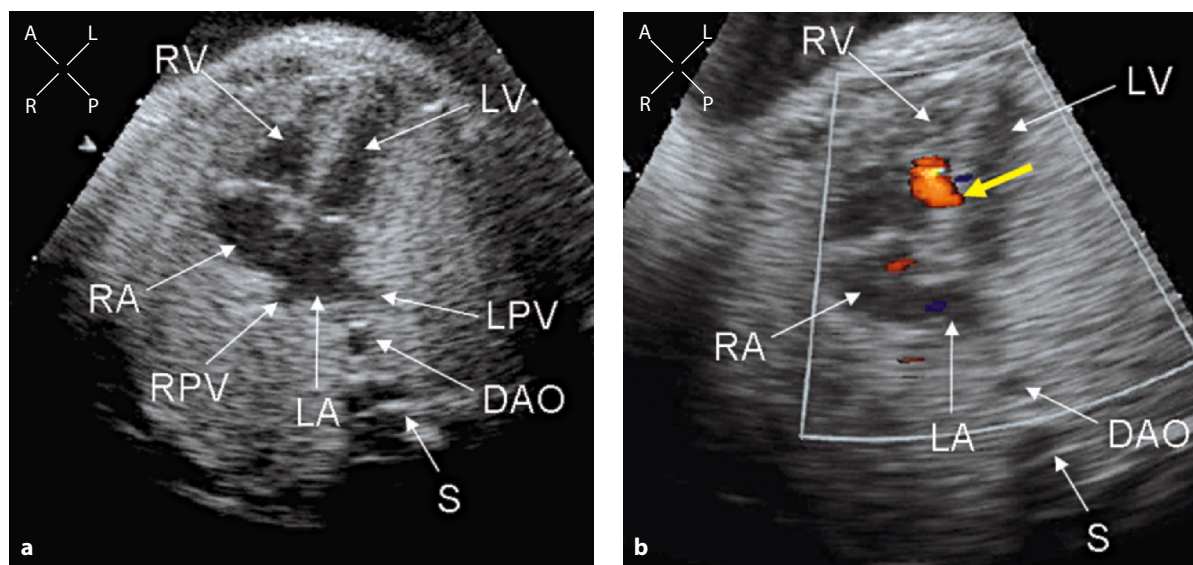
Fig. 7.27 • Apical view in a 30-week gestational-age fetus. The cross-sectional view (**a**) looks entirely normal. This systolic frame on color flow mapping (**b**) shows a small midmuscular ventricular septal defect (*yellow arrow*), undetectable on cross-sectional imaging. This aspecific defect motivated a third-level examination, which identified transposition of the great arteries. *DAO* descending aorta, *LA* left atrium, *LPV* left pulmonary vein, *LV* left ventricle, *RA* right atrium, *RPV* right pulmonary vein, *RV* right ventricle, *S* spine

during screening examination of the heart [38]. Figures 7.17 and 7.19 are associated with a substantial distortion of the four-chamber view, allowing detection during a routine obstetrical examination, even without the use of color flow mapping. The utility of Doppler investigation in such cases is to assess the severity of valvular dysfunction and follow the patient in order to optimize perinatal management.

In Figures 7.26 and 7.27, the use of color flow mapping in a first-level obstetrical scan arouses the first suspicion of a congenital heart disease that may otherwise go undetected.

The four-chamber view in several congenital heart diseases is shown in the appropriate section on the DVD-ROM. In the text pertaining to the slides is an information sheet on that particular disease.

References

1. Allan LD, Tynan MJ, Campbell S et al (1980) Echo-cardiographic and anatomical correlates in the fetus. Br Heart J 44:444-451

2. Cook AC, Yates RW, Anderson RH. (2004) Normal and abnormal fetal cardiac anatomy. Prenat Diagn 24:1032-1048

3. Paladini D, Chita SK, Allan LD (1990) Prenatal measurement of cardiothoracic ratio in evaluation of heart disease. Arch Dis Child 65:20-23

4. Rikitake N, Takechi T, Suzuki K et al (1981) Fetal echocardiography: structural evaluation of the fetal heart and prenatal diagnosis of congenital heart disease J Cardiogr 11:1319-1327

5. DeVore GR (1985) The prenatal diagnosis of congenital heart disease-a practical approach for the fetal sonographer J Clin Ultrasound 4:229-245

6. Copel JA, Pilu G, Green J et al (1987) Fetal echocardiographic screening for congenital heart disease: the importance of the four-chamber view. Am J Obstet Gynecol 157:648-655

7. Hess DB, Hess LW, Carter GA et al (1998) Obtaining the four-chamber view to diagnose fetal cardiac anomalies. Obstet Gynecol Clin North Am 25:499-515

8. Chaoui R, Bollmann R, Goldner B et al (1994) Fetal cardiomegaly: echocardiographic findings and outcome in 19 cases Fetal Diagn Ther 9:92-104

9. Allan LD, Joseph MC, Boyd EGC et al (1982) M-mode echocardiography in the developing human fetus. Br Heart J 47:573-583

10. Tan J, Silverman NH, Hoffman JI et al (1992) Cardiac dimensions determined by cross-sectional echocardiography in the normal human fetus from 18 weeks to term. Am J Cardiol 70:1459-1467

11. Gembruch U, Shi C, Smrcek JM (2000) Biometry of the fetal heart between 10 and 17 weeks of gestation. Fetal Diagn Ther 15:20-31

12. Firpo C, Hoffman JI, Silverman NH (2001) Evaluation of fetal heart dimensions from 12 weeks to term. Am J Cardiol 87:594-600

13. Veille JC, Sivakoff M, Nemeth M (1990) Evaluation of the human fetal cardiac size and function. Am J Perinatol 7:54-59

14. Sharland GK, Allan LD (1992) Normal fetal cardiac measurements derived by cross-sectional echocardiography. Ultrasound Obstet Gynecol 2:175-181

15. St. John Sutton MG, Gewitz MH, Shah B et al (1984) Quantitative assessment of growth and function of the cardiac chambers in the normal human fetus: a prospective longitudinal echocardiographic study. Circulation 69:645-654

16. Huhta JC (2004) Guidelines for the evaluation of heart failure in the fetus with or without hydrops. Pediatr Cardiol 25:274-286

17. Reed KL, Meijboom EJ, Sahn DJ et al (1986) Cardiac Doppler flow velocities in human fetuses. Circulation 73:41-46

18. Choi JY, Noh CI, Yun YS (1991) Study on Doppler waveforms from the fetal cardiovascular system. Fetal Diagn Ther 6:74-83

19. Van der Mooren K, Barendregt LG, Wladimiroff JW (1991) Fetal atrioventricular and outflow tract flow velocity waveforms during normal second half of pregnancy. Am J Obstet Gyencol 165:668-674

20. Copel JA, Hobbins JC, Kleinman CS (1991) Doppler echocardiography and color flow mapping. Obstet Gynecol Clin North Am 18:845-851

21. Rice MJ, McDonald RW, Sahn DJ (1993) Contributions of color Doppler to the evaluation of cardiovascular abnormalities in the fetus. Semin Ultrasound CT MR 14:277-285

22. Chaoui R, Bollmann R (1994) Fetal color-Doppler echocardiography. Part 1: general principles and normal findings. Ultraschall Med 15:100-104

23. Chaoui R, Bollmann R (1994) Fetal color Doppler echocardiography. Part 2: abnormalities of the heart and great vessels. Ultraschall Med 15:105-111

24. Marx GR (1995) Doppler color flow echocardiography: indispensable application to congenital heart disease. Echocardiography 12:413-424

25. Chaoui R, McEwing R (2003) Three cross-sectional planes for fetal color Doppler echocardiography. Ultrasound Obstet Gynecol 21:81-93

26. Allan L (2004) Technique of fetal echocardiography. Pediatr Cardiol 25:223-233

27. Messing B, Porat S, Imbar T et al (2005) Mild tricuspid regurgitation: a benign fetal finding at various stages of pregnancy Ultrasound Obstet Gynecol 26:606-609

28. Yagel S (2006) Mild tricuspid regurgitation: a benign fetal finding at various stages of gestation. Ultrasound Obstet Gynecol 27:102-103

29. Allan L, Anderson R, Sullivan I et al (1983) Evaluation of fetal arrhythmias by echocardiography. Br Heart J 50:240-245

30. Kleinman C, Donnerstein R, Jaffe C et al (1983) Fetal echocardiography. A tool for evaluation of in utero cardiac arrhythmias and monitoring of in utero therapy: analysis of 71 patients. Am J Cardiol 51:237

31. Steinfeld L, Rappaport H, RossbachH et al (1986) Diagnosis of fetal arrhythmias using echocardiographic and Doppler techniques. J Am Coll Cardiol 8:1425-1433

32. Strasburger JF, Huhta JC, Carpenter RJ et al (1986) Doppler echocardiography in the diagnosis and management of persistent fetal arrhythmias. J Am Coll Cardiol 7:1386-1391

33. Reed KL, Sahn DJ, Marx GR et al (1987) Cardiac Doppler flows during fetal arrhythmias: physiological consequences. Obstet Gynecol 70:1-6

34. Kenny JF, Plappert T, Doubilet P et al (1986) Changes in intracardiac blood flow velocities and right and left ventricular stroke volumes with ges-

tational age in the normal human fetus: a prospective Doppler echocardiographic study. Circulation 74:1208-1216

35. De Smedt MCH, Visser GHA, Meijboom EJ (1987) Fetal cardiac output estimated by doppler echocardiography during mid- and late gestation. Am J Cardiol 60:338-342

36. Schmidt KG, Silverman NH, Van Hare GF et al (1990) Two-dimensional echocardiographic determination of ventricular volumes in the fetal heart. Circulation 81:325-333

37. Chaoui R (2003) The four-chamber view: four reasons why it seems to fail in screening for cardiac abnormalities and suggestions to improve detection rate. Ultrasound Obstet Gynecol 22:3-10

38. Comstock CH (2000) What to expect from routine midtrimester screening for congenital heart disease. Semin Perinatol 24:331-342

The Five-Chamber View

The Section Plane

With cranial angulation from a four-chamber view, the left ventricular outflow tract appears wedged between the two atrioventricular valves. With further cranial angulation, the aortic valve and the aortic root are imaged (Fig. 8.1).

The Normal Morphology

The fifth chamber in this view refers to the aortic root, with its valve that is seen in the center of the heart, with the right and the left atria on its sides

(Figs. 8.2, 8.3). The inflow (through the mitral valve), outflow, and trabecular component of the left ventricle are displayed, whereas only a portion of the trabecular part of the right ventricle is seen anteriorly. Posteriorly, the junction of the two upper pulmonary veins with the left atrium and of the superior vena cava with the right atrium are seen.

The Normal Echocardiogram – 2D

In the normal five-chamber view, only a portion of the trabecular part of the right ventricle is seen anteriorly. In fact, when the lumen of the aortic root is visualized, the tricuspid valve and the inlet portion
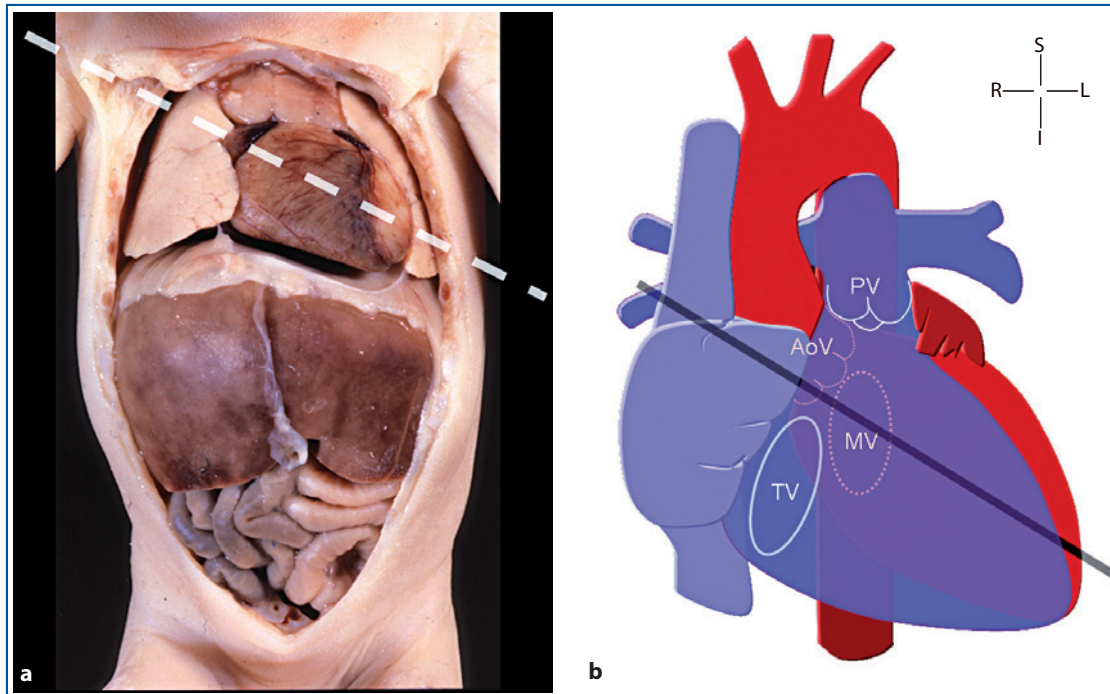
Fig. 8.1 • The plane of the five-chamber view on the fetal body (**a**) and on a heart diagram (**b**). *AoV* aortic valve, *MV* mitral valve, *PV* pulmonary valve, *TV* tricuspid valve
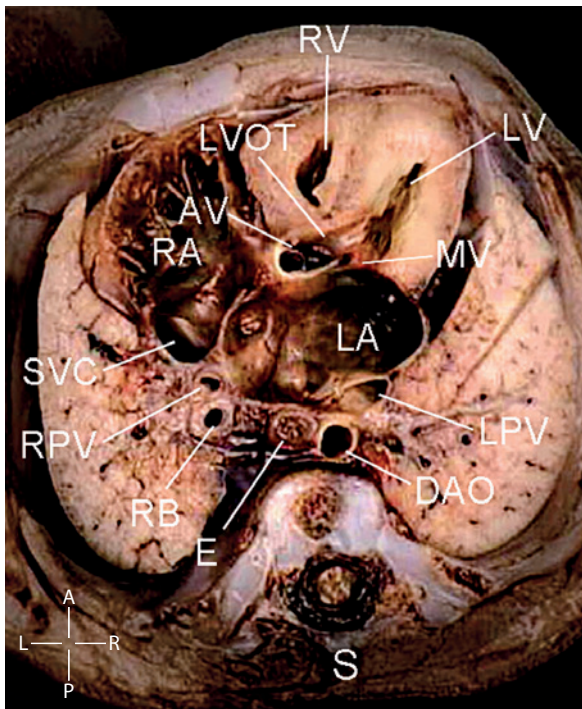
Fig. 8.2 • The five-chamber view is imitated in this specimen, viewed from below. The left ventricular outflow tract and the aortic valve are seen in the center of the heart. This figure illustrates how the inflow, the outflow, and the trabecular part of the left ventricle are included in this view, whereas only a minor portion of the trabecular part of the right ventricle is seen anteriorly. Posteriorly, the roof of both atria is shown. The opening of the superior vena cava in the right atrium and the junction between the upper left and right pulmonary vein and the left atrium are visible. The descending aorta, the esophagus, and the right bronchus are seen in cross section between the posterior wall of the left atrium and the spine. *AV* aortic valve, *DAO* descending aorta, *E* esophagus, *LA* left atrium, *LPV* left pulmonary vein, *LPV* left pulmonary vein, *LV* left ventricle, *LVOT* left ventricular outflow tract, *MV* mitral valve, *RA* right atrium, *RB* right bronchus, *RPV* right pulmonary vein, *RV* right ventricle, *S* spine, *SVC* superior vena cava

Fig. 8.3 • This specimen of an isolated heart has been cut to imitate the five-chamber view. This image shows how this section involves the mitral valve through its anterior (or aortic) (*1*) and posterior (or mural) (*2*) leaflet, showing the inflow of the left ventricle from the left atrium. The left ventricular outflow tract is also seen, separated by its inflow only by the anterior leaflet of the mitral valve. The inlet portion of the right ventricle is not involved in this section, and only the distal portion of the septal (*3*) and the anterolateral (*4*) leaflet of the tricuspid valve is seen. The trabecular portion of both ventricles is displayed. This specimen also shows continuity between the ventricular septum and the anterior wall of the aortic root and the continuity between the anterior leaflet of the mitral valve and the posterior wall of this artery. *AAO* ascending aorta, *AV* aortic valve, *LA* left atrium, *LV* left ventricle, *LVOT* left ventricular outflow tract, *MV* mitral valve, *RA* right atrium, *RPA* right pulmonary artery, *RV* right ventricle, *TV* tricuspid valve

of the right ventricle are not seen because they are located more caudal to this plane. Anteriorly and to the left, the left ventricle with its three components (inlet, trabecular, and outlet) is displayed. More posteriorly, the junction of the two upper pulmonary veins with the left atrium and the junction of the superior vena cava with right atrium are seen. The descending aorta is displayed between the posterior wall of the left atrium and the spine (Fig. 8.4a).

In the five-chamber view, the continuity between the anterior leaflet of the mitral valve and the root of the aorta is demonstrated. Moreover, this view is

particularly useful to assess the continuity between the outlet portion of the interventricular septum and the aortic root anteriorly (Fig. 8.4b). In association with the long axis view of the left ventricle – which is more difficult to obtain – this echocardiographic projection can demonstrate ventricular septal defects in the subarterial position with or without arterial overriding [1-4].

In the normal heart, the aortic root has a rightward takeoff from the long axis of the heart . In the five-chamber view, there is a wide angle between the major axis of the aortic root and that of the ventricular
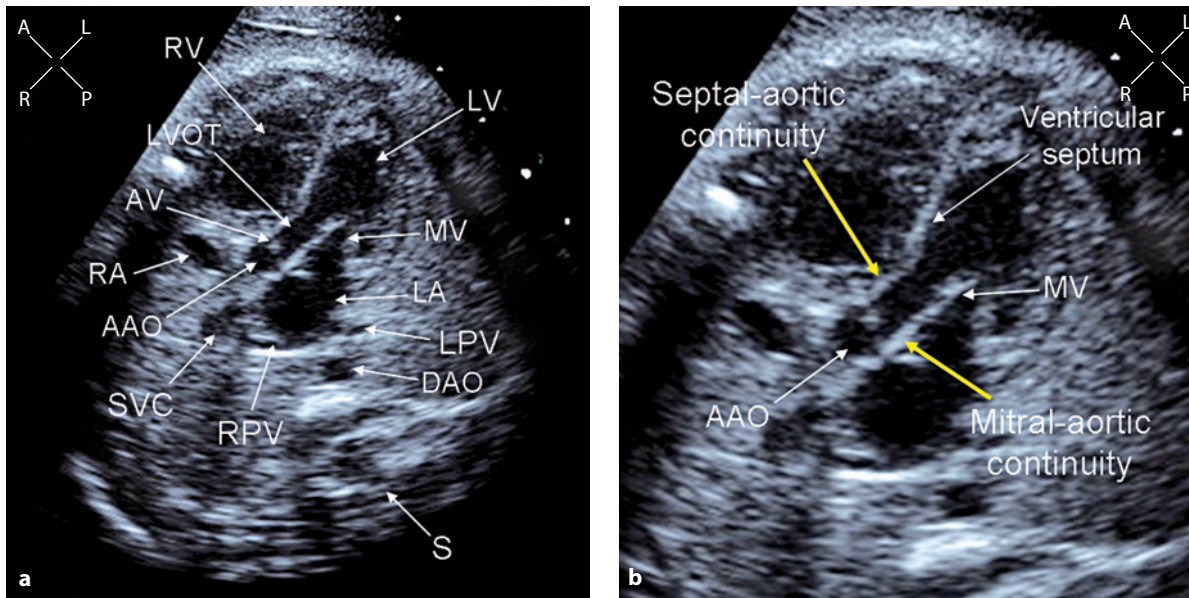
Fig. 8.4 • Cross-sectional five-chamber view in a normal 28-week gestational-age fetus (**a**). Most structures illustrated in the anatomical specimen of Figure 8.3 are seen. In a close-up view of the same image (**b**), the continuity between the outlet portion of the interventricular septum and the anterior wall of the aorta and the continuity between the anterior leaflet of the mitral valve and the posterior wall of the aorta are indicated (*yellow arrows*). *AAO* ascending aorta, *AV* aortic valve, *DAO* descending aorta, *LA* left atrium, *LPV* left pulmonary vein, *LV* left ventricle, *LVOT* left ventricular outflow tract, *MV* mitral valve, *RA* right atrium, *RPV* right pulmonary vein, *RV* right ventricle, *S* spine, *SVC* superior vena cava

septum. In complete transposition of the great arteries, this orientation is missed, and the major axis of the pulmonary artery, committed to the left ventricle, is almost parallel to the long axis of the ventricular septum [5] (Fig. 8.5).

The Normal Echocardiogram – Color Flow Mapping and Pulsed Doppler

With apical presentation, the five-chamber cut is ideal for Doppler and color Doppler assessment of the inflow and the outflow of the left ventricle. This view is useful for assessing the mitral valve, the left ventricular outflow, and the aortic valve (Fig. 8.6).

In this view, both diastolic inflow across the mitral valve and systolic outflow toward the aorta may be sampled by placing the sample volume in between the ventricular septum and the anterior leaflet of the mitral valve (Fig. 8.7a). This is a powerful tool for fetal heart rhythm assessment. For better results, the sample volume is kept intentionally more ample, between 5 and 10 mm. The atrial rate is indicated by the frequency of the A waves in the transmitralic inflow spectrum and the ventricular rate by the frequency of the V waves in the outflow spectrum from the left ventricle [6] (Fig. 8.7b). Two examples of arrhythmias assessed with this method are shown in Figure 8.8.

The five-chamber view is ideal for investigating obstructions to the left ventricular outflow at the valvular or subvalvular level. Two examples are shown in Figures 8.9, 8.10.

When a ventricular septal defect is detected in the subarterial position, this projection is not sufficient to precisely assess the type of ventriculoarterial connection (Figs. 8.11-8.14). In fact, similar images can be obtained in different cardiac malformations as isolated malalignment ventricular septal defect and tetralogy of Fallot with or without pulmonary atresia [7-9]. Moreover, because of the oblique orientation of this view, the degree of arterial overriding is best evaluated in the long-axis view of the left ventricle.
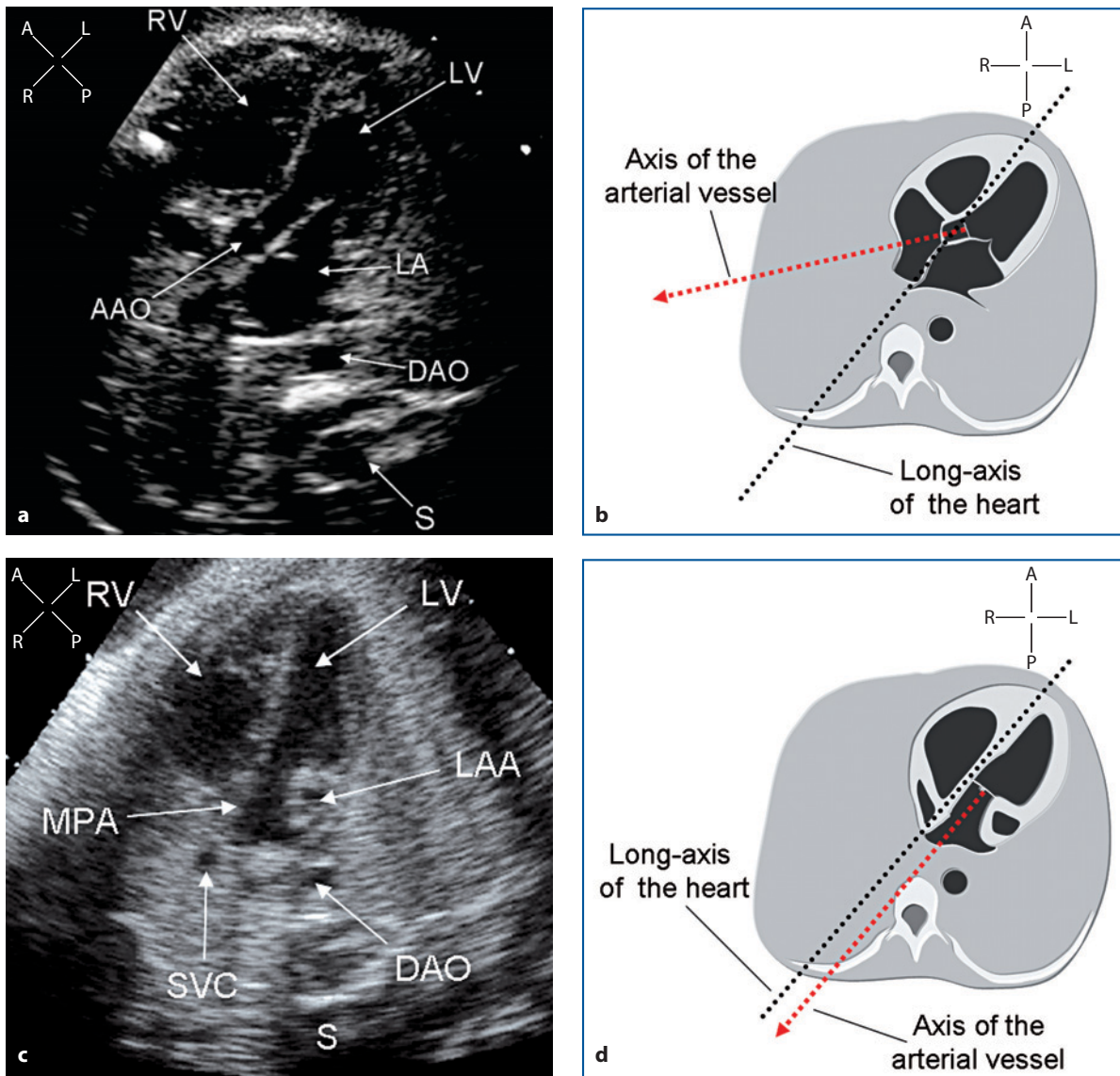
Fig. 8.5 • Cross-sectional view and a correlative diagram in a normal heart (**a**, **b**) and in transposition of the great arteries (**c**, **d**). The *black dashed line* indicates the long axis of the ventricular septum (and of the heart), whereas the *red dashed line* indicates the long axis of the arterial root connected with the left ventricle. In the normal heart, the major axis of the heart and that of the arterial vessel cross with a wide angle. In transposition of the great arteries, the major axis of the arterial vessel is nearly parallel to that of the heart. The pulmonary artery is recognized from its early bifurcation. *AO* ascending aorta, *DAO* descending aorta, *LAA* left atrial appendage *LV* left ventricle, *MPA* main pulmonary artery, *RV* right ventricle, *S* spine, *SVC* superior vena cava
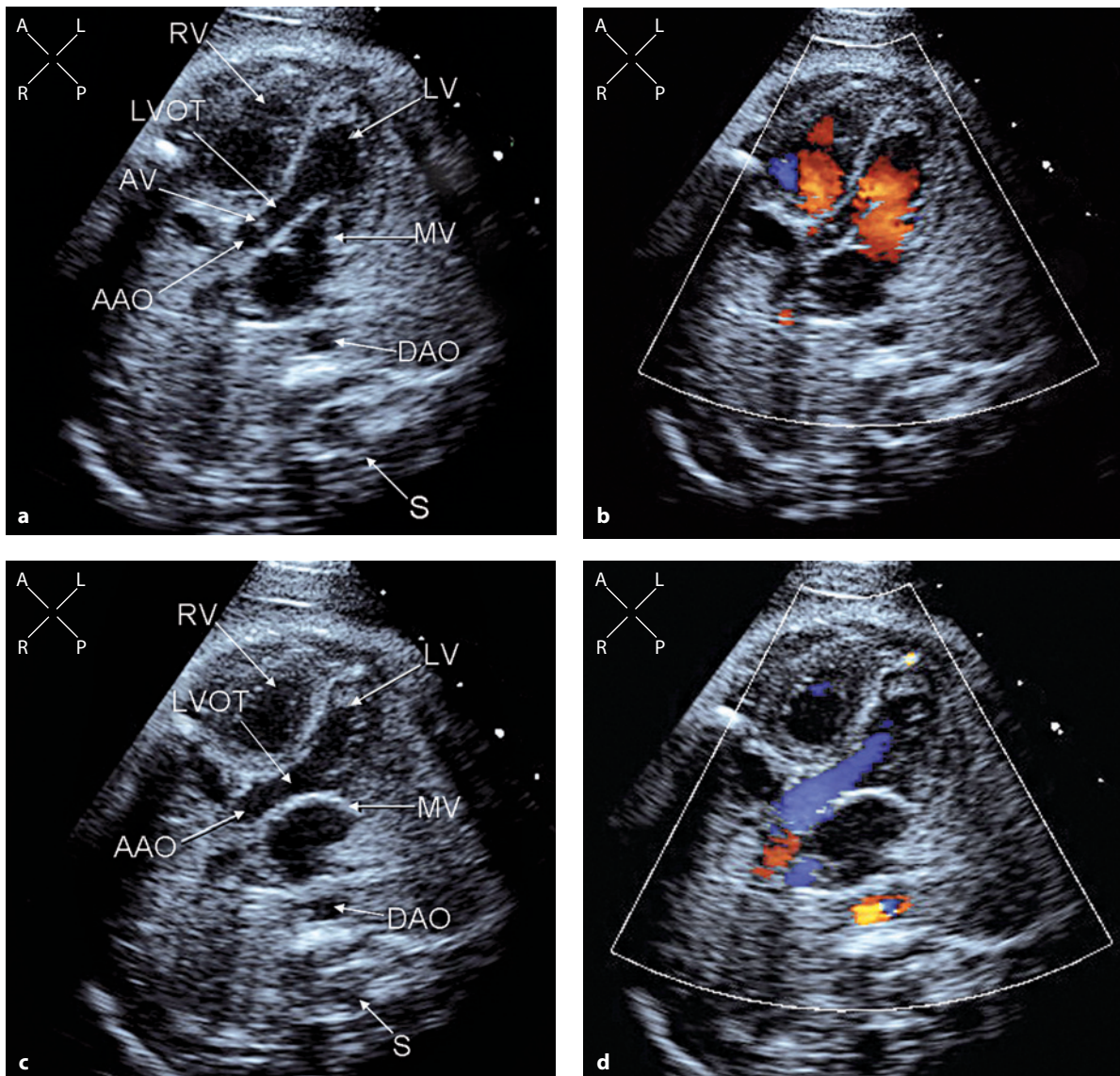
Fig. 8.6 • Cross-sectional and color flow mapping frames in apical presentation in a normal 22-week gestational-age fetus. The diastolic frames (**a**, **b**) show the opening of the mitral valve with filling of the left ventricle (*red*). There is no flow into the left ventricular outflow tract, and the aortic valve is closed. In the systolic frames (**c**, **d**), the mitral valve is closed, and the outflow from the left ventricle is seen, filling the root of the aorta (*blue*). *AAO* ascending aorta, *AV* aortic valve, *DAO* descending aorta, *LV* left ventricle, *LVOT* left ventricular outflow tract, *MV* mitral valve, *RV* right ventricle, *S* spine
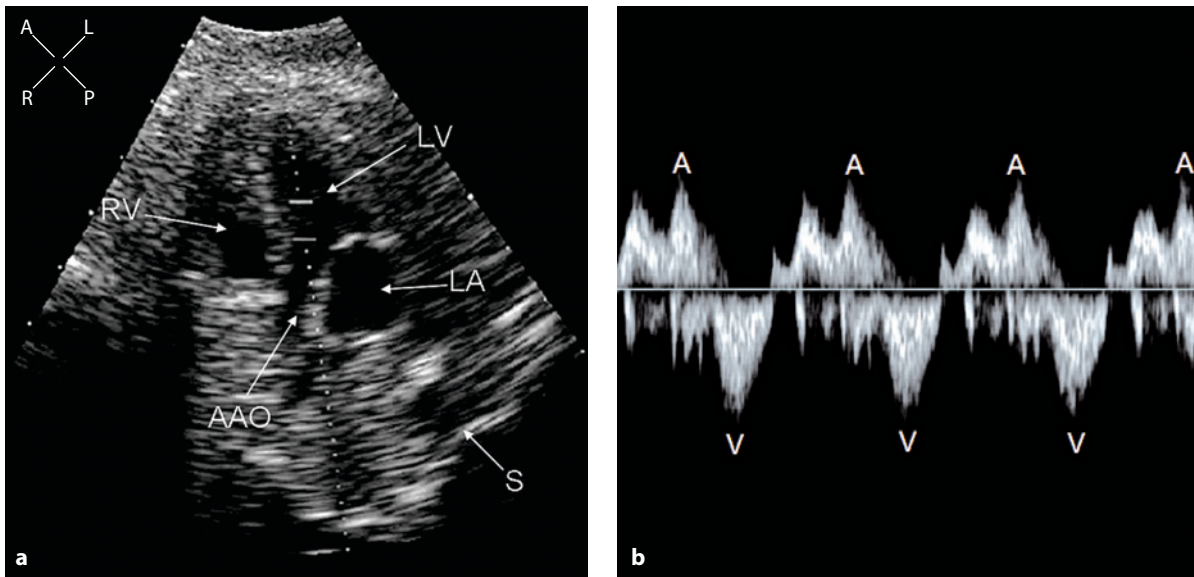
Fig. 8.7 • Cross-sectional view illustrating the position of the sample volume for Doppler assessment of the inflow-outflow of the left ventricle (**a**). Doppler tracing (**b**) shows, above the baseline, the inflow across the mitral valve, with the A waves (*A*) corresponding to atrial contractions. V waves (*V*), displayed below the baseline, correspond to the outflow from the left ventricle because of ventricular contractions. Because the rhythm of A waves is regular and every ventricular contraction is preceded by an atrial contraction, this is interpreted as normal sinus rhythm. *AAO* ascending aorta, *LA* left atrium, *LV* left ventricle, *RV* right ventricle, *S* spine
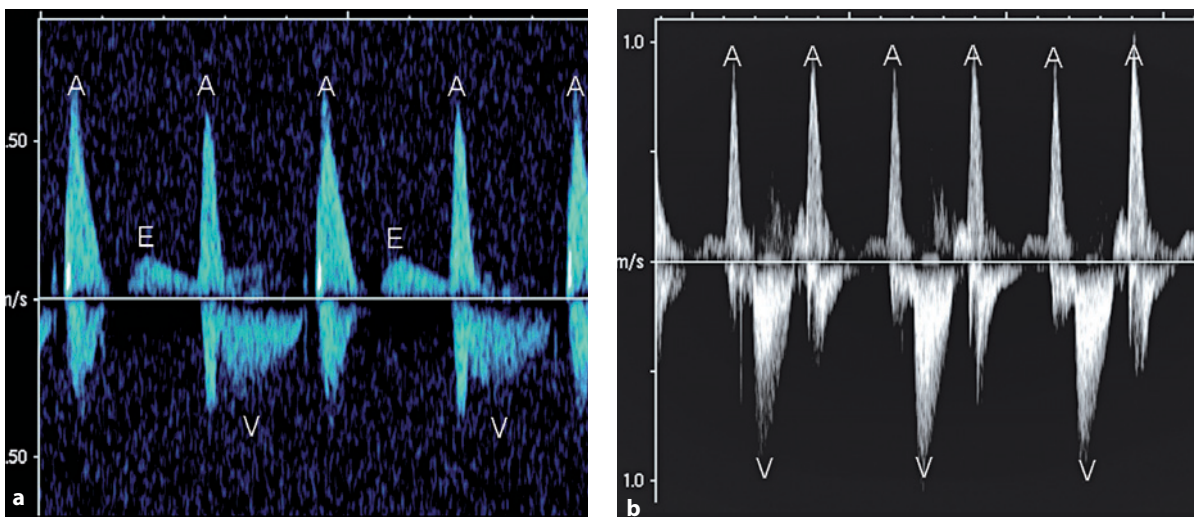
Fig. 8.8 • Inflow-outflow Doppler tracing of the left ventricle for fetal heart rhythm assessment. Bigeminal and blocked premature atrial contractions (**a**). The first, third, and fifth beats are anticipated, without early passive ventricular filling (*E*), and not followed by a ventricular contraction. Two to one atrioventricular block (**b**). The rhythm of atrial (*A*) and ventricular (*V*) contractions is regular, but every ventricular contraction is preceded by two regular atrial contractions
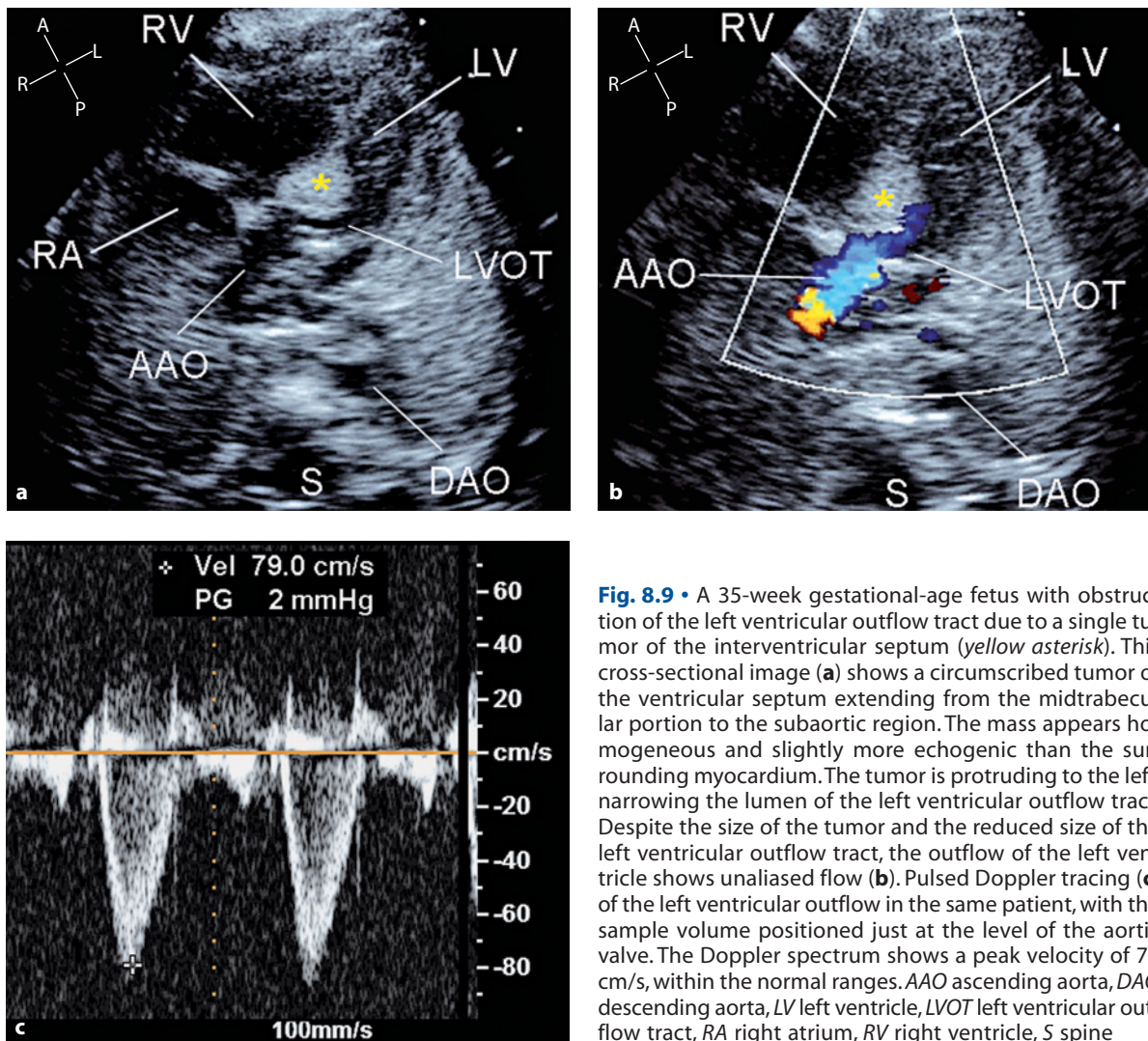
Fig. 8.9 • A 35-week gestational-age fetus with obstruction of the left ventricular outflow tract due to a single tumor of the interventricular septum (*yellow asterisk*). This cross-sectional image (**a**) shows a circumscribed tumor of the ventricular septum extending from the midtrabecular portion to the subaortic region. The mass appears homogeneous and slightly more echogenic than the surrounding myocardium. The tumor is protruding to the left, narrowing the lumen of the left ventricular outflow tract. Despite the size of the tumor and the reduced size of the left ventricular outflow tract, the outflow of the left ventricle shows unaliased flow (**b**). Pulsed Doppler tracing (**c**) of the left ventricular outflow in the same patient, with the sample volume positioned just at the level of the aortic valve. The Doppler spectrum shows a peak velocity of 79 cm/s, within the normal ranges. *AAO* ascending aorta, *DAO* descending aorta, *LV* left ventricle, *LVOT* left ventricular outflow tract, *RA* right atrium, *RV* right ventricle, *S* spine
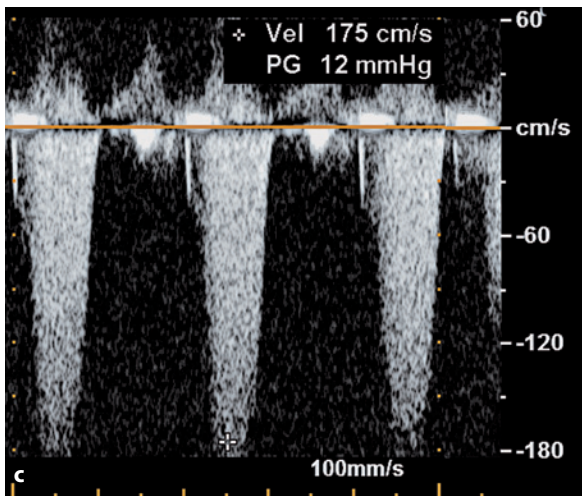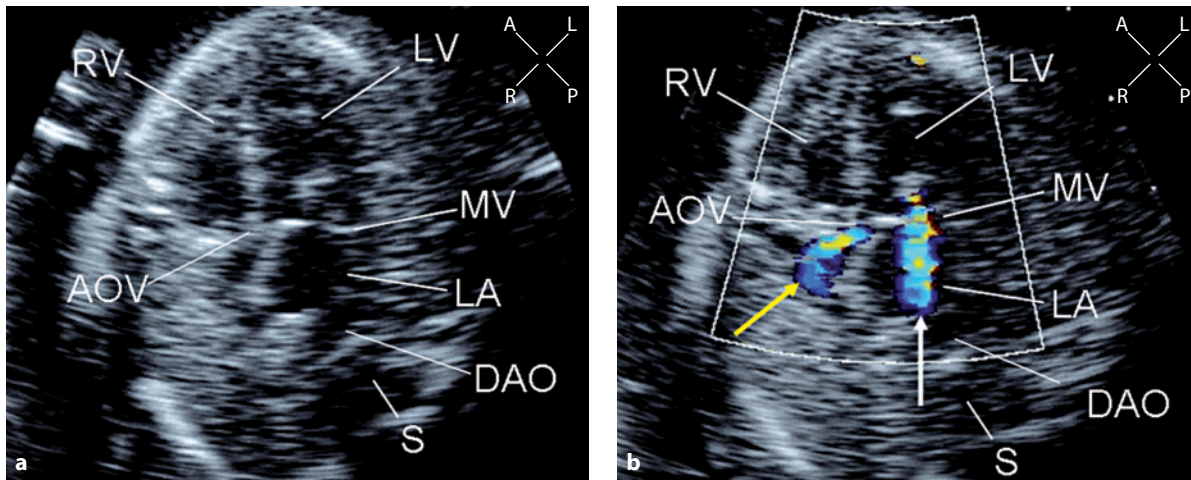
Fig. 8.10 • A 22-week gestational-age fetus with critical aortic stenosis. On cross-sectional view (**a**), the left chambers are moderately dilated. On moving images, the left ventricle shows a poor systolic function. The subvalvar apparatus of the mitral valve looks thickened and hyperechogenic because of endocardial fibroelastosis. The aortic valve is thickened and with fixed systolic doming. On color flow mapping (**b**), two different jets are distinguished: the anterograde flow through the stenotic aortic valve (*yellow arrow*) and the jet of mitral valve regurgitation (*white arrow*). Pulsed Doppler tracing (**c**) of the forward flow in the ascending aorta in the same case. The sample volume was placed in the jet above the plane of the aortic valve. Despite severe stenosis of this valve, a relatively low peak gradient (12 mmHg) is present because of the impaired systolic function of the left ventricle. *AOV* aortic valve, *DAO* descending aorta, *LA* left atrium, *LV* left ventricle, *MV* mitral valve, *RV* right ventricle, *S* spine
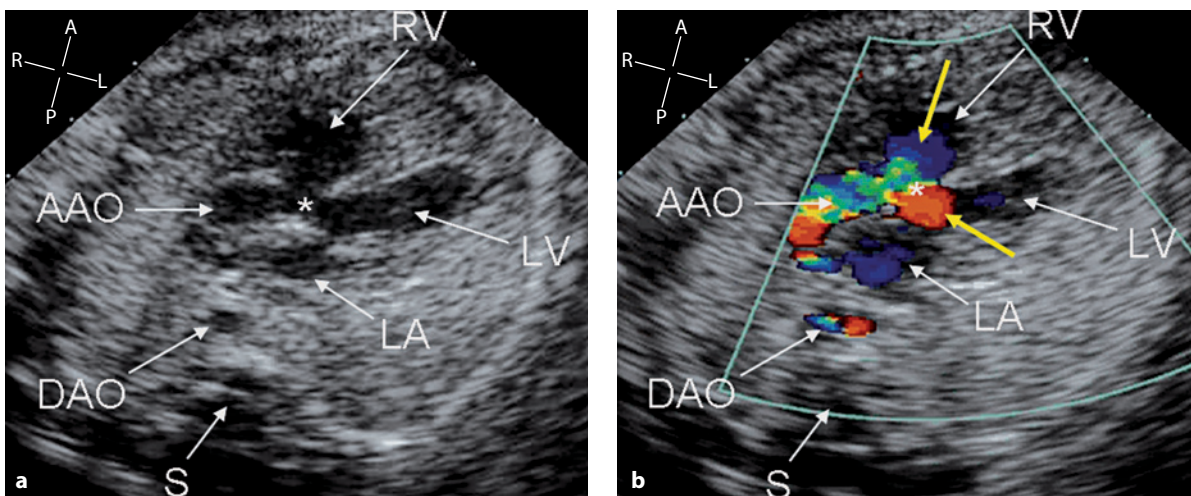
Fig. 8.11 • A 27-week gestational-age fetus with a classic type of tetralogy of Fallot. Subaortic ventricular septal defect (**a**) indicated by the *asterisk*; the aortic root overrides the crest of the interventricular septum. Posteriorly, the descending aorta is on the right side of the spine, anticipating a right-sided aortic arch. In the systolic frame with color flow mapping (**b**), the *two yellow arrows* indicate ejection of blood from both ventricles into the aorta. Because of the different orientation of the outflows relative to the ultrasound beam, the flow out from the right ventricle is represented in *blue*, whereas that from the left ventricle is represented in *red*. *AAO* ascending aorta, *DAO* descending aorta, *LA* left atrium, *LV* left ventricle, *RV* right ventricle, *S* spine
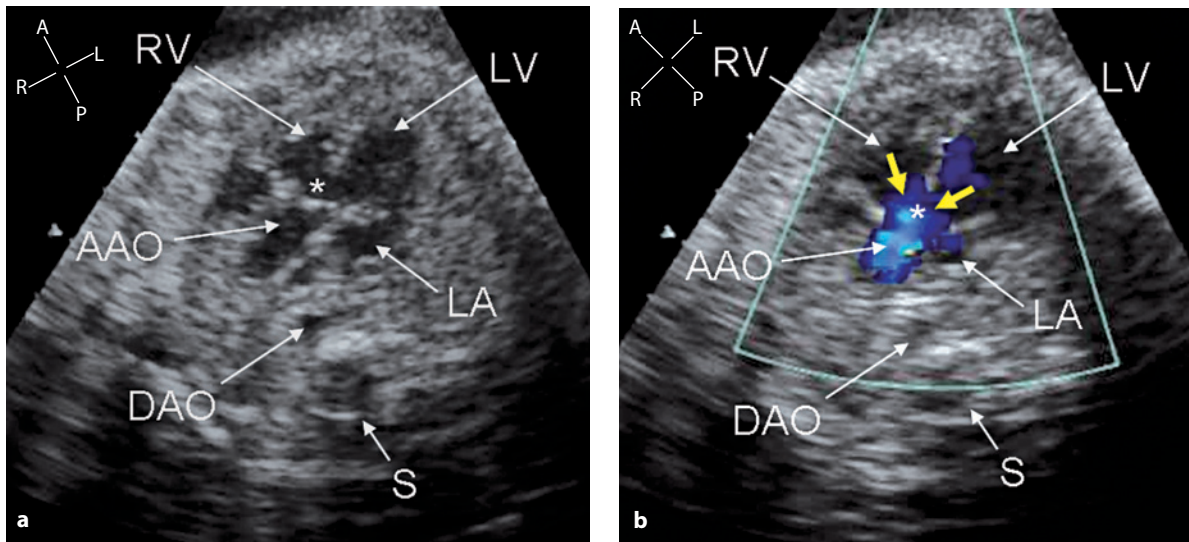
Fig. 8.12 • A 31-week gestational-age fetus with tetralogy of Fallot and pulmonary atresia. Tetralogy of Fallot with pulmonary atresia cannot be distinguished from classic tetralogy in this view (**a**). The cross-sectional picture shows a large subaortic ventricular septal defect (*asterisk*) with an oversized overriding aorta. The descending aorta is on the right anterior side of the spine due to a right-sided aortic arch. On color flow mapping (**b**), the ejection of blood into the aortic root from both ventricles is demonstrated (*yellow arrows*). Because of the similar orientation of the outflows relative to the ultrasound beam, the flow is represented in *blue* in both the right and left ventricles. *AAO* ascending aorta, *DAO* descending aorta, *LA* left atrium, *LV* left ventricle, *RV* right ventricle, *S* spine
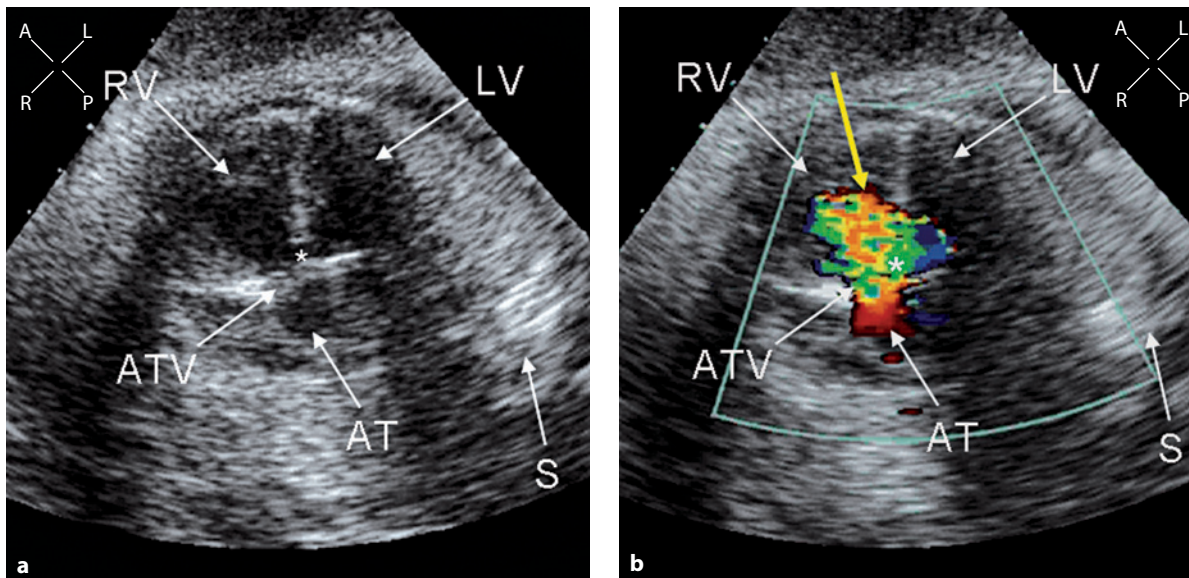
Fig. 8.13 • A 37-week gestational-age fetus with common arterial trunk. On cross-sectional examination (**a**), a subarterial ventricular septal defect (*asterisk*) is seen. There is a large arterial root that overrides the defect and appears mostly committed to the right ventricle. On moving images, the arterial valve looks thickened, with discrete systolic opening. This diastolic frame on color flow examination (**b**) shows severe regurgitation of the arterial valve into the right ventricle. *AT* arterial trunk, *ATV* arterial trunk valve, *LV* left ventricle, *RV* right ventricle, *S* spine
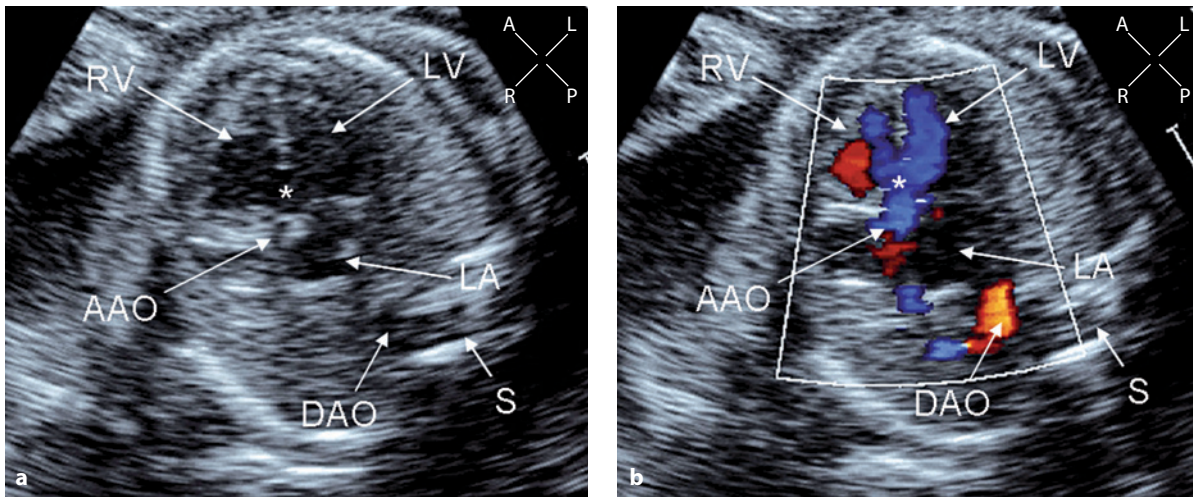
Fig. 8.14 • A 23-week gestational-age fetus with posterior malalignment ventricular septal defect. This defect is associated with interruption of the aortic arch and right aortic arch. On cross-sectional examination (**a**), both ventricles are well represented and in normal position. There is a large subarterial ventricular septal defect (*asterisk*). The arterial root looks small, as does the anulus of its semilunar valve. The descending aorta is on the right side of the spine, anticipating a right aortic arch. Color flow assessment (**b**) confirms a small anterograde flow through the arterial root and the sidedness of the descending aorta. *AAO* ascending aorta, *DAO* descending aorta, *LA* left atrium, *LV* left ventricle, *RV* right ventricle, *S* spine

References

1. Yoo SJ, Lee YH, Cho KS et al (1999) Sequential segmental approach to fetal congenital heart disease. Cardiol Young 9:430-444

2. Allan LD (2000) A practical approach to fetal heart scanning. Semin Perinatol 24:324-330

3. Barboza JM, Dajani NK, Glenn LG et al (2002) Prenatal diagnosis of congenital cardiac anomalies: a practical approach using two basic views. Radiographics 22:1125-1137

4. Sivanandam S, Glickstein JS, Printz BF et al (2006) Prenatal diagnosis of conotruncal malformations: diagnostic accuracy, outcome, chromosomal abnormalities, and extracardiac anomalies. Am J Perinatol 23:241-245

5. De Geeter B (2004) renatal diagnosis of transposition of great vessels. Arch Mal Coeur Vaiss 97:580-581

6. Steinfeld L, Rappaport H, Rossbach H et al (1986) Diagnosis of fetal arrhythmias using echocardiographic and Doppler techniques. J Am Coll Cardiol 8:1425-1433

7. Yoo SJ, Lee YH, Kim ES et al (1999) Tetralogy of Fallot in the fetus: findings at targeted sonography. Ultrasound Obstet Gynecol 14:29-37

8. Pepas LP, Savis A, Jones A et al (2003) An echocardiographic study of tetralogy of Fallot in the fetus and infant. Cardiol Young 13:240-247

9. Tongsong T, Sittiwangkul R, Chanprapaph P et al (2005) Prenatal sonographic diagnosis of tetralogy of Fallot. J Clin Ultrasound 33:427-431

The Three-Vessel View

Introduction

The three-vessel view is a transverse view of the fetal upper thorax. It can be obtained by sliding the scanning plane cephalad from the four-chamber view toward the fetal upper mediastinum. Obtaining this view is easy to teach and to learn, as its sonographic plane is orthogonal to the fetal body long axis. Because most of the significant lesions involving the ventricular outflow tracts and/or great arteries show an abnormal three-vessel view, this section is proposed as an alternative to the examination of the ventricular outflow tracts [1-8]. In Figure 9.1, the level of this section on the fetal body and on a heart diagram is illustrated.

The Normal Morphology

In the normal heart, the pulmonary trunk is the largest vessel and most anterior and to the left. The superior vena cava is the smallest vessel and most posterior and to the right. The ascending aorta is in between. The three-vessel view normally shows an oblique section of the pulmonary trunk and a round cross section of the ascending aorta and superior vena cava.

The right pulmonary artery arises almost at a right angle from the main pulmonary artery and runs behind the ascending aorta and superior vena cava to reach the hilum of the right lung. The left pulmonary artery arises as an extension of the main pulmonary
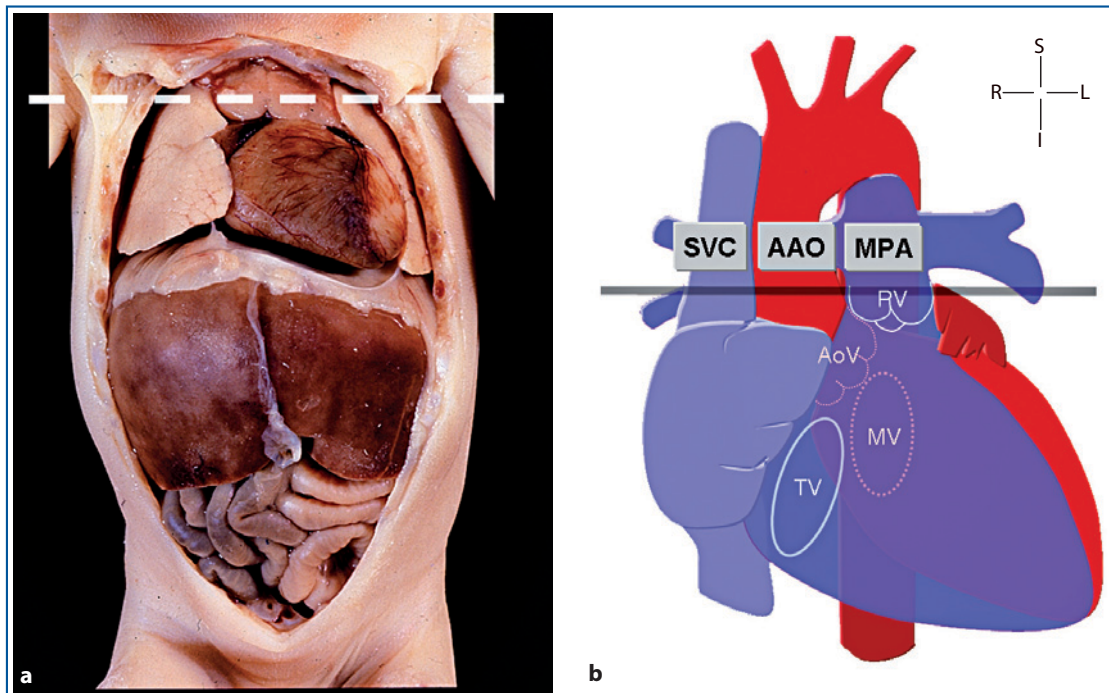
Fig. 9.1 • The level of the three-vessel view is shown on the fetal body (**a**) and on a heart diagram (**b**). Because of the crossing of the outflows, at the level of this section, the pulmonary artery is to the left of the ascending aorta. *AAO* ascending aorta, *AoV* aortic valve, *MPA* main pulmonary artery, *MV* mitral valve, *PV* pulmonary valve, *SVC* superior vena cava, *TV* tricuspid valve
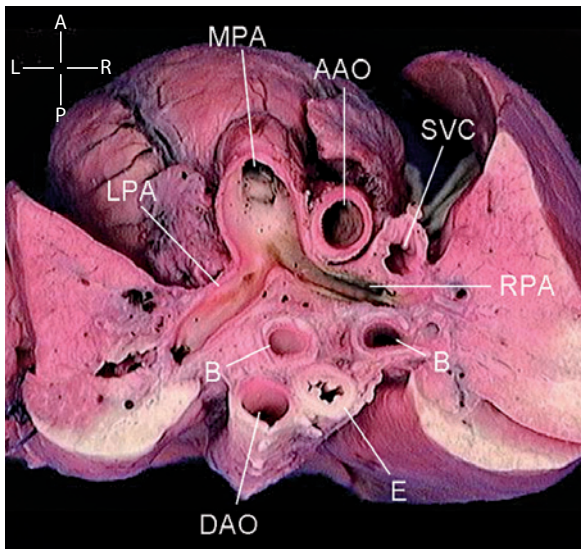
Fig. 9.2 • This anatomical specimen, viewed from above, is sectioned to imitate the three-vessel plane. *Anteriorly* and to the *left*, the oblique section of the main pulmonary artery is seen giving origin to its right and left branches. The right pulmonary artery is running behind the ascending aorta and the superior vena cava, which are seen in cross section. The superior vena cava is the vessel most posterior and to the right, whereas the ascending aorta is in between. In the posterior part of the mediastinum, the locations of the main stem bronchi, the esophagus, and the descending aorta are seen. *AAO* ascending aorta, *B* bronchus, *DAO* descending aorta, *E* esophagus, *LPA* left pulmonary artery, *MPA* main pulmonary artery, *RPA* right pulmonary artery, *SVC* superior vena cava

Fig. 9.3 • Echocardiographic frame of the three-vessel view in a normal 28-week gestational-age fetus (in caudocranial orientation). All the structures are labeled in the same fashion as in the anatomical specimen. In the normal fetus, the esophagus is usually difficult to identify with ultrasound because of its virtual lumen. Here the normal azygos vein in cross section lying in the right paravertebral position is seen. *AzV* azygos vein, *AAO* ascending aorta, *B* bronchus, *DAO* descending aorta, *E* esophagus, *LPA* left pulmonary artery, *MPA* main pulmonary artery, *RPA* right pulmonary artery, *S* spine, *SVC* superior vena cava

artery, lying on a more sagittal plane. In the posterior part of the mediastinum, seen in cross section, are the two main-stem bronchi, the descending aorta, and the esophagus (Fig. 9.2).

The Normal Echocardiogram – 2D

In this view, the normal echocardiogram shows the main pulmonary artery, the ascending aorta, and the superior vena cava aligned along an oblique line and in decreasing order of their diameter. The main pulmonary artery is the largest vessel, most anterior and to the left, and the superior vena cava, with the smallest diameter, is the vessel most posterior and to the right. The ascending aorta is of intermediate size and is seen in between. To visualize the bifurcation of the main trunk into its right and left pulmonary arteries, as in this example, a slight caudal and to the left angulation of the scan plane is usually necessary. The descending aorta is displayed on the left posterior side of the spine. With high-resolution ultrasound, the two main-stem bronchi are frequently seen in the posterior mediastinum and the normal azygos vein on the

right anterior side of the spine. Due to its virtual lumen in the normal fetus, the esophagus is usually difficult to identify by ultrasound (Fig. 9.3).

Normal ranges for diameters of the three vessels throughout gestation have been published [6, 8]. However, as a practical rule, to assess the anomalies of vessel size, the ascending aorta is defined as small if its diameter is equal to or smaller than the diameter of the superior vena cava or is smaller than the diameter of the descending aorta in the same image. The pulmonary artery is considered small if its diameter is equal to or smaller than the diameter of the ascending aorta. Diagrams in Figure 9.4 illustrate how spatial alignment, size, and shape of the three vessels are assessed in this view.

The Normal Echocardiogram – Color Flow Mapping and Pulsed Doppler

The usefulness of the three-vessel view is limited in assessing the flow with color flow mapping. When this section is truly horizontal, the superior vena ca-
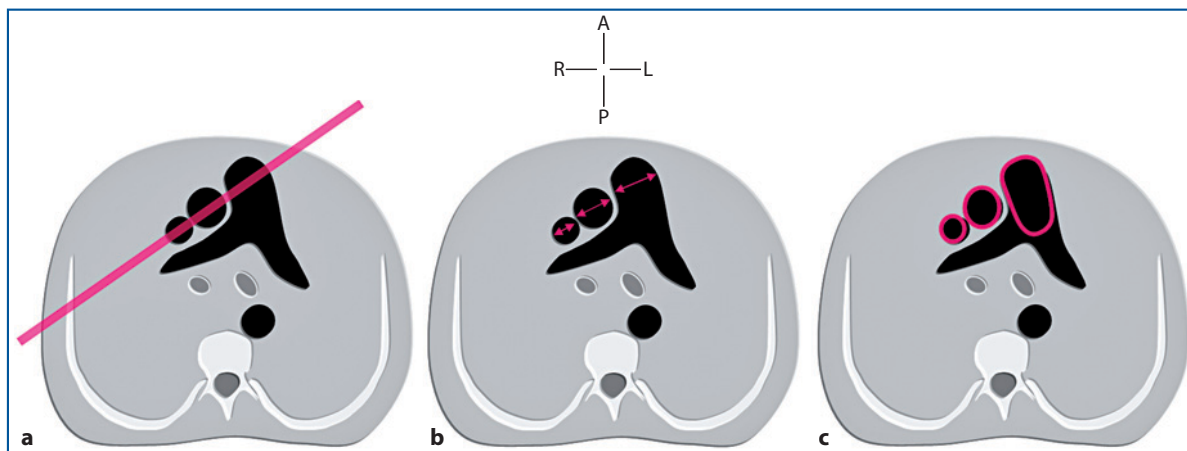
Fig. 9.4 • Diagrams in caudocranial orientation, illustrating how the spatial alignment (**a**), the relative size (**b**), and the different shape (**c**) of the pulmonary artery, ascending aorta, and superior vena cava can be assessed in this section

va and the ascending aorta are imaged at a right angle and therefore good color signal cannot be achieved. On the contrary, when this projection is obtained from an anterior approach to the fetal thorax, the main pulmonary artery is more parallel to the direction of the ultrasound beam, and its flow is easily shown on color flow mapping. With slight probe manipulation, the flow in the right and left pulmonary arteries is seen reaching the hilum of the respective lung (Fig. 9.5). Although Doppler assessment of the flow in the main pulmonary artery is achieved in this view, better control of the position of the cursor line and sample volume is obtained in sagittal or parasagittal view, as with the long-axis view of the arterial duct or the right ventricular outflow view, which will be described in the respective chapters. Conversely, the three-vessel view is ideal for Doppler study of the right pulmonary artery. Due to the anatomical orientation of this branch, parallel alignment of the ultrasound beam is best obtained with the lateral approach to the fetal thorax.

Fig. 9.5 • A normal 34-week gestational-age fetus. This systolic frame shows faint color in the ascending aorta and no color in the superior vena cava due to the unfavorable orientation of these vessels. On the contrary, the flow in the main pulmonary artery and its branches is clearly represented. *AzV* azygos vein, *AAO* ascending aorta, *B* bronchus, *DAO* descending aorta, *LPA* left pulmonary artery, *MPA* main pulmonary artery, *RPA* right pulmonary artery, *S* spine, *SVC* superior vena cava

Three-Vessel-View Abnormalities

According to Yoo and colleagues [1], abnormalities of the three-vessel view can be classified into four groups:
1. Abnormal vessel size: this occur because of enlarged or reduced size of one or more of the three vessels (Figs. 9.6-9.8).
2. Abnormal alignment, when the three vessels are not aligned in a straight line: abnormal vessel alignment occurs more commonly with subarterial ventricular septal defects of malalignment type, whether isolated or in the setting of tetral-

ogy of Fallot. Most of these defects are variably associated with anomalies of the vessel size (Figs. 9.9, 9.10). A very rare example of aorto-pulmonary window is shown in Figure 9.11.
3. Abnormal arrangement, when the normal left-to-right order of the three vessels is not preserved: this can occur in complete transposition, congenitally corrected transposition, and malposition
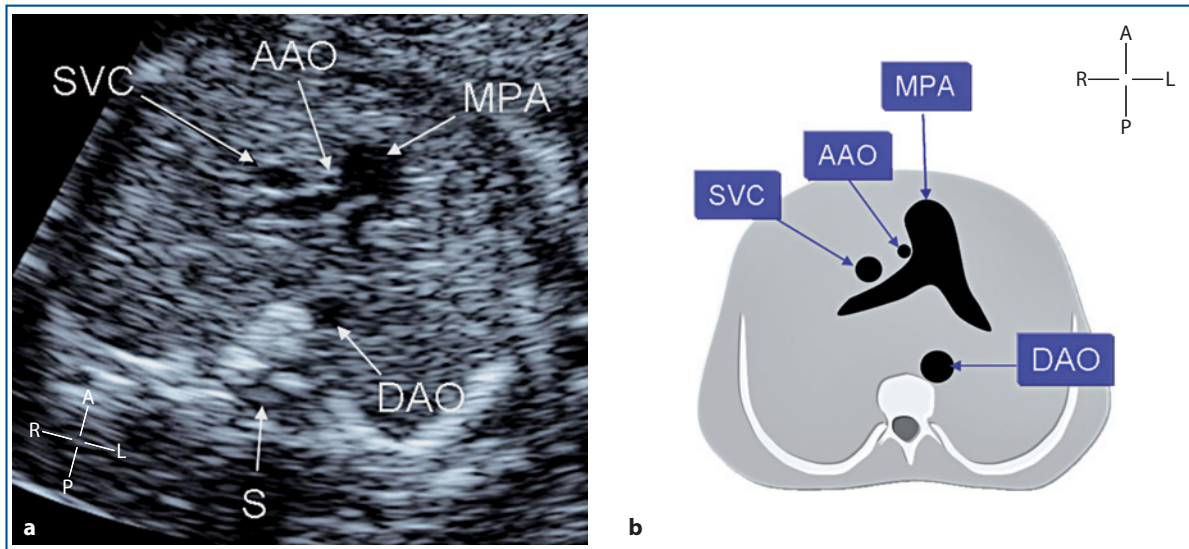
Fig. 9.6 • A 23-week gestational-age fetus with hypoplastic heart syndrome. The size of the ascending aorta is markedly inferior to that of the pulmonary artery and the superior vena cava. In second-trimester examinations, the vessel is often so small that it is difficult to identify, even on high-resolution ultrasound. *AAO* ascending aorta, *DAO* descending aorta, *MPA* main pulmonary artery, *S* spine, *SVC* superior vena cava
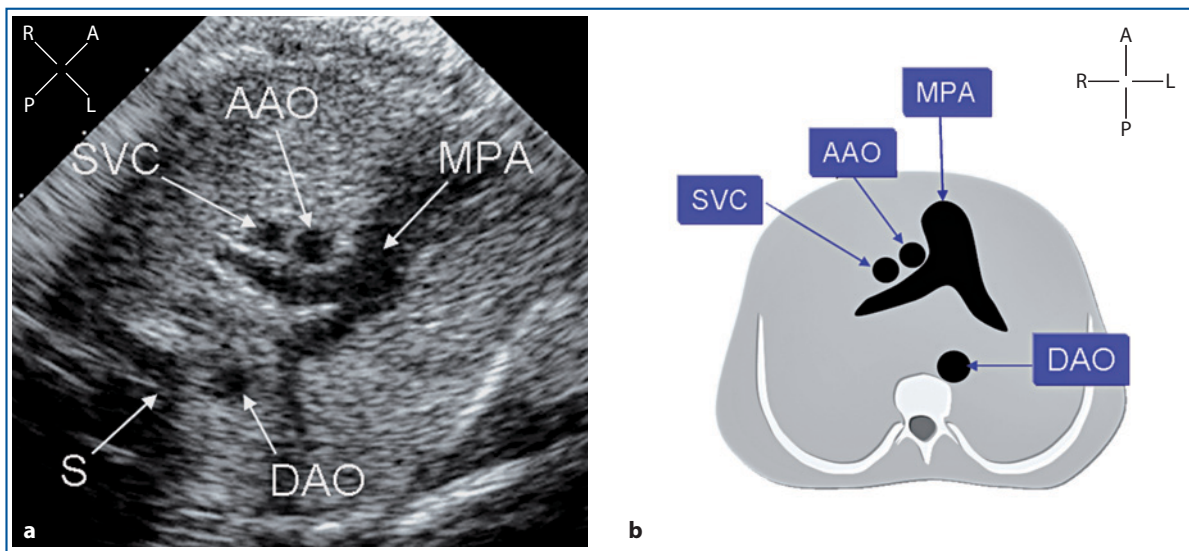
Fig. 9.7 • A 31-week gestational-age fetus with coarctation of the aorta. The size of the ascending aorta is relatively small and similar to that of the superior vena cava. Normal vessel alignment is maintained. *AAO* ascending aorta, *DAO* descending aorta, *MPA* main pulmonary artery, *S* spine, *SVC* superior vena cava

of the great artery, which is most commonly, although not exclusively, seen in double-outlet right ventricle (Figs. 9.12–9.14).

4. Abnormal vessel number, when the number of vessels is increased or decreased: this type of anomaly includes cases with only two or four vessels. Among the latter, the supernumerary vessel is more commonly a persistent left superior vena cava associated with a normal right superior vena cava. In rare cases, a dilated azygos vein or an anomalous venous channel can be noted, as in total anomalous venous connection of the supracardiac type. An example of each type is shown in Figures. 9.15–9.18.

The following figures show some examples of abnormalities of the three-vessel view in the different groups. Images are displayed in caudocranial presentation.
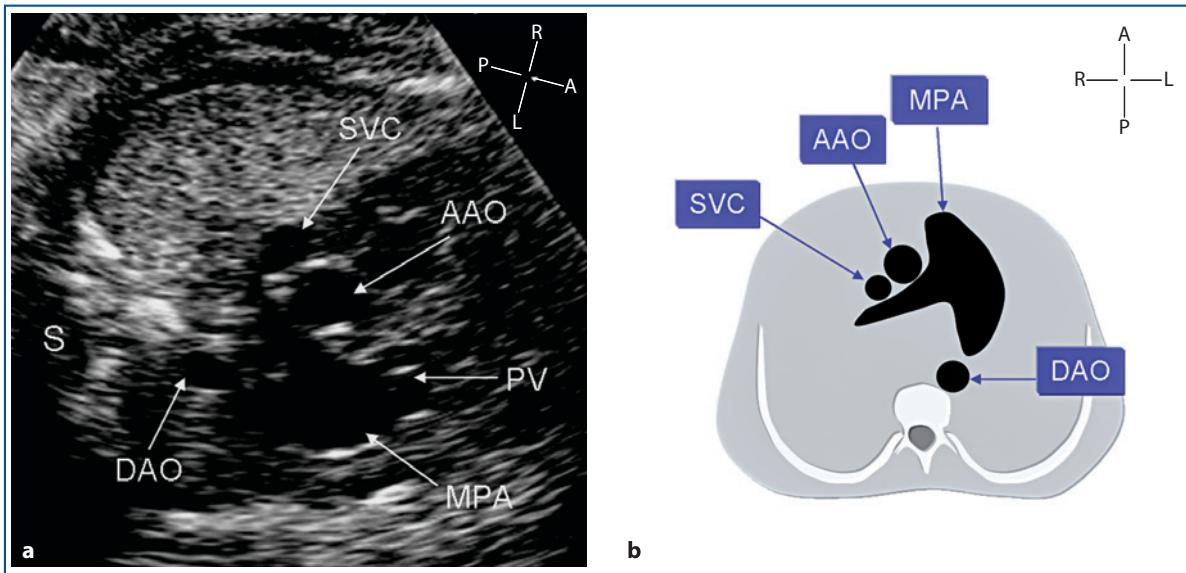
Fig. 9.8 • A 31-week gestational-age fetus with moderate stenosis of the pulmonary valve. Normal vessel alignment is maintained. The main pulmonary artery size is increased because of a poststenotic dilatation above the level of the pulmonary valve. *AAO* ascending aorta, *DAO* descending aorta, *MPA* main pulmonary artery, *PV* pulmonary valve, *S* spine, *SVC* superior vena cava
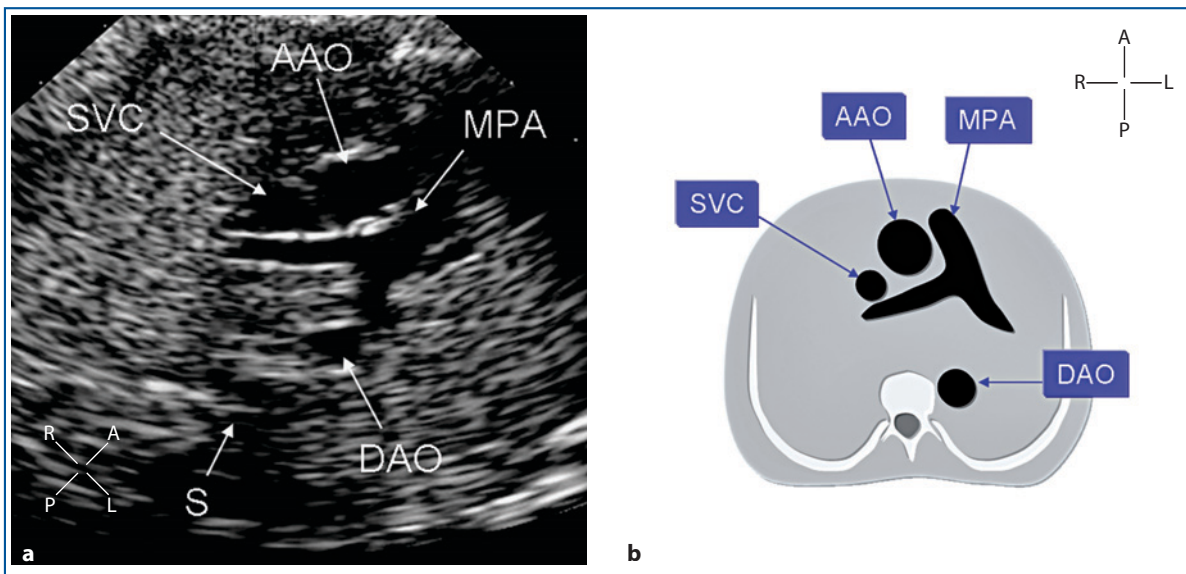
Fig. 9.9 • A 32-week gestational-age fetus with a "classic" type of tetralogy of Fallot. The size of the pulmonary artery is inferior to the size of the ascending aorta. The disproportion between the pulmonary artery and the aortic size is a useful means of predicting the severity of obstruction to the pulmonary flow. Interesting to note, there is also a certain degree of anteriorization of the ascending aorta. *AAO* ascending aorta, *DAO* descending aorta, *MPA* main pulmonary artery, *S* spine, *SVC* superior vena cava
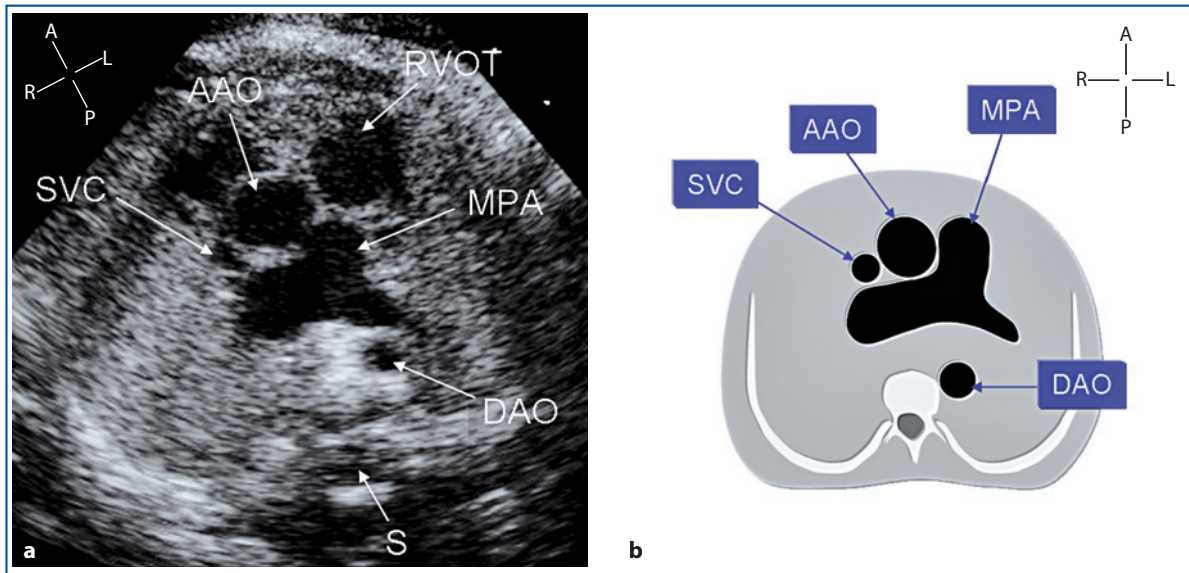
Fig. 9.10 • A 36-week gestational-age fetus with tetralogy of Fallot with "absent" pulmonary valve. The main pulmonary artery and its first branches show the characteristic aneurysmatic dilatation. The ascending aorta is also enlarged and anteriorly displaced. *AAO* ascending aorta, *DAO* descending aorta, *MPA* main pulmonary artery, *RVOT* right ventricular outflow tract, *S* spine, *SVC* superior vena cava
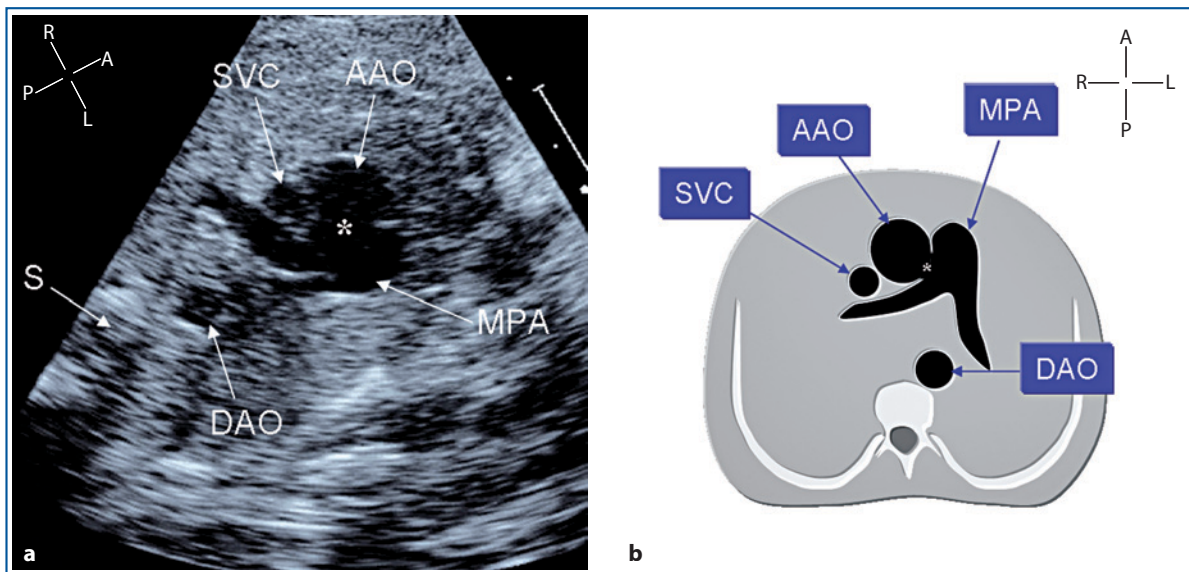
Fig. 9.11 • A 32-week gestational-age fetus with an aortopulmonary window. The ascending aorta is moderately dilated and more anterior and to the right than normal. There is lack of the normal wall separating the ascending aorta from the main pulmonary artery (*asterisk*). Both the great arteries show increased systolic pulsation on moving images. Associated interruption of the aortic arch cannot be anticipated from this view. *AAO* ascending aorta, *DAO* descending aorta, *MPA* pulmonary artery, *S* spine, *SVC* superior vena cava
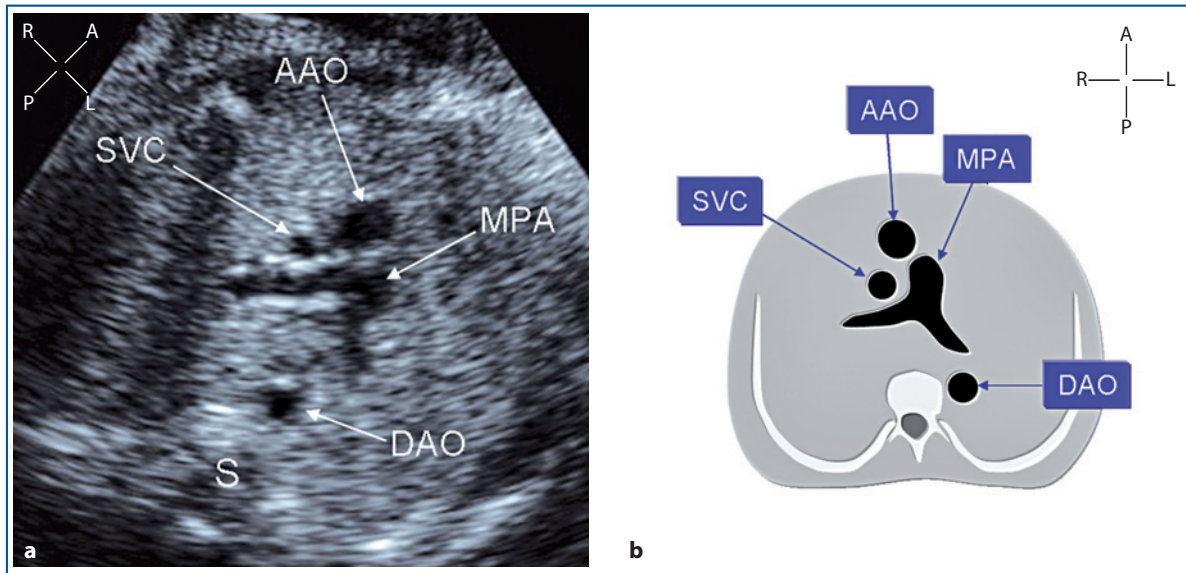
Fig. 9.12 • A 34-week gestational-age fetus with complete transposition of the great arteries (TGA). The ascending aorta is seen anteriorly and to the right relative to the main pulmonary artery. The three vessels appear "crowded" compared with the normal anatomical arrangement. In complete TGA, some exceptions can be found to the most common location of the great arteries shown in this case. *AAO* ascending aorta, *DAO* descending aorta, *MPA* main pulmonary artery, *S* spine, *SVC* superior vena cava

Fig. 9.13 • A 27-week gestational-age fetus with congenitally corrected transposition. The ascending aorta is the most anterior and to the left of the three vessels, whereas the main pulmonary artery is between the ascending aorta and the superior vena cava. *AAO* ascending aorta, *DAO* descending aorta, *MPA* main pulmonary artery, *S* spine, *SVC* superior vena cava
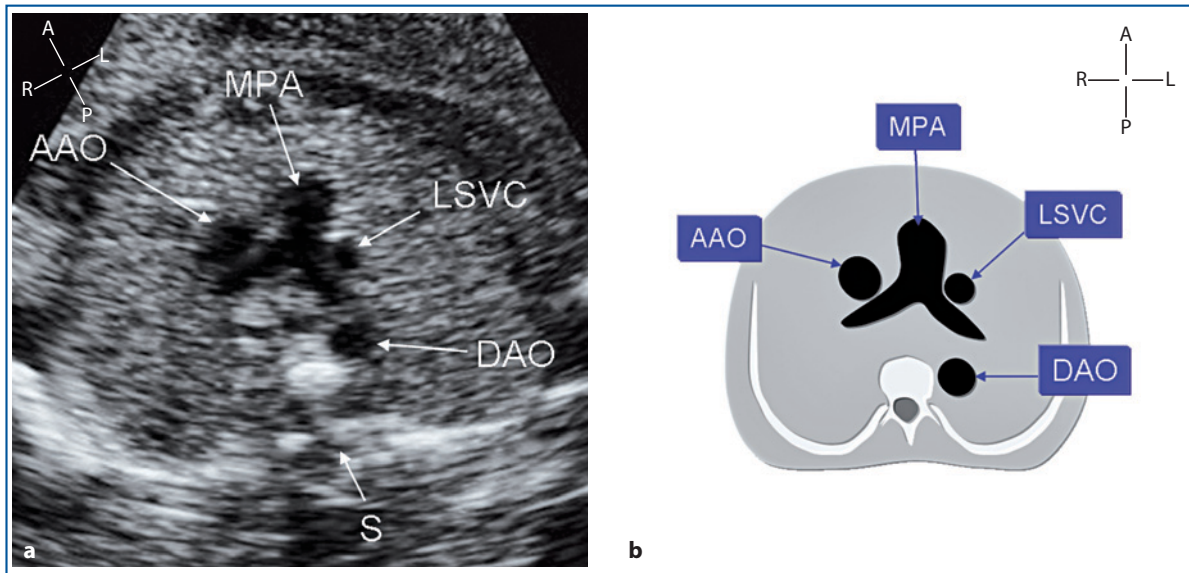
Fig. 9.14 • A 23-week gestational-age fetus who had persistent left superior vena cava with absence of the right superior vena cava. The relative size of the three vessels is normal, but their left-right order is distorted. The anomalous superior vena cava is seen to the left of the pulmonary artery. Double-outlet right ventricle is associated, but this anomaly cannot be anticipated from this view because the great arteries are normally related. *AAO* ascending aorta, *DAO* descending aorta, *LSVC* left superior vena cava, *MPA* main pulmonary artery, *S* spine

Fig. 9.15 • Three-vessel view in a 32-week gestational-age fetus with common arterial trunk. Only two vessels are seen: the large truncal root, which gives origin to the right pulmonary artery, and the superior vena cava. The left pulmonary artery is not seen because it originates in a more cranial plane. The position of the descending aorta on the right side of the spine predicts a right-sided aortic arch. *AT* arterial trunk, *DAO* descending aorta, *RAA* right atrial appendage, *RPA* right pulmonary artery, *S* spine, *SVC* left superior vena cava

Fig. 9.16 • A 32-week gestational-age fetus with abnormal vessel number due to the presence of a right superior vena cava and a persistent left superior vena cava. The supernumerary vessel is seen leftward of the pulmonary artery. The size of the ascending aorta is abnormally small, similar in size to one of the two vena cava. This fetus had postnatal confirmation of a complex type of coarctation, with tubular hypoplasia of the aortic arch. *AAO* ascending aorta, *DAO* descending aorta, *LSVC* left superior vena cava, *MPA* main pulmonary artery, *RSVC* right superior vena cava, *S* spine

Fig. 9.17 • A 35-week gestational-age fetus with total anomalous pulmonary venous connection of supracardiac type. An anomalous channel is easily identified behind the right pulmonary artery. This channel is a right vertical vein draining the confluence of the pulmonary veins upward into the superior vena cava via the left innominate vein. The superior vena cava is enlarged, draining the anomalous pulmonary venous return. The great arteries are malposed, with the ascending aorta anterior to the left of the pulmonary artery. The size of the pulmonary artery is slightly smaller than the ascending aorta, anticipating a certain degree of obstruction to the pulmonary flow. *AAO* ascending aorta, *DAO* descending aorta, *MPA* main pulmonary artery, *S* spine, *SVC* superior vena cava, *VV* vertical vein
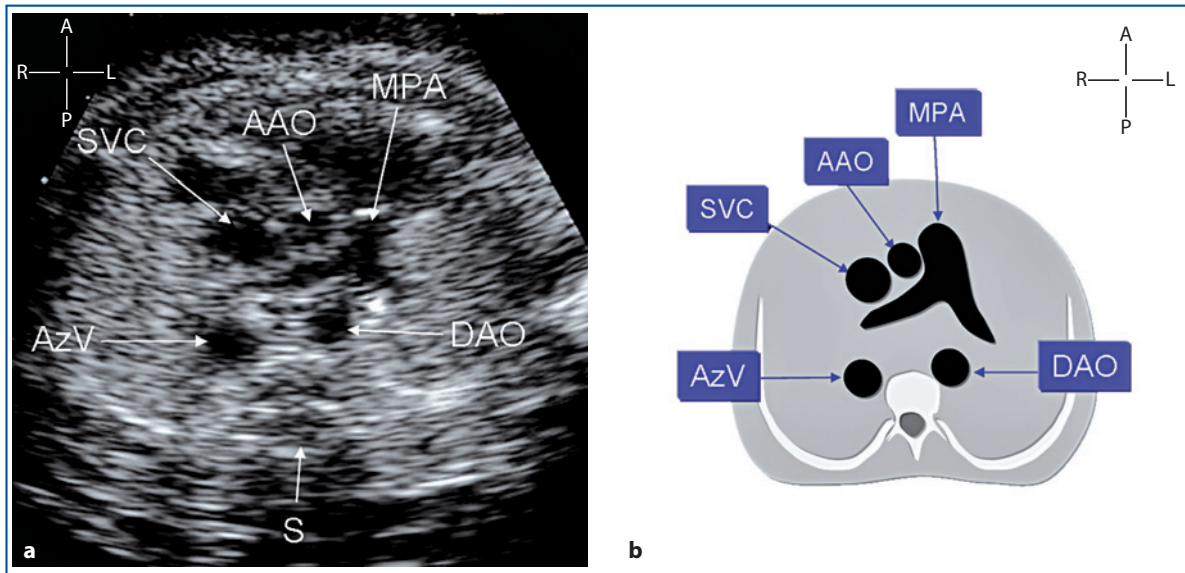
Fig. 9.18 • A 23-week gestational-age fetus in whom a persistent right umbilical vein drains anomalously into the superior vena cava via the azygos vein. This view shows the azygos vein as a large supernumerary vessel in right paravertebral position. The superior vena cava is severely enlarged because it is receiving (not seen in this view) the flow of the umbilical vein via the azygos vein. This is a rare case of anomalous drainage of the umbilical vein bypassing the liver. More commonly, a dilated azygos vein can be seen in cases with inferior vena cava interruption and azygos continuation. *AAO* ascending aorta, *AzV* azygos vein, *DAO* descending aorta, *MPA* main pulmonary artery, *S* spine, *SVC* superior vena cava

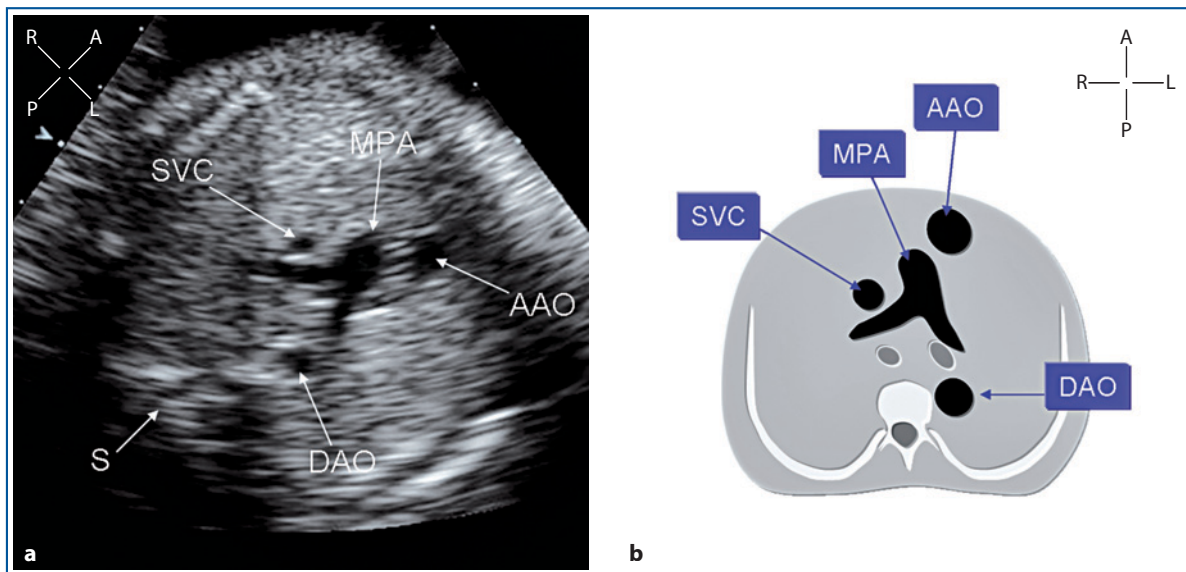## Ascending Aorta and Pulmonary Artery Disproportion

Independently from the type of alignment or arrangement, the disproportion between the size of the aorta and the pulmonary artery in the three-vessel view anticipates obstruction to the pulmonary or systemic outflow. Two examples with abnormal arrangement are shown in Figures 9.19, 9.20.

Aortic Arch Sidedness

The position of the descending aorta in the three-vessel view anticipates the laterality of the aortic arch. However the aortic arch sidedness is more easily assessed in the transverse view of the aortic arch. In Figures 9.15, 9.21b, two examples of right-sided aortic arch are illustrated. All other examples shown in this section have the aortic arch on the left side.

Relationship of the Great Arteries and Cardiac Connections

Normal relationship or malposition of the great arteries can occur in different types of atrioventricular and ventriculoarterial connections as double-outlet right ventricle, tricuspid atresia, or double-inlet left ventricle. Therefore, a similar pattern of three-vessel view can be seen with different types of congenital heart defects. The case in Figure 9.20, and that shown in Figure 9.22, are two example of this type. Despite different types of atrioventricular connections, both imitate the three-vessel-view aspect seen in complete transposition (Fig. 9.12).

In conclusion, the three-vessel view is very useful when anomalies of the ventriculoarterial connection are suspected. However, precise assessment of the type of connection cannot be predicted from this view but only through a complete sequential assessment of the heart.
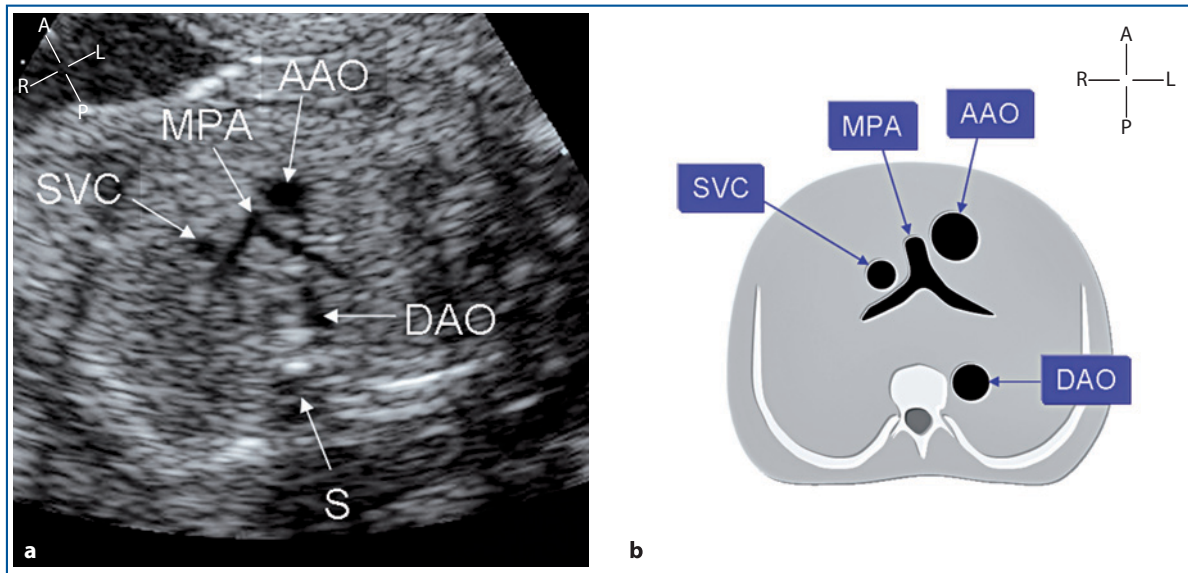
Fig. 9.19 • A 22-week gestational-age fetus with congenitally corrected transposition of the great arteries. The size of the pulmonary artery is markedly smaller than that of the ascending aorta, anticipating a severe obstruction to pulmonary flow. *AAO* ascending aorta, *DAO* descending aorta, *MPA* main pulmonary artery, *SVC* superior vena cava, *S* spine
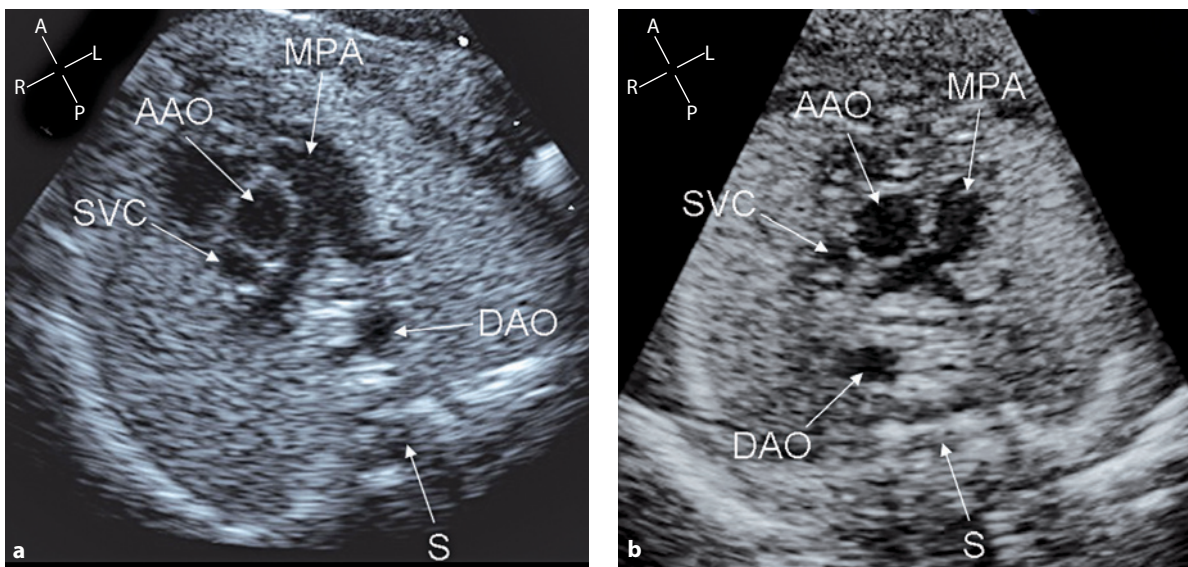
Fig. 9.20 • A normal case with left aortic arch (**a**) and a case of tetralogy of Fallot with right aortic arch (**b**). Tetralogy of Fallot is associated with right aortic arch in 25% of cases in postnatal series. Microdeletion of the chromosomal region 22q11 has been described more frequently in this setting. *AAO* ascending aorta, *DAO* descending aorta, *MPA* main pulmonary artery, *S* spine, *SVC* superior vena cava
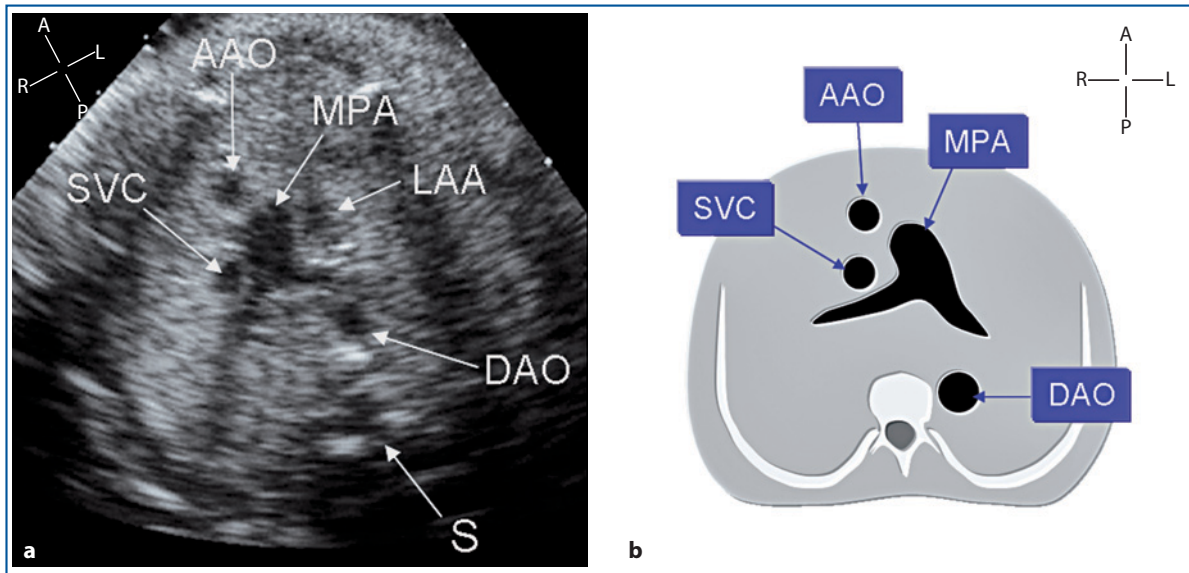
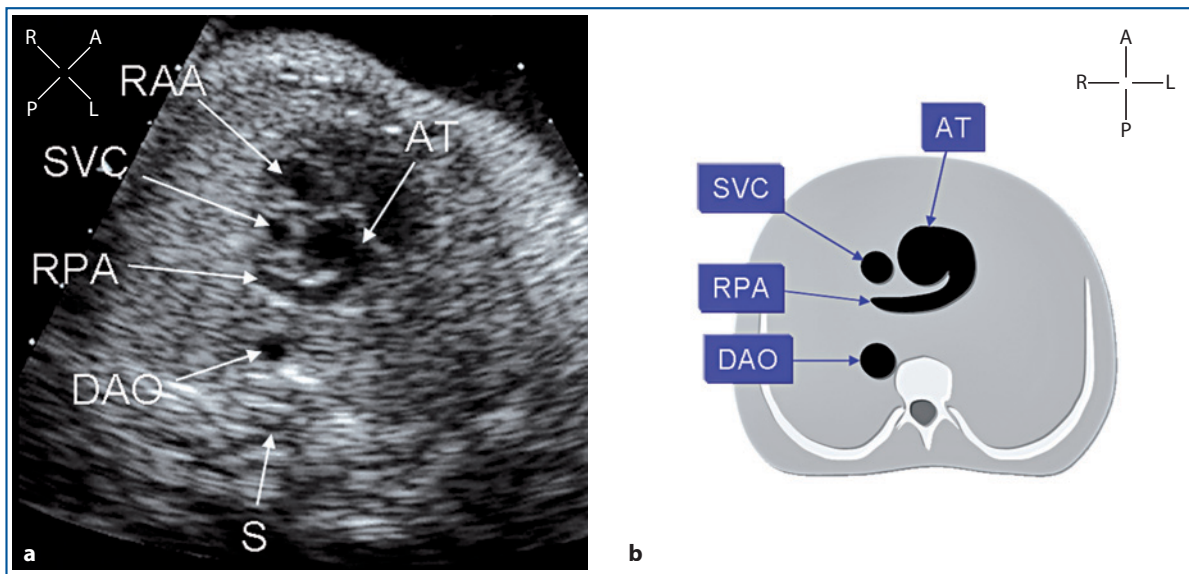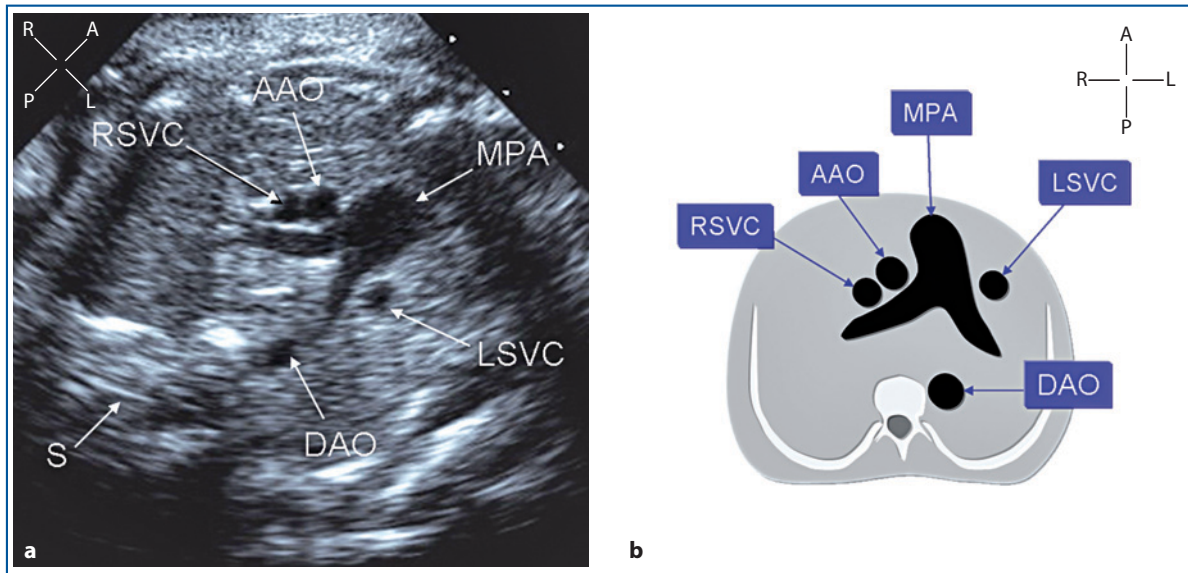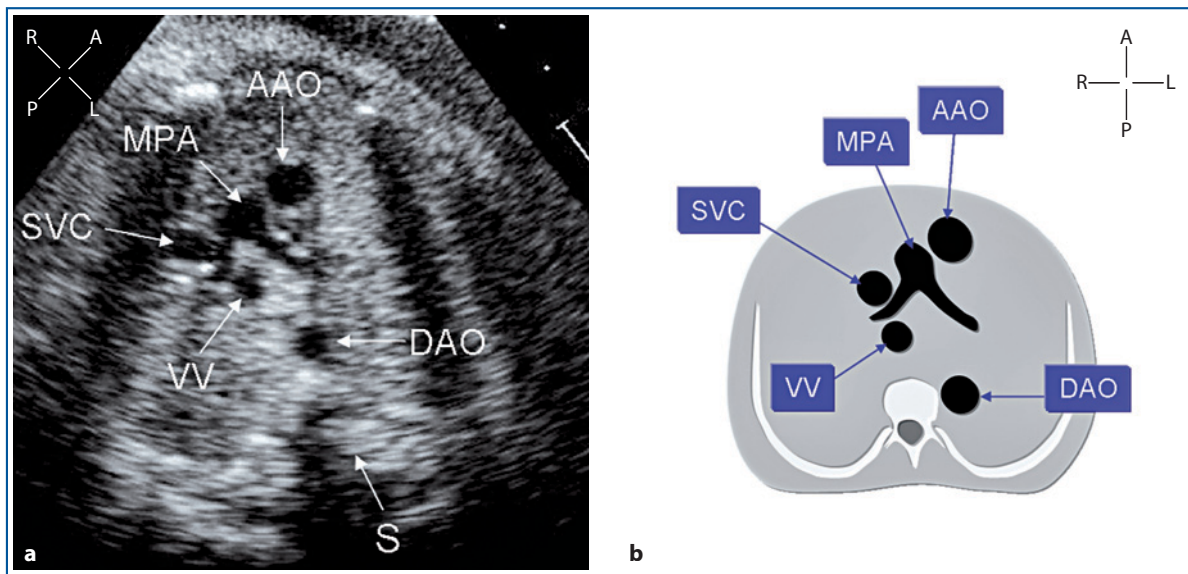**Fig. 9.21** • A 30-week gestational-age fetus with tricuspid atresia and discordant ventriculoarterial connection. The great arteries are malpositioned, with the ascending aorta anterior and to the right relative to the pulmonary artery. The size of the ascending aorta is small, similar to that of the superior vena cava, predicting obstruction to the systemic flow. This fetus had postnatal diagnosis of a complex type of aortic coarctation. *AAO* ascending aorta, *DAO* descending aorta, *LAA* left atrial appendage, *MPA* main pulmonary artery, *S* spine, *SVC* superior vena cava
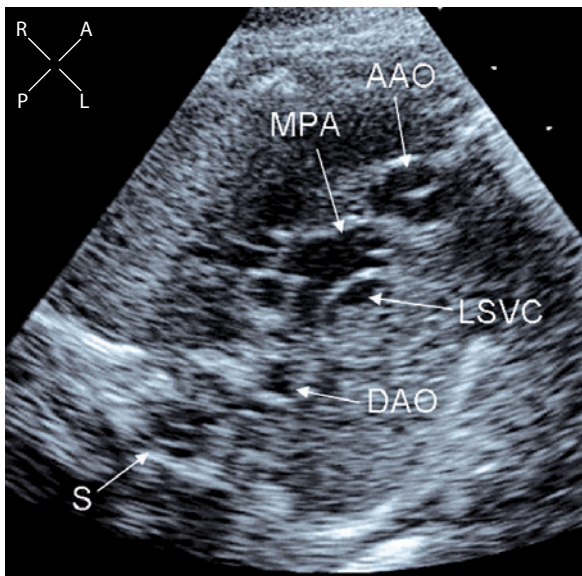
Fig. 9.22 • A 32-week gestational-age fetus with double-outlet right ventricle and malposition of the great arteries. On cross section, the ascending aorta is located anteriorly and slightly to the right of the pulmonary artery, thus imitating a case of complete transposition of the great arteries. A persistent left superior vena cava is seen leftward of the main pulmonary artery. *AAO* ascending aorta, *DAO* descending aorta, *LSVC* left superior vena cava, *MPA* main pulmonary artery, *S* spine

References

1. Yoo SJ, Lee YH, Kim ES et al (1997) Three-vessel view of the fetal upper mediastinum: an easy means of detecting abnormalities of the ventricular outflow tracts and great arteries during obstetric screening. Ultrasound Obstet Gynecol 9:173-183

2. Yoo SJ, Lee YH, Cho KS et al (1999) Sequential segmental approach to fetal congenital heart disease. Cardiol Young 9:430-444

3. Yoo SJ, Lee YH, Cho KS (1999) Abnormal three-vessel view on sonography: a clue to the diagnosis of congenital heart disease in the fetus. AJR Am J Roentgenol 172:825-830

4. Yagel S, Cohen SM, Achiron A (2001) Examination of the fetal heart by five short-axis views: a proposed screening method for comprehensive cardiac evaluation. Ultrasound Ostet Gynecol 17:367-369

5. Yagel S, Arbel R, Anteby EY et al (2002) The three vessels and trachea view (3VT) in fetal scanning. Ultrasound Ostet Gynecol 20:340-345

6. Vinals F, Hereida F, Giuliano A (2003) The role of the three vessels and trachea view (3VT) in the diagnosis of congenital heart defects. Ultrasound Ostet Gynecol 22:358-367

7. Zalel Y, Wiener Y, Gamzu R et al (2004) The three-vessel and tracheal view of the fetal heart: an in utero sonographic evaluation. Prenat Diagn 24:174-178

8. Moon MH, Cho JY, Park EJ et al (2007) Three-vessel view of the fetal heart: in utero development of the great vessels. Prenat Diagn 27:158-163

CHAPTER 10

The Arterial Duct Transverse View

The Section Plane

Although some authors include this section into the category of the three-vessel view [1, 2], here it is described separately. This cut is obtained with a slight cranial tilt from the classic three-vessel view. The level of this section is shown in Figure 10.1.

The Normal Morphology

In the normal fetus, a transverse section at this level usually should display a transverse section of the main pulmonary artery and the arterial duct join-ing the descending aorta on the left side of the spine. The ascending aorta and the superior vena cava appear in cross section on the right side, with their diameter in decreasing order. With a slight cranial orientation of the section plane, the upper part of the right atrial appendage seen anteriorly to these vessels, whereas the right pulmonary artery, sectioned along its major axis, appears posteriorly. In the posterior part of the mediastinum, the two main-stem bronchi and the esophagus are displayed in cross section. When the descending aorta is normally on the left side of the spine, the ductal arch does not cross the midline and shows a straight course, leaving these midline structures to its right side (Fig. 10.2).
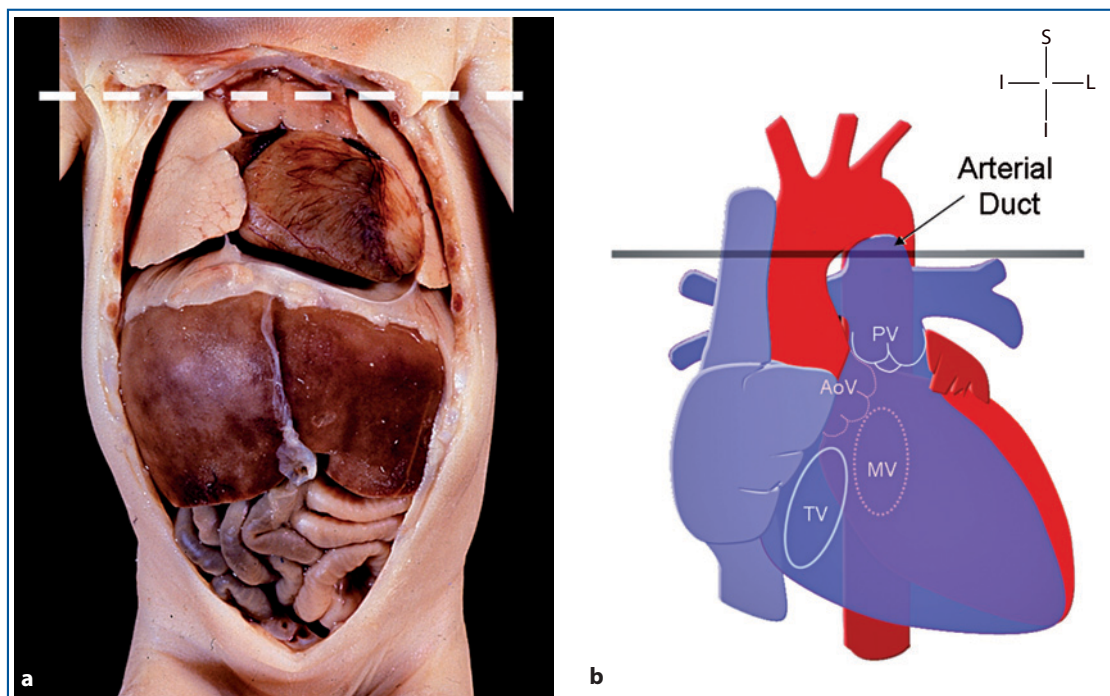
Fig. 10.1 • The level of the transverse section of the arterial duct is shown on the fetal body (**a**) and on a heat diagram (**b**). The latter shows that a true transverse cut lies above the level of left and right branch of the main pulmonary artery. *AoV* aortic valve, *MV* mitral valve, *PV* pulmonary valve, *TV* tricuspid valve
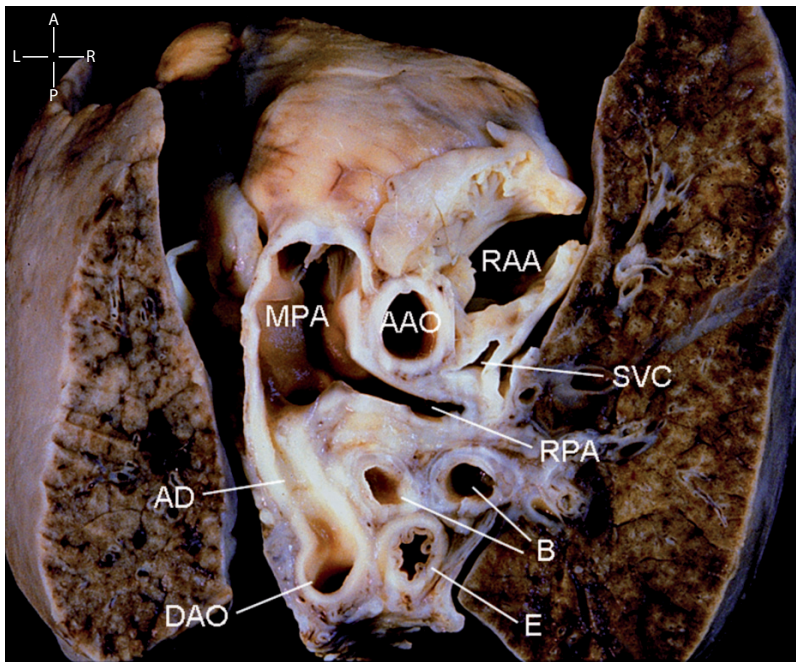
Fig. 10.2 • An anatomic specimen sectioned to imitate the transverse view of the ductal arch. This image demonstrates how the arterial duct connects the main pulmonary artery to the descending aorta. The cross section of the ascending aorta and the superior vena cava is seen anteriorly, and the two bronchi and the esophagus are seen posteriorly. The right pulmonary artery sectioned along its major axis is displayed between the ascending and the descending aorta. Anterior to the ascending aorta and the superior vena cava, the right atrial appendage is involved by this section. *AAO* ascending aorta, *AD* arterial duct, *B* bronchi, *DAO* descending aorta, *E* esophagus, *MPA* main pulmonary artery, *RAA* right atrial appendage, *RPA* right pulmonary artery, *SVC* superior vena cava

The Normal Echocardiogram – 2D

Echocardiographic sections along a true transverse plane of the fetal thorax (Figs. 10.3, 10.4) show only the main pulmonary artery joining the descending aorta through the arterial duct. The distal parts of the infundibulum, the pulmonary valve, and the right pulmonary artery are not seen because they lie on a more caudal plane.

True transverse sections of the fetal thorax are more difficult to obtain because of shadowing of the sternum and ribs. Consequently, it is easier to obtain a paratransverse section of the thorax from the upper abdomen with cranial tilt of the probe (Fig. 10.5). With such angulation, the transverse view of the ductal arch includes the pulmonary valve, the proximal part of the main pulmonary artery, and the right pulmonary branch, this latter being displayed along its major axis (Fig. 10.6).

The Normal Echocardiogram – Color Flow Mapping and Pulsed Doppler

The ductal flow can easily be assessed in transverse sections with color flow mapping, which shows the flow from the pulmonary artery toward the descend-
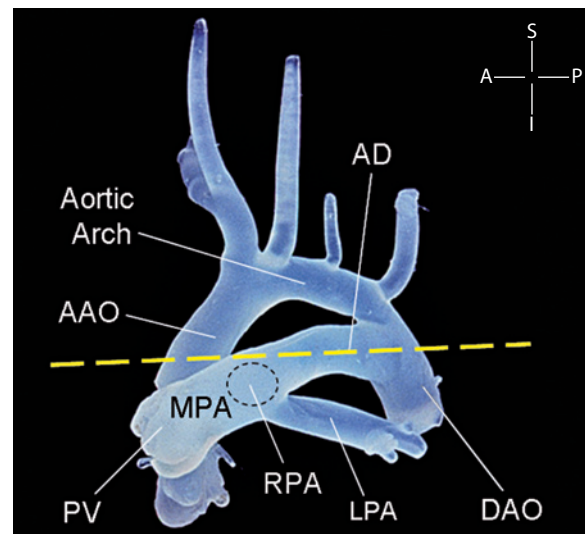
Fig. 10.3 • Silastic cast of the thoracic aorta and pulmonary artery in a fetus seen in laterolateral perspective from the left side. The *yellow dashed line* indicates the plane of the true transverse section of the arterial duct. The arch of the arterial duct lies more cranial relatively to the pulmonary valve and the major branches of the pulmonary artery (*dashed circle* indicates the origin of the right pulmonary artery). Moreover, the ductal arch lies caudal relatively to the aortic arch. *AD* arterial duct, *AAO* ascending aorta, *DAO* descending aorta, *LPA* left pulmonary artery, *MPA* main pulmonary artery, *PV* pulmonary valve, *RPA* right pulmonary artery
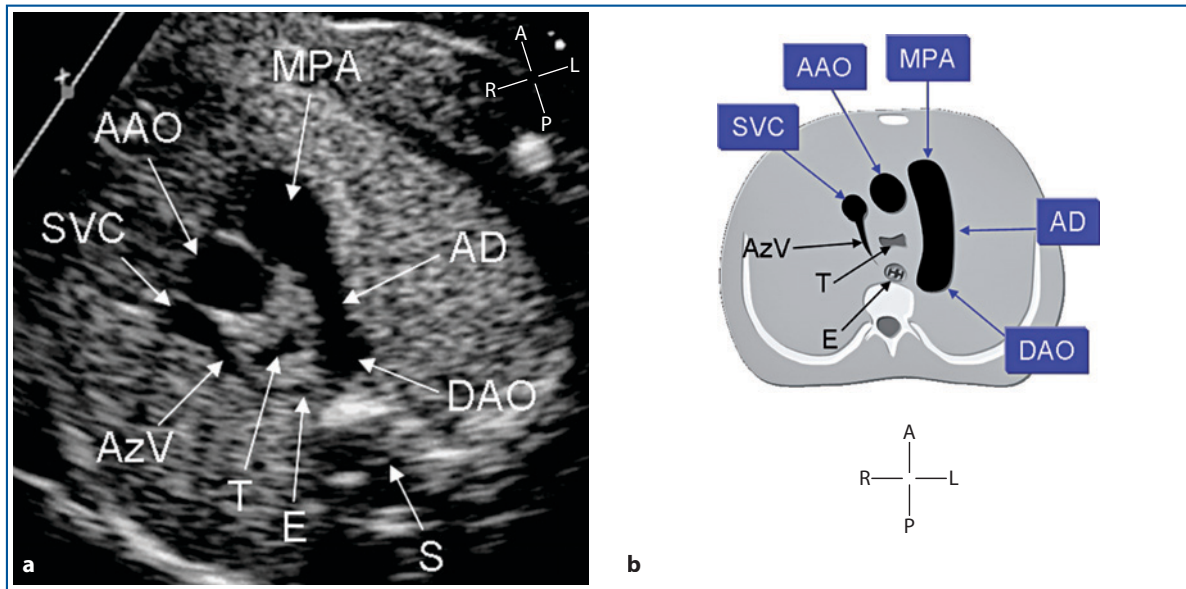
Fig. 10.4 • Cross-sectional frame (**a**) and a corresponding diagram (**b**) of the true transverse view of the arterial duct in a normal 23-week gestational-age fetus. The main pulmonary artery connects to the descending aorta via the arterial duct, thus forming the ductal arch. As in the three-vessel view, the ascending aorta and the superior vena cava are seen in cross section. With high-resolution ultrasound machines, it is common to visualize the distal portion of the azygos vein arching anteriorly to join the superior vena cava. If the descending aorta is on the left side of the spine, the ductal arch has a straight course, leaving to its right side the midline structures, the trachea, and the esophagus, which are seen in cross section in the posterior part of the mediastinum. However, the normal esophagus is usually very difficult to recognize by ultrasound because of its virtual lumen. *AAO* ascending aorta, *AD* arterial duct, *AzV* azygos vein, *DAO* descending aorta, *E* esophagus, *MPA* main pulmonary artery, *S* spine, *SVC* superior vena cava, *T* trachea
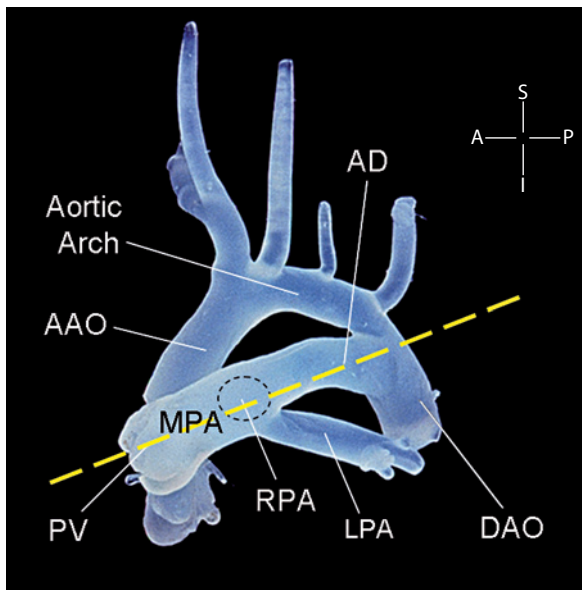
Fig. 10.5 • Same image as in Figure 10.3. The *yellow dashed line* indicates the plane of the paratransverse section of the arterial duct with cranial angulation. The plane of this cut intercepts the proximal part of the main pulmonary artery and the pulmonary valve. *Dashed circle* indicates the origin of the right pulmonary artery. *AAO* ascending aorta, *AD* arterial duct, *DAO* descending aorta, *LPA* left pulmonary artery, *MPA* main pulmonary artery, *PV* pulmonary valve, *RPA* right pulmonary artery

ing aorta via the ductus (Fig. 10.7). This view is sufficient to assess the presence of the normal forward flow in the arterial duct during routine examination [3].

Doppler assessment of the arterial ductal flow is easily obtained in transverse sections, demonstrating the characteristic spectrum of flow from the pulmonary artery toward the descending aorta via the ductus (Fig. 10.8) [4]. However, sagittal or parasagittal projections are preferable because they allow better control of the precise placement of the sample volume relative to the aortic arch above. Doppler flow features of the arterial duct are described in the chapter dealing with the arterial duct long-axis view. When the transverse view of the arterial duct is obtained with cranial angulation, the distal infundibulum and the pulmonary valve are seen. Therefore, dysfunction of this valve can be detected from this view.

The Arterial Duct – Reversed Flow

With severe obstructions of the pulmonary flow, the flow in the arterial duct is reversed. Usually, in congenital heart disease with pulmonary circulation dependent on the arterial duct, the shape of the ductus arteriosus is tortuous and more vertical than in the nor-
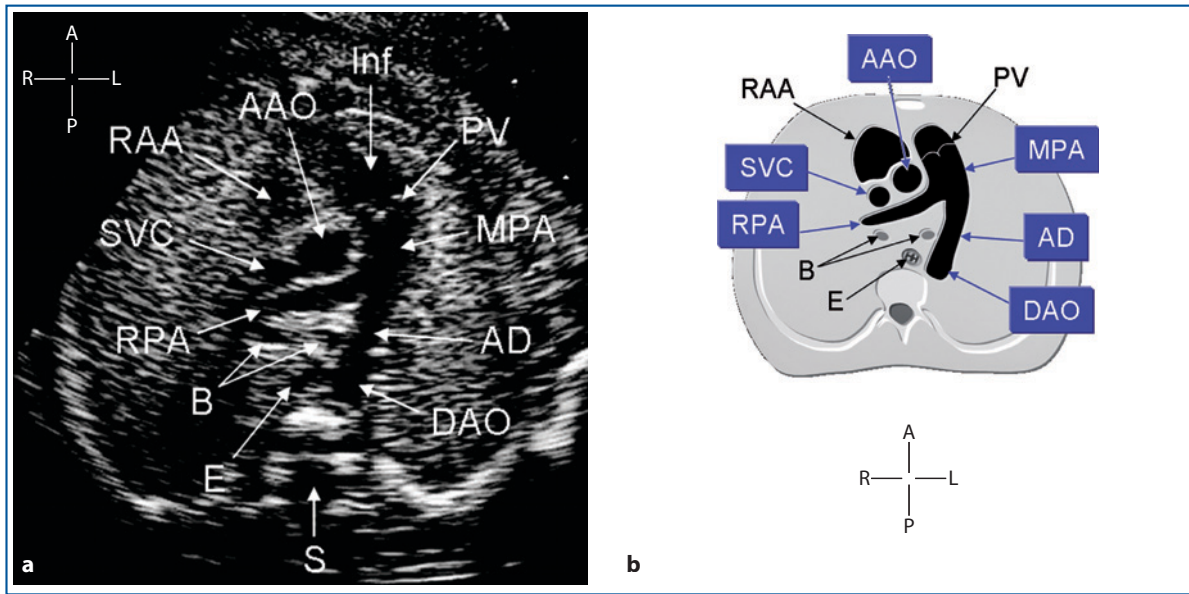
Fig. 10.6 • Cross-sectional view (**a**) and diagram (**b**) of a transverse section of the arterial duct in a normal 23-week gestational-age fetus. The section is obtained with the cranial tilt illustrated in Figure 10.5. With such angulation, besides a section of the main pulmonary artery, the arterial duct, the descending aorta forming the ductal arch, the pulmonary valve, and the distal infundibulum are seen. The upper part of the right atrial appendage is displayed anteriorly to the ascending aorta and the superior vena cava, whereas the long-axis section of the right pulmonary artery is seen posteriorly. In the posterior part of the mediastinum and on the right side of the ductal arch, the cross sections of the two bronchi and the esophagus are displayed. *AAO* ascending aorta, *AD* arterial duct, *B* bronchi, *DAO* descending aorta, *E* esophagus, *LPA* left pulmonary artery, *MPA* main pulmonary artery, *PV* pulmonary valve, *RAA* right atrial appendage, *RPA* right pulmonary artery, *S* spine, *SVC* superior vena cava
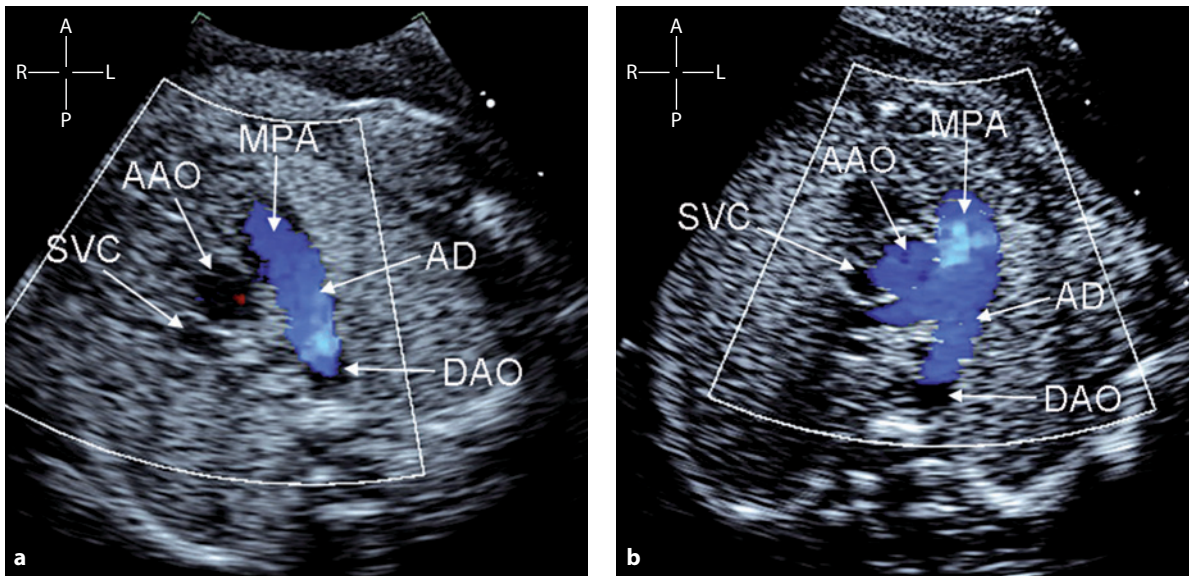
Fig. 10.7 • Color flow mapping systolic frames of the transverse view of the arterial duct in true transverse view (**a**) and with cranial tilt (**b**). The normal flow is from the pulmonary artery toward the descending aorta. With ventral presentation of the fetus, as in these examples, the flow is away from the transducer and is represented in *blue*. Good alignment can be obtained for Doppler assessment of both the flow in the main pulmonary artery and the arterial duct. *AAO* ascending aorta, *AD* arterial duct, *DAO* descending aorta, *MPA* main pulmonary artery, *SVC* superior vena cava
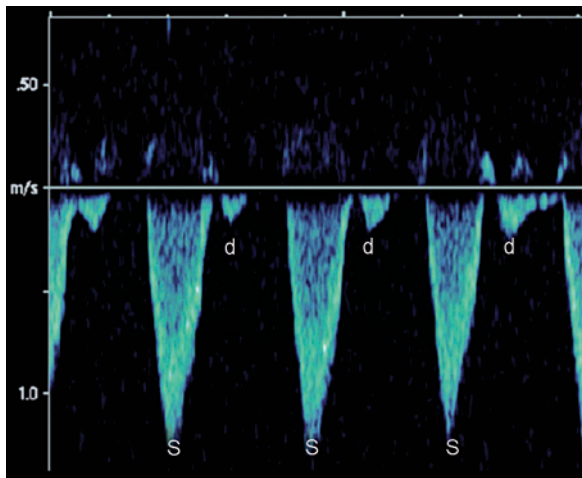
Fig. 10.8 • Pulse Doppler spectrum of the arterial duct obtained from a transverse view of the arterial duct. The systolic (*S*) and diastolic (*d*) peaks of flow are indicated
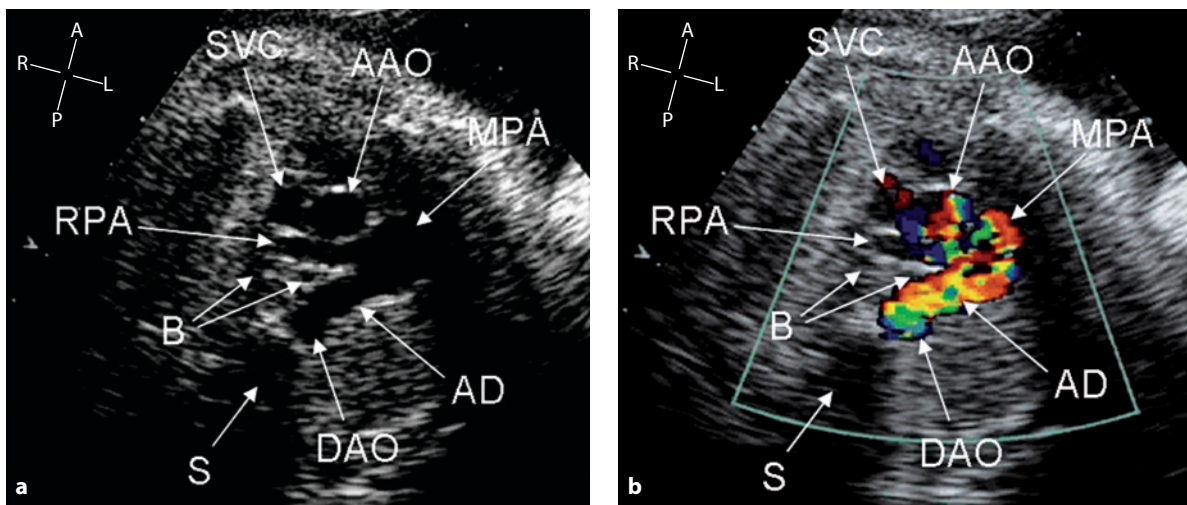
Fig. 10.9 • Transverse views of the arterial duct in a 28-week gestational-age fetus with pulmonary atresia and intact ventricular septum. On cross-sectional examination (**a**), the relative position, order, and size of the great arteries is maintained. In particular, the size of the main pulmonary artery is larger than the adjacent ascending aorta. There is a wide arterial duct joining the descending aorta with its full lumen. On color flow mapping (**b**), the main pulmonary artery is filled from the arterial duct in a reverse fashion. In fact, despite the ventral presentation of the fetus, the flow direction in the pulmonary artery is toward the transducer and represented in *red*. *AAO* ascending aorta, *AD* arterial duct, *B* bronchi, *DAO* descending aorta, *MPA* main pulmonary artery, *RPA* right pulmonary artery, *S* spine, *SVC* superior vena cava

mal fetus. Therefore, it can be difficult to visualize this vessel in transverse sections. In pulmonary atresia with intact ventricular septum or severe forms of Ebstein's malformation, which are among heart diseases with duct-dependent pulmonary circulation, the normal shape of the arterial duct can be maintained, and the reversed flow is more easily demonstrated [5]. One example is shown in Figure 10.9.

The Arterial Duct – Short Length

When the pulmonary artery is in the posterior position, the length of the arterial duct is shorter be-

cause this vessel is closer to the descending aorta. This can be seen in complete or congenitally corrected transposition (Figs. 10.10, 10.11).

The Arterial Duct – Abnormal Shape

On examination during the third trimester, the arterial duct often shows a certain degree of tortuosity (Fig. 10.12b). In rarer cases, this tortuosity can be particularly pronounced (Figs. 10.13, 10.14). Kinking of the arterial duct is better appreciated in transverse views than in long-axis views.
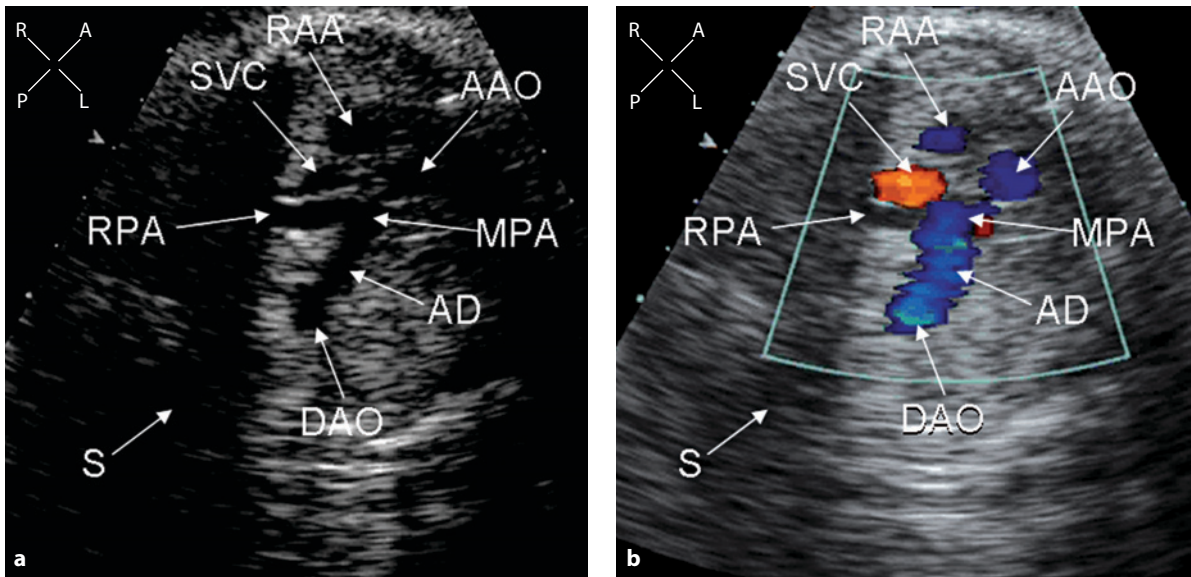
Fig. 10.10 • Transverse views of the arterial duct in a 36-week gestational-age fetus with transposition of the great arteries. On cross-sectional examination (**a**), the ascending aorta lies exactly anterior to the pulmonary artery. The pulmonary artery joins the descending aorta on the posterior side of the spine via a short arterial duct. On color flow mapping (**b**), the flow into the arterial duct is normal, from the pulmonary artery toward the descending aorta. *AAO* ascending aorta, *AD* arterial duct, *DAO* descending aorta, *MPA* main pulmonary artery, *RAA* right atrial appendage, *RPA* right pulmonary artery, *S* spine, *SVC* superior vena cava
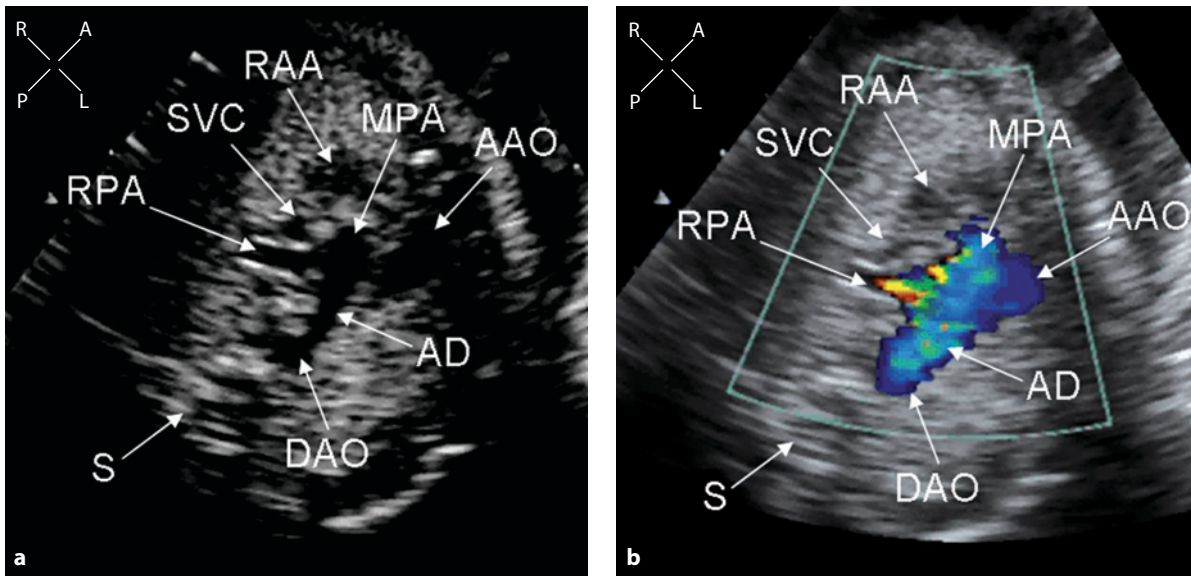
Fig. 10.11 • Transverse view of the arterial duct in a 27-week gestational-age fetus with congenitally corrected transposition. On cross-sectional view (**a**), the ascending aorta is located anteriorly and to the left relative to the pulmonary artery, as is typical in congenitally corrected transposition of the great arteries. Being in the posterior position, the pulmonary artery joins the descending aorta via a short arterial duct. On color flow mapping (**b**), the normal perfusion of the arterial duct, from the pulmonary artery toward the descending aorta, rules out a severe obstruction to the pulmonary flow. *AAO* ascending aorta, *AD* arterial duct, *DAO* descending aorta, *MPA* main pulmonary artery, *RAA* right atrial appendage, *RPA* right pulmonary artery, *S* spine, *SVC* superior vena cava
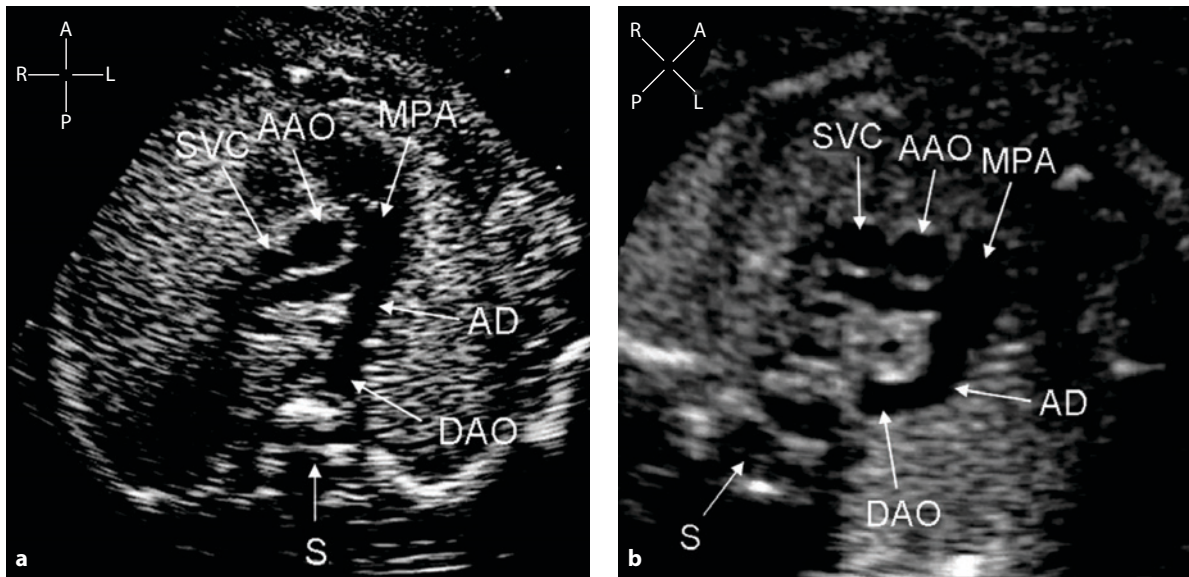
Fig. 10.12 • Cross-sectional transverse view of the arterial duct in a 21-week (**a**) and a 30-week (**b**) gestational-age fetus. In early pregnancy, the arterial duct is a straight channel but in the third trimester often becomes tortuous. *AAO* ascending aorta, *AD* arterial duct, *DAO* descending aorta, *MPA* main pulmonary artery, *S* spine, *SVC* superior vena cava
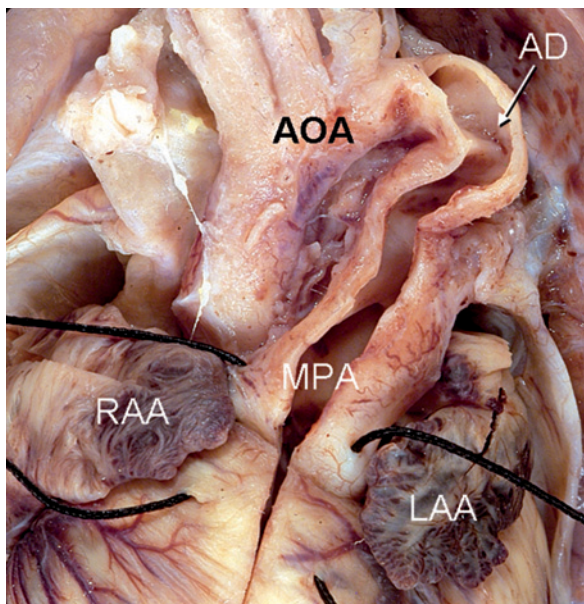
Fig. 10.13 • Morphological specimen of a fetus who underwent unexpected intrauterine death at 33 weeks of gestation. The image shows an elongated arterial duct with pronounced tortuosity. *AD* arterial duct, *AOA* aortic arch, *LAA* left atrial appendage, *MPA* main pulmonary artery, *RAA* right atrial appendage

Fig. 10.14 • Cross-sectional (**a**) and color flow mapping (**b**) frames of the transverse view of the arterial duct from left paravertebral approach. This 38-week gestational-age fetus had a striking S-shaped tortuosity of the arterial duct. The perinatal course was uneventful. *AAO* ascending aorta, *AD* arterial duct, *DAO* descending aorta, *MPA* main pulmonary artery, *S* spine, *SVC* superior vena cava, *T* trachea
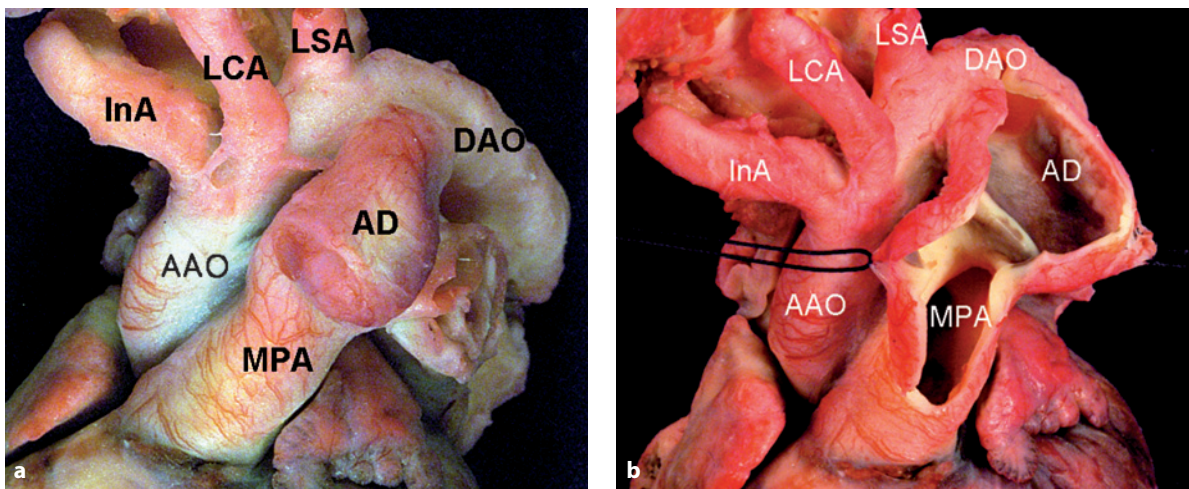
Fig. 10.15 • External view (**a**) and from inside (**b**) the arterial duct in a 39-week gestational-age stillborn fetus whose presumable cause of death was a diffuse subamniotic hemorrhage of the placenta. The arterial duct shows a large aneurysmatic dilatation with a prominent fold inside. *AAO* ascending aorta, *AD* arterial duct, *DAO* descending aorta, *InA* innominate artery, *LCA* left common carotid artery, *LSA* left subclavian artery, *MPA* main pulmonary artery

In rare cases, the arterial duct can reach aneurysmatic size (Fig. 10.15). Most cases of aneurysm of the arterial duct reported in the literature were incidental findings detected late in gestation [6-9]. The arterial duct closed spontaneously and did not require treatment. Some cases associated with complications have been reported. In transverse sections, the aneurism can appear as a cystic structure occupying the upper part of the left thorax [10]. With slight manipulation of the probe, the continuity with the main pulmonary artery should be demonstrated, with flow inside the lumen on color flow mapping (Fig. 10.16).

The Arterial Duct – Premature Constriction or Closure

Because Doppler assessment of arterial duct flow should be obtained in the long-axis view of the arterial duct, premature ductal constriction or closure will be discussed in the relative chapter. However, this type of complication can be suspected also in the transverse view, and one example is shown in Figure 10.17.
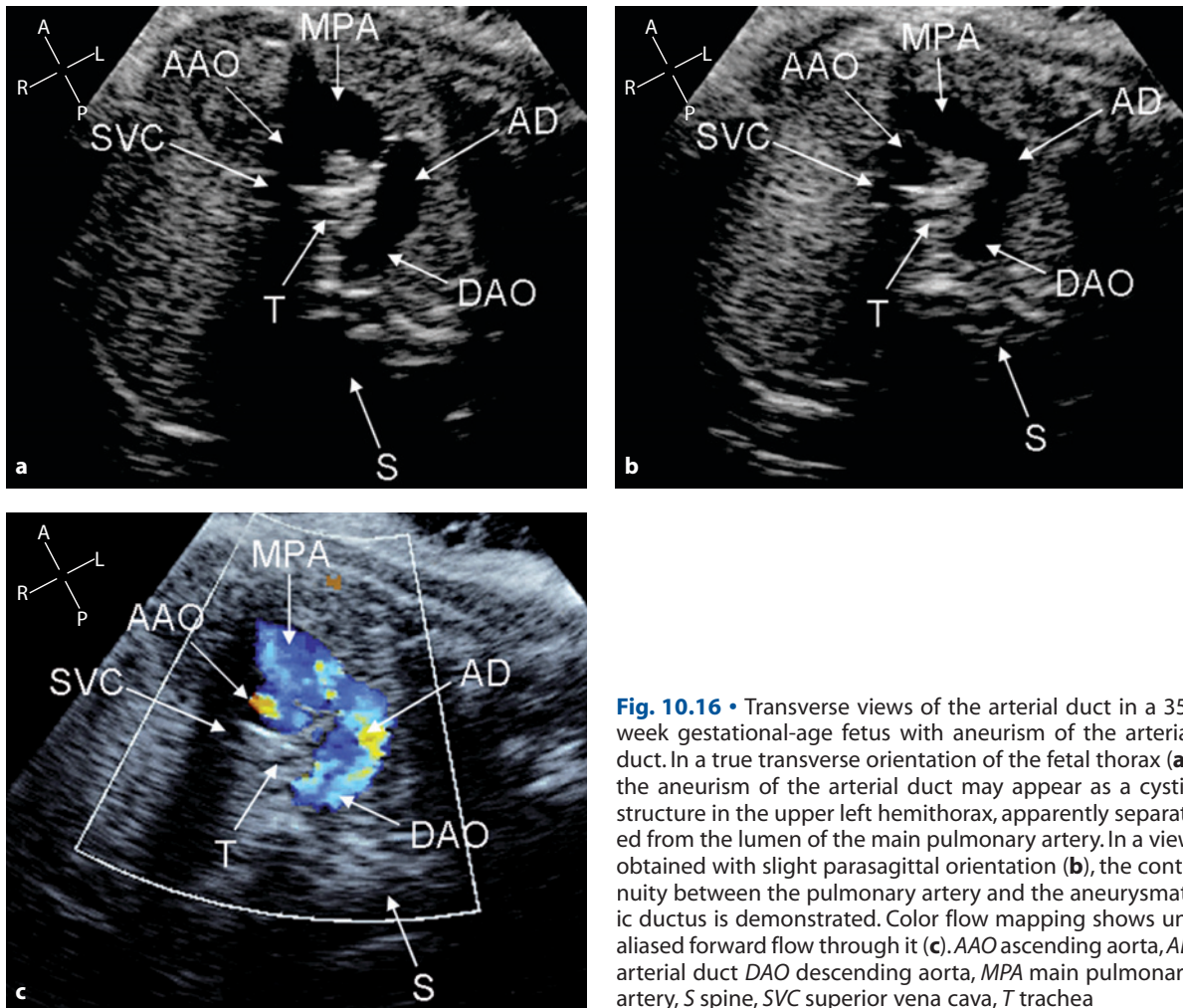
Fig. 10.16 • Transverse views of the arterial duct in a 35-week gestational-age fetus with aneurism of the arterial duct. In a true transverse orientation of the fetal thorax (**a**), the aneurism of the arterial duct may appear as a cystic structure in the upper left hemithorax, apparently separated from the lumen of the main pulmonary artery. In a view obtained with slight parasagittal orientation (**b**), the continuity between the pulmonary artery and the aneurysmatic ductus is demonstrated. Color flow mapping shows unaliased forward flow through it (**c**). *AAO* ascending aorta, *AD* arterial duct *DAO* descending aorta, *MPA* main pulmonary artery, *S* spine, *SVC* superior vena cava, *T* trachea
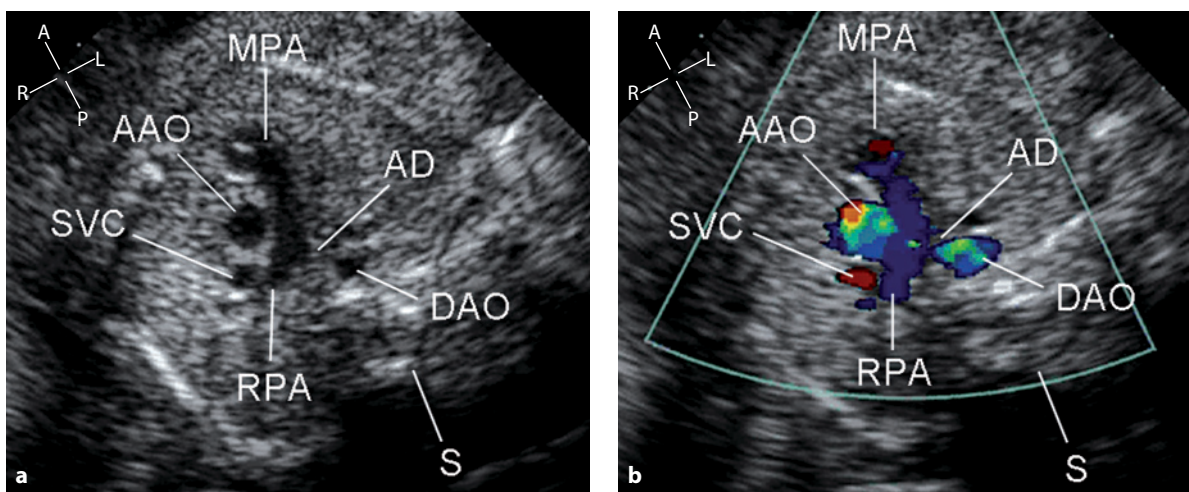
Fig. 10.17 • Transverse view of the arterial duct in a 29-week gestational-age fetus, with complete closure of the duct. On cross-sectional view (**a**), the lumen of the arterial duct is virtually closed. On color flow mapping (**b**), there is a faint flow into the main and right pulmonary artery because of the high resistances of the pulmonary circulation. Despite the unfavorable orientation of the ultrasound beam, the flow in the ascending and descending aortas is well visualized because of redistribution of the cardiac output on the left side of the heart. *AAO* ascending aorta, *AD* arterial duct, *DAO* descending aorta, *MPA* main pulmonary artery, *RPA* right pulmonary artery, *S* spine, *SVC* superior vena cava
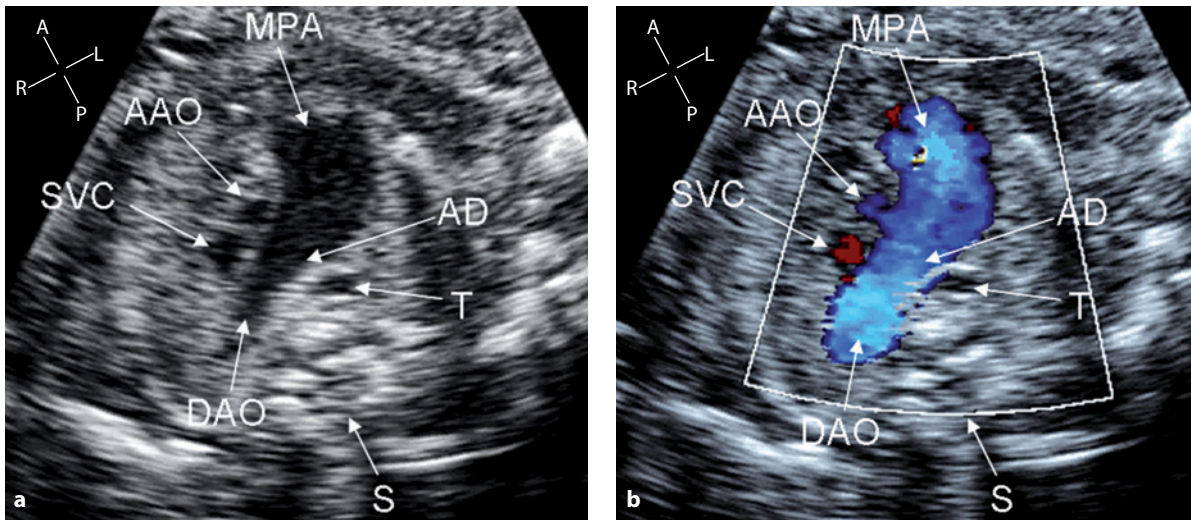
Fig. 10.18 • Transverse views of the arterial duct in a 23-week gestational-age fetus with aortic arch interruption. On cross-sectional examination (**a**), there is a small ascending aorta, similar in size to the superior vena cava. Due to a redistribution of flow to the right side of the heart, the size of the pulmonary artery and the arterial duct is increased. The arterial duct arch crosses the midline, joining the descending aorta on the right side of the spine and leaving the trachea to the left. These features identify a right-sided arch of the arterial duct and aorta. Color flow mapping (**b**) confirms a right-sided arch with increased size of the pulmonary artery and arterial duct. *AAO* ascending aorta, *AD* arterial duct, *DAO* descending aorta, *MPA* main pulmonary artery, *S* spine, *SVC* superior vena cava, *T* trachea
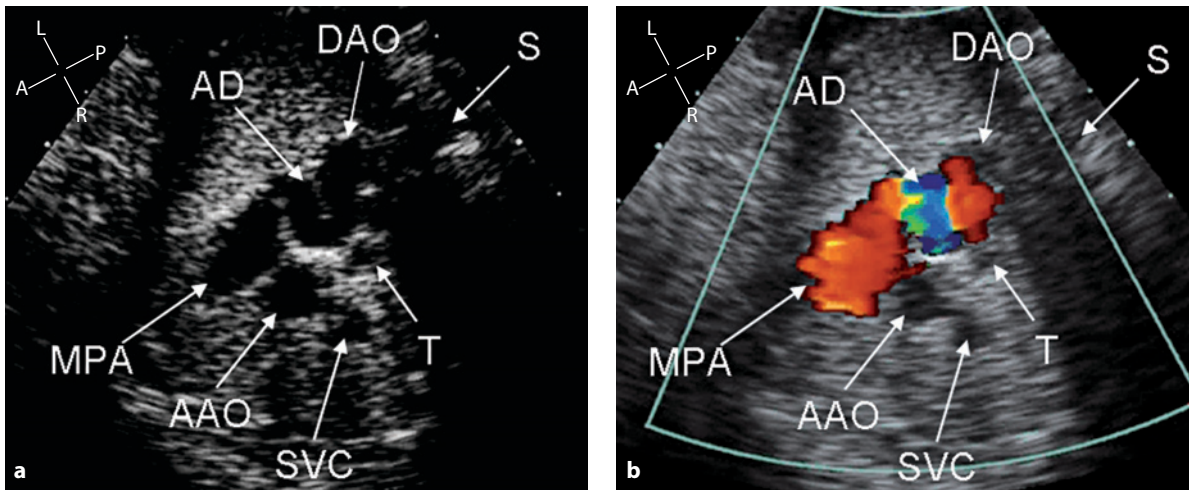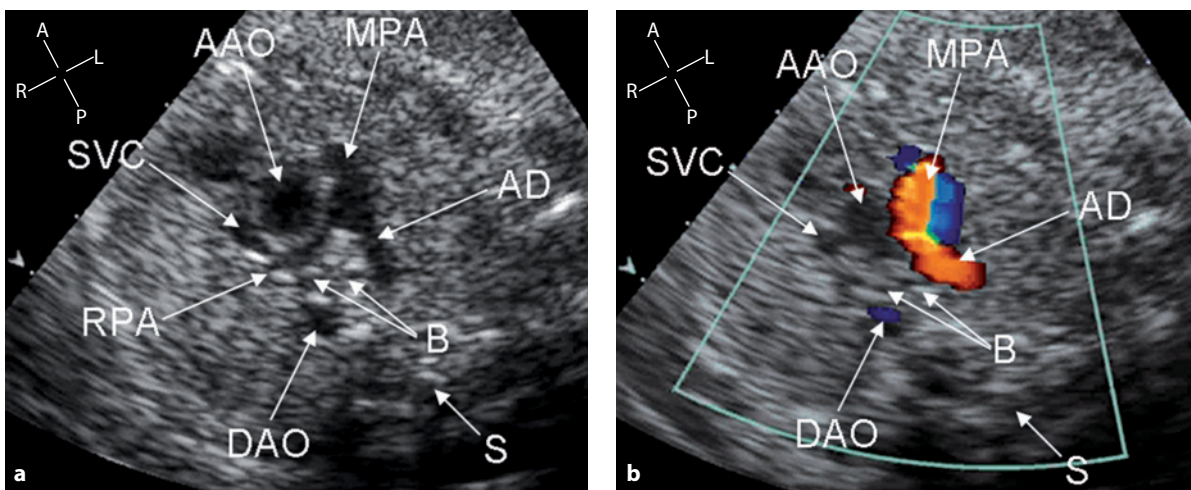

Fig. 10.19 • Transverse views of the arterial duct in a 31-week gestational-age fetus with tetralogy of Fallot with pulmonary atresia. On cross-sectional view (**a**), the main pulmonary artery is abnormally small, having a size inferior to that of the ascending aorta. The descending aorta is on the right side of the spine, anticipating a right-sided aortic arch. Although this cross-sectional view may appear at first sight as a three-vessel view of the pulmonary artery bifurcation, the left branch is represented by an oblique section of the arterial duct. In fact, the arterial duct, as is common in tetralogy of Fallot and right aortic arch, originated from the foot of the left subclavian artery and was located in the left side of the mediastinum. Color flow mapping (**b**) shows a reversed flow into the arterial duct, filling the pulmonary artery retrogradely. *AAO* ascending aorta, *AD* arterial duct, *B* bronchi, *DAO* descending aorta, *MPA* main pulmonary artery, *RPA* right pulmonary artery, *S* spine, *SVC* superior vena cava

The Arterial Duct – Abnormal Position

The arterial duct may show abnormal orientation or position. For instance, in aortic arch interruption with right descending aorta, the arterial duct arch will not be lying on a sagittal plane but on a parasagittal plane orienting rightward and crossing the midline (Fig. 10.18). As to abnormal position, cases with tetralogy of Fallot and right aortic arch may have the arterial duct originating from the foot of the left subclavian artery (Fig. 10.19).

References

1. Vinals F, Heredia F, Giuliano A (2003) The role of the three vessels and trachea view (3VT) in the diagnosis of congenital heart defects. Ultrasound Obstet Gynecol 22:358-367

2. Zalel Y, Wiener Y, Gamzu R et al (2004) The three-vessel and tracheal view of the fetal heart: an in utero sonographic evaluation. Prenat Diagn 24:174-178

3. Chaoui R, McEwing R (2003) Three cross-sectional planes for fetal color Doppler echocardiography. Ultrasound Obstet Gynecol 21:81-93

4. Van der Mooren K, Barendregt LG, Wladimiroff JW (1991) Flow velocity waveforms in the human fetal ductus arteriosus during the normal second half of pregnancy. Pediatr Res 30:387-390

5. Hornberger LK, Benacerraf BR, Bromley BS et al (1994) Prenatal detection of severe right ventricular outflow tract obstruction: pulmonary stenosis and pulmonary atresia. J Ultrasound Med 13:743-750

6. Mielke G, Peukert U, Krapp M et al (1995) Fetal and transient neonatal right heart dilatation with severe tricuspid valve insufficiency in association with abnormally S-shaped kinking of the ductus arteriosus. Ultrasound Obstet Gynecol 5:338-341

7. Dyamenahalli U, Smallhorn JF, Geva T et al (2000) Isolated ductus arteriosus aneurysm in the fetus and infant: a multi-institutional experience. J Am Coll Cardiol 36:262-269

8. Tseng JJ, Jan SL (2005) Fetal echocardiographic diagnosis of isolated ductus arteriosus aneurysm: a longitudinal study from 32 weeks of gestation to term. Ultrasound Obstet Gynecol 26:50-56

9. Tongprasert F, Tongsong T, Sittiwangkul R (2005) Prenatal sonographic diagnosis of congenital ductus arteriosus aneurysm: a case report. J Med Assoc Thai 88:541-544

10. Jackson CM, Sandor GG, Lim K et al (2005) Diagnosis of fetal ductus arteriosus aneurysm: importance of the three-vessel view. Ultrasound Obstet Gynecol 26:57-62

The Aortic Arch Transverse View

The Section Plane

Cranially to the transverse view of the ductal arch, the transverse view of the aortic arch is obtained. The level of this section is shown in Figures 11.1, 11.2. These images illustrate that when the plane of this section is truly horizontal, the arterial duct and the pulmonary artery are no longer visible because they are lying in an inferior plane.

The Normal Morphology

In the normal fetus, this plane shows a transverse section of the aortic arch with an oblique direction from right anterior to left posterior (Fig. 11.3). The upper portion of the superior vena cava is seen in cross section on the right anterior side of the arch. Posteriorly, the cross section of the trachea at the level of the carina and of the esophagus is seen. The normal left-sided aortic arch crosses the midline to join the descending aorta in front of the spine and leaves the trachea and the esophagus on its right side.

The Normal Echocardiogram – 2D

In the normal heart, the aortic arch is relatively short and starts in the middle of the chest, at nearly half of the anteroposterior diameter between the sternum and the spine. This is because the aorta is connected with the posterior left ventricle (Fig. 11.4). The normal left-sided aortic arch shows an oblique course crossing the midline and merging into the descending aorta in front of the spine and leaves the trachea and the esophagus
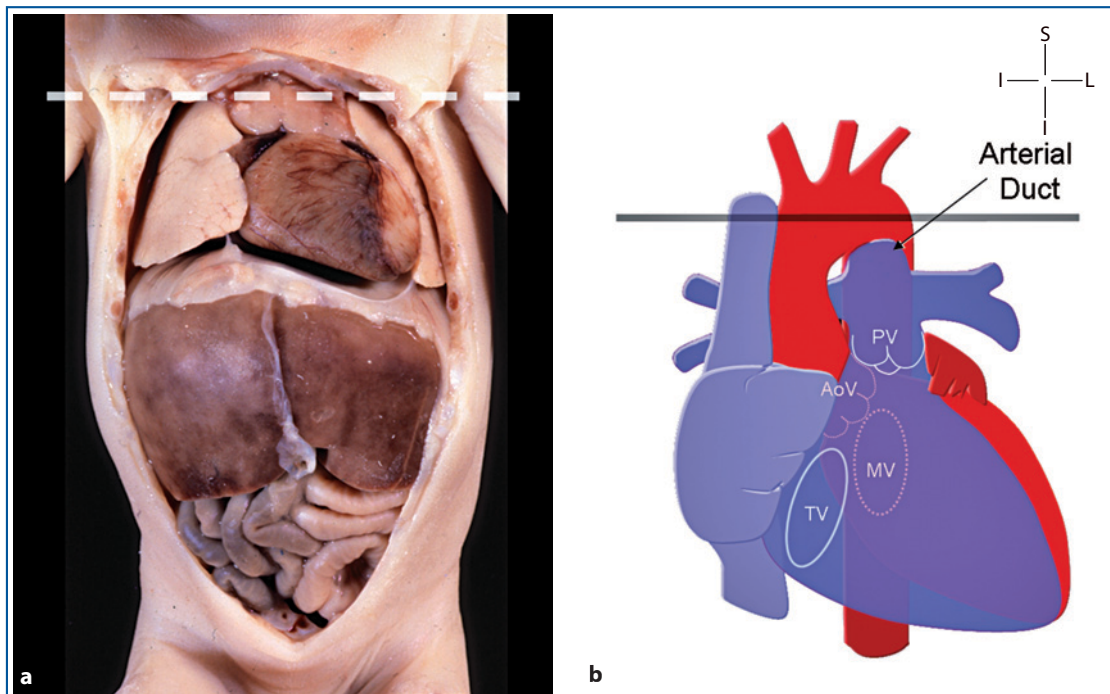
Fig. 11.1 • The level of the transverse view of the aortic arch is shown on the fetal body and a heart scheme. *AoV* aortic valve, *MV* mitral valve, *PV* pulmonary valve, *TV* tricuspid valve
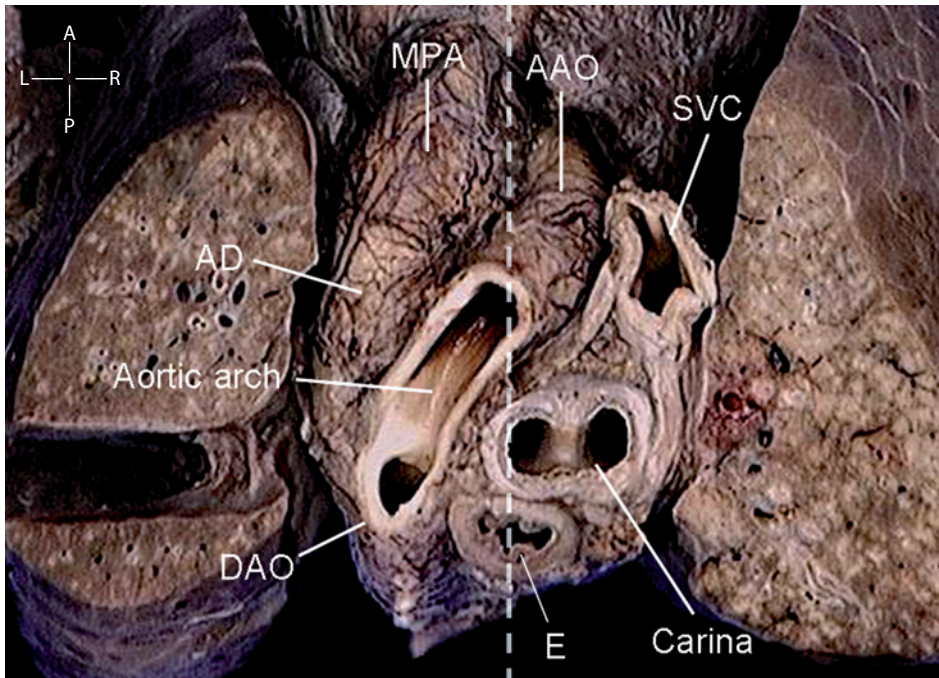
Fig. 11.3 • This normal specimen, viewed from above, is sectioned to imitate the transverse view of the aortic arch. The aortic arch and the superior vena cava are involved by this section, but the arterial duct and the main pulmonary artery are not, as they lie in a slightly caudal plane. The normal relationship between the aortic arch and the ascending and the descending aorta is seen. The trachea, close to its bifurcation (the carina), and the esophagus are seen in the posterior part of the mediastinum. The *dashed line* indicates the midline. *AAO* ascending aorta, *AD* arterial duct, *DAO* descending aorta, *E* esophagus, *MPA* main pulmonary artery, *SVC* superior vena cava
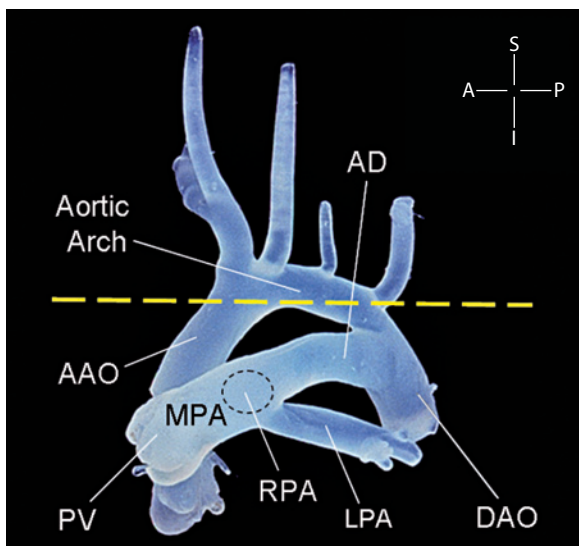
Fig. 11.2 • Silastic cast of the thoracic aorta and pulmonary artery seen in laterolateral perspective from the left side. The *yellow dashed line* indicates the plane of the transverse section of the aortic arch. The aortic arch lies more cranially to the arch of the arterial duct. When this section is truly horizontal, the pulmonary artery and the arterial duct are not involved. *AAO* ascending aorta, *AD* arterial duct, *DAO* descending aorta, *LPA* left pulmonary artery, *MPA* main pulmonary artery, *PV* pulmonary valve, *RPA* right pulmonary artery

on its right side. Being filled with amniotic fluid, the trachea can be visualized sonographically. It can be differentiated from a vessel because of its bright walls, due to its cartilaginous rings, and because the lumen does not code in color on color flow mapping [1, 2]. Due to its virtual lumen, the normal esophagus is difficult to identify on ultrasound examination.

The Thymus

The anterosuperior part of the mediastinum is mostly occupied by the thymus, just above the heart and in front of the three vessels. With high-resolution ultrasound systems, it can be visualized and assessed after 15 weeks of gestation. From the second trimester, it appears slightly less echoic than the adjacent lungs, and its parenchyma is visible, containing scattered spindle-shaped foci. On close observation, the interface between the thymus and the lung can be identified (Fig. 11.5). The normal diameter and perimeter of the fetal thymus have been published [3, 4]. Agenesia or hypoplasia of the thymus is a marker for 22q11.2 deletion in conotruncal anomalies (tetralogy of Fallot in all subtypes, double-outlet right ventricle, common arte-
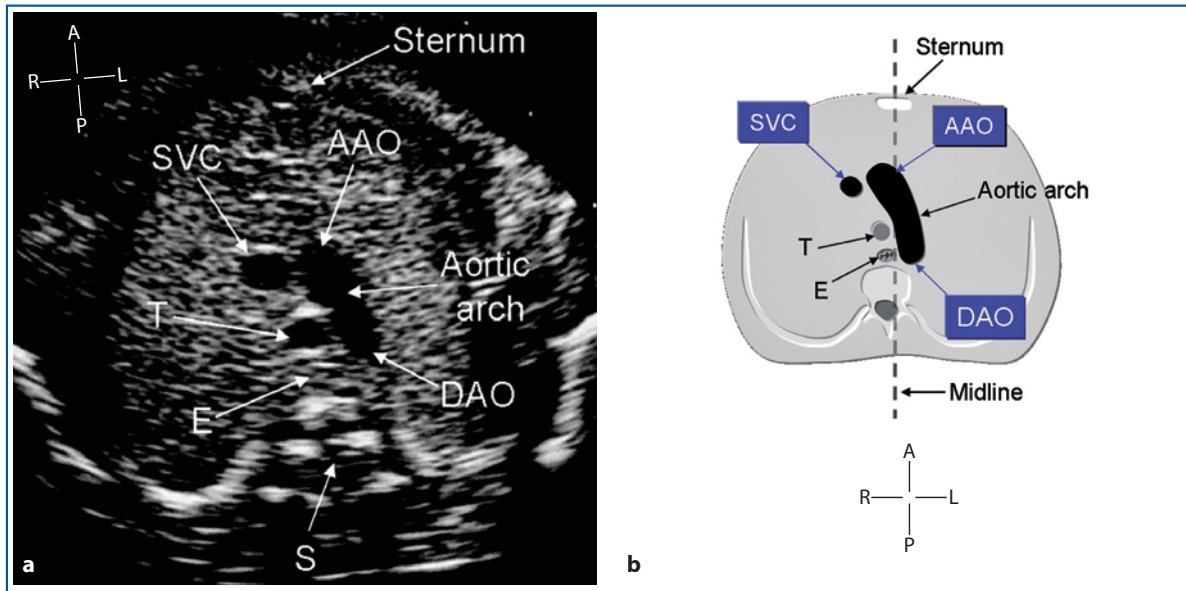
Fig. 11.4 • Cross-sectional frame and diagram of the transverse view of the normal aortic arch in a 23-week gestational-age fetus, seen in caudocranial presentation. The aortic arch is relatively short and starts in the middle of the chest. When the arch is to the left, the trachea lies on its right side. The cross section of the trachea is distinguished from a section of a vessel by its brighter walls and because its lumen does not code in color on color flow mapping. *AAO* ascending aorta, *DAO* descending aorta, *E* esophagus, *S* spine, *SVC* superior vena cava, *T* trachea
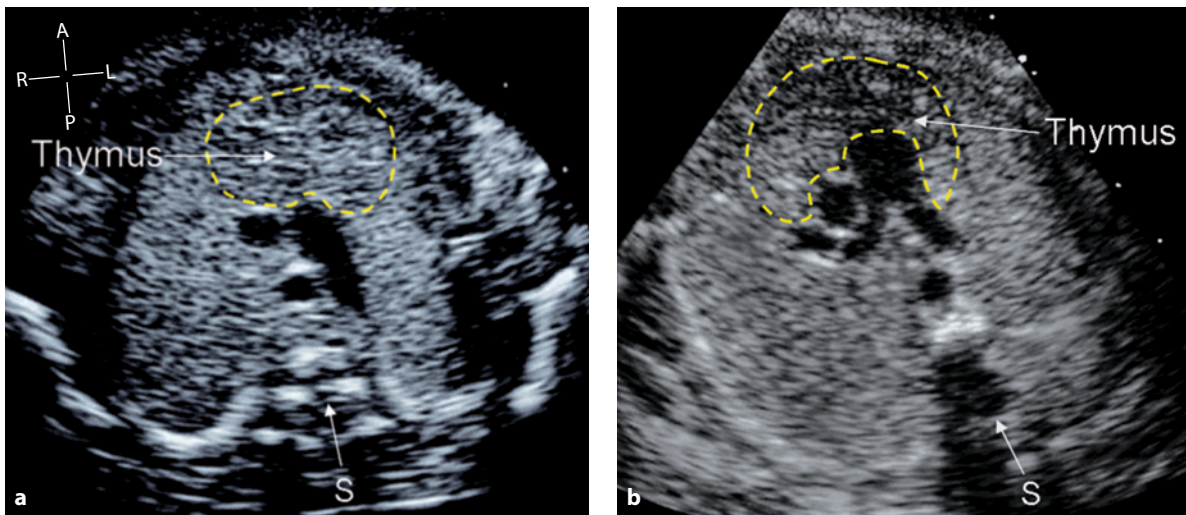
Fig. 11.5 • The *yellow-shaded area* indicates the position of the normal thymus in the anterior part of the mediastinum in a transverse section of the aortic arch (**a**) and in a three-vessel view (**b**). *S* spine

rial trunk, aortic arch interruption, and ventricular septal malalignment defects). Prenatal assessment of thymic hypoplasia or aplasia identifies a group of congenital heart diseases at high risk for 22q11.2 deletion [5-8]. However, rare false positive and false negative cases are possible. In a retrospective study of conotruncal anomalies prenatally detected, 90% sensitivity and 98.5% specificity have been reported [7]. The thymus can be best assessed in the fetus with a high-frequency probe (8-5 MHz) utilizing a general preset with low contrast and wide dynamic range.

The Normal Echocardiogram – Color Flow Mapping and Pulsed Doppler

On color flow mapping, in the aortic arch, there should be nonturbulent forward flow from the ascending aorta toward the descending aorta. The direction of blood in the aortic arch should be from anterior to posterior, in the same direction as that in the arch of the arterial duct (Fig. 11.6). Doppler assessment of the aortic arch can be obtained in transverse view. However, the sample Doppler can be better positioned in long-axis
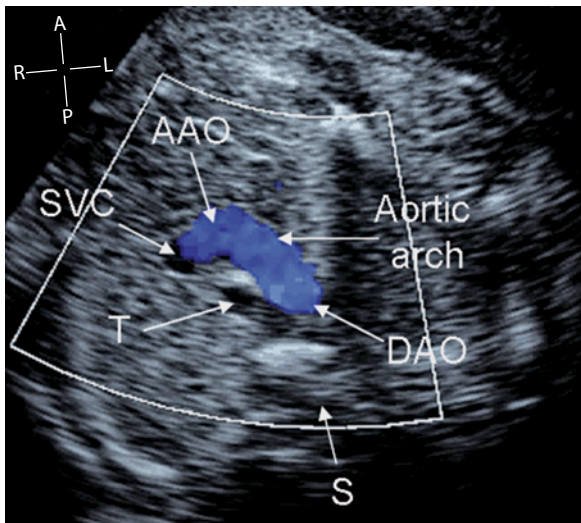
Fig. 11.6 • Aortic arch in a 23-week gestational-age fetus. Colour flow mapping shows unaliased flow, which is from the aortic arch. The flow is anterior to posterior, away from the transducer, and therefore is represented in *blue*. *AAO* ascending aorta, *DAO* descending aorta, *S* spine, *SVC* superior vena cava, *T* trachea

views of the aortic arch, which avoids sampling the flow of the ductal arch below. Therefore, Doppler study of the aortic arch is discussed in the chapter pertaining to the long-axis view of the aortic arch.

Aortic Arch Abnormal Size

Due to the physiological shortcuts of the fetal circulation, the systemic or pulmonary output can be redistributed, partially or even totally, into the opposite arterial vessel when severe obstruction to the pulmonary or aortic outflow is present. The pul-monary flow can be diverted into the ascending aorta in severe obstruction to the pulmonary circulation. In such cases, the ascending aorta and its arch are enlarged (Fig. 11.7), whereas the arterial duct is usually smaller than normal, with inverted curvature and retrograde perfusion. On the contrary, the aortic flow may be diverted into the pulmonary artery in severe obstruction to the aortic flow. In such cases, the ascending aorta and its arch is small, with partial or total retrograde perfusion through the arterial duct and the aortic isthmus (Fig. 11.8). In hypoplastic aortic arches, transverse sections involving the aortic arch only are virtually impossible to
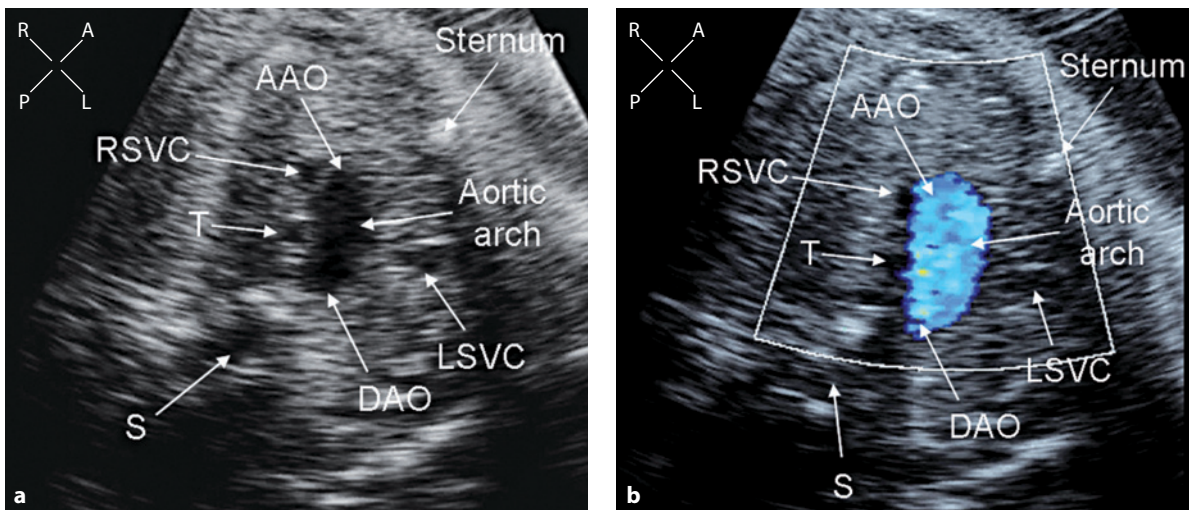
Fig. 11.7 • Aortic arch in a 28-week gestational-age fetus with severe pulmonary valve stenosis in the setting of double-outlet right ventricle with normally related great arteries. Due to the significant obstruction to the pulmonary flow, the aortic arch is enlarged and appears disproportionate to the fetal thorax on cross-sectional examination (**a**). The arch, to the left, crosses the midline, leaving the trachea on its right. Right and left superior vena cava are seen on both sides of the aortic arch. Color flow mapping confirms the enlarged aortic arch, which shows increased systolic pulsations on moving images (**b**). *AAO* ascending aorta, *DAO* descending aorta, *LSVC* left superior vena cava, *RSVC* right superior vena cava, *S* spine, *T* trachea
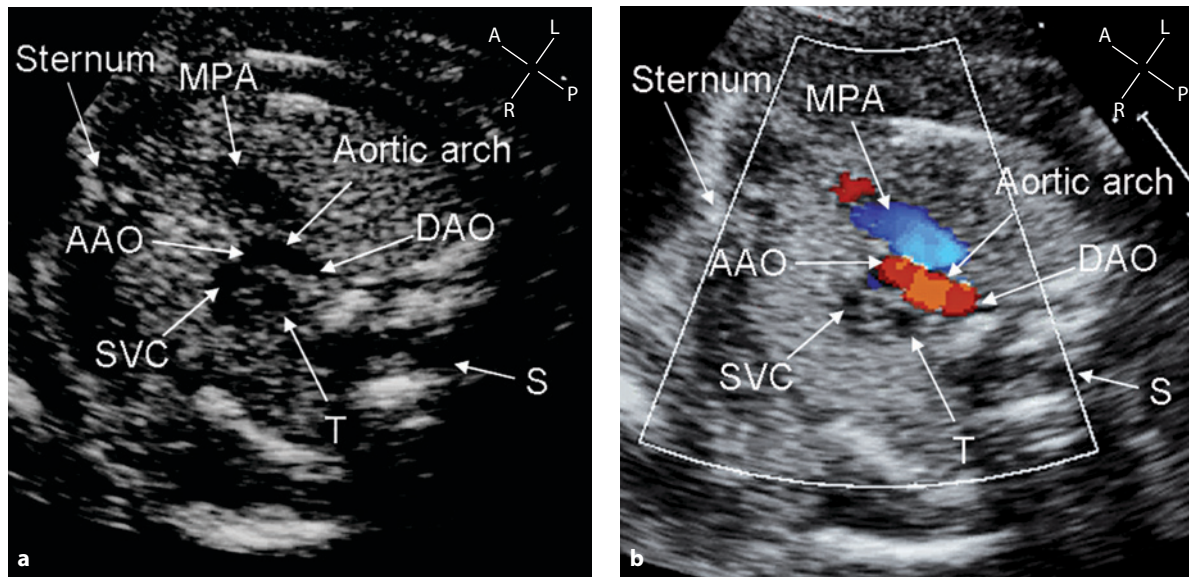
Fig. 11.8 • Aortic arch in a 21-week gestational-age fetus with critical aortic valve stenosis in the setting of a hypoplastic left heart. Although the aortic arch is very small, on cross-sectional examination (**a**), its left-sidedness is easily appreciated. In fact, it crosses the midline, leaving the trachea on its right. The upper portion of the dilated pulmonary artery is seen. Color flow mapping (**b**) shows a reversed flow into the aortic arch. The flow is from posterior to anterior, approaching the transducer and therefore represented in *red*. The normal anterograde flow in the main pulmonary artery is represented in *blue*. *AAO* ascending aorta, *DAO* descending aorta, *MPA* main pulmonary artery, *S* spine, *SVC* superior vena cava, *T* trachea

obtain. Usually, these sections also involve the superior portion of the main pulmonary artery and/or the arterial duct. This is due to dilatation and cranial elongation of the main pulmonary artery and arterial duct because of the redistribution of the aortic output on this artery.

Aortic Arch Interruption

Interruption of the aortic arch can be suspected in transverse views of the fetal thorax when the normal "oblique sausage" appearance of the transverse aortic arch cannot be obtained. Cranially to a transverse section of the arterial duct, a cross section of a very small ascending aorta is obtained (Fig. 11.9), which usually ends in the two common carotid arteries.

Aortic Arch Sidedness

Provided the examiner includes assessment of the trachea location, the transverse view of the aortic arch is particularly useful in determining the side of the aortic arch. Achiron et al. first described the usefulness of the three vessels and trachea view in assessing the prevalence of aortic arch abnormalities in an un-

selected population [9]. In the last 10 years, a growing number of papers have been published dealing with this subject [10-16].

In hearts with normally related great arteries, a right-sided aortic arch lies closer to a sagittal plane of the body and does not cross the midline. The midline structures, the trachea and the esophagus, are seen on its left side (Fig. 11.10). In tetralogy of Fallot with aortic arch to the right, the origin of the arterial duct is frequently from the foot of the left subclavian artery. A cross section of the arterial duct is seen in this view on the left side of the midline (Fig. 11.11). This can be difficult to identify, even for the experienced examiner.

When the ascending aorta is malposed and in anterior position, the aortic arch is elongated, with a takeoff behind the sternum (Figs. 11.12-11.14) If the ascending and descending aortas are on opposite sides, the aortic arch crosses the midline (Fig. 11.12). Conversely, when the ascending and descending aortas are on the same side, whether to the left or to the right, the arch lies in a sagittal plane and does not cross the midline (Fig. 11.13). However, the most reliable sign to assess the laterality of the aortic arch is to identify its relative position with the trachea. This is particularly useful when the aorta is in anterior position and the arch runs in neutral position close to the midline (Fig. 11.14).
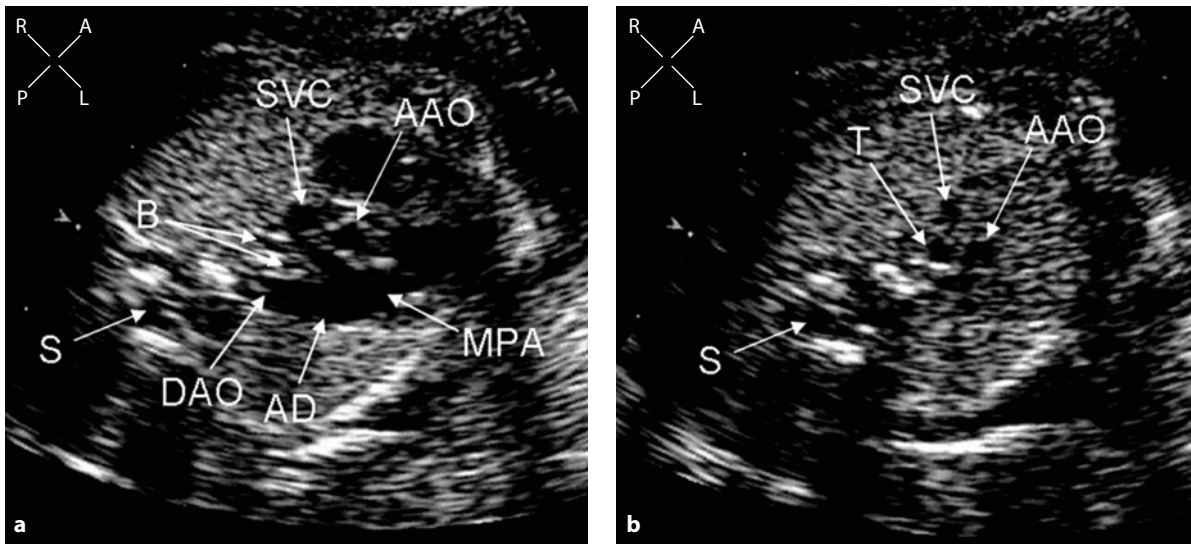
Fig. 11.9 • Upper mediastinum in a 21-week gestational-age fetus with interruption of the aortic arch. On transverse view of the arterial duct (**a**), the ascending aorta is small, similar in size to the superior vena cava. With slight cranial angulation (**b**), the transverse section of the aortic arch is not obtained, only a cross section of a very small ascending aorta, which is visible ending in the two common carotid arteries on a superior plane (not seen in this image). *AAO* ascending aorta, *AD* arch arterial duct arch, *B* bronchi, *DAO* descending aorta, *MPA* main pulmonary artery, *S* spine, *SVC* left superior vena cava, *T* trachea
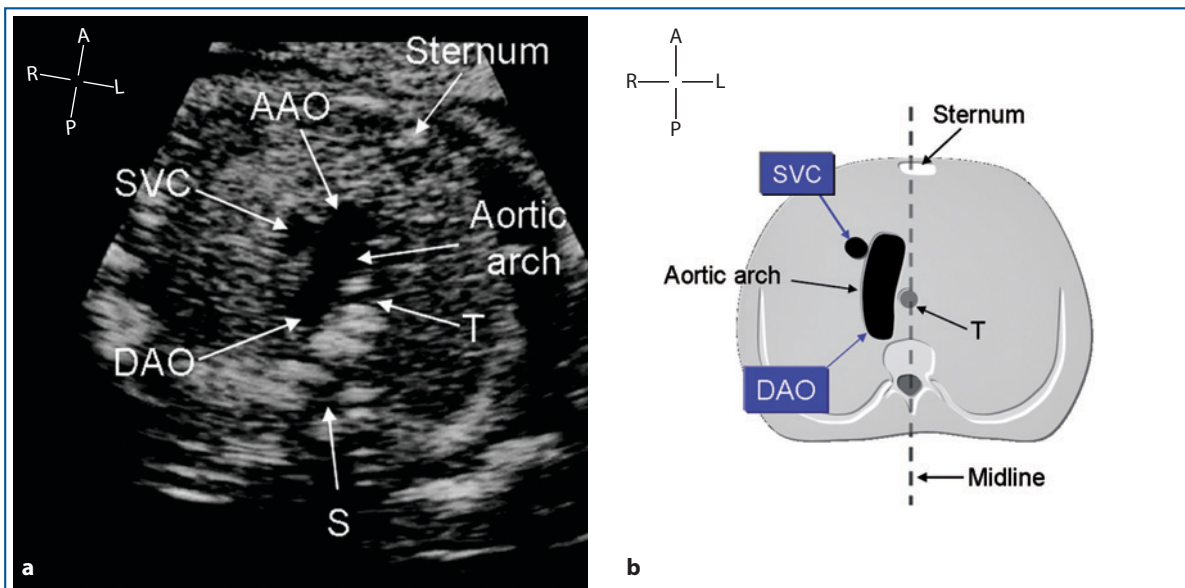
Fig. 11.10 • Aortic arch in a 22-week gestational-age fetus with a classic type of tetralogy of Fallot (**a**), and a correlative diagram (**b**). The takeoff of the aortic arch is in its normal position in the middle of the thorax, as in aortic arches in normal relationship to the posterior ventricle. The arch is right sided, lying parallel to the midline and leaving the trachea on its left. *AAO* ascending aorta, *DAO* descending aorta, *S* spine, *SVC* superior vena cava, *T* trachea
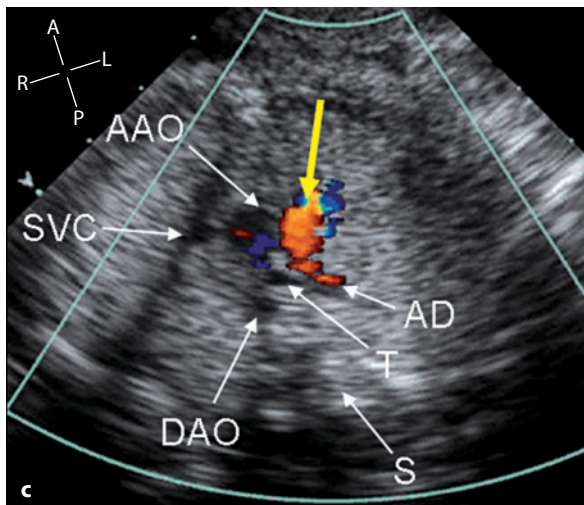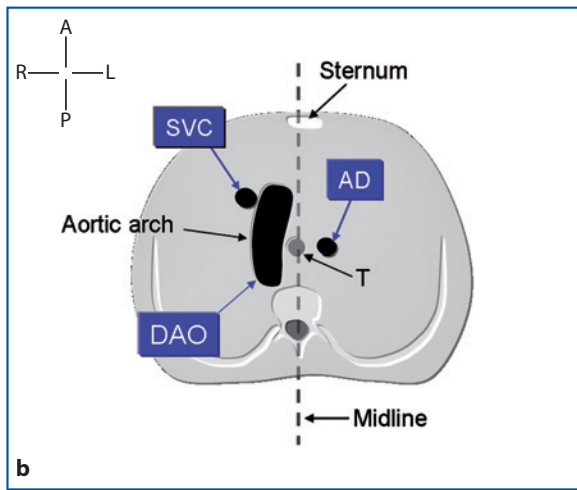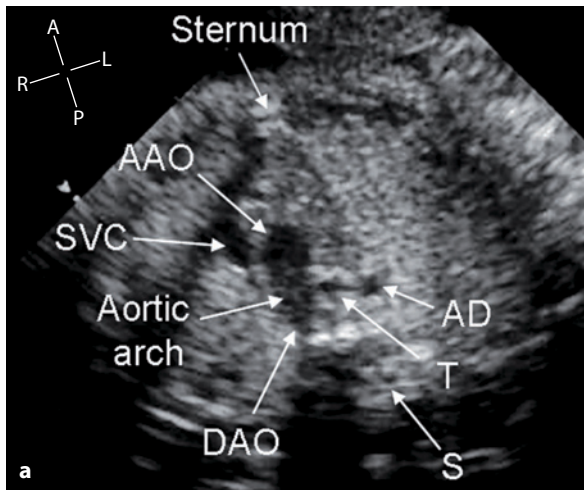
Fig. 11.11 • Aortic arch in a 31-week gestational-age fetus with tetralogy of Fallot and pulmonary atresia (**a**, **c**) and a correlative diagram (**b**). On cross-sectional view, the takeoff of the aortic arch is in the normal position in the middle of the thorax, as in aortic arches in normal relationship to the posterior ventricle. The arch is right sided, lying parallel to the midline and leaving the trachea on its left side. The arterial duct originates from the foot of the left innominate artery (not visible in this image). A cross section of the arterial duct is seen between its origin and the junction with the pulmonary artery (**a**). Color flow mapping (**c**) demonstrates the reversed flow in *red* (*yellow arrow*) in the arterial duct flowing toward the main pulmonary artery (not seen in this picture). *AAO* ascending aorta, *AD* arterial duct, *DAO* descending aorta, *S* spine, *SVC* superior vena cava, *T* trachea
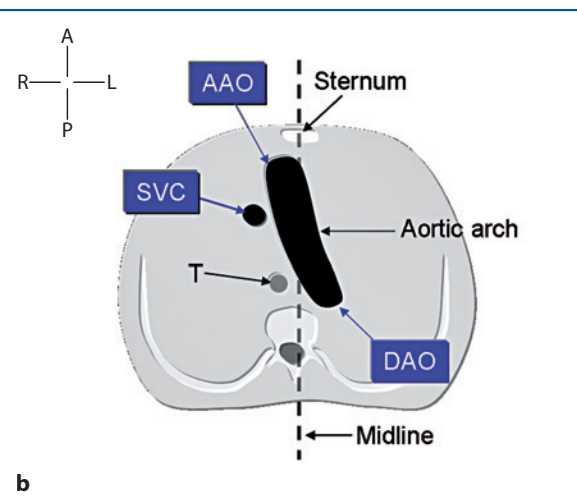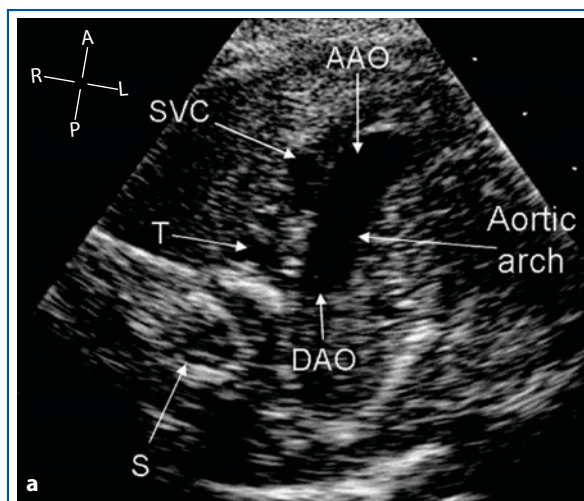
Fig. 11.12 • Aortic arch in a 32-week gestational-age fetus with malposition of the great arteries (**a**) in the setting of double-outlet right ventricle and correlative diagram (**b**). The ascending aorta is anterior and to the right. Cross-sectional examination shows an elongated left aortic arch crossing the midline and leaving the trachea on its right side. *AAO* ascending aorta, *DAO* descending aorta, *S* spine, *SVC* superior vena cava, *T* trachea
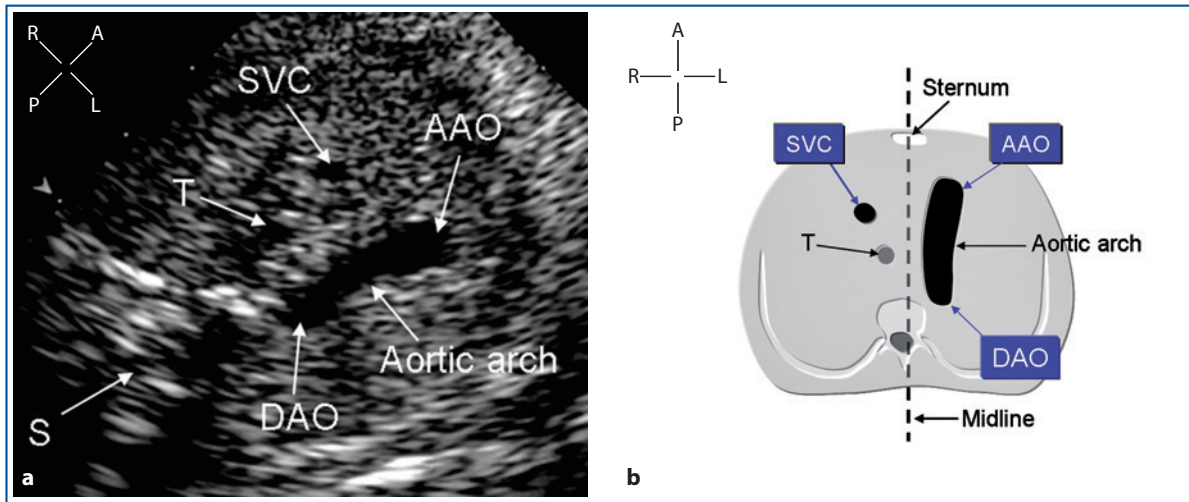
Fig. 11.13 • Aortic arch in a 25-week gestational-age fetus with transposition of the great arteries (**a**) and a correlative diagram (**b**). The ascending aorta is anterior to the left, a very rare but possible position in complete transposition of the great arteries. The aortic arch is longer than normal and does not cross the midline, lying, instead, on a left sagittal plane. The position of the trachea on the right side confirms the left sidedness of the aortic arch. *AAO* ascending aorta, *DAO* descending aorta, *S* spine, *SVC* superior vena cava, *T* trachea
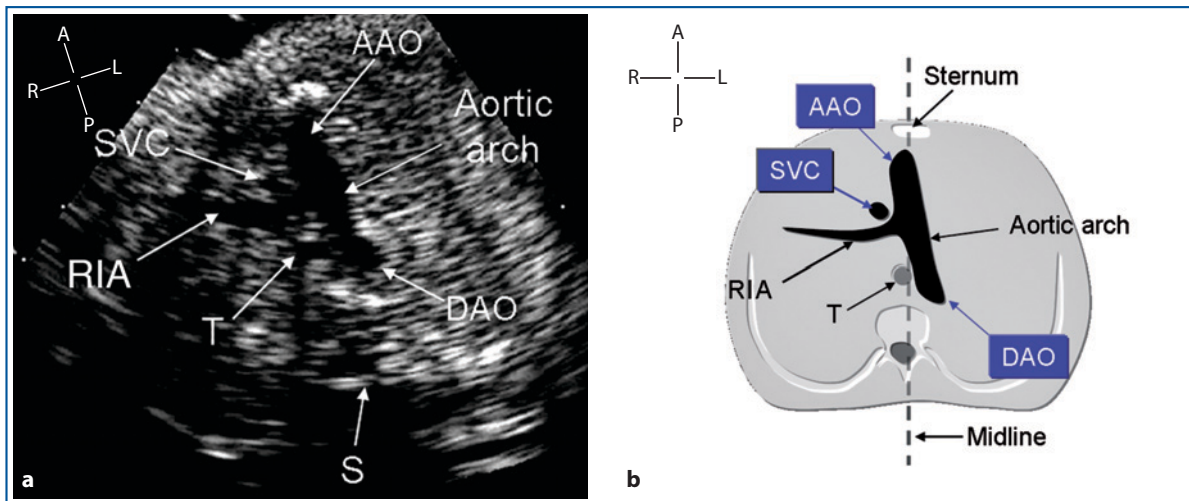
Fig. 11.14 • Aortic arch in a 25-week gestational-age fetus with tricuspid atresia and discordant ventriculoarterial connections. Cross-sectional frame (**a**) and a correlative diagram (**b**). The ascending aorta is in anterior position. The aortic arch shows a long takeoff, which starts immediately behind the sternum and runs in neutral position close to the midline. However, the arch is clearly to the left because it leaves the trachea on its right side. The origin of the right innominate artery is also visible. *AAO* ascending aorta, *DAO* descending aorta, *RIA* right innominate artery, *S* spine, *SVC* superior vena cava, *T* trachea

References

1. Petrikovsky BM, Kaplan GP, Pestrak H (1995) The application of color Doppler technology to the study of fetal swallowing. Obstet Gynecol 86:605-608

2. Kalache KD, Chaoui R, Marcks B et al (2000) Differentiation between human fetal breathing patterns by investigation of breathing-related tracheal fluid flow velocity using Doppler sonography. Prenat Diagn 20:45-50

3. Zalel Y, Gamzu R, Mashiach S et al (2002) The development of the fetal thymus: an in utero sonographic evaluation. Prenat Diagn 22(2):114-117

4. Cho JY, Min JY, Lee YH et al (2007) Diameter of the normal fetal thymus on ultrasound Ultrasound Obstet Gynecol 29:634-638

5. Chaoui R, Korner H, Bommer C et al (2002) Fetal thymus and the 22q11.2 deletion. Prenat Diagn 22:839-840

6. Barrea C, Yoo SJ, Chitayat D et al (2003) Assessment of the thymus at echocardiography in fetuses at risk for 22q11.2 deletion. Prenat Diagn 23:9-15

7. Chaoui R, Kalache KD, Heling KS et al (2002) Absent or hypoplastic thymus on ultrasound: a marker for deletion 22q11.2 in fetal cardiac defects. Ultrasound Obstet Gynecol 20:546-552

8. Volpe P, Marasini M, Caruso G et al (2003) 22q11 deletions in fetuses with malformations of the outflow tracts or interruption of the aortic arch: impact of additional ultrasound signs. Prenat Diagn 23:752-757

9. Achiron R, Rotstein Z, Heggesh J et al (2002) Anomalies of the fetal aortic arch: a novel sonographic approach to in-utero diagnosis. Ultrasound Obstet Gynecol 20:553-557

10. Bronshtein M, Lober A, Berant M (1998) Sonographic diagnosis of fetal vascular rings in early pregnancy. Am J Cardiol 81:101-103

11. Chaoui R, Schneider MBE, Kalache KD (2003) Right aortic arch with vascular ring and aberrant left subclavian artery: prenatal diagnosis assisted by three-dimensional power Doppler ultrasound. Ultrasound Obstet Gynecol 22:661-663

12. Yoo SJ, Min JY, Lee YH et al (2003) Fetal sonographic diagnosis of aortic arch anomalies. Ultrasound Obstet Gynecol 22:535-546

13. Patel CR, Spector ML, Smith PC (2006) Fetal echocardiographic diagnosis of vascular rings. J Ultrasound Med 25:251-257

14. Berg C, Bender F, Soukup M et al (2006) Right aortic arch detected in fetal life. Ultrasound Obstet Gynecol 28:882-889

15. Zidere V, Tsapakis EG, Huggon IC et al (2006) Right aortic arch in the fetus. Ultrasound Obstet Gynecol 28:876-881

16. Gardiner HM (2006) Mind the gap! What we don't know about right aortic arches and aberrant branches Ultrasound Obstet Gynecol 28:868-869

CHAPTER 12 | The Arterial Duct and Aortic Arch Transverse View

The Section Plane

From the transverse view of the aortic arch, with slight angulation of the ultrasound beam caudal and to the left, a simultaneous section of the aortic arch and arterial duct can be obtained. Figure 12.1 shows the level of this section.

The Normal Morphology

The aortic and ductal arches merge together into the descending aorta, with an acute angle between the two. The arterial duct is slightly larger than the aortic isthmus. Both arches sit on the left side relative to the midline structures, which are the trachea and the esophagus. In the normal anatomy, there is no vascular structure coursing behind the trachea (Fig. 12.2).

The Normal Echocardiogram – 2D

On cross-sectional examination of the normal fetus, this view shows, as a *V* shape, the confluence of the ductal and aortic arch, with the descending aorta at the left anterior corner of the spine. The left arm of the *V* is formed by the main pulmonary artery and the arterial duct, and the right arm is formed by the aortic arch. In the normal fetus, the arterial duct arch is slightly larger than the aortic arch. Both arches are on the left side of the trachea, which is seen in cross section, filled with amniotic fluid (Fig. 12.3). This view was designated by
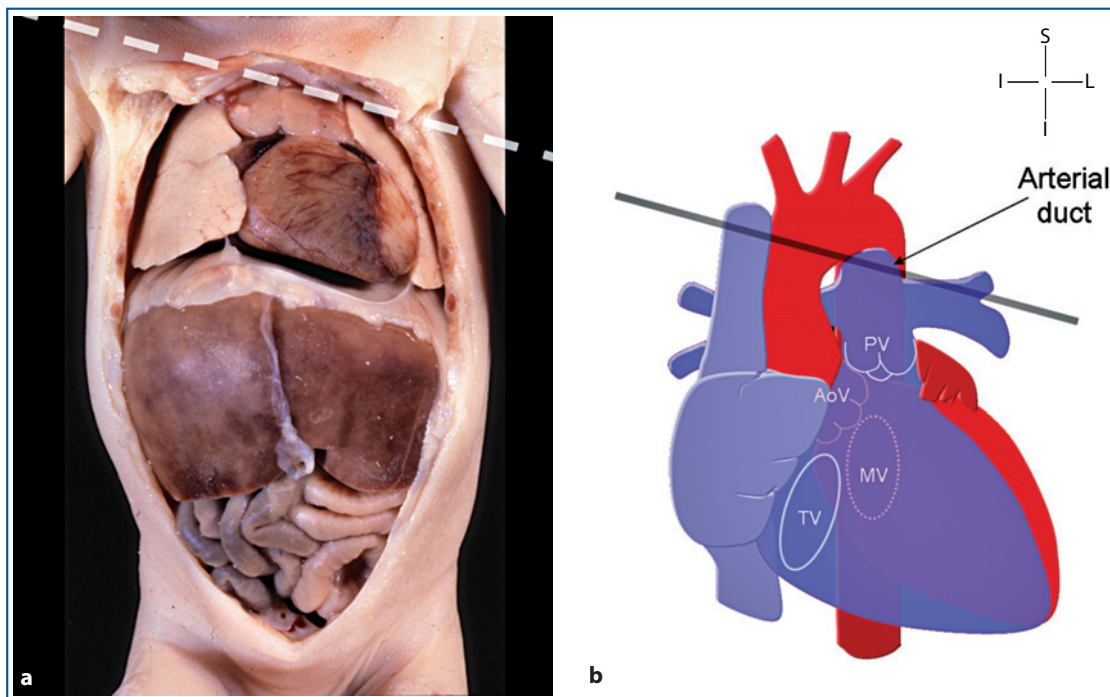
Fig. 12.1 • Level of the transverse view of the arterial duct and the aortic arch. Because the arterial duct lies on a plane that is inferior and to the left relative to the aortic arch, this section is obtained with leftward and caudal tilt of the scan plane from the true horizontal view of the aortic arch. *AoV* aortic valve, *MV* mitral valve, *PV* pulmonary valve, *TV* tricuspid valve
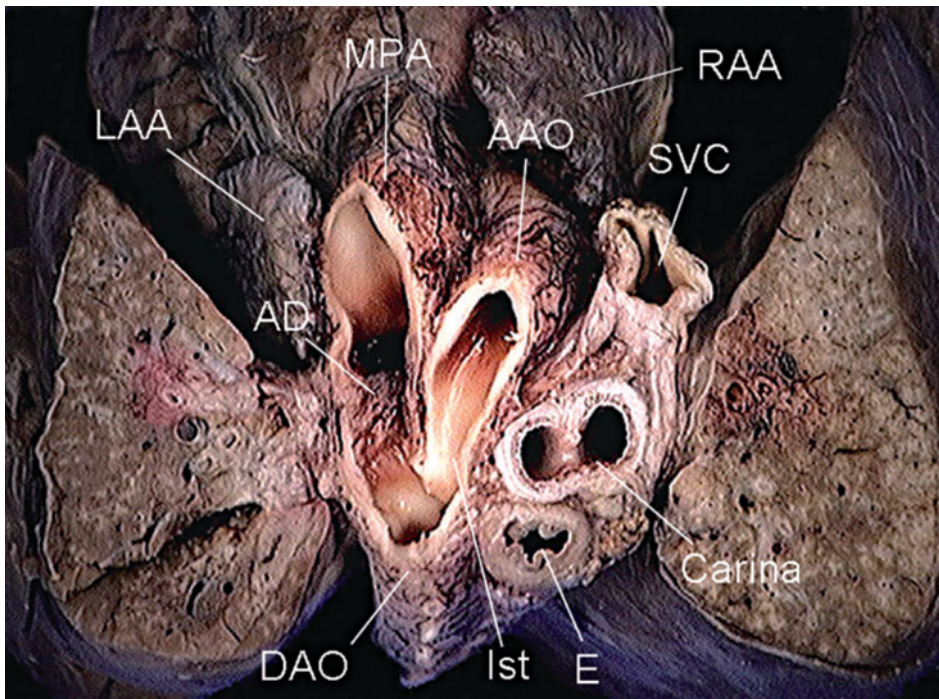
Fig. 12.2 • This normal anatomical specimen, seen from above, is cut to imitate the transverse view of the ductal and aortic arches. The ductal arch is formed by the confluence of the main pulmonary artery into the descending aorta via the arterial duct. In the normal heart, the ductal and aortic arches merge together into the descending aorta close to the anterior left side of the spine. The arterial duct is slightly larger than the aortic isthmus. In this fetus, who had an unexpected spontaneous death at 38 weeks gestation, the arterial duct shows well-formed endothelial folds, which are the anatomical substrate preparing the vessel for postnatal closure. The relationship between the two arches and the bifurcation of the trachea (carina) and esophagus are demonstrated. No vascular structure is coursing behind the trachea. *AAO* ascending aorta, *AD* arterial duct, *DAO* descending aorta, *E* esophagus, *Ist* isthmus, *LAA* left atrial appendage, *MPA* main pulmonary artery, *RAA* right atrial appendage, *SVC* superior vena cava

Yagel et al. [1, 2] as the three-vessel and trachea view (3VT). In the normal fetus, no vascular structure should be seen behind the trachea, and any branch coursing behind it should be considered an aberrant vessel. The diameter of the two arches can be compared in this view, and significant discrepancies between the two can be detected. However, due to the oblique nature of this view, absolute assessment of the size of the great arteries is not reliable. Thus, they are better evaluated in views with the beam at right angle to the structure to be measured. Although measurement of the dimensions of the great arteries is not necessary during a normal fetal scan, this should be done whenever a suspicious disproportion is noted. Values should be compared with normal ranges, plotted against gestational age, of large published series [3, 4].

The Normal Echocardiogram – Color Flow Mapping

Whether the fetus is in ventral or dorsal presentation, in the normal heart, the aortic and ductal arches show the same direction of blood flow on color flow mapping examination (Figs. 12.4, 12.5). In dorsoanterior presentation and when the aortic arch is normally to the left, this view is obtained only with the left paravertebral approach (Fig. 12.5).

In the normal fetus approaching term, there can be a brief reversed flow into the isthmus of the aorta in early diastole (Fig. 12.6). This is thought to be the result of the changing ratio between cerebral and placental resistance with advancing gestation. This observation per se does not reinforce suspicion of systemic outflow obstruction [5].
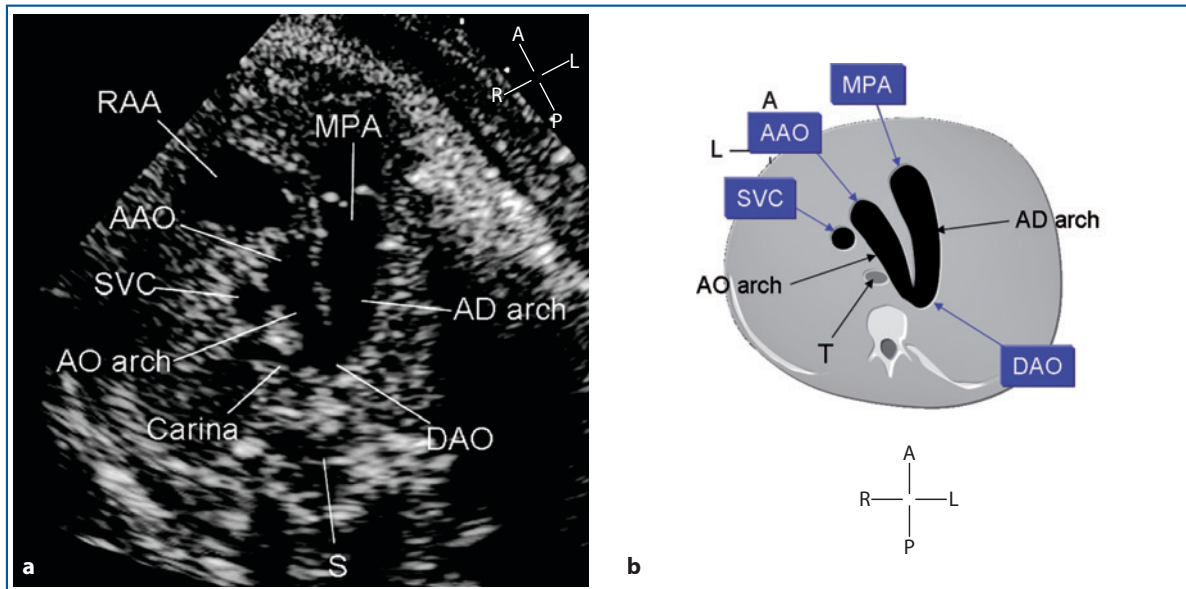
Fig. 12.3 • Cross-sectional echocardiographic frame and corresponding diagram of the transverse view of the arterial duct and aortic arches, shown in caudocranial presentation. The *V*-shaped confluence of the two arches in the descending aorta at the left anterior corner of the spine is displayed. Both arches are located to the left of the trachea. *AAO* ascending aorta, *AD arch* arterial duct arch, *AO arch* aortic arch, *DAO* descending aorta, *MPA* main pulmonary artery, *RAA* right atrial appendage, *S* spine, *SVC* superior vena cava, *T* trachea
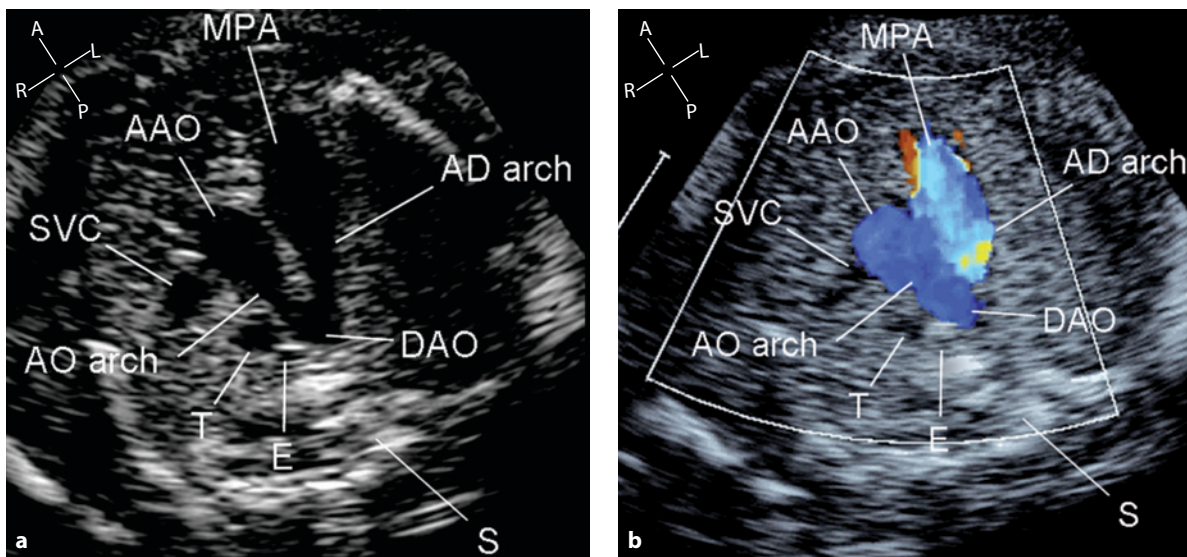
Fig. 12.4 • Transverse view of the arterial duct and aortic arch in a 23-week gestational-age normal fetus with ventral presentation: cross-sectional (**a**) and systolic frame on color flow mapping (**b**). Because the flow in both arches is moving away form the probe, it is represented in *blue*. *AAO* ascending aorta, *AD arch* arterial duct arch, *AO arch* aortic arch, *DAO* descending aorta, *E* esophagus, *MPA* main pulmonary artery, *S* spine, *SVC* superior vena cava, *T* trachea
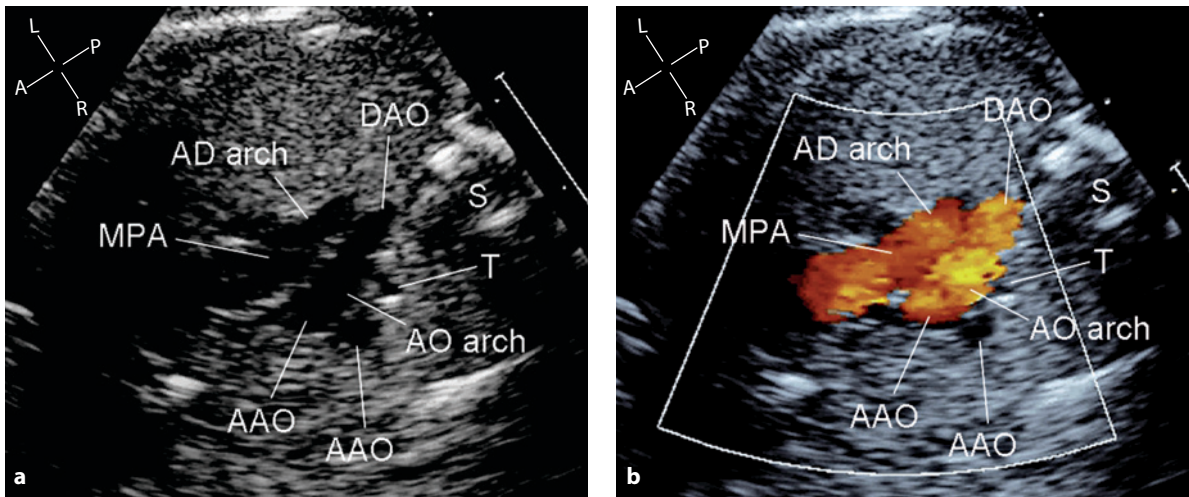
Fig. 12.5 • Transverse view of the arterial duct and aortic arch in a normal fetus with dorsoanterior presentation: cross-sectional (**a**) and systolic frame with color flow mapping (**b**). Because the flow in both arches is approaching the probe, which is placed in the left paravertebral position, it is represented in *red*. *AAO* ascending aorta, *AD arch* arterial duct arch, *AO arch* aortic arch, *DAO* descending aorta, , *MPA* main pulmonary artery, *S* spine, *SVC* superior vena cava, *T* trachea
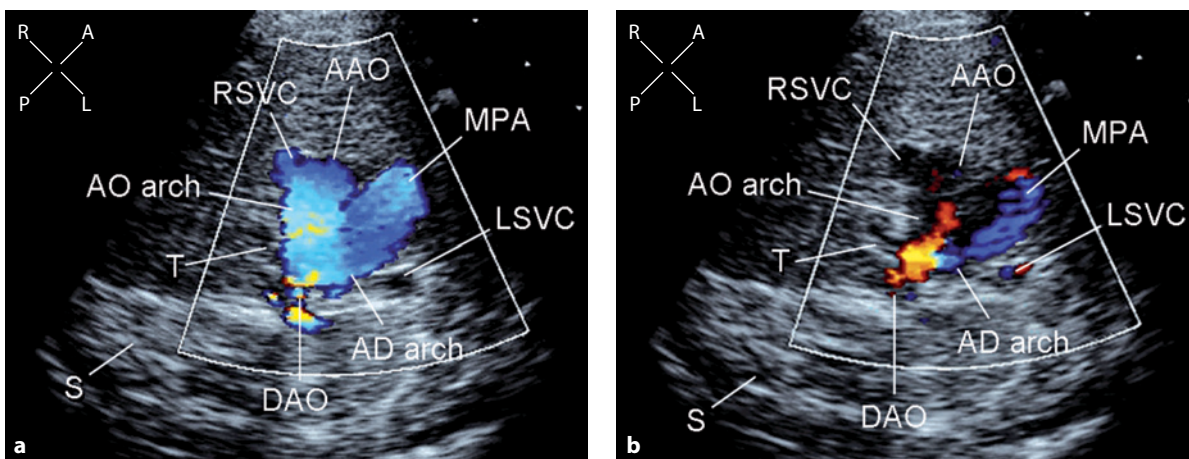
Fig. 12.6 • Transverse view of the aorta and arterial duct in a 36-week gestational-age fetus with bilateral superior vena cava. His fetal and postnatal echocardiogram is otherwise normal. This early systolic frame (**a**) shows in *blue* the normal forward flow into the to arches. In this early diastolic frame (**b**), the brief reversed flow into the aortic isthmus is shown in *red*. This observation is relatively common in fetuses approaching term. *AAO* ascending aorta, *AO arch* aortic arch, *AD arch* arterial duct arch, *DAO* descending aorta, *LSVC* left superior vena cava, *MPA* main pulmonary artery, *RSVC* right superior vena cava, *S* spine, *T* trachea

The Aortic Arch Abnormalities

Severe Aortic Outflow Obstruction

With severe aortic outflow obstruction, as in critical aortic valve stenosis or atresia, the ascending aorta and the aortic arch are partially or totally perfused retrogradely through the arterial duct. Usually, the aortic arch shows a degree of hypoplasia proportional to obstruction severity (Fig. 12.7).

Severe Pulmonary Outflow Obstruction

With severe pulmonary flow obstruction, as in pulmonary atresia or critical pulmonary stenosis, the pulmonary artery is partially or totally perfused retrogradely through the arterial duct. Usually, the transverse view of the arterial duct is difficult to obtain together with the aortic arch, because the arterial duct in these cases is tortuous and lies in a more vertical plane (Fig. 12.8).
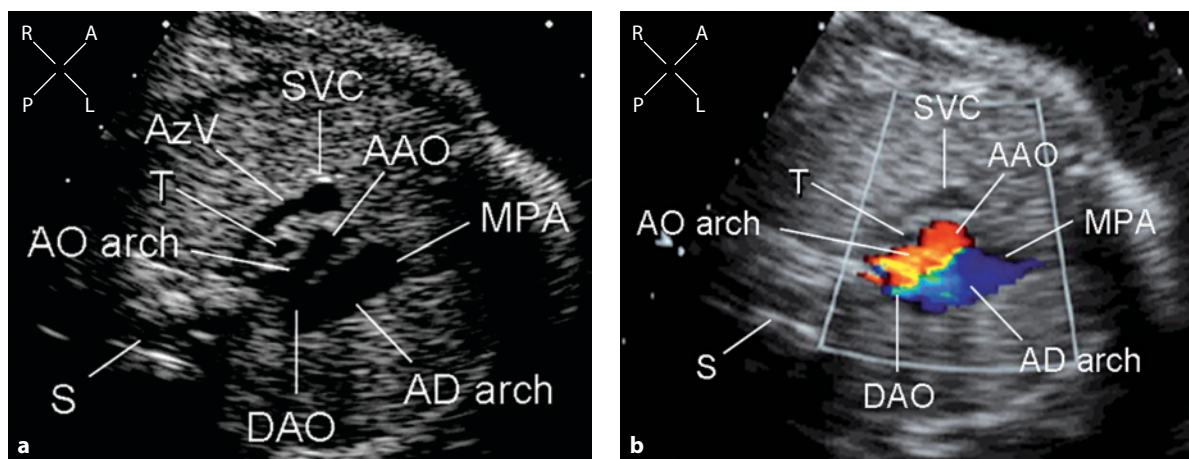
Fig. 12.7 • Cross-sectional and color flow mapping transverse view of the arterial duct and aortic arch in a 30-week gestational-age fetus with aortic atresia and hypoplastic left heart. The aortic arch (**a**) shows a normal takeoff in the middle of the thorax, but it is very small compared with the ductal arch. The aortic arch is normally left-sided, leaving the trachea on its right side. The distal part of the azygos vein is seen, describing a sagittal arch, from the right-posterior paravertebral space to join the superior vena cava anteriorly. On color flow mapping (**b**), flow direction into the arterial duct arch is normal from the pulmonary artery toward the descending aorta, and is represented in *blue*. The small aortic arch is perfused retrogradely in posteroanterior fashion and is represented in *red*. *AAO* ascending aorta, *AD arch* arterial duct arch, *AO arch* aortic arch, *AzV* azygos vein, *DAO* descending aorta, *MPA* main pulmonary artery, *S* spine, *SVC* superior vena cava, *T* trachea
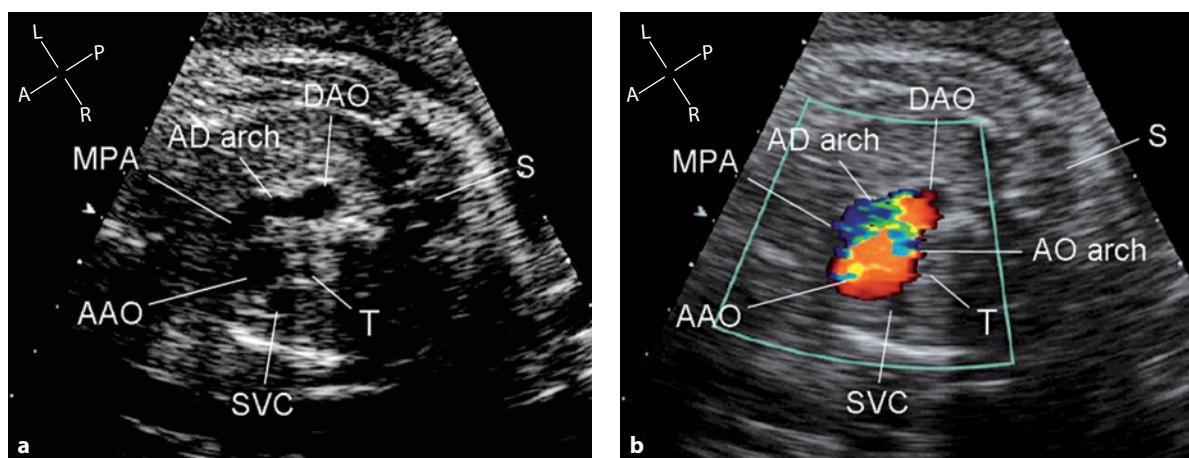
Fig. 12.8 • Arterial duct and aortic arch transverse views in a 33-week gestational-age fetus with pulmonary atresia and intact ventricular septum, with the fetus in dorsoanterior presentation. On cross-sectional scanning (**a**), this is in reality a transverse section of the arterial duct because the aortic arch is not seen, being on a more cranial plane. The arterial duct is small and tortuous, whereas the ascending aorta is enlarged. On color flow mapping (**b**), the arterial duct is perfused in retrograde fashion. Although the transverse aortic arch is not seen on 2D images, on color flow mapping, its flow is well represented because it is sampled by color Doppler on the azimuthal plane. *AAO* ascending aorta, *AD arch* arterial duct arch, *AO arch* aortic arch, *DAO* descending aorta, *MPA* main pulmonary artery, *S* spine, *SVC* superior vena cava, *T* trachea

Pseudoatresia of the Pulmonary Valve

With severe tricuspid valve regurgitation, as is common in Ebstein's malformation or tricuspid valve dysplasia, the pulmonary artery can be totally perfused retrogradely through the arterial duct, even in the absence of organic obstructions to right ventricular outflow. Pseudoatresia of the pulmonary valve can be the consequence of tricuspid valve regurgitation, with inability of the right ventricle to generate sufficient systolic pressure to open the pulmonary valve (Fig. 12.9) [6, 7]. Reversed flow in the arterial duct and the main pulmonary artery is not sufficient to distinguish between functional and organic atresia of the pulmonary valve, which can coexist with tricuspid valve incompetence. Pseudoatresia is suspected when the pulmonary valve, investigated in other views, does not show systolic opening but diastolic regurgitation is present.

Vascular Ring

Aortic arch anomalies include a variety of congenital abnormalities of aortic arch position or branching or both. Some patterns are simple positional anomalies, but others form a complete or incomplete vascular ring around the trachea and esophagus. The ductal and aortic arch transverse view is most useful in diagnosing these cases [8-10]. After right aor-

tic arch with mirror image branching, the second most common anomaly is a right aortic arch associated with an aberrant left subclavian artery and left-sided arterial duct. On transverse views, the aortic arch and arterial duct are seen forming a *U*-shaped vascular loop around the trachea (Fig. 12.10). A coronal longitudinal view of the fetal body, ventrally from the spine, and the use of power Doppler ultrasound, hare been proposed as an alternative ultrasound technique for prenatal assessment of this vascular anomaly [11]. Although aberrant left subclavian artery and left-sided arterial duct realize a vascular ring, the majority of these cases have no symptoms, as the vascular ring is loose.

Azygos Vein Dilatation

The normal azygos vein can be imaged in nearly 50% of normal fetuses in the second trimester and in 98% of cases in the third trimester [12]. The most common cause of azygos vein dilatation is interruption of the inferior vena cava with azygos continuation, a condition most commonly seen in left isomerism of the atrial appendages [13, 14]. More rarely, the flow into the azygos vein can increase for different reasons, as in some forms of anomalous drainage of the pulmonary veins or umbilical vein. A dilated azygos vein can be seen in this transverse
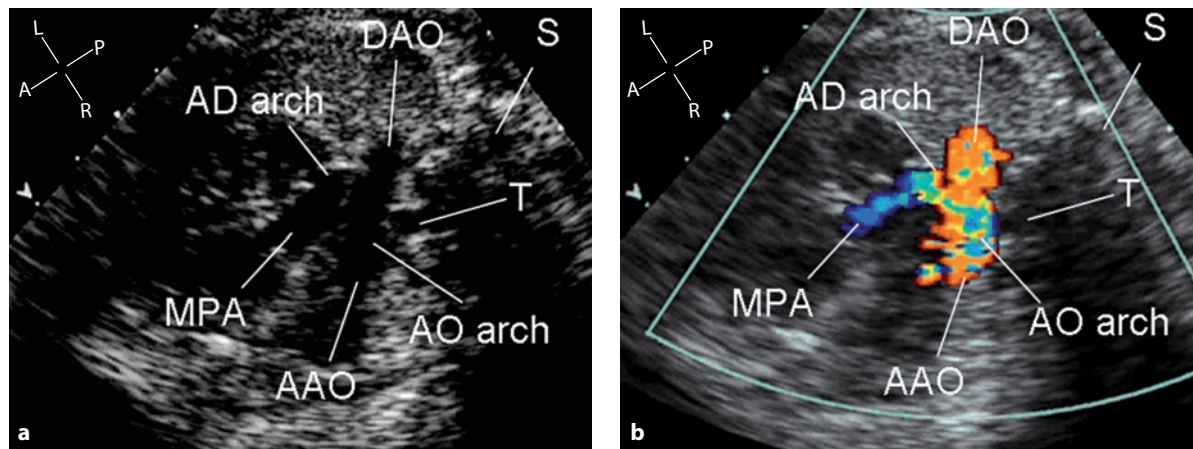
Fig. 12.9 • Arterial duct and aortic arch transverse view in a 37-week gestational-age fetus with Ebstein's malformation of the tricuspid valve, with the fetus in dorsoanterior presentation. On cross-sectional examination (**a**), the pulmonary artery is smaller than the aorta. On moving images, the pulmonary valve cusps show little systolic motion, with incomplete opening. This was the consequence of significant tricuspid valve regurgitation with negligible forward flow and functional atresia of the pulmonary valve. Color flow mapping (**b**) confirms the different sizes of the two great arteries. The arterial duct is retrogradely perfused and is therefore represented in *blue*, whereas the normal flow in the aortic arch is represented in *red*. *AAO* ascending aorta, *AD arch* arterial duct arch, *AO arch* aortic arch, *DAO* descending aorta, *MPA* main pulmonary artery, *S* spine, *T* trachea
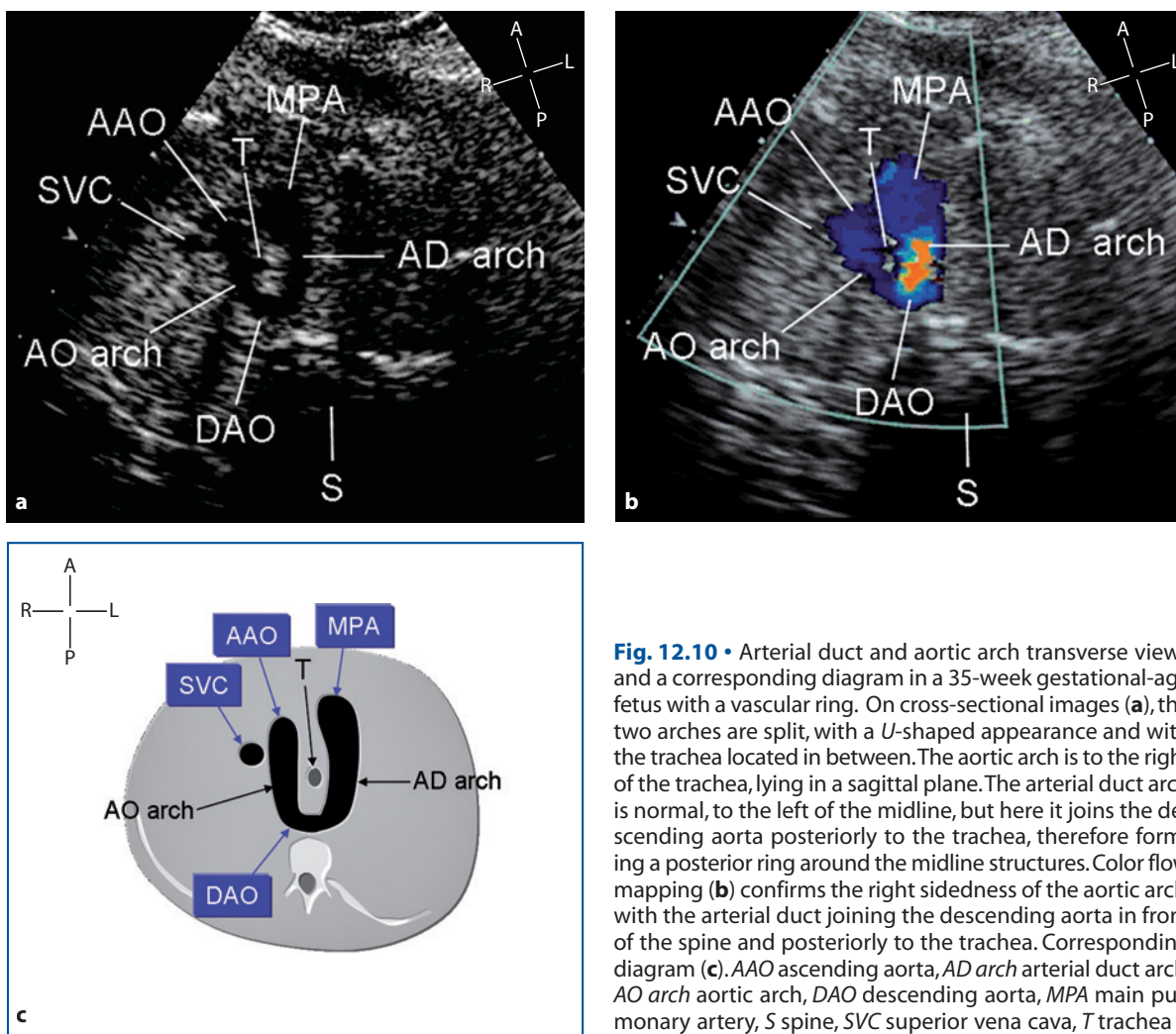
Fig. 12.10 • Arterial duct and aortic arch transverse views and a corresponding diagram in a 35-week gestational-age fetus with a vascular ring. On cross-sectional images (**a**), the two arches are split, with a *U*-shaped appearance and with the trachea located in between. The aortic arch is to the right of the trachea, lying in a sagittal plane. The arterial duct arch is normal, to the left of the midline, but here it joins the descending aorta posteriorly to the trachea, therefore forming a posterior ring around the midline structures. Color flow mapping (**b**) confirms the right sidedness of the aortic arch, with the arterial duct joining the descending aorta in front of the spine and posteriorly to the trachea. Corresponding diagram (**c**). *AAO* ascending aorta, *AD arch* arterial duct arch, *AO arch* aortic arch, *DAO* descending aorta, *MPA* main pulmonary artery, *S* spine, *SVC* superior vena cava, *T* trachea

section forming a third arch on the right side of the trachea, with flow direction opposite that into the aortic and ductal arches (Fig. 12.11).

The Transverse Views of the Fetal Body: an Overview

Summary

The diagram in Figure 12.12 summarizes the transverse and paratransverse views discussed so far in this and previous chapters in which the fetal echocardiographic examination is based on short-axis views of the heart. Long-axis views often represent the most difficult and time-consuming part of the examination, which lengthens examination time and often necessitates waiting until the fetus assumes a more favorable presentation. Because transverse views are more quickly and easily obtained, it has been proposed that the fetal heart be examined on transverse planes [1]. The examiner can obtained these sections by sliding the scanning plane in a continuous motion cephalad, from the upper abdomen to the upper part of the thorax.
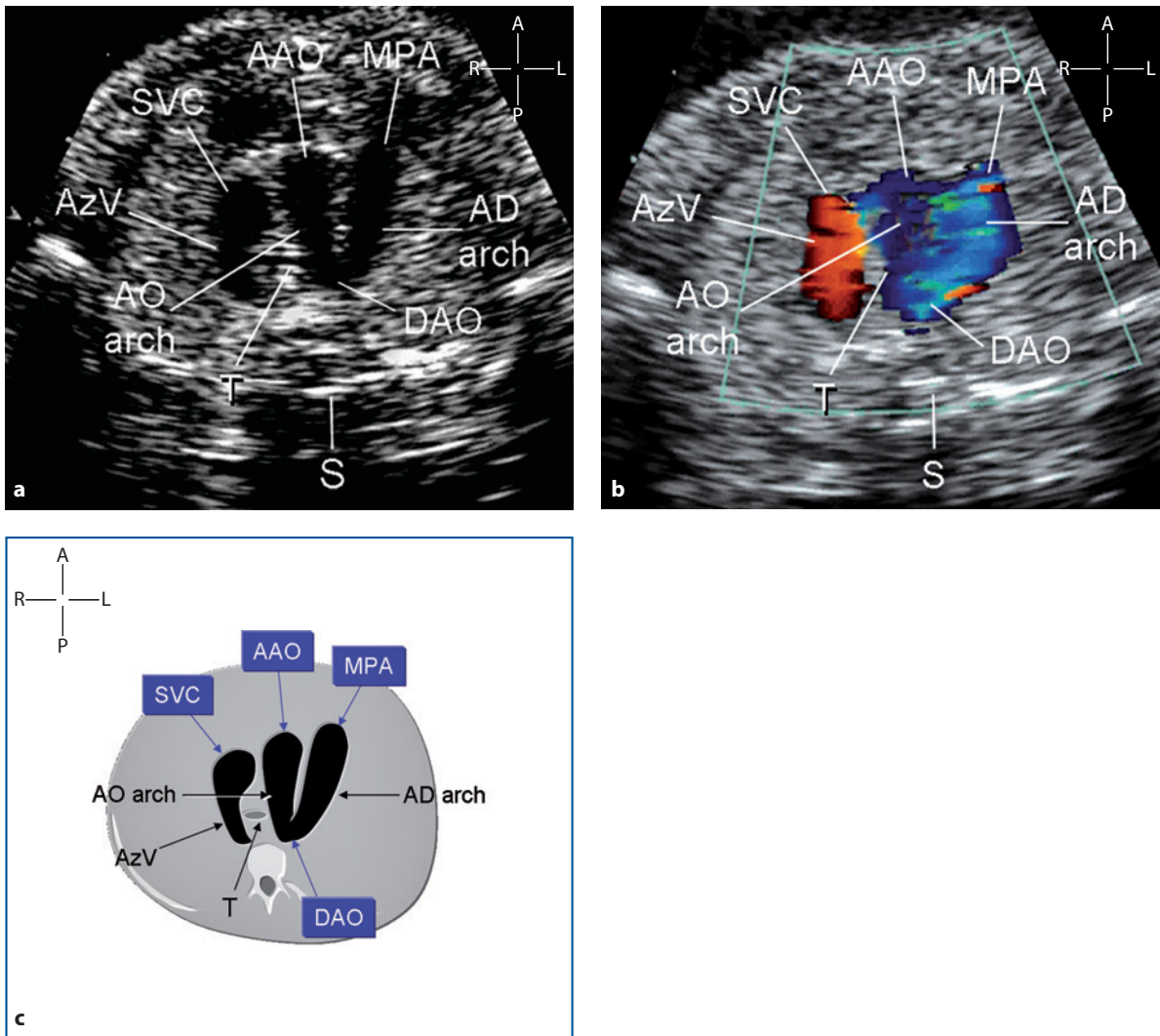
Fig. 12.11 • Transverse views of the arterial duct and aortic arch in a 23-week gestational-age fetus with absence of the venous duct with persistent right umbilical vein draining into the superior vena cava via the azygos vein. On cross-sectional examination (**a**), three arches are seen. The aortic arch is in the middle. It is in the normal left-sided position because it crosses the midline and leaves the trachea on its right side. Due to high cardiac output circulation, it appears slightly dilated and with increased pulsation on moving images. The arterial duct arch, which in the normal heart joins the descending aorta in front of the spine, is on the left. The arch on the right side of the midline is formed by an exceptionally dilated azygos vein that arches anteriorly and joins the superior vena cava. On color flow mapping (**b**), the flow into the aortic arch and that of the arterial duct show a normal anteroposterior direction, from the ascending aorta and main pulmonary artery toward the descending aorta. It is therefore represented in *blue*. The flow into the azygos vein has a posteroanterior direction, from the right paravertebral space toward the front where the vein merges into the superior vena cava. It is therefore represented in *red*. Corresponding diagram (**c**). *AAO* ascending aorta, *AD arch* arterial duct arch, *AO arch* aortic arch, *AzV* azygos vein, *DAO* descending aorta, *MPA* main pulmonary artery, *S* spine, *SVC* superior vena cava, *T* trachea
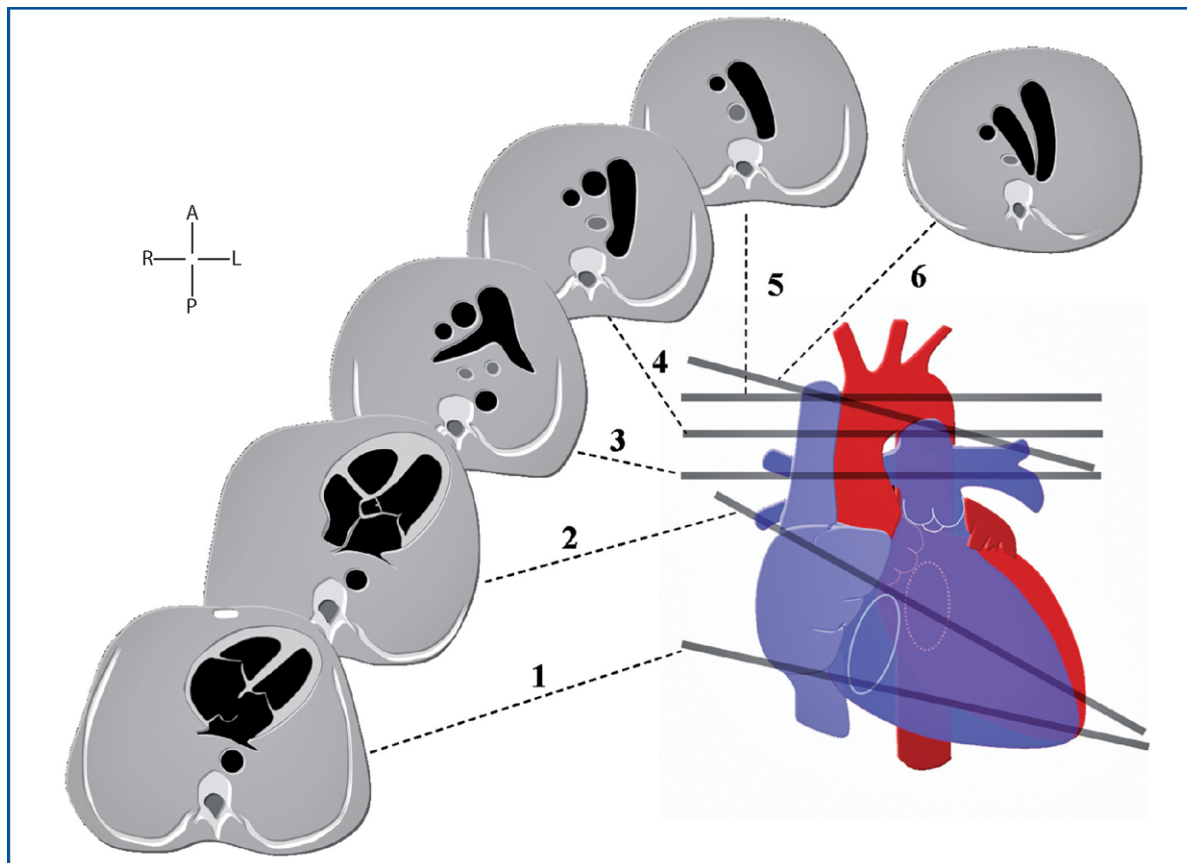
Fig. 12.12 • This diagram summarizes the transverse and paratransverse section of the fetal thorax for heart assessment: the four-chamber view (*1*), the most caudal section; the five-chamber view (*2*), with its cranial angulation relative to the true transverse plane; the three-vessel view (*3*), with the bifurcation of the main pulmonary artery; the arterial duct transverse view (*4*); the aortic arch transverse view (*5*); the arterial duct and aortic arch transverse view (*6*), with its left and caudal angulation

References

1. Yagel S, Cohen SM, Achiron R (2001) Examination of the fetal heart by five short-axis views a proposed screening method for comprehensive cardiac evaluation. Ultrasound Obstet Gynecol 17:67-69
2. Yagel S, Arbel R, Anteby EY et al (2002) The three vessel and trachea view (3VT) in fetal cardiac scanning. Ultrasound Obstet Gynecol 20:340-345
3. Zalel Y, Wiener Y, Gamzu R et al (2004) The three-vessel and tracheal view of the fetal heart: an in utero sonographic evaluation. Prenat Diagn 24:174-178
4. Moon MH, Cho JY, Park EJ et al (2007) Three-vessel view of the fetal heart: in utero development of the great vessels. Prenat Diagn 27:158-163
5. Fouron JC (2003) The unrecognized physiological and clinical significance of the fetal aortic isthmus. Ultrasound Obstet Gynecol 22 (5):441-447
6. Lee CL, Hsieh KS, Huang TC et al (1999) Recognition of functional pulmonary Atresia by color Doppler echocardiography. Am J Cardiol 83:987-988
7. Hiraumi Y, Watanabe K, Tomita H et al (2002) Doppler echocardiographic differentiation of functional from anatomical pulmonary atresia analysis using quantitative parameters, Circ J 66:665-667
8. Achiron R, Rotstein Z, Heggesh J at al (2002) Anomalies of the fetal aortic arch: a novel sonographic approach to in-utero diagnosis. Ultrasound Obstet Gynecol 20:553-557
9. Yoo SJ, Min JY, Lee YH, Roman K et al (2003) Fetal sonographic diagnosis of aortic arch anomalies. Ultrasound Obstet Gynecol 22:535-546
10. Patel CR, Lane JR, Spector ML, Smith PC (2006) Fetal echocardiographic diagnosis of vascular rings. J Ultrasound Med 25:251-257
11. Chaoui R, Schneider MBE, Kalache KD (2003). Right aortic arch with vascular ring and aberrant left subclavian artery: prenatal diagnosis assisted by three-dimensional power Doppler ultrasound. Ultrasound Obstet Gynecol 22:661-663

12. Belfar HL, Hill LM, Peterson C et al (1990) Sonographic imaging of the fetal azygous vein. Normal and pathologic appearance. J Ultrasound Med 9(10):569-573

13. Sheley RC, Nyberg DA, Kapur R (1995) Azygous continuation of the interrupted inferior vena cava: a clue to prenatal diagnosis of the cardiosplenic syndromes. J Ultrasound Med 14(5):381-387

14. Berg C, Geipel A, Kamil D et al (2005) The syndrome of left isomerism: sonographic findings and outcome in prenatally diagnosed cases. J Ultrasound Med 24(7):921-931

CHAPTER 13

The Inferior and Superior Vena Cava Long-Axis View (The Bicaval View)

The Section Plane

This view is obtained by orienting the scan plane along the true sagittal plane of the fetal body immediately to the right of the midline (Fig. 13.1). Alternatively, it is easily obtained with slight translation from a long-axis view of the aortic arch obtained from a parasagittal view of the right chest (Fig. 13.2b). Because this view shows the connection of superior and inferior vena cava with the right atrium, it is also called the bicaval view.

The Normal Morphology

In the specimen shown in Figure 13.3, the fetal thorax is cut in a simulated echocardiographic plane in the bicaval view. The right atrium sits on the diaphragm above the right lobe of the liver, where a section of the umbilical vein and the ductus venosus is visible. Inside the cavity of the right atrium, the terminal crest is shown, with pectinate muscles branching at a right angle and running anteriorly into the right atrial appendage. Posteriorly to the terminal crest, the venous part of the right atrium is displayed, receiving the superior and inferior vena cava. The proximal portion of the inferior vena cava is enlarged because it drains the flow from the venous duct and the suprahepatic veins and is overridden by the crista dividens, which is the superior portion of the interatrial septum. The upper atrial septum separates the right from the left atrium and represents the superior rim of the foramen ovale. The short axis of the right pulmonary artery is visible behind the superior vena cava, close to its junction with the right atrium. A section of the thymus is seen between the anterior wall of the thorax and the superior vena cava.
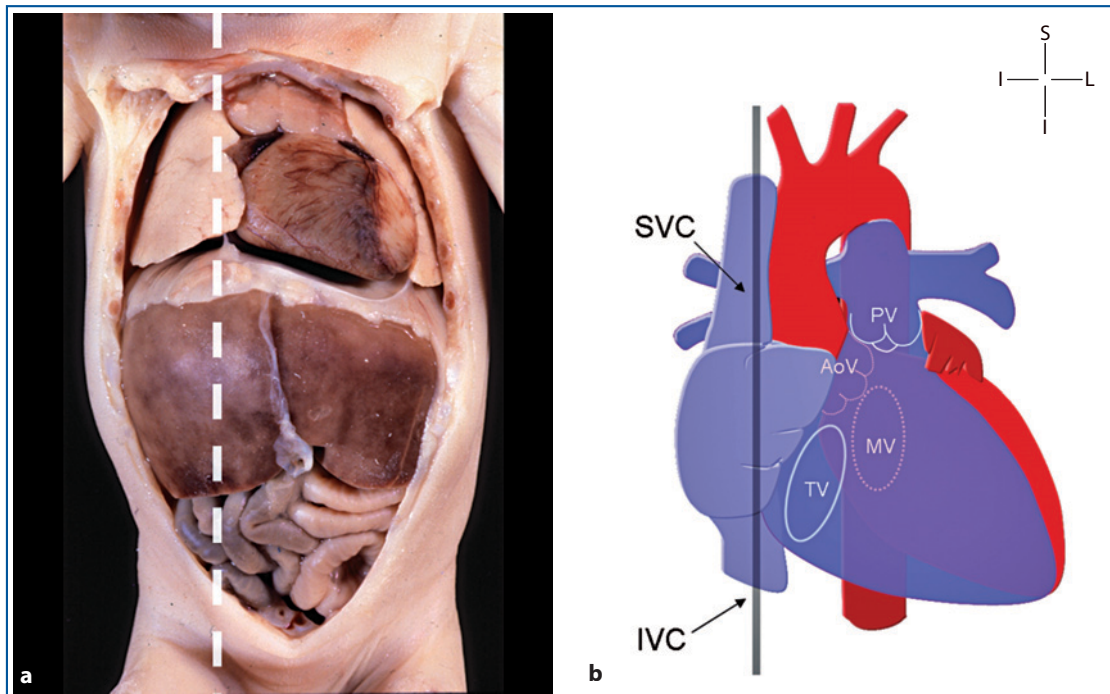
Fig. 13.1 • The plane of the bicaval view along a true sagittal plane is shown on the fetal body (**a**) and on a heart diagram (**b**). *AoV* aortic valve, *IVC* inferior vena cava, *MV* mitral valve, *PV* pulmonary valve, *SVC* superior vena cava, *TV* tricuspid valve
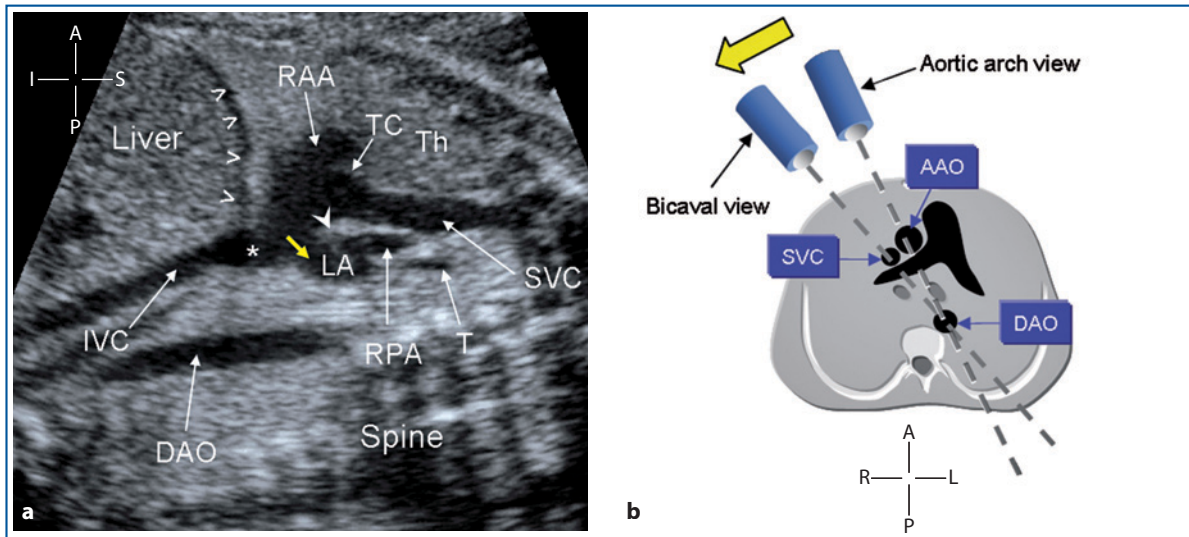
Fig. 13.2 • Normal bicaval view in a 36-week gestational-age fetus (**a**). *Open arrowheads* indicate the anterior portion of the diaphragm. The *arrowhead* indicates the posterosuperior portion of the interatrial septum, which delimits superiorly the foramen ovale (*yellow arrow*) and overrides the proximal portion of the inferior vena cava (*asterisk*). A short tract of the descending aorta is seen posteriorly, in front of the spine. The diagram (**b**) shows the small angle between the plane of the long-axis view of the aortic arch and that of the bicaval view. From the long-axis view of the aortic arch, the bicaval view is easily obtained with slight rightward angulation (*yellow arrow*) of the scanning plane, maintaining the descending aorta as the center of this rotation. *AAO* ascending aorta, *DAO* descending aorta, *IVC* inferior vena cava, *LA* left atrium, *RAA* right atrial appendage, *RPA* right pulmonary artery, *SVC* superior vena cava, *T* trachea, *TC* terminal crest, *Th* thymus
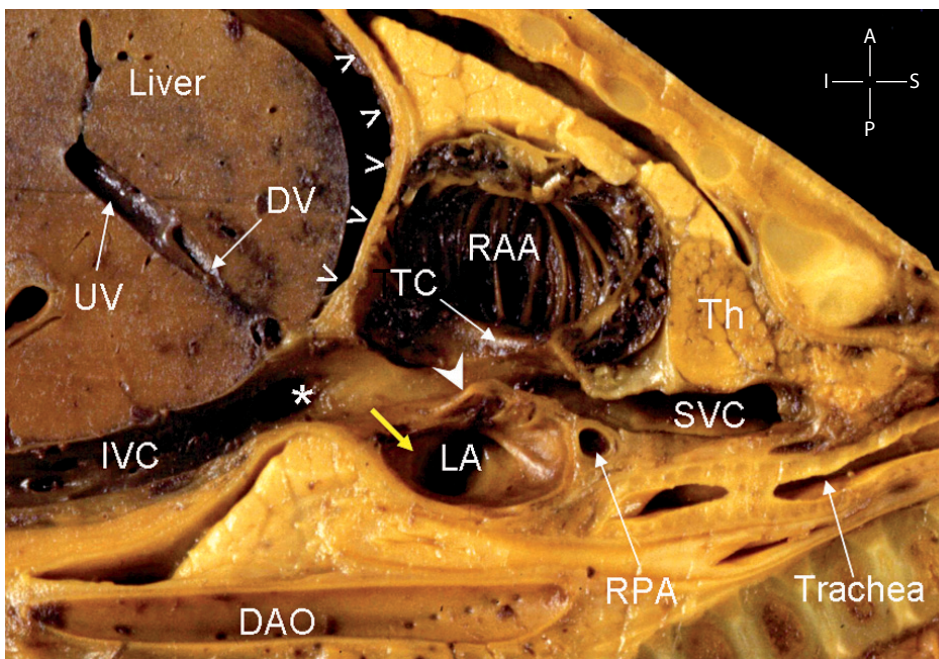
Fig. 13.3 • Anatomical specimen of the normal fetal thorax sectioned along a parasagittal plane to imitate the long-axis view of the superior and inferior vena cava. The relationship of the two vena cavas with the right atrium and the upper portion of the interatrial septum (*arrowhead*) is shown. The size of the inferior vena cava increases above the level of the confluence of the ductus venosus and the suprahepatic veins (*asterisk*). The *yellow arrow* indicates the foramen ovale, the natural opening between the two atria. Below the level of the diaphragm (*open arrowheads*), the terminal part of the umbilical vein and the ductus venosus is seen. Due to a left oblique angulation of this section, the descending aorta is displayed in the bottom part of the picture (see text for details). *DAO* descending aorta, *DV* ductus venosus, *IVC* inferior vena cava, *LA* left atrium, *RAA* right atrial appendage, *RPA* right pulmonary artery, *SVC* superior vena cava, *TC* terminal crest, *Th* thymus, *UV* umbilical vein

The Normal Echocardiogram – 2D

On echocardiographic assessment, the bicaval view shows the superior and inferior vena cava in a longitudinal section, along with their junction with the right atrium. In the normal fetus, the size of the vena cavas is similar, with the exception of the proximal part of the inferior vena cava, which enlarges when receiving the flow from the umbilical and suprahepatic veins. The right atrial appendage is displayed anteriorly and a small portion of the left atrium posteriorly, separated by the posterosuperior part of the atrial septum. The pectinated muscles are not visible on cross-sectional echocardiography. The right pulmonary artery is imaged in cross section behind the superior vena cava and above the roof of the left atrium [1].

With slight manipulation of the transducer, the distal portion of the umbilical vein, the ductus venosus, and usually one suprahepatic vein is visible inside the liver. The Eustachian valve is seen in the right atrium close to the mouth of the inferior vena cava. When this view is obtained from the right chest and with right-to-left angulation, a portion of the descending aorta is visible posteriorly along the spine (Figs. 13.2, 13.4).

The Normal Echocardiogram – Color Flow Mapping and Pulsed Doppler

Transducer positions that provide the best representation of the anatomical structures often are not those that provide the best flow detection on Doppler examination. In fact, anatomic imaging is most effective when the echocardiographic targets are perpendicular to the ultrasound beam, whereas flow detection by Doppler is most effective when targets (red blood cells) are parallel to the ultrasound beam. The bicaval view is one of the best examples in which anatomical study and flow investigations require different approaches with the ultrasound beam.

When the bicaval view is obtained by an approach to the fetal body at the heart level, the two vena cava are investigated at a right angle by the ultrasound beam. Figures 13.2 and 13.4 show how many anatomical details are detected by this approach. On the other hand, with this angulation, the flow inside the two veins appears relatively faint on color Doppler examination due to the unfavorable interrogation angle. Black areas can appear inside the color map on the vessel not only because no Doppler shift is detected but also because the flow velocity may be inferior to the minimal threshold. Moving the transducer caudally or cranially improves flow representation by reducing the interrogation angle. Moreover, keeping the scale threshold as low as 20 cm/s highlights the low-velocity flow of the vena cava (Fig. 13.5).

Fig. 13.4 • This slightly modified bicaval view shows the Eustachian valve and a section of one suprahepatic vein below the diaphragm (*open arrowheads*). Also in this section, a short tract of the descending aorta is seen posteriorly to the left atrium. *DAO* descending aorta, *EV* Eustachian valve, *HV* hepatic vein, *IVC* inferior vena cava, *LA* left atrium, *RPA* right pulmonary artery, *SVC* superior vena cava

Fig. 13.5 • Color flow mapping of a bicaval view in a normal 36-week gestational-age fetus. The scale setting was intentionally set at 34 cm/s. Due to the larger flow and slightly more favorable insonation angle, the flow inside the inferior vena cava is better represented. Aliased flow is seen inside the adjacent aortic arch. *AOA* aortic arch, *DAO* descending aorta, *IVC* inferior vena cava, *IMA* internal mammary artery, *LA* left atrium, *RAA* right atrial appendage, *RPA* right pulmonary artery, *SVC* superior vena cava

Sagittal or parasagittal views of the fetal body are the best projections to evaluate the flow of the inferior or superior vena cava. Even in the presence of a favorable fetal position, it is rarely possible to align the ultrasound beam with the flow in the vena cava at an angle less than 30°. The flow from the inferior vena cava in the intrathoracic area is joined to that of the proximal ductus venosus and the suprahepatic veins. Animal-model studies have demonstrated how these flows have different velocities and tend not to mix with one another [2]. The blood from the left suprahepatic vein (which receives the ductus venosus blood flow) drains into the left dorsal portion of the caval flow and is oriented toward the foramen ovale by the Eustachian valve and the upper portion of the interatrial septum (crista dividens). Therefore, the left sections of the heart receive a significant portion of the placental blood flow, with a higher oxygen concentration, which is distributed to the coronary and cerebral circulation through the ascending aorta. Blood coming from the abdominal portion of the inferior vena cava and the other two suprahepatic veins (middle and right) drain into the right ventral portion of the caval flow of the superior vena cava and is oriented in the right cardiac cavity. Due to this double source of flow in its terminal tract, evaluation of the inferior vena cava should ideally be done by positioning the sample volume in the abdominal tract between the renal veins and the outlet of the ductus venosus (Fig. 13.6a). However, as this is no easy technical feat, imaging the flow in the suprahepatic vein as been proposed as a valid alternative [3].

The caval flow shows a triphasic profile (Fig. 13.6b). A systolic anterograde peak (S wave) is observed due to the atrial "suction" produced by the movement of the tricuspid valve plane in an base-to-apex direction during ventricular systole. A lower anterograde peak (D wave) is observed during early diastole, which corresponds to the reduction in atrial pressure produced by the opening of the atrioventricular valve and the subsequent passive filling of the ventricle. A small retrograde wave (A wave) is observed in late diastole during atrial contraction. In the normal fetus, the ratio of the reverse flow during atrial contraction to the forward flow (systolic and diastolic) decreases as gestation advances. In the third trimester, this ratio should be 10% or less of the anterograde flow [4].

As it is difficult to obtain correct alignment of the ultrasound beam, the absolute velocities of the vena cava are usually not evaluated. Instead, some indices, such as the ratio between systolic and diastolic peak velocities, are used. This ratio, which expresses flow pulsatility, is more or less constant with a value of 1.8 ± 0.2 throughout the entire gestation period [5-7]. The flow profile of the superior vena cava is similar to that of the inferior vena cava, although with less inversion during atrial contraction.
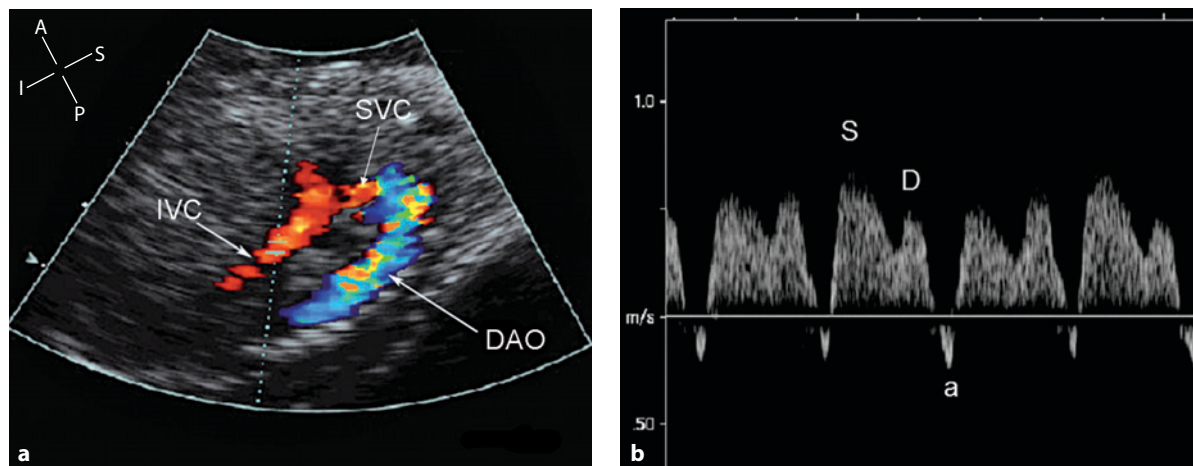
Fig. 13.6 • Sagittal view of the inferior vena cava in a 22-week gestational-age fetus illustrating the position of the sample volume for inferior vena cava Doppler assessment (**a**). This view is obtained with an approach to the superior part of the fetal thorax that keeps the angle between the ultrasound beam and the flow into the vena cava as small as possible. Color flow mapping facilitates the position of the sample volume inside the vessel for pulsed Doppler assessment. Corresponding pulsed Doppler flow profile (**b**) showing systolic (*S*) and diastolic (*D*) waves of the forward flow and reversed flow (*a*) during atrial contraction. *DAO* descending aorta, *IVC* inferior vena cava, *SVC* superior vena cava
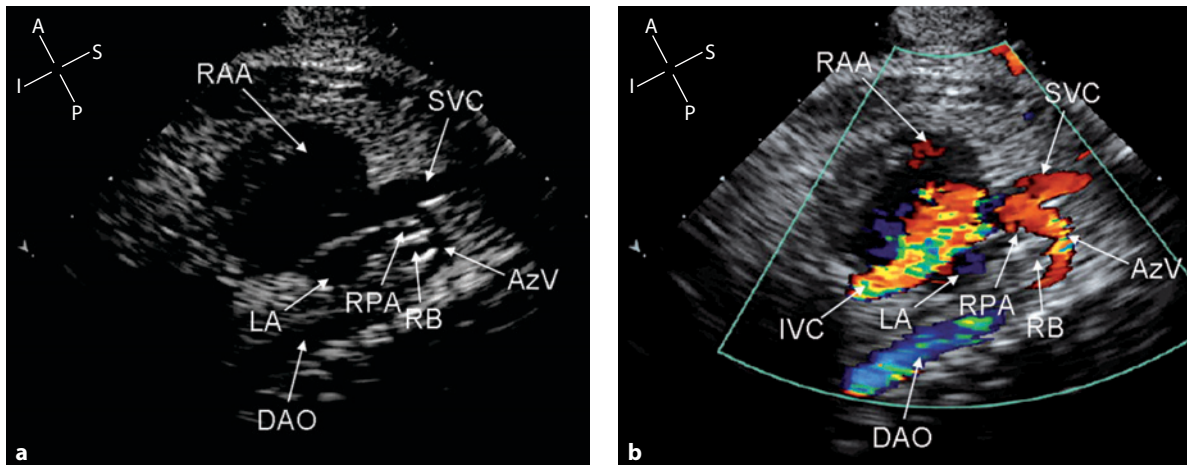
Fig. 13.7 • An example of long-axis view of the azygos vein in a normal 36-week gestational-age fetus. On cross-sectional examination (**a**), the azygos vein is seen coming from the posterior paravertebral space and arching anteriorly above the right pulmonary artery and bronchus. The vein joins the posterior aspect of the superior vena cava near its junction with the right atrium. Because of the oblique angulation of this view, the inferior vena cava is not seen, whereas a small portion of the descending aorta is seen along the spine. Color flow mapping (**b**) shows the flow into the arch of the azygos vein coded in *red*. Although the inferior vena cava is not visible, the flow from this vein is well seen coming from the floor of the right atrium. The runoff into the descending aorta is displayed in *blue* along the spine. *AzV* azygos vein, *DAO* descending aorta, *IVC* inferior vena cava, *LA* left atrium, *RAA* right atrial appendage, *RB* right bronchus, *RPA* right pulmonary artery, *SVC* superior vena cava

The Azygos Vein

The azygos vein connects the suprarenal portion of the inferior vena cava with the right superior vena cava. It can originate from the right lumbar or renal vein or from the inferior vena cava. After entering the thorax through the aortic opening of the diaphragm, it runs medial to the thoracic vertebrae and to the right of the aorta. Along its intrathoracic course, it receives the lower ten right intercostal veins. At the level of the fourth thoracic vertebra, it arches anteriorly to connect the posterior surface of the superior vena cava. (See Figure 3.8, Chapter 3).

With favorable fetal presentation, the azygos vein is visible echocardiographically on a modified bicaval view with slight medial orientation. It is seen arching above the right bronchus and the right pulmonary artery and veins to join the superior vena cava. On color Doppler, the flow in the azygos vein arch is coded in opposite color to that in the aortic arch (Fig. 13.7a, b).

Vena Cava Disproportion

In the normal fetus, the two vena cavas have a similar diameter with the exception of the terminal part of the inferior vena cava. When one vena cava is disproportionately large, increased flow from different causes is suspected: arteriovenous fistulas; large tumors with increased vascular supply; anomalous systemic or pulmonary venous drainage [8, 9]. The disproportion between the two veins must be confirmed by color Doppler assessment. Some examples are shown in Figures 13.8-13.10.

Azygos Vein Dilatation

The most common cause of azygos vein dilatation is the interruption of the inferior vena cava with azygos continuation. This is one of the most consistent features in left isomerism, observed in 78% of cases in postnatal series [10]. A dilated azygos vein can occur also when this vein is an alternative route to the heart, for example, because of kinking of the inferior vena cava due to liver herniation in large omphalocele. An interrupted inferior vena cava is often associated with direct hepatic vein drainage into the atrial floor. More rarely, the azygos vein can dilate when it is part of an anomalous drainage of the pulmonary veins or the umbilical vein (Fig. 13.11).

A dilated azygos vein is first suspected by the detection of two vessels nearly equal in size – the aorta and the azygos vein – lying behind the heart on transverse or long-axis views of the fetal thorax. The vessel more posterior and to the right is the azygos vein (Fig. 13.12) [11].
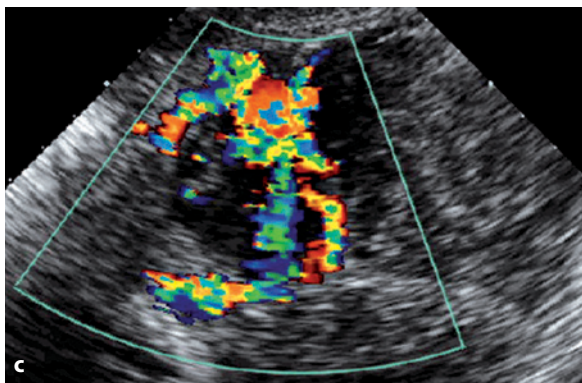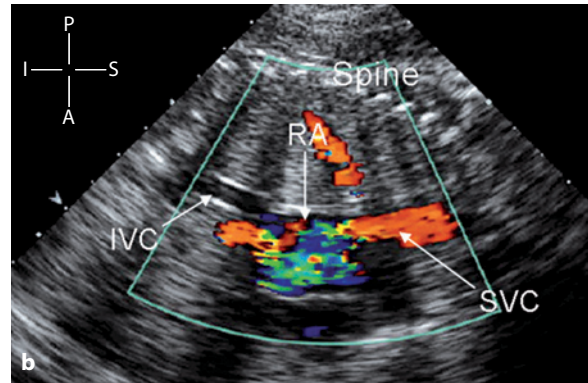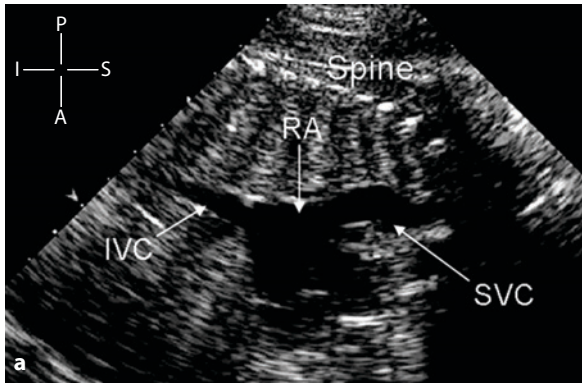
Fig. 13.8 • Bicaval view, with dorsoanterior presentation, in a 33-week gestational-age fetus with a large intracranial arteriovenous malformation. On cross-sectional image (**a**), the superior vena cava is enlarged and tortuous, being the efferent vessel of a large intracranial arteriovenous fistula. Despite the more unfavorable insonation angle, only the flow of the superior vena cava is well represented because of the large flow in this vessel coming from the arteriovenous malformation (**b**). Transverse section (**c**) of the fetal head showing a large arteriovenous malformation. On color Doppler, there are multiple vessels connecting with an ovoid "aneurism" located in the posterosuperior part of the fetal brain. *IVC* inferior vena cava, *RA* right atrium, *SVC* superior vena cava
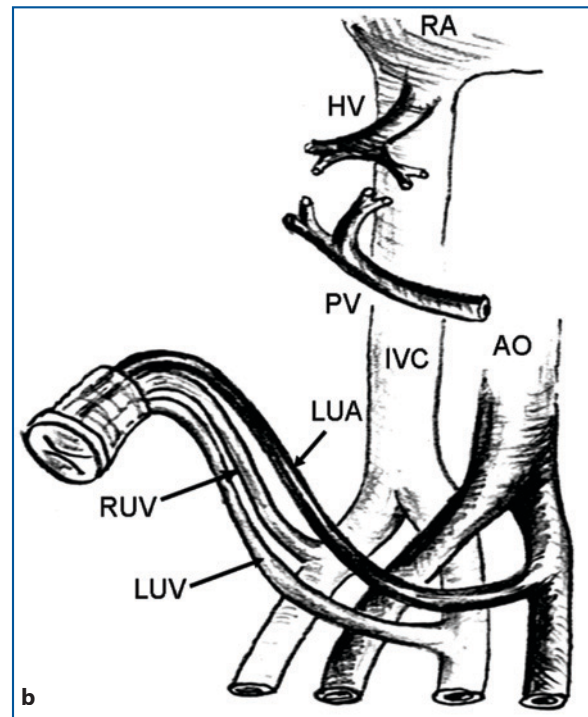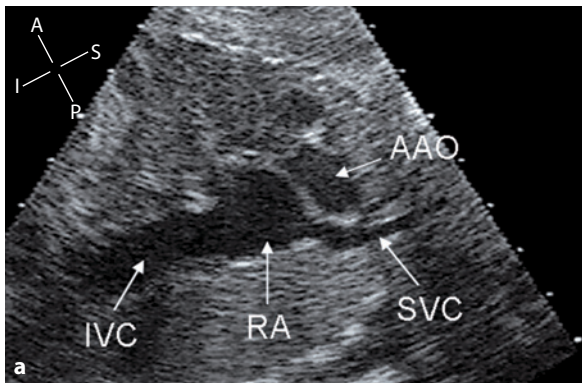
Fig. 13.9 • Bicaval view in a 30-week gestational-age fetus with a single umbilical artery and two umbilical veins bypassing the liver and joining the iliac vessel. Multiple arteriovenous fistulas of the placenta are associated. On cross-sectional imaging (**a**), a very large inferior vena cava is visible. Because of the considerable venous return from the placenta draining directly into iliac veins, the size of the inferior vena cava is uniformly large, even well before its terminal portion. Diagram (**b**) of the umbilical vessels of the case in **a**. The ductus venosus is absent and the hepatic veins are draining into the terminal part of the inferior vena cava. There is a single left umbilical artery and two umbilical veins draining into the iliac veins. *AAO* ascending aorta, *AO* aorta, *HV* hepatic veins, *IVC* inferior vena cava, *LUA* left umbilical artery, *LUV*, left umbilical vein, *PV* portal vein, *RA* right atrium, *RUV* right umbilical vein, *SVC* superior vena cava
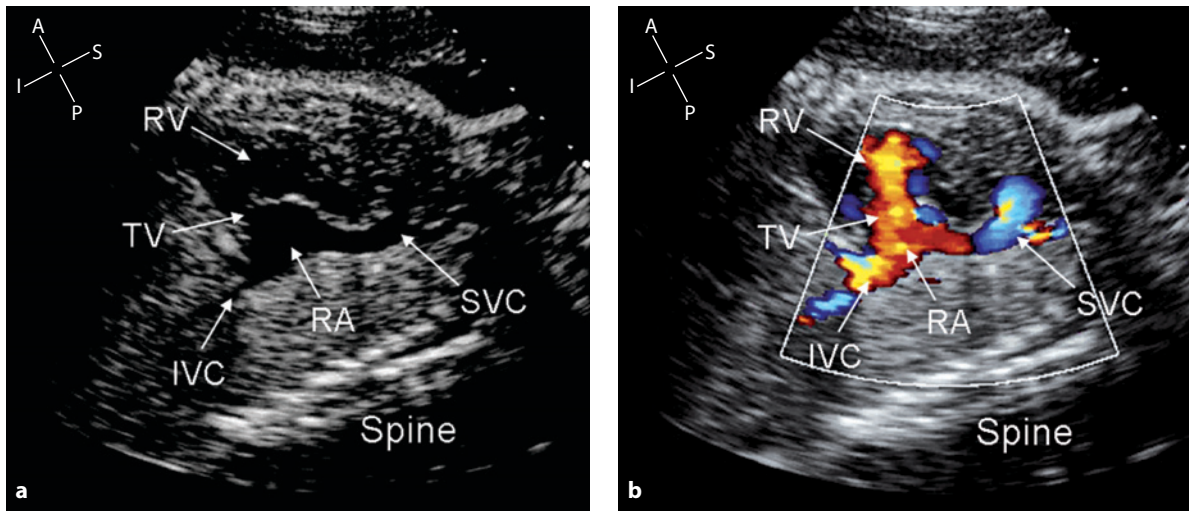
Fig. 13.10 • Bicaval view in a 35-week gestational-age fetus with total anomalous drainage of the pulmonary veins to the right superior vena cava. On cross-sectional image (**a**), the superior vena cava, and its cranial portion in particular, appears disproportionately large. Color flow mapping (**b**) confirms the unusual size of the first tract of the superior vena cava. Due to a more cranial approach on the fetal chest, the flow inside the first portion of the superior vena cava is represented in *blue*. *IVC* inferior vena cava, *RA* right atrium, *RV* right ventricle, *SVC* superior vena cava, *TV* tricuspid valve
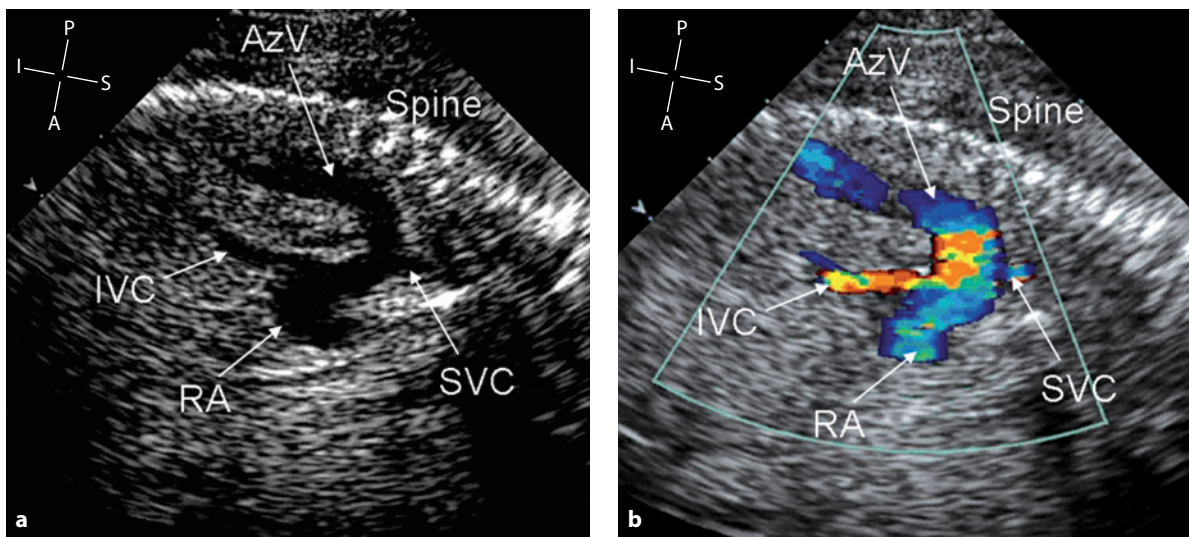
Fig. 13.11 • Long-axis view of the azygos vein in a 21-week gestational-age fetus with dorsoanterior presentation. The ductus venosus is absent, and a persistent right umbilical vein drained into the superior vena cava via a lower intercostal vein and the azygos vein. On cross-sectional examination (**a**), a very large azygos vein is seen joining the superior vena cava, whose terminal portion is consequently enlarged. Color flow mapping (**b**) confirms the large flow from the azygos vein. A small flow from a suprahepatic vein is visible entering the right atrium. *AzV* azygos vein, *IVC* inferior vena cava, *RA* right atrium, *SVC* superior vena cava
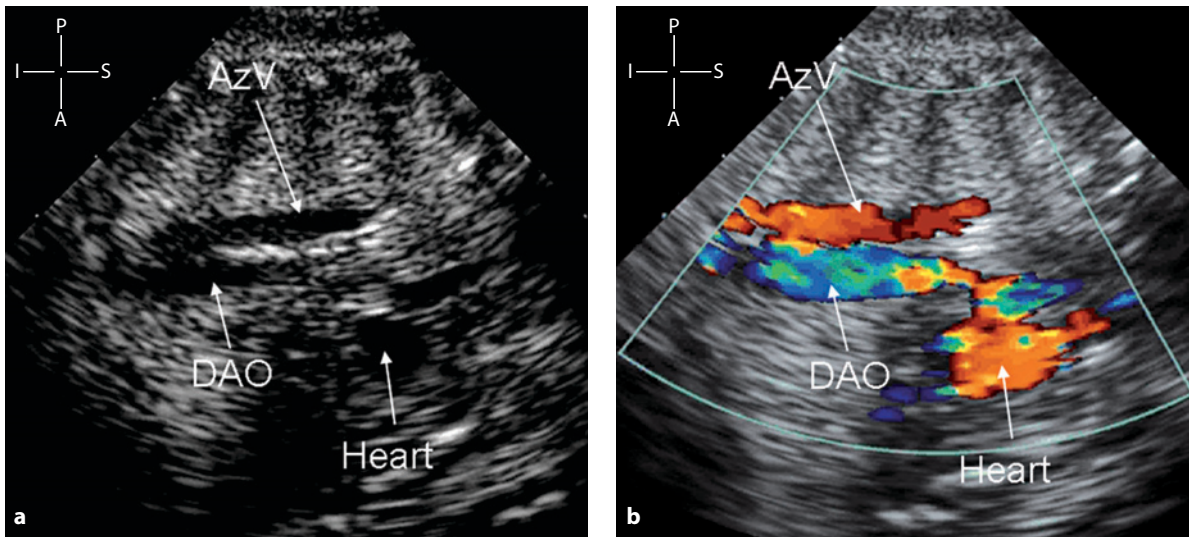
Fig. 13.12 • Long-axis view of the fetal thorax, with dorsoanterior presentation, in a 31-week gestational-age fetus who had interruption of the inferior vena cava and azygos continuation. On cross-sectional scanning (**a**), two vessels nearly equal in size are visible in the posterior mediastinum behind the heart. On color flow mapping (**b**), the two vessel are filled in *red* and *blue* because of the opposite flow direction. On still frame, it is not possible to identify which vessel is which. On the moving images, the more anterior vessel reveals a pulsatile flow, characteristic of the aorta. The azygos vein, posteriorly, shows a typical subcontinuous and low-velocity venous flow. *AzV* azygos vein, *DAO* descending aorta

References

1. Yoo SJ, Lee YH, Cho KS, Kim DY (1999) Sequential segmental approach to fetal congenital heart disease. Cardiol Young 9:430-444

2. Schimdt KG, Silverman NH, Rudolph AM (1996) Assessment of flow events at the ductus venosus-inferior vena cava junction and at the foramen ovale in fetal sheep by use of multimodal ultrasound. Circulation 93:826-833

3. Nagueh SF, Kopelen HA, Zoghbi WA (1996) Relation of mean right atrial pressure to echocardiographic and Doppler parameters of right atrial and right ventricular function. Circulation 93:1160-1169

4. Hecher K, Campbell S (1996) Characteristics of fetal venous blood flow under normal circumstances and during fetal disease. Ultrasound Obstet Gynecol 7:68-83

5. Reed KL, Appleton CP, Anderson CF et al (1990) Doppler studies of vena cava flows in human fetuses. Circulation 81:498-505

6. Huisman TWA, Stewart PA, Wladimiroff JW (1991) Flow velocity waveforms in the fetal inferior vena cava during the second half of normal pregnancy. Ultrasound Med Biol 17:679-682

7. Huisman TWA, Stewart PA, Wladimiroff JW et al (1993) Flow velocity waveforms in the ductus venosus, umbilical vein and inferior vena cava in normal human fetuses at 12-15 weeks of gestation. Ultrasound Med Biol 19:441-445

8. Sau A, Sharland G, Simpson J (2004) Agenesis of the ductus venosus associated with direct umbilical venous return into the heart – case series and review of literature. Prenat Diagn 24:418-423

9. Chiappa E, Viora E, Botta G et al (1998) Arteriovenous fistulas of the placenta in a singleton fetus with large atrial septal defect and anomalous connection of the umbilical veins. Ultrasound Obstet Gynecol 12:132-135

10. Uemura H, HO SY, Devine WA, Kilpatrik LL et al (1995) Atrial appendages and venoatrial connections in hearts from patients with visceral heterotaxy. Ann Thorac Surg 60:561-569

11. Sheley RC, Nyberg DA, Kapur R (1995) Azygos continuation of the interrupted inferior vena cava: a clue to prenatal diagnosis of the cardiovascular syndromes. J Ultrasound Med 14:381-387

The Aortic Arch Long-Axis View

The Section Plane

This view is obtained by cutting the fetal body in a parasagittal plane with transducer angulation from the right of the sternum to the left shoulder. As to the heart chambers, the diagram shows how this view includes inferiorly an oblique section of the two atria together with the long-axis view of the aortic arch (Fig. 14.1).

The Normal Morphology

In the normal heart, the aortic arch long-axis view shows the ascending aorta arising in the center of the chest and forming the aortic arch, characterized by the three head and neck vessels originating from its superior aspect in the following order: the innominate artery, the left common carotid artery, and the left subclavian artery. Posteriorly to the arch, the cross section of the right pulmonary artery and the right bronchus are seen. Anterosuperiorly, just in front of the origin of the innominate artery, the innominate vein is displayed in cross section. This vein is the largest vessel of the upper mediastinum and is anteriorly embraced by the thymus.

The sagittal view of the aortic arch is a short-axis view of the heart at the level of the two atria or at the atrioventricular junction. Usually, a larger portion of the right atrium with its appendage is seen anteriorly and a smaller portion of the left atrium posteriorly. This view displays the superior portion of the interatrial septum (crista dividens) that forms the roof of the foramen ovale. Inferiorly, the junction between the inferior vena cava and the right atrium is visible (Fig. 14.2).
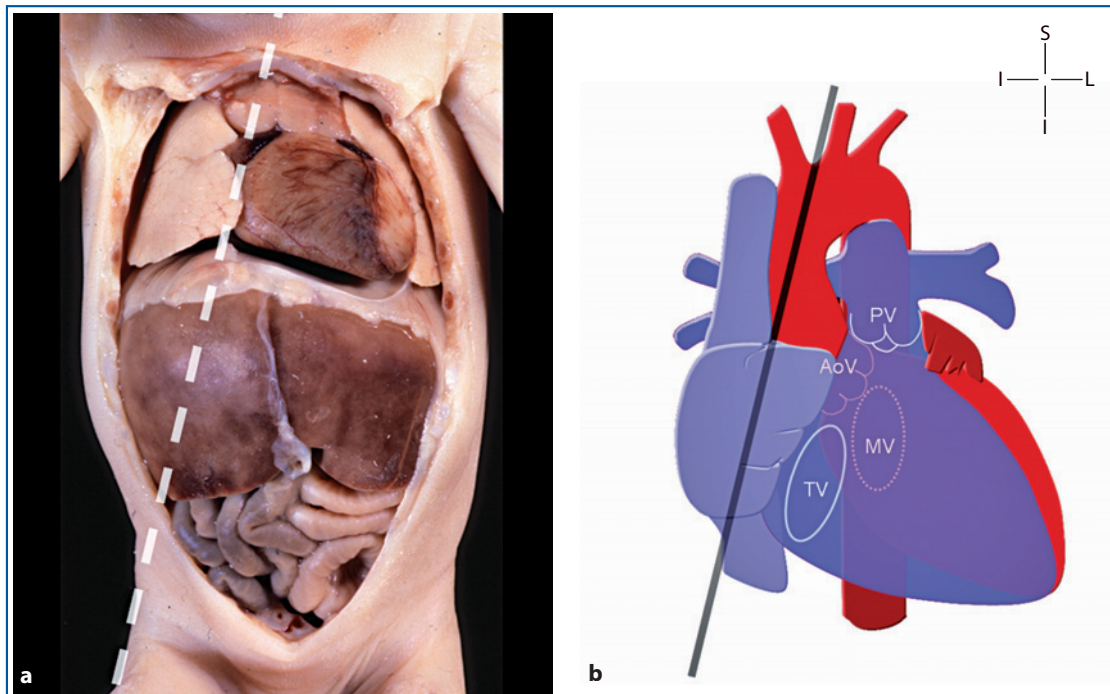
Fig. 14.1 • Lines show the plane of the long-axis view of the aortic arch on the fetal body (**a**) and a heart diagram (**b**). *AoV* aortic valve, *MV* mitral valve, *PV* pulmonary valve, *TV* tricuspid valve
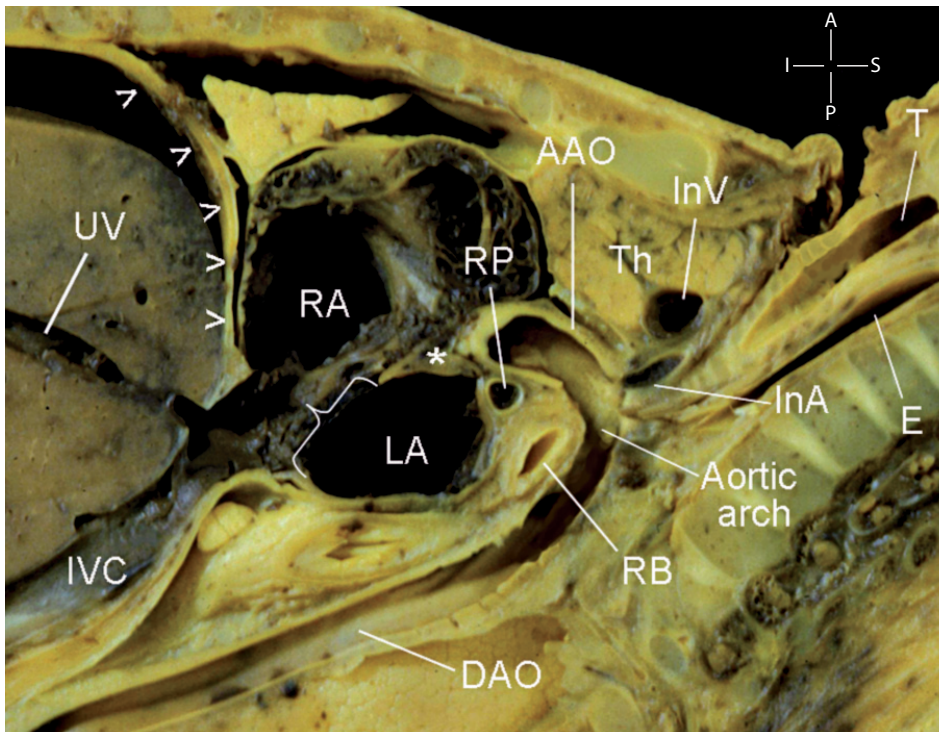
Fig. 14.2 • This section is obtained with a parasagittal cut of the fetal thorax to imitate the long-axis view of the aortic arch. The aortic arch is seen arising with a narrow curvature between the two atria in the center of the chest. Due to difficulties in obtaining this section in the whole fetal body, only the origin of the innominate artery is seen among the neck vessels. In the anterosuperior part of the mediastinum, the thymus embraces the innominate vein displayed in cross section. The oblique section of the trachea and esophagus in the neck region are indicated. Behind the arch, the right pulmonary artery and the right bronchus are displayed. The *white asterisk* indicates the upper portion of the interatrial septum, which superiorly delimits the foramen ovale (*white bracket*) and overrides the opening of the inferior vena cava below. The *open arrowheads* indicate the diaphragm, with the right lobe of the liver below. *AAO* ascending aorta, *DAO* descending aorta, *E* esophagus, *InA* innominate artery, *InV* innominate vein, *IVC* inferior vena cava, *LA* left atrium, *RA* right atrium, *RB* right bronchus, *RPA* right pulmonary artery, *Th* thymus, *T* trachea, *UV* umbilical vein

The thoracic aorta can be distinguished in its different segments: the ascending aorta, the proximal arch, the distal arch, the isthmus, and the descending aorta. These segments are illustrated in Figure 14.3. The isthmus is the aortic segment between the left subclavian artery and the aortic end of the arterial duct. In the normal newborn, the aortic arch shows progressive tapering of its diameter, with the smallest diameter at the isthmus, which can be up to 60% smaller than that of the ascending aorta. The progressive reduction of the aortic arch diameter is believed to reflect the proportion of the cardiac output transversing each segment in the fetal life, with the smallest amount crossing the isthmus because most of the blood ejected in the ascending aorta is taken by the cerebral circulation. In the fetal lamb, only 10% of the combined ventricular output passes through the isthmus, compared with 32% of the ascending aorta and 57% of the arterial duct [1]. Doppler flow studies have demonstrated in the human fetus that the flow at the isthmus decreases as gestation progresses, and an early reverse flow can be observed in diastole, particularly near term [2, 3].

The aortic isthmus is a crucial vascular structure in the fetal circulation, situated between the circulation of the upper part and that of the inferior part of the body. Circulation of the upper part is characterized by the left ventricle as pumping chamber and the major peripheral resistance produced by cerebral circulation. The circulation of the inferior part is supported by the right ventricle as pumping chamber and the major peripheral resistance given by placental circulation (Fig. 14.4). The aortic isthmus may show flow abnormalities not only in case
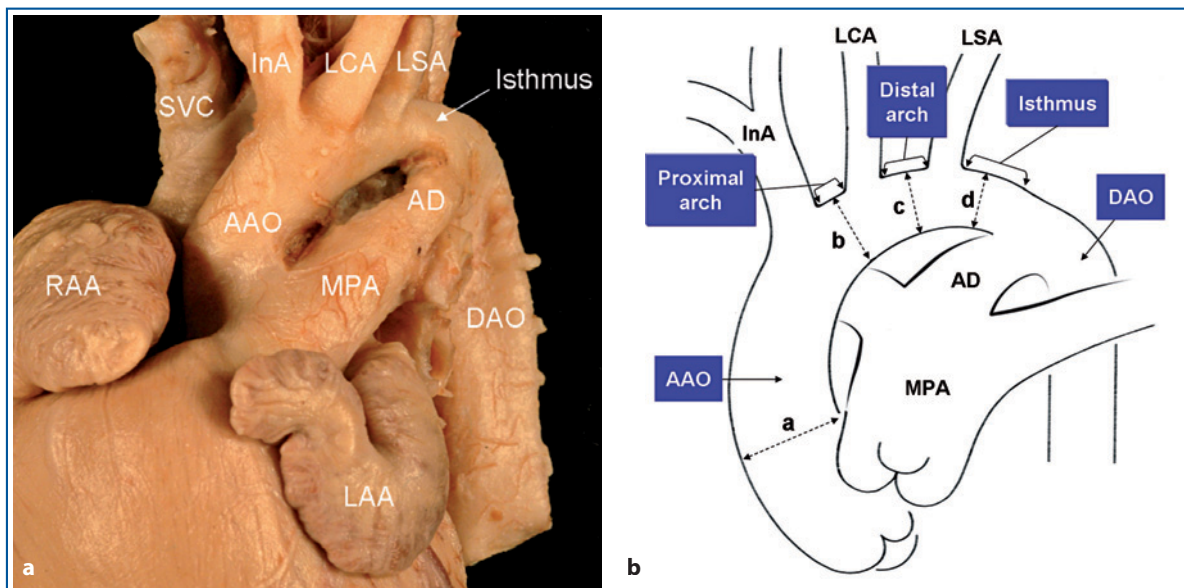
Fig. 14.3 • This anatomical specimen (**a**) shows the three head and neck arteries originating from the aorta. The aortic arch is continuous with the descending aorta and receives the arterial duct beyond the isthmus, the segment included between the origin of the left subclavian artery and the duct itself. The diagram (**b**) shows the different thoracic aorta segments (*a-d*) and their diameters. At the isthmus, the aorta reaches its smallest size. *AAO* ascending aorta, *AD* arterial duct, *DAO* descending aorta, *InA* innominate artery, *LAA* left atrial appendage, *LCA* left carotid artery, *LSA* left subclavian artery, *MPA* main pulmonary artery, *RAA* right atrial appendage, *SVC* superior vena cava

of major ventricular dysfunction and/or obstruction but also due to imbalance between cerebral and placental resistance.

The Normal Echocardiogram – 2D

Because in the normal heart the aorta arises from the posterior ventricle, the aortic arch shows on cross-sectional examination as a narrow curvature that has been suggested as having a "candy-cane" or a "walking-cane" appearance. However, a narrow curvature is not a sufficient feature to characterize the aorta. In hearts with malposition of the great arteries and the aorta in anterior position, the aortic arch curvature is wider. Therefore, the most specific feature of the aortic arch is the origin of the three head and neck vessels from the superior part of this arch. Even with the best presentation of the fetus, it is difficult to visualize all three vessels at the same time. More frequently, they will be imaged in a sequential manner with slight manipulation of the scan plane. During this examination, the integrity of the aortic arch has to be assessed. Being a section along the major axis of the fetal body, this view shows posteriorly an oblique section of the spine with several vertebral bodies (Fig. 14.5a).

The long-axis view of the aortic arch can be obtained from a bicaval view with slight leftward tilt
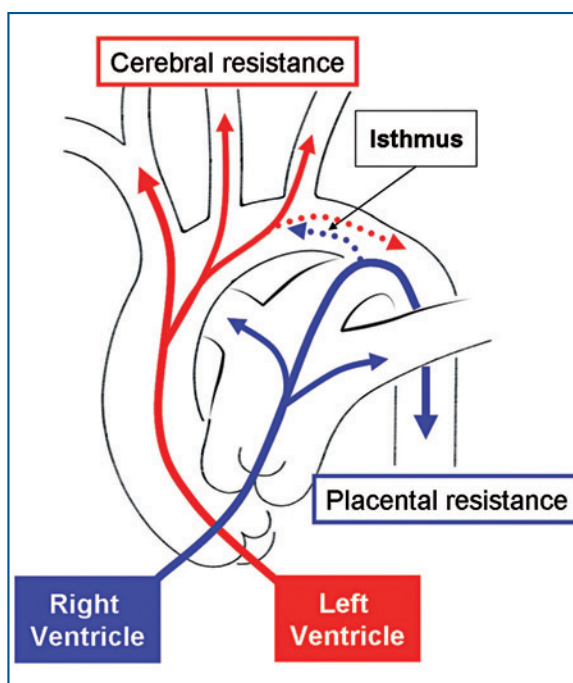
Fig. 14.4 • Circulation in the upper part of the fetal body is mostly supported by the left ventricle pumping against vascular resistance of the cerebral circulation. The inferior part of the body is mostly supported by the right ventricle pumping blood against vascular resistance of the placental circulation. The isthmus can receive blood flow from the two sources depending on the circulatory needs
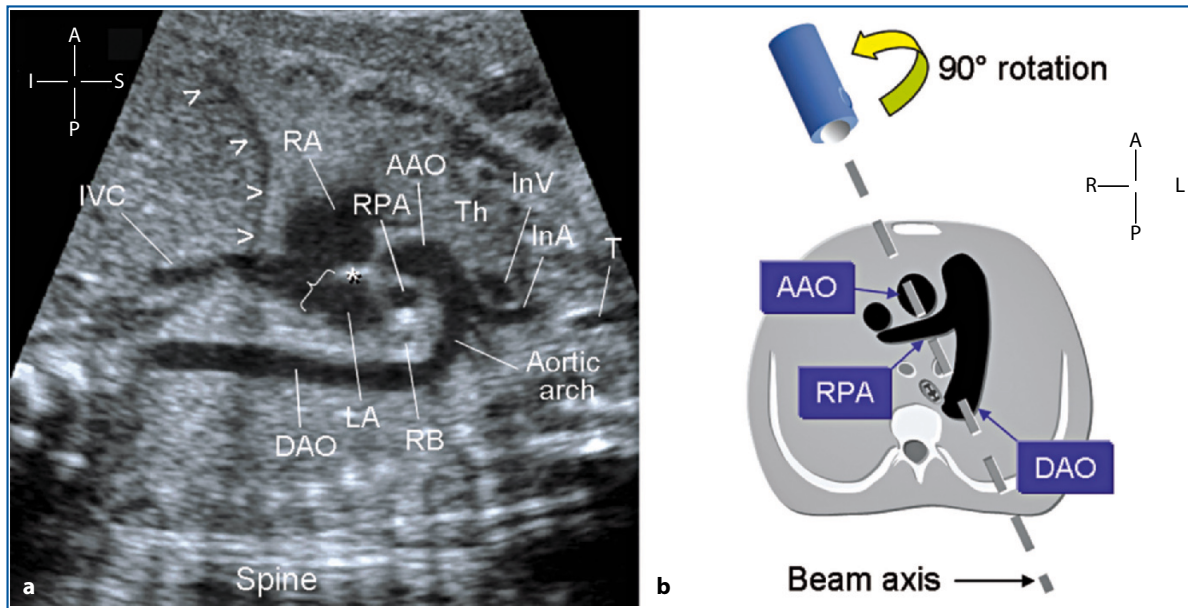
Fig. 14.5 • Long-axis view of the aortic arch in a normal 28-week gestational-age fetus (**a**). The "candy-cane" appearance of the arch is shown. All structures described in Fig. 14.2 are visible. The upper part of the interatrial septum (*asterisk*) is seen, representing the superior rim of the oval fossa (*bracket*). The *open arrowheads* indicate the outline of the diaphragm. The diagram (**b**), depicting the transverse view of the arterial duct, illustrates where the probe must be placed and how the beam axis is to be oriented to obtain the long-axis view of the aortic arch by 90° rotation of the scan plane. A right parasternal approach on the fetal thorax is needed. *AAO* ascending aorta, *DAO* descending aorta, *InA* innominate artery, *InV* innominate vein, *IVC* inferior vena cava, *LA* left atrium, *RA* right atrium, *RB* right bronchus, *RPA* right pulmonary artery, *Th* thymus, *T* trachea

of the scan plane. An alternative method is to start from a transverse view of the thorax. By placing the probe on the right side of the sternum and aligning the ascending and the descending aorta on the ultrasound beam, the long-axis view is obtained after 90° rotation of the scan plane (Fig. 14.5b).

The long-axis view of the aortic arch can be obtained even when the fetus is in dorsoanterior presentation, particularly in the mid trimester when ossification of the rib cage is less pronounced. In the normal fetus with a left-sided aortic arch, this cut can be obtained only with a left paravertebral approach. The scanning plane should have a parasagittal orientation from left posterior to right anterior. The scanning technique is further discussed in the following chapter. Due to substantial absorption of the ultrasound energy by the vertebral bodies, scapulae, and ribs, the morphologic details with this orientation are poorer than those obtained with a ventral approach. Nevertheless, many details can be still recognized. An example of this view with the paravertebral approach is shown in Figure 14.6.

The long-axis view of the aortic arch is useful to assess the shape of the entire arch, to measure the size of its segments, and for Doppler assessment from the aortic valve to the descending aorta.

The Normal Echocardiogram – Color Flow Mapping and Pulsed Doppler

Because the flow in the normal aortic arch changes direction up to 180°, on color flow mapping, different segments of the aorta are represented in opposite colors. Color flow should be laminar in all segments and, with the appropriate setting, a small filling should be seen at the origin of the three head and neck vessels (Fig. 14.7).

Doppler flow study of the proximal and distal aortic arch is ideally performed by this view. The Doppler spectrum is characterized by a monophasic wave, similar to that of the aortic valve, but with a diastolic forward flow (Fig. 14.8) [4]. This is due to diastolic recoil of the aortic walls and the low placental resistance.
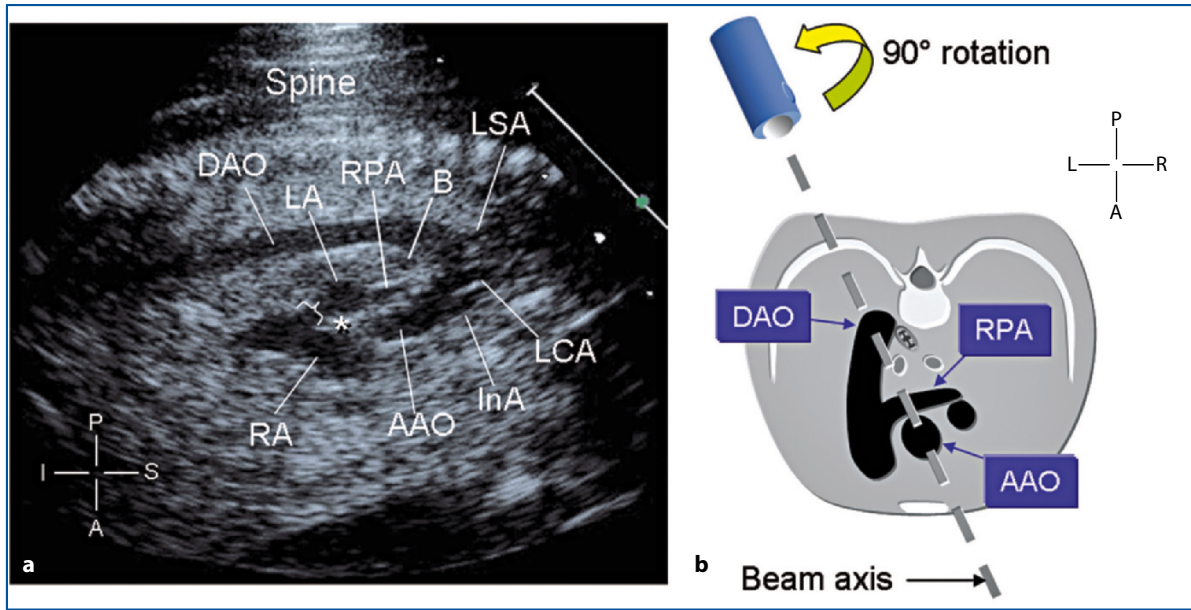
Fig. 14.6 • Long-axis view of the aortic arch in a normal 23-week gestational-age fetus with dorsoanterior presentation (**a**). Despite the inferior resolution to that of ventral presentation, several anatomical details are recognizable. The upper part of the interatrial septum (*white asterisk*) is seen, delimiting superiorly the oval fossa (*white bracket*). The diagram (**b**), depicting the transverse view of the fetal thorax with dorsoanterior presentation, illustrates where the probe must be placed and how the beam axis is to be oriented to obtain the long-axis view of the aortic arch by 90° rotation of the scan plane. A left paravertebral approach on the fetal thorax is necessary. *AAO* ascending aorta, *B* bronchus, *DAO* descending aorta, *InA* innominate artery, *LA* left atrium, *LCA* left carotid artery, *LSA* left subclavian artery, *RA* right atrium, *RPA* right pulmonary artery
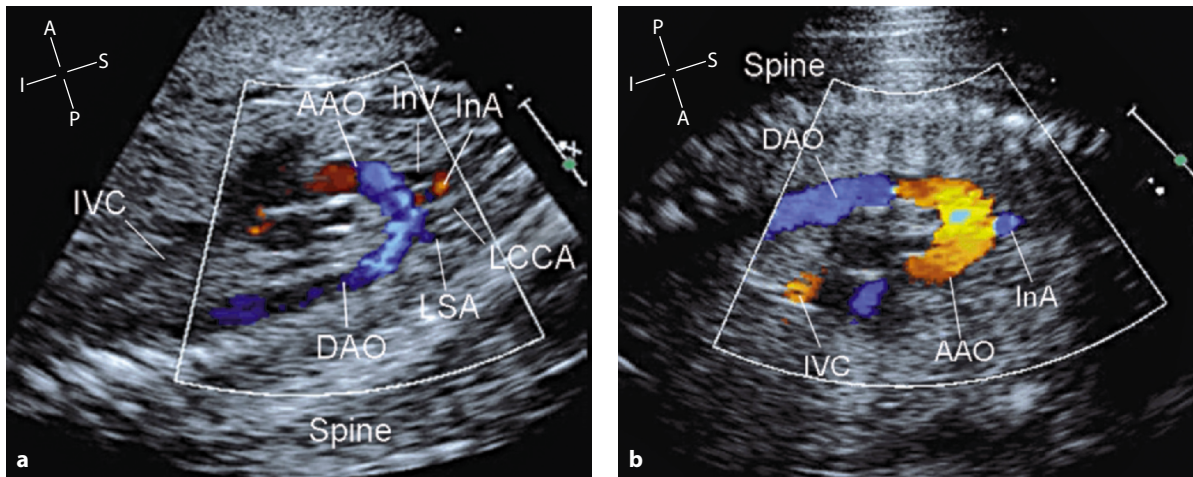
Fig. 14.7 • Color flow mapping systolic frames of the long-axis view of the aortic arch in two normal 23-week gestational-age fetuses with spine-posterior (**a**) and spine-anterior (**b**) presentation. The ascending and descending aortas are visible in opposite colors, with laminar flow in the transverse arch and small filling at the origin of some of the neck vessels. *AAO* ascending aorta, *DAO* descending aorta, *InA* innominate artery, *InV* innominate vein, *IVC* inferior vena cava, *LCCA* left common carotid artery, *LSA* left subclavian artery
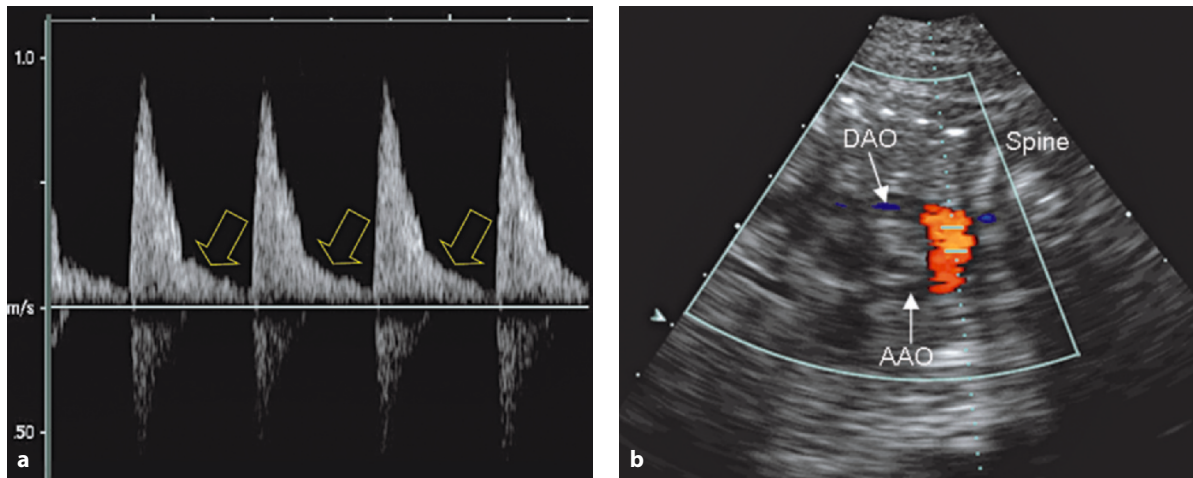
Fig. 14.8 • Pulsed Doppler tracing (**a**) showing the flow pattern in the distal aortic arch in a normal 20-week gestational-age fetus**.** The image being obtained in the paravertebral approach to the fetal thorax, the flow is seen approaching the probe and therefore is represented above the baseline. *Yellow open arrows* indicate diastolic runoff from the aorta. The sample volume is placed in the distal aortic arch with the fetus in dorsoanterior presentation (**b**). *AAO* ascending aorta, *DAO* descending aorta
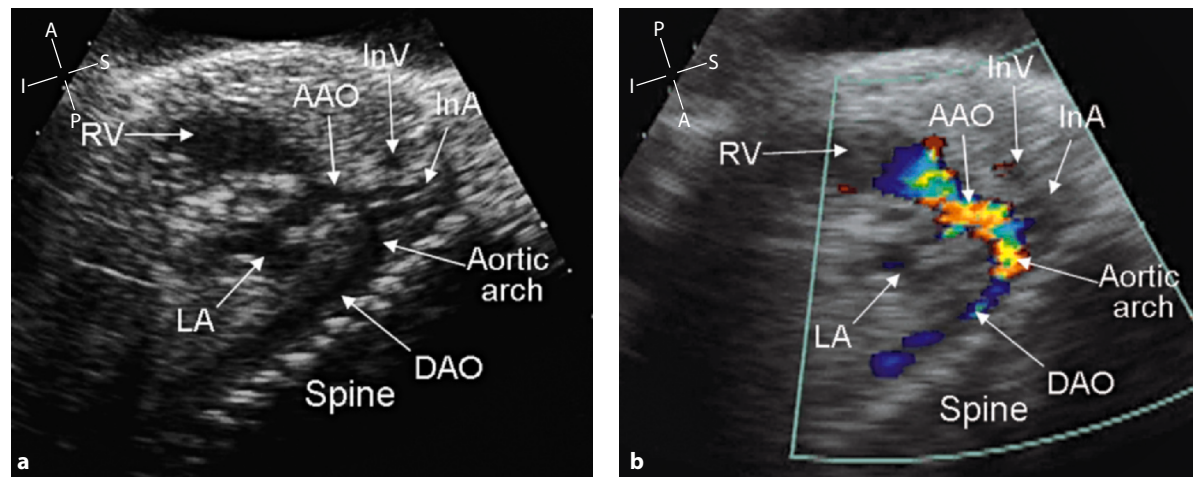
Fig. 14.9 • Long-axis view of the aortic arch in a 33-week gestational-age fetus with hypoplastic left heart. On cross-sectional examination (**a**), the ascending aorta and the proximal aortic arch are markedly hypoplastic. The narrow curvature of the aortic arch is maintained, and the origin of the head and neck vessel from its superior margin is demonstrated. The size of the descending aorta is normal. On color flow mapping (**b**), the aortic arch is perfused retrogradely by the arterial duct (not seen in this view). *AAO* ascending aorta, *DAO* descending aorta, *InA* innominate artery, *InV* innominate vein, *LA* left atrium, *RV* right ventricle

The Aortic Arch Abnormalities

In the following sections of common abnormalities of the aortic arch are shown in this echocardiographic projection.

Severe Aortic Outflow Obstructions

With severe obstruction to the aortic outflow, the size of the proximal aorta is generally reduced. Partial or complete retrograde perfusion through the arterial duct is seen (Fig. 14.9, 14.10).

Coarctation of the aorta is a common congenital heart disease, accounting for nearly 7% of congenital heart disease in postnatal series. Despite the published information, coarctation of the aorta remains a challenging lesion to detect in utero [5]. Even with optimal technique, coarctation of the aorta is one of the most frequent false positive and false negative diagnoses in prenatal cardiac assessment. The incidence of false negative cases is higher in simple lesions and lower in complex cases. Prenatal diagnosis of coarctation of the aorta relies on direct and/or indirect echographic signs. Direct signs include visualization
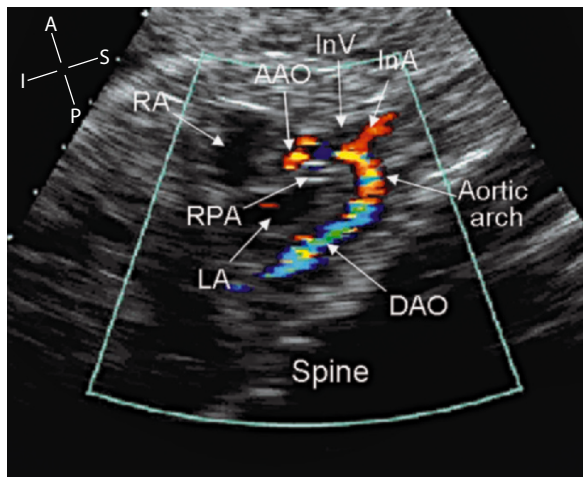
Fig. 14.10 • Long-axis view of the aorta in a 24-week gestational-age fetus with critical aortic valve stenosis. This systolic frame shows a tiny jet of flow passing through the aortic valve into the aortic root. This jet can be easily missed with low-resolution ultrasound machines or inappropriate settings. Due to the insufficient anterograde flow, there is retrograde perfusion of the distal and proximal aortic arch through the arterial duct (not visible in this view). *AAO* ascending aorta, *DAO* descending aorta, *InA* innominate artery, *InV* innominate vein, *LA* left atrium, *RA* right atrium, *RPA* right pulmonary artery
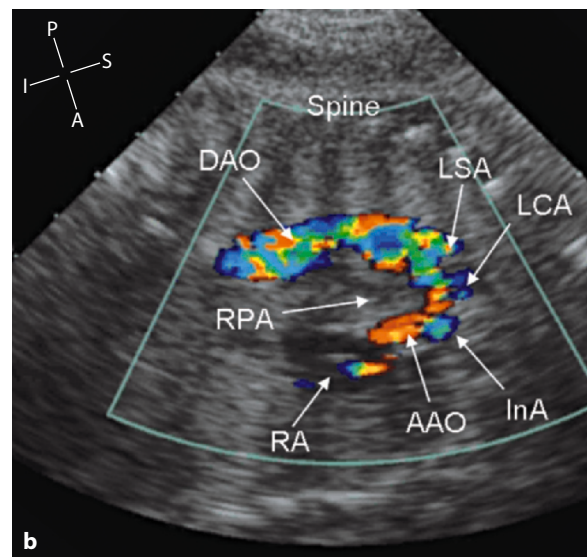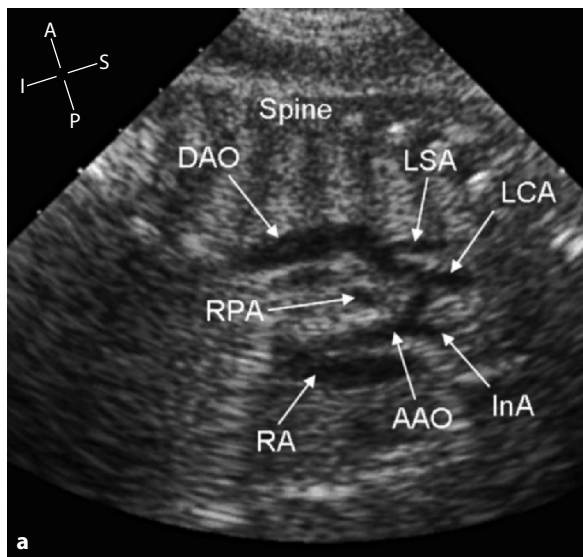
Fig. 14.11 • Long-axis view of the aortic arch in a 33-week gestational-age fetus with complex aortic coarctation. The arch is seen from the posterior approach to the fetal thorax. The cross-sectional image (**a**) shows a tubular hypoplasia of the aortic arch, which is particularly narrow at its distal segment. The origins of the head and neck vessels are widely spaced. Below the confluence of the arterial duct (not visible in this view), the size of the descending aorta is normal. On color flow mapping (**b**), there is anterograde unaliased flow in the ascending aorta and a retrograde perfusion (*blue*) of the distal aortic arch. *AAO* ascending aorta, *DAO* descending aorta, *InA* innominate artery, *LCA* left carotid artery, *LSA* left subclavian artery, *RA* right atrium, *RPA* right pulmonary artery

of a contraductal shelf of the aorta or hypoplasia of the aortic arch and isthmus (Fig. 14.11) [5, 6]. Although they are the most specific, imaging of these signs during a routine obstetric examination is often not practical. Initial suspicion must therefore rely on indirect signs, which include dominant size of the right ventricle and pulmonary artery over the size of the left ventricle and the ascending aorta [7-9].

When the aortic arch is interrupted, the continuity between segments of the aortic arch cannot be demonstrated (Fig. 14.12) [10].

Severe Pulmonary Outflow Obstructions

In contrast to normal fetuses in which the ascending and the descending thoracic aorta are relatively similar in size, in most lesions with ductal-dependent pulmonary circulation, the ascending aorta is disproportionately large. This is because both ventricles eject into the aorta or the pulmonary flow is redistributed to the systemic ventricle at the atrial level through the foramen ovale. Pulmonary flow is provided by retrograde perfusion of the arterial duct or through collateral arteries (Fig. 14.13).
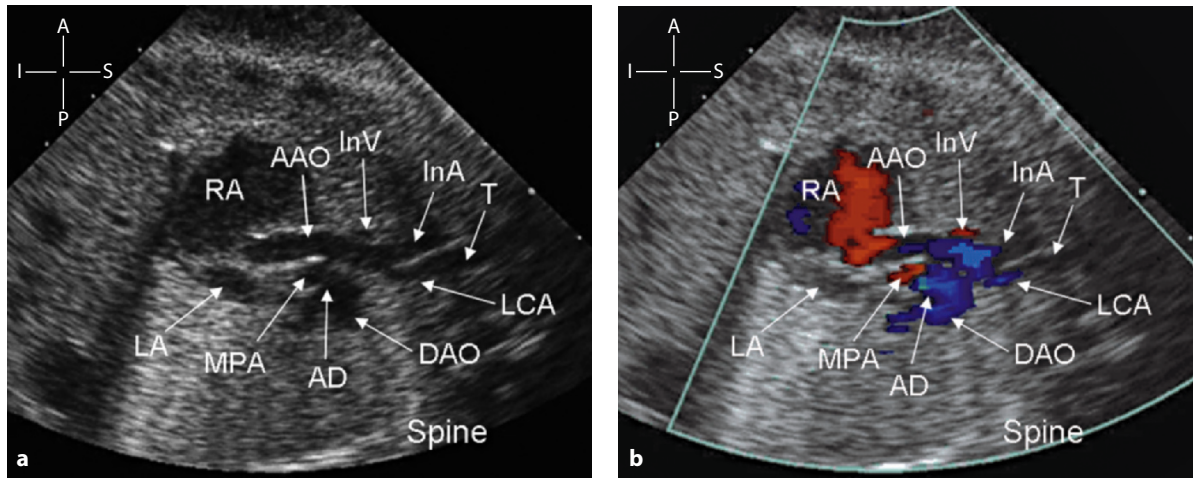
Fig. 14.12 • Aortic arch long-axis view in a 30-week gestational-age fetus with interruption of the aortic arch. The interruption was between the left common carotid artery and the left subclavian artery (type B). A ventricular septal defect with posterior malalignment of the infundibular septum was associated. There was a left-sided aortic arch. Postnatal fluorescence in situ hybridization investigation revealed a chromosome 22q11 deletion. On cross-sectional examination (**a**), the ascending aorta is mildly hypoplastic and shows a straight course ending in the left carotid artery. No continuity of the aortic arch with the descending aorta is demonstrated. The main pulmonary artery is in continuity with the descending aorta through the arterial duct. On color flow mapping (**b**), both great arteries show unaliased flow. Discontinuity between the proximal aortic arch and the descending aorta is confirmed. *AAO* ascending aorta, *AD* arterial duct, *DAO* descending aorta, *InA* innominate artery, *InV* innominate vein, *LA* left atrium, *LCA* left carotid artery, *MPA* main pulmonary artery, *RA* right atrium, *T* trachea
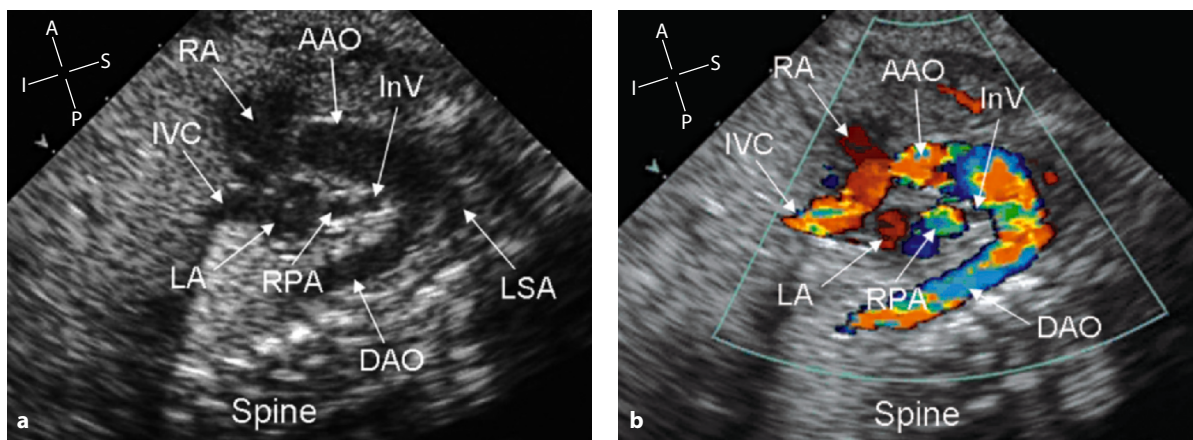
Fig. 14.13 • Long-axis view of the aortic arch in a 27-week gestational-age fetus with tetralogy of Fallot. A right aortic arch is associated. On cross-sectional examination (**a**), the ascending aorta and the proximal arch are disproportionately large. Behind the ascending aorta, two vessels are displayed in cross section. The inferior vessel is a relatively small right pulmonary artery, and the superior vessel is an innominate vein with a retroaortic course. The aortic arch is right sided, but laterality of the aortic arch is not appreciated in sagittal views of the fetal body. A retroaortic innominate vein was seen in three cases in our series, all with tetralogy of Fallot and right aortic arch. Color flow mapping (**b**) confirms the large size of the aortic arch, with increased systolic pulsation on the moving images. Due to low-velocity flow, the innominate vein is not coded in color, whereas a turbulent flow, due to pulmonary valve stenosis, fills the right pulmonary artery. *AAO* ascending aorta, *DAO* descending aorta, *InV* innominate vein, *IVC* inferior vena cava, *LA* left atrium, *LSA* left subclavian artery, *RPA* right pulmonary artery, *RA* right atrium

Variability of the Plane of the Aortic Arch Long-Axis View

Left- or right-sided aortic arch can occur in normal and abnormal hearts. Moreover, malposition of the great arteries can occur in different types of abnormal connections such as complete transposition, double-outlet right ventricle, tricuspid atresia, or double-inlet right ventricle. The plane of this view shows wide variability, from a true sagittal plane to a parasagittal plane with right or left angulation. This depends not only on the position of the ascending aorta but also on that of the descending aorta. The orientation of the scan plane can be defined precisely with a transverse view of the thorax and by aligning the ascending and the descending aorta on the ultrasound beam axis before rotating the scan plane 90°. Some schematic examples are shown in Figure 14.14. Echocardiographic examples of the different orientations of the aortic arch plane are provided in the chapter describing the transverse view of the aortic arch.

When the aorta is anteriorly positioned, the aortic arch curvature widens, losing its normal narrow curvature. Consequently, the aorta must be recognized not from the width of its curvature per se but from the origin of the neck vessels, which is its more constant feature. The neck vessels can be imaged only in the long-axis view of the aortic arch (Figs. 14.15, 14.16).

The Aortic Arch in Mitral Valve Atresia with Ventricular Septal Defect

When mitral valve atresia and concordant ventriculoarterial connection is associated with a ventricular septal defect, the size of the ascending aorta and aortic arch depends on the dimensions of the defect of the ventricular septum. If this defect is wide, the size of the ascending aorta and its arch is usually normal despite the rudimentary dimensions of the left ventricle. Figure 14.17 shows an example of this type of defect.
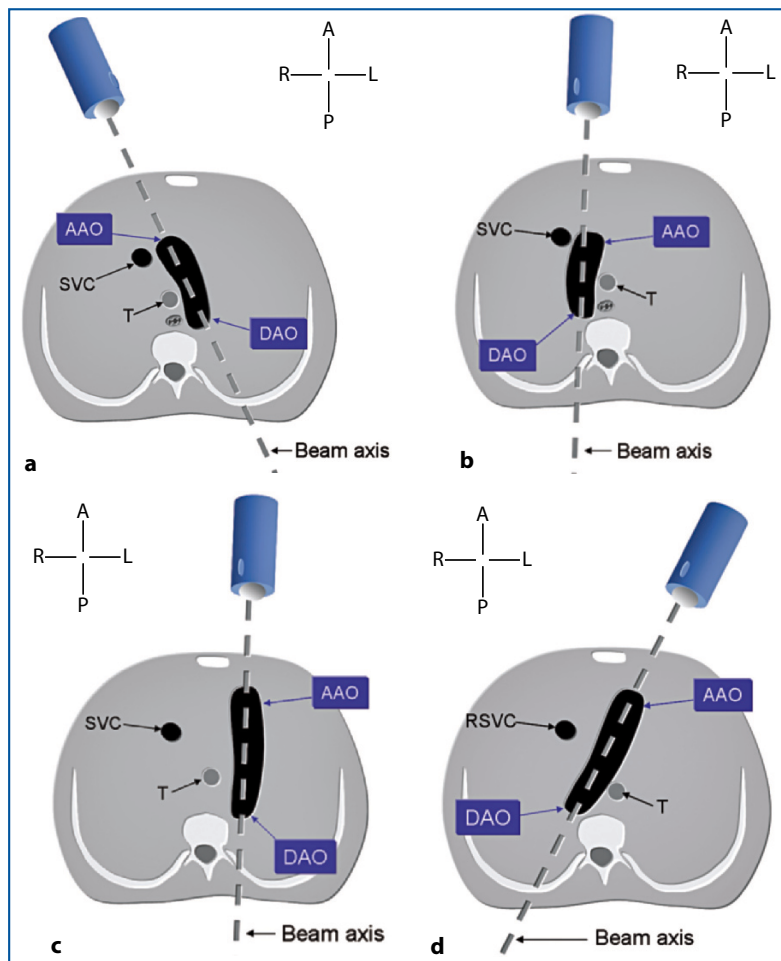
Fig. 14.14 • Diagrams imitating a transverse view of the aortic arch show the different orientation of the beam axis necessary to obtain the long-axis view of the aortic arch with 90° rotation of the scan plane. Left-sided (**a**) and a right-sided (**b**) aortic arch with normal posterior aorta. Left (**c**) or right (**d**) arch when the ascending aorta is anterior and to the left. The long-axis view of the aortic arch is obtained with a sagittal orientation of the scan plane in (**b**) and (**c**), whereas while a parasagittal cut is necessary in (**a**) and (**d**) with an approach from the right and left side of the sternum, respectively. *AAO* ascending aorta, *DAO* descending aorta, *SVC* superior vena cava, *T* trachea
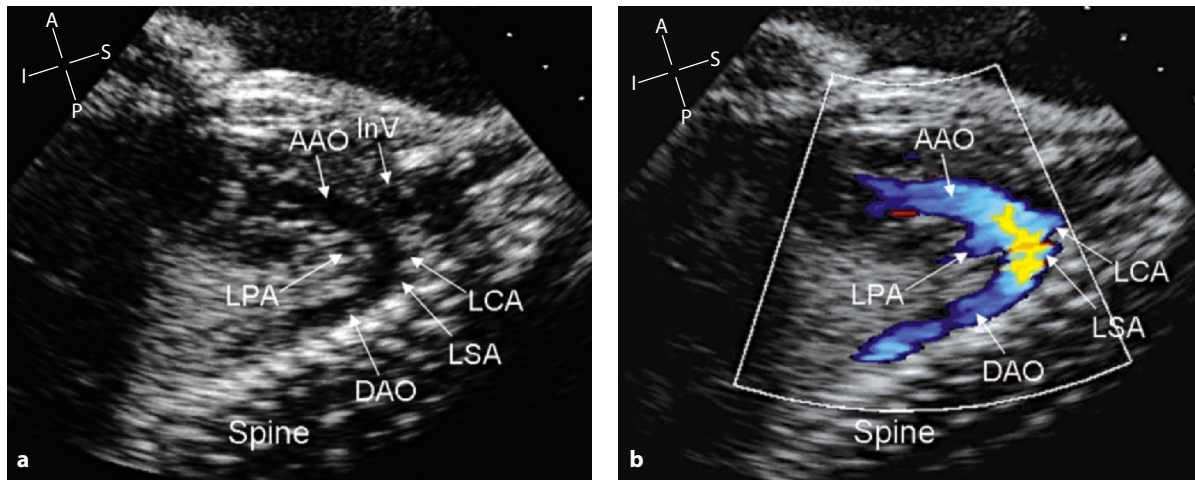
Fig. 14.15 • Long-axis view of the aortic arch in a 35-week gestational-age fetus with double-outlet right ventricle and malposition of the great arteries. The aorta is anterior and to the left relative to the pulmonary artery. On cross-sectional examination (**a**), the aorta, recognized by the origin of the head vessels, shows a curvature wider than normal because this artery is committed to the anterior right ventricle. The aortic arch is regular in all its segments. Color flow mapping (**b**) confirms that this anterior vessel is the aorta, with color filling the origin of the head and neck vessels. The artery shows normal perfusion by unaliased flow. *AAO* ascending aorta, *DAO* descending aorta, *InV* innominate vein, *LSA* left subclavian artery, *LCA* left carotid artery, *LPA* left pulmonary artery
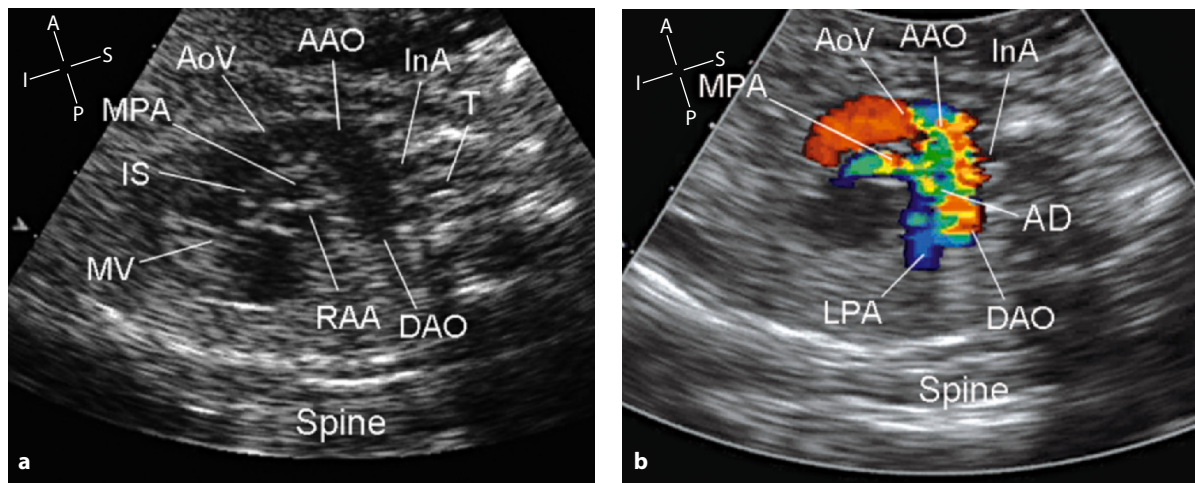
Fig. 14.16 • Long-axis view of the aortic arch in a 25-week gestational-age fetus with tricuspid atresia and ventriculoarterial discordance. The ascending aorta is anterior and to the right of the pulmonary artery. On cross-sectional examination (**a**), the most anterior arterial vessel is the aorta because it gives origin to the head and neck vessels. This is despite the wide curvature of its arch and its connection with the infundibulum behind the sternum. The aorta is far larger than the main pulmonary artery and runs parallel behind. The infundibular septum is posteriorly deviated and contributes to the obstruction of the pulmonary flow. This view sections the heart on the atrioventricular junction where a single atrioventricular valve is seen with a two-leaflet morphology on moving images. Color flow mapping (**b**) confirms the small size of the pulmonary artery, filled with turbulent anterograde flow, originating at the subarterial conus. Due to the significant obstruction to the pulmonary flow, the small arterial duct shows diastolic inversion of its flow. *AAO* ascending aorta, *AD* arterial duct, *AoV* aortic valve, *DAO* descending aorta, *InA* innominate artery, *IS* infundibular septum, *LPA* left pulmonary artery, *MPA* main pulmonary artery, *MV* mitral valve, *RAA* right atrial appendage, *T* trachea
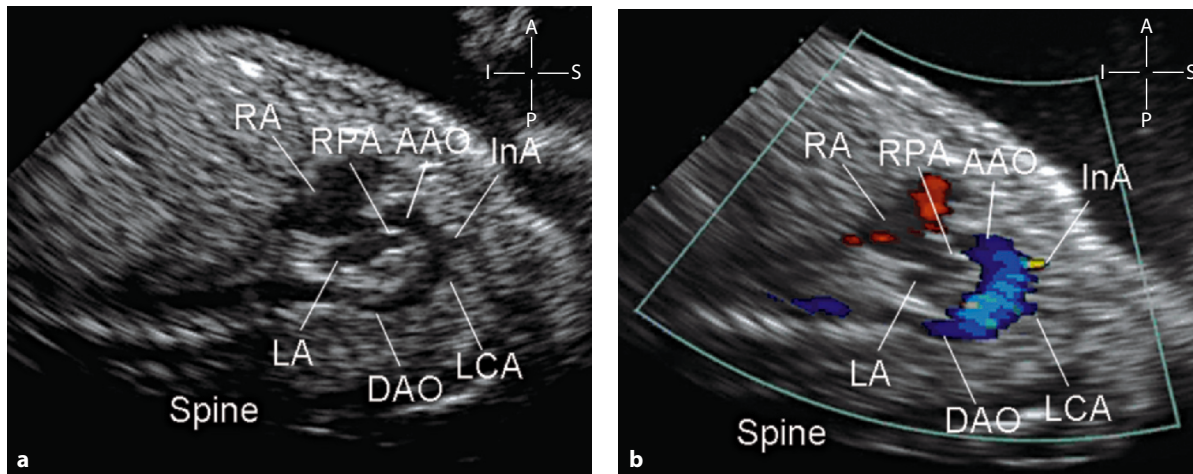
Fig. 14.17 • Long-axis view of the aortic arch in a 23-week gestational-age fetus with atresia of the mitral valve associated with ventricular septal defect. On cross-sectional examination (**a**), all aortic segments are mildly hypoplastic, with a normal curvature of the arch. The origin of the head and neck vessels is demonstrated. The foraminal flap, bulging from left to right, testifies to a restrictive foramen ovale, a common feature of left-ventricle inflow obstructions. On color flow mapping (**b**), the entire aorta is seen perfused by unaliased flow despite mitral valve atresia. This is not surprising, because anterograde perfusion of the ascending aorta is possible through a subaortic ventricular septal defect. *AAO* ascending aorta, *DAO* descending aorta, *InA* innominate artery, *LA* left atrium, *LCA* left carotid artery, *RA* right atrium, *RPA* right pulmonary artery

References

1. Heymann MA (1989) Fetal and neonatal circulations. In: Adams FH, Emmanouillides GC, Riemenschneider TA (eds) Heart disease in infants, children, and adolescents. Williams & Wilkins, Baltimore, pp 24-35

2. Fouron JC, Zarelli M, Drblik SP et al (1994) Lessard M. Normal flow velocity profile through the fetal aortic isthmus. Am J Cardiol 74:483-486

3. Fouron JC (2003) The unrecognized physiological and clinical significance of the fetal aortic isthmus. Ultrasound Obstet Gynecol 22(5):441-447

4. Choi JY, Noh CI, Yun YS (1991) Study on Doppler waveforms from the fetal cardiovascular system. Fetal Diagn Ther 6:74-83

5. Sharland GK, Chan KY, Allan LD (1994) Coarctation of the aorta: difficulties in prenatal diagnosis. Br Heart J 71:70-75

6. Hornberger LK, Sahn DJ, Kleinman CS et al (1994) Antenatal diagnosis of coarctation of the aorta: a multicenter experience. J Am Coll Cardiol 23:417-423

7. David N, Iselin M, Blaysat G et al (1997) Disproportion in diameter of the cardiac chambers and great arteries in the fetus. Contribution to the prenatal diagnosis of coarctation of the aorta. Arch Mal Coeur Vaiss 90:673-678

8. Brown DL, Durfee SM, Hornberger LK (1997) Ventricular discrepancy as a sonographic sign of coarctation of the fetal aorta: how reliable is it? J Ultrasound Med 16:95-99

9. Hornung TS, Heads A, Hunter AS (2001) Right ventricular dilatation in the fetus: a study of associated features and outcome. Pediatr Cardiol 22:215-217

10. Volpe P, Marasini M, Caruso G et al (2002) Prenatal diagnosis of interruption of the aortic arch and its association with deletion of chromosome 22q11. Ultrasound Obstet Gynecol 20:327-331

The Arterial Duct Long-Axis View

The Section Plane

This family of sections is obtained when the chest is cut sagittally slightly to the left of the midline of the fetal body or parasagittally with slight angulation toward the left fetal shoulder. The two extreme planes of these sections are indicated on the fetal body and a heart diagram in Figure 15.1. The diagram illustrates how all sections within these two planes pass through the main pulmonary artery, the arterial duct, and its junction with the descending aorta. However, these sections differ from the structures sectioned inside the body of the heart. In fact, parasagittal sections include the inlet portion of the right ventricle, the tricuspid valve, and a transverse section of the aortic root. True sagittal sections pass through the trabecular part of the right ventricle anteriorly, the mitral valve, and the left atrium posteriorly.

The Normal Morphology

These sections show superiorly the main pulmonary artery that sweeps posteriorly where it splits into two branches. The inferior branch is the left pulmonary artery, and the superior branch is the arterial duct, which merges into the descending aorta. The vascular continuity between the main pulmonary artery, the arterial duct, and the descending aorta forms the so-called ductal arch.
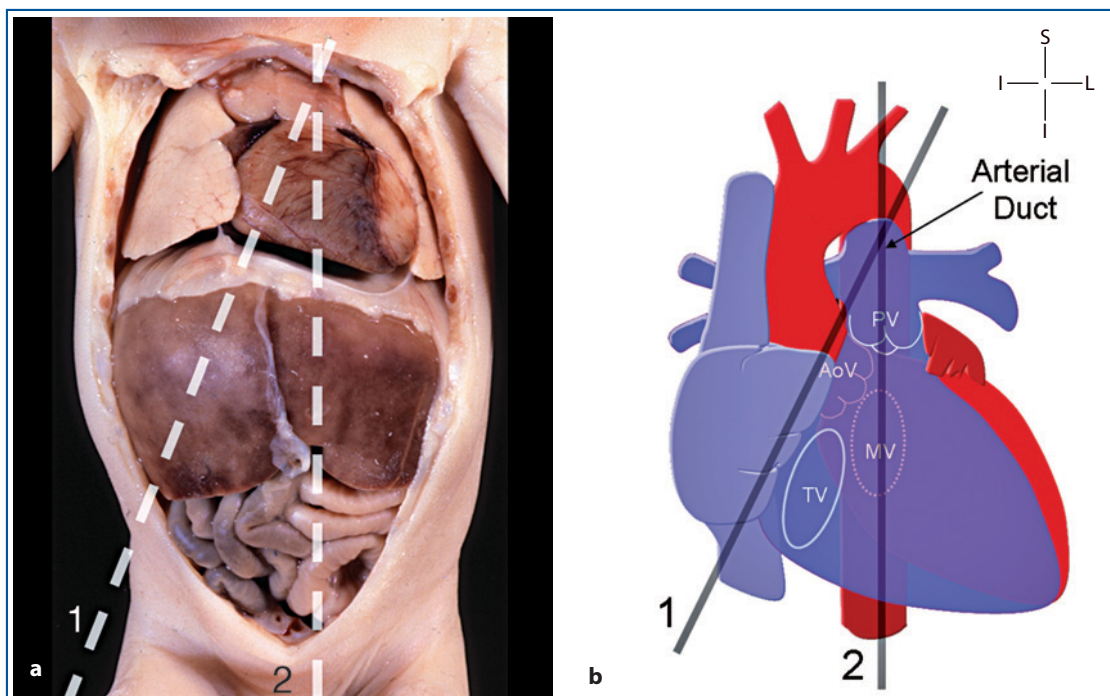
Fig. 15.1 • The two extreme planes for obtaining a long-axis view of the arterial duct are shown on the fetal body (**a**) and on a heart diagram (**b**). *Line 1* indicates the plane along a parasagittal cut, and *line 2* indicates the true sagittal section of the fetal body. *AoV* aortic valve, *MV* mitral valve, *PV* pulmonary valve, *TV* tricuspid valve

When the examining plane is oriented along a true sagittal plane, an oblique cut of the outflow of the left ventricle appears in the center of this section. Inferiorly, the left atrium is seen, separated from the left ventricular outflow by the anterior leaflet of the mitral valve. Anteriorly, a transverse section of the right ventricle is displayed apically to the tricuspid valve and the inlet portion (Fig. 15.2).

When the section plane is parasagittal, a cross section of the aortic root and its valve is displayed in the center of the heart, and a section of the two atria is seen inferiorly. With further clockwise rotation, the plane of this section becomes the short-axis view of the heart at the level of the right ventricular outflow tract.

Sagittal and parasagittal sections close to the midline of the fetal body are characterized by a long-axis view of the spine, with a long series of vertebral bodies displayed in the posterior part of the section and with the descending aorta in front of it.

The Normal Echocardiogram – 2D

In the normal fetus, the arterial duct arch arises in a more anterior position in the chest compared with the aortic arch. This is because its anterior branch, the main pulmonary artery, is connected with the infundibulum of the right ventricle, which is the heart's
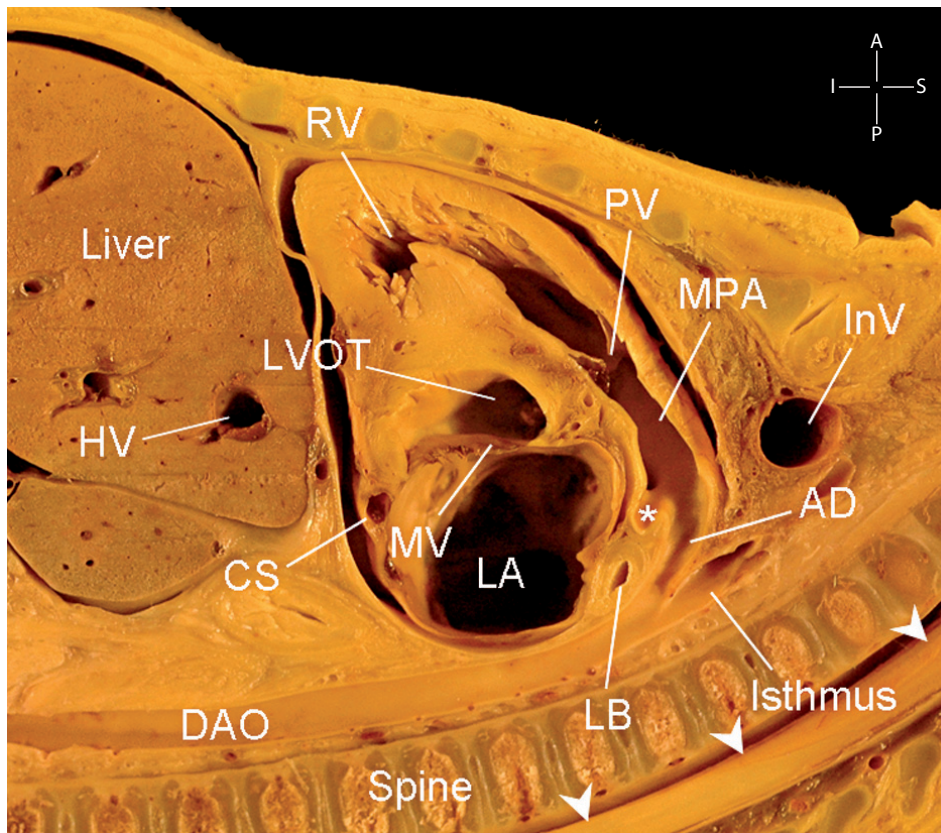
Fig. 15.2 • The fetal thorax is sectioned along a true sagittal plane slightly to the left of the sternum. Superiorly, a long-axis view of the main pulmonary artery and the arterial duct is seen joining the descending aorta (the ductal arch). The *white asterisk* indicates the origin of the left pulmonary artery. A cross section of the innominate vein is shown in the superior part of the mediastinum. The left ventricular outflow tract is seen in the center of the section separated from the left atrium by the anterior leaflet of the mitral valve. Anteriorly, a transverse section of the right ventricle is displayed. Posteriorly, a long tract of the descending aorta is seen in front of a longitudinal section of the spine. The *white arrowheads* indicate the spinal cord. *AD* arterial duct, *CS* coronary sinus, *DAO* descending aorta, *HV* hepatic vein, *InV* innominate vein, *LA* left atrium, *LB* left bronchus, *LVOT* left ventricular outflow tract, *MPA* main pulmonary artery, *MV* mitral valve, *PV* pulmonary valve, *RV* right ventricle

most anterior structure. Consequently, the arterial duct arch has a wider curvature than that of the aortic arch and is often referred to as having a "hockey-stick" appearance on ultrasound examination. Inferiorly to the pulmonary end of the arterial duct, the origin of the left pulmonary artery can be imaged. The most important feature of the ductal arch is that it does not give origin to the head and neck vessels. Only the left subclavian artery is often seen to enter the distal aortic arch (isthmus) above the aortic end of the arterial duct.

As already stated, parasagittal and sagittal sections differ as to the structures inside the heart that are displayed together with the arterial duct arch. In parasagittal sections, the left atrium, the right atrium, the tricuspid valve, and the right ventricle are seen wrapping around the aortic valve, which is seen in cross section in a central position. With high-resolution machines, a portion of the interatrial septum can be imaged between the two atria, with the flap valve protruding into the left atrium. Inside the right atrium, the Eustachian valve is often seen, simulating a membrane that divides this chamber in two portions: the posterior portion, which receives the inferior vena cava and the hepatic veins, and the anterior portion, the so-called vestibule, which gives access to the right ventricle through the tricuspid valve. In parasagittal section, a short tract of the descending aorta and a limited number of vertebral bodies can be imaged at the same time (Fig. 15.3).

When the section plane is along a truly a sagittal plane of the fetal body, the central position is occupied by an oblique cut of the left ventricular outflow tract. Posteriorly, the left atrium is seen, separated from the left ventricular outflow by the anterior leaflet of the mitral valve. True sagittal orientation of the scan plane is also characterized by a long-axis view of the descending aorta, which is displayed for a long tract in front of a row of thoracic and lumbar vertebral bodies (Fig. 15.4a).

In our experience, a true sagittal view of the arterial duct is easier to obtain than a parasagittal view. To obtain a projection of this type, it is helpful to start from a transverse view of the fetal thorax. With the fetus in ventral presentation, the probe must be placed on the left side of the sternum and the ultrasound beam aligned on the main pulmonary artery and descending aorta. The long-axis view of the arterial duct is obtained after 90° rotation of the scan plane (Fig. 15.4b).

Together with its transverse view, the long-axis view of the arterial duct is useful to assess the size, shape, and flow of the arterial duct. Together with the right ventricle outflow view, it allows evaluation of the right ventricular infundibulum, the pulmonary valve, and the main pulmonary artery.

The Normal Echocardiogram – Color Flow Mapping and Pulsed Doppler

With the fetus in dorsoposterior presentation, the arterial duct arch is coded in blue. When the descending aorta is oriented at a right angle to the ultrasound beam, the flow is represented with color only in the main pulmonary artery and arterial duct (Fig. 15.5). If the approach to the fetal body is more cranial, the entire course of the descending aorta is seen in col-

Fig. 15.3 • Long-axis view of the arterial duct obtained with parasagittal orientation in a normal 28-week gestational-age fetus. The ductal arch is displayed, formed by the main pulmonary artery, the arterial duct, and the descending aorta. A cross section of the aortic valve is seen in the center of this view, with the two atria, the tricuspid valve, and the right ventricle wrapping around. The *yellow arrowhead* indicates the flap valve of the atrial septum, which protrudes inside the left atrium. The *white arrowhead* indicates the Eustachian valve, between the posterior part (*1*) and the vestibule (*2*) of the right atrium. The *asterisk* is placed at the origin of the left pulmonary artery. *AD* arterial duct, *AV* aortic valve, *DAO* descending aorta, *HV* hepatic vein, *LA* left atrium, *MPA* main pulmonary artery, *PV* pulmonary valve, *RA* right atrium, *RV* right ventricle, *TV* tricuspid valve
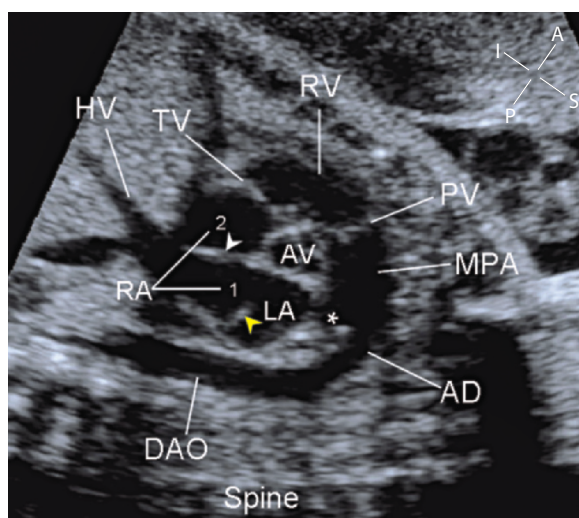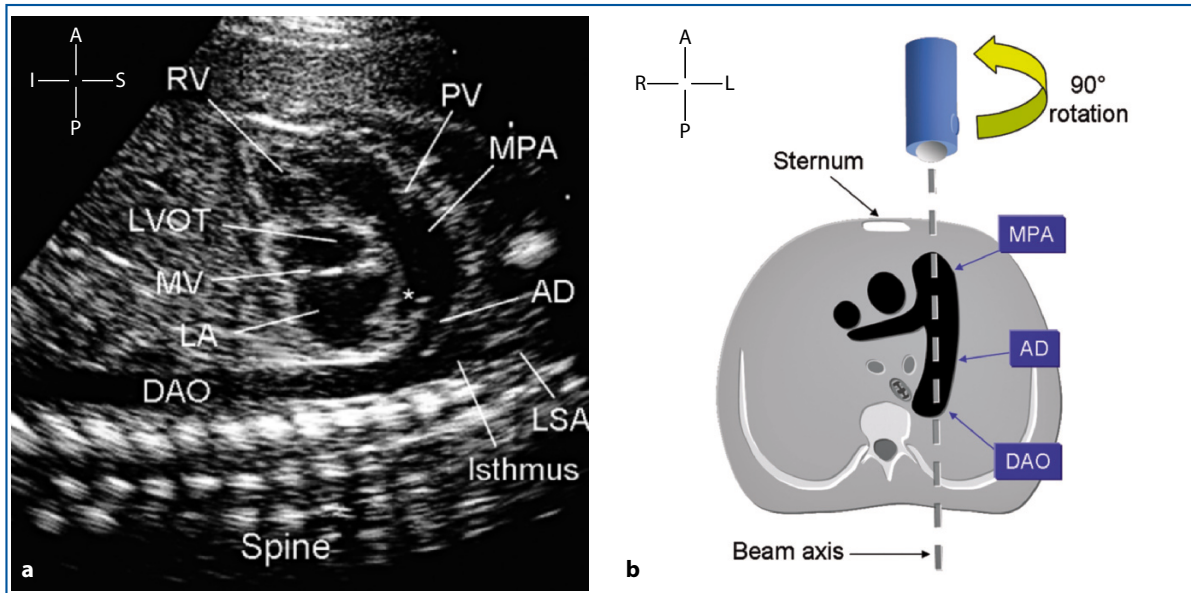
Fig. 15.4 • Cross-sectional image (**a**) of the long-axis view of the arterial duct obtained with true sagittal orientation of the scan plane in a 23-week gestational-age fetus. The "hockey-stick" appearance of the arterial duct arch is visible. The origin of the left subclavian artery is seen above the junction of the arterial duct with the descending aorta. The *asterisk* indicates the origin of the left pulmonary artery. The diagram (**b**), imitating the transverse view of the arterial duct, illustrates where the probe must be placed and how the beam axis must be oriented to obtain the long-axis view of the arterial duct by 90° rotation of the scan plane. A left parasternal approach on the fetal thorax is needed. *AD* arterial duct, *DAO* descending aorta, *LA* left atrium, *LSA* left subclavian artery, *LVOT* left ventricular outflow tract; *MPA* main pulmonary artery, *MV* mitral valve, *PV* pulmonary valve, *RV* right ventricle
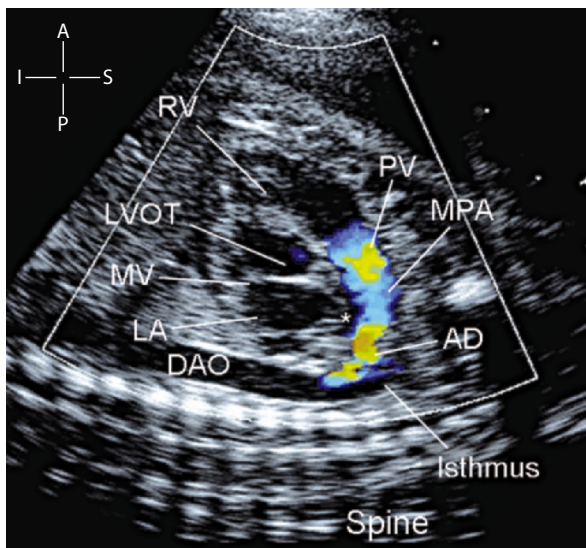
Fig. 15.5 • Color flow mapping from the long-axis view of the arterial duct in a normal 23-week gestational-age fetus. This early systolic frame shows a slightly aliased flow at the level of the pulmonary valve and of the arterial duct. The Nyquist limit is 42 cm/s. The *asterisk* indicates the origin of the left pulmonary artery. *AD* arterial duct, *DAO* descending aorta, *LA* left atrium, *LVOT* left ventricular outflow tract; *MPA* main pulmonary artery, *MV* mitral valve, *PV* pulmonary valve, *RV* right ventricle
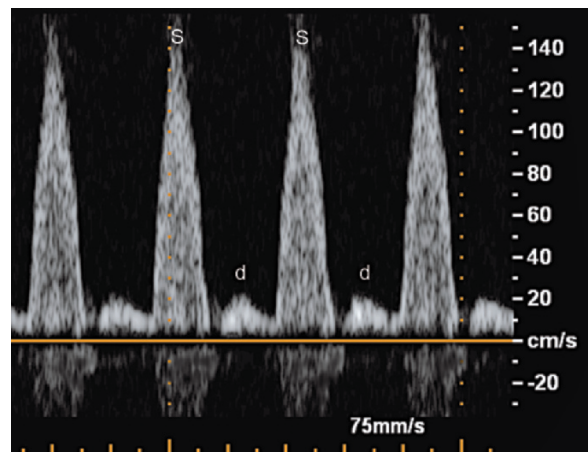
Fig. 15.6 • Pulsed Doppler tracing of the arterial duct flow in a normal 36-week gestational-age fetus obtained in a long-axis view of the arterial duct. Because of the left paravertebral approach, the arterial duct flow approaches the probe and therefore is represented as a positive wave. The image shows the higher systolic waves (*S*) reaching 140 cm/s and the smaller diastolic waves (*d*) below 20 cm/s
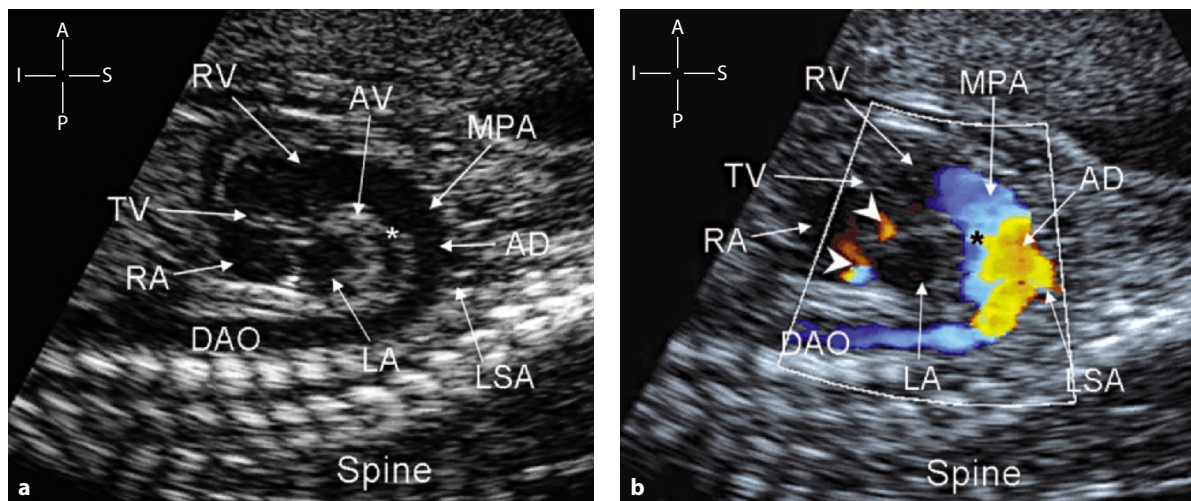
Fig. 15.7 • Parasagittal long axis-views of the ductal arch in a 23-week gestational-age fetus with hypoplastic left heart. On cross-sectional examination (**a**), the size of the ductal arch is disproportionately large because of redistribution of the total cardiac output on the right ventricle. The aortic root, seen in cross section, is so small it is difficult to identify. The *asterisk* indicates the origin of the left pulmonary artery. Color flow mapping (**b**) confirms the increased size of the ductal arch, with some aliased flow at the level of the duct. The *white arrowheads* indicate two small jets of flow from the left atrium to the right atrium through a restrictive foramen ovale. *AD* arterial duct, *AV* aortic valve, *DAO* descending aorta, *LA* left atrium, *LSA* left subclavian artery, *MPA* main pulmonary artery, *RA* right atrium, *RV* right ventricle, *TV* tricuspid valve

or. Because the peak velocity of arterial duct flow reaches the highest values in the fetal circulation, it is common to see an aliased flow in the arterial duct in early systole.

The arterial duct flow is characterized by systolic and diastolic anterograde waves. The peak velocity of this vessel reaches the highest value of the entire fetal cardiovascular system. Due to the high pulmonary vascular resistance and the reduced pulmonary perfusion, a large portion of the output from the right ventricle is diverted through the arterial duct into the descending aorta. The peak acceleration time of the arterial duct's systolic wave is higher than that of both the aorta and pulmonary arteries, reflecting the low resistances of the placenta downstream. Once the systolic wave has returned to baseline, a second anterograde wave, of much smaller width than the first, is observed during diastole (Fig. 15.6). This wave is thought to be the result of the rebound of the energy potentially stored by the walls of the main pulmonary artery and its branches, which produces a further flow from the pulmonary artery toward the aorta [1]. The systolic peak velocity usually varies from less than 50 cm/s at 6 weeks to 130-160 cm/s at the end of the pregnancy. The diastolic peak velocity for the same period ranges from close to zero early in gestation to 30-40 cm/s near term. The pulsatility index is rather constant throughout gestation, varying between 1.9 and 3.0 [2].

Duct-Dependent Systemic Circulation

In congenital heart disease with duct-dependent systemic circulation, the arterial duct shows an increased size due to redistribution of the total cardiac output to the right side of the heart. The position and the shape of the arterial duct is usually normal (Figs. 15.7, 15.8).

Duct-Dependent Pulmonary Circulation

In duct-dependent pulmonary circulation, the arterial duct frequently shows abnormalities of size, shape, and origin. When it is normally located, the size is generally reduced and shows an inverted curvature that lies on a more vertical plane [3]. This abnormal shape is due to reversed arterial duct perfusion from the aorta (Fig. 15.9). Arterial ducts of this kind cannot be visualized on the standard long-axis view of the arterial duct but can often be seen on a long-axis view of the aortic arch (Fig. 15.10).

Critical pulmonary valve stenosis or atresia with intact ventricular septum sometimes shows a normal-shaped duct. Many authors agree that cases with severe pulmonary valve stenosis or atresia at term are less severe and have better forward flow in the first part of pregnancy [4], thus explaining the normal size and shape of the arterial duct in some these cases (Fig. 15.11).
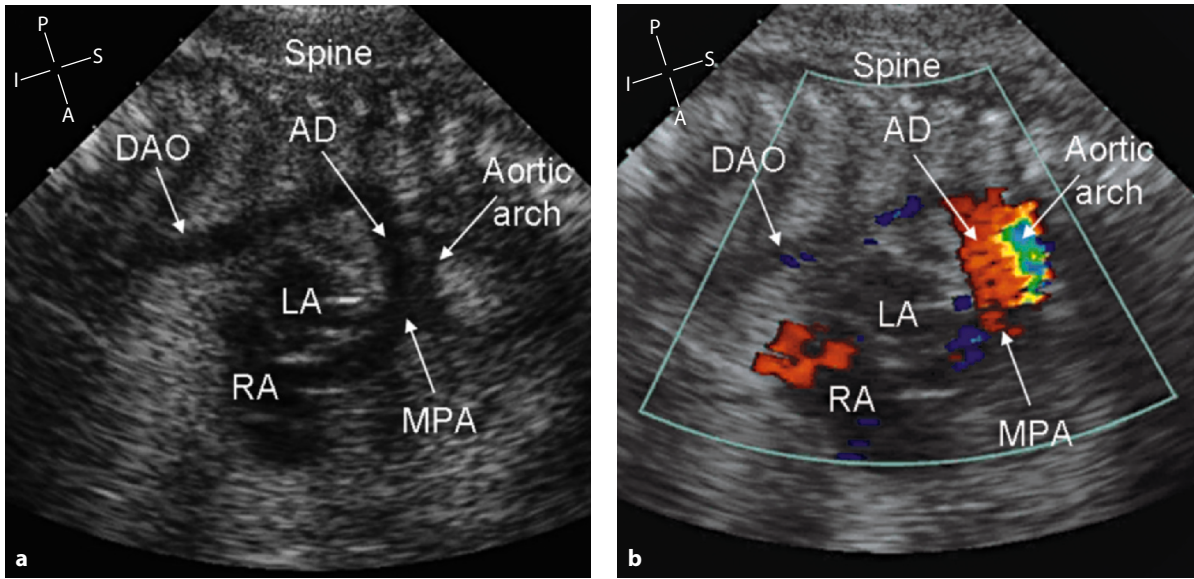
Fig. 15.8 • Long-axis view of the arterial duct in a 33-week gestational-age fetus with a complex type of aortic coarctation. These views are obtained from a left paravertebral approach. Due to the oblique nature of this cut, the aortic and ductal arches are seen on cross-sectional examination (**a**). The size of the transverse arch of the aorta is markedly smaller than the size of the pulmonary artery and the arterial duct. On color flow mapping **(b)**, the ductal arch is normally perfused in *red*, whereas the aortic arch is retrogradely perfused in *blue* through the arterial duct. *AD* arterial duct, *DAO* descending aorta, *LA* left atrium, *PA* main pulmonary artery, *RA* right atrium
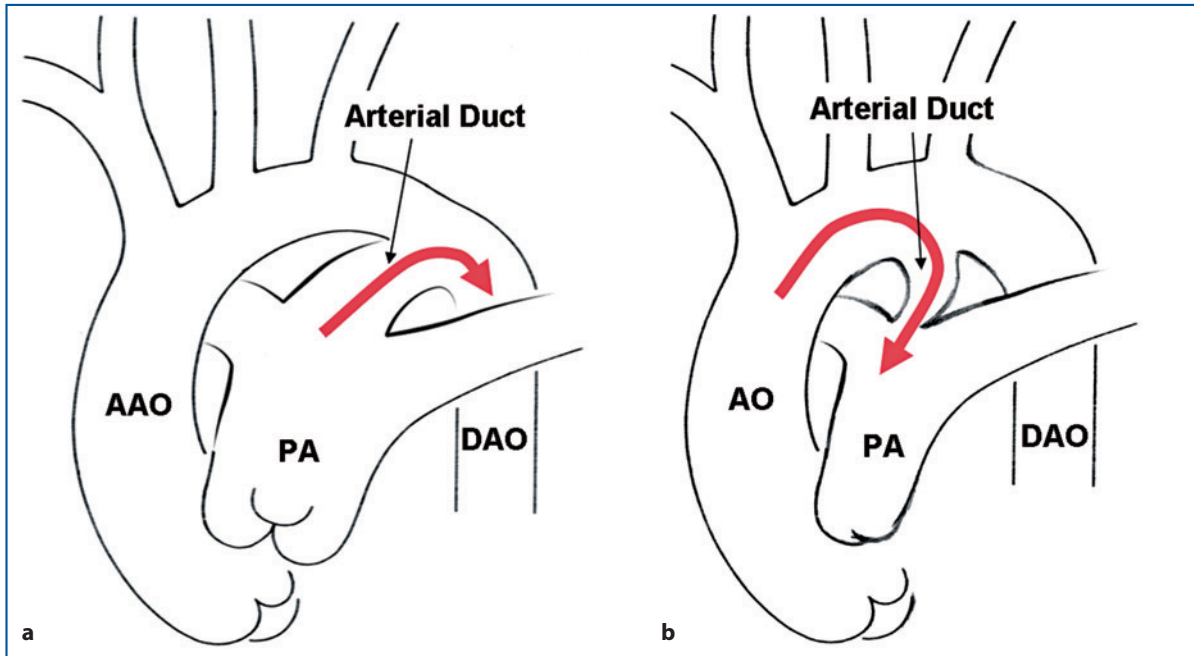
Fig. 15.9 • In the normal heart (**a**), the arterial duct merges into the descending aorta in a nearly horizontal plane. The direction of blood flow is from the pulmonary artery to the descending aorta. In pulmonary atresia (**b**), the arterial duct frequently is more vertical and the direction of blood flow is from the aortic arch to the pulmonary artery. *AAO* ascending aorta, *DAO* descending aorta, *PA* pulmonary artery
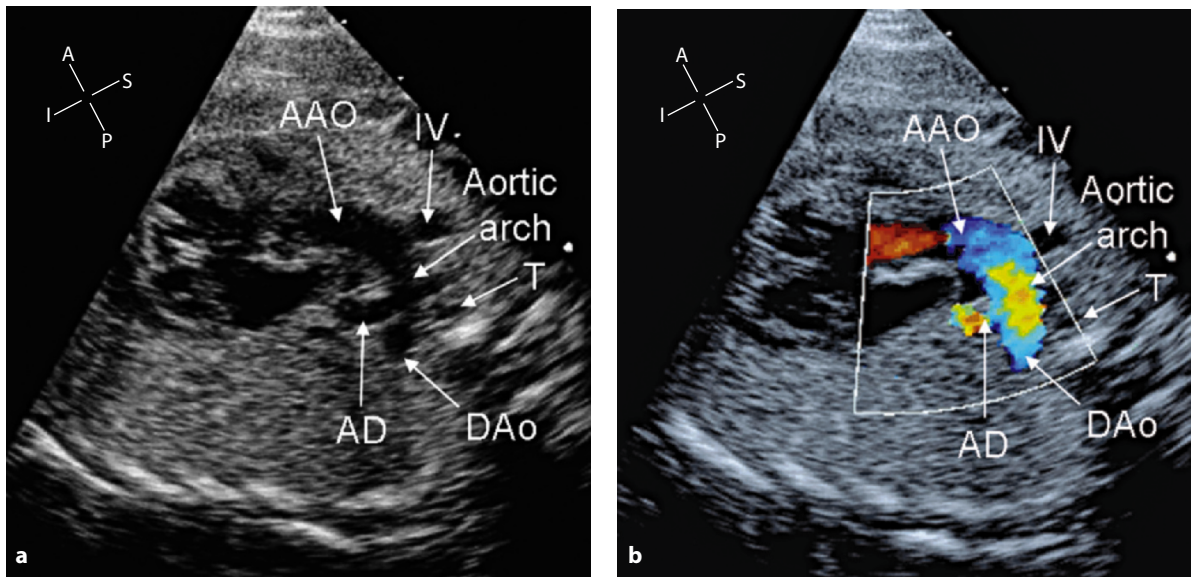
Fig. 15.10 • Long-axis view of the aortic arch in a 27-week gestational-age fetus with pulmonary valve atresia associated with complete atrioventricular septal defect. On cross-sectional examination (**a**), the arterial duct lies in a more vertical plane coming from the concavity of the aortic arch. Compared with the size of the aortic arch, the duct is relatively small and shows an inverted curvature. Color flow mapping (**b**) demonstrates reversed perfusion of the duct from the aorta. *AAO* ascending aorta, *AD* arterial duct, *DAO* descending aorta, *IV* innominate vein, *T* trachea
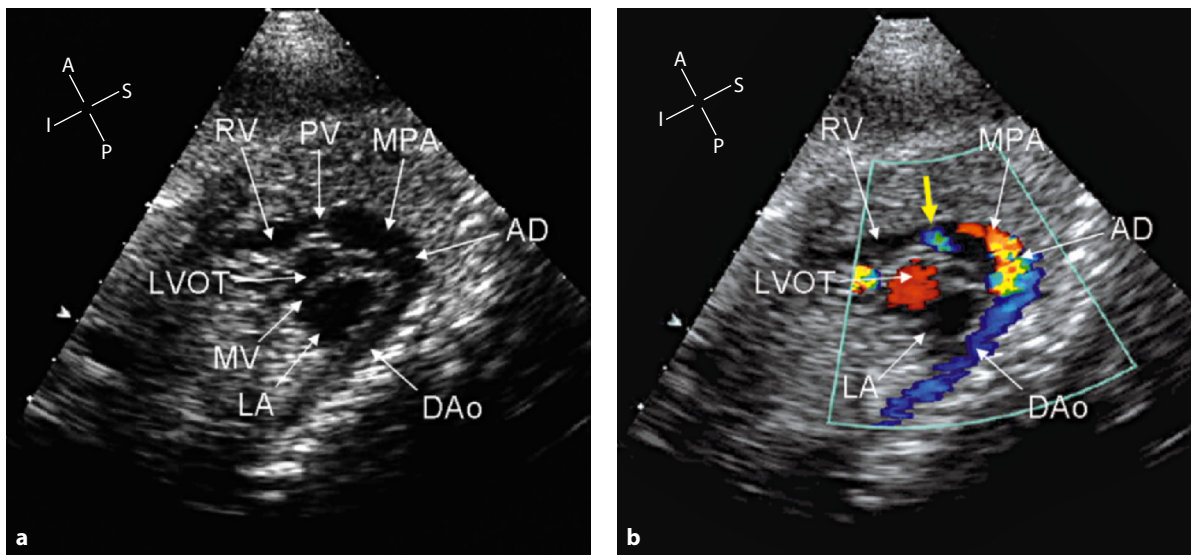
Fig. 15.11 • Cross-sectional long-axis view (**a**) of the arterial duct in a 23-week gestational-age fetus with critical pulmonary stenosis. The main pulmonary artery is a good size, as is common in this type of congenital valve malformation. Despite severe obstruction to the pulmonary outflow, the arterial duct maintained a normal curvature. Systolic frame on color flow mapping (**b**) shows a tiny jet of forward flow (*yellow arrow*) through the pulmonary valve in early systole. This small jet is easily overlooked if a high-resolution ultrasound machine with appropriate setting is not employed. Moreover, such a brief jet is easily missed on moving images and is better identified on frame-by-frame assessment. The main pulmonary artery is retrogradely perfused through the arterial duct, and this flow is represented in *red*. Even a very small patency of the pulmonary valve improves the probability of successful transcatheter balloon dilation and lowers the risk of complication. *AD* arterial duct, *DAO* descending aorta, *LA* left atrium, *LVOT* left ventricular outflow tract; *MPA* main pulmonary artery, *MV* mitral valve, *PV* pulmonary valve, *RV* right ventricle
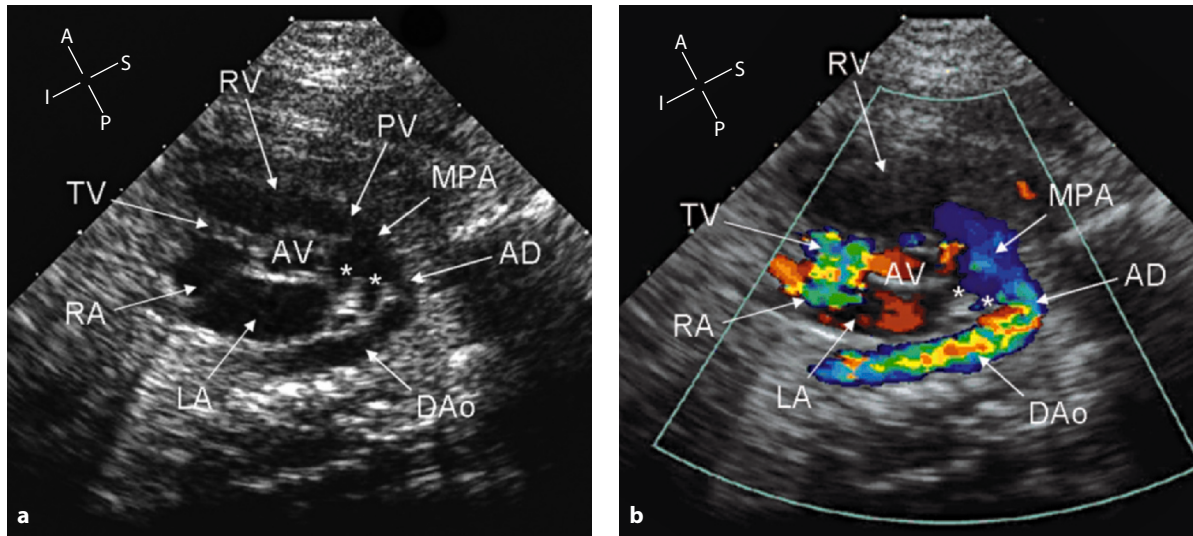
Fig. 15.12 • Parasagittal view of the arterial duct in a 32-week gestational-age fetus with premature duct constriction. Cross-sectional examination (**a**) is not particularly striking, and this complication is easily missed. Only with careful examination does the aortic end of the arterial duct appear narrowed. This systolic frame on color flow mapping (**b**) confirms the narrowing of the arterial duct at its aortic end, where a jet of accelerated flow originates and extends into the descending aorta. A second jet of tricuspid-valve regurgitation is seen inside the right atrium. The *white asterisks* indicate the origin of the right and left pulmonary artery. *AD* arterial duct, *AV* aortic valve, *DAO* descending aorta, *LA* left atrium, *MPA* main pulmonary artery, *PV* pulmonary valve, *RA* right atrium, *RV* right ventricle, *TV* tricuspid valve

The Arterial Duct – Premature Constriction or Closure

Arterial duct patency in the fetus is the result of an active process due to the release of prostaglandins from the placenta and, to a lesser degree, from the duct wall.

Premature arterial duct constriction or closure can occur in the human fetus. Maternal treatment with prostaglandin synthetase inhibitors can produce fetal ductal constriction. Indomethacin has been implicated in many published cases with ductal constriction/closure [5-7]. The risk of this complication increases with advanced gestational age and is dose dependent [8]. However, other anti-inflammatory agents can also cause this effect, blocking the cyclooxygenase enzymes that produce prostaglandins [9, 10]. It can occur, however, even without exposure to prostaglandin synthetase inhibitors (Fig. 15.12). Recently, arterial duct constriction in the fetus as been associated with maternal ingestion of herbal teas and grape juice during pregnancy [11]. Prenatal ductal constriction/closure can lead to progressive right ventricular dysfunction, with secondary tricuspid regurgitation, congestive heart failure, and fetal death. Persistent pulmonary hypertension of the newborn has

been linked to in utero arterial duct constriction. Although the long-term prognosis appears to be good in survivors, there is a risk of neonatal death. Prompt delivery after diagnosis is advocated to avoid such complications.

When suspected in the transverse section, ductal constriction or closure must be confirmed in longitudinal sections. False positive images for constriction can be obtained if the section plane does not pass through the vessel lumen. Suspicion on cross-sectional images needs to be confirmed by Doppler assessment [12, 13]. In case of arterial duct constriction, longitudinal sections are usually the best way to evaluate the size and flow of the arterial duct and to align the cursor line to the jet for pulsed or continuous Doppler assessment. In cases with severe arterial duct constriction, continuous Doppler system may be necessary, because the maximal velocities of the flow through the narrowed duct can be greater than 3 m/s (Fig. 15.13). In case of ductal closure, one must be careful not to mistake the flow into the left pulmonary artery for the arterial duct flow (Fig. 15.14). Indirect signs of ductal closure/constriction can be identified from the four-chamber view. These include hypertrophy and dysfunction of the right ventricle and regurgitation of the tricuspid valve.
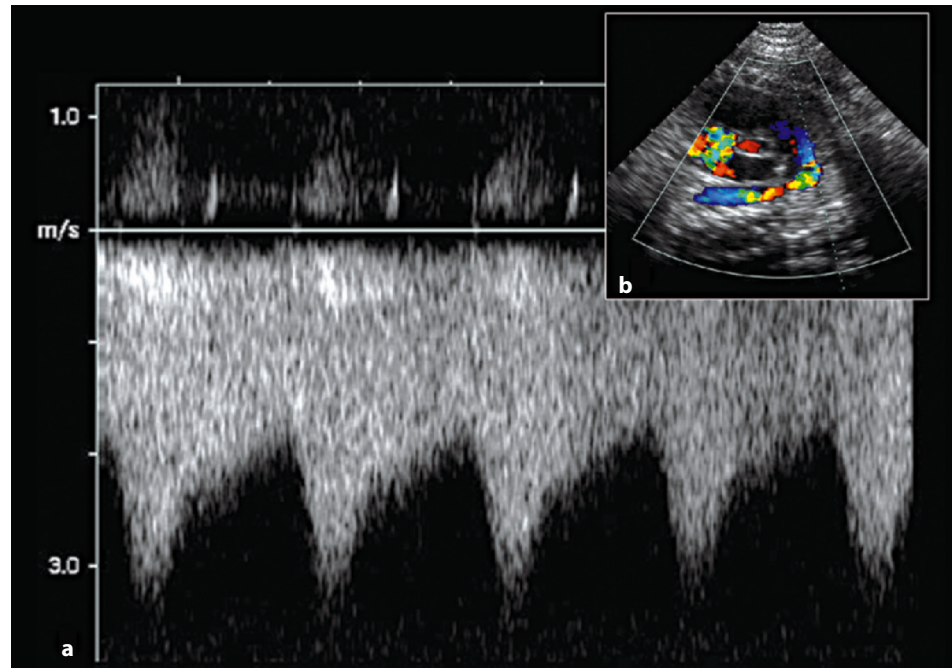
Fig. 15.13 • Continuous-wave Doppler spectrum (**a**) of the arterial duct jet in the same case shown in Figure 15.7. The systolic velocity is approximately 3 m/s, well above the normal upper limits for the arterial duct, whereas the diastolic velocity is 1.8 m/s. The *small frame* (**b**) indicates the cursor-line position (*dashed line*)
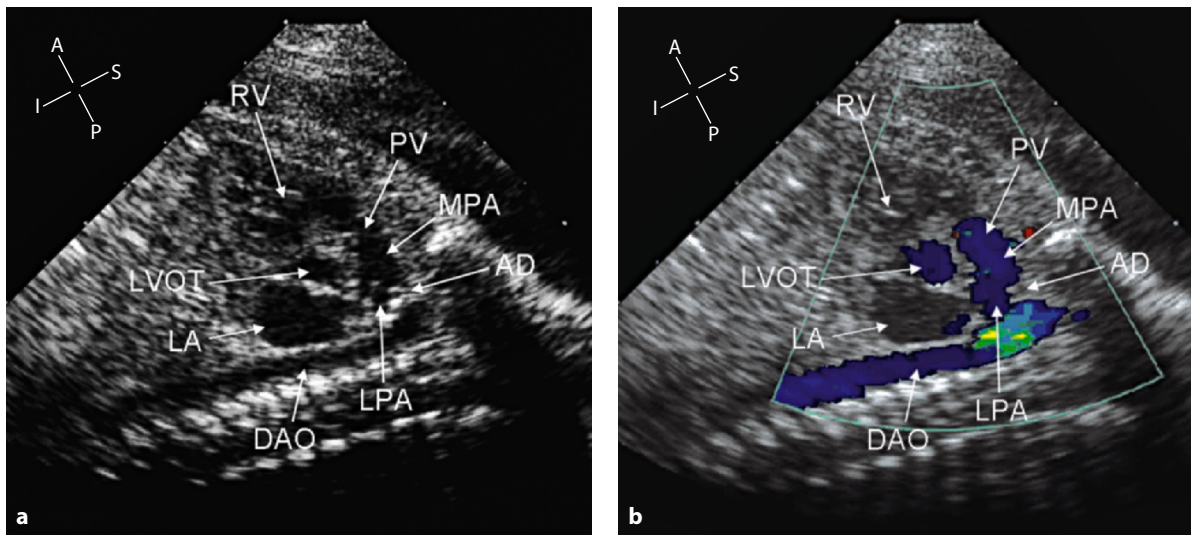
Fig. 15.14 • Arterial duct long-axis view in a 29-week gestational-age fetus with complete closure of the arterial duct. On cross-sectional examination (**a**), the arterial duct walls are thickened and have a virtual lumen, as in a postnatal examination. On color flow mapping (**b**), this complication was overlooked by an experienced examiner, because the flow into the proximal left pulmonary artery was mistaken for the forward flow into the arterial duct. *AD* arterial duct, *DAO* descending aorta, *LA* left atrium, *LPA* left pulmonary artery, *LVOT* left ventricular outflow tract, *MPA* main pulmonary artery, *PV* pulmonary valve, *RV* right ventricle

References

1. Van der Mooren K, Barendregt LG, Wladimiroff JW (1991) Flow velocity waveforms in the human fetal ductus arteriosus during the normal second half of pregnancy. Pediatr Res 30:387-390
2. Huta JC (1995) The fetal ductus arteriosus. In: Copel JA, Reed KL (eds) Doppler ultrasound in obstetrics and gynecology. Raven Press, New York, pp 325-331
3. Santos MA, Moll JN, Drumond C et al (1980) Development of the ductus arteriosus in the right ventricular outflow tract obstruction. Circulation 62:818
4. Hornberger LK, Benacerraf BR, Bromley BS et al (1994) Prenatal detection of severe right ventricular outflow tract obstruction: pulmonary stenosis and pulmonary atresia. J Ultrasound Med 13:743-750
5. Eronen M, Pesonen E, Kurki T et al (1991) The effects of indomethacin and a beta-sympathomimetic agent on the fetal ductus arteriosus during treatment of premature labor: a randomized double-bind study. Am J Obstet Gynecol 164:141-146
6. Mohen D, Newham JP, D'Orsogna L (1992) Indomethacin for the treatment of polydramnios: a case of constriction of the ductus arteriosus. Aust NZ J Obstet Gynaecol 32:243-246
7. Shehata BM, Bare JB, Denton TD et al (2006) Premature closure of the ductus arteriosus: variable response among monozygotic twins after in utero exposure to indomethacin. Fetal Pediatr Pathol 25:151-157
8. Moise KJ (1993) Effect of advancing gestational age on the frequency of fetal ductal constriction in association with maternal indomethacin use. Am J Obstet Gynecol 168:1350-1353
9. Paladini D, Marasini M, Volpe P (2005) Severe ductal constriction in the third-trimester fetus following maternal self-medication with nimesulide. Ultrasound Obstet Gynecol 25:357-361
10. Auer M, Brezinka C, Eller P et al (2004) Prenatal diagnosis of intrauterine premature closure of the ductus arteriosus following maternal diclofenac application. Ultrasound Obstet Gynecol 23:513-516
11. Zielinsky P, Piccoli Jr AL, Manica JL et al (2006) Ingestion of herbal teas and grape juice during pregnancy is associated to fetal ductal constriction: a clinical approach. Cardiol Young 17(I):8
12. Huhta JC, Moise KJ, Fisher DJ et al (1987) Detection and quantitation of constriction of the fetal ductus arteriosus by Doppler echocardiography. Circulation 75:406-412
13. Tulzer G, Gudmundsson S, Sharkey AM et al (1991) Doppler echocardiography of fetal ductus arteriosus constriction versus increased right ventricular output. J Am Coll Cardiol 18:532-536

CHAPTER 16

Special Considerations on the Arterial Duct and Aortic Arch Views

Technique

Visualization of the long-axis views of the aorta and arterial duct is facilitated in the fetus if one refers to a transverse section of the upper mediastinum as the starting point. For instance, the long-axis view of the aortic arch is obtained from the transverse view of the fetal thorax by rotating the scan plane 90° when the ascending and the descending aorta are aligned with the ultrasound-beam axis. In the normal fetus in ventral presentation, this alignment is obtained by placing the transducer on the right parasternal area (Fig. 16.1).

On the other hand, the long-axis view of the arterial duct is obtained after 90° rotation of the scan plane when the main pulmonary artery and descending aorta are aligned with the ultrasound-beam axis in a transverse view of the fetal thorax. When the fetus is in ventral presentation, this alignment is possible by placing the transducer on the left side of the sternum (Fig. 16.2).

In the normal fetus in dorsoanterior presentation, the sagittal view of the aortic arch and the ductal arch is obtained with a left paravertebral approach (Fig. 16.3a). The right paravertebral approach is useful to obtain the bicaval view from the back (Fig. 16.3b). Figure 16.4 shows a sagittal echocardiographic view of the aortic arch with left paravertebral approach to the fetal body.
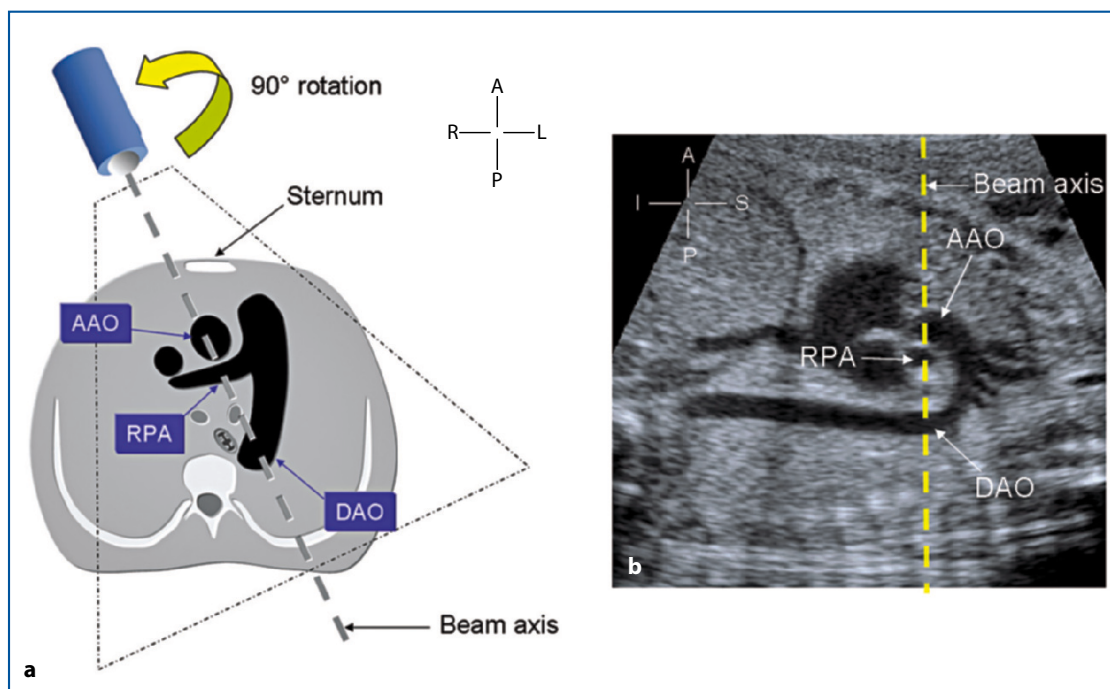
Fig. 16.1 • Diagram illustrating the arterial duct transverse view with the fetus in ventral presentation (**a**). Right parasternal probe position is necessary to align the ascending and descending aorta with the ultrasound-beam axis. By rotating the probe 90°, the aortic arch long-axis view is obtained (**b**). *AAO* ascending aorta, *DAO* descending aorta, *RPA* right pulmonary artery
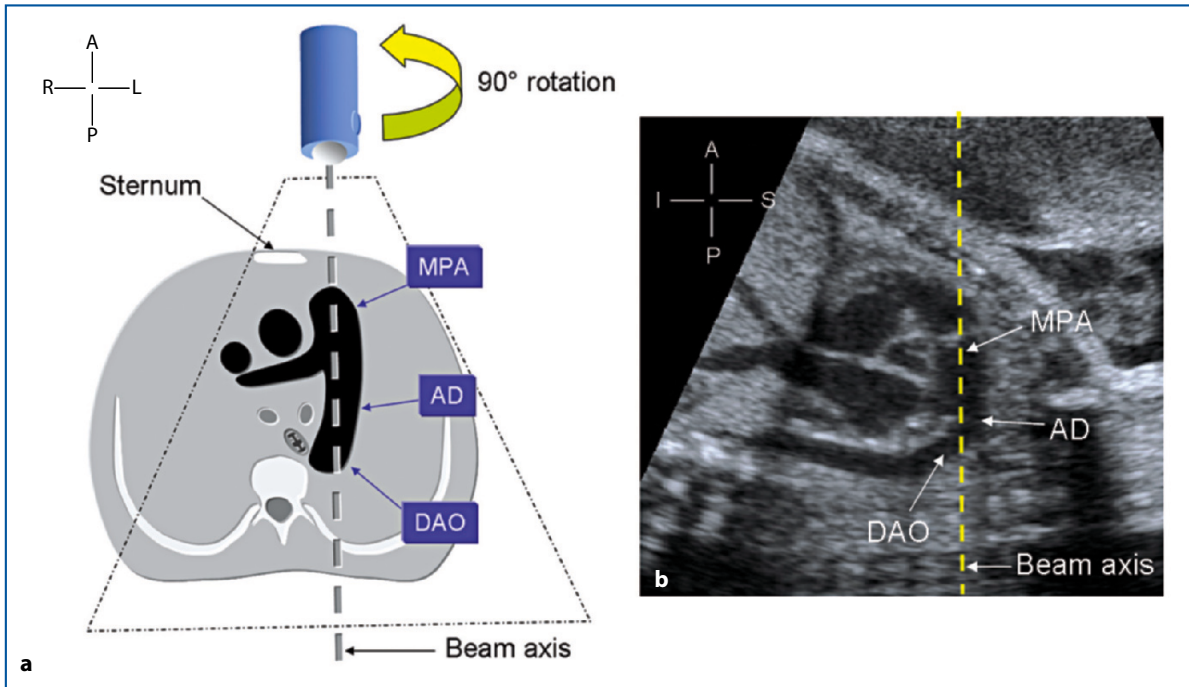
Fig. 16.2 • Diagram of the arterial duct transverse view with the fetus in ventral presentation (**a**). Left parasternal approach necessary to align the pulmonary artery and descending aorta with the ultrasound-beam axis. By rotating the probe 90°, the ductal arch long-axis view is obtained (**b**). *AD* arterial duct, *DAO* descending aorta, *MPA* main pulmonary artery
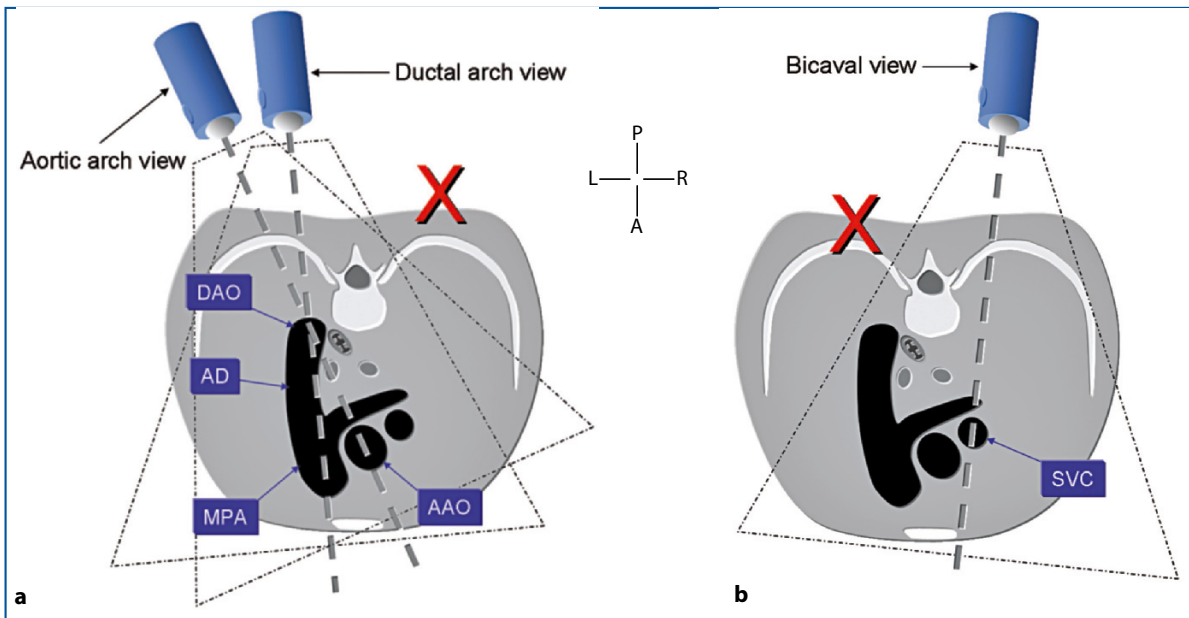
Fig. 16.3 • Diagrams of the arterial duct transverse view with the fetus in dorsoanterior presentation. Sagittal views (**a**) of the aortic arch and arterial duct are obtained with appropriate orientation of the scan plane with left paravertebral approach because the descending aorta is located on the left side of the spine. These views cannot be obtained with right paravertebral approach (*red cross*). Conversely, a right paravertebral approach (**b**) is usually necessary to obtain the bicaval view from the back and cannot be obtained from the right side of the spine (*red cross*). *AAO* ascending aorta, *AD* arterial duct, *DAO* descending aorta, *MPA* main pulmonary artery
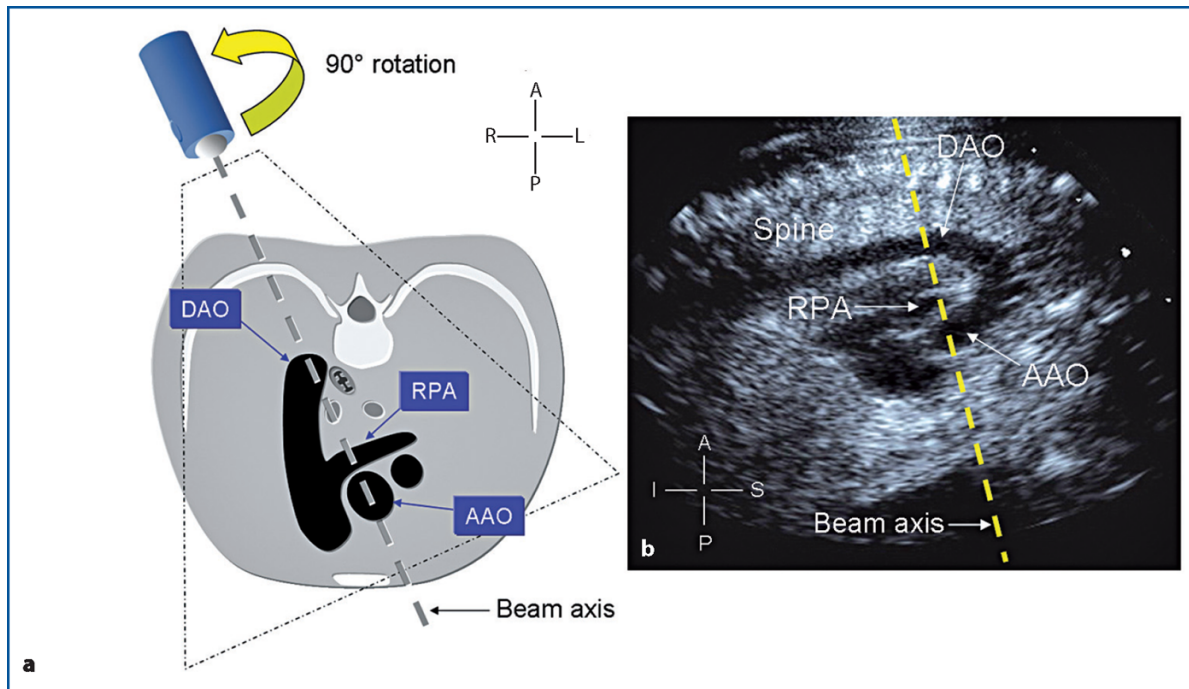
Fig. 16.4 • Diagram of the arterial duct transverse view with the fetus in dorsoanterior presentation (**a**). Left paravertebral probe position is necessary to align the ascending and descending aorta with the beam axis. After 90° rotation of the scan plane, a long-axis view of the aortic arch is obtained, with the spine in anterior position (**b**). *AAO* ascending aorta, *DAO* descending aorta, *RPA* right pulmonary artery
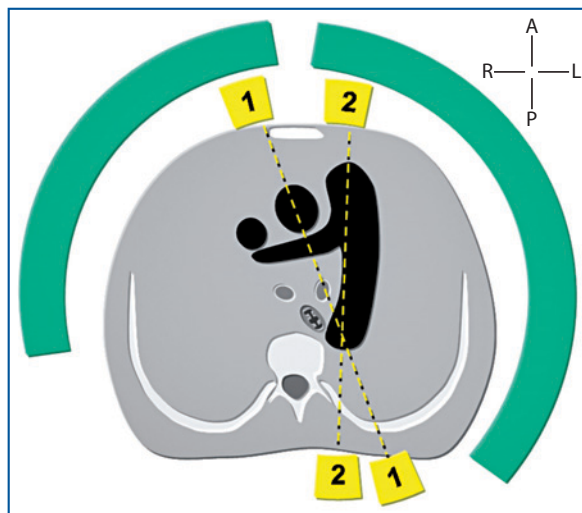
Fig. 16.5 • *Green sectors* indicate the area of approach to the fetal thorax that provides transverse sections of the aortic arch and arterial duct. *Yellow sectors* indicate the limited areas where the long axis of the aortic arch (*1*) and arterial duct (*2*) are obtained

It is therefore evident that the long-axis view of the aortic arch and the arterial duct arch is obtained only from limited positions of the transducer. With unfavorable fetal presentation, achieving these views can be an exhausting procedure for the examiner and the patient. Moreover, the sagittal views of the fetal thorax are limited by shadows of the ribs and sternum, which is particularly the case with advanced gestational age. On the other hand, a transverse section of the aortic and arterial duct arches is more easily obtained from a wide range of lateral approaches to the fetal thorax (Fig. 16.5). Better penetration of the ultrasound beam between intercostal spaces is often possible, even in third-trimester examinations (Figs. 16.6, 16.7). However, these views are often limited by the position of the upper limbs and the scapulae. Also, it is better to avoid the very anterior portion of thorax because of the noisy shadowing of the sternum (Fig. 16.8).
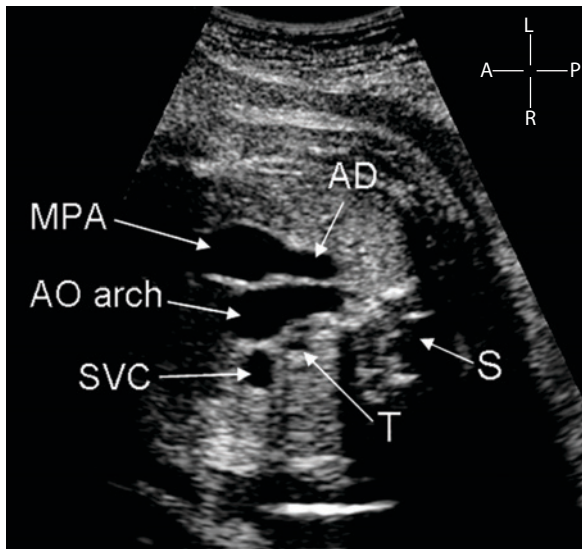
Fig. 16.6 • Normal transverse view of the arterial duct and aortic arch in a 35-week gestational-age fetus obtained with the left-sided approach to the fetal thorax. Despite advanced gestational age, this transverse section allows assessment of the two arches. *AO* aorta, *AD* arterial duct, *MPA* main pulmonary artery, *S* spine, *SVC* superior vena cava, *T* trachea
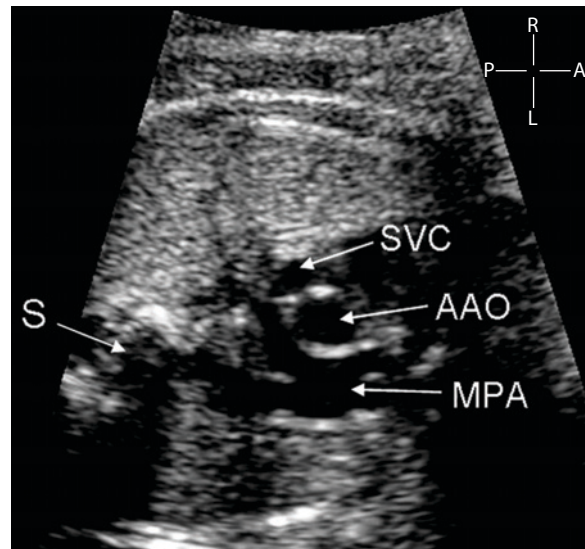
Fig. 16.7 • Normal three-vessel view in a 34-week gestational-age fetus with transverse approach on the right side of the fetal thorax. The normal size, shape, and alignment of the vessels is shown. To obtain sagittal views of the two arches would be impossible if the fetal position remains unchanged. *AAO* ascending aorta, *MPA* main pulmonary artery, *S* spine, *SVC* superior vena cava
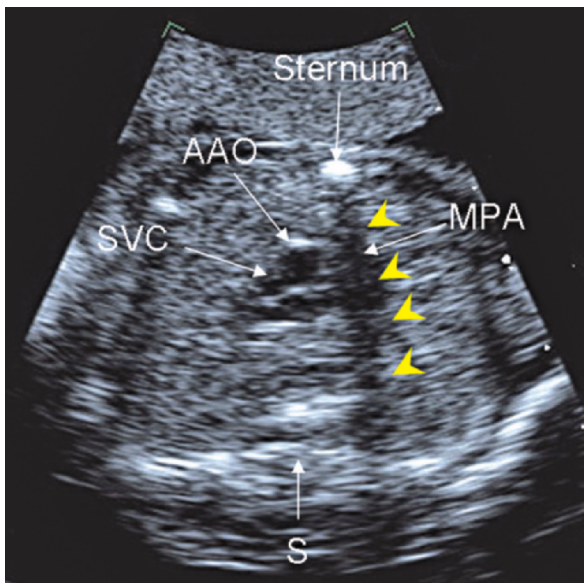
Fig. 16.8 • This three-vessel view shows shadowing of the sternum because of the direct approach of the ultrasound beam to the midline of the fetal thorax. The pulmonary artery is not defined because it is covered by a strong ultrasound shadow (*yellow arrowheads*) generated by the sternal cartilage. *AAO* ascending aorta, *MPA* main pulmonary artery, *S* spine, *SVC* superior vena cava

CHAPTER 17

The Right Ventricle Outflow View

The Section Plane

Because of the horizontal position of the fetal heart, sections along its short axis lie on planes close to a sagittal plane of the fetal body. From a sagittal plane parallel to the fetal spine, these sections are obtained with a slight rotation toward the left side of the fetus, so that the examining plane is from the right hypochondrium to the left shoulder. By maintaining this orientation and by translating the scanning plane leftward on the fetal thorax, a series of sections from the base of the heart to its apex is obtained.

This short-axis section of the heart is obtained by sweeping the section plane leftward from the long-axis view of the aortic arch. The section level is in-dicated in Figure 17.1. Because the aortic root is near-ly parallel to the long axis of the heart, the short-axis view displays the aortic root in cross section (Fig. 17.1b). Moreover, because the right ventricular outflow is nearly orthogonal to the left outflow, the right ventricular outflow is seen in long axis, hence the name of this view. This is because in the normal heart, the great arteries are wrapped around one another and their outflows cross (Fig. 17.2).

The Normal Morphology

In the right ventricular outflow view, structures of the right side of the heart are displayed arranged around the aortic root, as seen in the center of the section (Fig. 17.3).
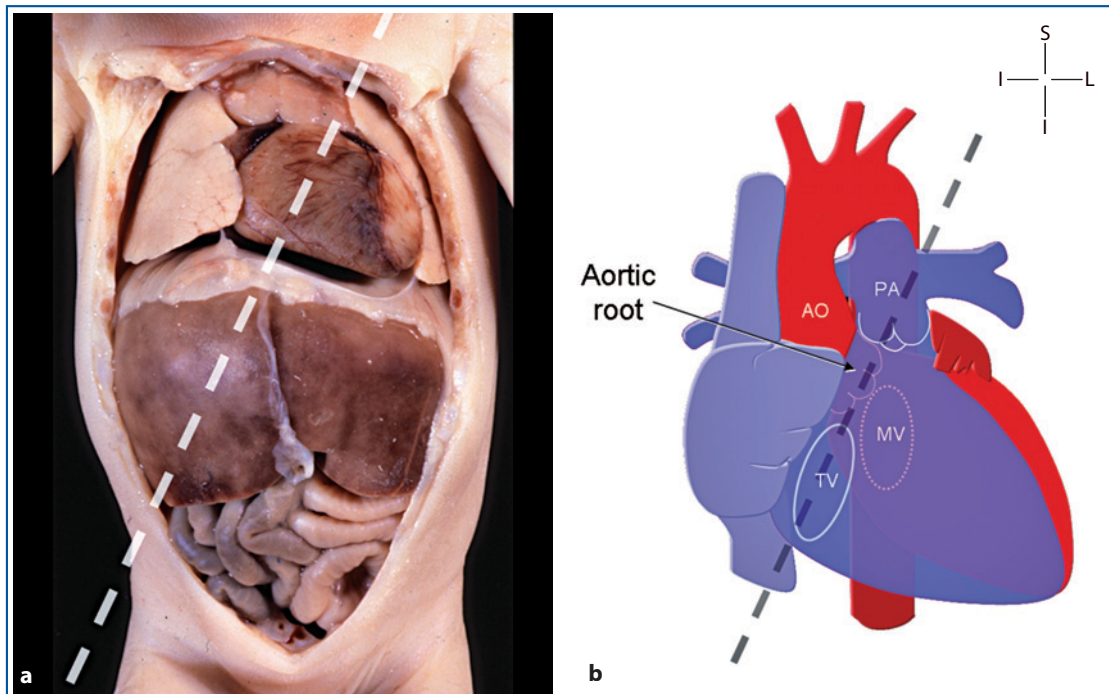
Fig. 17.1 • The *dashed line* indicates the plane of the right ventricular outflow view on the fetal body (**a**) and on a heart diagram (**b**). *AO* ascending aorta, *MV* mitral valve, *PA* main pulmonary artery, *TV* tricuspid valve
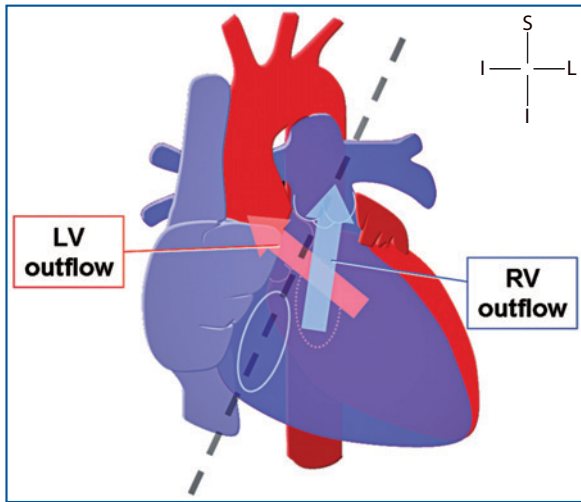
Fig. 17.2 • This heart diagram shows the nearly orthogonal orientation of the outflow of the left (*red arrow*) and right (*blue arrow*) ventricle. The major axis of the latter is almost parallel to the plane of this view (*dashed line*)
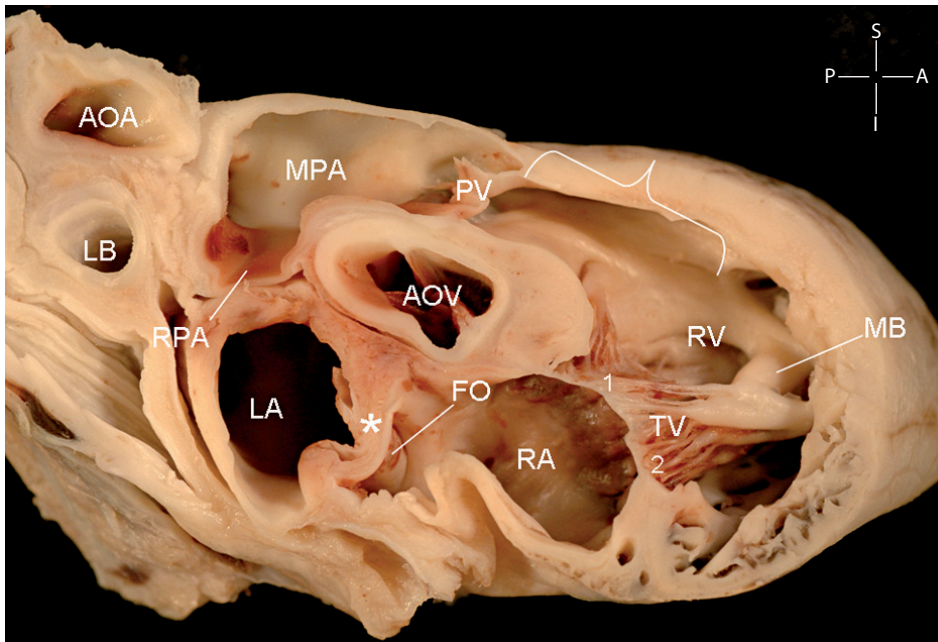
Fig. 17.3 • This specimen is sectioned along a parasagittal plane of the fetal body to imitate the outflow view of the right ventricle. In the center, the aortic root is seen in cross section at the level of its valve. Superiorly, the pulmonary valve is shown where the infundibulum (*bracket*) joins the main pulmonary artery. Posterosuperiorly, the origin of the right branch from the main pulmonary artery is seen. Inferiorly, an oblique section of the left and right atrium is seen, with the interatrial septum in between (*asterisk*). Inferoanteriorly, the tricuspid valve, sectioned along its septal (*1*) and mural (*2*) leaflets, connects the right atrium to the inlet portion of the right ventricle. Anteriorly, the right ventricle wraps around the aortic root with its inlet and outlet component (the infundibulum). *AOA* aortic arch, *AOV* aortic valve, *FO* foramen ovale, *LA* left atrium, *LB* left bronchus, *MB* moderator band, *MPA* main pulmonary artery, *PV* pulmonary valve, *RA* right atrium, *RPA* left pulmonary artery, *RV* right ventricle, *TV* tricuspid valve

The Normal Echocardiogram – 2D

As stated, most structures of the right heart can be investigated in this view. These structures include the right atrium, the tricuspid valve, the infundibulum, the pulmonary valve, and the main pulmonary artery. Because the root of the great arteries is imaged, this view is ideal for measuring the diameter of the root of the aorta and the pulmonary artery. Moreover, it

allows assessment of defects of the membranous part of the interventricular septum and deviation of the infundibular septum. Posteriorly, the main pulmonary artery is often seen bifurcating into the right pulmonary artery and arterial duct. Behind the aortic root, a section of the left atrium and the atrial septum is imaged. With high-resolution equipment, the flap valve is seen flickering into the body of the left atrium on moving images (Fig. 17.4b). Due to the oblique orientation of this section relative to the long axis of the fetus, few vertebral bodies are displayed.

Fig. 17.4 • Right ventricular outflow view in a normal 22-week gestational-age fetus (**a**). Comments are provided in the text. A close-up view of the same image (**b**) shows the flap valve (*yellow arrowhead*) of the foramen ovale bulging inside the body of the left atrium. *AD* arterial duct, *AOV* aortic valve, *Ist* isthmus of the aorta, *LA* left atrium, *MPA* main pulmonary artery, *PV* pulmonary valve, *RA* right atrium, *RV* right ventricle, *S* spine, *TV* tricuspid valve

The Normal Echocardiogram – Color Flow Mapping and Pulsed Doppler

This view highlights the wide angle between the direction of the inlet and outlet portion of the right ventricle, approximately at right angles to each other. When the inner curvature of the heart is toward the apex of the echocardiographic fan, this view is particularly suitable for Doppler assessment of the inflow and outflow of the right ventricle, with favorable interrogation angle (Fig. 17.5). This allows assessment of the flow of the tricuspid valve, the right ventricular outflow, and the pulmonary valve (Fig. 17.6).

Figures 17.7-17.11 show some examples of congenital heart disease seen in the right ventricle outflow view.
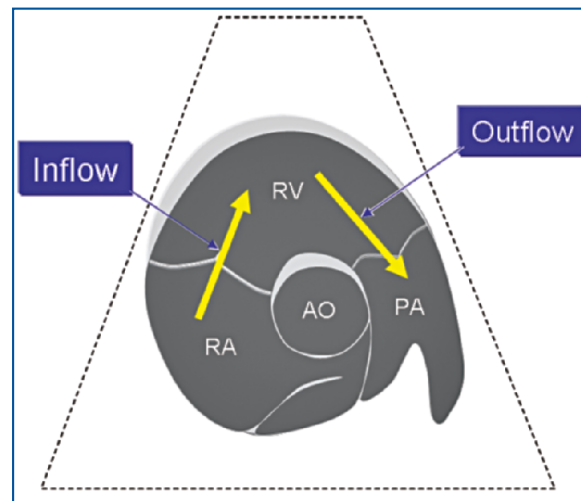
Fig. 17.5 • This diagram, imitating a right ventricular outflow view, shows how the inflow and outflow of the right ventricle are investigated with a ventral approach to the fetal heart. The directions of the inflow and outflow (*yellow arrows*) of the right ventricle are approximately at right angles with each other. *AO* aorta, *PA* pulmonary artery, *RA* right atrium, *RV* right ventricle
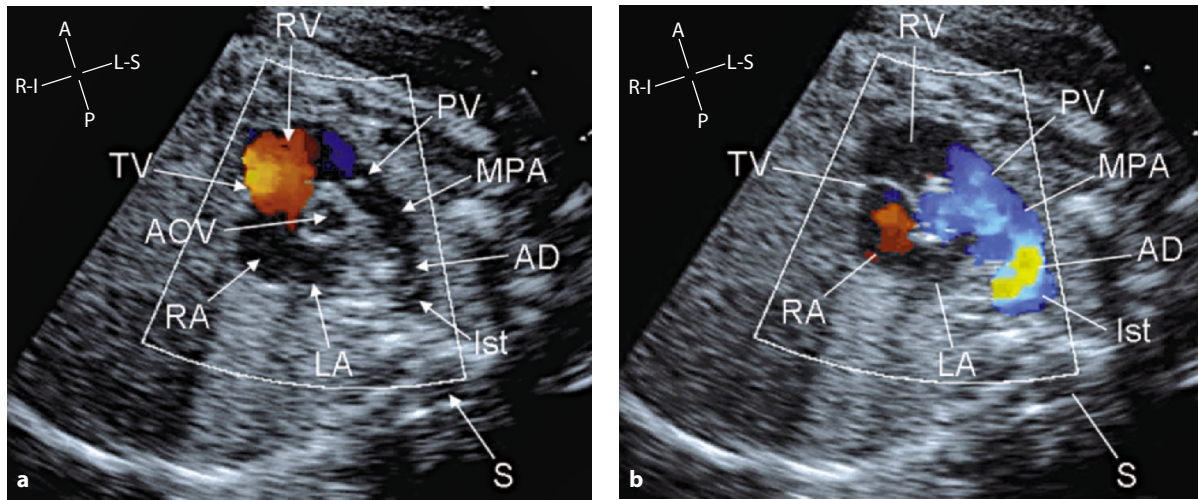
Fig. 17.6 • Color flow mapping in ventral presentation in a normal 22-week gestational-age fetus. The diastolic frame (**a**) shows the opening of the tricuspid valve, with the right ventricle filling in *red*. A faint flow is seen in *blue* filling the right ventricular outflow, and the pulmonary valve is closed. In this systolic frame (**b**), the tricuspid valve is closed, and the outflow from the right ventricle is seen in *blue* filling anterogradely the main pulmonary artery. The flow is slightly aliased at the level of the arterial duct, where it reaches its highest velocity. *AD* arterial duct, *AOV* aortic valve, *Ist* isthmus of the aorta, *LA* left atrium, *MPA* main pulmonary artery, *PV* pulmonary valve, *RA* right atrium, *RV* right ventricle, *S* spine, *TV* tricuspid valve
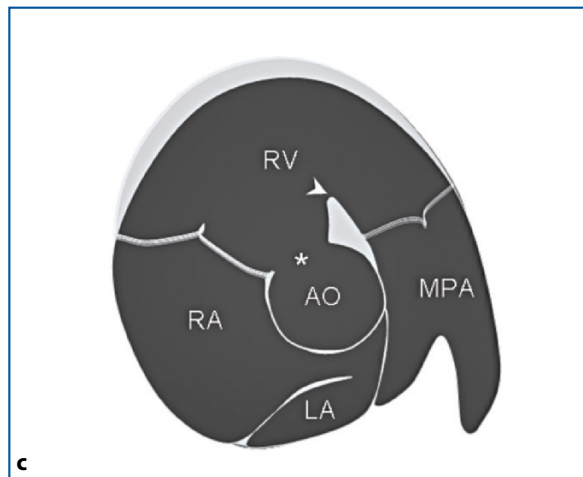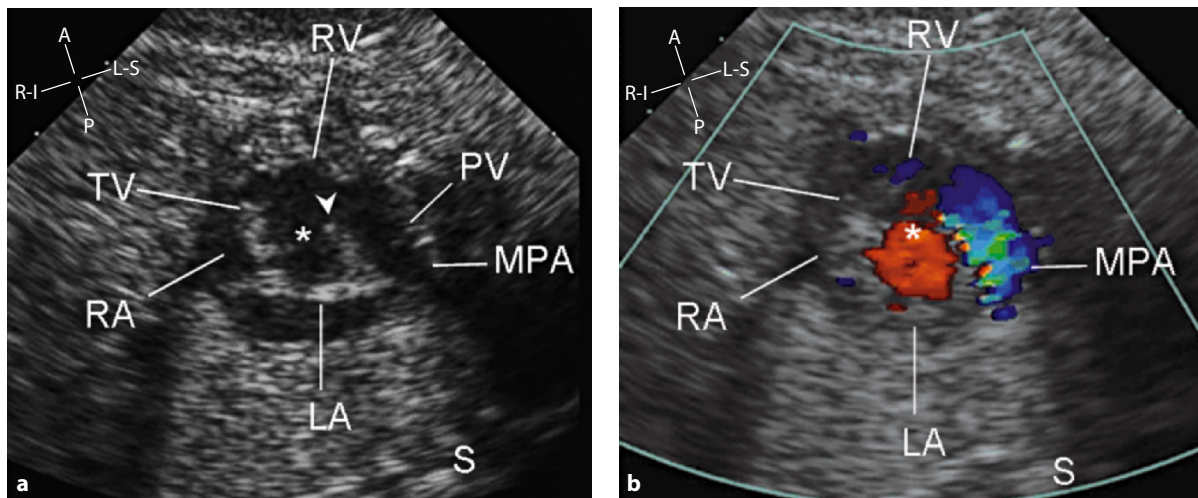
Fig. 17.7 • Right ventricular outflow view in a 27-week gestational-age fetus with malalignment ventricular septal defect. The cross-sectional frame (**a**) shows the subaortic ventricular septal defect (*asterisk*) with anterior malalignment of the infundibular septum (*arrowhead*). The infundibulum is wide open, and the diameter of the main pulmonary artery is normal. Color flow mapping (**b**) demonstrates an unobstructed forward flow through the pulmonary valve. On moving images, the ventricular septal defect shows a bidirectional shunt. A correlative diagram (**c**). *AO* aorta, *LA* left atrium, *MPA* main pulmonary artery, *PV* pulmonary valve, *RA* right atrium, *RV* right ventricle, *S* spine, *TV* tricuspid valve
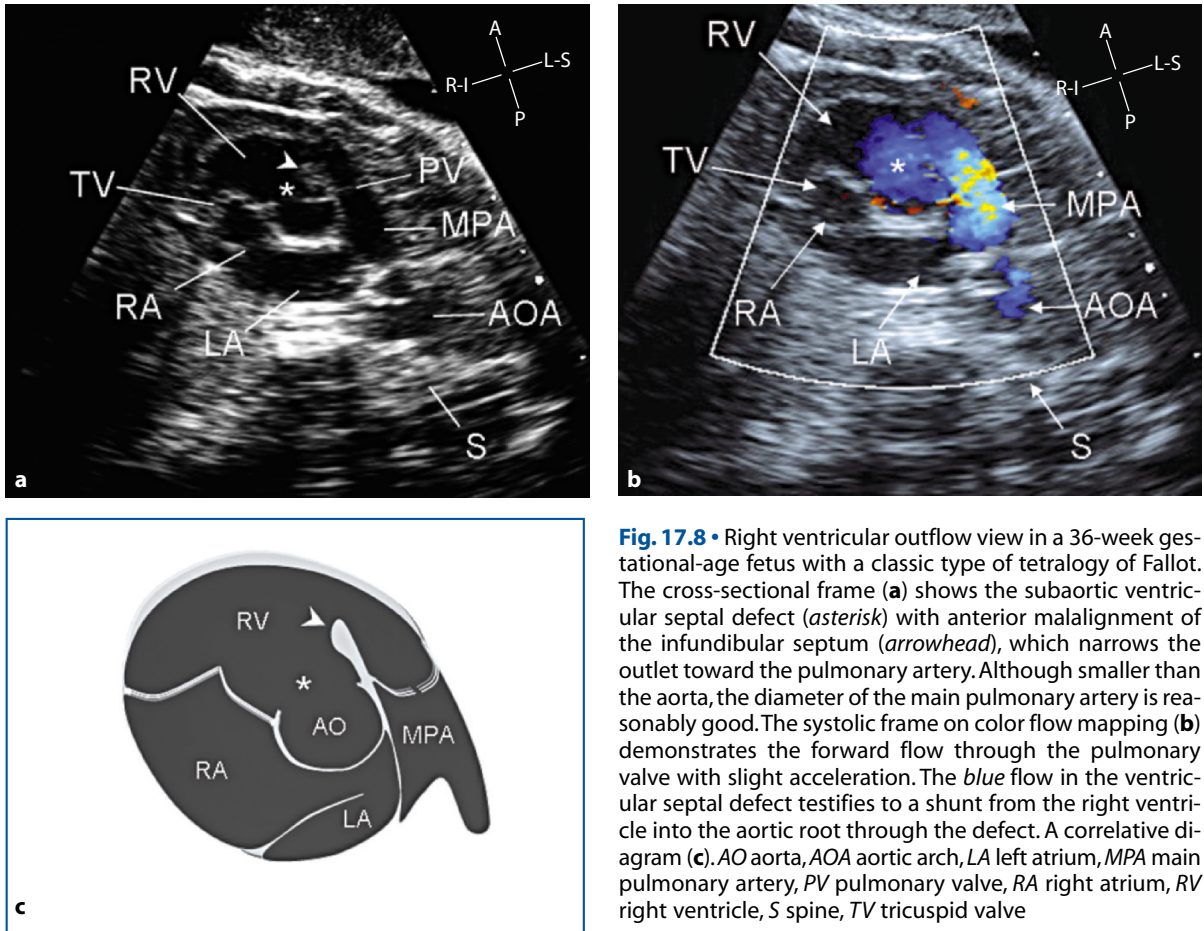
Fig. 17.8 • Right ventricular outflow view in a 36-week gestational-age fetus with a classic type of tetralogy of Fallot. The cross-sectional frame (**a**) shows the subaortic ventricular septal defect (*asterisk*) with anterior malalignment of the infundibular septum (*arrowhead*), which narrows the outlet toward the pulmonary artery. Although smaller than the aorta, the diameter of the main pulmonary artery is reasonably good. The systolic frame on color flow mapping (**b**) demonstrates the forward flow through the pulmonary valve with slight acceleration. The *blue* flow in the ventricular septal defect testifies to a shunt from the right ventricle into the aortic root through the defect. A correlative diagram (**c**). *AO* aorta, *AOA* aortic arch, *LA* left atrium, *MPA* main pulmonary artery, *PV* pulmonary valve, *RA* right atrium, *RV* right ventricle, *S* spine, *TV* tricuspid valve
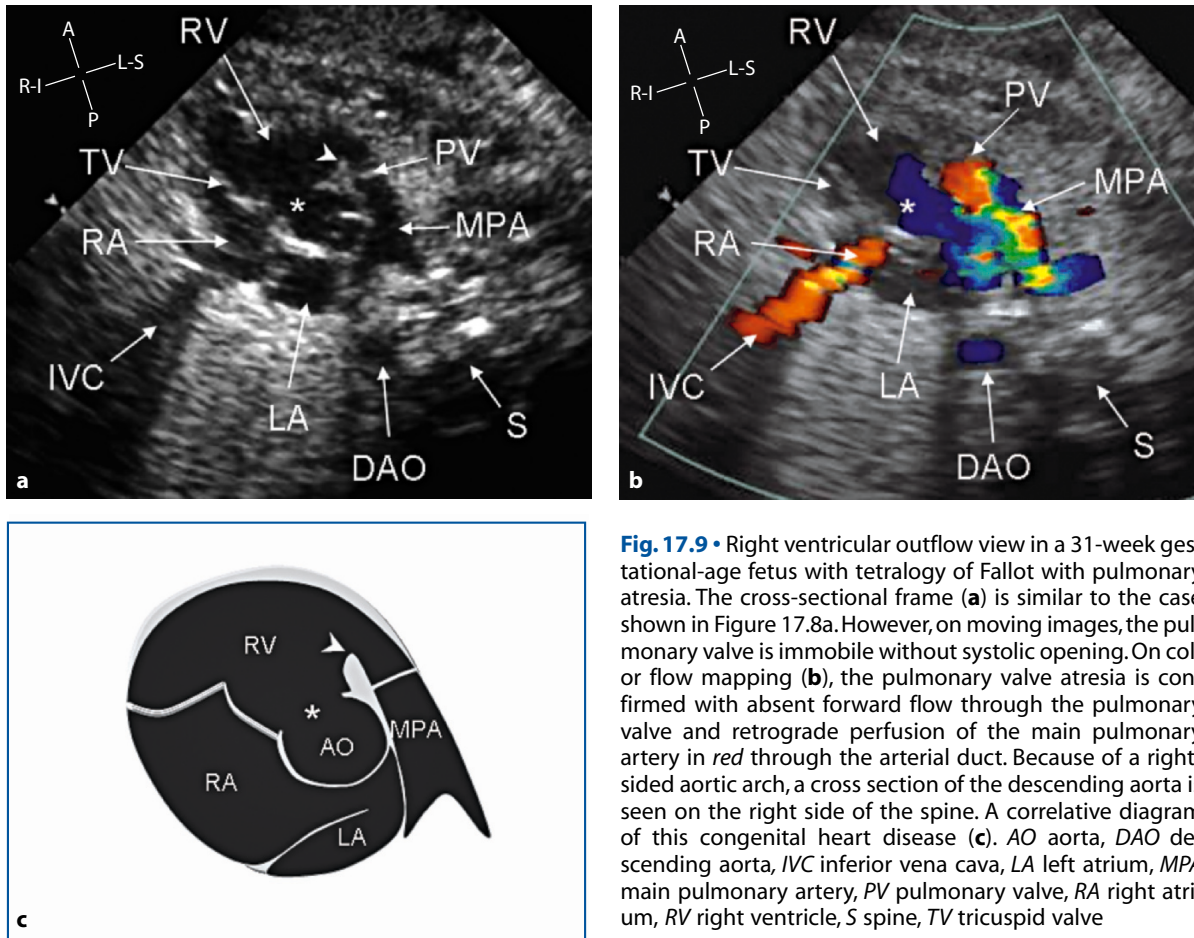
Fig. 17.9 • Right ventricular outflow view in a 31-week gestational-age fetus with tetralogy of Fallot with pulmonary atresia. The cross-sectional frame (**a**) is similar to the case shown in Figure 17.8a. However, on moving images, the pulmonary valve is immobile without systolic opening. On color flow mapping (**b**), the pulmonary valve atresia is confirmed with absent forward flow through the pulmonary valve and retrograde perfusion of the main pulmonary artery in *red* through the arterial duct. Because of a right-sided aortic arch, a cross section of the descending aorta is seen on the right side of the spine. A correlative diagram of this congenital heart disease (**c**). *AO* aorta, *DAO* descending aorta, *IVC* inferior vena cava, *LA* left atrium, *MPA* main pulmonary artery, *PV* pulmonary valve, *RA* right atrium, *RV* right ventricle, *S* spine, *TV* tricuspid valve

Fig. 17.10 • Right ventricular outflow view in a 33-week gestational-age fetus with pulmonary atresia and intact ventricular septum. The cross-sectional image (**a**) shows a right ventricle with a reduced cavity and hypertrophic walls. The membranous septum is intact. Although small, the cavity of the infundibulum is represented beneath the plane of an imperforate pulmonary valve. The size of the main pulmonary artery is reasonably good. On color flow mapping (**b**), the pulmonary artery is retrogradely perfused through the arterial duct in *red*. A correlative diagram (**c**). *AD* arterial duct, *AOA* aortic arch, *LA* left atrium, *MPA* main pulmonary artery, *PV* pulmonary valve, *RA* right atrium, *RV* right ventricle, *S* spine, *TV* tricuspid valve
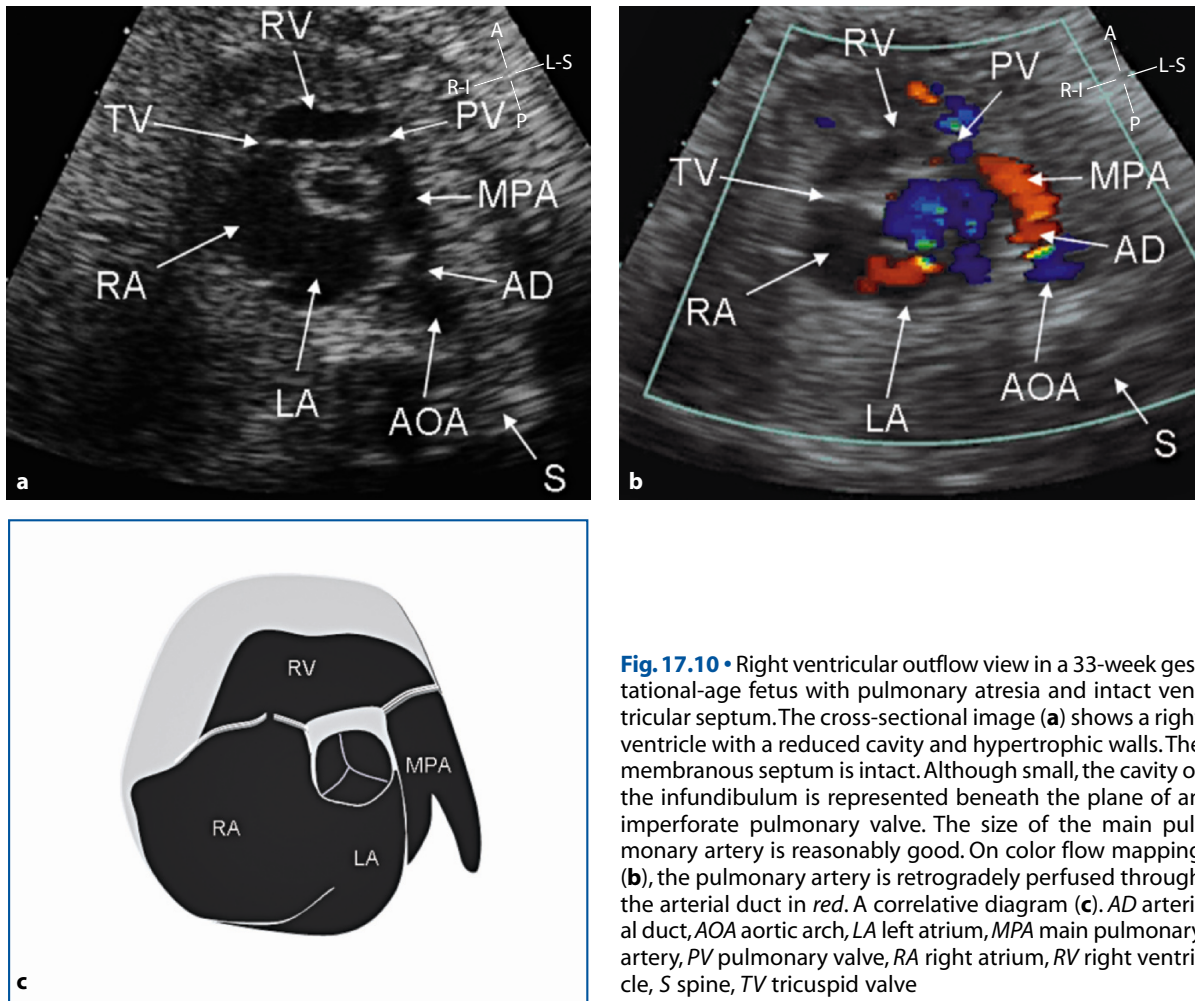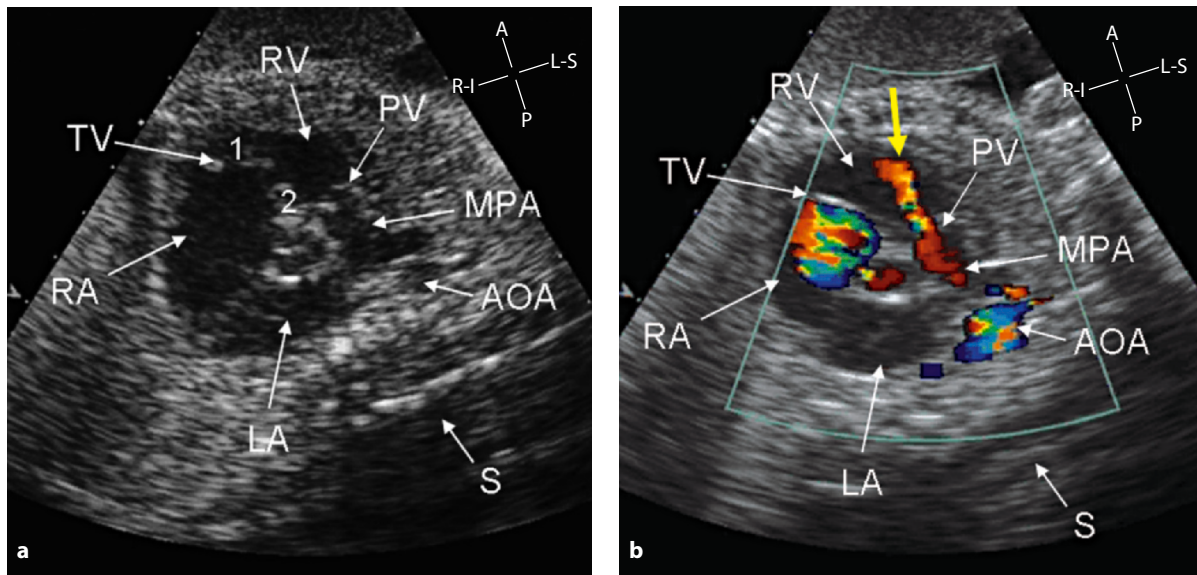
Fig. 17.11 • Right ventricular outflow view in a 33-week gestational-age fetus with Ebstein's malformation. The cross-sectional image (**a**) shows significant dilatation of the right atrium. On moving images, the tricuspid valve leaflets appear elongated and dysplastic. The anterolateral leaflet (*1*) is inserted normally, whereas the septal leaflet (*2*) is displaced, reaching the plane of the pulmonary valve. The pulmonary artery shows a reasonably good size despite the fact the pulmonary valve cusps do not show a clear systolic opening. On color flow mapping (**b**) the main pulmonary artery is perfused retrogradely in *red* through the arterial duct. A regurgitating jet (*yellow arrow*) indicates the functional nature of the pulmonary valve atresia. The turbulent flow (*yellow-blue*) in the right atrium is produced by a severe tricuspid regurgitation, better assessed in the four-chamber view. *AOA* aortic arch, *LA* left atrium, *MPA* main pulmonary artery, *PV* pulmonary valve, *RA* right atrium, *RV* right ventricle, *S* spine, *TV* tricuspid valve

The Left Ventricle Short-Axis View

The Section Plane

This view is obtained with the scan plane perpendicular to the long axis of the left ventricle. Because of the horizontal position of the fetal heart, these views lie on planes close to the sagittal plane of the fetal body. In normal hearts, this is obtained by cutting the fetal body on a parasagittal plane slightly rotated to the left shoulder. Two sections, which are easy to recognize, are: (1) at the level of the atrioventricular valves, and (2) at the level of the papillary muscles of the left ventricle. These sections can be sequentially obtained by translating the scan plane from the midline toward the left side of the fetal body (Fig. 18.1).

The Normal Morphology

In the normal fetus, the short-axis view of the left ventricle shows the heart lying on the diaphragm, with the left lobe of the liver and the stomach underneath and the left lung posteriorly. When the heart sits in its normal position, the spine is not seen posteriorly, but a section of the left thoracic cage is visible (Fig. 18.2).

The Level of the Mitral and Tricuspid Valves

When the scan plane is close to the atrioventricular junction, the different morphologic features of the two ventricles are shown: anteriorly, the right
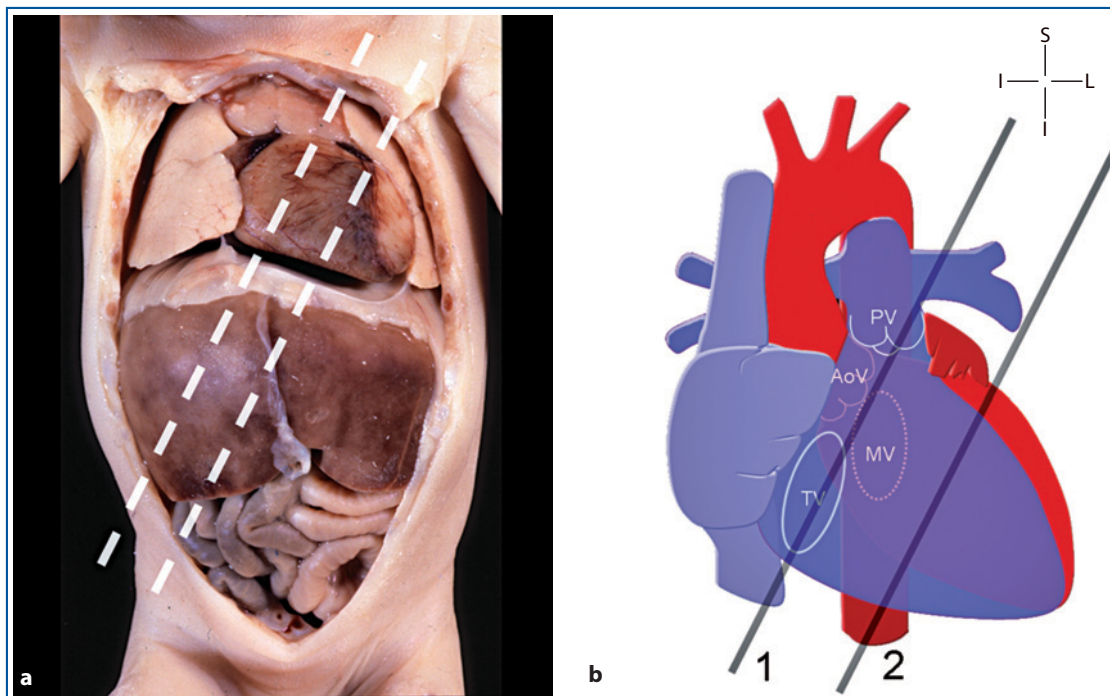
Fig. 18.1 • Planes of the short-axis views of the left ventricle are illustrated on the fetal body (**a**) and on a heart diagram (**b**). *Line 1* indicates the section at the level of the atrioventricular valves, and *line 2* is at the level of the papillary muscles of the left ventricle. *AOV* aortic valve, *MV* mitral valve, *PV* pulmonary valve, *TV* tricuspid valve
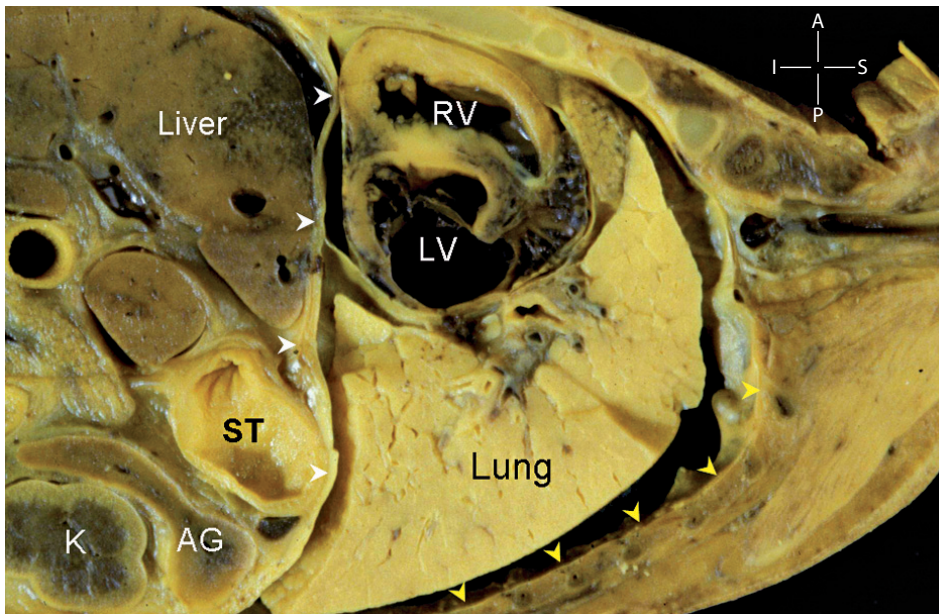
Fig. 18.2 • This specimen is sectioned along a parasagittal plane on the left side of the fetal body. Although the section is not exactly in the short-axis plane of the left ventricle, the image shows the position of the heart on the diaphragm (*white arrowheads*), with the stomach and the left lobe of the liver underneath. Behind the heart, a sagittal section of the left lung is seen bordered posteriorly by the thoracic cage (*yellow arrowheads*). *AG* adrenal gland, *K* kidney, *LV* left ventricle, *RV* right ventricle, *St* stomach

ventricle with semilunar shape and posteriorly, the left ventricle with a more circular section. The two atrioventricular valves reveal their different characteristics: the tricuspid valve with three leaflets and septal insertions, and the mitral valve with two leaflets and without insertion on the ventricular septum. The inlet portion of the interventricular septum is seen between the two atrioventricular valves, with a flattened appearance due to equal ventricular pressure. It is quite common that the short-axis views of the left ventricle at this level also shows the junction of the infundibulum with the main pulmonary artery and its homonym valve (Figs. 18.3, 18.4).

Although this view is less intuitive than the four-chamber view to inexperienced examiners, it is very useful for assessing the type of atrioventricular connection and disproportions between the ventricles and their respective atrioventricular valves.

The Level of the Papillary Muscles

In short-axis sections of the heart more toward the apex, the different shape of the ventricles is still ap-preciated, but the infundibulum is no longer visible (Fig. 18.5). The subvalvular apparatus of the mitral valve shows two papillary muscles in the left ventricle and a transverse section of the moderator band in the right ventricle. When the atrioventricular valves are inserted normally at their atrioventricular junction, the tricuspid and mitral valve leaflets are not imaged at this level. Between the right and the left ventricle, the midportion of the interventricular septum is seen. Therefore, the whole trabecular and perimembranous portion of the interventricular septum is investigated with this family of views by moving the scanning plane from the base to the apex of the heart. Because the septum is imaged at right angle to the ultrasound beam, these sections are particularly reliable in distinguishing true defects of the septum from false dropouts. Moreover, ventricular septal defects can also be assessed on color flow mapping, because the flow through the septal defect is mostly parallel to the ultrasound beam.

Figures 18.6-18.12 are examples of short-axis views of the left ventricle in some congenital heart diseases.
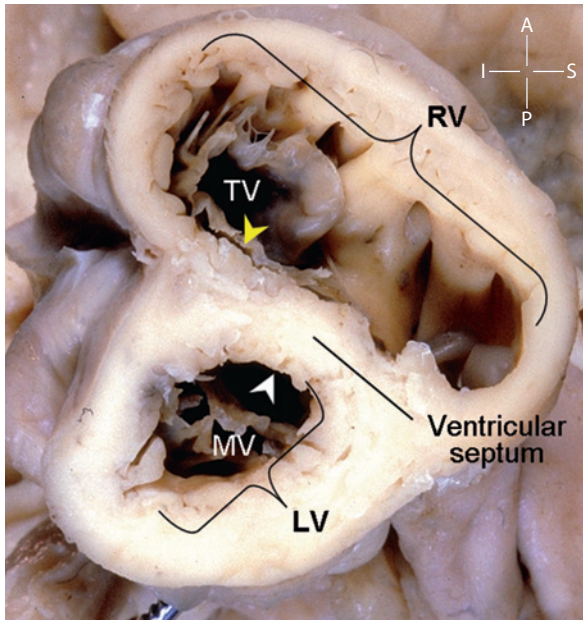
Fig. 18.3 • In this specimen, the heart is sectioned to imitate the short-axis view of the left ventricle at the level of the mitral and tricuspid valve leaflets. The different morphologic features of the ventricles are shown: crescent-like for the right ventricle, and more circular for the left ventricle. The close relationship of the tricuspid valve septal leaflet (*yellow arrowhead*) with the right side of the interventricular septum is demonstrated, whereas the left side is free from the mitral valve apparatus (*white arrowhead*). *LV* left ventricle, *MV* mitral valve, *RV* right ventricle, *TV* tricuspid valve
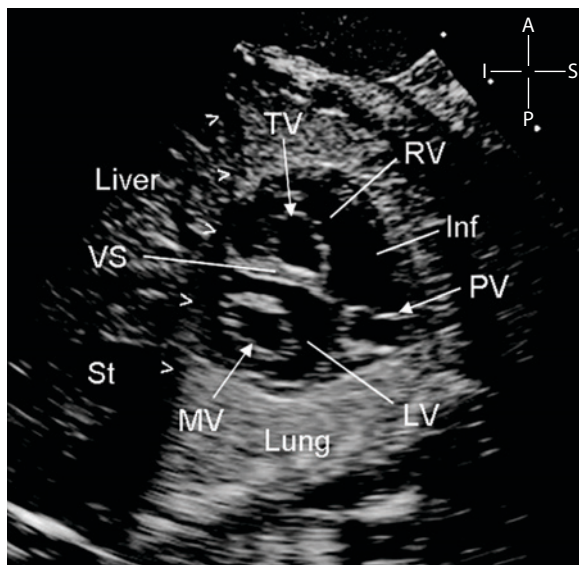
Fig. 18.4 • Echocardiograph of a normal short-axis view of the heart at the level of the mitral and tricuspid valves. The heart is lying on the diaphragm (*open arrowheads*), with the stomach and left lobe of the liver underneath. Posteriorly, a sagittal section of the left lung is imaged. The different relationship of the mitral and tricuspid valves with the ventricular septum is demonstrated. The anterior ventricle gives rise to the infundibulum and the pulmonary artery, with the pulmonary valve in between. *Inf* infundibulum, *LV* left ventricle, *MV* mitral valve, *PV* pulmonary valve, *RV* right ventricle, *St* stomach, *TV* tricuspid valve, *VS* ventricular septum
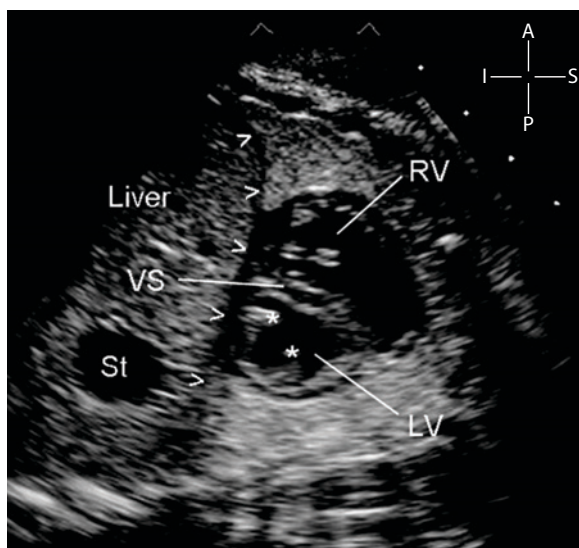
Fig. 18.5 • Short-axis view of the left ventricle at the level of the papillary muscles (*asterisks*). The *open arrowheads* indicate the diaphragm. The infundibulum is no longer seen at this level. *LV* left ventricle, *RV* right ventricle, *St* stomach, *VS* ventricular septum
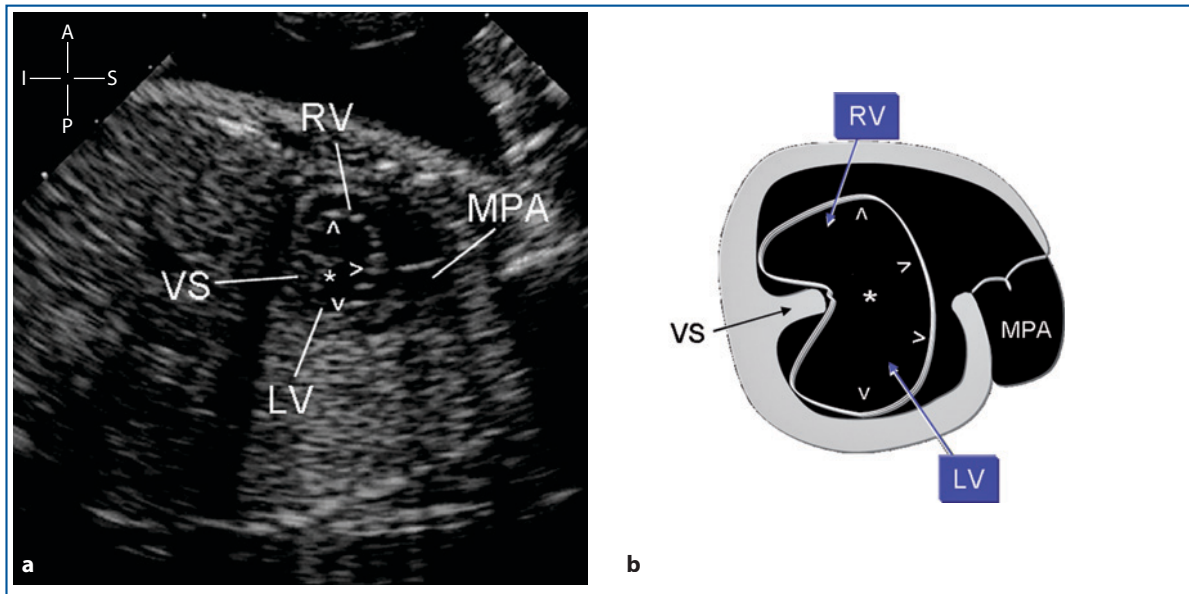
Fig. 18.6 • Short-axis view of the left ventricle at the level of the atrioventricular junction in a 24-week gestational-age fetus with atrioventricular septal defect with atrial and ventricular component (**a**). A correlative diagram (**b**). This section shows an *en face* view of the common atrioventricular valve (*open arrowheads*) opening across a defect in the inferior part of the ventricular septum (*asterisk*). On moving images, the anterior bridging leaflet of the common valve is attached to the septum, as in Rastelli classification type A. *LV* left ventricle, *MPA* main pulmonary artery, *RV* right ventricle, *VS* ventricular septum
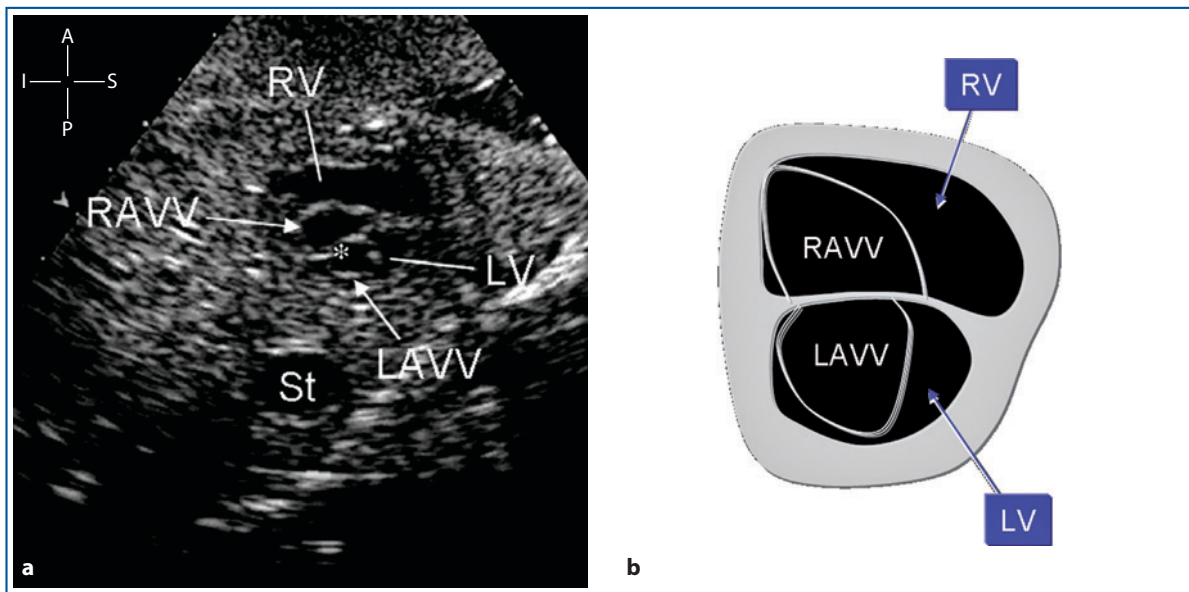
Fig. 18.7 • Short-axis view of the heart in a 28-week gestational-age fetus with atrioventricular septal defect and atrial component only. This cross-sectional view (**a**), at the level of the atrioventricular junction, shows two separate atrioventricular-valve orifices. However, both the right and left components of the atrioventricular valve show insertion toward what seems to be the ventricular septum. This, in reality, is a thin tongue of valvular tissue (*asterisk*) dividing the two atrioventricular valve components. This is a case with normal karyotype and familial recurrence, the father being affected by an identical congenital heart disease. However, this type of congenital heart defect may also be associated with chromosome anomalies. *LV* left ventricle, *LAVV* left atrioventricular valve, *RAVV* right atrioventricular valve, *RV* right ventricle, *St* stomach

Fig. 18.8 • Short axis-views of the left ventricle in a 33-week gestational-age fetus with Ebstein's malformation of the tricuspid valve. On cross-sectional examination (**a**), the left ventricle is imaged at the level of the papillary muscles. Nevertheless, the anterolateral leaflet of the tricuspid valve (*open arrowheads*) is still visible inside the cavity of the right ventricle. This indicates the apical displacement of the tricuspid valve leaflets, which also appear tethered to the corresponding wall of the right ventricle. Ascites is seen below the diaphragm. On color flow mapping (**b**), the *yellow arrow* indicates the origin of a significant regurgitant jet of tricuspid valve, which is the cause of fetal hydrops. *LV* left ventricle, *RV* right ventricle, *VS* ventricular septum

Fig. 18.9 • Short-axis view at the level of the atrioventricular valves in a 34-week gestational-age fetus with congenitally corrected transposition. This view demonstrates the inverted position of the ventricles and their respective atrioventricular valves. The posterior ventricle is morphologically right, with a crescent-like morphology and the atrioventricular valve attached to the interventricular septum. The anterior ventricle is morphologically left, with a more circular shape and the atrioventricular valve unattached to the septum. *mLV* morphologically left ventricle, *mRV* morphologically right ventricle, *MV* mitral valve, *St* stomach, *TV* tricuspid valve, *VS* ventricular septum
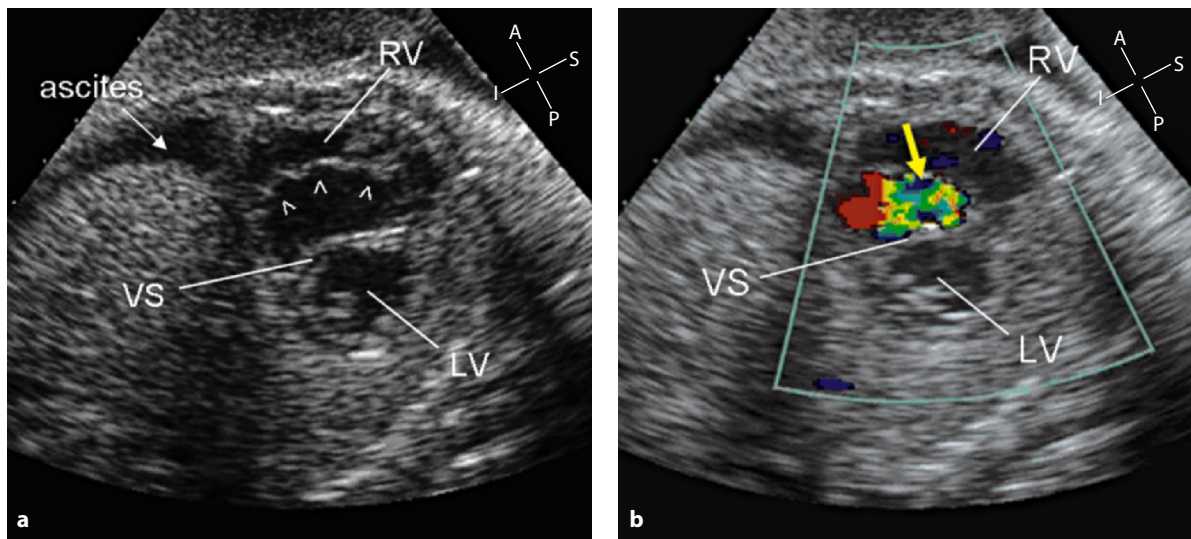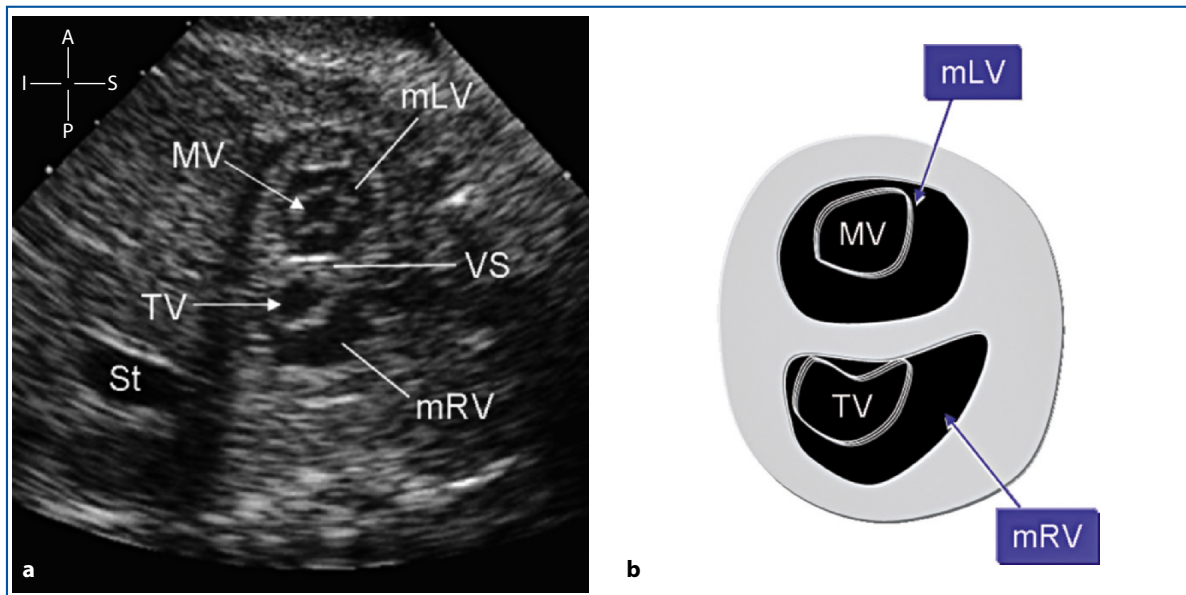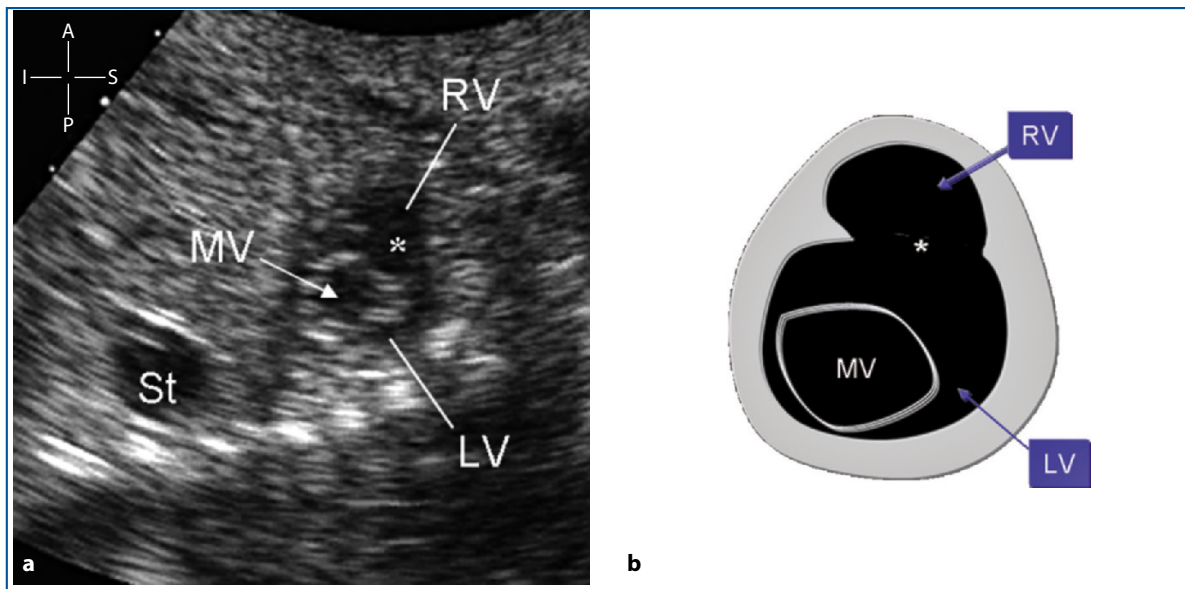
Fig. 18.10 • Short-axis section at the level of the atrioventricular junction in a 25-week gestational-age fetus with tricuspid atresia (**a**) and a correlative diagram (**b**). This section shows a single, bileaflet, atrioventricular valve indicative of a mitral valve, opening into a large, posterior left ventricle. The rudimentary right ventricle, in anterosuperior position, lacks its atrioventricular valve. The large ventricle and the rudimentary ventricle communicate through a wide ventricular septal defect (*asterisk*). The outflow toward the arterial vessel (not seen in this image), committed to the rudimentary ventricle, is unobstructed. *LV* left ventricle, *MV* mitral valve, *RV* right ventricle, *St* stomach
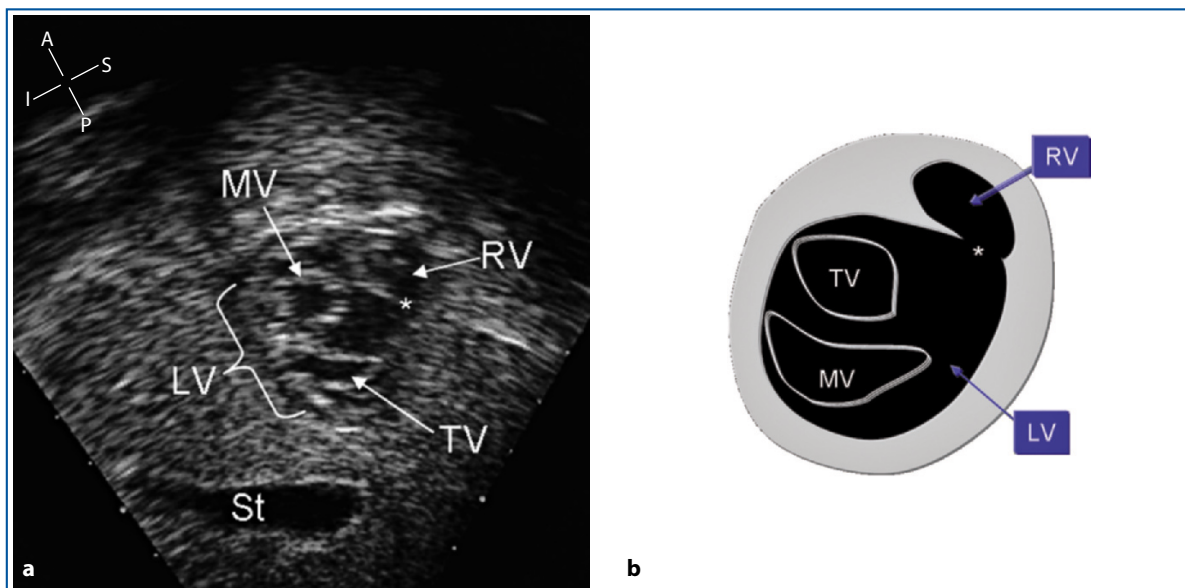
Fig. 18.11 • Short-axis section at the level of the atrioventricular junction in a 36-week gestational-age fetus with double-inlet left ventricle (**a**) and a correlative diagram (**b**). This cut shows the univentricular atrioventricular connection in this case, with the two atrioventricular valves opening into the large cavity of the left ventricle (*bracket*). The left ventricle communicates with a rudimentary right ventricle, in anterosuperior position, through a restrictive ventricular septal defect (*asterisk*). The outflow toward the arterial vessel connected with the rudimental ventricle is severely impaired**.** Correlative diagram (**b**). *LV* left ventricle, *MV* mitral valve, *RV* right ventricle, *St* stomach, *TV* tricuspid valve
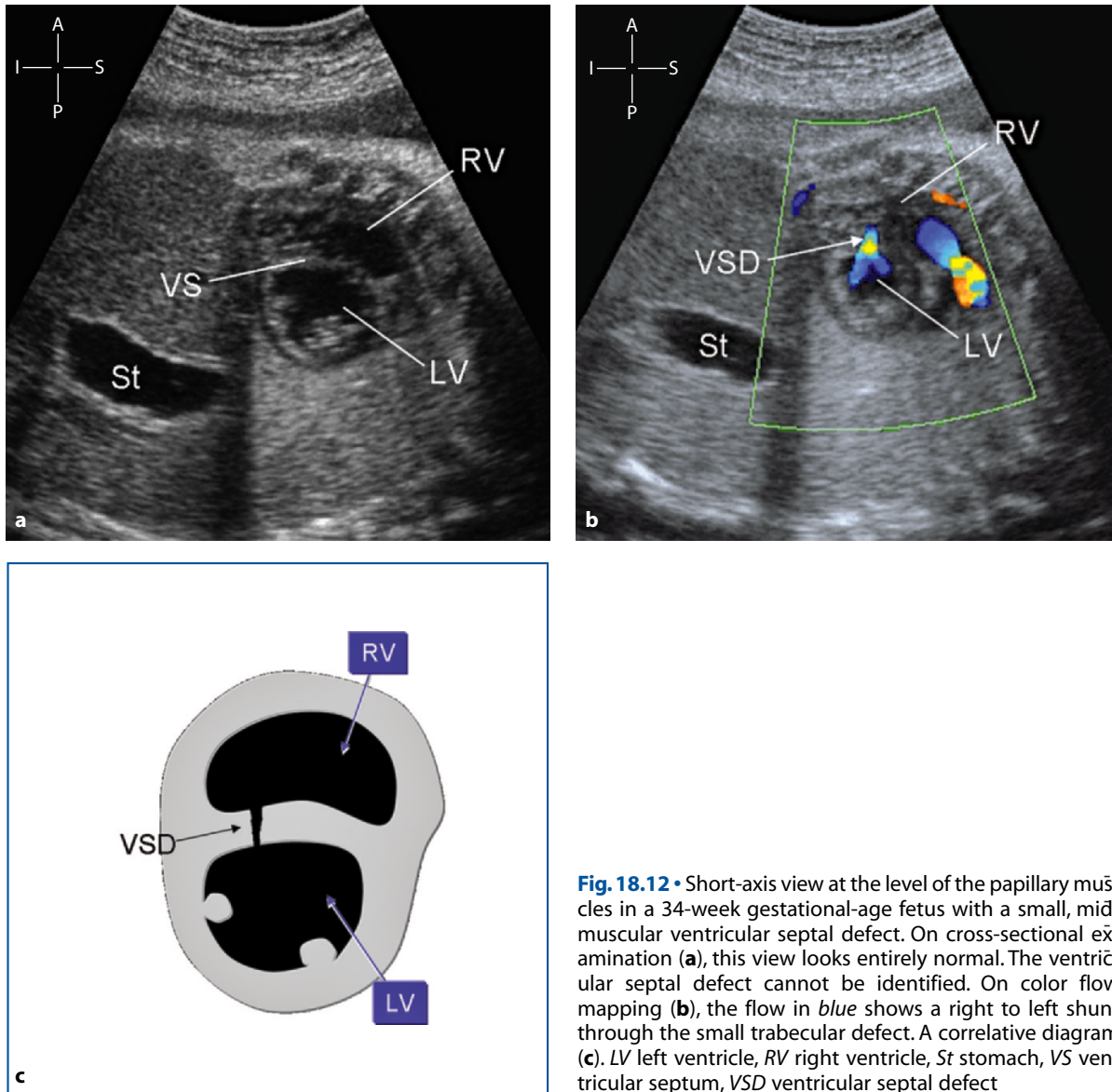
Fig. 18.12 • Short-axis view at the level of the papillary muscles in a 34-week gestational-age fetus with a small, mid-muscular ventricular septal defect. On cross-sectional examination (**a**), this view looks entirely normal. The ventricular septal defect cannot be identified. On color flow mapping (**b**), the flow in *blue* shows a right to left shunt through the small trabecular defect. A correlative diagram (**c**). *LV* left ventricle, *RV* right ventricle, *St* stomach, *VS* ventricular septum, *VSD* ventricular septal defect

The Left Ventricle Long-Axis View

The Section Plane

This projection lies on an intermediate plane, between the transverse and sagittal plane of the fetal body, in a plane that runs from the left hypochondrium to the right shoulder. The standard long-axis view passes through the long axis of the left ventricle, hence its name. It is obtained by rotating the transducer 90° from the apical four-chamber view and tilting it toward the right shoulder (Fig. 19.1). In the fetus, where the proximal ribs and part of the sternum are not ossified, this view can be obtained even from the anterior part of the chest.

The Normal Morphology

The parasagittal orientation of this plane is better appreciated in sections of the whole fetal body, where abdominal and thoracic structures are displayed (Fig. 19.2). In the left inferior part of these cuts, the left lobe of the liver and the stomach are usually seen below the diaphragm. Posteriorly, an oblique section of the left lung is seen above the diaphragm, with the descending aorta and esophagus in the posterior part of mediastinum. As to the heart, a whole section of the left atrium and left ventricle in its full length is usually shown; therefore,
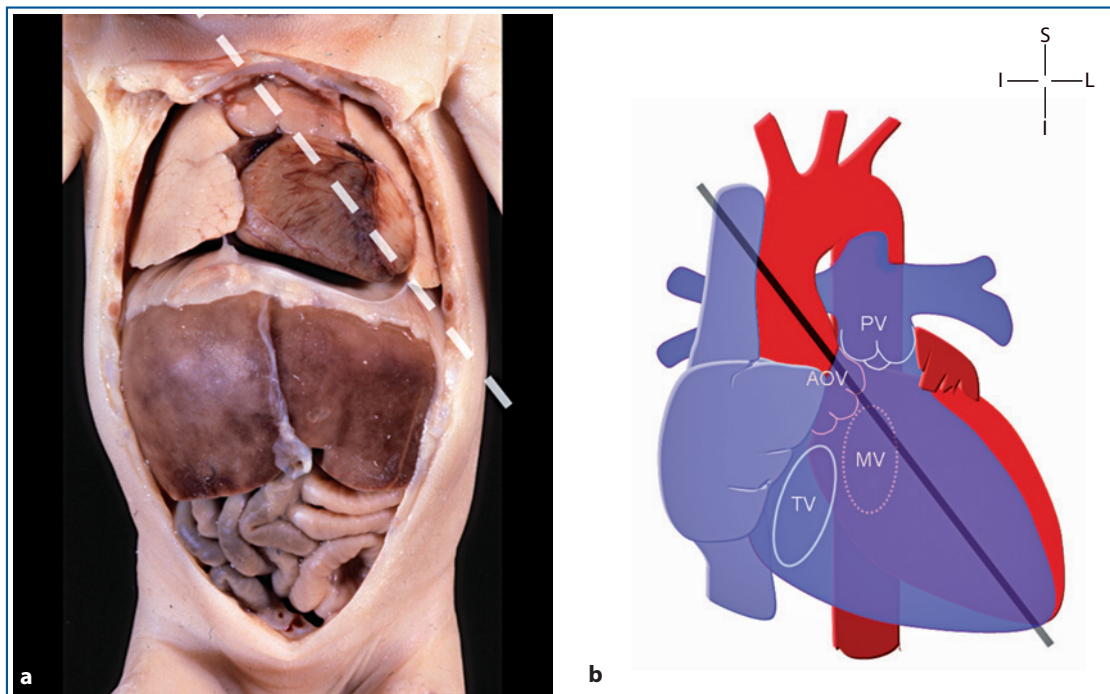
Fig. 19.1 • Section plane of the long-axis view of the left ventricle is shown on the fetal body (**a**) and a heart diagram (**b**). The image of the fetal body shows how the section plane is oriented from the left hypochondrium to the right upper part of the chest. *AOV* aortic valve, *MV* mitral valve, *PV* pulmonary valve, *TV* tricuspid valve
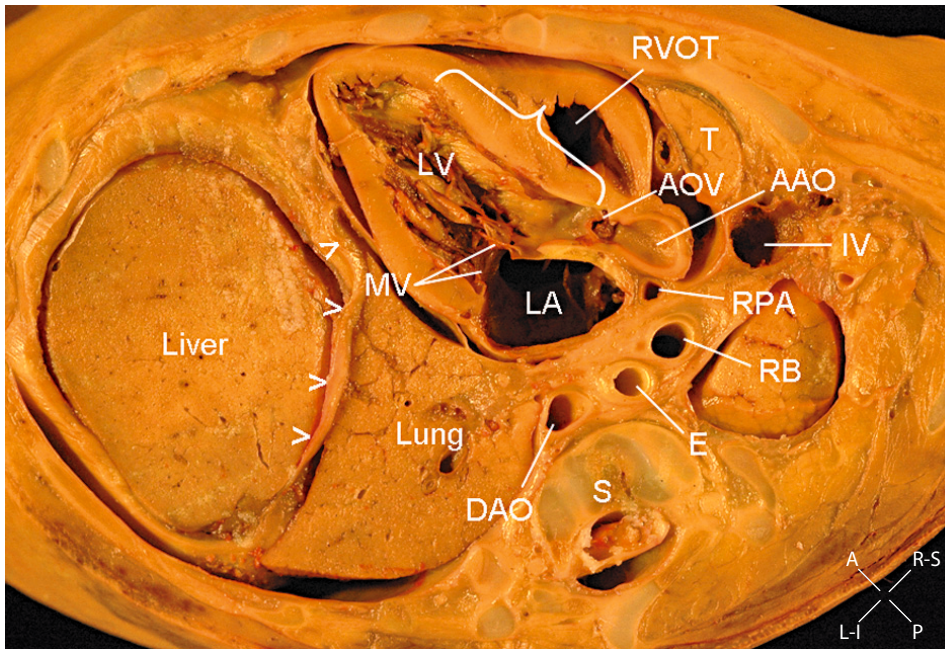
Fig. 19.2 • Fetal body sectioned to imitate the long-axis view of the left ventricle. The parasagittal orientation of this section is appreciated in this image, where abdominal and thoracic structures are displayed at the same time. In the bottom left, the left lobe of the liver is seen below the diaphragm (*open arrowheads*) and the inferior lobe of the left lung above. In the upper right, the aortic root and innominate vein, structures of the right profile of the heart, are displayed. The left atrium and ventricle are seen in their full length. The continuity between the interventricular septum (*white bracket*) and the anterior wall of the aortic root and between the anterior leaflet of the mitral valve and posterior wall of the aorta is appreciated. In the posterior part of the mediastinum, from left to right, respectively, an oblique section of the descending aorta, the esophagus, and the right bronchus is seen. *AAO* ascending aorta, *AOV* aortic valve, *DAO* descending aorta, *E* esophagus, *IV* innominate vein, *LA* left atrium, *LV* left ventricle, *MV* mitral valve, *RB* right bronchus, *RPA* right pulmonary artery, *RVOT* right ventricular outflow tract, *S* spine, *T* thymus

this projection is also called the two-chamber view. The perimembranous and anterior parts of the interventricular septum are displayed together with the origin of the arterial vessel from the left ventricle. In the normal heart, the ascending aorta sweeps anteriorly and rightward from the left ventricle. Continuity of the anterior wall of the aorta with the interventricular septum and the posterior wall with the anterior leaflet of the mitral valve are appreciated. Anteriorly to the ventricular septum, the right ventricular outflow tract is seen, lying almost perpendicular to the left outflow tract. This view allows appreciation of the narrow angle between the inflow and outflow of the left ventricle, separated only by the anterior leaflet of the mitral valve (Fig. 19.3).
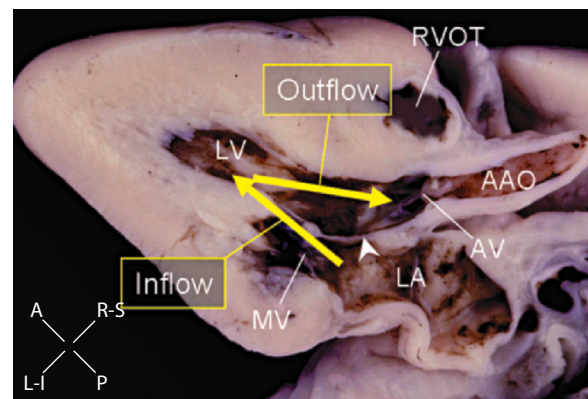
Fig. 19.3 • This specimen of an isolated heart is sectioned to imitate the long-axis view of the left ventricle. The *yellow arrows* show orientation of inflow and outflow of the left ventricle, separated only by the anterior leaflet of the mitral valve (*white arrowhead*) and with a narrow angle between the two. The right superior sweep of the ascending aorta is appreciated. *AAO* ascending aorta, *AV* aortic valve, *LA* left atrium, *LV* left ventricle, *MV* mitral valve, *RVOT* right ventricular outflow tract

Fig. 19.4 • Long-axis view of the left ventricle in a normal 22-week gestational-age fetus. In the left-inferior part of this section, the stomach is seen below the diaphragm. The left atrium and left ventricle are imaged in the central part, with the mitral valve in between. The aortic root is seen sweeping superiorly and to the right beneath the innominate vein, which is seen in cross section. Anteriorly, an oblique section of the right ventricular outflow tract is seen behind the anterior thoracic wall. Posteriorly, the descending aorta is displayed between the left atrium and the spine. In the central part of the image, the *arrowhead* indicates the membranous portion of the interventricular septum where subarterial defects are located. The mitroaortic and septal-aortic continuity is clearly demonstrated. *AAO* ascending aorta, *AOV* aortic valve, *DAO* descending aorta, *IV* innominate vein, *LA* left atrium, *LV* left ventricle, *MV* mitral valve, *RB* right bronchus, *RPA* right pulmonary artery, *RVOT* right ventricular outflow tract, *St* stomach
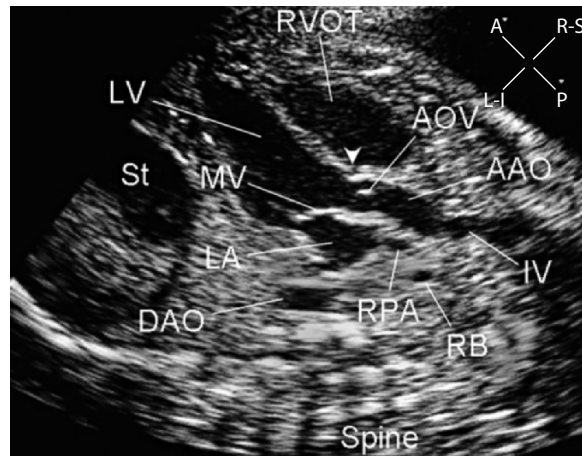
The Normal Echocardiogram – 2D

Most structures described in the morphological section can be evaluated by ultrasound (Fig. 19.3). The long-axis view of the left ventricle is particularly useful in assessing the inlet and outlet portion of the left ventricle. Moreover, defects in the anterior trabecular and subarterial portions of the interventricular septum can be investigated. When obtained with transverse orientation (Fig. 19.4), this view is the most reliable echocardiographic projection to assess the degree of arterial overriding in subarterial defects, because this part of the septum and the arterial root are seen nearly at a right angle to the ultrasound beam.
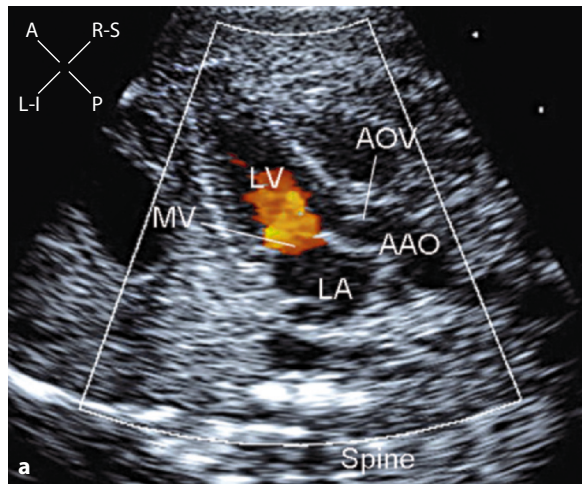
The Normal Echocardiogram – Color Flow Mapping and Pulsed Doppler

When obtained with the cardiac apex toward the echocardiographic fan, this section is ideal for color flow mapping and pulsed Doppler assessment of the inflow and outflow of the left ventricle with favorable Doppler interrogation angle (Fig. 19.5). Pulsed Doppler tracing on this view is very similar to that described in the section on the five-chamber view.

Figures 19.6-19.14 are examples of congenital heart disease shown in the long-axis view of the left ventricle.

The long-axis view of the left ventricle with transverse orientation is particularly suitable for fetal cardiac rhythm assessment with the M-mode and color M-mode techniques. The cursor line must be aligned in such a way as to intercept the atrial wall, to asses atrial contraction, and through the aortic root where the opening of the aortic valve testifies to ventricular contraction. Figure 19.15 shows one example of normal color M-mode tracing obtained from this projection.
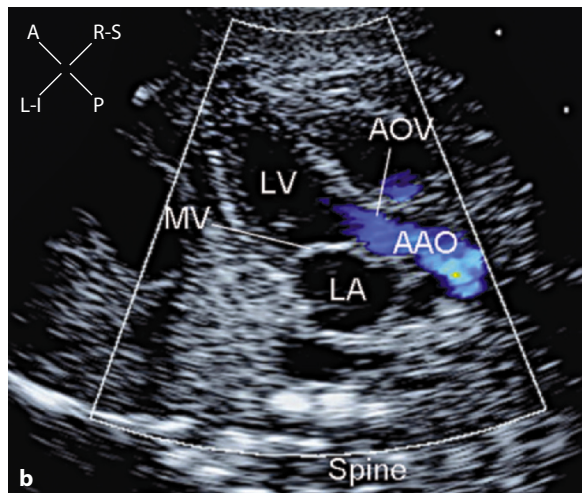
Fig. 19.5 • Long-axis view of the left ventricle in a 23-week gestational-age fetus with apical presentation. The diastolic frame (**a**) shows the inflow of the left ventricle through the mitral valve (*red*). The aortic valve is closed. In the systolic frame (**b**), the outflow from the left ventricle is shown filling the aortic root through the homonym valve (*blue*). The mitral valve is closed. *AAO* ascending aorta, *AOV* aortic valve, *LA* left atrium, *LV* left ventricle, *MV* mitral valve
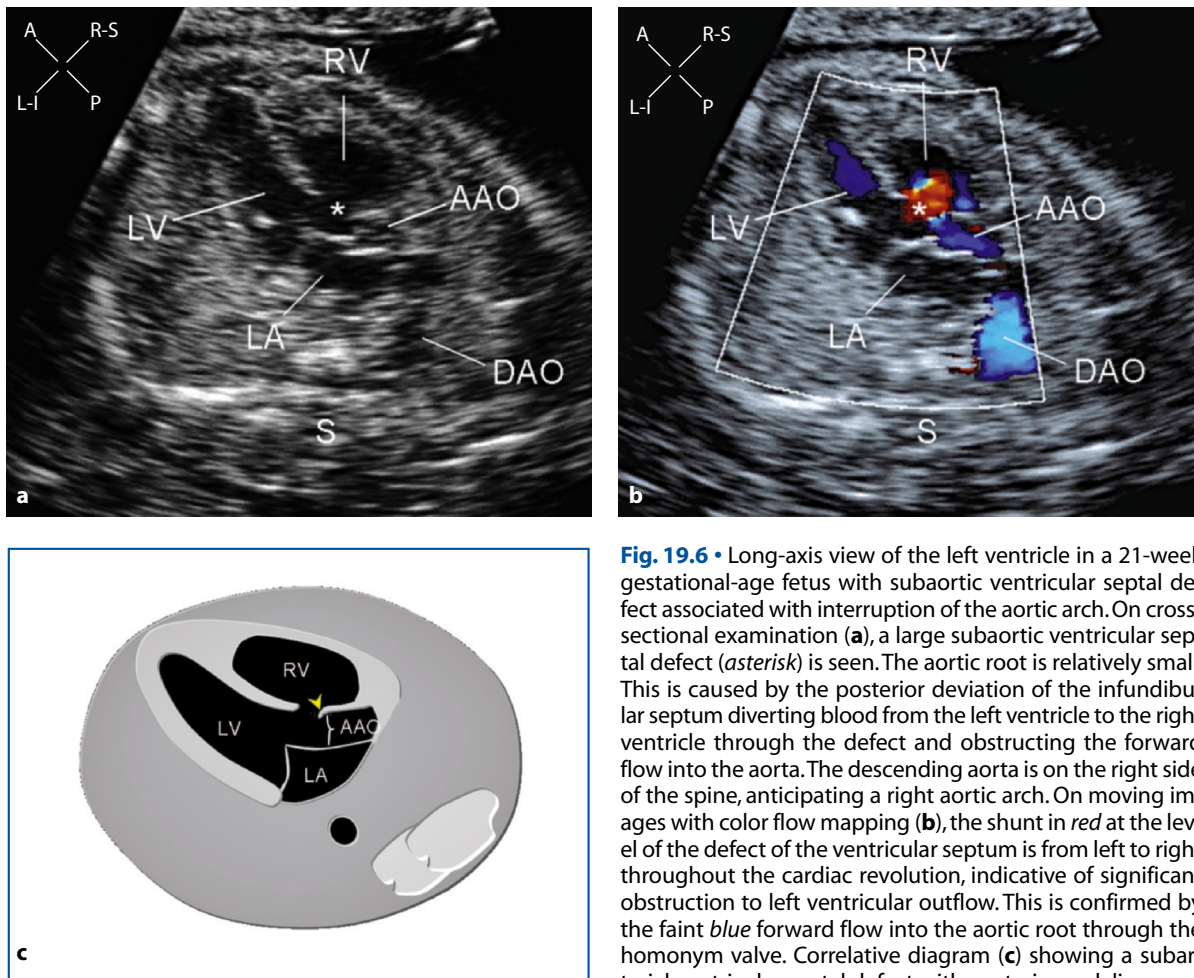
Fig. 19.6 • Long-axis view of the left ventricle in a 21-week gestational-age fetus with subaortic ventricular septal defect associated with interruption of the aortic arch. On cross-sectional examination (**a**), a large subaortic ventricular septal defect (*asterisk*) is seen. The aortic root is relatively small. This is caused by the posterior deviation of the infundibular septum diverting blood from the left ventricle to the right ventricle through the defect and obstructing the forward flow into the aorta. The descending aorta is on the right side of the spine, anticipating a right aortic arch. On moving images with color flow mapping (**b**), the shunt in *red* at the level of the defect of the ventricular septum is from left to right throughout the cardiac revolution, indicative of significant obstruction to left ventricular outflow. This is confirmed by the faint *blue* forward flow into the aortic root through the homonym valve. Correlative diagram (**c**) showing a subarterial ventricular septal defect with posterior malalignment of the infundibular septum (*yellow arrowhead*). *AAO* ascending aorta, *DAO* descending aorta, *LA* left atrium, *LV* left ventricle, *RV* right ventricle, *S* spine

Fig. 19.7 • Long-axis view of the left ventricle in a 36-week gestational-age fetus with tetralogy of Fallot of classic type. Cross-sectional examination (**a**) displays a subaortic ventricular septal defect (*asterisk*) with aortic overriding. The ascending aorta is oversized. On color flow mapping (**b**), the right ventricle is seen ejecting blood (*blue*) into the aorta through the ventricular septal defect. Correlative diagram (**c**) showing a subarterial ventricular septal defect with anterior malalignment of the infundibular septum (*yellow arrowhead*) and aortic overriding. *AAO* ascending aorta, *AOV* aortic valve, *DAO* descending aorta, *LA* left atrium, *LV* left ventricle, *RV* right ventricle, *S* spine

Fig. 19.8 • Long-axis view of the left ventricle in a 31-week gestational-age fetus with tetralogy of Fallot and pulmonary atresia. The cross-sectional view (**a**) shows an enlarged aortic root overriding on a subarterial ventricular septal defect (*asterisk*). The aortic root is enlarged. On color flow mapping (**b**), both the left and right ventricles are seen ejecting (*blue*) into the aorta through the ventricular septal defect. *AAO* ascending aorta, *DAO* descending aorta, *LA* left atrium, *LV* left ventricle, *MV* mitral valve, *RV* right ventricle, *S* spine

Fig. 19.9 • Long-axis view of the left ventricle in a 31-week gestational-age fetus with common arterial trunk type 1. On cross-sectional examination (**a**), a large arterial root overriding a subarterial ventricular septal defect (*asterisk*) is shown. The ascending aorta and pulmonary artery originate from this common trunk. On color flow mapping (**b**), the left and the right ventricle are seen ejecting into the common arterial trunk, which represents the single outlet from both ventricles. The common origin of the ascending aorta and pulmonary artery is demonstrated. Diagram (**c**) in the long-axis view of the left ventricle imitating a common arterial trunk of this type. *AAO* ascending aorta, *AT* arterial trunk, *DAO* descending aorta, *LA* left atrium, *LV* left ventricle, *PA* pulmonary artery, *RV* right ventricle, *S* spine
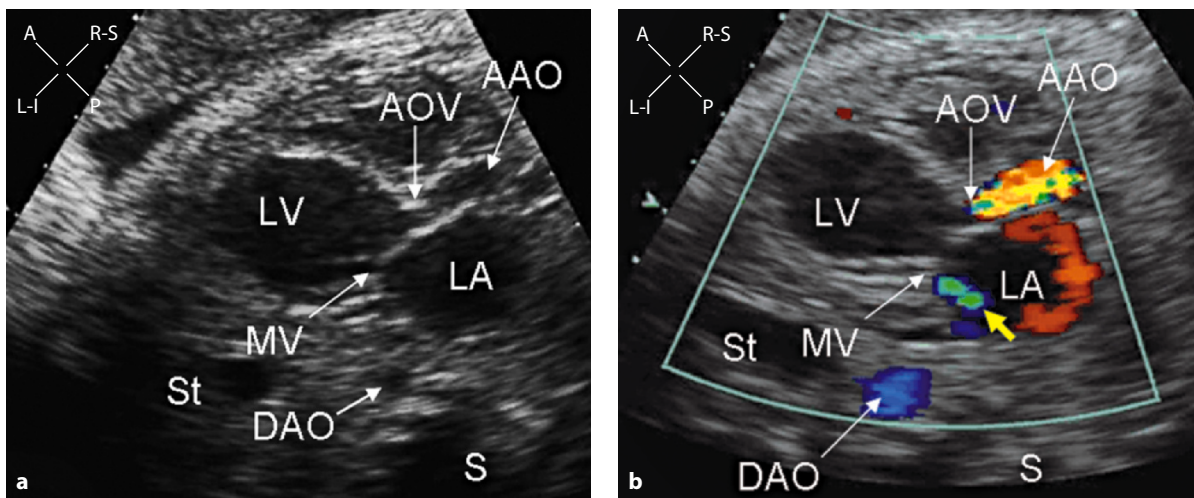
Fig. 19.10 • Long-axis view of the left ventricle in a 34-week gestational-age fetus with critical aortic stenosis. On cross-sectional examination (**a**), there is left atrial and ventricular dilatation. On moving images, the left ventricle shows poor systolic function, with focal areas of endocardial fibroelastosis. The mitral valve appears abnormal, with restricted diastolic opening. The aortic cusps are dysplastic, with barely appreciable systolic motion. The ascending aorta is a reasonably good size. This systolic frame on color flow mapping (**b**) shows an eccentric jet of mitral regurgitation (*yellow arrow*) and turbulent flow across the aortic valve filling the aortic root. *AAO* ascending aorta, *AOV* aortic valve, *DAO* descending aorta, *LA* left atrium, *LV* left ventricle, *MV* mitral valve, *S* spine, *St* stomach
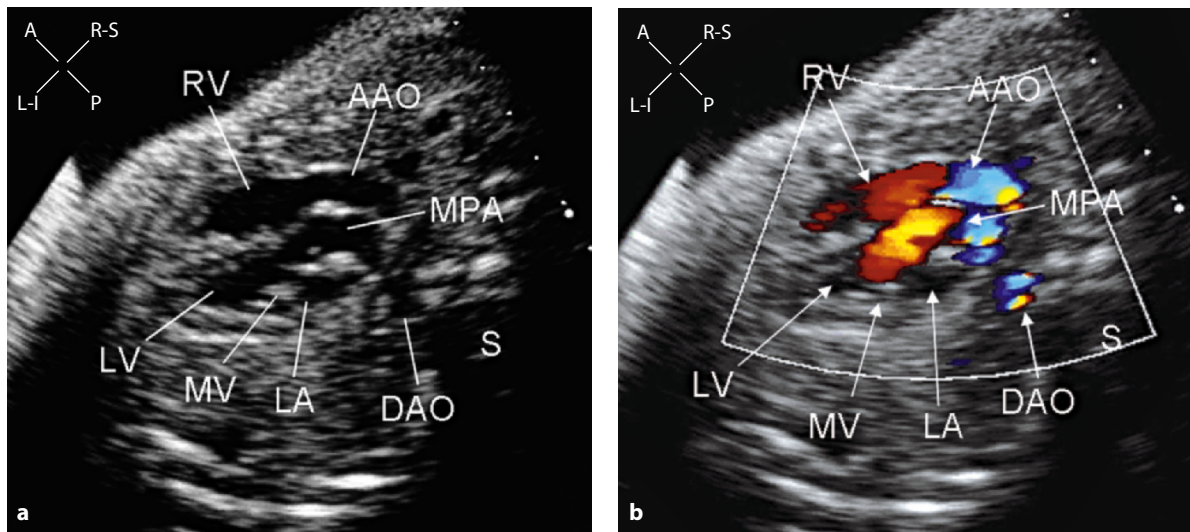
Fig. 19.11 • Long-axis view of the left ventricle in a 32-week gestational-age fetus with transposition of the great arteries. On cross-sectional examination (**a**), the orientation of the root of the arterial vessel, committed to the left ventricle, arouses suspicion of transposition of the great arteries because it sweeps posteriorly, in the opposite direction of a normally located aorta. Moreover, the two great arteries show a parallel course in their first tract. The subarterial ventricular septum looks intact. Color flow mapping (**b**) highlights the parallel course of the two great arteries. *AAO* ascending aorta, *DAO* descending aorta, *LA* left atrium, *LV* left ventricle, *MPA* main pulmonary artery, *MV* mitral valve, *RV* right ventricle, *S* spine
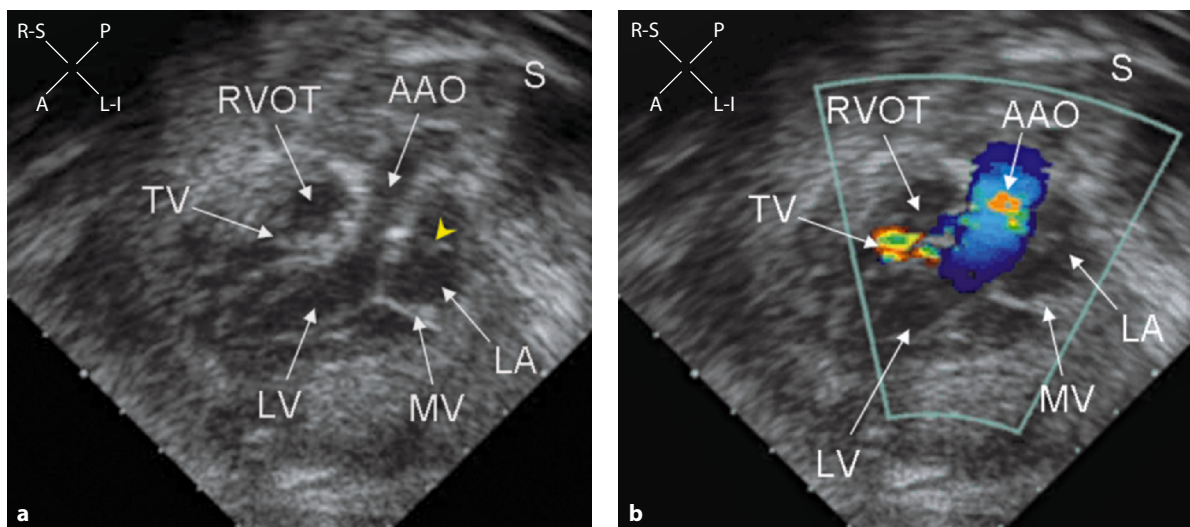
Fig. 19.12 • Long-axis view of the left ventricle in a 37-week gestational-age fetus with Ebstein's malformation and regurgitation of the tricuspid valve. On cross-sectional examination (**a**), the left heart chamber seems unaffected in this case. On moving images, the foraminal flap constantly protrudes inside the left atrium (*yellow arrowhead*) because of the high right-to-left shunt. A portion of the tricuspid valve leaflet is seen displaced into the right ventricular outflow tract. In this systolic frame, color flow mapping (**b**) shows in *yellow* the regurgitant jet, which originates at the level of the displaced tricuspid valve. The ascending aorta has an increased anterograde flow because of the redistribution of flow from right to left at the level of the foramen ovale. *AAO* ascending aorta, *LA* left atrium, *LV* left ventricle, *MV* mitral valve, *RVOT* right ventricular outflow tract, *TV* tricuspid valve, *S* spine
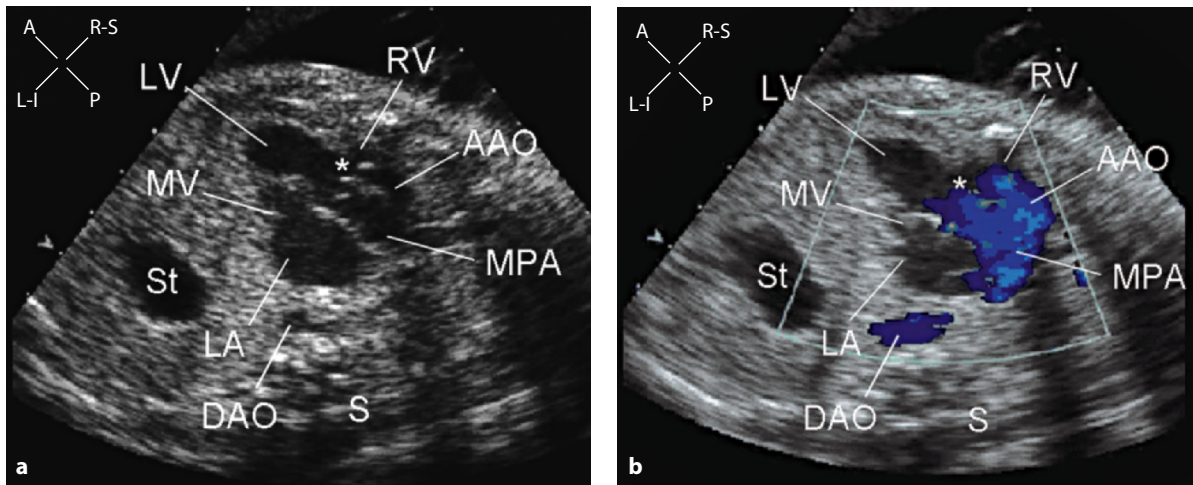
Fig. 19.13 • Long-axis view of the left ventricle in a 30-week gestational-age fetus with tricuspid valve atresia and discordant ventriculoarterial connections. On cross-sectional examination (**a**), the left atrium is committed to a large, morphologically left ventricle through a normal mitral valve. There is a rudimentary right ventricle in anterosuperior position. The two ventricles communicate through a small ventricular defect (*asterisk*). Although this view does not show any characteristic features that allow one to distinguish which artery is which, these arteries show a parallel course indicative of an anterior aorta. The ventriculoarterial connections are therefore discordant. The diameter of the ascending aorta is relatively small compared with the pulmonary artery. Color flow mapping (**b**) shows a normally competent mitral valve with apparently unobstructed systolic flow in *blue* into the two great arteries. *AAO* ascending aorta, *DAO* descending aorta, *LA* left atrium, *LV* left ventricle, *MPA* main pulmonary artery, *MV* mitral valve, *RV* right ventricle, *S* spine, *St* stomach
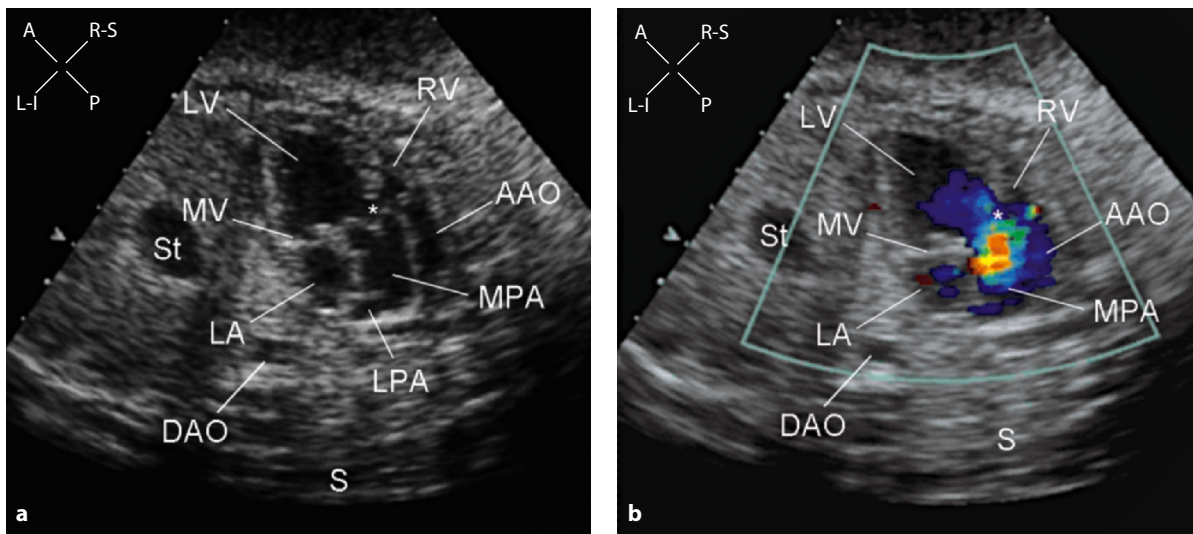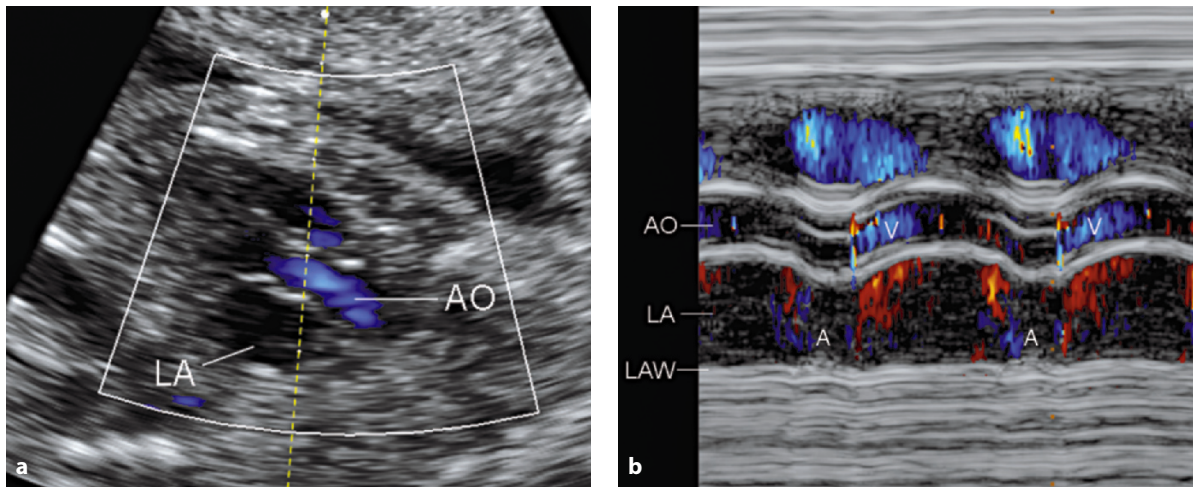

Fig. 19.14 • Long-axis view of the left ventricle in a 37-week gestational-age fetus with double-inlet left ventricle and discordant ventriculoarterial connection. On cross-sectional examination (**a**), this view is very similar to the case in Fig. 19.12. In fact, tricuspid atresia and double-inlet left ventricle cannot be distinguished by this view. There is a large, morphologically left ventricle and a rudimentary right ventricle in superoanterior position. The two ventricles communicate through a small ventricular defect (*asterisk*). The left ventricle is committed to a large pulmonary artery, which bends posteriorly and shows early bifurcation. The ascending aorta, which originates from the rudimentary ventricle, is significantly smaller than the main pulmonary artery. A complex type of aortic coarctation is associated. Color flow mapping (**b**) confirms the disproportion in size between the two arterial vessels. *AAO* ascending aorta, *DAO* descending aorta, *LA* left atrium, *LPA* left pulmonary artery, *LV* left ventricle, *MPA* main pulmonary artery, *MV* mitral valve, *RV* right ventricle, *S* spine, *St* stomach

Fig. 19.15 • Fetal thorax approached from the anterior side. In a long-axis view of the left ventricle (**a**), the cursor line is placed across the aortic root first and the left atrium second. Therefore, these structures are represented in this order, from top to bottom, in the M-mode tracing (**b**). Contractions of the left atrial wall are clearly seen (*A*), followed by regular ventricular contractions, indicated by the opening of the aortic valve (*V*). The systolic flow through the aortic valve is easily demonstrated (*blue*) by color M-mode tracing. *AO* aorta, *LA* left atrium, *LAW* left atrial wall

PART III

Echocardiographic and Morpologic Overview

Three-Dimensional Ultrasound Assessment of the Fetal Heart

Rabih Chaoui

Introduction

In the last 10 years, 3D and live 3D ultrasound – also called 4D ultrasound (3D/4D) – became popular in prenatal diagnosis but focused mainly on the demonstration of the fetal face and other external fetal body parts (hands, feet, etc.). The use of the 3D/4D in assessing the fetal heart evolved rapidly with the advent of the new technique called spatial and temporal image correlation (STIC), which enabled acquisition of a volume data set with information pertaining to the beating fetal heart [1, 2]. Matrix transducers for live 4D examination are already available, but the resolution is still too low to be routinely used in fetal studies, and the expenses are still high.

A detailed fetal echocardiogram includes visualization of different cross-sectional planes, either as parallel transverse slices or oblique short- and long-axis views [3, 4], as shown in the different chapters of this book. With a systematically segmental approach, venoatrial, atrioventricular, and ventriculoarterial connections are assessed. The use of color Doppler completes the examination in confirming the regular blood flow at the level of the valves, chambers, and vessels [5]. Such planes on 2D or color Doppler are today acquired online during live examination but could be generated off-line from a 3D volume data set [5-7].

This chapter discusses the use of 3D/4D fetal echocardiography in assessing normal cardiac anatomy, and the potential of its application in fetuses with cardiac defects is emphasized.

Technical Principles of 3D/4D Fetal Echocardiography

When 3D ultrasound is used, three steps should be considered separately: volume acquisition, volume display, and volume manipulation (Table 20.1).

Volume Acquisition

Fetal heart volume data set acquisition is achieved either in static 3D, real-time 3D (direct volume scan real time: online 4D), or STIC (indirect volume scan, motion gated: off-line 4D).

Table 20.1 • The three steps in 3D/4D fetal echocardiography

Steps	Possibilities	
Volume acquisition	Static 3D gray-scale, static 3D combined with color Doppler, B-flow, and others Real-time 3D (online 4D) STIC (off-line 4D) STIC combined with color Doppler, B-flow, and others	
Volume display	Planes – One plane – Multiplanar orthogonal – Multiplanar tomography	Rendering – Surface mode – Glass-body mode with color Doppler – Minimum transparent mode – Inversion mode – B-flow mode
Volume manipulation	Cutting parts of the thorax to see the heart (MAGICUT tool) Turning the volume box to see the valves or septum Selectively cutting gray scale to emphasize the color Doppler information	
STIC spatial and temporal image correlation		

Static 3D

In this acquisition, still images are stored as a volume data set, and neither heart rate nor motion is considered during acquisition and rendering. A quick, instead of slow, rapid volume acquisition enables motion artefacts to be avoided and provides acceptable images. This technique cannot be used for assessing events related to the heart cycle or to myocardial wall or valve movement. However, size and relationship of cardiac structures are valuable for diagnostic purposes. This static 3D gray scale can be combined with color Doppler, but we prefer to use it with uniform (one color) power Doppler or B-flow. For such purposes, the problem of motion artefacts appears to be insignificant in vascular 3D visualization, especially when attention is taken to reduce vessel pulsation during acquisition [8]. This is achieved by increasing the persistence of color Doppler and reducing the gain.

Real-Time 3D (Direct Volume Scan Real Time: Online 4D)

This is achieved either with a mechanical 2D transducer with rapid acquisition of 20-30 volumes/s or with a matrix 3D transducer, which allows real-time dynamic 3D evaluation. Both techniques have limitations in image resolution, frame rate, and lack of combination with color Doppler. In the future, when computer technology improves, they may partially replace STIC acquisition.

STIC (Indirect Volume Scan, Motion Gated: Off-Line 4D)

Volume STIC acquisition is a slow acquisition of image slices (duration 7.5-15 s) that allows acquisition of numerous planes, including additional information from a whole cardiac cycle. Spatial and temporal image correlation calculates the mean heart rate acquired, and images in the volume are rearranged according to their temporal event within the heart cycle. This slice-reconstruction method is completed directly after a volume scan, and the 4D information is available within seconds. The displayed volume includes a single "hypothetical" heart cycle, which is reconstructed from single selected images at the different intervals of the heart cycle [1, 2, 6, 9]. Therefore, STIC cannot be applied when ectopic beats are present. STIC can be used with gray-scale fetal echocardiography but can be also combined with color Doppler, power Doppler, B-flow, etc.

Volume Display

Planes: One Plane, Multiplanar Orthogonal, and Multiplanar Tomography

A 3D volume data set contains digital information of the cardiac structures and their spatial arrangement. In addition, STIC volume contains information on the temporal relationship of the cardiac structures. Thus, from a 3D/4D data set, cross-sectional views can be obtained at any desired orientation, direction, and depth. In a STIC volume, the reconstructed cardiac volume is displayed as a single hypothetical real-time cardiac cycle played in a cine loop. The loop may also be played in slow motion or stopped at any time for detailed analysis of specific phases of the cardiac cycle.

In such a volume data set, each plane of interest ("any plane") can be demonstrated by scrolling through the volume and orienting the views to obtain the plane of interest. In a good volume, the four-chamber, five-chamber, transverse, and long-axis views of the arterial duct and aortic arch, the three-vessel and tracheal view, etc., can be visualized off-line both in cine loop or as still images. The display format (Fig. 20.1) can be either the single-plane view or a multiplanar view showing three planes perpendicular to each other, or multiplanar tomography imaging showing parallel slices of the heart cavities and vessels.

The main limitations of reconstructed views are, on one hand, lower image quality in comparison with originally acquired 2D images and, on the other hand, dependency on possible artefacts. Such artefacts can be caused by fetal or maternal movements during acquisition, by shadowing in the region of interest, or by inaccurate volume reconstruction when acquisition time is too long or too short.

Studies on multiplanar analysis from a cardiac cycle at a remote station using STIC volume acquisition were shown to be reliable in assessing the different cardiac planes [6, 7], in screening studies [10], and in evaluating fetal cardiac anomalies [2, 7, 11, 12]. The advantages of using such a volume for an Internet link evaluation are emphasized as well, showing potential for a second opinion in the future [13]. Efforts were made recently to standardize the fetal cardiac examination on 3D, and the possibility of an automated cardiac image analysis from a volume data set was proposed [14, 15].

Color and power Doppler were added to gray-scale STIC technology, permitting possible assessment of hemodynamic changes throughout the cardiac cycle in the different cardiac cavities. Advan-
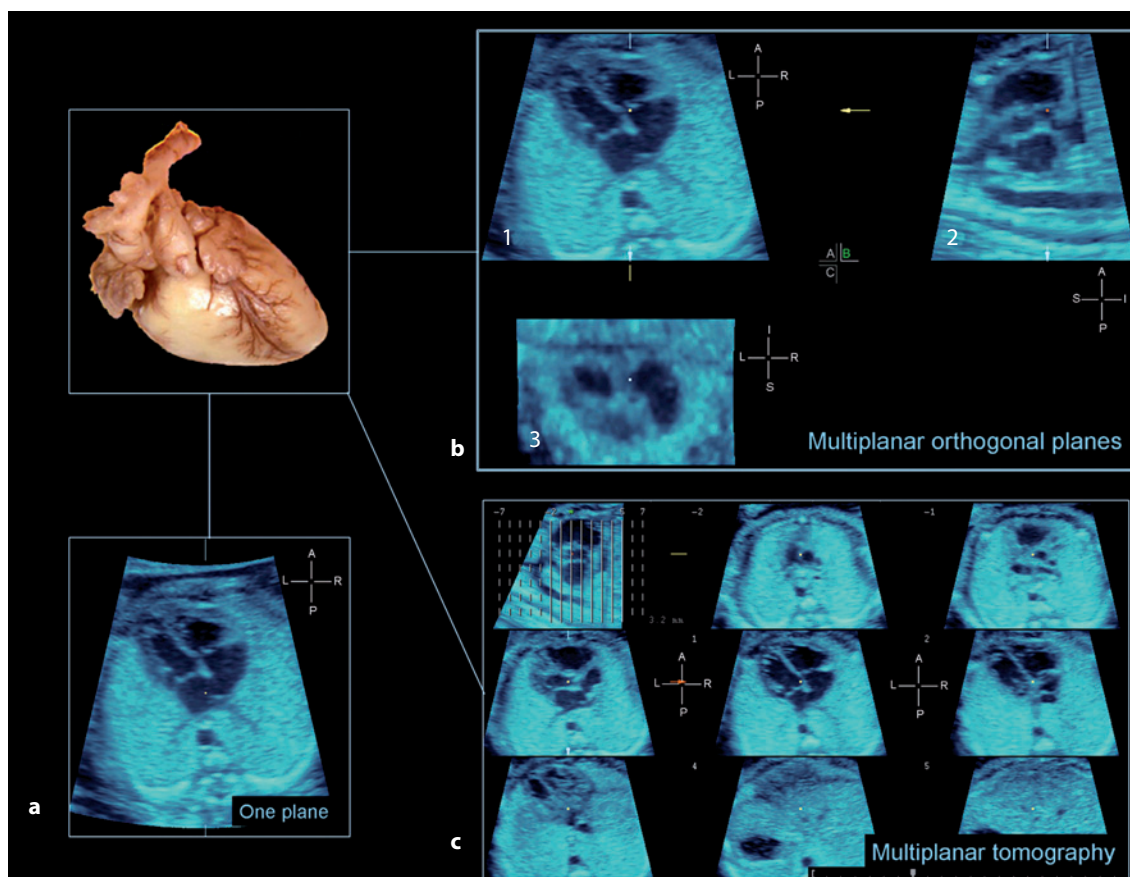
Fig. 20.1 • From a 3D or spatial and temporal image correlation (STIC) volume of a fetal heart, it is possible to display on postprocessing one single plane (**a**), which can be arbitrarily chosen by the examiner. The display can be multiplanar orthogonal planes (**b**) with one transversal (*1*), one longitudinal (*2*), and one coronal (*3*) plane, as well as multiplanar tomography view (**c**) with parallel slices, here seen as transversal planes. In a STIC volume, the period within the cardiac cycle can be selected also

tages and limitations of this technique have been reported elsewhere [2], but once a volume is properly acquired, display in the tomographic mode [12] provides rapid information on the three essentials planes in color Doppler, namely, the four-chamber, five chamber, and three-vessel trachea views (compare Figure 20.2 of a normal heart with Figure 20.3 of a heart with transposition of the great arteries).

Generally, fetal echocardiography is performed by obtaining numerous planes, such as transverse, oblique, and longitudinal cross sections, as demonstrated in this book.

For the obstetrician and sonographer not very familiar with these cardiac planes adapted from pediatric and adult cardiology, it has been shown that the main information for a cardiac exam can also be achieved by obtaining parallel transverse views [3, 4, 5, 16]. Such parallel transverse views are ideally demonstrated from a 3D/4D volume data set

using the tomographic display (Figs. 20.1, 20.2). This approach was shown to demonstrate at a glance cardiac anomalies affecting the four-chamber planes as well as conotruncal anomalies involving transverse views of the upper mediastinum, such as the three-vessel view and the aortic arch transverse view [11, 12, 17].

Rendering

Surface Mode

In surface-mode rendering, cardiac cavities are well visualized due to the different echogenicity of blood and cardiac walls. The render view direction (green line in Figure 20.4) is placed within the heart as a thick slice. If the slice is too slim, cardiac walls are emphasized, but the impression of a volume image
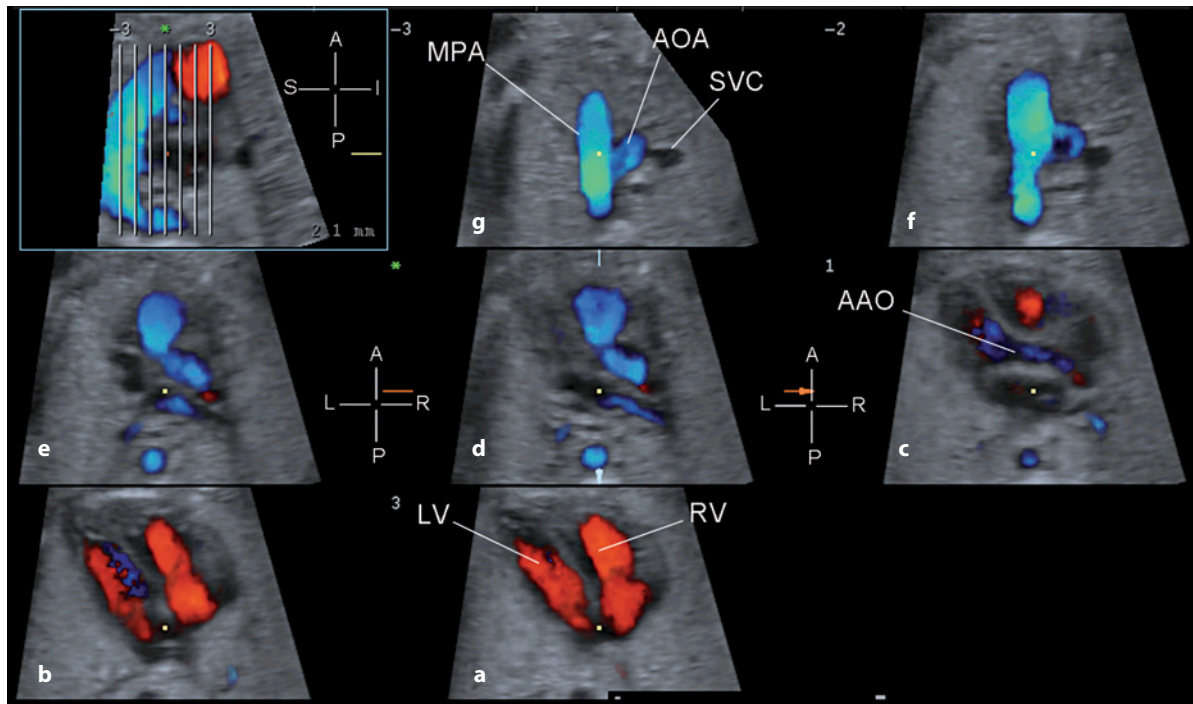
Fig. 20.2 • Tomographic view of spatial and temporal image correlation (STIC) volume showing a normal fetal heart in color Doppler. In plane **a**, the heart is seen in the four-chamber view in early diastole. Plane **c** shows the five-chamber view, and plane **g**, the arterial duct and aortic arch transverse view. *AAO* ascending aorta, *AOA* aortic arch, *LV* left ventricle, *MPA* main pulmonary artery, *RV* right ventricle, *SVC* superior vena cava
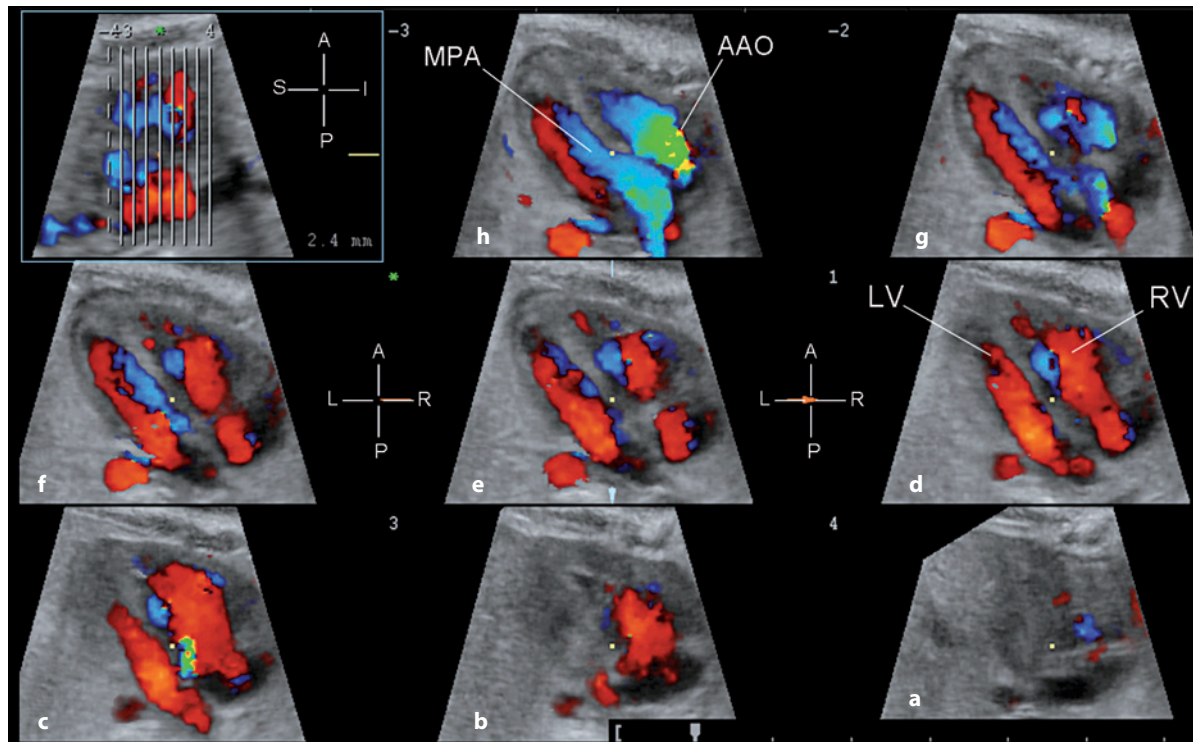
Fig. 20.3 • Tomographic view of a spatial and temporal image correlation (STIC) volume showing a fetal heart with transposition of the great arteries in color Doppler. Plane **d** shows the normal four-chamber view, whereas plane **h** shows the typical finding of the parallel course of both aorta and pulmonary artery. *AAO* ascending aorta, *LV* left ventricle, *MPA* main pulmonary artery, *RV* right ventricle
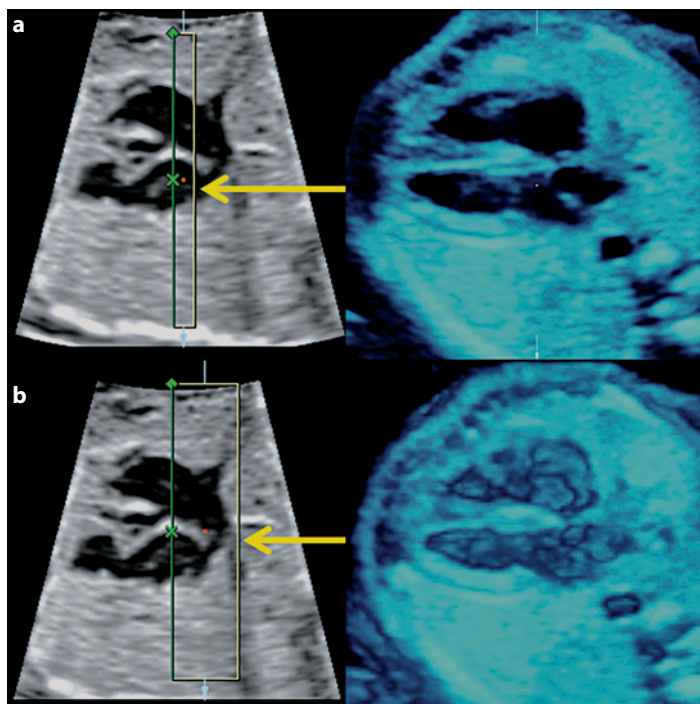
Fig. 20.4 • Volume rendering in surface mode. If the slice (*3D box*) is chosen narrow (**a**) the image does not show the same 3D effect as if the box is larger (**b**) and includes the inferior wall of the ventricles

is lacking (Fig. 20.4). The render view line is placed wherever the examiner wishes, and typical views of the upper abdomen (Fig. 20.5), the four-chamber view, the left and right ventricular outflow tract, and the arterial duct and aortic arch transverse views (Fig. 20.6) are demonstrated. Fetal cardiac anomalies are well demonstrated in these views, as shown for the atrioventricular septal defect (Fig. 20.7a) and the hypoplastic left-heart syndrome (Fig. 20.7b).

Besides the typical views used in 2D echocardiography, this technique allows reconstruction of new views, providing new insights into the normal and abnormal fetal heart. One possibility is to place the render view direction into the atrium and ventricle to visualize *en face* the atrial and ventricular septum from the left or right side (Figs. 20.8, 20.9). In the future, this view may allow better assessment of the size and shape of a ventricular septal defect (Fig. 20.9b) or other septal or valvular anomalies. In another view, the "base of the heart view" [18], the render view direction is placed in the atria at the level of the valves and enables the *en face* view of both atrioventricular and semilunar valves (Fig. 20.10). This view may be helpful in demonstrating the common atrioventricular valve in atrioventricular septal defect (Fig. 20.11). In one study, this view was shown to help differentiate the different Rastelli types in fetuses with atrioventricular septal defect [19]. This view is also helpful in demonstrating the caliber and relative position of the great

arteries, as found in transposition of the great arteries (Fig. 20.12) or in double-outlet right ventricle and other congenital heart diseases [18]. In a recent study on fetuses with transposition of the great arteries, this view used in combination with color Doppler identified the different patterns of position of the great arteries [20].

Glass-Body Mode with Color Doppler

Volume acquisition combining 2D and color (or power) Doppler provides a volume data set with structural and hemodynamic information of the fetal heart [2]. Volume data can be rendered in three ways: either gray scale information alone (see Surface Mode), color information alone, or the combination of both as a so-called "glass-body" mode (Fig. 20.13) [2]. A prerequisite for good volume is optimal presetting of color during 2D scan before acquiring a volume. One of the main application fields of this mode is to demonstrate the great-vessel arrangement. The clinical use of such new techniques, however, remains to be evaluated: Using 3D power Doppler ultrasound, we recently demonstrated the aberrant origin of the left and right subclavian artery in fetuses [8]. Figure 20.14 shows a heart seen from the anterior, with both chambers and crossing arteries and a trabecular ventricular septal defect.
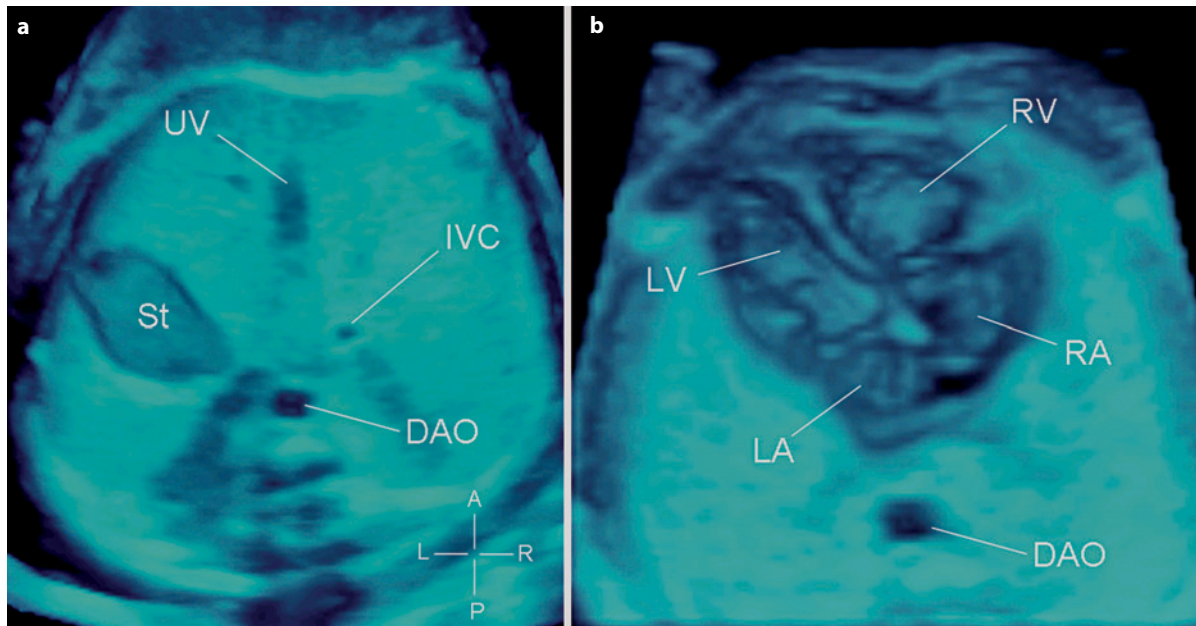
Fig. 20.5 • Three-dimensional surface view of the upper abdomen (**a**) and four-chamber view (**b**). In the upper abdomen view (**a**), the stomach, descending aorta, inferior vena cava, and intrahepatic umbilical vein are demonstrated. In the four-chamber view, the cardiac axis points to the left, the descending aorta is on the left of the spine, and the right and left atria are well visualized, as are the right and left ventricles. *DAO* descending aorta, *IVC* Inferior vena cava, *LA* left atrium, *LV* let ventricle, *RA* right atrium, *RV* right ventricle, *St* stomach, *UV* umbilical vein
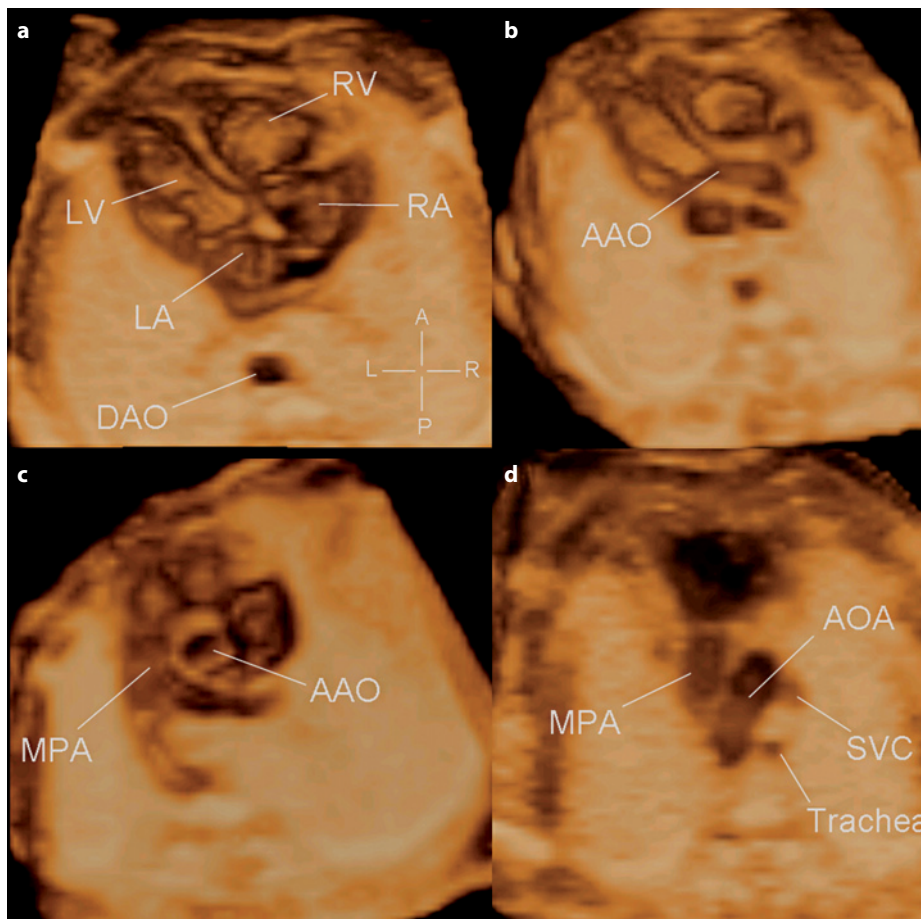
Fig. 20.6 • Three-dimensional surface view of the different common planes in the four-chamber view (**a**), five-chamber view (**b**), right ventricle outflow view (**c**), and arterial duct and aortic arch transverse view (**d**). *AAO* ascending aorta, *AOA* aortic arch, *DAO* descending aorta, *LA* left atrium, *LV* let ventricle, *MPA* main pulmonary artery, *RA* right atrium, *RV* right ventricle
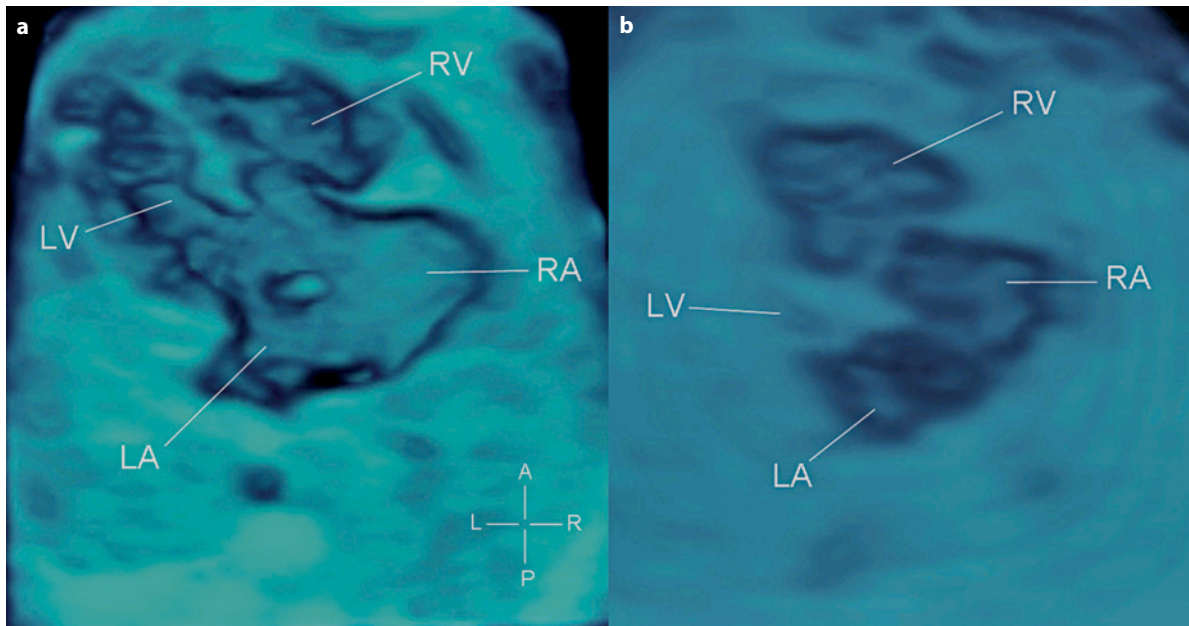
Fig. 20.7 • Three-dimensional surface of two cardiac anomalies detectable in the four-chamber view: complete atrioventricular septal defect (**a**) and hypoplastic left heart syndrome (**b**). *LA* left atrium, *LV* let ventricle, *RA* right atrium, *RV* right ventricle
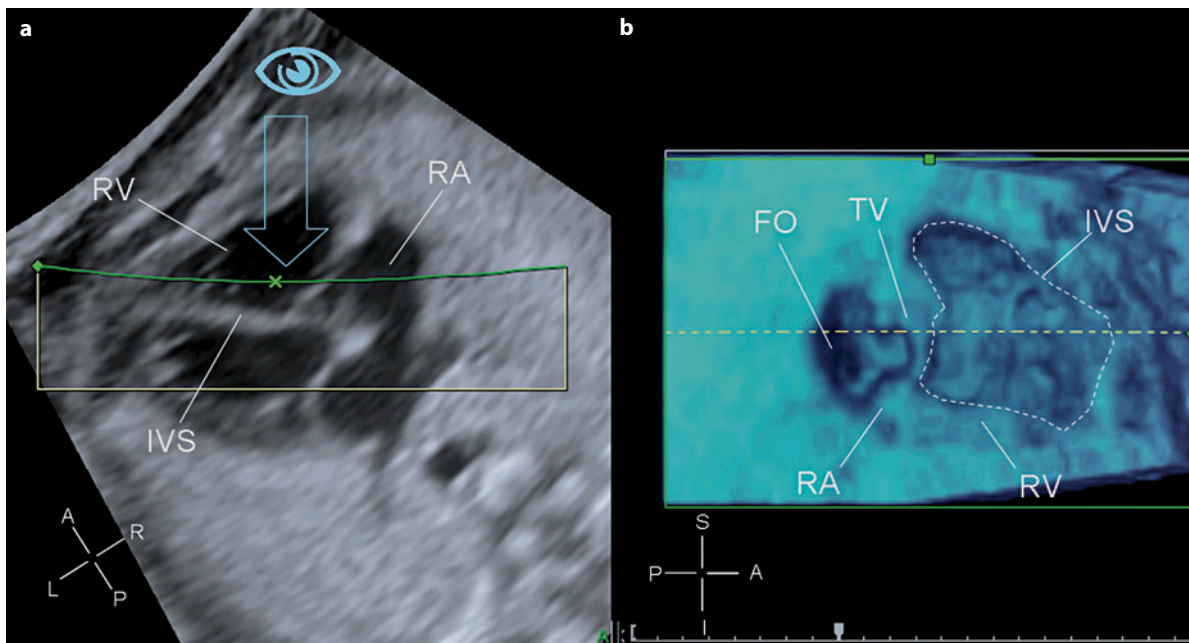
Fig. 20.8 • *En face* view of the interventricular septum. The 3D box is placed over the interventricular septum (**a**), with the rendering view from the right side (*green line* and *opened arrow with eye symbol*). Visualization of the right atrium with foramen ovale and the tricuspid valve (**b**) is seen, as well as the complete area of the interventricular septum (*dashed line*) within the right ventricle. *FO* foramen ovale, *IVS* interventricular septum, *RA* right atrium, *RV* right ventricle, *TV* tricuspid valve
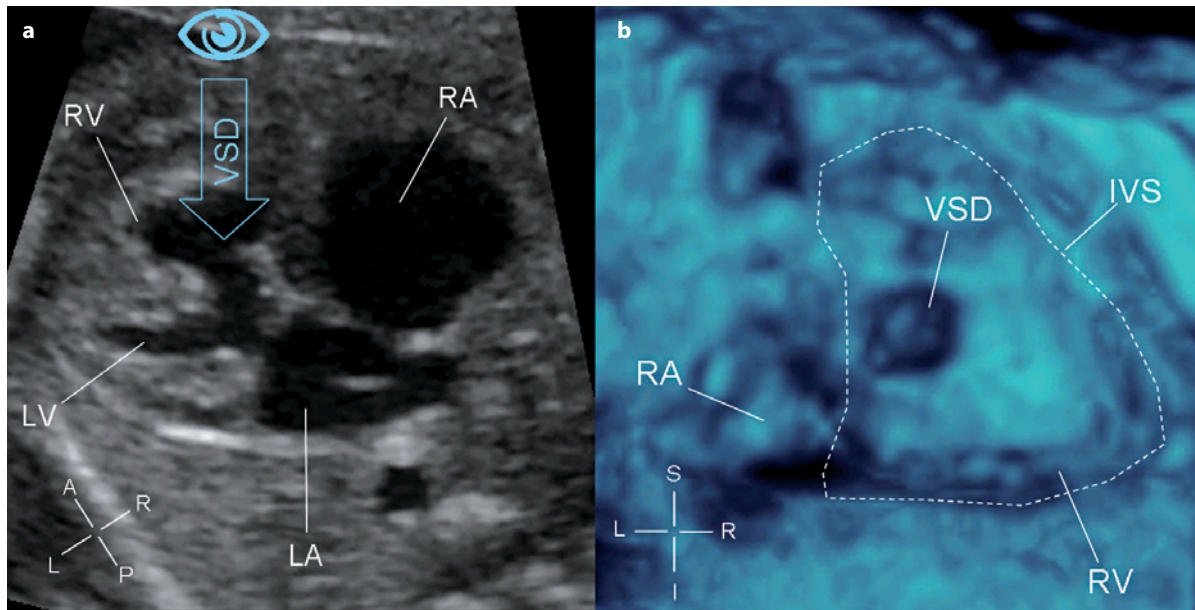
Fig. 20.9 • *En face* view of the interventricular septum in a fetus with interventricular septal defect. Ventricular septal defect is recognized in the four-chamber view (**a**) (*open arrow*). With the same rendering technique as in Figure 20.8, the *en face* view of the interventricular septum (**b**) demonstrates clearly the circular shape of this ventricular septal defect and the complete area of the interventricular septum (*dashed line*) within the right ventricle. *IVS* interventricular septum, *LA* left atrium, *LV* left ventricle, *RA* right atrium, *RV* right ventricle, *VSD* ventricular septal defect
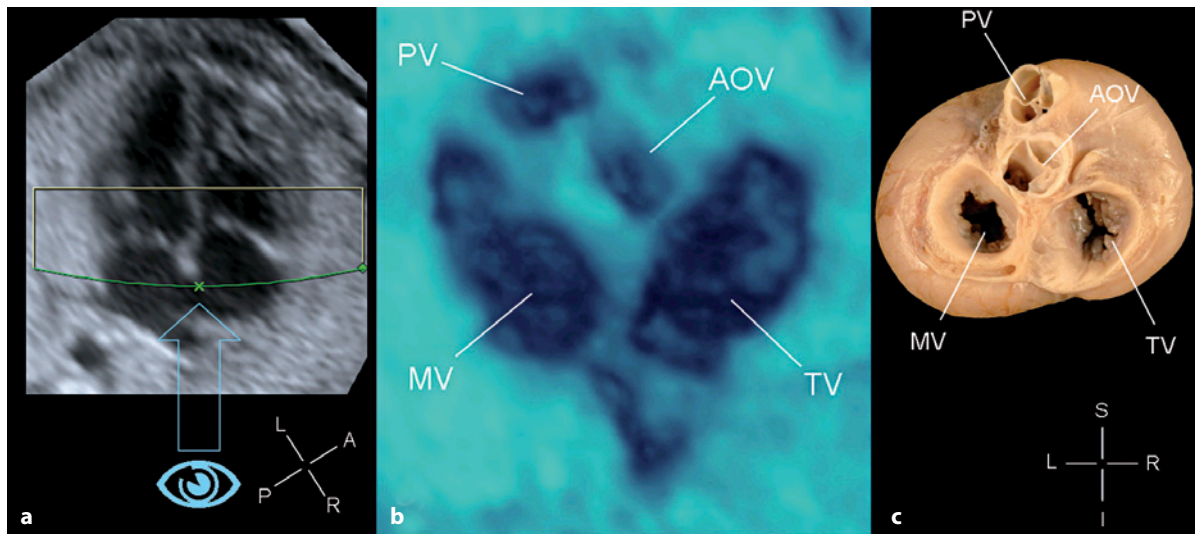
Fig. 20.10 • Base of the heart on the atrioventricular plane. The volume-rendering box is placed in the four-chamber view (**a**) over the atrioventricular valves, and the view direction (*green line*) is from the atria to the ventricles. Three-dimensional *en face* view (**b**) of the tricuspid and mitral valve seen from the base of the heart. Embedded between both ventricles is the aortic root, and anterior and on the left of the aorta is the pulmonary trunk. Pathologic specimen of a normal fetal heart (**c**) showing the base of the heart view demonstrated on 3D. *AOV* aortic valve, *MV* mitral valve, *PV* pulmonary valve , *TV* tricuspid valve
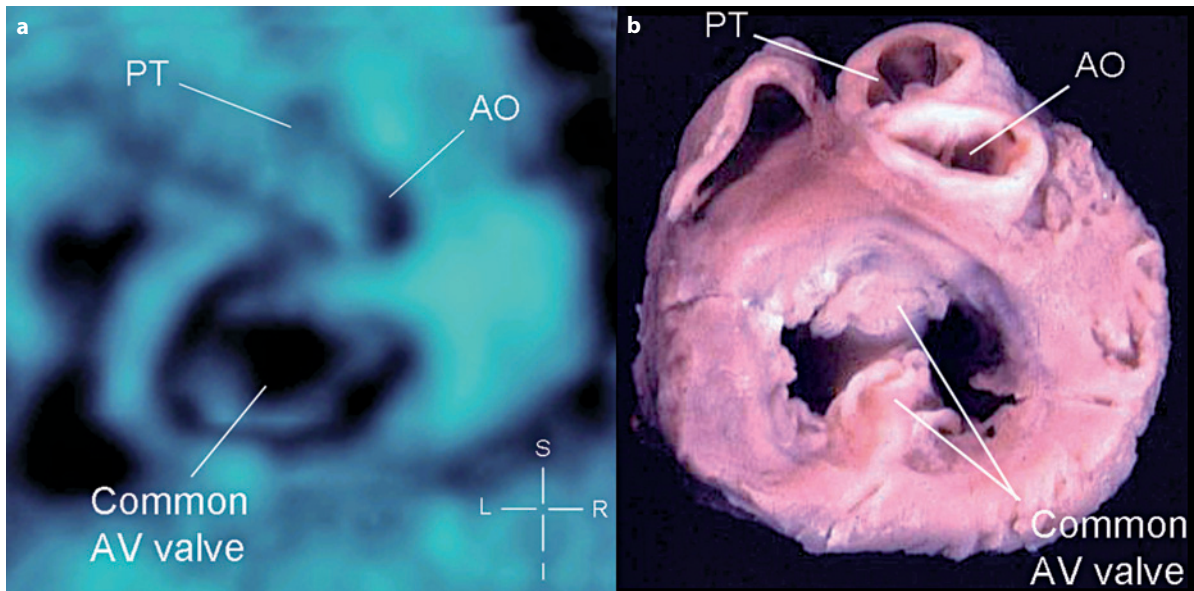
Fig. 20.11 • Base of the heart view in a fetus with atrioventricular (*AV*) septal defect showing the common AV valve on 3D rendering (**a**). Pathologic specimen of a similar case (**b**) showing the common valve. Compare with the normal finding in Figure 20.10b. *AO* aorta, *PT* pulmonary trunk
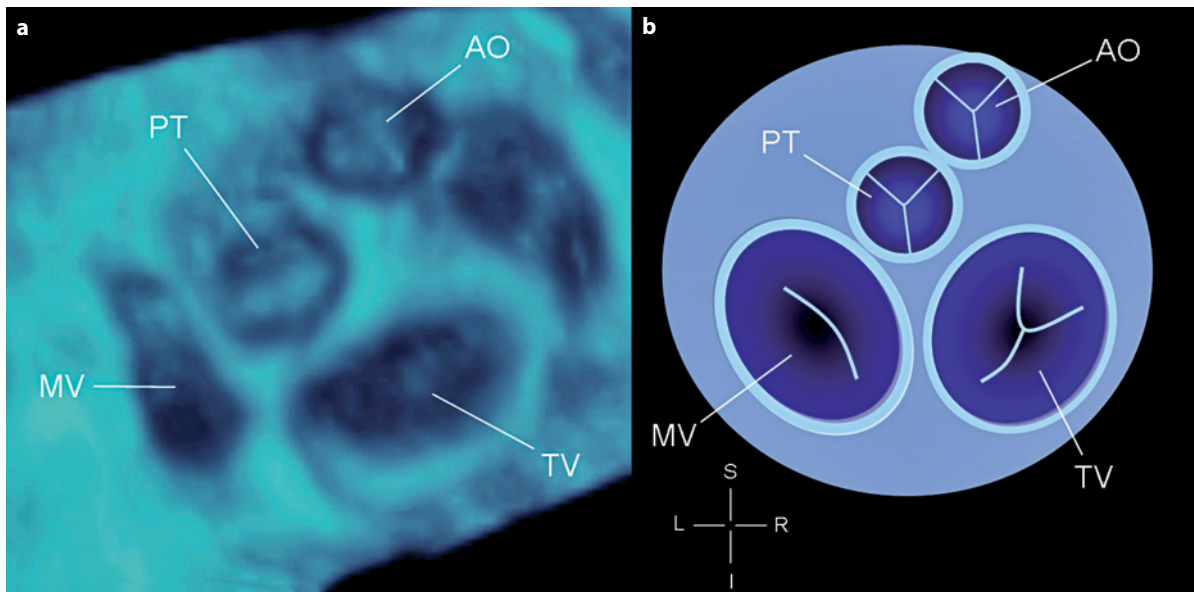
Fig. 20.12 • Base of the heart view in a fetus with transposition of the great arteries in the 3D rendering (**a**) with the corresponding diagram (**b**). This view shows the aortic root to the right side and anterior to the pulmonary trunk. Compare with the normal finding in Figure 20.10. *AO* aorta, *MV* mitral valve, *PT* pulmonary trunk, *TV* tricuspid valve
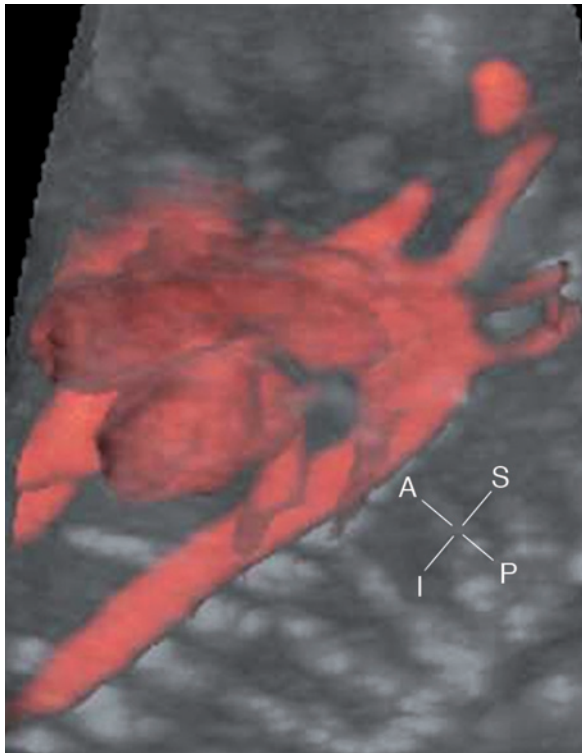
Fig. 20.13 • Glass-body mode showing the aortic arch within the thoracic cavity on power Doppler

Fig. 20.14 • Anterior view of the heart in power Doppler showing a muscular ventricular septal defect (*VSD*) and the crossing of the aorta and main pulmonary artery. The upper part of the heart was removed from the image to improve visualization of the VSD. *AAO* ascending aorta, *LV* left ventricle, *MPA* main pulmonary artery, *RV* right ventricle, *VSD* ventricular septal defect

Minimum Transparent and Inversion Mode
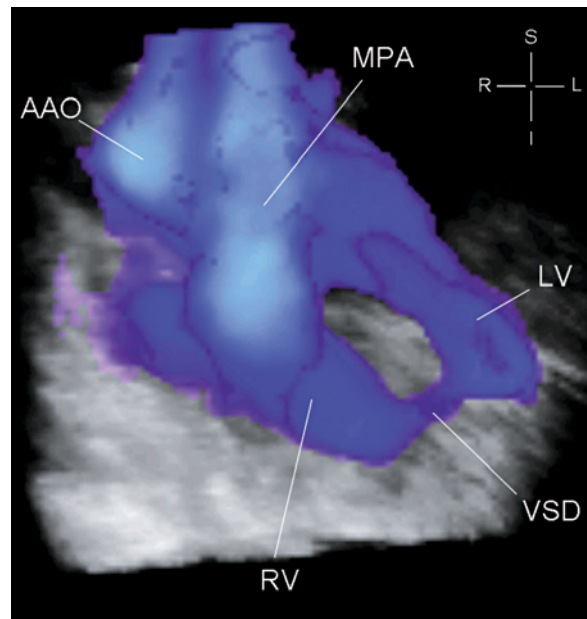
Transparent minimum-mode rendering is a display in which heart and blood vessels are seen in a transparent projection, mainly emphasizing structures with highest transparency (anechoic) in a 3D projection of black-appearing vessels (Fig. 20.15a), cysts, bladders, etc. [21]. In the recently introduced inversion display mode, however, the minimum mode rendering information is simply inverted (as in a negative/positive film) (Fig. 20.15b), thus presenting the hypoechoic structures as echogenic solid and eliminating into black most of the surrounding tissue information [22]. By changing some presets, such as increasing the threshold and decreasing the transparency, the image is improved. Artefacts are eliminated by using the electronic scalpel Magicut® during volume manipulation (Table 20.1).

The image is similar to that acquired with color/power Doppler but is very easy to obtain, as it is a gray-scale acquisition with 3D or STIC. The disadvantage of inversion is that tiny vessels, such as pulmonary or brachiocephalic vessels, are not well demonstrated due to the limited visualization on 2D image at acquisition. Figure 20.16 shows a normal heart with normally arising great vessels (Fig. 20.16a) and a heart with transposition of the great arteries

(Fig. 20.16b), with a parallel course of the aorta and main pulmonary artery.

Conclusion

In the recent years, 3D and 4D facilities have been used in fetal echocardiography, especially with the advent of the exciting acquisition technique STIC, which allows imaging of a beating fetal heart. From a volume data set, it is possible to obtain any plane within the fetal heart at anytime during the cardiac cycle. Volume data display can be achieved in planes (single, orthogonal, tomography) and also as a rendered 3D volume in surface, glass-body, and minimum or inversion modes. The examiner should, however, know how to choose the appropriate slice thickness within the volume, the region of interest, and the display mixture. As one might imagine, this new technique may improve future detection rates of fetal cardiac anomalies and our understanding of spatial relationships of cardiac structures in complex cardiac malformations.

Clinically, the 3D/4D technique is used to store volumes of cardiac anomalies for review of the findings at a later occasion or for a second opinion. In some institutions, it is used as a tool for controlling
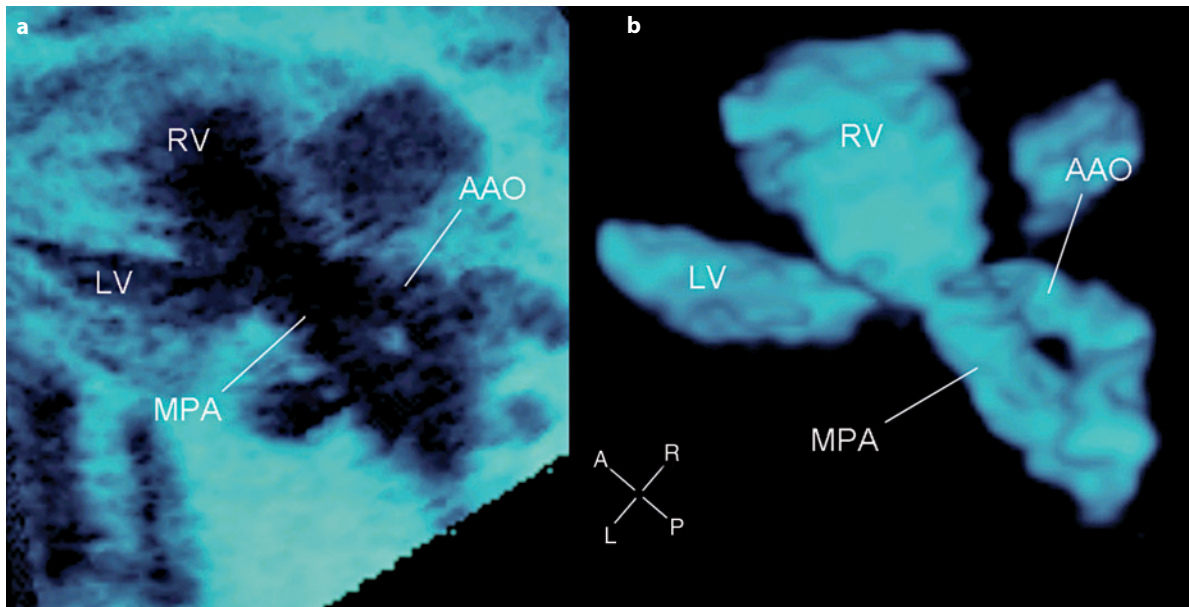
Fig. 20.15 • Two displays of a fetal heart volume: The transparent minimum mode (**a**) highlights the hypoechoic structures and shows a slice over the aorta and main pulmonary artery crossing each other. The inversion mode (**b**) is shown in the same volume, which is the negative image of the minimum mode with a modelling of the surface. Without using Doppler ultrasound, the crossing of the aorta and pulmonary trunk is demonstrated. *AAO* ascending aorta, *LV* left ventricle, *MPA* main pulmonary artery, *RV* right ventricle
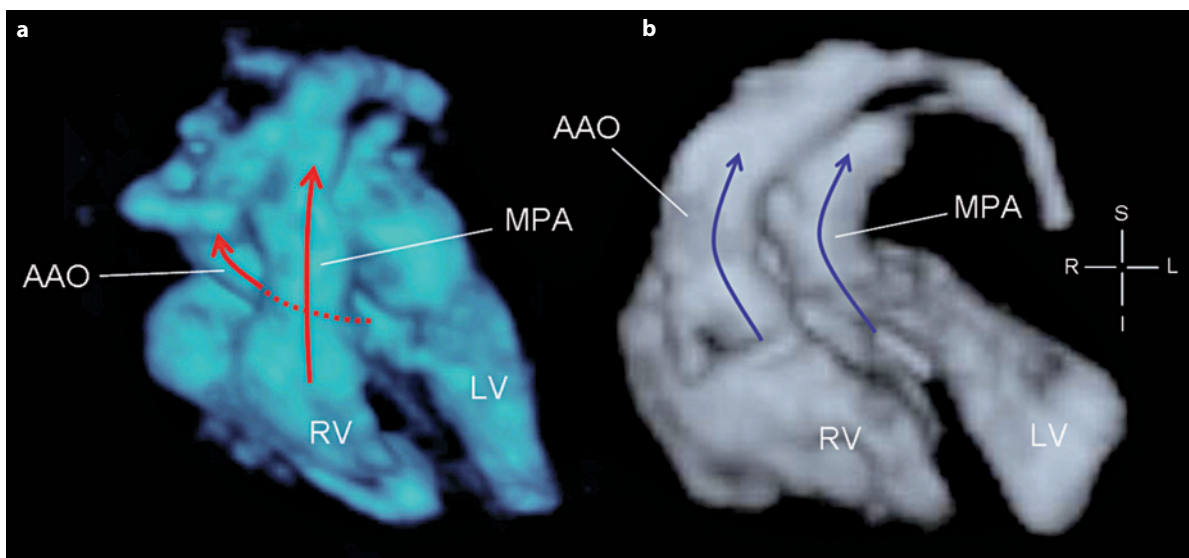
Fig. 20.16 • Inversion mode of two hearts rendered from an anterior view. In the normal heart (**a**), the left and right ventricles and the crossing of the aorta and main pulmonary artery (*red arrows*) are clearly seen. Transposition of the great arteries (**b**) with the parallel course of both aorta and main pulmonary artery, with the aorta arising from the right and the main pulmonary artery from the left ventricle. *AAO* ascending aorta, *LV* left ventricle, *MPA* main pulmonary artery, *RV* right ventricle

screening examinations, where STIC is acquired by the sonographers and reviewed by the specialist. It is used in teaching courses, mimicking a live scan, for fetal echocardiography to allow students to scroll through volumes of cardiac anomalies and determine the diagnosis. Finally, it is used in research to measure the volume of cardiac cavities and develop a step-by-step approach to demonstrate cardiac anomalies.

References

1. Devore GR, Falkensammer P, Sklansky MS, Platt LD (2003) Spatio-temporal image correlation (STIC): new technology for evaluation of the fetal heart. Ultrasound Obstet Gynecol 22:380-387

2. Chaoui R, Hoffmann J, Heling KS (2004) Three-dimensional (3D) and 4D color Doppler fetal echo-cardiography using spatio-temporal image correlation (STIC). Ultrasound Obstet Gynecol 23:535-545

3. Chaoui R (2003) The examination of the fetal heart using two-dimensional echocardiography. In: Yagel S, Silvermann N, Gembruch U (eds) Martin Dunitz, London, pp 141-149

4. Yagel S, Cohen SM, Achiron R (2001) Examination of the fetal heart by five short-axis views: a proposed screening method for comprehensive cardiac evaluation. Ultrasound Obstet Gynecol 17:367-369

5. Chaoui R, McEwing R (2003) Three cross-sectional planes for fetal color Doppler echocardiography. Ultrasound Obstet Gynecol 21:81-93

6. Goncalves LF, Lee W, Espinoza J et al (2003) Four-dimensional fetal echocardiography with spatio-temporal image correlation (STIC): a systematic study of standard cardiac views assessed by different observers. Ultrasound Obstet Gynecol 22(Suppl):50

7. Devore GR, Polanco B, Sklansky MS, Platt LD (2004) The 'spin' technique: a new method for examination of the fetal outflow tracts using three-dimensional ultrasound. Ultrasound Obstet Gynecol 24:72-82

8. Chaoui R, Schneider MBE, Kalache KD (2003) Right aortic arch with vascular ring and aberrant left subclavian artery: prenatal diagnosis assisted by three-dimensional power Doppler ultrasound. Ultrasound Obstet Gynecol 22:661-663

9. Chaoui R, Heling KS (2005) New developments in fetal heart scanning: three- and four-dimensional fetal echocardiography. Semin Fetal Neonatal Med 10:567-577

10. Vinals F, Poblete P, Giuliano A (2003) Spatio-temporal image correlation (STIC): a new tool for the prenatal screening of congenital heart defects. Ultrasound Obstet Gynecol 22:388-394

11. Goncalves LF, Espinoza J, Romero R et al (2006) Four-dimensional ultrasonography of the fetal heart using a novel tomographic ultrasound imaging display. J Perinat Med 34:39-55

12. Paladini D, Vassallo M, Sglavo G et al (2006) The role of spatio-temporal image correlation (STIC) with to-mographic ultrasound imaging (TUI) in the sequential analysis of fetal congenital heart disease. Ultrasound Obstet Gynecol 27:555-561

13. Vinals F, Mandujano L, Vargas G, Giuliano A (2005) Prenatal diagnosis of congenital heart disease using four-dimensional spatio-temporal image correlation (STIC) telemedicine via an Internet link: a pilot study. Ultrasound Obstet Gynecol 25:25-31

14. Abuhamad A (2004) Automated multiplanar imaging: a novel approach to ultrasonography. J Ultrasound Med 23:573-576

15. Abuhamad A, Falkensammer P, Zhao Y (2007) Automated sonography: defining the spatial relationship of standard diagnostic fetal cardiac planes in the second trimester of pregnancy. J Ultrasound Med 26:501-507

16. Chaoui R, Bollmann R, Hoffmann H, Heling KS (1991) [Sonoanatomy of the fetal heart. Proposal of simple cross-sectional planes for the non-cardiologists]. Ultraschall Klin Prax 6:59-67

17. Espinoza J, Romero R, Kusanovic JP et al (2008) Standardized views of the fetal heart using four-dimensional sonographic and tomographic imaging. Ultrasound Obstet Gynecol 31:233-242

18. Chaoui R, Hoffmann J, Heling KS (2004) Basal cardiac view on 3D/4D fetal echocardiography for the assessment of AV-valves and great vessels arrangement. Ultrasound Obstet Gynecol 22:228 (Abstract)

19. Vinals F, Pacheco V, GiulianoA (2006) Fetal atri-oventricular valve junction in normal fetuses and in fetuses with complete atrioventricular septal defect assessed by 4D volume rendering. Ultrasound Obstet Gynecol 28:26-31

20. Paladini D, Volpe P, Sglavo G et al (2008) Transposition of the great arteries in the fetus: assessment of the spatial relationships of the arterial trunks by four-dimensional echocardiography. Ultrasound Obstet Gynecol 31:271-276

21. Espinoza J, Goncalves LF, Lee W et al (2004) The use of the minimum projection mode in 4-dimensional examination of the fetal heart with spatio-temporal image correlation. J Ultrasound Med 23:1337-1348

22. Goncalves LF, Espinoza J, Lee W et al (2004) Three- and four-dimensional reconstruction of the aortic and ductal arches using inversion mode: a new rendering algorithm for visualization of fluid-filled anatomical structures. Ultrasound Obstet Gynecol 24:696-698

CHAPTER 21

The Role of the Pathologist in the Diagnosis of Fetal Heart Disease

Introduction

The importance of autopsy in the event of fetal or neonatal death is widely demonstrated in several studies [1-3]. Thanks to the diagnostic power now provided by cross-sectional echocardiography, most structural and functional congenital heart diseases can be identified during fetal life. However, it is unreasonable to expect 100% sensitivity in all cases. In fact, many drawbacks can limit the ultrasonic examination, such as gestational age at the time of scan, fetal position, ultrasonic impedance of the maternal abdomen, examiner experience, and types of equipment used. In case of termination or spontaneous intrauterine death autopsy is still a valuable tool that provides clinicopathological correlation for clinicians and gives information to families regarding the risk of recurrence of specific diseases in future pregnancies. In the latter instance, evaluations can be made earlier in gestation, allowing informed decisions that will be in the best interest of the mother and fetus. Performing autopsies also provides the opportunity to create archives of heart specimens with congenital diseases, which are extremely useful for improving clinical practice, research, and education. Despite their small size, fetal hearts with congenital heart disease are invaluable in teaching because they are free from surgical manipulation, which usually modifies the native morphology in most postnatal specimens. Fetal autopsies and specimen archives should be obtained after informed consent of the families according to their religious beliefs and according to local laws, avoiding the inappropriate retention of organs such as that which came to light in Europe a few years ago [4, 5].

The pathologist who addresses congenital heart diseases in the fetus should be adequately trained and maintain his or her expertise with a high workload. Moreover, it is crucial to be familiar with the physiology and morphology of both normal and malformed hearts, even the most complex malformations [6]. Ideally, the pathologist's practice should be located at a tertiary level in a pathology department and have close links with other relevant subspecialties, such as fetal medicine, obstetrics, pediatric cardiology and cardiothoracic surgery, and clinical genetics.

The Morphologic Study

Instrumentation

Because of the small dimensions of the fetal heart, a suitable set of instruments is needed:

– a ruler, small scissors with at least one sharp point, small scissors with two sharp points, fine probe with rounded ends, blades, scalpel, needles, syringes, floppy guidewire, etc. (Fig. 21.1);
– a magnifying lens, and/or a dissecting microscope preferably equipped with a camera;
– photographic equipment: camera, lenses, camcorder, image archiving systems;
– pathologist time and patience.

When a prenatal ultrasound diagnosis is available, it should not influence the pathologist's judgment but offer, instead, the opportunity for a positive confrontation between echographer and pathologist. Knowing the ultrasound diagnosis before starting the autopsy is often useful to plan the best approach for dissection.
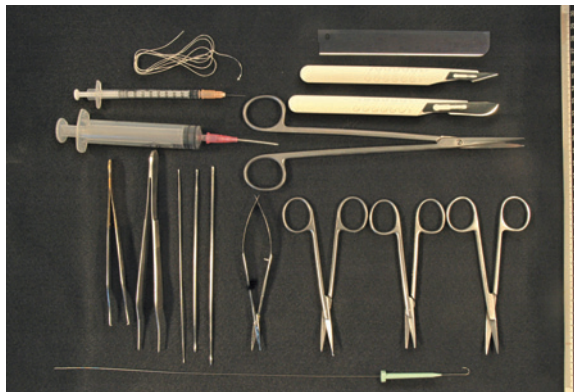
Fig. 21.1 • A set of instruments commonly used for dissecting fetal hearts

Exposure of the Heart and Great Vessels

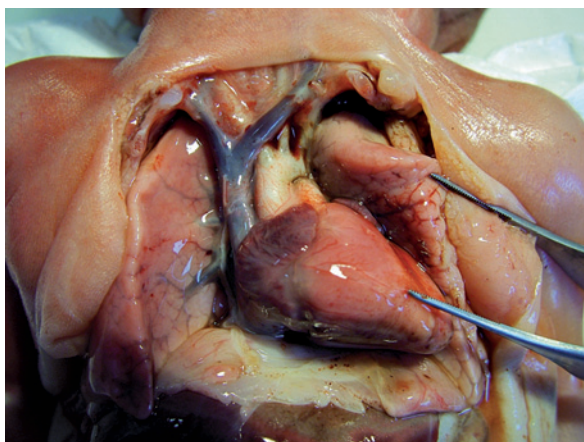The chest plate is removed by separating the sterno-clavicular joint on each side while preserving the jugular veins. Removing the pericardium and thymus together allows exposure of the heart and great vessels (Fig. 21.2). The pericardium is nicked, and a cut is made parallel to the diaphragm, extending it to the terminal part of the inferior vena cava on the right side and to the pulmonary veins on the left side. On the right side, the pericardium is removed as close as possible to the inferior vena cava and toward the superior vena cava by reaching, without cutting, the left innominate vein. On the left side, the scissors are placed perpendicular to the diaphragm toward where the pulmonary veins enter the left atrium. The pericardium, with the thymus attached, is dissected from the left pulmonary artery and innominate vein without opening the lumen. If the innominate vein is absent, a persistent left superior vena cava should be suspected. At the end, the pericardium is completely removed as close as possible to vascular insertions.

A sterile needle can be inserted in the lateral wall of the right atrium to obtain blood culture if necessary. In general, we suggest removing the blood inside the heart and replacing it with a fixative solution, such as methyl-Carnoy's solution. This procedure also allows enhancement of the coronary morphology.

Heart Examination In Situ

Examining the heart in situ may provide crucial information. Many congenital heart diseases can be suspected from the outside, which allows planning

for the most appropriate anatomic dissection. The following list summarizes the most important points to annotate during external examination:
–   heart position and axis orientation;
–   cardiothoracic ratio;
–   visceroatrial arrangement;
–   systemic and pulmonary vein connection;
–   great arteries' position and size;
–   external morphology of atrial and ventricular chambers;
–   pattern of coronary arteries.

To best examine the heart and, in particular, to inspect the aortic arch, the arterial duct, and the descending aorta, we suggest moving the left lung to the left (Fig. 21.2). If the heart can be moved from the chest without displacing the lungs, an anomalous pulmonary connection should be suspected (Taussig maneuver). External examination of the heart in situ must be performed thoroughly, and every abnormality should be annotated and possibly photographed, as many of them are difficult or even impossible to identify once the heart is removed from the thorax (Fig. 21.3).
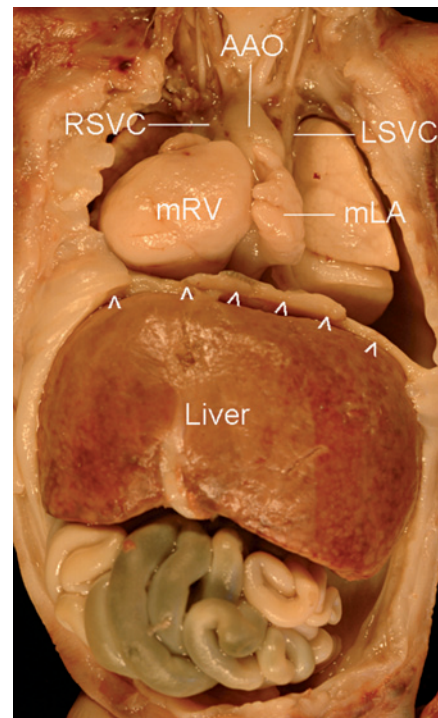
Fig. 21.3 • Chest and abdominal organs in situ. The liver is a central structure with two nearly symmetrical lobes. The intestines are malrotated. On external inspection, the heart is in the right side of the chest, and there is a bilateral superior vena cava. The great arteries are malposed, with an enlarged anterior aorta. The *open arrowheads* indicate the diaphragm. *AAO* ascending aorta, *LSVC* left superior vena cava, *mLA* morphologically left atrium, *mRV* morphologically right ventricle, *RSVC* right superior vena cava

Fig. 21.2 • The chest plate has been removed to expose the heart and the great vessels. The left lung is moved to the left to inspect the aortic arch, arterial duct, and descending aorta

Removal of the Heart and Lung Block

The organs can be eviscerated in anatomically related groups (Ghon method) or en bloc (Letulle method), as in adult autopsy [7]. We usually prefer to eviscerate thoracic organs together with the trachea, the larynx, and the esophagus. The carotid arteries should be tied just above their bifurcation. To maintain separation between thoracic and abdominal organs, the esophagus, aorta, and great veins are sectioned just under the diaphragm (Fig. 21.4).

Methods of Heart Dissection

Different dissection methods can be employed [8, 9]. The method can be chosen on the basis of which type of heart disease is suspected and specimen size. More than one method is possible on the same specimen.
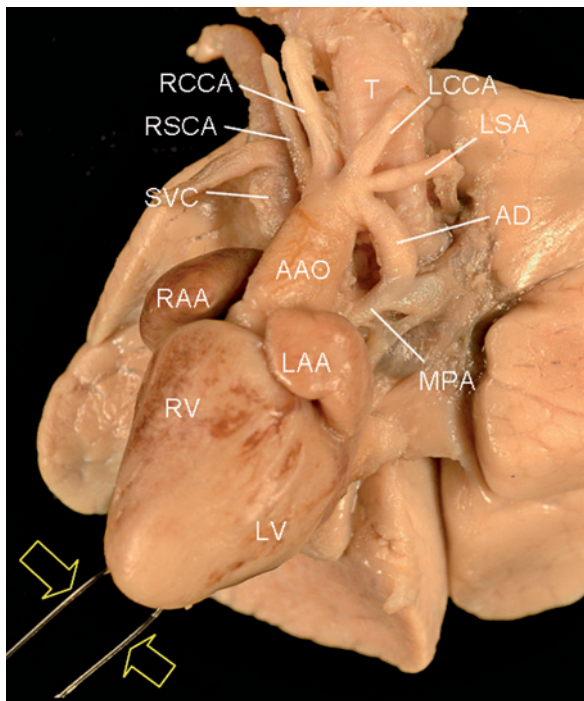
Fig. 21.4 • The heart and lung block in a fetal heart with tetralogy of Fallot and pulmonary valve atresia. With the help of a surgical suture (*yellow open arrows*), the apex of the heart is rotated to the right. The presence of the trachea allows recognition of a right-sided aortic arch and an anomalous arterial duct that originates from the foot of the left subclavian artery. *AAO* ascending aorta, *AD* arterial duct, *LAA* left atrial appendage, *LCCA* left common carotid artery, *LSCA* left subclavian artery, *LV* left ventricle, *MPA* main pulmonary artery, *RAA* right atrial appendage, *RCCA* right common carotid artery, *RSCA* right subclavian artery, *SVC* superior vena cava, *T* trachea

Dissection Following Blood Flow

With this method, the heart is opened chamber after chamber (examining each chamber as it is opened) following the stream of blood and using the epicardial coronary arteries as marker of the position of the ventricular septum. This method should be performed following sequential segmental analysis from the venous to the arterial side. It usually requires a heart specimen of sufficient dimension, which is rare in prenatal diagnosis. Even if this type of dissection can be performed immediately after the heart is removed from the chest, specimen fixation is recommended (Fig. 21.5). In fact, when fixation is performed after dissection, it results in distortion of the dissected edges and alters the relationship of the cardiac structures. This makes comprehensive pictures of the specimen and morphologic study at a later stage difficult.

Tomographic Method

Sections of this type allow morphologic sections comparable with the echocardiographic views and can be obtained from very small hearts. However, accurate perfusion and fixation is required. Dissection should be performed with a sharp knife, avoiding a sawing motion, no earlier than 1-7 days after fixation. Should the section so obtained be incorrect, a new section can be performed after repairing mistakes. This can be done in a few hours after carefully gluing together the dried surface of the two halves of the specimen with commercially available cyanoacrylate glue.

Following are some examples of congenital heart diseases displayed on different tomographic sections of the heart.

Short-Axis Section

The heart is placed on its diaphragmatic surface, and serial cuts are made parallel to the atrioventricular groove. Slices so obtained correspond to the short axis plane of the heart produced by cross-sectional echocardiography. This method is indicated in a limited number of conditions, such as cardiomyopathy or ischemic myocardial damage (Fig. 21.6).

The Four-Chamber Section

In this section, the cut begins at the cardiac apex along a plane that passes through the acute and obtuse
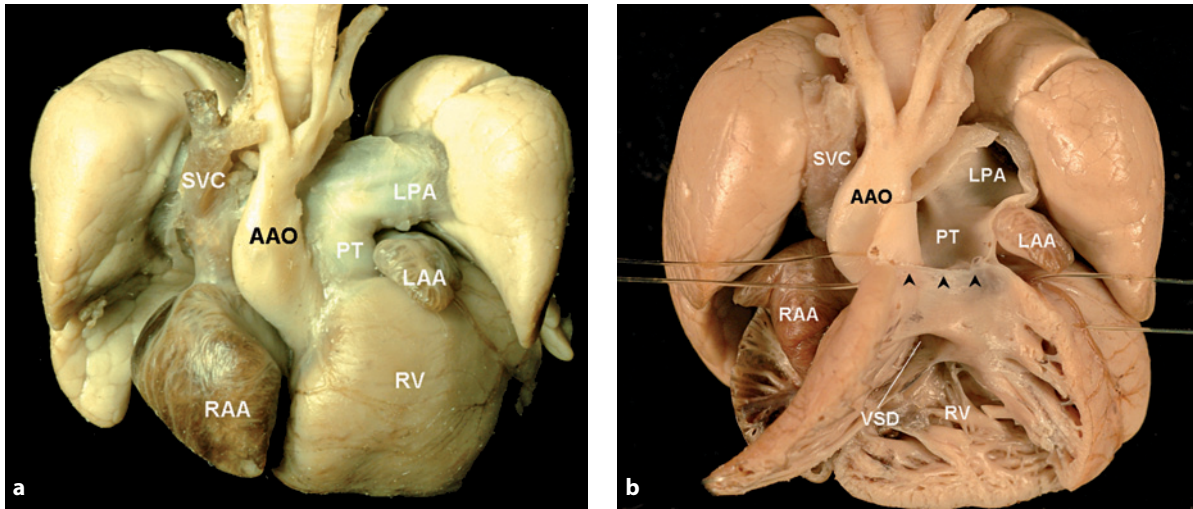
Fig. 21.5 • Outside (**a**) and inside (**b**) in a heart specimen of a fetus with tetralogy of Fallot and the so-called absent pulmonary valve. This specimen was fixated before dissection. Following the flow-of-blood method, the infundibulum and pulmonary trunk are opened from the apex of the right ventricle (**b**). This cut allows evaluation of the ventricular septal defect and the rudimentary pulmonary valve (*arrowheads*). To emphasize dilatation of the pulmonary trunk and left pulmonary artery and the absence of the arterial duct – a common finding in cases with congenital heart disease of this type – the lumens of these vessels are windowed. *AAO* ascending aorta, *LAA* left atrial appendage, *LPA* left pulmonary artery, *PT* pulmonary trunk, *RAA* right atrial appendage, *RV* right ventricle, *SVC* superior vena cava, *VSD* ventricular septal defect
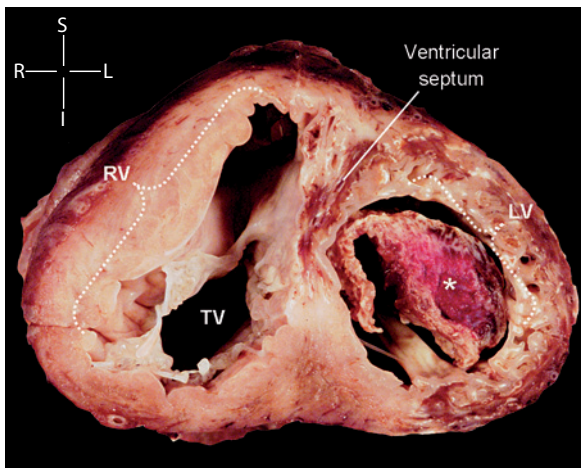
Fig. 21.6 • Short-axis section of the heart in a 32-week gestational-age fetus who suffered a large myocardial infarction of the left ventricle due to thrombosis of the left main coronary artery. The anterior portion of the interventricular septum and the anterolateral wall of the left ventricle show extensive ischemic damage. A very large thrombus fills the cavity of the left ventricle (*asterisk*). *LV* left ventricle, *RV* right ventricle, *TV* tricuspid valve
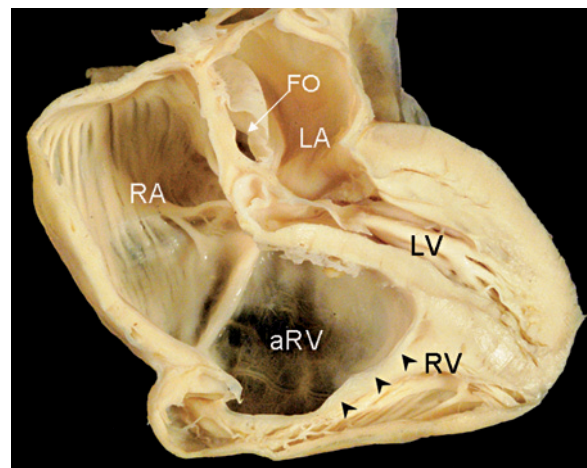
Fig. 21.7 • Ebstein's malformation in a 31-week gestational-age fetus This specimen is cut in a simulated four-chamber section. Displacement of the tricuspid valve leaflets and the atrialized portion of the right ventricle are well demonstrated (*arrowheads*). The enlarged foramen ovale with a redundant flap valve testifies to the obligatory right-to-left shunt due to functional obstruction to the right ventricular outflow. *aRV* atrialized right ventricle, *FO* foramen ovale, *LA* left atrium, *LV* left ventricle, *RA* right atrium, *RV* right ventricle

margins of the heart and perpendicular to the inlet and trabecular ventricular septum. This dissection allows assessment of the size of the cardiac chambers, the atrioventricular junction and its valves, and the atrial and ventricular septum (Fig. 21.7). After a section of this type, the ventriculoarterial junction and great arteries should be examined with other methods of dissection, such as following the blood flow.

The Base of the Heart Section

Both atria are removed a few millimeters above the mitral and tricuspid valve plane. This cut allows assessment of the atrioventricular junction and valves, the relative position of the great arteries, and morphology and size of the semilunar valves (Fig. 21.8).

Tomographic Section of the Whole Body

In echocardiography textbooks, tomographic sections of fetal cardiac specimens are usually compared with their corresponding echographic projections. These sections are generally obtained from isolated hearts. However, tomographic sections of the whole body are among the best techniques by which to understand the relationship between cardiac and extracardiac structures. This understanding is particularly necessary in fetal echocardiography where the number of visible structures is much greater and approaches to the fetal thorax are variable. Nevertheless, specimens of the whole body are rarely used because the process of fixation and the methods by which to obtain these sections are technically difficult and time consuming. In fact, the section plane should be chosen with unforeseeable

result on the inner organs and with limited possibility of correction after the first cut has been performed. Sections of the whole fetal body are generally not applicable in abnormal cases, because the standard reference lines on the external surface of the body cannot be applied in most cases with congenital heart disease.

Sections of the whole fetal body, shown in other chapters of this book, have been obtained – according to Italian law and with maternal consent – from four fetuses who underwent termination before 20 weeks of gestational age. The fetal body was perfused through the umbilical vein and trachea with Bouin solution, a liquid that allows good tissue fixation and satisfactory decalcification of the skeleton. After fixation for 1 week, a series of parallel sections of the fetal body were performed with a long blade along the horizontal plane, the true sagittal plane, the parasagittal plane with 40° clockwise orientation, and the parasagittal plane with 60° counterclockwise orientation from the sagittal midline in one fetus each. Each section was classified and photographed using a professional, digital, single-lens reflex camera with a macro lens, mounted on a standard photographic stand. Sections shown in this volume are the result of the close collaboration between the pathologist and the pediatric cardiologist (Fig. 21.9).
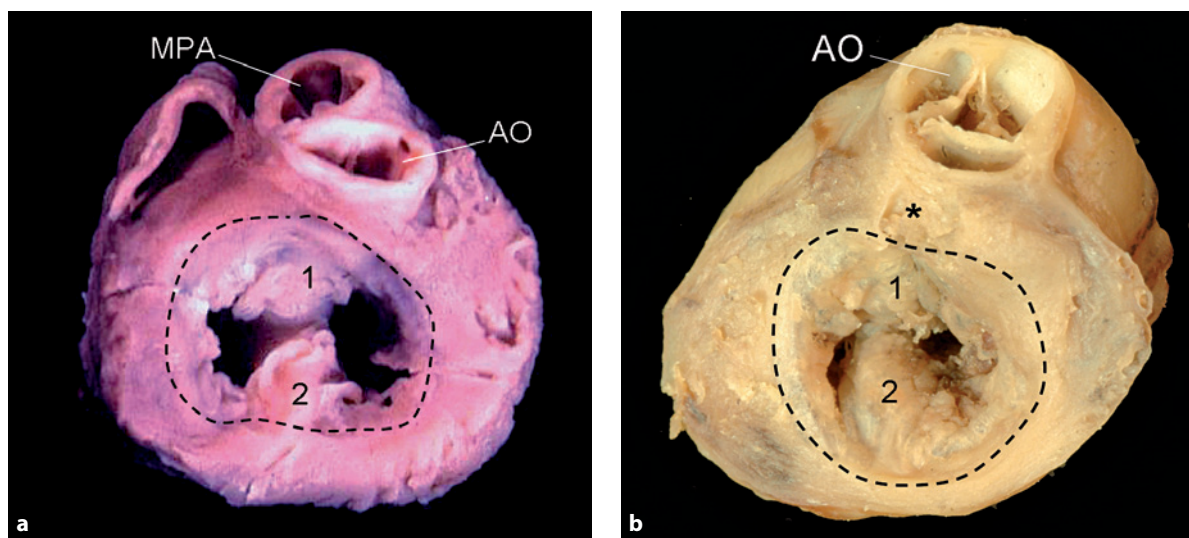
Fig. 21.8 • Base of the heart in two fetal specimens with atrioventricular septal defect. Both images show the common atrioventricular orifice (*black broken line*) and the anterior (*1*) and posterior (*2*) bridging leaflet of the common valve. The ventriculoarterial connection is concordant without obstruction to ventricular outflow (**a**). The great arteries are therefore normally related and of equal size. However, the aorta is displaced anteriorly, compared with its position in the normal heart where it is wedged between the two atrioventricular valves. A case with right isomerism (**b**). The ventriculoarterial connection is double outlet from the right ventricle. The aorta is enlarged and malposed, in anterior position. The *black asterisk* indicates the root of the atretic main pulmonary artery, located posteriorly. *AO* aorta, *MPA* main pulmonary artery
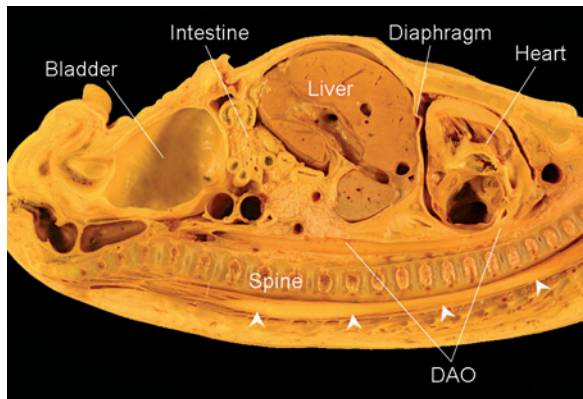
Fig. 21.9 • Section of the whole fetal body obtained along a true left parasternal sagittal plane. The relationship between the heart and the thoracic and abdominal organs is well depicted. The *cranial portion* of this image shows the long-axis view of the arterial duct. *Arrowheads* indicate the spinal cord
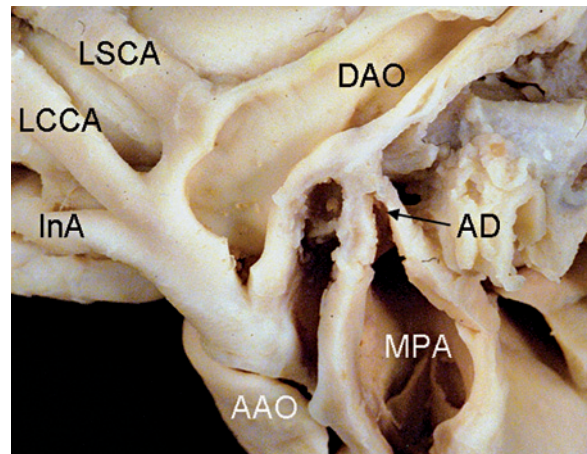
Fig. 21.10 • In this fetal specimen, the distal aortic arch, the first portion of the descending aorta, and the main pulmonary artery are windowed to highlight an in utero closure of the arterial duct. *AAO* ascending aorta, *AD* arterial duct, *DAO* descending aorta, *InA* innominate artery, *LCCA* left common carotid artery, *LSCA* left subclavian artery, *MPA* main pulmonary artery

Windowing the Heart

This method allows a "window" to be opened with a scalpel or scissors in the cardiac chambers or vessels by cutting out a portion of their wall to show abnormalities inside. This type of dissection can be applied to small hearts (Fig. 21.10).

## New Technique for the Autopsy

The rate of postmortem examinations of newborns and children has been declining over the last 30 years for different reasons, including the steady decline of parental consent and the reluctance of physicians to subject the corpse to internal examination of organs [10, 11]. In 1990, Ros et al. [12] proposed the use of magnetic resonance imaging (MRI) as an alternative to the perinatal necropsy. In fact, MRI provides good soft-tissue imaging, and there are several advantages in the postmortem setting compared with its use in life: the absence of motion artifacts, the unlimited acquisition time, and the possibility of placing the receiver coil close to the area of interest without concern for exposure dosage, which allows high-resolution images. Several studies have reported that MRI in the fetus provides a detailed insight into fetal anatomy, pathology, and etiology in a wide range of abnormalities [13]. Computed tomography (CT) scanning is superior to MRI for assessing bony structures and pro-

vides excellent visualization of skeletal abnormalities, allowing data acquisition for further three-dimensional reconstruction. Excellent anatomical evaluation is obtained by a combination of postmortem MRI and CT scanning. The documentation and analysis of postmortem findings with CT and MR imaging and postprocessing techniques (the so-called virtual autopsy) is noninvasive, less investigator dependent, and will probably lead to qualitative improvement in forensic pathologic investigation [14].

As to the cardiovascular system, there is general agreement that cardiac anomalies are difficult to identify on postmortem fetal MRI [15–17]. This is due to poor resolution of the technique for very small structures, the loss of circulation, and clotting inside the cardiac chambers. A learning curve is necessary also, because image interpretation must be adapted to postmortem conditions and the admitted inexperience with complex congenital heart diseases of most investigators.

Because of the limited availability of the instrumentation, high costs, and limited experience of investigators, it is highly unlikely that MR/CT imaging will replace, in the foreseeable future, traditional autopsy examination of the fetal heart. However, the new methodologies represent a new frontier and will be a promising substitute for autopsy if combined with minimal tissue sampling [18]. The role of the pathologist in the field of the congenitally malformed heart has been recently reviewed [19].
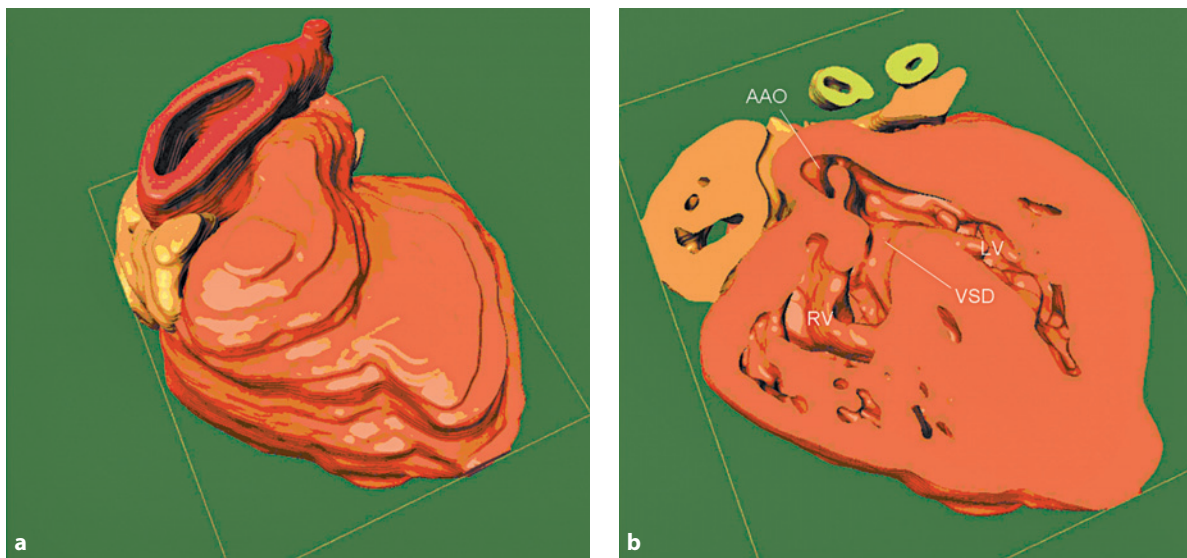
Fig. 21.11 • General view (**a**) of a tridimensional model in a 12-week gestational-age fetal heart. A ventricular septal defect associated with aortic overriding (**b**) virtual sectioning by a clipping plane passing through the 3D model, revealing the defects. *AAO* ascending aorta, *LV* left ventricle, *RV* right ventricle, *VSD* ventricular septal defect

Because of the growing number of pregnancy terminations for fetal malformations detected very early in gestation, there is a growing interest to obtain reliable autopsic studies on the hearts of very small fetuses. A new technique, applicable in this setting, was recently reported by Bussolati and colleagues [20]. The technique first requires paraffin embedding of the whole heart. Then, to allow proper alignment of the sections, fiducial markers are introduced in the block, close to the specimen. Three to four tissue cores of anthracotic lymph node are introduced in the block using a tissue micro arrayer, then serial sections are performed. Sections are stained with hematoxylin and eosin and scanned. Digital color pictures are stored in JPEG format to be processed with dedicated software for 3D reconstruction [20, 21]. Three-dimensional-model elaboration is obtained as a mesh polygonal structure using a specific algorithm model rendering. This is obtained with a rough wireframe model, with texture characterized by a specific color and a particular degree of sheen and transparency. Once the model is created, the software allows navigation and, most importantly, virtual sectioning by clipping planes (Fig. 21.11). However, this technique requires longer technical work time.

cur in isolation or are variably associated, an approach based on "pattern recognition" is doomed to be unsuccessful. An embryogenetic approach to diagnosing and classifying cardiovascular defects is confusing rather than helpful to the pathologist. Pathologists need to apply the same type of approach as the echocardiographer does, as most congenital heart diseases show disordered morphology rather than histological changes.

Diagnosis of any congenital heart malformation requires the ability to recognize the morphological features of each cardiac segment independently of its location and to investigate the heart sequentially. Since the first report – which revolutionized the diagnosis of congenital heart disease [22] – sequential analysis has been reviewed [23, 24] on the basis of a new concept that has proven its value in several fields. In essence, one particular feature of the heart, which is itself variable, should not be used as the defining feature for that particular cardiac component. Instead, the component should be defined on the basis of its most constant feature. Such sequential analysis is a simple descriptive approach that allows accurate and reproducible description of every heart, even those with the most complex abnormalities.

Description of Cardiovascular Defects

Congenital heart malformations are usually considered to be too difficult to diagnose and describe. Because of the wide range of cardiac lesions that oc-

Iconographic Documentation

Good photographic documentation of the heart is recommended, whether in situ or isolated, from the outside before cutting and from the inside after

cutting [25]. Such documentation is useful for diagnostic, research, teaching, and sometimes legal, purposes. No descriptive words can replace the information obtained from high-quality images, either still-frame or video. Some technical suggestions follow.

Choice of Equipment

Digital techniques now outweigh traditional photographic techniques. Digital images can be checked immediately after the shot is taken, and pictures are easily transmitted to other parties though different forms of media and are more practical for archiving. Moreover, by avoiding the use of film, the process of developing and printing is more economical. The use of a single-lens reflex camera with interchangeable lenses is preferable, as it allows total control over angle, depth of field, and exposure time. Because they are so small, fetal hearts require the use of macro lenses.

Lighting

Two diffused light sources at a 45° angle should be used for general lighting of the subject to be photographed. An additional spotlight can be employed to highlight specific details and increase the 3D effect. Whenever possible, a flashlight is to be avoided. To prevent reflections, every surface to be pho-

tographed should be dried carefully. A polarizing filter on the camera lens and the light sources is recommended. This filter is useless if a flashlight is employed.

Background

In general, the background should be black and without reflections. Black velvet or flat black cloth is suitable (Figs. 21.12, 21.13).

Image Quality

All digital cameras compress the photos before storing them on a flash memory card. The most common compression format is JPEG (Joint Photographic Experts Group), which has the advantage of drastically reducing the size of an image but the disadvantage of losing part of the content. The higher the compression, the lower the size of memory occupied. Nearly all cameras provide at least three bands of quality, which relate to different levels of compression. These levels are usually identified by the words basic (the lowest), normal (standard), and fine (the highest). The more sophisticated digital cameras also allow saving in TIFF (Tagged Image File Format) format. TIFF is very widespread in the world of graphics and publishing. This format allows a low degree of compression and preserves all the information from the original snapshot. However, it has
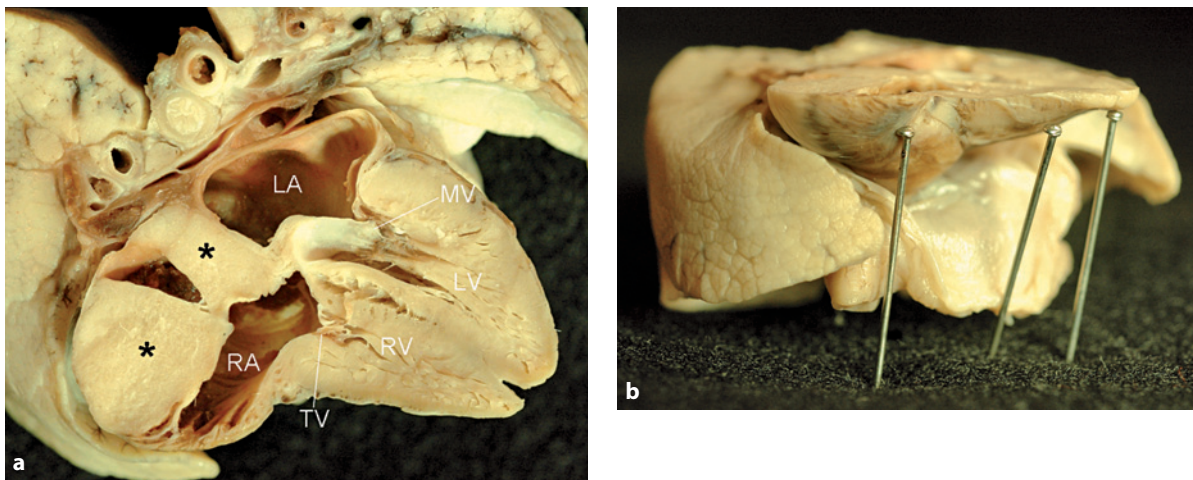
Fig. 21.12 • The heart and lung block cut in a simulated four-chamber section to show a very large tumor filling the cavity of the right atrium (*black asterisk*) (**a**). To avoid reflections during photography, the surface of this specimen has been thoroughly dried. The background is black velvet. The surface of the specimen is maintained horizontal by suspending it on pins, which are hidden behind the photographed surface (**b**). *LA* left atrium, *LV* left ventricle, *MV* mitral valve, *RA* right atrium, *RV* right ventricle, *TV* tricuspid valve
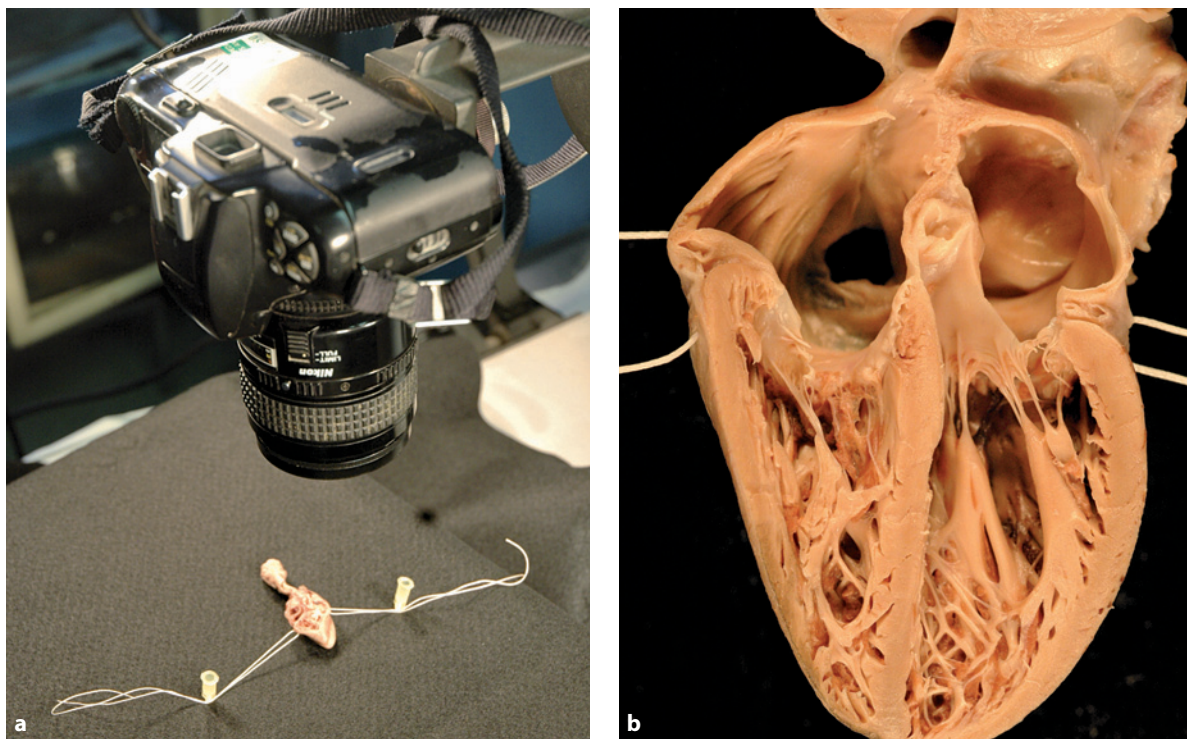
Fig. 21.13 • Light sources (outside the field of this picture) and camera are mounted on a stand (**a**). To open the lumen of the cardiac chambers, the heart specimen is distended with a surgical suture fixed to two hypodermic needles stuck into a foam board covered with black velvet as background. Close-up of the cardiac specimen shows atrioventricular valves distended by the sutures (**b**)

the disadvantage of producing very large files. As an alternative to TIFF, a third format is often available, called RAW (crude). This format preserves all the original information of the image, but it is not standard and may change depending on the manufacturer. Computer software may be necessary to convert RAW files into an international format. Contrary to what one might assume, RAW and TIFF format files offer very few tangible benefits over JPEG and conversely increase consumption of memory and battery and image processing time. For everyday practice, we recommend the JPEG format in fine or normal mode, which virtually guarantees images of good quality and occupies less space. Using JPEG format, one should remembered that repeatedly saving the same picture implies a loss of data, because the image is compressed after every change. It is therefore good practice to keep the original image and produce as many copies as there are changes one wants to obtain. Fine standard is recommended for scientific purposes when quality is essential and the maximum resolution available is required. This is the only setting that allows enlarging a picture for small details without losing definition.

Exposure Time and Depth of Field

Using a camera that allows setting the exposure time and diaphragm is recommended. To achieve a high depth of field, such as bringing into focus every plane of the subject to be represented, a small lens openings is required, usually F/8, F/11, F/16. Macro lenses with small lens openings require long exposure times, even with strong light sources. Because the shortest time for freehand shooting is 1:60 s, a tripod or other stabilizer is essential if a longer exposure time is required. In general, the best results are obtained with strong light sources, small diaphragm, and long exposure time, with the camera fixed on a stand.

To hold the small specimens to be photographed in the proper position, some tricks are useful. We suggest using a foam or cork board covered with the material chosen as background (see above). Long straight pins can be used to fix or raise the specimen in the required position (Fig. 21.12b). Sometimes it is necessary to open the lumen of a cardiac chamber or a vessel to improve the visual angle inside. For this purpose, a very thin tensioned
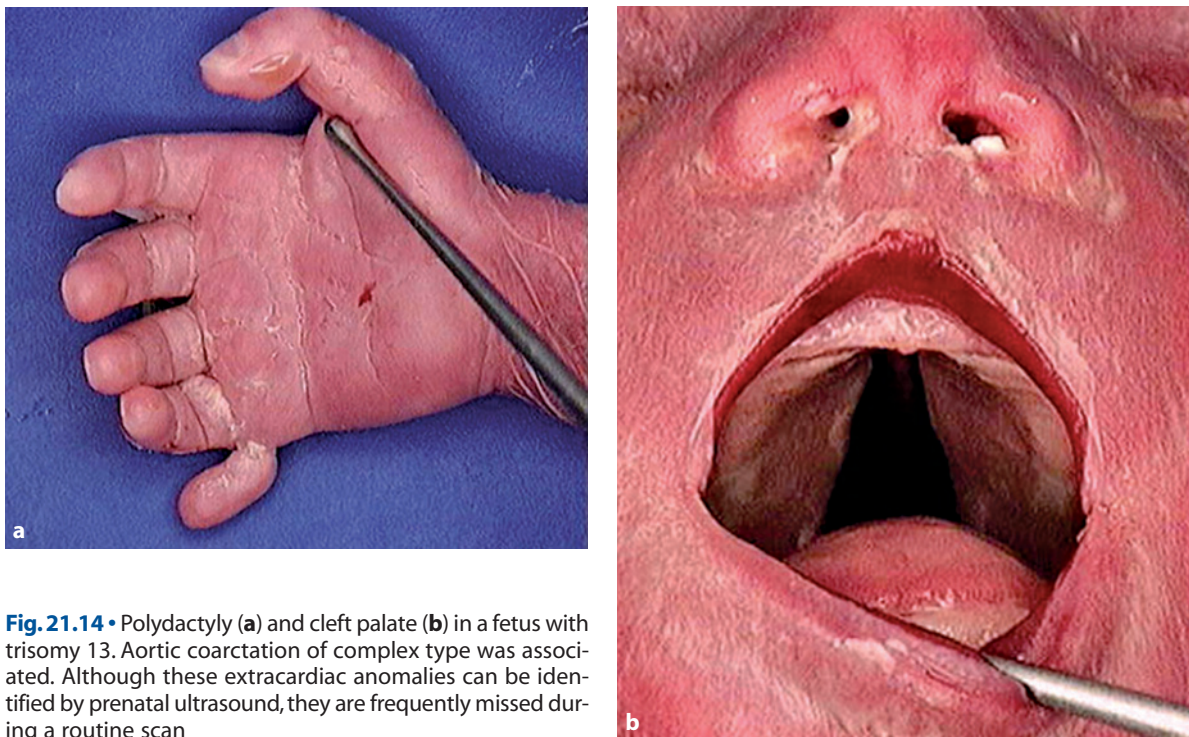
Fig. 21.14 • Polydactyly (**a**) and cleft palate (**b**) in a fetus with trisomy 13. Aortic coarctation of complex type was associated. Although these extracardiac anomalies can be identified by prenatal ultrasound, they are frequently missed during a routine scan

suture on both edges of the cavity may enlarge the cavity to be photographed. The end of the suture can be fixed to the board with a hypodermic needle or a large pin (Fig. 21.13).

Conclusion

Despite major progress in imaging technologies in prenatal diagnosis, clinical usefulness of traditional autopsy examination is still irreplaceable in the field of fetal heart disease. Autopsy often provides crucial information that allows identification of unsuspected associated anomalies (Fig. 21.14) and the understanding of pathogenetic mechanisms of an anomaly, thus affecting genetic counseling. Correlation between ultrasound and autopsy findings provides valuable educational information and improved accuracy of prenatal diagnostic imaging. Among the new techniques, postmortem MR/CT imaging will probably become an alternative to traditional autopsy, or at least an integral part of postmortem examination of the fetus and infant, indi-

cating the type of further examination necessary for a given case.

Whatever the future scenario, a growing interaction between experts in the field of cardiology, fetal medicine, pathology, and radiology will be required. We agree with Dr. Sebire [18] that a new subspecialty will probably develop in which the knowledge of the fetal/pediatric pathologist, an expert of direct examination of the fetus with postmortem changes, organ-specific pathology, and histopathological findings, will be shared with that of the perinatal cardiologist and the fetal medicine specialist, who are more confident with examining the morphology and physiology of the fetal cardiovascular system with cross-sectional and 3D ultrasound, and finally with the radiologist, who is best equipped in the technical aspect of MR/CT image generation, acquisition, and manipulation. It is our belief that the approach to the study of the fetal heart by projections, described in the pages of this book, will be the common "language" for these experts, independent of the type of imaging technique (morphological, ultrasonographic, radiological, or by magnetic resonance) used.

References

1. Bove KE (1997) Practice guidelines for autopsy pathology: the perinatal and pediatric autopsy. Autopsy Committee of the College of American Pathologists. Arch Pathol Lab Med 121:368–376

2. Gordijn SJ, Erwich JJHM, Khong TY (2002) Value of perinatal autopsy: critique. Pediatr Devel Pathol 5:480–488

3. Siebert JR, Kapur RP (2000) Congenital anomalies in the fetus: approaches to examination and diagnosis. Path Case Rev 5:3–13

4. Redfern M, Keeling JW, Powell E (2001) The Royal Liverpool Children's Inquiry Report. The Stationary Office, Norwich, UK

5. Kennedy L (2001) The report of the public inquiry into children's heart surgery at The Bristol Royal Infirmary 1984–1995. Learning from Bristol. The Stationary Office, Norwich, UK

6. Cook CA, Yates RW, Anderson RH (2004) Normal and abnormal fetal cardiac anatomy. Prenat Diagn 24:1032–1048

7. Sheaff MT, Hopster DJ (2005) Post mortem technique handbook. Springer, London, pp 119–140

8. Gilbert-Barness E, Debich-Spicer DE (2005) Handbook of pediatric autopsy pathology, Humana Press, Totowa, pp 191–250

9. Gilbert-Barness E (2007) Potter's pathology of the fetus, infant and child, 2nd edn. Mosby Elsevier, Philadelphia, pp 969–1071

10. Brodlie M, Laing IA, Keeling JW, et al (2002) Ten years of neonatal autopsies in a tertiary referral centre: retrospective study. BMJ 324:761–763

11. Okah FA (2002). The autopsy: experience of a regional neonatal intensive care unit. Paediatr Perinat Epidemiol;16:350–354

12. Ros PR, Li KC, Vo P et al (1990) Preautopsy magnetic resonance imaging: initial experience. Magn Reson Imaging 8:303–308

13. Brookes JS, Hagmann C (2006) MRI in fetal necroscopy. J Magn Reson Imag 24:1221-1228

14. Jackowski C, Schweitzer W, Thali M et al (2005) Virtopsy; postmortem imaging of the human heart in situ using MSCT and MRI. Forensic Sci Int 149:11-23

15. Woodward PJ, Sohaey R, Harris DP et al (1997) Postmortem fetal MR imaging: comparison with findings at autopsy. AJR Am J Roentgenol 168:41–46

16. Alderliesten ME, Peringa J, van der Hulst VP et al (2003) Perinatal mortality: clinical value of postmortem magnetic resonance imaging compared with autopsy in routine obstetric practice. BJOG 110:378–382

17. Huisman TA, Wisser J, Stallmach T et al (2002) MR autopsy in fetuses. Fetal Diagn Ther 17:58–64

18. Sebire NJ (2006) Towards the minimally invasive autopsy? Ultrasound Obstet Gynecol 28: 865-867

19. Aiello VD, Debich-Spicer D, Anderson RH (2007) Is there still a role for cardiac autopsy in 2007? Cardiol Young 17:97-10

20. Bussolati G, Marchiò C, Volante M (2005) Tissue arrays as fiducial markers for section alignment in 3-D reconstruction technology. J Cell Mol Med 9:438-445

21. Fredouille C, Morice JE, Delbecque K et al (2006) New fetopathological section of the heart. Correlated to the ultrasonographic 4-chamber view in fetuses. Ann Pathol 26(1):60-65

22. Van Praagh R (1972) The segmental approach to diagnosis in congenital heart disease. In: Bergsma D (ed) Birth defects original article series, vol VIII, no. 5, The National Foundation – March of Dimes. Williams & Wilkins, Baltimore, pp 4-23

23. Anderson RH, Ho SY (1997) Continuing medical education, Sequential segmental analysis - description and categorization for the Millenia. Cardiol Young 7:98-116

24. Anderson RH (2000) Nomenclature and classification; sequential segmental analysis. In: Moller JH, Hoffman JIE (eds) Pediatric cardiovascular medicine. Churchill Livingstone, New York, pp 263-274

25. Varetto L, Gargallo C, Botta G et al (2008) Photographic documentation of autopsies. Minerva Medicoleg 128:1-7

Credits for Figures

Credits for Figures - DVD

Slide 3: G. Botta and A.C. Cook
All other pictures (still frames and moving images), E.M. Chiappa

7. The Five-Chamber View
Slide 1: left picture, A.C. Cook; right diagram, E.M. Chiappa
Slide 2: small left picture, A.C. Cook; large section, G. Botta
Slide 3: G. Botta
All other pictures (still frames and moving images), E.M. Chiappa

8. The Three-Vessel View
Slide 1: left picture, A.C. Cook; right diagram, E.M. Chiappa
Slide 2: G. Botta
All other pictures (still frames and moving images), E.M. Chiappa

9. The Arterial Duct Transverse View
Slide 1: left picture, A.C. Cook; right diagram, E.M. Chiappa
Slide 2: A.C. Cook
Slide 3: small frame, A.C. Cook; still frames and moving images, E.M. Chiappa
Slide 4: small frame, A.C. Cook; still frames and moving images, E.M. Chiappa
Slide 5: small frame, A.C. Cook; still frames and moving images, E.M. Chiappa
Slide 6: small frame, A.C. Cook; still frames and moving images, E.M. Chiappa
All other pictures (still frames and moving images), E.M. Chiappa

10. The Aortic Arch Transverse View
Slide 1: left picture, A.C. Cook; right diagram, E.M. Chiappa
Slide 2: G. Botta
Slide 3: small frame, A.C. Cook; still frames and moving images, E.M. Chiappa
Slide 4: still frames and moving images, E.M. Chiappa
Slide 5: small frame, A.C. Cook; still frames and moving images, E.M. Chiappa
All other pictures (still frames and moving images), E.M. Chiappa

11. The Arterial Duct and Aortic Arch Transverse View
Slide 1: left picture, A.C. Cook; right diagram, E.M. Chiappa

Slide 2: G. Botta
All other pictures (still frames and moving images), E.M. Chiappa

12. The Inferior and Superior Caval Vein Long-Axis View (The Bicaval View)
Slide 1: left picture, A.C. Cook; right diagram, E.M. Chiappa
Slide 2: G. Botta
All other pictures (diagrams, still frames, and moving images), E.M. Chiappa

13. The Aortic Arch Long-Axis View
Slide 1: left picture, A.C. Cook; right diagram, E.M. Chiappa
Slide 2: G. Botta
Slide 3: G. Botta
All other pictures (diagrams, still frames, and moving images), E.M. Chiappa

14. The Arterial Duct Long-Axis View
Slide 1: left picture, A.C. Cook; right diagram, E.M. Chiappa
Slide 2: G. Botta
All other pictures (drawing, still frames, and moving images), E.M. Chiappa

15. The Right Ventricular Outflow View
Slide 1: left picture, A.C. Cook; right diagram, E.M. Chiappa
Slide 2: G. Botta
All other pictures (still frames and moving images), E.M. Chiappa

16. The Left Ventricle Short-Axis View
Slide 1: left picture, A.C. Cook; right diagram, E.M. Chiappa
Slide 2: G. Botta
Slide 3: A.C. Cook
All other pictures (still frames and moving images), E.M. Chiappa

17. The Left Ventricle Long-Axis View
Slide 1: left picture, A.C. Cook; right diagram, E.M. Chiappa
Slide 2: G. Botta
All other pictures (still frames and moving images), E.M. Chiappa